Ludger O. Figura
Arthur A. Teixeira

Food Physics

Physical Properties – Measurement and Applications

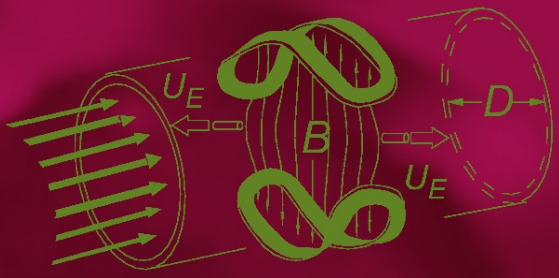

Springer

Food Physics

Physical Properties – Measurement and Applications

Ludger O. Figura
Arthur A. Teixeira

Food Physics

Physical Properties – Measurement and Applications

With 131 Figures and 208 Tables

Springer

Professor Dr. Ludger O. Figura
Hochschule Bremerhaven
University of Applied Sciences
An der Karlstadt 8
27568 Bremerhaven
Germany
lfigura@hs-bremerhaven.de

Professor Arthur A. Teixeira Ph.D., P.E.
Agricultural and Biological Engineering Department
University of Florida
207 Frazier Rogers Hall
P.O. Box 110570
Gainesville, FL 32611-0570
USA
atex@ufl.edu

Library of Congress Control Number: 2007925693

ISBN 978-3-540-34191-8 Springer Berlin Heidelberg New York
DOI 10.1007/b107120

Springer is a part of Springer Science+Business Media
springer.com

Cover-Design: WMXDesign GmbH, Heidelberg
Typesetting: PTP-Berlin Protago-TEX-Production GmbH, Germany
Production: LE-TEX Jelonek, Schmidt & Vöckler GbR, Leipzig, Germany
Printed on acid-free paper 52/3180/YL - 5 4 3 2 1 0

Foreword

This new book, *Food Physics: Physical Properties – Measurement and Applications*, is an expanded version of the text in German, *Lebensmittelphysik* (Springer, 2004), by the first author, Ludger Figura. It is the result of collaboration between Ludger Figura and Art Teixeira who have been teaching food physics and physical properties of foods at the Bremerhaven Hochschule (Germany) and the University of Florida (USA), respectively. The book is a timely addition that will serve as a useful resource on the physics and physical properties of foods. It should be useful worldwide to teach junior- or senior-level undergraduate students. In addition, it should find use in food companies because, as the authors point out: "it is essential that food companies be able to design and control their processing operations to assure maximum product quality and safety and to develop new and improved food products and quality attributes desired by the consuming public."

There are fourteen chapters, in order: Water Activity, Mass and Density, Geometric Properties: Size and Shape, Rheological Properties, Interfacial Phenomena, Permeability, Thermal Properties, including Heat Transfer in Food, Electrical Properties, Magnetic Properties, Electromagnetic Properties, Optical Properties, Acoustical Properties, Radioactivity, and On-Line Sensing. Each subject was given its due weight. The first seven chapters cover about 62% of the book. In addition, there are several appendices on relevant topics, such as: Units and their Conversion, Distribution Functions, Complex Numbers, Greek Letters, Properties of Water, and Conversion Charts for: Temperature, Sugar Concentration, as well as Relevant Literature references.

I enjoyed reading an early draft of *Food Physics: Physical Properties – Measurement and Applications*. I am sure that students and researchers of Food Physics and Physical Properties will find it to be a useful and worthy text.

M.A. Rao
Emeritus Professor (Active), Food Engineering
Cornell University, Geneva, NY

Preface

Why should there be a book about food physics and the physical properties of foods? In order for the food processing industry to increase food safety and to be competitive in an ever expanding global market place, it is essential that food companies be able to design and control their processing operations to assure maximum product quality and safety and to develop new and improved food products with quality attributes desired by the consuming public. The food scientists and engineers entrusted with the responsibility for developing the means by which these results can be achieved will have to have mastered a fundamental knowledge base in the physical properties of food materials, and the science of food physics, which provides the scientific principles upon which these properties can be understood and applied. This book was conceived with this purpose in mind.

The book is intended for both food scientists and food engineers, as reflected in the chosen title and subtitle for the book. The title *Food Physics* is directed to food scientists who recognize the importance of food physics as a core part of a food science curriculum, along side food chemistry and food microbiology, for understanding the physical behavior of food materials. The subtitle *Physical Properties – Measurement and Applications* is directed to food engineers who are always in need of physical properties for process design and control applications, and recognize that such physical properties can only come from the study of food physics. In fact, it has been the relatively recent introduction of food engineering into the food process industries over the past few decades that called attention to the need for physical properties and the study of food physics in the combined fields of food science and engineering.

Food physics offers considerable breadth in the range of topics covered, as well as depth of coverage in each topic. The book contains fourteen chapters with each chapter related to a different field of physics in which physical properties of foods are important. Nearly all areas of physics are covered, beginning with water activity and the role of moisture content in foods, followed by basic properties of mass and density and size and shape, and then continuing through mechanical, rheological, thermal, and electromagnetic radiation properties and their applications, including electrical, magnetic, optical, acoustical, and ionizing radiation properties. The final chapter of the book introduces the reader to the exciting new world of in-line sensors for the on-line measurement of physical phenomena that can be used as indirect indicators of food

properties or quality attributes that must be controlled in closed-loop feed back control systems for on-line process control in food process automation.

The material in each chapter is presented at several levels of depth so that the book can serve as an instructional text for students at one level, a source book on theory and scientific principles for researchers at another level, and a handy reference book for practicing professionals in the field on a third level. The presentation of material in each chapter has been crafted with the undergraduate college student in mind first. Basic scientific principles and theory are explained in simple clear language, drawing on examples of every day life experiences to help students understand the concepts. The derivation of mathematical expressions is carried out in a step-by-step sequence of logic so that students can fully appreciate the subsequent use of these expressions in making the necessary calculations, and most chapters include examples for the students to gain exercise in the calculations. Each chapter also contains further discussion of scientific principles and theory with suggestions and examples of possible new applications with the research graduate student and scientist in mind. Also included in each chapter are cited references to which the reader may go for more detailed information on specific applications of the related physical properties.

The authors have combined their experience of more than thirty years teaching food properties to undergraduate food science and engineering students to make this book possible. The book, itself, is primarily an English translation of the recent German text *Lebensmittelphysik* by Figura, published by Springer in 2004. At the time that first book was published, Figura and Teixeira had already teamed up to begin collaboration on an English language version of the book through a series of exchange visits. This new book, *Food Physics: Physical Properties – Measurement and Applications* is the result of that collaboration.

Quakenbrück, Germany — Ludger Figura
June 2007 — Arthur Teixeira

Contents

1 Water Activity

1.1 Introduction

Water is an important component of nearly all food materials, and plays a decisive role in dictating the physical properties, quality and microbial, chemical and biochemical degradation of the food material [1]. For most food materials, unless the moisture content is reduced below 50% (wet basis), much of the water content is freely available to behave physically as pure water with properties such as vapor pressure equal to pure water. As moisture content is lowered further, a point will be reached at which the water becomes less active in that it cannot act physically or chemically as pure water. For example, it cannot freeze or act as a solvent or reactant. In this state, it is considered to be bound water.

The way in which water is bound to the internal structure of the food, the degree to which it is freely available to act as a solvent, to vaporize or freeze, or the degree to which it is chemically bound and unavailable can all be reflected by an ability to specify the water activity of a food material. The matrix presented in Table 1.1 attempts to illustrate the range of conditions under which water may be bound and the role it can play under each condition [6]. The water activity of a food can be thought of as the equilibrium relative humidity of the food material. When a food sample comes into equilibrium with the atmosphere surrounding it, the water activity in the food sample becomes equal to the relative humidity of the atmosphere surrounding it. Once this equilibrium is reached, the food sample neither gains nor loses moisture over time. A more comprehensive definition of water activity will be given later in this chapter.

1.1.1 Time to Reach Equilibrium

The equilibrium relative humidity described above comes about as a result of a two-step process involving transfer of water vapor between the food sample and the surrounding fluid atmosphere. In one step, water vapor must transfer across the boundary surface of the sample in the form of adsorption or desorption, depending upon whether water vapor is entering or exiting the sample.

Table 1.1. Types of water binding and related heats of binding [6]

	adhering water droplets	capillary water		water as a solute	adsorbed water	crystal water	water of constitution
description	water dropping from bodies	water in coarse capillaries	water in fine capillaries	water between molecules	water sitting on surfaces	water belonging to a crystal lattice	water in a compound
binding	none	mechanical	physical	physicochemical		chemical	
binding type			nonstoichiometric			stoichiometric	
water mobility	free	nearly free		decreased		none mobile	
heat of binding in J/g H_2O	0	0	0–300	0–1000	100–3300	300–2200	1000–6000
examples	wet surfaces of solids	wet sand	wet filter tissue	starch gel, gelatin gel	solid surfaces in atmospheric air	crystalline glucose-mono-hydrate	$Ca(OH)_2$

The second step involves diffusion, or absorption, of the water vapor into or out of the interior tissue structure of the sample. These two combined processes require considerable time to be accomplished, especially the diffusion process. A classic method for bringing a food sample to a specified water activity is first to weigh it and then place it in a closed chamber maintained at the controlled relative humidity desired to be reached at equilibrium. Depending on whether the sample has an initial water activity above or below the controlled target relative humidity it will either lose or gain moisture over time as it approaches equilibrium. This loss or gain of moisture will be evident as weight loss or gain, which can be monitored over time by periodically weighing the sample until no further change in weight can be detected from one day to the next. Normally, several days may be required to reach equilibrium. Therefore, it is important to understand more fully the transport phenomena of adsorption, desorption and diffusion, discussed in the following subsections.

1.1.2 Solid–Fluid Boundary Surfaces

Recall that the first of the transport phenomena mentioned above (adsorption and desorption) occur on the boundary surface at the interface between the solid food material and fluid atmosphere surrounding it (liquid or gas). Such boundary conditions in mass transfer are known as solid–liquid or solid–gas boundary surfaces. When fluid molecules are attracted to the solid surface and begin to adhere to it, the process is called adsorption with respect to the solid. When the same molecules are already present on the solid surface and are escaping from the surface by being attracted to the fluid phase, the process is called desorption with respect to the solid (Figure 1.2). For example, when a fresh moist food sample is being dried to produce a dehydrated product, it is placed into an environment of very low relative humidity. Under that condition, the free water molecules on the surface begin to escape into the relatively dry fluid atmosphere surrounding it in attempt to reach equilibrium relative humidity, and the food sample is undergoing desorption. Alternatively, when a previously dehydrated food sample is being rehydrated by being placed into a relatively humid environment or surrounded by water, the water molecules from the surrounding fluid will be attracted to the dry surface and begin to adhere to it in attempt to reach equilibrium relative humidity, and the food sample is undergoing adsorption.

The rate at which these adsorption and desorption processes take place is governed largely by the physical and chemical characteristics of the surface boundary. For example, how readily the fluid molecules can either adhere or escape from the surface can depend upon special features of the surface physical structure, such as roughness, smoothness, and porosity (having a porous structure affecting absorbance, etc.). Besides physical adsorption, there can also be chemical binding that can enhance or interfere with the surface adsorption / desorption process (chemisorption), as shown in Figure 1.2. These

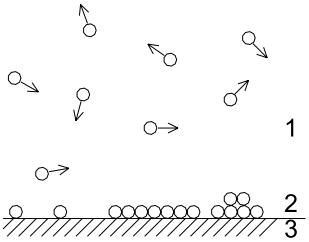

Figure 1.1. Solid surface in adsorption equilibrium with the surrounding atmosphere (schematic). **1:** gaseous phase, **2:** sorbate, **3:** sorbent

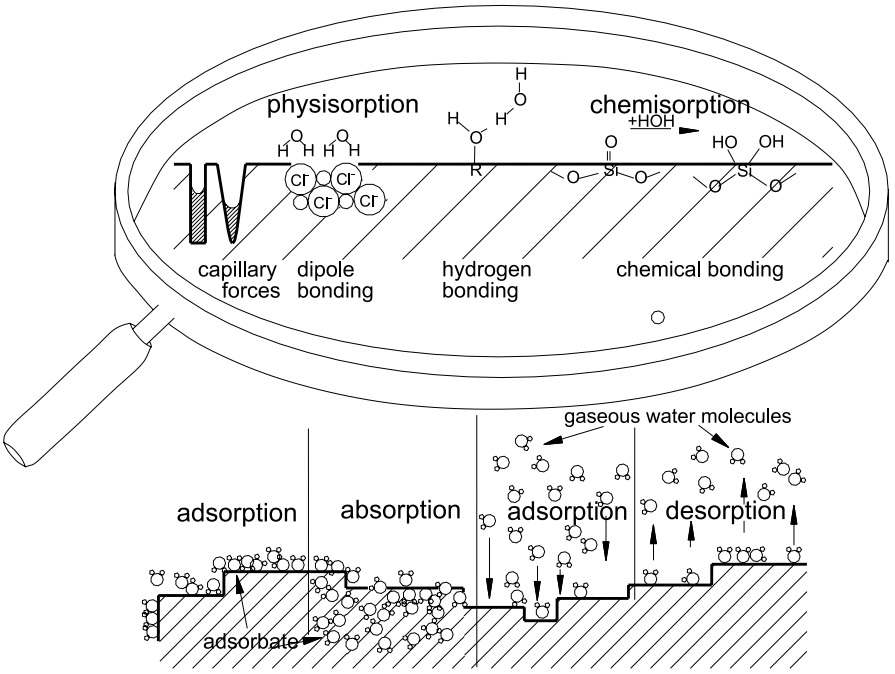

Figure 1.2. Types of binding and terms used in sorption

phenomena of adsorption and absorption will be explored more fully in the following section.

1.2 Adsorption Equilibrium

The term adsorption equilibrium refers to the steady state condition that is ultimately reached when adsorption and desorption are going on at the same time. This is a dynamic state, in which molecules are leaving the surface in a desorption process, while other molecules are attaching themselves to the surface in an adsorption process. Eventually, a dynamic equilibrium state is reached when the number of molecules leaving the surface and those attaching

themselves to the surface is the same, and the number of molecules resting on the surface remains constant on average. This is adsorption equilibrium. The various factors affecting the rate at which this equilibrium can come about are discussed in the following subsections.

1.2.1 Surface Adhesion

Another way to describe the behavior of water in foods is by the mechanisms of molecular adsorption, corresponding to "bound water" and capillary adsorption corresponding to "free water" described earlier. Molecular adsorption occurs under very low water activity when water molecules adhere to specific points in the molecular structure of the cell walls within the solid food material. When the distance between the water molecule and the cell wall becomes small enough, the force of attraction is large enough to draw the water molecule into the micelle network of the cell wall. The force of attraction at such low moisture content is so high that an "adsorption compression" results in a net decrease in volume of the solid–water aggregate. As the moisture content increases, the molecular attraction lessens and there is a volume increase, which is roughly equal to the volume of water added. Because of the initial adsorption compression, however, the total volume of the aggregate remains smaller than that of the sum of the constituents. Normally, it is undesirable to bring water activity of food materials to such low levels that irreversible damage from adsorption compression will occur.

The extent and nature of the surface on which adsorption compression can take place are likely the primary factors governing molecular adsorption. Molecular attraction can be due to electronic and VAN DER WAALS' attraction, but it is mostly due to hydrogen bonding in the case of water in foods. Thus, the greater the number of ionic or polar type molecules, the more water is held in the food material in this form. Molecular adsorption is the primary cause of swelling in hygroscopic food materials, such as starches.

At still higher moisture contents, where the vapor pressure has not yet reached the saturation point, most of the available attraction sites have been filled with water molecules, and further holding of water molecules is possible only through the formation of "water bridges," chains of water molecules extending between those molecules which have been directly adsorbed.

Nonporous Surfaces

In the case of solid food materials with nonporous surfaces when placed in contact with a gaseous phase at a different relative humidity, adsorption or desorption will take place freely at the solid–fluid boundary surface, as described earlier. During adsorption, gaseous molecules will be attracted to the solid surface and begin diffusion to the interior once the surface becomes saturated with gas-phase molecules. In the case of desorption, water molecules

from within the solid phase will be attracted to the surface, and freely escape into the gaseous phase once they reach the surface. The degree to which the molecules disperse themselves about the surface before escaping to the gaseous phase will depend upon the strength of bonding at the surface. In the case of a nonporous surface with no interference from porosity, this bonding strength is a function of the energy or enthalpy of adsorption or heat of vaporization.

Both adsorption and desorption processes take place at the same time, but very different rates, depending on the initial difference in relative humidity of the two phases. At a constant temperature and partial pressure of the gaseous phase, equilibrium will be reached when the results from both processes compensate for themselves, and conditions at the boundary surface remain constant. If partial pressure of the gaseous phase is increased, the equilibrium is disrupted, and adsorption will begin once again until the surface becomes saturated with gaseous molecules forming a complete monolayer of molecules. This is known as monomolecular adhesion of a complete monolayer. If partial pressure is increased even further, then further adsorption from the gaseous phase causes formation of multiple molecular layers. These multiple layers are held by much weaker bonds, and begin to give rise to term "free water" referred to drying technology that can be most easily evaporated. When only lower layers are present approaching only the monolayer, then the binding forces are very strong giving rise to "bound water" that is difficult to remove by evaporation. Table 1.1 shows how these levels of binding depend upon the way the water is held within the material.

Porous Surfaces

Surfaces with porous structure contain voids that promote transport of water by capillary adsorption. Capillary adsorption occurs when voids in the cellular structure are of the size to hold water in liquid form by forces of surface tension. Normally, these pore sizes would fall in meso- to macro-pore size ranges listed in Table 1.2 [2]. The size of capillaries that will fill with water under different levels of relative humidity can be estimated by the KELVIN equation below:

$$\ln \frac{p}{p_0} = \frac{2 \cdot \sigma \cdot V_m}{r_p \cdot R \cdot T} \tag{1.1}$$

with

Table 1.2. Pore size classes according to IUPAC [2]

Term	pore radius in nm
Micro-pores	< 1
meso-pores	1...25
macro-pores	> 25

$$\frac{V_m}{R} = \frac{V}{n \cdot R_s \cdot M} = \frac{V}{m \cdot R_s} = \frac{1}{\rho \cdot R_s} \tag{1.2}$$

and so

$$\ln \frac{p}{p_0} = \frac{2 \cdot \sigma}{r_p \cdot \rho \cdot R_s \cdot T} \tag{1.3}$$

where

p	vapor pressure above curved interface
p_0	saturation vapor pressure
σ	surface tension at capillary wall in $\mathrm{N \cdot m^{-1}}$
R	universal gas constant in $\mathrm{J \cdot K^{-1} \cdot mol^{-1}}$
R_s	specific gas constant in $\mathrm{J{\cdot}K^{-1} \cdot kg^{-1}}$
M	molar mass of liquid in $\mathrm{kg \cdot mol^{-1}}$
ρ	density of the liquid in $\mathrm{kg \cdot m^{-3}}$
T	temperature in K
r_P	pore radius in m
n	amount of liquid substance in mol
V	volume in $\mathrm{m^3}$
V_m	molar volume in $\mathrm{m^3 \cdot mol^{-1}}$

Example 1.1. Relative water vapor pressure in cylindrical pores for water vapor adsorption at room temperature:

$$\ln \frac{p}{p_0} = \frac{1}{r_p} \cdot \frac{2 \cdot \sigma}{\rho \cdot R_s \cdot T} = \frac{1}{r_p} \cdot \frac{2 \cdot 72.25 \cdot 10^{-3} \mathrm{N m^{-1}}}{999\,\mathrm{kg \cdot m^{-3}} \cdot 461.9\,\mathrm{J \cdot K^{-1} \cdot kg^{-1}} \cdot 293.15\,\mathrm{K}}$$

so

$$\ln \frac{p}{p_0} = \frac{1.0682\,\mathrm{mm}}{r_p}$$

This is Kelvin's equation for calculating the relative vapor pressure of droplets. Droplets have a convex shaped surface whereas liquid surfaces in capillaries have a concave shaped surface (for details refer to Section 5.1.1 and also Table 5.2). In mathematics the difference is the sign of the radius only. That is why we have to put into Kelvin's equation here negative values of the cylindrical pores, e.g.

$$\ln \frac{p}{p_0} = \frac{1.0682\,\mathrm{mm}}{-10\,\mathrm{nm}} = -0.10682 \rightarrow \frac{p}{p_0} = 0.899$$

Based on this equation, the sizes of capillaries for various relative vapor pressures are given in Table 1.3.

We can see from Table 1.3 that the vapor pressure of a liquid in a coarse capillary is slightly lower than that of unbound water. For meso-pores and micro-pores, the vapor pressure depression is remarkable.

Table 1.3. Relative vapor pressures in cylindrical pores

r_P in nm	$\ln \frac{p}{p_0}$	p/p_0
1	−1.0682	0.344
10	−0.10682	0.899
100	−0.010682	0.989
1000	−0.0010682	0.998

Bottle or Flask Shaped Pores

Reference to cylindrical-shaped pores in the previous section is only an ideal case to help explain the mechanism of capillary adsorption. A way to explain hysteresis of the sorption isotherm is to assume surfaces having pores with the shape of a bottle or flask, whose opening has a considerably smaller radius than the bottom of the pore (see Figure 1.3). Recall that the relative vapor pressure required for capillary adsorption will depend upon the pore radius. In the case of such bottle-shaped pores, the smaller radius at the top of the pore will govern the vapor pressure needed for the process of desorption (drying), in which water molecules must be drawn out from the bottom of the pore. However, in the case of the adsorption process when the material starts out in the dry form and the pores are initially empty of free water, the water molecules adsorb at the larger radius at the bottom of the pore. This will require a greater vapor pressure to reach the same level of moisture content during desorption than was required during adsorption. This difference in vapor pressure that is needed to reach the same level of moisture content depending on the direction of the process (adsorption or desorption) is often given as a possible explanation for the hysteresis observed in most sorption isotherms of food materials (graph IV in Table 1.4). Sorption isotherms will be discussed at some length in the following sections.

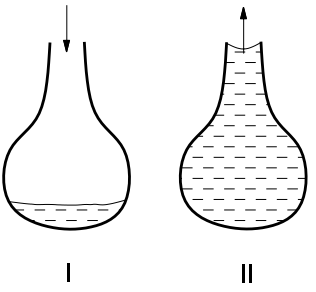

Figure 1.3. The capillary radius on adsorption (I) is different from that on desorption (II) when a pore has the shape of a bottle or flask (schematic)

1.2.2 Sorption Isotherms

Sorption isotherms are graphical plots of the equilibrium between surface adhesion forces and the partial pressure of the gaseous adsorbent at the boundary surface over a range of partial pressures at a constant temperature. Four classic types of sorption isotherms encountered in scientific studies are shown in Table 1.4 along with names of the mathematical models that are used to characterize each type [4].

Table 1.4. Four main types of sorption isotherms

I	II	III	IV
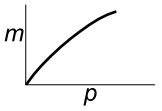	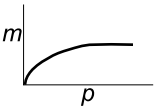	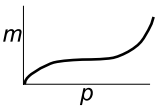	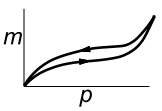
Freundlich	Langmuir	BET / GAB	BET / GAB with pores

1.2.3 Freundlich Model

The Freundlich model is given by equation (1.4), and is intended to characterize the isotherm when it shows nearly no saturation behavior (Type I) when adhesion at the boundary surface takes place. Since the Freundlich model is a simple power law equation, taking logarithms of both sides will produce a linear equation (1.4) from which the Freundlich constants (a_F and b_F) in the model can be obtained by linear regression of a log–log plot of equation (1.5). The constant b_F is taken from the slope of the straight line log–log plot, and the constant a_F can then be found by substitution. The Freundlich model is the model of choice when sorption isotherms are to be analyzed in regions of very low partial pressure. However, when regions of higher partial pressure are important, other models like the Langmuir and BET / GAB models described in the following discussion are better suited.

$$m = a_F \cdot p^{b_F} \tag{1.4}$$

or

$$\lg m = \lg a_F + b_F \cdot \lg p \tag{1.5}$$

where

m	mass of adsorbent in kg
a_F, b_F	Freundlich constants ($0 < b_F < 1$)
p	partial pressure in Pa

1.2.4 Langmuir Model

The Langmuir model focuses on characterizing the saturation behavior of the sorption process. This is the region in the sorption isotherm where the curve tends to flatten out (Type II). This region of the isotherm is often explained by realizing that it normally covers the range of partial pressures over which molecular adhesion at the boundary surface is a saturated monolayer. Under this condition a relatively wide shift in partial pressure may produce relatively little change in molecular adhesion at the surface. The model is based upon the assumption that in adsorption equilibrium the rates of adsorption k and desorption k' must produce an equal end result, as reflected in equations (1.6) and (1.7):

$$k \cdot p \cdot (1 - m) = k' \cdot m \tag{1.6}$$

$$m = \frac{k \cdot p}{k \cdot p + k'} \tag{1.7}$$

Over the range of the curve:

$$m = m_{\max} \frac{p}{p + b} \tag{1.8}$$

where

M	mass of adsorbent in kg
$m_{\max}$	maximum mass of adsorbent in kg
k, k'	rate constants
b	Langmuir constant in Pa
p	partial pressure in Pa

The Langmuir model starts out with the assumption of a homogeneous monomolecular layer in which the adsorbent is held with maximum adhesion at the surface $m_{\max}$. The model parameters ($b, m_{\max}$) can be determined by writing the equation in the form of

$$\frac{1}{m} = \frac{1}{m_{\max}} + \frac{b}{m_{\max}} \cdot \frac{1}{p} \tag{1.9}$$

This is the equation of a straight line in a graph of $\frac{1}{m}$ versus $\frac{1}{p}$. The slope $\frac{b}{m_{\max}}$ and intercept $\frac{1}{m_{\max}}$ will give the constants.

The saturation behavior described by the Langmuir model applies to gas and liquid phase adsorption, particularly in the case of chemisorption (see Figure 1.2) when the monomolecular layer covering the boundary surface cannot be exceeded. If the monolayer were to become covered with additional molecular layers, this would give rise to multilayer adsorption, as in the case of physisorption (see Figure 1.2). In this case the Langmuir model would fail, and the Brunnauer, Emmet and Teller (BET) model, described next, should be used instead. Table 1.5 gives an overview of the applicability of these various models at increasing partial pressure.

Table 1.5. Adsorption models and its range of application

General: $\frac{m}{m_{max}} = \frac{p}{p+b}$		
for small p	for middle p	for higher p
$\frac{m}{m_{max}} = \frac{1}{1+\frac{b}{p}}$	$m = m_{max}\frac{1}{1+\frac{b}{p}}$	$\frac{m}{m_{max}} = \frac{p}{p+b}$
$\frac{m}{m_{max}} \approx \frac{p}{b}$	$m = m_{max} \cdot k' \cdot p^{b_F}$	$\frac{m}{m_{max}} \approx \frac{p}{p} = \text{const.}$
$m = k \cdot p$	$m = a_F \cdot p^{b_F}$	$m = m_{max}$
Henry's law	Freundlich model	Langmuir model

Note that the Langmuir model changes into the Freundlich model as partial pressures decrease from the intermediate range. At very low partial pressures the Freundlich model becomes practically identical with Henry's law.

1.2.5 BET Model

Once multilayer molecular adsorption is reached, further increase in partial pressures will cause the isotherm to depart from the relatively flat region characterized earlier by the Langmuir model, and it will begin to increase dramatically reflecting the weakening bonds of multilayer adhesion. When the isotherm is examined over the full range of partial pressure, it will take on a sigmoid shape (Types III and IV in Table 1.4). The best known and most widely used mathematical representation of the complete adsorption phenomenon in biological materials is given by the BET equation (1.10), after Brunnauer, Emmet and Teller [5], because it mathematically characterizes the entire isotherm over all three regions:

$$\frac{p}{V \cdot (p_s - p)} = \frac{1}{V_a \cdot C} + \frac{C-1}{V_a \cdot C} \cdot \frac{p}{p_S} \tag{1.10}$$

with

$$V \cdot \frac{1}{\rho} = m \tag{1.11}$$

and the abbreviation

$$\frac{p}{p_S} = \varphi \tag{1.12}$$

it is

$$\frac{\frac{p}{p_S}}{m \cdot \left(1 - \frac{p}{p_S}\right)} = \frac{1}{m_a \cdot C} + \frac{C-1}{m_a \cdot C} \cdot \frac{p}{p_S} \tag{1.13}$$

respectively

$$\frac{\varphi}{m \cdot (1-\varphi)} = \frac{1}{m_a \cdot C} + \frac{C-1}{m_a \cdot C} \cdot \varphi \tag{1.14}$$

where

p	partial pressure in Pa
ρ	density of the adsorbent in kg · m^{-3}
φ	relative partial pressure
V_a	volume of the monolayer in m^3
m_a	mass of the monolayer in kg
C	BET constant
m	mass of adsorbent in kg
V	Volume of adsorbent in m^3
p_S	saturation vapor pressure in Pa

The BET equation can undergo a linear transformation by creating a graphical plot of $\frac{1}{m} \cdot \frac{\varphi}{1-\varphi}$ against φ, as shown in Figure 1.4. This produces a straight line having an equation in the form $y = a + b \cdot \varphi$.

The BET constant C can be obtained from the slope and intercept of this straight line using the expression, $C = \frac{b}{a} + 1$, the monolayer mass m_a from equation (1.15):

$$m_a = \frac{1}{a\left(\frac{b}{a} + 1\right)} = \frac{1}{a+b} \tag{1.15}$$

The BET model has a strong advantage over the Freundlich or Langmuir models because of its validity over the full range of partial pressures. It has become a very useful tool for estimating the volume or mass of the monolayer on the surface boundary of powders or materials with porous surfaces with meso-pore size. For example if we adsorb nitrogen onto a powder surface, the

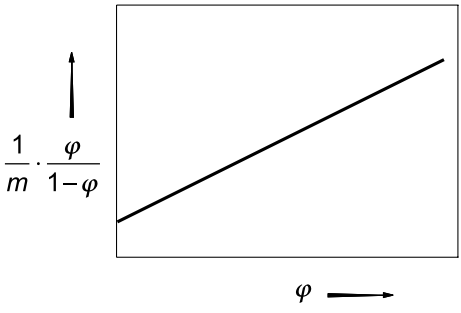

Figure 1.4. BET plot of adsorbed mass versus relative vapor pressure

monolayer area can be calculated from the known area of a nitrogen molecule $A_{N_2} = 1.62 \cdot 10^{-19}\text{m}^2$ [38]. If water vapor is used as the adsorbent, then the relative partial pressure $\frac{p}{p_S} = \varphi$ takes on the meaning of equilibrium relative humidity (or water activity), which will be explained further.

When isotherm data points taken from an adsorption process are plotted on the same graph as those taken from a desorption process on the same material at the same temperature, the two isotherms will follow different pathways revealing the hysteresis behavior shown in Type IV isotherms (Table 1.4). Sorption isotherm hysteresis is far from being understood [136]. As explained earlier, the presence of bottle-shaped pores with openings that are much narrower than their interior is a possible cause of this type of hysteresis. Another possible cause is that irreversible changes may occur in the food material during the adsorption/desorption experiment.

Both desorption and adsorption isotherms can be characterized well by the BET equation. The desorption isotherm relates to a drying process, in which a fresh food sample with initial high moisture content is exposed to a gaseous surrounding of lower and lower partial pressures. The desorption isotherm relates to a rehydration process, in which an initially dry food sample is exposed to a surrounding fluid of higher and higher partial pressure. Understanding the distinction between both cases is a necessary prerequisite for undertaking the experimental procedures used to obtain the sorption isotherm for a given material.

Thermodynamics of Sorption Isotherms

Another feature of the BET isotherms is that thermodynamic information can also be obtained from further analysis. This type of information can be very useful in the engineering design of drying processes for food dehydration. One of the assumptions upon which the model is based is that the adsorbate (water) is initially held in a liquid state within the moist food material to be dried, and must first undergo phase transition to the gaseous or vapor phase before being desorbed from the boundary surface. In order to remove a monolayer of water molecules from the solid boundary surface, the energy required to provide sufficient heat (enthalpy) of vaporization Δh_{vap} must be delivered to the boundary surface. In addition to the enthalpy of vaporization, energy will be needed to break the adhesion forces bonding the monolayer to the surface boundary, discussed earlier. This monolayer-bonding enthalpy Δh_C will depend upon the chemical and physical characteristics affecting the bonding forces between the two substances at the boundary surface monolayer (see Table 1.1), and must be delivered in excess of the enthalpy of vaporization in order to drive the desorption process. Thus, the total energy required is the monolayer-desorption enthalpy, and is simply the sum of these two enthalpies, as expressed in equation (1.16):

$$\Delta h_{s,mono} = \Delta h_{vap} + \Delta h_C \tag{1.16}$$

In the reverse direction when the substance is undergoing the adsorption process, water vapor molecules must first condense into liquid at the monolayer surface, giving up their enthalpy of vaporization, as well as the enthalpy for building the monolayers (monolayer-building enthalpy). These enthalpies are given up freely during the adsorption process, and together are known as the specific sorption enthalpy of the monolayers $\Delta h_{s,mono}$.

Recall that sorption isotherms are obtained and reported at a constant temperature. When obtained at different constant temperatures, they will become different for the same substance. The constant C in the BET equation is the key parameter that is temperature dependent in this equation. Its temperature dependency follows the classic ARRHENIUS relationship, which characterizes the temperature dependency of most chemical, physical, biochemical, and microbiological reactions. The ARRHENIUS equation for temperature dependency can be derived from a semi-log plot, in which the logarithm of the temperature dependent parameter is plotted against the reciprocal of absolute temperature, as indicated by equations (1.17)–(1.21):

$$C = C' \cdot e^{\frac{\Delta h_C}{R_s \cdot T}} \tag{1.17}$$

or

$$\ln C = \ln C' + \frac{\Delta h_C}{R_s \cdot T} \tag{1.18}$$

By drawing an ARRHENIUS diagram with $\log C$ plotted against $1/T$ a straight line will result. From the slope of this straight line we can obtain the excess enthalpy Δh_C term. The slope is:

$$m = \frac{\Delta h_C}{2.3 \cdot R_s} \tag{1.19}$$

where

Δh_C	specific bonding enthalpy of monolayer in $J \cdot kg^{-1}$ (desorption)
Δh_{vap}	specific vaporization enthalpy of adsorbate in $J \cdot kg^{-1}$ (desorption)
$\Delta h_{s,mono}$	specific sorption enthalpy of monolayers in $J \cdot kg^{-1}$ (desorption)
T	absolute temperature in K
R_s	specific gas constant of adsorbate in $J \cdot K^{-1} \cdot kg^{-1}$
C, C'	constants in BET equation

Therefore, the specific sorption enthalpy of the monolayer can be determined from the temperature dependency of the constants (C, C') in the BET equation. The "excess" monolayer bonding enthalpy Δh_C disappears and plays no further role in the case of multilayer adsorption. In this case, other values of Δh_C apply depending on the adhesive bonding of the second, third and additional multiple layers. With each additional layer, less and less bonding energy (enthalpy) is needed until the adsorbed water becomes freely available to behave as normal water (vaporize, condense, freeze, sublime and thaw), and only the enthalpy of vaporization (or condensation) applies.

1.2.6
Sorption of Water Vapor in Foods

Much of the previous section was aimed at introducing many of the basic scientific principles of sorption phenomena in general. Although frequent reference was made to the processes of drying and rehydration (implying sorption of water) to help explain the distinction between desorption and adsorption, references to any specific substances were rarely made. Sorption processes can occur at the interface between solids and fluids (gases or liquids), or between fluids (gas–liquid, liquid–liquid). However, in the fields of food technology and engineering, an understanding of the sorption of water vapor in foods is of paramount importance in the design and specification of many food processing, packaging, storage and handling systems. In the case of water vapor adsorption (rehydration) in foods, we have sorption at a solid–fluid interface with water molecules being adsorbed onto the boundary surface of a dry solid material. Once monolayer saturation is achieved at the boundary surface and multilayers begin to form, the initially dry solid material will begin to absorb the water molecules through the porous structure into the interior of the material, just as a dry towel will absorb water from a wet surface. Thus, the initially dry solid material is called the "adsorbent." When the process comes to an end at equilibrium, the resulting adsorbed water is called the "adsorbate" (see Figure 1.5).

Just as in the previous section, the sorption of water vapor in foods is characterized by the sorption isotherms for water vapor in food materials, called vapor sorption isotherms. These vapor sorption isotherms are graphical plots showing the relationship between moisture content and water activity over a range of water activities at constant temperature for a given substance. For most food and biological materials the data points on these plots normally fall on a smooth curve of sigmoid shape, which becomes the sorption isotherm at that temperature for that substance. The precise shape and position of the sorption isotherm on the graphical plot is specific to each type of food material or substance, and can be considered a signature physical property of that substance.

Figure 1.6 shows some examples of different sorption isotherms. Curve 1 shows a strong sorbent, which takes up large amounts of water although in a region of very low water activity or equilibrium relative humidity. After the rapid water uptake we see a plateau, which is the result of the monolayer that has formed becoming stable. Silica for example would have a curve of this

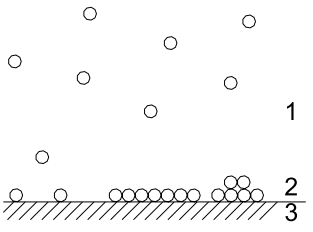

Figure 1.5. Sorption of water vapor to a solid food surface. **1:** gaseous water molecules, **2:** adsorbed water (adsorbate), **3:** food (adsorbent)

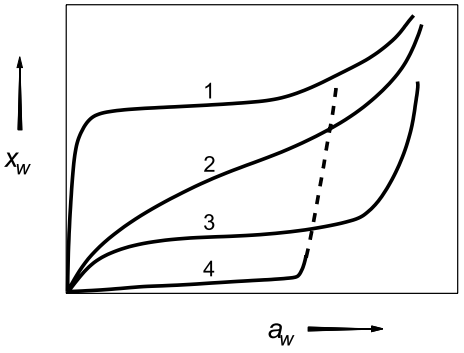

Figure 1.6. Examples of water vapor sorption isotherms. **1:** silica (strong sorbent), **2:** milk powder (multilayer forming material), **3:** black tea (monolayer forming material), **4:** fructose (nearly impervious to water, then rapid uptake of water until a syrup is formed)

shape. Curve 3 shows a similar behavior, but not with such extreme water uptake. When a material does not stop to adsorb water when a monolayer is formed and continues on to form second, third and additional multilayers without pausing, we see a shape like that shown in curve 2. Some materials such as PVC powder do not adsorb very large amounts of water, and they behave like a substance impervious to water. Curve 4 shows crystalline fructose which, in regions of lower water activity shows nearly impervious behavior, but on exceeding a certain level of water activity starts to dissolute and form a syrup. The isotherm in this region is a dashed line because the original sample (in the form of dry crystals) does not exist any longer.

Examples of sorption isotherms for specific food and agricultural materials are given in Figure 1.7 (from [133]).

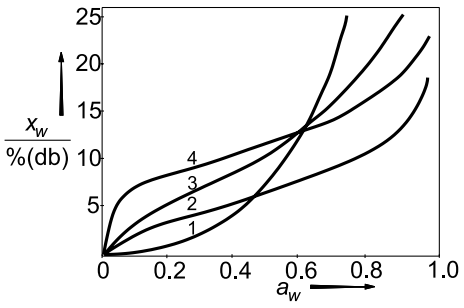

Figure 1.7. Examples of sorption isotherms: **1:** dried peaches, **2:** cotton, **3:** soybeans, **4:** wheat [133]

Note the sigmoid shape is similar to other isotherms described by the BET model. However, in the case of the classic isotherms discussed in the previous section, the plotted parameters were adsorbent mass on the vertical axis, and partial pressure on the horizontal axis. In the case of water vapor sorption isotherms in food system applications, these parameters are replaced by moisture content and water activity, respectively. Therefore, a full understanding of these two properties (water activity and moisture content) is needed before proceeding further.

1.2.7 Water Activity

Recall that water activity was first mentioned in the introduction to this chapter as a property parameter that could be used to reflect the way in which water is bound to the internal structure of the food. The degree to which water is freely available to act as a solvent, to vaporize or freeze, or the degree to which it is chemically bound and unavailable can all be reflected by an ability to specify the water activity of a food material. Recall that a simple working definition for water activity was given at the beginning of this chapter as the equilibrium relative humidity of the food material when it has come into equilibrium with the relative humidity of the atmosphere surrounding it. Once this equilibrium is reached, the food sample neither gains nor loses moisture over time [133].

Recall further that the definition of relative humidity in a mixture of air and water vapor is the ratio of amount of water vapor in the mixture divided by the maximum amount of water vapor that could be held by the air at that condition (saturation). Mathematically, this ratio is the same as the ratio of water vapor partial pressure divided by saturation pressure, as expressed in equation (1.20):

$$\frac{p}{p_S} = \varphi = a_W \tag{1.20}$$

By substituting this definition in the BET equation, expression (1.21) is derived, and transformation of variables plotted on the graph in Figure 1.4, allows for the determination of the constants, as shown in the previous section. Thus, we can see how water activity (or equilibrium relative humidity) can take the place of partial pressure as the parameter plotted on the x-axis for obtaining water vapor sorption isotherms.

$$\frac{1}{m} \cdot \frac{a_W}{1 - a_W} = \frac{1}{m_a \cdot C} + \frac{C - 1}{m_a \cdot C} \cdot a_W \tag{1.21}$$

Recall that the BET plot is a graph of versus $\frac{1}{m} \cdot \frac{a_W}{1-a_W}$. Another possibility to further simplify the use of water sorption isotherms, is to use the water content instead of m (mass of the water absorbed). The water content is what we know as moisture content of the food.

1.2.8 Moisture Content

For general purposes, the moisture content of a food is normally expressed simply as the percent moisture in the food substance. Mathematically, this is the ratio of the mass of water contained in the food sample (adsorbent) over the total mass of food sample containing the moisture (adsorbate), expressed as a percent. However, moisture content used as the variable plotted on the vertical axis of vapor sorption isotherms often is expressed as the ratio of mass of

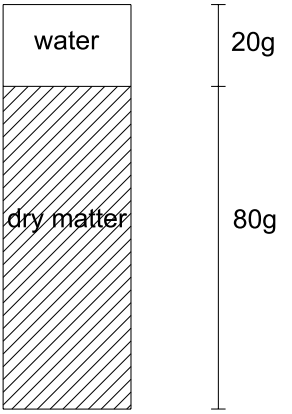

Figure 1.8. Food material with 20% moisture (wb) and 25% moisture (db)

water m_W (adsorbate) divided by mass of dry matter m_{dm}, only (absorbent), as expressed in equation (1.22):

$$x_W = \frac{m_W}{m_{dm}} \tag{1.22}$$

These two different methods for expressing moisture content in a food sample are known as "wet basis" (wb) and "dry basis" (db), respectively. The distinction between both methods of expression, as well as the ability to quickly calculate one from the other must be well understood. The illustration in Figure 1.8, shows a vertical bar representing a 100 g food sample composed of 20 g water and 80 g dry matter, and shows how these quantities are used to correctly express moisture content on either basis. For example, in this case the moisture content on a wet basis is 20/100 = 20%. But, on a dry basis it is 20/80 = 25%. Refer also to Table 1.6 for further elaboration on the difference between the two expressions and how to convert the quantities from one to another.

Example 1.2. Moisture content of corn flakes (dry basis)
A sample of corn flakes has a moisture content of 7.5% (wet basis). Express this moisture content on a dry basis.

$$x_{W,db} = \frac{m_W}{m_{total} - m_W} = \frac{7.5\,\text{kg}}{100\,\text{kg} - 7.5\,\text{kg}} = \frac{7.5\,\text{kg}}{92.5\,\text{kg}} = 0.081$$

so

$$x_{W,db} = 8.1\,\text{g}\,H_2O/100\,\text{g dm} = 8.1\%\,\text{(db)}$$

or more simply

$$x_{W,db}\frac{1}{\frac{1}{0.075} - 1} = 0.081$$

Table 1.6. Conversion of moisture content on dry basis and wet basis

dry basis (db)	wet basis (wb)
$x_{W,db} = \frac{m_W}{m_{dm}}$	$x_{W,wb} = \frac{m_W}{m_{total}}$
$x_{W,db} = \frac{m_W}{m_{total} - m_W}$	$x_{W,wb} = \frac{m_W}{m_{dm} + m_W}$
division by m_W yields	
$x_{W,db} = \frac{1}{\frac{1}{x_{W,wb}} - 1}$	$x_{W,wb} = \frac{1}{\frac{1}{x_{W,db}} + 1}$
possibilities to present the result	
x_W (db)	x_W (wb)
x_W on dry basis	x_W on wet basis
x_W in g H_2O/g dry matter	x_W in g H_2O/g

Example 1.3. Moisture of corn flakes (wet basis):
A sample of corn flakes has a moisture content of 21.2% (dry basis). Express the moisture content on a wet basis.

$$x_{W,wb} = \frac{m_W}{m_{dm} + m_W} = \frac{21.2\,\text{kg}}{100\,\text{kg} + 21.2\,\text{kg}} = 0.175$$

$$x_{W,wb} = 17.5\,\text{g}\,H_2O/100\,\text{g} = 17.5\%\,\text{(wb)}$$

When we refer to moisture content in food sorption phenomena in this book, we always mean moisture content on a dry basis.

1.2.9 Hygroscopicity

Hygroscopicity is a term used to describe how readily a material will take up moisture when subjected to a given shift (change) in relative humidity. The term is often used in industrial practice to indicate materials that quickly become problematic in the presence of the least increase in surrounding relative humidity. For example, certain powdered ingredients are said to be very hygroscopic if they become sticky and cause caking problems that prevent free flowing from the storage hopper in a food process.

In this regard the term is used in a relative qualitative sense, and no quantitative scale has ever been assigned to hygroscopicity. We have no means to quantify what is the difference between strong and weak hygroscopic behavior. It may be possible to consider hygroscopicity as a material property that could be quantified if we understand that this type of moisture uptake behavior in response to change in relative humidity can be observed from the shape of the sorption isotherm for this material. For example, a highly hygroscopic powder will show a much higher uptake of water when shifted from 45% to 75% relative humidity than a powder would with lower hygroscopicity.

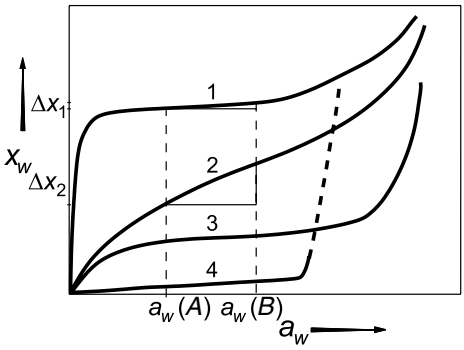

Figure 1.9. Exposing four materials exhibiting different degrees of hygroscopicity to a shift in water activity from $a_W(A)$ to $a_W(B)$. The same shift causes different amounts of water uptake Δx

To help better understand this, consider the four different sorption isotherms shown in Figure 1.9. Each isotherm belongs to a different material, and all four materials exhibit different degrees of hygroscopicity. Let us assume that we shift the equilibrium relative humidity (water activity) from water activity $a_W(A)$ to water activity $a_W(B)$ on all four materials. Then, we can observe the different quantities of water uptake experienced by each material as an indicator of different degrees of hygroscopicity.

It clearly can be seen that material 2 will have greater water uptake than material 1. The slope of the secant in the segment of the curve between the starting point and final point of the shift in water activity can be taken as a water uptake potential (w_P-value) of the given material. The w_P-value serves only as an indicator of the moisture difference Δx, which occurs on a given change Δa_W. It does not take into account the level of moisture already absorbed into the material earlier. So, when we examine Figure 1.9 once again, we would have to note that although material 1 is a very good sorbent, when we make our shift in water activity $a_W(A) \rightarrow a_W(B)$ experiment, material 2 will show the higher water uptake. Therefore, we can say that material 2 has a greater w_P than material 1 in the range of water activities of our experiment. When we use w_P as an indicator of hygroscopicity, the points A and B have to be clearly specified. Also, a constant temperature was assumed throughout this example.

1.2.10 BET Equation for Foods

In the case of water vapor sorption in foods, when the isotherms are obtained as plots of moisture content (db) versus water activity, the BET equation gets the form

$$\frac{1}{x_W} \cdot \frac{a_W}{1 - a_W} = \frac{1}{x_{W,a} \cdot C} + \frac{C - 1}{x_{W,a} \cdot C} \cdot a_W \tag{1.23}$$

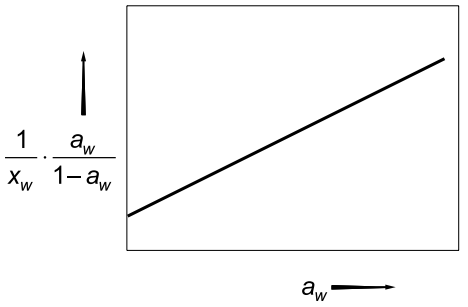

Figure 1.10. BET plot of adsorbed moisture content versus water activity

where

a_W	water activity
x_W	moisture content (db) in kg/kg dry matter
C	BET constant
$x_{W,a}$	monolayer moisture content (db) in kg/kg dry matter

If the quantity $\frac{1}{x_W} \cdot \frac{a_W}{1-a_W}$ were plotted against water activity a_W, a straight line is obtained (see Figure 1.10). The monolayer moisture content $x_{W,a}$ as well as the BET constant, can then be obtained from the slope and intercept of the line. The value of $x_{W,a}$ is usually the moisture content at which the water is tightly bound with water molecules in a single monolayer, and it cannot participate as a solvent. Thus, it is the moisture content that should be reached for maximum stability of dehydrated foods (see also Section 1.3).

The evaluation of the plot is performed again by obtaining the intercept and slope of the straight line curve in the diagram.

$$\text{intercept:} \quad a = \frac{1}{x_{W,a} \cdot C} \qquad \text{slope:} \quad b = \frac{C-1}{x_{W,a} \cdot C}$$

Because of $\frac{b}{a} = C - 1$ or $C = \frac{b}{a} + 1$ the moisture content of the food at the point where a complete monolayer exists is

$$x_{W,a} = \frac{1}{a \cdot \left(\frac{b}{a} + 1\right)} = \frac{1}{a+b}$$

The monolayer moisture content $x_{W,a}$ and BET constant C are the only two parameters needed to describe the sorption isotherm for a given food product. Published tables or on-line data bases listing values of these parameters for various food stuffs can be found in references [7–9]. Also, sorption enthalpies needed for estimating energy requirements in the engineering design of drying or dehydration processes can be obtained from the ARRHENIUS temperature dependency of these parameters [10].

Example 1.4. BET – isotherm for a food product:
The moisture content (dry basis) of the product in equilibrium with different relative humidity is listed below: Construct the BET plot from these data, and calculate the values for the monolayer moisture content $x_{W,a}$ and BET constant C.

φ/% r.h.	x_W/% (db)
0	0.0
10	2.5
20	4.3
30	5.2
50	8.3
75	18.8

First we prepare a table of values; then we draw the BET diagram:

φ/% r.h.	x_W/% (db)	x_W (db)	a_W	$\frac{a_W}{1-a_W}$	$\frac{1}{x_W}\frac{a_W}{1-a_W}$
0	0.0	0	0	0	–
10	2.5	0.025	0.1	0.11	4.4
20	4.3	0.043	0.2	0.25	5.8
30	5.2	0.052	0.3	0.43	8.3
50	8.3	0.083	0.5	1.0	12.0
75	18.8	0.188	0.75	3.0	16.0

For the slope, we get $b = 19.0$ and for the intercept $a = 2.4$. So the monolayer moisture content is

$$x_{W,a} = \frac{1}{a+b} = \frac{1}{2.4+19.0} = 0.0467$$

and the BET constant C is

$$C = \frac{b}{a} + 1 = \frac{19.0}{2.4} + 1 = 8.92$$

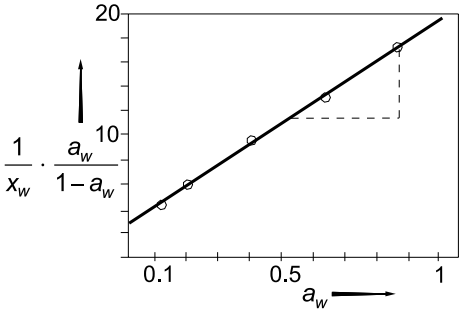

Figure 1.11. Evaluation of Example 1.4

BET – One-Point Method

For the purpose of rough estimation, the straight line BET plot can be approximated by constructing a straight line from the origin of the coordinate axes through a single data point. The single data point should be taken at value of water activity at which the monolayer is fully developed (saturated) but no multiple layer formation exists. As a rule of thumb for most foods, this value is normally chosen in the range of water activity between 0.3–0.4. The BET parameters for the monolayer moisture content $x_{W,a}$ and BET constant C can be estimated from the slope of this straight line, and will normally serve sufficiently well for most purposes of approximating the profile of the sorption isotherm for the given food substance, as shown by equation (1.24). Because of $a = 0$ we can say:

$$x_{W,a} = \frac{1}{b} \tag{1.24}$$

and

$$C = \frac{b}{a} + 1 = \infty \tag{1.25}$$

Example 1.5. Sorption isotherm of a food using the BET – one-point method:
A food product has a moisture content of 5.2% (db) in equilibrium with air at a relative humidity of 30% r.h. Construct the one-point BET straight line, and estimate the monolayer moisture content $x_{W,a}$ for this food.

With that single point we get the following:

φ/% r.h.	x_W/% (db)	x_W (db)	a_W	$\frac{a_W}{1-a_W}$	$\frac{1}{x_W}\frac{a_W}{1-a_W}$
30	5.2	0.052	0.3	0.43	8.2

Therefore, without diagram we see the slope will be $b = \frac{8.2-0}{0.3-0} = 27$. The intercept was set to zero: $a = 0$. So the monolayer moisture content can be estimated to be about $x_{W,a} = \frac{1}{b} = \frac{1}{27} = 0.037$

Thermodynamics of Water Vapor Sorption in Foods

Similar to the discussion on thermodynamics of sorption isotherms presented earlier in this chapter, the temperature dependency of the BET constant C can be obtained from an Arrhenius plot of $\log C$ over reciprocal absolute temperature T. The excess enthalpy of adsorption, or monolayer-bonding enthalpy Δh_C, can be obtained from the slope m of the straight-line Arrhenius semi-log plot, as given by equation (12.6):

$$m = -\frac{\Delta h_C}{2.3 \cdot R_s} \tag{1.26}$$

with

$$\Delta h_C = \Delta h_{s,mono} - \Delta h_{vap} \tag{1.27}$$

respectively

$$\Delta h_{s,mono} = \Delta h_{vap} + \Delta h_C \tag{1.28}$$

where

Δh_C	specific bonding enthalpy of H_2O monolayer in $J \cdot kg^{-1}$ (desorption)
Δh_{vap}	specific vaporization enthalpy H_2O in $J \cdot kg^{-1}$(desorption)
$\Delta h_{s,mono}$	specific sorption enthalpy H_2O monolayer in $J \cdot kg^{-1}$(desorption)
T	absolute temperature in K
R_s	specific gas constant of H_2O ($461\ J \cdot kg^{-1} \cdot K^{-1}$)

The specific sorption enthalpy $\Delta h_{s,mono}$ will be found at the drying condition which leaves only the monolayer, but fully intact. At this point the monolayer is a complete layer of water molecules tightly bound to the boundary surface of the food material, and the enthalpy at this point marks the distinction between "free" and "bound" water in the food. As explained earlier, the BET theory covers a monolayer only and there is no regard for multilayers (like in the GAB model, see below). That means water in the second layer is treated like "free" water. So in the BET theory the "excess" monolayer bonding enthalpy Δh_C disappears and plays no further role. In this case, water is freely available to behave as normal water (vaporize, condense, freeze, sublime and thaw), and only the enthalpy of vaporization (in the case of desorption), or condensation (in the case of adsorption) applies. In the opposite direction when the "excess" monolayer bonding enthalpy Δh_C takes on high values, the bonding strength at the monolayer surface becomes very strong. Further water removal beyond this point through normal drying processes becomes very costly and time consuming. Therefore, it is of critical importance to identify this point of distinction with respect to the "excess" monolayer bonding enthalpy Δh_C in order to design and specify optimum drying, storage and packaging conditions to assure long-term stability of dehydrated foods.

A fast method for quickly estimating this "excess" monolayer bonding enthalpy Δh_C is possible by comparing water activity of a food at different temperatures, and determining the temperature dependency of water activity for the given food. This can be done with the Clausius–Clapeyron equation [11]:

$$\left(\frac{d \ln a_W}{d \frac{1}{T}} \right)_{x_W} = -\frac{\Delta h_C}{R_s} \tag{1.29}$$

or in approximation

$$\frac{\Delta \log a_W}{\Delta \frac{1}{T}} = -\frac{\Delta h_C}{2.3 \cdot R_s} \tag{1.30}$$

where

Δh_C	specific bonding enthalpy of H_2O monolayer in $J \cdot kg^{-1}$ (desorption)
Δh_{vap}	specific vaporization enthalpy H_2O in $J \cdot kg^{-1}$ (desorption)
$\Delta h_{s,mono}$	specific sorption enthalpy H_2O monolayer in $J \cdot kg^{-1}$ (desorption)
a_W	water activity
T	absolute temperature in K
R_s	specific gas constant of H_2O

Example 1.6. Starch powder monolayer sorption enthalpy
From two sorption isotherms taken at different temperatures we read the water activities at moisture content $x_W = 10\%$ (db):

ϑ/°C	a_W
30	0.25
80	0.45

We transform these data to

ϑ_1/°C	T_1/K	$\frac{1}{T_1}/K^{-1}$	a_{W1}	$\log a_{W1}$
30	303.15	$3.299 \cdot 10^{-3}$	0.25	–0.602

ϑ_2/°C	T_2/K	$\frac{1}{T_2}/K^{-1}$	a_{W2}	$\log a_{W2}$
80	353.15	$2.832 \cdot 10^{-3}$	0.45	–0.347

From equation (1.29) we get

$$\Delta h_C = -2.3 \cdot R_s \cdot \frac{\Delta \log a_W}{\Delta \frac{1}{T}}$$

or

$$\Delta h_C = -2.3 \cdot \frac{\log a_{W2} - \log a_{W1}}{\frac{1}{T_2} - \frac{1}{T_1}}$$

so

$$\Delta h_C = -2.3 \cdot 0.461\,\text{kJ} \cdot \text{kg}^{-1} \cdot \frac{-0.34678 - (-0.6020)}{2.832 \cdot 10^{-3}\,\text{K}^{-1} - 3.299 \cdot 10^{-3}\,\text{K}^{-1}}$$

that is

$$\Delta h_C = 579\,\text{kJ} \cdot \text{kg}^{-1}$$

The result is a positive enthalpy. It means that have $579\,kJ \cdot kg^{-1}$ to be introduced into the material to overcome the sorption of the monolayer molecules. To bring the water molecules from the monolayer phase into the gaseous phase according to equation (1.28) we need the total enthalpy of $\Delta h_{s,mono} = 2200\,kJ \cdot kg^{-1} + 579\,kJ \cdot kg^{-1} = 2779\,kJ \cdot kg^{-1}$.

When we calculate a monolayer sorption enthalpy based on two points only (here 30 °C and 80 °C) we should not overestimate the precision of the result. Although in this example we got the information that the heat needed for desorption of the monolayer molecules is about 20 to 30% higher than for free water:

$$\frac{\Delta h_C}{\Delta h_{vap}} = \frac{579}{2200} = 0.26$$

Recall that vapor sorption isotherms, as well as the BET model, provide information on the relationship between moisture content and water activity only in the region of relatively low moisture content. Food with intermediate moisture content can contain water adsorbed in multilayers. Because the BET model does not address multilayers, it is not valid in these regions of higher water activity, and the following GAB model is better suited for this purpose.

1.2.11 GAB Model

The GAB model (after Guggenheim, Anderson, and deBoer [12]) is a semi-theoretical multimolecular adsorption model intended for use over a wide range of water activity, and can be written as a three-parameter model:

$$\frac{a_W}{m \cdot (1 - k \cdot a_W)} = \frac{1}{m_a \cdot C \cdot k} + \frac{C - 1}{m_a \cdot C} \cdot a_W \tag{1.31}$$

where

a_W	water activity
m	mass of adsorbate in kg
k	GAB correction factor (0.7–1.0)
C	Guggenheim constant
m_a	mass of monolayer in kg

The GAB isotherm equation is an extension of the two-parameter BET model which takes into account the modified properties of the adsorbate in the multilayer region and bulk liquid ("free" water) properties through the introduction of a third parameter k. If k is less than 1, a lower sorption is predicted than that by the BET model, and allows the GAB isotherm to be successful up to water activity of 0.9. The GAB equation reduces to the BET equation when $k = 1$. The constants in the GAB equation (k and C) are temperature dependent, and are the means by which we can extract information when we construct and refer to sorption isotherms at different temperatures.

Thermodynamics of Sorption Phenomena

Temperature dependency of the GAB model is approached in the same way as with the BET model, in that the Guggenheim constant is analogous to the BET constant with respect to being temperature dependent according to the Arrhenius relationship, as shown in equations (1.32), (1.33) and (1.34):

$$C = C' \cdot e^{\frac{\Delta h_C}{R_s \cdot T}} \tag{1.32}$$

respectively

$$\ln C = \ln C' + \frac{\Delta h_C}{R_s \cdot T} \tag{1.33}$$

So, by drawing an ARRHENIUS plot with $\log C$ versus $1/T$ we can get the monolayer bonding enthalpy Δh_C from the slope (same way as done in the BET model).

$$m = \frac{\Delta h_C}{2.3 \cdot R_s} \tag{1.34}$$

Unlike the BET model, the GAB model takes into account the fact that when multimolecular layers begin to develop, adsorbed water molecules does not instantly behave as free water. But instead, bonding forces gradually weaken with increasing multilayers, such that vapor pressure is slightly reduced from that of pure water. This is taken into account by the parameter k, which is used as a multiplier coefficient that serves as a correction factor (with values between 0.7 and 1.0) in order to take this behavior into account. The BET model neglects this effect. From the temperature dependency of the GAB parameter k, we can determine the excess enthalpy from bonding of the multilayers:

$$k = k' \cdot e^{\frac{\Delta h_k}{R_s \cdot T}} \tag{1.35}$$

So by making the ARRHENIUS plot $\log k$ versus $1/T$ from the slope m we can get this excess enthalpy Δh_k.

$$m = -\frac{\Delta h_k}{2.3 \cdot R_s} \tag{1.36}$$

where Δh_k is the mean bonding enthalpy of layers above the monolayer. When such a n-layer shall be removed from a surface the enthalpy $\Delta h_{S,multi}$ is necessary, which is the sum of enthalpy of vaporization and that bonding enthalpy Δh_k, in other words,

$$\Delta h_k = \Delta h_{S,multi} - \Delta h_{vap} \tag{1.37}$$

where

$\Delta h_{S,multi}$	mean specific sorption enthalpy of the water multilayer in $\mathrm{J \cdot kg^{-1}}$ (desorption)
Δh_{vap}	specific enthalpy of vaporization for water in $\mathrm{J \cdot kg^{-1}}$
Δh_k	mean specific bonding enthalpy of the water multilayer in $\mathrm{J \cdot kg^{-1}}$ (desorption)
R_s	specific gas constant for water in $\mathrm{J \cdot kg^{-1}\ K^{-1}}$
T	absolute temperature in K

The GAB model is most appropriate when we deal with water activities above 0.4–0.5. A little disadvantage of this model is the increased mathematical complexity in dealing with a three-parameter equation compared to the BET model [14].

One can also use the expression for moisture content on a dry basis from equation (1.31) to further simplify the GAB equation into the form of equation (1.38), respectively (1.39):

$$x_W = \frac{x_{W,a} \cdot C \cdot k \cdot a_W}{(1 - k \cdot a_W)\,(1 + (C - 1) \cdot k \cdot a_W)} \tag{1.38}$$

so

$$x_W = \frac{x_{W,a} \cdot C \cdot k \cdot a_W}{(1 - k \cdot a_W)(1 - k \cdot a_W + C \cdot k \cdot a_W)} \tag{1.39}$$

where

a_W	water activity
x_W	moisture content (db) in kg · kg^{-1} dry matter
C	GUGGENHEIM constant
k	GAB correction factor (0.7–1.0)
$x_{W,a}$	monolayer moisture content (db) in kg · kg^{-1} dry matter

Other workers [13] have transformed the GAB equation into a quadratic form, as shown by equations (1.40)–(1.43).

$$\frac{a_W}{x_W} = \alpha \cdot {a_W}^2 + \beta \cdot a_W + \gamma \tag{1.40}$$

By taking experimental data of x_W versus a_W and bringing them into a function like equation (1.40) we can determine the coefficients α, β, γ of the polynomial, and from it we can calculate the GAB parameters [15]:

$$\alpha = \frac{k}{x_{W,a}} \left(\frac{1}{C} - 1 \right) \tag{1.41}$$

$$\beta = \frac{1}{x_{W,a}} \left(1 - \frac{2}{C} \right) \tag{1.42}$$

$$\gamma = \frac{1}{x_{W,a} \cdot C \cdot k} \tag{1.43}$$

$$x_{W,a} = \left(\frac{1}{\beta^2 - 4\alpha \cdot \gamma} \right)^{\frac{1}{2}} \tag{1.44}$$

$$k = -\frac{2 \cdot \alpha \cdot x_{W,a}}{\beta \cdot x_{W,a} + 1} \tag{1.45}$$

$$C = \frac{1}{x_{W,a} \cdot \gamma \cdot k} \tag{1.46}$$

With the aid of appropriate computer software, these parameters can be calculated within a few seconds for daily routine use of the BET or GAB models. With the use of such software and appropriate data input, food engineers and scientists can quickly determine the information needed to design and specify optimum processing, packaging, storage and handling conditions with respect to water activity requirements for shelf life stability of foods [16].

1.2.12 Other Models

Several other models to mathematically describe the profile of sorption isotherms in foods have been proposed and reported in the literature [15,17]. They differ in regard to their physical approach, method for mathematical derivation, and number of parameters. Tables 1.7 to 1.9 contain a listing of these other models organized by the number of parameters required of each model. Models with only two parameters are listed in Table 1.7, three-parameter models are listed in Table 1.8, and four-parameter models in Table 1.9.

Sometimes for special recipes other models can be applied, for example for sugar syrups or confectionery products there are special models in use. For more information and examples refer, e.g. to [134,135].

Table 1.7. Two-parameter models for sorption isotherms

Freundlich (1906)	$x_W = A \cdot a_W^B$
Langmuir (1916)	$x_W = x_{\max}\left(\frac{a_W}{a_W + B}\right)$
Smith (1947)	$x_W = A + B \cdot \ln(1 - a_W)$
Oswin (1946)	$x_W = A\left(\frac{a_W}{1 - a_W}\right)^B$
Henderson (1952)	$x_W = \left[\frac{\ln(1 - a_W)}{-A}\right]^{\frac{1}{B}}$
Brunauer, Emmet, Teller (1938) (BET)	$x_W = \frac{x_{W,a} \cdot C \cdot a_W}{(1 - a_W)(1 + (C - 1)a_W)}$
	$\frac{1}{x_W} \cdot \frac{a_W}{1 - a_W} = \frac{1}{x_{W,a} \cdot C} + \frac{C - 1}{x_{W,a} \cdot C} \cdot a_W$
Halsey (1948)	$x_W = \left[-\frac{A}{\ln a_W}\right]^{\frac{1}{B}}$
Chung, Pfost (1967)	$x_W = -\frac{1}{B} \cdot \ln\left[-\frac{\ln a_W}{A}\right]$
Iglesias, Chirife (1978)	$\ln\left[x_W + (x_W^2 + x_{0.5W})^{\frac{1}{2}}\right] = A \cdot a_W + B$
Lewicki (2000)	$x_W = A \cdot \left[\frac{1}{a_W} - 1\right]^{B-1} - 1$

Table 1.8. Three-parameter models for sorption isotherms

Cubic model	$x_W = p_1 + p_2 \cdot a_W + p_3 \cdot a_W^2 + p_4 \cdot a_W^3$
GAB: Guggenheim (1966), Andersen (1946), De Boer (1953)	$x_W = \dfrac{x_{W,a} \cdot C \cdot k \cdot a_W}{(1 - k \cdot a_W)(1 + (C-1) \cdot k \cdot a_W)}$
expressed by Bizot as:	$\dfrac{a_W}{x_W} = \alpha \cdot a_W^2 + \beta \cdot a_W + \gamma$

Table 1.9. Four-parameter models for sorption isotherms

Peleg (1993)	$x_W = A \cdot a_W^C + B \cdot a_W^D$
Isse (1993)	$\ln x_W = A \cdot \ln \dfrac{a_W}{1 - a_W} + B$

where

x_W	moisture content (db) in $kg \cdot kg^{-1}$ dry matter
a_W	water activity
x_m	monolayer moisture content (db) in $kg \cdot kg^{-1}$ dry matter
$x_{0.5m}$	moisture content in $kg \cdot kg^{-1}$ (db) at $a_W = 0.5$
A, B, C, D	Constants

1.3 Shelf Life of Food Related to Water Activity

The normally high moisture content in most fresh foods is largely the reason they are so perishable. If left unprotected without being processed or preserved in any way, they will deteriorate rapidly as a result of various microbial, chemical and biochemical reactions. In order for these reactions to proceed, most of them require abundant availability of free water to act as a solvent and for hydraulic transport of molecules across semi-permeable membranes, essential for microbial metabolism, within the food [1]. For this reason one of the most effective methods of food preservation is to reduce the moisture content until the water activity is low enough that the amount of free water needed to support any of the degradation reactions that might take place is not available. This is the principle behind the storage stability and long shelf life of dehydrated foods.

As the water activity is brought below 1 and lowered further in a food, the rates of these reactions begin to slow down. They proceed more slowly with further lowering water activity, which translates into longer and longer shelf life. The actual shelf life of any specific food product at a given water activity may vary depending on structure and composition of the food material, and spoilage mechanism of concern. The shelf life of a food will be limited by any one of a series of spoilage mechanisms that can destroy the food. These include microbial activity (bacteria, yeasts and moulds), enzyme activity, browning reactions, and lipid oxidation (rancidity). Of all these reactions, microbial

Table 1.10. Minimum water activity for population growth [109]

a_W	lower limit for growth of
0.91–0.95	most bacteria
0.88	most yeasts
0.80	most moulds
0.75	halo-tolerant bacteria
0.70	osmo-tolerant yeasts
0.65	xero-tolerant moulds

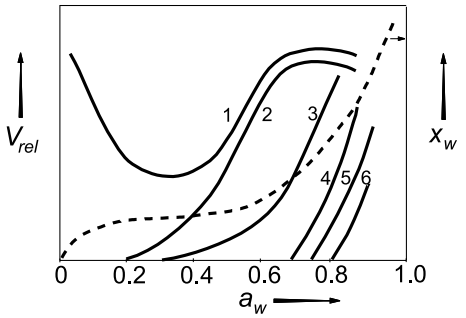

Figure 1.12. Relative rate (V_{rel}) of different spoilage reactions as a function of water activity a_W in food. **1:** lipid oxidation, **2:** browning reactions, **3:** enzymatic reactions, **4:** moulds, **5:** yeasts, **6:** bacteria. The dashed line indicates the sorption isotherm of the sample material

activity is by far the most sensitive to water activity, having the greatest need for available free water. Table 1.10 lists the minimum values of water activity needed for the growth of different microorganisms.

The relative rate of activity of these various spoilage reactions (microbial, enzymatic, browning, oxidation) as a function of water activity is portrayed in Figure 1.12 after Labuza [18]. Wide reference is made to this diagram by food engineers and scientists for the purpose of estimating the range of water activity that may be needed to prevent a given spoilage reaction [14–19].

Table 1.11 shows typical values of water activity for various food products:

It can now be apparent how all the different relationships discussed in this chapter begin to fit together. Water activity dictates whether or not a reaction will take place in a food, and if so, at what rate. Therefore the objective of most food dehydration processes is to bring the food product to a specified water activity. However, the engineer responsible for the design and operation of the food dehydration process can only be concerned about moisture content. The food drying equipment is designed only to remove moisture, and only moisture content can be measured and controlled on the factory floor (not water activity). The sorption isotherm becomes the fundamental tool by which it is possible to specify the moisture content needed that will assure the required water activity.

Table 1.11. Typical water activities of food (examples, average data), from [109] and [131]

a_W	
≈ 0.99	milk, meat, fish, juice, fruits, vegetables
≈ 0.95	sausage, liverwurst, camembert
≈ 0.8–0.9	ketchup, jam, bread, syrup, salami
≈ 0.7–0.8	prunes, marzipan
≈ 0.6–0.7	honey, raisins, nuts, dried fruits
≈ 0.5	bakery products, spices
≈ 0.4	egg powder
≈ 0.3	cookies
≈ 0.2	milk powder

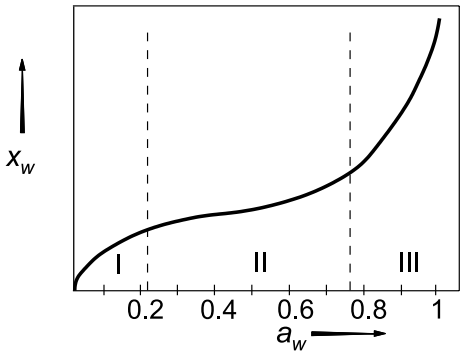

Figure 1.13. Generic sorption isotherm showing main regions of water bonding

The shape of the sorption isotherm also helps us to know what to expect about the quality of physical characteristics of a food product as a function of water activity. For example, we often divide a sorption isotherm into the three regions of water bonding states, as shown in Figure 1.13.

Region I is the region of very lowest water activity and moisture content. In this region, the very small amount of water in the material is completely bound within the monolayer, and unavailable to contribute any kind of moisture behavior to the material. Most food materials would be completely shrunken, hard and brittle in this state. It is also very difficult and costly to attempt to remove sufficient water by drying processes to reach such low levels of water activity. For these reasons, we often avoid to bring foods into Region I of their sorption isotherms.

Region II is the region in which the water activity is sufficiently low that most food spoilage reactions cannot proceed. This is the region in which the monolayer is completely saturated, but no free moisture is available for supporting any chemical, biochemical or biological activity. Therefore, this is the region into which we bring dehydrated foods for long term storage stability, such as food powders and dry snacks. These dry foods normally have a crispy or crunchy texture.

Region III is the region in which moisture uptake occurs most rapidly as multilayers are formed and the moisture content reaches the levels in which the water can act freely once again to support chemical and biological reactions. This is also the region in which the food material will exhibit the textural properties of being "fresh" with soft to firm elastic properties while being moist and swollen (fresh fruit and vegetables).

Some foods called "intermediate moisture" foods are dehydrated to a carefully controlled intermediate level of water activity in the region of transition between Regions II and III. The precise level of water activity is chosen to be sufficiently low so that no free moisture is available for supporting any spoilage reactions, but sufficiently high to still give a soft flexible texture. These foods are ready to eat and require no rehydration (beef jerky, salami, etc.). At the same time they are shelf stable for long periods of storage just as any dehydrated foods.

1.4 Laboratory Determination of Sorption Isotherms

In order to obtain a sorption isotherm for any material substance, it is necessary to be able to accurately measure both the moisture content and the water activity of a sample after it has come into equilibrium relative humidity at different known levels of relative humidity. The moisture content must be on a dry basis (db), as described in Table 1.6.

Measurement of Water Activity

Different procedures are available for measuring water activity [20], but they usually fall into one of three general methods of approach. Water activity can be measured through:

- Sample being brought into equilibrium with a closed atmosphere of known constant relative humidity (isopiestic technique or desiccators method)
- Equilibrium head space atmosphere surrounding sample is measured for its relative humidity with the sample (water activity meter)
- Dynamic method in which samples are exposed to atmospheres of various relative humidity and weighed simultaneously.

The first method of approach involves samples of known initial moisture content which go through the process of moisture gain (adsorption) or loss (desorption) in a constant controlled relative humidity atmosphere. The sample weight will change over time as it gains or loses moisture, and is measured and recorded periodically until the sample has come into equilibrium with the relative humidity of the surrounding atmosphere. At this point, when the sample will neither gain nor lose moisture with further time, the sample will have a water activity equal to the controlled constant relative humidity used

throughout the experiment therefore this approach sometimes is called isopiestic technique.

The second approach is to place the food sample of known constant moisture content into a sealed enclosure with small head space. The atmosphere in the head space is then probed for measurement and monitoring of changes in relative humidity or partial pressure until equilibrium is reached. The relative humidity measured at equilibrium is taken as the water activity of the sample. Because time to reach equilibrium can be long e.g. several hours, some instruments are equipped with software for extrapolation to the water activity at which the sample will neither gain nor lose moisture.

In the third approach (dynamic method), samples of food can be exposed for a short period of time to flowing air at various relative humidity and weighed automatically. For this purpose, isothermal thermogravimetric methods are useful techniques (see Section 7.9.1).

Regardless of the different approaches, it is important in all three methods to remember that sorption is strongly temperature dependent, and the temperature must be kept constant and controlled while all the experiments are being carried out. It is also important to determine and note the distinction if the experiment is for the purpose of constructing a desorption (drying) or adsorption (wetting) isotherm, because of hysteresis effects explained earlier. In the case of a desorption isotherm, the food sample will initially be very fresh with relatively high moisture content (fully hydrated), and will lose moisture and weight during the experiment. In the case of an adsorption isotherm, the food sample will initially be very dry (dehydrated), and will gain moisture and weight during the experiment.

Measurement of Moisture Content

The standard classic procedure for accurate determination of the moisture content in a sample of food material is the gravimetric oven method [103]. In this method, a sample of known initial weight is placed into a drying oven at 103 °C, and weighed periodically until no further weight loss is detected.

There are various types of laboratory "moisture meters" available for more rapid determination of moisture content (within 10–30 minutes). These work on the principles of either measuring electrical conductivity (see, e.g. [110]), which depends on moisture content, or by driving the moisture out of the sample more rapidly than a drying oven using infrared radiation from an infrared lamp. These methods, however, can often give erroneous results because of various limitations, and must be used with great caution.

Laboratory Apparatus for Determination of Sorption Isotherms

Of all the methods described earlier for measuring water activity, the "desiccator jar" method in which the sample is brought into equilibrium in a closed system with a known constant relative humidity, is considered to be the classic

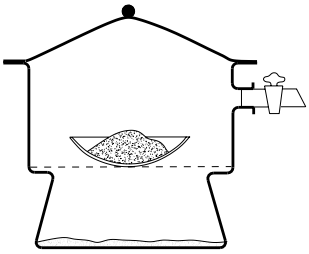

Figure 1.14. Taking a point of the sorption isotherm. The sample is placed in a closed chamber with a humidity standard (at the bottom, schematic). After water activity equilibration of sample and atmosphere in the chamber the sample is weighed to get its moisture content

standard for the purpose of constructing sorption isotherms with the greatest accuracy. In order to construct a sorption isotherm several data points are needed, each point defined by the moisture content (db) measured at a specified water activity, over a range of specified water activities. Samples are brought to specified water activities by placing them in hermetically sealed desiccator jars, shown in Figure 1.14. Each jar maintains a sealed headspace atmosphere around the sample at known constant relative humidity. Samples are then periodically weighed to monitor weight gain or loss until equilibrium is reached when no further weight gain or loss occurs over time.

The covers on these jars are designed in such a way that they can be easily opened and re-closed quickly for removal and replacement of the samples during the few minutes required for periodic weighings. More sophisticated desiccator jar systems allow for continuous monitoring of weight change by having the samples resting upon electronic load cells within the jar, so there is no need to open the jar during the experiment. The relative humidity in jar head space can be measured accurately by means of a hygrometer. The time period between sample weighings will depend upon how rapidly equilibrium will be reached. The time required to reach equilibrium at any given relative humidity can vary widely depending upon the size and shape as well as physical and chemical make-up of the food sample. Sometimes this can be a problem with many fresh food samples that are highly perishable [21, 35]. They may begin to deteriorate as a result of microbial spoilage activity before equilibrium is reached. This would compromise the validity of the data.

In a laboratory experiment for determining a sorption isotherm on a food sample, several desiccator jars are needed, one for each data point that will be used to construct the isotherm with each jar maintaining a different controlled relative humidity. The method most commonly chosen for establishing a different relative humidity in each jar is to place within each jar a saturated solution of a given salt. Saturated salt solutions are frequently used as relative humidity standards. Table 1.12 shows some salts frequently used for this purpose, and their water activities (equilibrium relative humidities) at different temperatures.

Another isopiestic technique is to bring a droplet of an indicator liquid into water activity equilibrium with the sample. The sample is placed in a small jar and a small amount of the indicator liquid is placed in glassware in the same jar. Now the indicator fluid will take up water from the sample head space

Table 1.12. Water activity standards

saturated aqueous solution of:	from	water activity a_W at					
		10 °C	15 °C	20 °C	25 °C	30 °C	35 °C
NaOH	[37]	–	0.0957	0.0891	0.0824	0.0758	0.0692
Sodium hydroxide			±0.028	±0.024	±0.021	±0.017	±0.015
LiCl	[37]	0.1129	0.1130	0.1131	0.1130	0.1128	0.1125
Lithium chloride		±0.0041	±0.0035	±0.0031	±0.0027	±0.0024	±0.0022
$ZnCl_2$	[134]	–	–	0.119	–	–	–
Zinc chloride							
K-CH_3CO_2	[37]	0.2338	0.2340	0.2311	0.2251	0.2161	–
Potassium acetate		±0.0053	±0.0032	±0.0025	±0.0032	±0.0053	
$MgCl_2$	[37]	0.3347	0.3330	0.3307	0.3278	0.3244	0.3205
Magnesium chloride		±0.0024	±0.0021	±0.0018	±0.0016	±0.0014	±0.0013
K_2CO_3	[37]	0.4314	0.4315	0.4316	0.4316	0.4317	–
Potassium carbonate		±0.0039	±0.0033	±0.0033	±0.0039	±0.0050	
$MgNO_3$	[37]	0.5736	0.5587	0.5438	0.5289	0.5140	0.4991
Magnesium nitrate		±0.0033	±0.0027	±0.0023	±0.0022	±0.0024	±0.0029
NH_4NO_3		–	–	0.66	0.66	–	–
Ammonium nitrate							
NaCl	[134]	0.7567	0.7561	0.7547	0.7529	0.7509	0.7487
Sodium chloride		±0.0022	±0.0018	±0.0014	±0.0012	±0.0011	±0.0012
KCl	[37]	0.8677	0.8592	0.8511	0.8434	0.8362	0.8295
Potassium chloride		±0.0039	±0.0033	±0.0029	±0.0026	±0.0025	±0.0025
KNO_3	[37]	0.9596	0.9541	0.9462	0.9358	0.9231	0.9079
Potassium nitrate		±0.014	±0.0096	±0.0066	±0.0055	±0.0060	±0.0083

until equilibrium is reached. Then the indicator fluid is taken out and analyzed by a refractometer for its water content. Having the sorption isotherm of the indicator fluid (water content versus its water activity) the water activity of the sample can be determined very simply and quickly [22]. Note that a high quality constant-temperature refractometer is needed for this procedure.

It is also important to note that sample size has a great effect on time required to reach equilibrium because of time needed for diffusion of molecules through the interior tissue structure of the sample. Laboratory methods and procedures that permit very small sample sizes, have the advantage that they are likely to produce valid results far more quickly [36].

Standards for Measuring Sorption Isotherms

In order to validate the accuracy of any given laboratory procedure or analytical method for measuring a physical or chemical property, most laboratories

rely upon testing their procedures with a "standard" sample to see if the result is in accordance with the expected known outcome for the standard. In the case of water vapor sorption isotherms in foods, the recommended standard is microcrystalline cellulose (MCC). This material is widely available to the scientific community under the trade name "Avicel," and possesses a signature isotherm, that is published in books on physical properties of foods [23]. Figure 1.15 shows the sorption isotherm for this standard material. Equation (1.47) gives the mathematical model for this isotherm when the numerical value of the constants A and b are taken as 0.0540 and –0.4343, respectively (Avicel PH1 at 25 °C).

$$x_W = A\left(\frac{1}{a_W - 1}\right)^b \tag{1.47}$$

The following table compares model predicted with experimentally measured moisture content of a sample of Avicel.

Table 1.13. Predicted and measured data of Avicel

a_W	x_W in % (db) predicted	x_W in % (db) measured (from [23])
0.1	2.80	2.0 ± 0.5
0.2	2.96	3.0 ± 0.5
0.4	4.53	5.0 ± 0.5
0.6	6.44	7.0 ± 0.5
0.8	9.86	10.0 ± 0.5
0.9	14.02	–

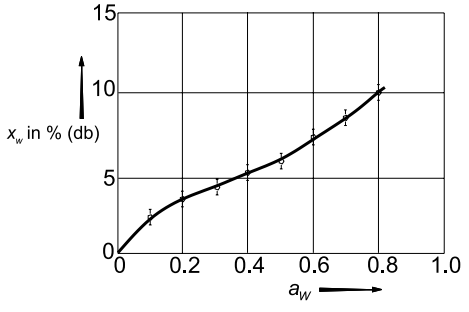

Figure 1.15. Sorption isotherm of microcrystalline cellulose (25 °C, adsorption) (from [23])

1.5 Applications

sugar and sugar replacers: phase transitions by water uptake	[24]
lupinus: sorption isotherms and monolayer bonding enthalpy	[25]
potato: sorption isotherms and monolayer bonding enthalpy	[26,27]
starch powders: sorption isotherms	[28]
agar gels: sorption isotherms, monolayer bonding enthalpy, HENDERSON model	[29]
strawberries: GAB sorption isotherm and glass transition	[30]
poultry meat: sorption isotherm and glass transition	[31]
pineapple: sorption isotherm, sorption enthalpy	[32]
pepper: sorption enthalpy	[33]
starch and wheat gluten: GAB sorption isotherms	[34]
pineapple: water desorption thermodynamic properties	[39]
corn starch: modeling of water sorption isotherm	[40]

Literature

1. Lewicki PP (2004) Water as the determinant of food engineering properties. A review. J Food Engineering, 61:483–495
2. Gregg SJ, Sing KSW (1982) Adsorption, Surface Area and Porosity. Academic Press, London
3. Luy B (1991) Vakuum Wirbelschicht. Dissertation, Universität Basel
4. Korte F (ed) (1973) Methodicum chimicum Bd 1 Teil 2. Thieme, Stuttgart
5. Brunauer S, Emmet PH, Teller E (1938) J Am Chem Soc 60:309
6. Bauer KH, Frömming KH, Führer C (1999) Pharmazeutische Technologie. Deutscher Apotheker Verlag, Stuttgart
7. Cazier JB, Gekas V (2001) Water activity and its prediction: a review. Intern J Food Properties 4:35
8. Iglesias HA, Chirife J (1982) Handbook of Food Isotherms: Water Sorption Parameters for Food and Food Components. Academic Press, New York
9. Nesvadba P, Houska M, Wolf W, Gekas V, Jarvis D, Sadd PA, Johns AI (2004) Database of physical properties of agro-food materials. J Food Engineering 61: 497–503
10. Taylor AJ (1998) Physical chemistry of flavour. Int J Food Sci Tech 33:53–62
11. Atkins PW (1990) Physikalische Chemie. VCH Weinheim
12. Van den Berg, Bruin S (1981) Water activity and its estimation in food systems. In: Rockland LB, Stewart GF (eds) Water Activity: Influence on Food Quality. Academic Press, New York
13. Bizot H (1983) in: Jowitt R, Escher F, Hallström B, Meffert HFTh, Spiess WEL, Vos G (1983) Physical Properties of Food. Applied Science Publishers, Barking
14. Timmermann EO, Chirife J, Iglesias HA (2001) Water sorption isotherms of foods and foodstuffs: BET or GAB parameters? J Food Engineering 48:19–31
15. Isengard HD, Rückold S, Grobecker KH (2001) Water as a source of errors in reference materials. Fresenius J Anal Chem 370:189–193
16. Labuza Th, University of Minnesota, available online from: http://www.fsci.umn.edu/Ted_Labuza/CV/tplcv.htm [cited 2003–12–24]

17. Lewicki PP (2000) Raoult's law based food water sorption isotherm. J Food Engineering 43:31–40
18. Labuza TP (1971) Kinetics of lipidoxidation in foods. Crit Rev Food Technol 2:355
19. Troller JA, Christian JHB (1978) in: Water Acivity and Food. Academic Press, New York
20. Hofer AA (1962) Zur Aufnahmetechnik von Sorptionsisothermen und ihre Anwendung in der Lebensmittelindustrie. Dissertation, Universität Basel
21. Chirife J, Buera MP (1995) A critical review of some non-equilibrium situations and glass transitions on water activity values of foods in the microbiological growth range. J Food Engineering 25:531–552
22. Steele RJ (1987) Use of polyols to measure equilibrium relative humidity. Int J Food Sci Technol 22:377–384
23. Spiess (1983) in: Jowitt R, Escher F, Hallström B, Meffert HFTh, Spiess WEL, Vos G (1983) Physical Properties of Food. Applied Science Publishers, Barking
24. Cammenga HK, Gehrich K (2003) Glatt, rau oder klebrig? Zeitschrift für Lebensmittel- und Verpackungstechnik (LVT) 48:28
25. Vázquez G, Chenlo F, Moreira R (2003) Sorption isotherms of lupine at different temperatures. J Food Engineering 60:449–452
26. McMinn WAM, Magee TRA (2003) Thermodynamic properties of moisture sorption of potato. J Food Engineering 60:157–165
27. McLaughlin CP, Magee TRA (1998) The determination of sorption isotherm and the isosteric heats of sorption for potatoes. Journal of Food Engineering 35:267–280
28. Al-Muhtaseb AH, McMinn WAM, Magee TRA (2004) Water sorption isotherms of starch powders: Part 1: mathematical description of experimental data. J Food Engineering 62:135–142
29. Iglesias O, Bueno JL (1999) Water agar–agar equilibrium: determination and correlation of sorption isotherms. Int J Food Sci Tech 34:209–216
30. Moraga G, Martínez-Navarrete N, Chiralt A (2004) Water sorption isotherms and glass transition in strawberries: influence of pre-treatment. J Food Engineering 62:315–321
31. Delgado AE, Sun DW (2002) Desorption isotherms and glass transition temperature for chicken meat. J Food Engineering 5:1–8
32. Hossain MD, Bala BK, Hossain MA, Mondol MRA (2001) Sorption isotherms and heat of sorption of pineapple. J Food Engineering 48, 2:103–107
33. Kaymak-Ertekin F, Sultanoglu M (2001) Moisture sorption isotherm characteristics of peppers. J Food Engineering 47:225–231
34. Viollaz E, Rovedo CO (1999) Equilibrium sorption isotherms and thermodynamic properties of starch and gluten. J Food Engineering 40:287–292
35. Rückold S, Grobecker, KH, Isengard, HD (2001) Water as a source of errors in reference materials. Fresenius J Analytical Chemistry 370:189–193.
36. Czepirski L, Komorowska-Czepirska E, Szymonska J (2005) Adsorptive properties of biobased adsorbents. Adsorption 11:757–761
37. Greenspan L (1977) Humidity fixed points of binary saturated aqueous solutions. Journal of Research of the National bureau of Standards A: Physics and Chemistry, Vol 81A:89
38. DIN ISO 9277 (2003) Determination of the specific surface area of solids by gas adsorption using the BET method, in [101]
39. Simal S, Femenia A, Castell-Palou A, Rosselló C (2007) Water desorption thermodynamic properties of pineapple. J Food Engineering 80:1293–1301
40. Guilan Peng, Xiaoguang Chen, Wenfu Wu, Xiujuan Jiang (2007) Modeling of water sorption isotherm for corn starch. J Food Engineering 80:562–567

2 Mass and Density

2.1 Mass

Mass is a measure for inertia and heaviness of a body. Heaviness is caused by the Earth's gravitational attraction for a body. The force between the body of interest and the planet Earth is called the weight force of the body. Mathematically, this force can be expressed as the product of the body's mass and the Earth's acceleration due to gravity, as shown by equation (2.1).

$$G = m \cdot g \tag{2.1}$$

where

G	weight force in N
m	mass in kg
g	gravitational acceleration in $\mathrm{m} \cdot \mathrm{s}^{-2}$

Because the density of planet Earth varies with location and the planet is slightly pear-shaped and not in the shape of a perfect sphere, the value of gravitational acceleration differs slightly with location on the Earth's surface. Considering the rotation of the planet, a body resting at the equator will have a greater tangential speed and centrifugal force than in regions far north or south of the equator. The value of Earth's gravitational acceleration in Zurich, Switzerland is used as a standard for calculations, and is called standard gravitational acceleration having the value $g = 9.80665\ \mathrm{m} \cdot \mathrm{s}^{-2}$ [107]. When a balance which was adjusted in Zurich, is taken to another place on the Earth, but is not corrected for the local gravitational acceleration, the displayed weight may be in error. Table 2.1 illustrates this concept for a body having a mass of 1 kg. To avoid erroneous weight measurements of this type, a balance has to be recalibrated at the location in which it will be used. For this purpose, commercial mass standards are produced with the help of national standards organizations around

Table 2.1. Weighing a 1 kg mass in different places

City	g in $\mathrm{m} \cdot \mathrm{s}^{-2}$	balance displays
Zurich, Switzerland	9.80665	1000.0 g
Bogota, Columbia	9.77390	996.7 g
Reykjavik, Iceland	9.82265	1001.6 g

Table 2.2. Metrological institutes, examples

ISO	International Organization for Standardization	www.iso.org
NIST	National Institute of Standards and Technology (USA)	www.nist.gov
PTB	Physikalisch-Technische-Bundesanstalt (Germany)	www.ptb.de
AIST	National Institute of Advanced Industrial Science and Technology (Japan)	www.aist.go.jp
NPL	National Physical Laboratory (UK)	www.npl.co.uk
IEN	Istituto Elettrotecnico Nazionale Galileo Ferraris (Italy)	www.ien.it
NRC	National Research Council (Canada)	http://inms-ienm.nrc-cnrc.gc.ca
METAS	Bundesamt für Metrologie und Akkreditierung (Switzerland)	www.metas.ch
CSIRO	Division of Telecommunication & Industrial Physics (Australia)	www.csiro.au
NML	National Metrology Laboratory (South Africa)	www.csir.co.za
NMi	Nederlands Meetinstituut (Netherlands)	www.nmi.nl

the world. These organizations assume responsibility for control and uniformity of standards from different countries. For example the national 1 kg mass standards that are used throughout Europe are copies of a platinum iridium prototype, which is kept at BIPM (Bureau International des Poids et Mesures) in Sevres near Paris, France. Similar organizations/institutes responsible for national standards in other parts of the world are identified in Table 2.2.

2.2 Weighing and Atmospheric Buoyancy

A balance is an instrument measuring the weighing force of a body. However, it usually does not display a force signal (e.g. newtons), but a mass signal (e.g. kilograms). This is due to the principle of calibration used for balances: A mass standard is placed on the balance that causes a deformation, which can be read as an angle, a distance or an electric voltage, depending on the type of balance. With different mass standards a mass versus reading data set is obtained. This can be used to generate a scale to be mounted on the balance. With that scale in place, the balance operates as though it were an instrument for measuring mass. This procedure is called a calibration. A calibration has to be performed for every type of sensing/measuring instrument. For this purpose, appropriate respective standard materials and procedures are needed, that make it possible to perform calibration of an instrument in any laboratory. However, in many parts of the world, calibration of balances or check weighers, that are to be used in commerce (sale of products) often has to be done by official institutions with official standards depending on national laws.

From a scientific point of view the calibration procedure described for a balance is basically to use the instrument as a "force meter," then divide the force G measured by the value of the local gravitational acceleration g, and display the result (equation volume of hydrometer in m^3).

$$\frac{G}{g} = m \tag{2.2}$$

Since the middle ages the weight of a body has been a manifold of a reference weight. So weighing is simply a comparison to a given mass standard. From this point of view weighing is dividing the weight force of the given body and weight force of a mass standard and the result is a dimensionless number. That is the principle of all mechanical and electronic balances up to today, and a consequence of lacking an expression for mass with fundamental natural constants.

$$\frac{G_K}{G_R} = \frac{m_K \cdot g}{m_R \cdot g} = n \tag{2.3}$$

where

G_K	weight force in N
G_R	weight force of mass standard in N
m_K	mass of body in kg
m_R	mass of mass standard in kg
n	ratio
g	gravitational acceleration in $m \cdot s^{-2}$

Most weight measurements are carried out with body and balance surrounded by atmospheric air, which is a gaseous fluid possessing density. Only bodies of material with density greater than atmospheric air at the Earth's surface can impart a force when placed upon a balance. For example a rubber balloon filled with helium gas (less dense than air) possesses mass, but it will not rest on a balance. It will rise upward into the atmosphere in search of an altitude at which the density of the atmosphere is in equilibrium with itself. His upward force caused the density of the Earth's atmosphere is known as buoyancy. This atmospheric buoyancy causes a body resting on a balance when surrounded by atmospheric air to exhibit a slightly smaller weight measurement than if it were in a vacuum (Figure 2.1).

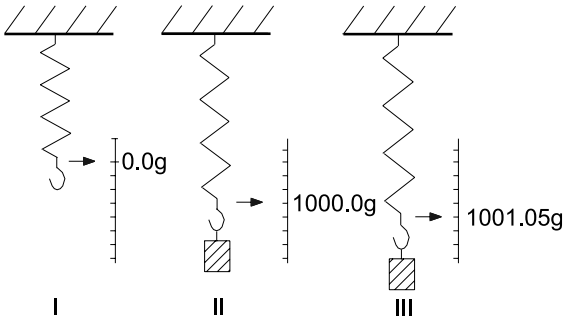

Figure 2.1. A balance is adjusted to zero weight (picture I). A mass of 1 kg is weight in atmosphere (picture II) and in vacuum (picture III)

The calculation needed to correct for this buoyancy effect in order to yield the true mass of a body is called atmospheric buoyancy correction. The true mass of a body m_K is the product of the displayed mass m_K^* and a correctional factor K. The value of the correctional factor K depends on the density of the air surrounding the balance. Because weight measurement is a comparison of a body of interest and a mass standard, the densities of both materials also influence the correctional factor (equations (2.4) to (2.6):

$$m_K = m_K^* \cdot K \tag{2.4}$$

$$K = 1 + \rho_L \cdot \frac{\frac{1}{\rho_K} - \frac{1}{\rho_R}}{1 - \frac{\rho_L}{\rho_K}} \tag{2.5}$$

$$K \approx 1 + \rho_L \cdot \left(\frac{1}{\rho_K} - \frac{1}{\rho_R}\right) \tag{2.6}$$

where

m_K^*	displayed weight of the body in kg
m_K	true mass of the body in kg
ρ_L	density of air in kg · m^{-3}
ρ_K	density of the body in kg · m^{-3}
ρ_R	density of mass standard in kg · m^{-3}
K	correctional factor for atmospheric buoyancy

The density of air depends on its pressure, temperature, humidity and its concentration of CO_2. Values are listed (see, e.g. [105]) or can be approximated with empirical equations (see e.g. [106]). For practical purposes, the density of atmospheric air at normal room temperature and sea level (standard conditions) can be taken to be approximately 1.2 kg · m^{-3}. A simple approach to calculate the density of air more precisely (on the basis of [1]) is given by equation (2.7):

$$\rho_L/\text{kg} \cdot \text{m}^{-3} = 3.4849 \cdot 10^{-3} \, \frac{p/\text{Pa}}{T/\text{K}} \cdot \left(1 - 0.3780 \, \frac{p^*}{p}\right) \tag{2.7}$$

where

p	air pressure in Pa
p^*	water vapor partial pressure in Pa
T	temperature in K

Example 2.1. Estimation of air density

air pressure	$p = 10^5$ Pa
air temperature	$\vartheta = 20\,^\circ$C i.e. $T = 293.15$ K
air humidity	$\varphi = 50\%$ r.h.
water vapor partial pressure	$p^* = \varphi \cdot p_s = 0.5 \cdot 23.27$ Pa $= 11.7$ Pa

Table 2.3. Atmospheric buoyancy correctional factor, examples

food material	ρ/kg · m^{-3}	K	m_K^*/g	m_K	difference
cocoa butter	915	1.00116	1000.00	1001.16	0.12%
water	1000	1.00105	1000.00	1001.05	0.11%
sucrose	1590	1.00091	1000.00	1000.91	0.09%

Values of water vapor pressure p_s are listed in water vapor steam tables, see, e.g. Appendix 15.8.

$$\rho_L/\mathrm{kg}\cdot\mathrm{m}^{-3} = 3.4849\cdot 10^{-3}\frac{10^5}{293.15}\cdot\left(1-0.3780\cdot\frac{11.7}{10^5}\right) = 1.1887$$

so

$$\rho_L = 1.189\,\mathrm{kg}\cdot\mathrm{m}^{-3}$$

In contrast to air, the density of water is 1000 times greater (1000 kg · m^{-3}). Therefore, the density range of most food, agricultural and biological materials is in the same order of magnitude as that of water, about 1200 ± 300 kg · m^{-3}. The densities of materials with high water content are in a range more closely to that of water (between 1000 and 1100 kg · m^{-3}) while dry materials like agricultural grains, seeds and dry beans consisting of proteins, carbohydrates, starch or cellulose are often in the range 1400–1600 kg · m^{-3}. Since these density ranges are one thousand times greater than the density of air, the correctional factor for atmospheric buoyancy can be estimated to be approximately 0.1%. Table 2.3 shows some examples calculated with an air density of $\rho_L = 1.2$ kg · m^{-3} and density of a mass standard used for calibration of the balance of $\rho_R = 8000$ kg · m^{-3}. Note that the density of the mass standard used in calibration is far greater than the range of most food materials because these mass standards are fabricated from very dense metals (brass, stainless steel, chromium, etc.). Because of the small effect of atmospheric buoyancy in most food technology applications, the systematic error of atmospheric buoyancy is frequently neglected. Often this error is overshadowed by other factors, such as uncertainty of weighing accuracy and lack of precision, which may be larger. However, for the fabrication of mass standards to be used in calibration, and in commercial trade of highly expensive materials it must be taken into account.

2.3 Density

Frequent reference to the physical property of density was made in the previous subsection with the expectation that the reader would have an intuitive "operational definition" of density. In this subsection, a more scientific definition is presented. The density of a substance is the quotient of mass over volume. The standard international (SI) units for expressing density are kg · m^{-3}. The same

definition is valid for solid, liquid, gaseous and disperse systems like foams, bulk goods or powders. The reciprocal of density is called specific volume and the units are $m^3 \cdot kg^{-1}$ (equations (2.8) and (2.9).

$$\rho = \frac{m}{V} \tag{2.8}$$

$$\frac{V}{m} = v = \frac{1}{\rho} \tag{2.9}$$

where
m mass in kg
V volume in m^3
ρ density in $kg \cdot m^{-3}$
v specific volume in $m^3 \cdot kg^{-1}$

2.3.1 Temperature Dependency of Density

Many materials undergo thermal expansion when heated, meaning they increase in volume without any change in mass. For this reason, the density of a given material often depends on temperature. Since the volume of a material normally increases with temperature, the density usually decreases with temperature. This effect is much larger in gaseous systems than in liquid or solid systems.

Ideal Gases

For many engineering applications air can be assumed to behave as an ideal gas, meaning that the ideal gas law can be used for calculating the density of air as a function of temperature and pressure (equations (2.10) and (2.11).

$$p \cdot V = m \cdot R_S \cdot T \tag{2.10}$$

$$\rho = \frac{p}{R_S T} \tag{2.11}$$

where
p pressure in Pa
R_s specific gas constant in $J \cdot K^{-1} \cdot kg^{-1}$
ρ density $kg \cdot m^{-3}$
T temperature in K
m mass in kg
V volume in m^3

In case of low temperatures and humid air the ideal gas law loses accuracy, and will lead to error. To calculate the density of air more precisely as a function of water vapor partial pressure and atmospheric pressure, equation (2.7) can be used.

Solids and Liquids

The density of liquids and solids is a function of temperature. Small changes in volume caused by temperature change can be calculated with the aid of the thermal expansion coefficient:

$$\gamma = \frac{1}{V} \cdot \frac{dV}{dT} \tag{2.12}$$

where

γ	thermal expansion coefficient in K^{-1}
T	temperature in K
V	volume in m^3

For numerous materials, values of density at different temperatures are published in tables (e.g. for air [105,106], water [105,108], milk [109]), or can be calculated with polynomial functions (see Section 15.9).

Water shows abnormal behavior in a narrow range of temperature near its freezing point at atmospheric pressure. When lowering the temperature of water from 4 °C and 0 °C, the density of water actually decreases rather than increases. This abnormal behavior of water (see Figure 2.2 and Figure 2.3 is taken into account within the polynomial function of Bertsch (1983) for calculation of the density of liquid water [106] (equation (2.13):

$$\begin{aligned} \rho/\mathrm{kg \cdot m^{-3}} = 1000.22 &+ 1.0205 \cdot 10^{-2} \cdot (\vartheta/^\circ\mathrm{C}) \\ &- 5.8149 \cdot 10^{-3} \cdot (\vartheta/^\circ\mathrm{C})^2 \\ &+ 1.496 \cdot 10^{-5} \cdot (\vartheta/^\circ\mathrm{C})^3 \end{aligned} \tag{2.13}$$

A further abnormality of water is that the solid phase (ice) has a lower density than the liquid phase at the same temperature. This behavior has important consequences for the biosphere.

Because of this temperature dependency of density, control or measurement and recording of temperature is necessary when density is measured for

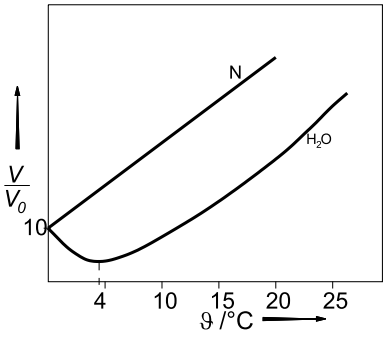

Figure 2.2. Normal (N) and abnormal (H_20) thermal expansion (schematic)

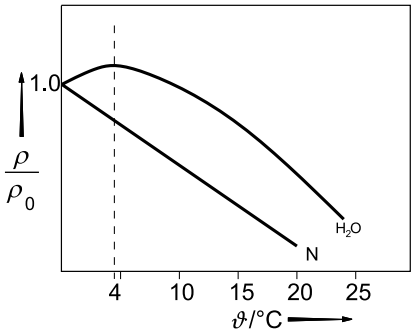

Figure 2.3. Abnormality of water (H_2O): Temperature dependency of density compared to normal behavior (N)

process control and quality control purposes (e.g. in-line sensors during food processing, see Chapter 14).

2.3.2 Pressure Dependency of Density

Materials are compressible. On application of pressure their volume decreases, causing the density to be a function of pressure as well as temperature. Gases are far more compressible than liquids and solids. Over a normal temperature range many gases can be assumed to behave like ideal gases:

Ideal Gases

For ideal gases the density is directly proportional to the pressure:

$$p \cdot V = m \cdot R_S \cdot T \tag{2.14}$$

$$\frac{m}{V} = \frac{p}{R_S T} \tag{2.15}$$

$$\rho = \frac{p}{R_S T} \tag{2.16}$$

so the density of the ideal gas is

$$\rho \sim p \tag{2.17}$$

The negative slope of the volume–pressure curve divided by the initial volume is called the compressibility κ. It is the inverse compression modulus K of a material.

$$\kappa = -\frac{1}{V} \cdot \frac{dV}{dp} \tag{2.18}$$

$$\frac{1}{\kappa} = K \tag{2.19}$$

Liquids and Solids

Ideal liquids and solids show an elastic behavior. That means their volume can decrease by a certain amount when a pressure is applied, but that it will fully recover to the initial volume when the pressure is restored. For this type of material the change in volume on increasing the pressure can be calculated based on equation (2.20):

$$\frac{\Delta V}{V} = -\kappa \cdot \Delta p \tag{2.20}$$

with (2.8) and because of m = const the relative density is:

$$\frac{\Delta \rho}{\rho} = \left| \frac{\Delta V}{V} \right| = |\kappa \cdot \Delta p| \tag{2.21}$$

where

p	pressure in Pa
R_s	specific gas constant in $J \cdot K^{-1} \cdot kg^{-1}$
ρ	density in $kg \cdot m^{-3}$
T	temperature in K
m	mass in kg
V	volume in m^3
κ	compressibility in Pa^{-1}
K	modulus of compression in Pa

Liquids and solids with very low compressibility κ show a very small volume reduction and often are treated in practice as incompressible materials.

Water has very low compressibility with a value of $\kappa \approx 5 \cdot 10^{-10}$ Pa^{-1}. So, up to pressures in the order of 10 MPa (100 bar), the reduction of the volume in water is so small that it can be neglected. Although in high pressure processing of food, where the pressure will range to some 100 MPa, the compressibility of water cannot be neglected [2] (see Example 2.2), and also must be taken into account because the mechanical energy of compression is converted to heat (see Example 2.3 and Example 2.4).

Example 2.2. Change in density of water under high pressure operations

$$\frac{\Delta\rho}{\rho} = |\kappa \cdot \Delta p|$$

With this equation the relative change in density is:

	Δp	result
10 bar	$\frac{\Delta\rho}{\rho} = 5 \cdot 10^{-10}\ Pa^{-1} \cdot 10^6\ Pa = 5 \cdot 10^{-4} =$	0.05%
100 bar	$\frac{\Delta\rho}{\rho} = 5 \cdot 10^{-10}\ Pa^{-1} \cdot 10^7\ Pa = 5 \cdot 10^{-3} =$	0.5%
1000 bar	$\frac{\Delta\rho}{\rho} = 5 \cdot 10^{-10}\ Pa^{-1} \cdot 100 \cdot 10^6\ Pa = 5 \cdot 10^{-2} =$	5.0%
10000 bar	$\frac{\Delta\rho}{\rho} = 5 \cdot 10^{-10}\ Pa^{-1} \cdot 1000 \cdot 10^6\ Pa = 50 \cdot 10^{-2} =$	50%

The modulus of compression can also be used to characterize the firmness or stiffness of materials (see Section 4.1.3).

Example 2.3. Energy input by compression of 1 kg water by Δp = 300 MPa (3000 bar)

$$dW = -p \cdot \mathrm{d}V$$

$$W = -\int p \cdot \mathrm{d}V$$

$$W = -\int p \cdot (-\kappa \cdot V) \cdot \mathrm{d}p$$

$$W = \kappa \int p \cdot V \cdot \mathrm{d}p$$

$$W = \kappa \cdot V \int p \cdot \mathrm{d}p$$

$$W = \frac{1}{2}\kappa \cdot V \cdot p^2$$

The dimensional units for this term are:

$$\mathrm{Pa}^{-1} \cdot \mathrm{m}^3 \cdot \mathrm{Pa} = \frac{\mathrm{N}}{\mathrm{m}^2} \cdot \mathrm{m}^3 = \mathrm{N} \cdot \mathrm{m}$$

$$3000\,\mathrm{bar} = 300\,\mathrm{MPa} = 3 \cdot 10^8\,\mathrm{Pa}$$

sample: 1 kg Water

$$\kappa \approx 5 \cdot 10^{-10}\,\mathrm{Pa}^{-1}$$

$$\frac{W}{m} = \frac{1}{2}\kappa \cdot \frac{V}{m} \cdot p^2$$

$$\frac{W}{m} = \frac{1}{2} \cdot 5 \cdot 10^{-10} \frac{10^{-3}}{1} \cdot \left(3 \cdot 10^8\right)^2 \frac{\mathrm{J}}{\mathrm{kg}} = 22.5 \frac{\mathrm{kJ}}{\mathrm{kg}}$$

Example 2.4. How high will temperature rise in response to this energy input?

$$Q = m \cdot c_p \cdot \Delta T$$

$$\frac{Q}{m} = c_p \cdot \Delta T$$

$$\Delta T = \frac{Q}{m \cdot c_p}$$

$$\Delta T = 22.5 \frac{\mathrm{kJ}}{\mathrm{kg}} \cdot \frac{1\,\mathrm{kg}}{4.18\,\mathrm{kJ}} \cdot \mathrm{K}$$

$$\Delta T = 5.4\,\mathrm{K}$$

For calculation of temperature increase during high pressure processing of food refer also to reference [24].

2.3.3 Specific Gravity (Relative Density)

The ratio of the absolute density of a material to the density of a reference material is called relative density d. Water at 4 °C or 20 °C is most often used

as the reference material for this purpose. In the USA and Canada, when water is used as the reference standard, the term "relative density" is not used, and is replaced by the term "specific gravity." Since water is nearly always chosen as the reference standard world-wide, for practical purposes the terms "relative density" and "specific gravity" may be considered as synonymous.

$$d = \frac{\rho}{\rho_R} \tag{2.22}$$

where

d relative density (specific gravity)
ρ density in $\mathrm{kg \cdot m^{-3}}$
ρ_R density of reference material in $\mathrm{kg \cdot m^{-3}}$

It is important to note that both density and specific gravity (relative density) relate to the same physical property. However, density must be reported in dimensional units of mass per unit volume (e.g. $\mathrm{g \cdot cm^{-3}}$ or $\mathrm{kg \cdot m^{-3}}$), while specific gravity (relative density) is a ratio of densities, and is always a dimensionless number. In the case where density is being reported in dimensional units of $\mathrm{g \cdot cm^{-3}}$ and with the density of the reference material being 1 $\mathrm{g \cdot cm^{-3}}$ or nearly 1 $\mathrm{g \cdot cm^{-3}}$ it is interesting to note that numerical values of both density and specific gravity (relative density) will be the same, respectively, nearly the same (see Example 2.5).

Example 2.5. Specific gravity of potatoes

density of potatoes	specific gravity $d = \frac{\rho}{\rho_R}$ with	
	$\rho_R = 1000\ \mathrm{kg \cdot m^{-3}}$ (water of 4 °C)	$\rho_R = 997.1\ \mathrm{kg \cdot m^{-3}}$ (water of 20 °C)
$\rho = 1000\ \mathrm{kg \cdot m^{-3}}$	$d = 1.080$	$d = 1.083$

2.3.4 Methods for Laboratory Measurement of Density

Table 2.4 shows examples of different methods used for density measurement.

Pycnometric Measurement

By weighing a known volume of a liquid, the density of that liquid can be measured in a simple way. Glass bulbs with precisely known volume that are used for this purpose are called pycnometers. A pycnometer can also be any other instrument designed for the same purpose that may have sample chambers of precisely known volume, but made of other materials (not glass bulbs). The glass bulb or sample chamber will have a marker to which the liquid sample must be carefully filled. Then the density of the fluid can be calculated by:

Table 2.4. Techniques of density measurement

name	pycnometer	hydrostatic balance	submersion balance for viscous liquids	hydrometer	density gradient column
	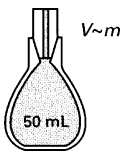	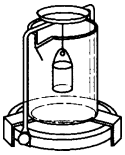	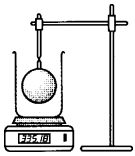	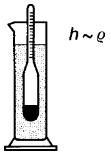	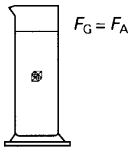
for	fluids, solids	fluids, solids	fluids	fluids	Solid particles
	Mohr–Westphal balance	X-ray technique	bulk density	tapped bulk density	resonator frequency
	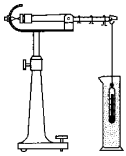	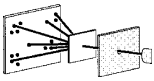	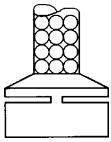	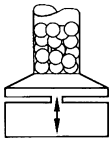	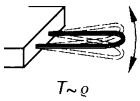
for	fluids	solids	solids	solids	gases, fluids

$$\rho_F = \frac{m_F - m_0}{V} \tag{2.23}$$

Because of thermal expansion of the glass, the pycometer volume is known for the temperature at which it was calibrated, only. So, for measurement of the absolute density, pycnometers should be used at the same temperature at which they were calibrated. Another way is to measure the relative density (specific gravity) rather than the absolute density. For this purpose, the pycnometer is weighed with the sample liquid and again weighed with the reference liquid (often water). The ratio of both weights gives the relative density d, or specific gravity of the sample.

$$\frac{m_F}{m_W} = \frac{m_F \cdot V}{V \cdot m_W} = \frac{\rho_F}{\rho_W} = d \tag{2.24}$$

The advantage of the latter approach is that neither the weight of the empty pycnometer nor the volume needs to be known. So, if there is no opportunity to adjust temperature to accommodate pycnometer calibration, the instrument should be used to measure relative density (specific gravity). In this case, the weighing of the sample and weighing of the reference material must be carried out at the same temperature.

m_0 mass of empty pycnometer in kg
m_F mass of pycnometer filled with sample in kg
m_W mass of pycnometer filled with water in kg
V volume in m^3
ρ_F density of sample in $kg \cdot m^{-3}$

ρ_W density of water in $kg \cdot m^{-3}$
d relative density of sample (specific gravity)

Once the relative density d, or specific gravity, of the sample is known, and the density of the reference material is known from the literature, the absolute density of the sample can be calculated:

$$\rho_F = d \cdot \rho_W \tag{2.25}$$

As mentioned in Section 2.2 a weighing result can be corrected for the effect of atmospheric buoyancy. The corrected mass is the true mass of a body, and is slightly higher than the mass which the balance displays. When a true mass is used to calculate density this is called a true density. If the atmospheric buoy-

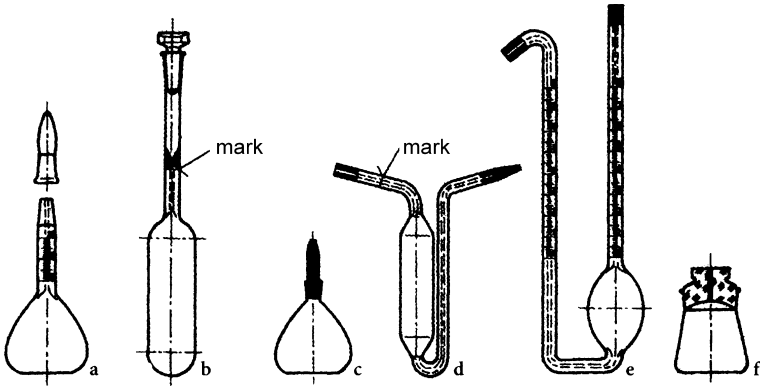

Figure 2.4. Pycnometer designs: (**a**) Reischauer, (**b**) Bingham, (**c**) Gay-Lussac, (**d**) Sprengel, (**e**) Lipkin, (**f**) Hubbard [5,6]

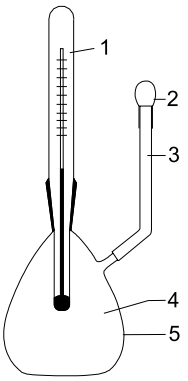

Pycnometer:
1 thermometer, 2 cap, 3 capillary,
4 sample, 5 glass bulb

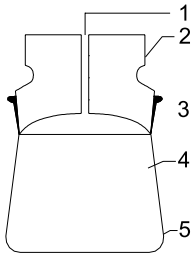

Hubbard pycnometer:
1 capillary, 2 glass stopper, 3 wide opening,
4 sample, 5 glass bulb

Figure 2.5. Examples of pycnometers from [5]. The right one is for viscous samples and powders

ancy correction is not applied, the result can be called an apparent mass, and respectively, an apparent density. When relative density is measured by using the same pycnometer for both sample and reference material, the buoyancy effect is eliminated by forming the weight ratio. Figure 2.4 and Figure 2.5 show different designs of glass pycnometers.

Hydrostatic Balances (Buoyancy Weighing)

The principle of a hydrostatic balance is based on ARCHIMEDES law of buoyancy. If a body is submersed in a fluid its weight will be lowered because of the buoyancy force. The buoyancy force is directly proportional to the volume of the submersed body and the density of the fluid. By measurement of the buoyancy force with the balance, the volume of the body can be determined quite accurately, and together with the measured mass of the body, the density is obtained. A simple technique for making this type of measurement is to place a beaker partially filled with water on top of a top-loading balance, with the weight of beaker and water tared-out to read zero on the display. Then, fully submerge the solid body beneath the water surface, taking care that it neither touches the bottom nor the sides of the beaker. The weight reading shown on the display of the balance will be the weight of the volume of water displaced by the solid body. Since density of water is known, the precise volume of the solid body is determined.

$$\rho_K = \frac{m_L}{V_K} \tag{2.8}$$

$$F_A = \rho_F \cdot V_K \cdot g \tag{2.26}$$

with Δm as the difference in weight (in kg) of the body before and after submersion:

$$\Delta m = m_L - m_F \tag{2.27}$$

$$F_A = \Delta m \cdot g \tag{2.28}$$

$$V_K = \frac{(m_L - m_F)g}{\rho_F \cdot g} = \frac{m_L - m_F}{\rho_F} \tag{2.29}$$

$$\rho_K = \frac{m_L}{m_L - m_F} \cdot \rho_F \tag{2.30}$$

where

m_L	mass of the body in air in kg
m_F	mass of the body submersed in fluid in kg
F_A	buoyancy force in N
g	gravitational acceleration in $\mathrm{m \cdot s^{-2}}$
V_K	volume of body in $\mathrm{m^3}$
ρ_F	density of fluid in $\mathrm{kg \cdot m^{-3}}$
ρ_K	density of body in $\mathrm{kg \cdot m^{-3}}$
d	relative density

So the density of a body can be obtained by taking first the weight prior to submersion (that means weighing in air) and its weight when submersed in a fluid with a known density ρ_F using equation (2.30).

With the ratio

$$\frac{\rho_K}{\rho_F} = \frac{m_L}{m_L - m_F} \tag{2.31}$$

the relative density d (specific gravity) of the body is

$$d = \frac{\rho_K}{\rho_F} \tag{2.32}$$

or

$$d = \frac{m_L}{m_L - m_F} \tag{2.33}$$

That means d can be calculated very quickly after two readings from the balance.

If the weight in air m_L is not corrected for atmospheric buoyancy, the density obtained by hydrostatic weighing can be called apparent density of the body. If that correction made, then m_L and ρ_K will be slightly higher, and can be called true mass and true density.

On the other hand when a body of known volume is submersed in a fluid, the difference in weight of the body in air and the weight of fluid displaced by the body can be used to determine the density of the fluid, and can be calculated with equation (2.34):

$$\rho_F = \frac{m_L - m_F}{V_K} \tag{2.34}$$

Figure 2.6 shows a special design of hydrostatic balance that is suitable for measuring the density of a solid or the density of the liquid in the reservoir when used with a solid body of precisely known volume. To obtain the density

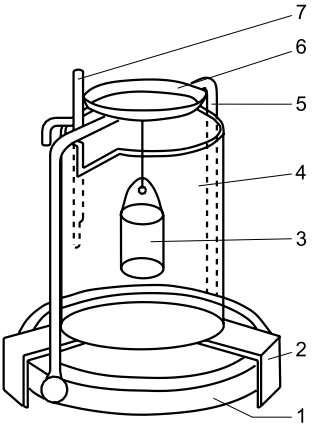

Figure 2.6. Hydrostatic balance design. **1:** balance, **2:** platform, **3:** small beaker, **4:** large beaker, **5:** support bracket, **6:** pan, **7:** thermometer

of a solid, the sample is weighed first in air, and then it is submersed and the weight is taken again. As can be seen in Figure 2.6 there is a small pan mounted on the weighing plate of the balance. A small beaker on a cable is suspended within a larger beaker containing the fluid of interest. The large beaker is resting on a raised platform so its weight is not transmitted to the balance.

To obtain the fluid density in the large beaker, a test body with known volume is first placed on the pan and its weight in air is measured. Then the test body is placed into the small beaker, submersed in the fluid and weighed once again. Then the density of the liquid is calculated using equation (2.34). It should be remembered that the density of the fluid is dependent on temperature so the temperature must be controlled and recorded.

Here are two examples of application the principle of a hydrostatic balance.

Example 2.6. Starch in corn kernels
Agronomists have determined that degree of ripeness of an ear of corn can be closely correlated with density (or specific gravity) of individual corn kernels. A specific gravity (relative density) between 1.080 and 1.118 is the range expected at peak ripeness. Values below that range would indicate insufficient ripeness, while values above would indicate the corn has gone beyond peak ripeness [110]. With a hydrostatic balance a fast check of incoming raw material is possible.

Example 2.7. Starch in potatoes
Another application is in checking the quality of incoming potatoes for a potato processing facility. The density of potatoes also is a function of the starch content. By weighing a basket with potatoes in air, and then submersed in water, the starch content can be estimated quickly.

The diagram in Figure 2.7 shows the relationship between the relative density (specific gravity) of potatoes and their starch content. For convenience, the scale on the left side vertical axis of the diagram shows the underwater weight m_{UW} of a potato sample weighing 5050 g in air. A standard test with that sample size is published by the EU [3]. The fact that the weight of the basket in air and under water is not the same is neglected.

The underwater weight force of the sample is the weight force in air G_L lowered by the buoyancy force F_A:

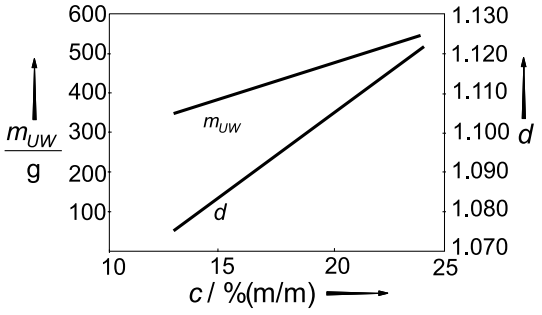

Figure 2.7. Relative density d of potatoes versus starch content. The scale on the left shows the underwater weight of a 5050 g sample

$$G_{UW} = G_L - F_A \tag{2.35}$$

Hence

$$m_{UW} \cdot g = m_L \cdot g - \rho_F \cdot V_K \cdot g \tag{2.36}$$

so the volume of the sample is

$$V_K = \frac{m_L - m_{UW}}{\rho_F} \tag{2.37}$$

and the density of the sample is

$$\rho_K = \frac{m_L}{V_K} = \frac{\rho_F \cdot m_L}{(m_L - m_{UW})} \tag{2.38}$$

The relative density then is

$$d = \frac{\rho_K}{\rho_F} = \frac{m_L}{m_L - m_{UW}} \tag{2.39}$$

where

g	gravitational acceleration in $\mathrm{m} \cdot \mathrm{s}^{-2}$
G_{UW}	underwater weight force in N
G_L	weight force in air in N
F_A	buoyancy force in N
m_{UW}	apparent mass of submersed sample in kg
m_L	mass of sample in air in kg
ρ_F	density of fluid in $\mathrm{kg} \cdot \mathrm{m}^{-3}$
V_k	volume of sample in m^3
d	relative density (specific gravity) of sample

Mohr–Westphal Balance

The Mohr–Westphal balance (see Figure 2.8) is another type of hydrostatic balance. It is designed as a nonsymmetric beam balance for measuring the density of liquids.

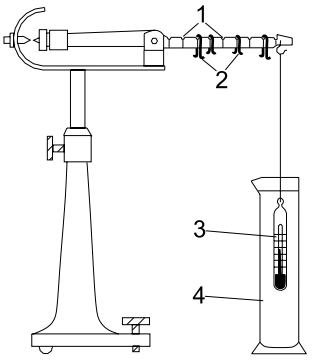

Figure 2.8. Mohr–Westphal balance. **1:** beam, **2:** weights, **3:** buoyancy body, **4:** liquid sample

At the free end of the arm of the balance a "buoyancy body" is suspended in air. The buoyancy body is normally made of glass and can have a built-in thermometer. Then the buoyancy body is submersed into the liquid of interest. Because of the effect of buoyancy, the weight of the submersed glass body will appear lower than it was in air, and will bring the balance out of zero. The buoyancy force can be measured by successively adding small weights to the arm until the balance is restored to zero. The measurement is then repeated with water as a reference liquid. The ratio of both readings provides the relative density or specific gravity of the liquid as can be shown below. With the buoyancy force

$$F_A = \rho \cdot V \cdot g \tag{2.40}$$

$$F_A = m \cdot g \tag{2.41}$$

with the fluid of interest

$$F_{A,F} = \rho_F \cdot V_K \cdot g = m_F \cdot g \tag{2.42}$$

with water as reference material

$$F_{A,W} = \rho_W \cdot V_K \cdot g = m_W \cdot g \tag{2.43}$$

so the ratio is

$$\tau = \frac{m_F}{m_W} \tag{2.44}$$

Because the volume of the glass body is the same for both readings, then

$$\tau = \frac{m_F}{m_W} = \frac{m_F \cdot V}{V \cdot m_W} = \frac{\rho_F}{\rho_W} = d \tag{2.45}$$

so the specific gravity is simply

$$d = \frac{m_F}{m_W} \tag{2.46}$$

where

m	mass of weights in kg
V	volume in m^3
F_A	buoyancy force in N
ρ	density in $kg \cdot m^{-3}$
g	gravitational acceleration in $m \cdot s^{-2}$
τ	submersed weights ratio
d	relative density (specific gravity)
subscript F	for fluid
subscript W	for reference material (mostly water)

The result should be recorded along with the temperature of the measurement. Often both readings are taken at 20 °C and the result is written as $d_{20/20}$. The quantity $d_{20/4}$ would mean that the density of the liquid was compared to the density of water at 4 °C:

$$d_{20/20} = \frac{\rho_{F,20\,^\circ C}}{\rho_{W,20\,^\circ C}}$$

$$d_{20/4} = \frac{\rho_{F,20\,^\circ C}}{\rho_{W,4\,^\circ C}}$$

The Mohr–Westphal balance can also be used to measure the density of a solid sample which is submersed in a fluid with known density. For this purpose, equation (2.37) would be used to calculate the volume of the sample.

Hydrometer

Hydrometers (sometimes called areometers) are hollow glass bodies with the shape of a buoy. Hydrometers are designed with a volume to mass ratio in such a way that the glass body will float at a certain depth in the liquid under investigation. Depending upon the density of that liquid the hydrometer will float at a higher or lower position. The upper part of the hydrometer has a scale for reading the nonsubmersed part h of the floating glass body.

The floating depth position of the hydrometer depends on weight force and interfacial force (force due to surface tension, see Section 5.1). It is

$$F_G + F_\sigma = F_A \tag{2.47}$$

which means:

$$m \cdot g + \sigma \cdot \pi \cdot d = V_S \cdot \rho \cdot g \tag{2.48}$$

so

$$m \cdot g + \sigma \cdot \pi \cdot d = \left(V - \frac{\pi \cdot d^2}{4} \cdot h \right) \cdot \rho \cdot g \tag{2.49}$$

The nonsubmersed part of the hydrometer has the length

$$h = \frac{4}{\pi \cdot d^2} \left(V - \frac{m \cdot g + \sigma \cdot \pi \cdot d}{\rho \cdot g} \right) \tag{2.50}$$

which means

$$h = \text{function}\,(\rho) \tag{2.51}$$

The nonsubmersed length of the hydrometer can be read with the aid of a scale on the upper part of the hydrometer. A weight at the bottom of the hydrometer acts like the keel of a sailboat to ensure that it will float in the liquid in a vertical orientation.

The scale can be calibrated directly in units of density or, e.g. in concentration units (see Figure 2.10). Hydrometers with special scales are available for specific applications, such as for sugar solutions (saccharimeter), alcohols (alcoholometer), acids (acid hydrometer), Baumé hydrometer for salt solutions, milk (Quevenne lactometer), beer wort hydrometer, urine checker, liquid gas aerometer, etc.

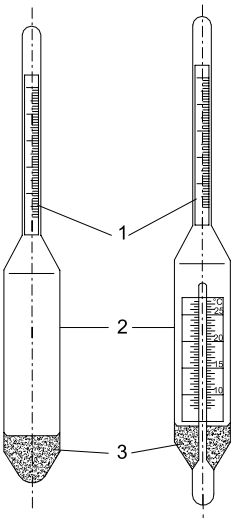

Figure 2.9. Hydrometer. **1:** scale, **2:** body (with and without thermometer), **3:** keel

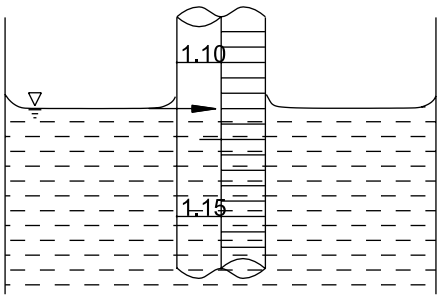

Figure 2.10. Reading of a hydrometer scale at the liquid surface (example)

Sometimes the combination of two physical properties will give the information needed about a process or a product. For example, by knowing both the density and refractive index of beer wort, the alcohol content can be calculated, and by this, the progress of fermentation [101,111].

m	mass of hydrometer in kg
V	total volume of hydrometer in m^3
V_S	volume of hydrometer submersed in m^3
F_G	weight force of hydrometer in N
F_A	buoyancy force in N
F_σ	interfacial tension force (force of surface tension) in N
σ	interfacial tension (surface tension) in $N \cdot m^{-1}$
d	diameter of hydrometer neck in m
ρ	density of liquid $kg \cdot m^{-3}$
g	gravitational acceleration in $m \cdot s^{-2}$
h	length of hydrometer neck not submersed in m

Without consideration of interfacial tension effects the hydrometer equation simplifies to

$$h = \frac{4}{\pi \cdot d^2}\left(V - \frac{m}{\rho}\right) \tag{2.52}$$

There are hydrometers available which are corrected for interfacial tension offered in different range categories called L (low, 15–35 $mN \cdot m^{-1}$), M (medium, 35–65 $mN \cdot m^{-1}$) and H (high, for higher values).

Submersion Technique

Pycnometers and hydrometers do not work very well with liquids of high viscosity. For highly viscous liquids, measurement of density can be performed with the submersion technique (see Table 2.4). A beaker with the viscous liquid sample is put on a balance. The display value is recorded, or the display may be set to zero (tare). Then a test body with known volume is pressed into the sample. The buoyancy force caused by the submerged test body is transferred to the balance and appears on the display as an apparent increased weight Δm. This increased weight force is the buoyancy force, and is the weight of the displaced liquid, which is equal in volume to the volume of the submersed solid body:

$$\Delta G = F_A \tag{2.53}$$

and

$$\Delta m \cdot g = \rho \cdot V_K \cdot g \tag{2.54}$$

so

$$\rho = \frac{\Delta m}{V_K} \tag{2.55}$$

where

ΔG	apparent weight force increase in kg
Δm	apparent mass increase in kg
V_K	volume of test body in m^3
ρ	density of liquid $kg \cdot m^{-3}$

For precision measurement, the buoyancy body can be a hollow metal sphere with calibrated volume. To avoid errors from buoyancy of the mounting rod there is normally a depth mark on the rod which indicates the right depth position for immersion so that the submerged section of rod is accounted for in the calibrated volume.

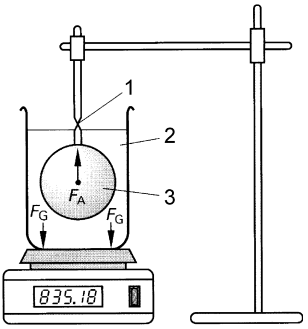

Figure 2.11. Submersion technique for density measurement. **1:** depth mark, **2:** liquid sample, **3:** buoyancy body of known volume

Particle Floating Technique

A solid particle will remain suspended within a liquid (meaning it will neither rise to float at the surface nor sink to rest at the bottom) when both the liquid and solid particle have the same density. Then the buoyancy force acting upward on the particle will be equal to the gravitational force acting downward, and the particle will remain suspended. To measure the density by the floating method, two different liquids must be chosen so that one has a density lower than the particle, and the other higher. Also both liquids must be miscible with each other when mixed together, and remain optically transparent in order to observe the particle when placed into the liquids. The liquids must also have no adverse effect on the particle, meaning the particle will not dissolve or be altered in any way. Appropriate liquids for this purpose are listed in Table 2.5.

Table 2.5. Liquids for the floating technique (examples)

liquid	density at 20 °C in $kg \cdot m^{-3}$ [137]
water	998.2
aqueous sucrose solution 50% (m/m)	1229.5
aqueous NaCl solution 20% (m/m)	1147.8
ethanol 90% (m/m)	818.0

The solid particle of unknown density is first placed into a beaker partially filled with the low density liquid. Since the liquid density is lower than that of the particle, the particle should sink to rest at the bottom of the beaker. Then, small amounts of the high-density liquid are lowly added and gently mixed until the particle just begins to float upward. When this point is reached the density of the liquid mixture and the solid sample are the same (Figure 2.12). By measuring the density of the liquid mixture, e.g. by a pycnometric method, the density of the solid particle sample is known. For measuring the density of agricultural materials or food products, the floating method liquids will need to have densities ranging between 900 and 1500 $kg \cdot m^{-3}$. This range of densities can be obtained e.g. with mixtures of water and alcohols or with sugar solutions or salt solutions.

The temperature of the liquid mixture must be held constant for this procedure to yield accurate results. If this is ensured there is no need to perform the floating technique at a fixed or controlled temperature so it can be carried out very easily. The floating technique is recommended for solid samples which cannot be handled in a hydrostatic balance. Problems may arise because the sample may dissolve or alter in aqueous solutions. In that cases the samples should be packaged or coated or another liquid should be chosen.

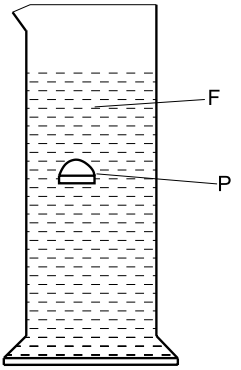

Figure 2.12. Floating technique. The sample P is suspended in the fluid F

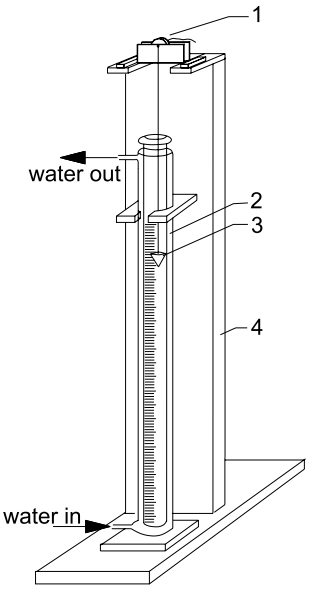

Figure 2.13. Density gradient column (from [133]). **1:** clock motor, **2:** water jacket, **3:** elevating basket, **4:** stand

Density Gradient Column

An interesting variation of the floating technique is the use of a density gradient column as a fast and accurate method for determining the density of small solid particles like agricultural seeds and grains. The method is based on observing the depth to which a particle will remain suspended in a tall column of liquid that exhibits a gradual change in density along the depth of the column, as shown in Figure 2.13. The column is first prepared by filling it carefully with layers of mixtures in different proportions of two miscible transparent liquids of different densities similar to those used in the floating methods. The first layer at the bottom would consist only of the high density liquid. The next layer above would be a mixture of 10% low density liquid and 90% high density liquid, followed by a layer of 20% low density with 80% high density, and so on, until the layer at the top would consist only of the low density liquid. In this way, the column will exhibit a gradual gradient in density ranging from the high density at the bottom up to the low density at the top. The column is normally calibrated with color-coded glass beads of known density commercially available for this purpose. The calibration beads are dropped into the column, and each bead comes to rest suspended at the depth to which the liquid density is the same as the bead. A graph of bead density versus column depth serves to calibrate the column. Then, small particles of unknown density are dropped into the column. They will come to rest suspended at the depth to which the liquid density is the same as the particle. This depth is read from the gradu-

Table 2.6. Liquids suitable for density gradient column (from [133])

liquid	specific gravity
isopropanol–water	0.79 to 1.00
isopropanol–diethylene glycol	0.79 to 1.11
water–calcium nitrate	1.00 to 1.60

ated scale on the column. The particle density is obtained from the calibration graph, which will give the density at that depth. Table 2.6 gives a listing of various liquid mixtures suitable for preparation of a density gradient column.

Resonator Frequency Techniques

When we have an oscillating tube filled with the fluid of interest, its resonant frequency depends on the density of the liquid. So with electronic means and appropriate calibration, it is possible to measure the density of a fluid by monitoring the resonant frequency of a oscillating (vibrating) tube. Density meters based on this effect are available as stationary laboratory devices, portable hand-held sensors and as in-line process sensors. The working principle is described in detail in Section 14.3.1.

Overrun

Overrun is a term used in the manufacture of products involving whipping or aeration, such as in ice cream or whipped dairy toppings. The whipping process causes air to become incorporated into the liquid being mixed causing the physical phenomenon of foaming. The density is an important process parameter which is directly related to the degree foaming. Foaming causes the volume of the foamed liquid to increase far beyond the original volume of the liquid prior to whipping. This volume increase, when divided by the original volume, is called overrun A. It is a dimensionless ratio, and can be mathematically expressed as follows:

$$A = \frac{V_{foam} - V_{liquid}}{V_{liquid}} \tag{2.56}$$

since:

$$m_{foam} = m_{liquid} + m_{gas} \approx m_{liquid} \tag{2.57}$$

and with

$$m = m_{foam} \approx m_{liquid} \tag{2.58}$$

with

$$\frac{1}{\rho} = \frac{V}{m}$$

the overrun can be expressed:

$$A = \frac{\frac{m}{V_{foam}} - \frac{m}{V_{liquid}}}{\frac{m}{V_{liquid}}} \tag{2.59}$$

i.e.

$$A = \frac{\frac{1}{\rho_{foam}} - \frac{1}{\rho_{liquid}}}{\frac{1}{\rho_{liquid}}} \tag{2.60}$$

which means

$$A = \frac{\rho_{liquid}}{\rho_{foam}} - \frac{\rho_{liquid}}{\rho_{liquid}} \tag{2.61}$$

so

$$A = \frac{\rho_{liquid}}{\rho_{foam}} - 1 \tag{2.62}$$

Equation (2.62) yields a dimensionless ratio. The equation was developed from (2.56) which indicates that the ratio is a volume ratio. So when the overrun is calculated in %, the meaning is a percentage of volume.

$$A \text{ in } \% = \left(\frac{\rho_{liquid}}{\rho_{foam}} - 1\right) \cdot 100 \tag{2.63}$$

where

A	overrun
m	mass in kg
V	volume in m^3
ρ	density in $kg \cdot m^{-3}$

Example 2.8. Overrun of ice cream
Ice cream is produced by whipping and freezing of a liquid mixture (see e.g. [109]). Typical values are given to $\rho_{ice\ cream} = 550\ kg \cdot m^{-3}$ and $\rho_{ice\ mix} = 1150\ kg \cdot m^{-3}$. The overrun is calculated using equation (2.62) to

$$A = \left(\frac{\rho_{liquid}}{\rho_{foam}} - 1\right) \cdot 100\ \%$$

$$A = \left(\frac{1150\ kg \cdot m^{-3}}{550\ kg \cdot m^{-3}} - 1\right) \cdot 100\ \% = 109\ \%$$

This value for the overrun means the volume of the liquid ice cream mix was raised by 109%, or more than doubled.

Density of Solids

Many agricultural materials and food and feed ingredients are in the form of granular materials (grains, meals and powders), which are bulk solids made up of small particles. The weight or size of the individual particles within any of these types of materials may vary over a large range e.g. from frozen diced vegetables to corn cornels to fine powder particles. The term "solid density" means the density of the solid material of which a particle is made, no matter what type of fluid or other material may exist between the particles. On the other hand if the solid particles contain pores or hollow cavities filled with gases or liquids, this contributes to the density of the solid. When pores or cavities occur, it is important to state whether they are closed or open. If they are closed, meaning they are located completely within the solid particle, they belong to the solid. If they are open to the surroundings at the particle surface, e.g. the atmosphere, they do not belong to the solid body. To avoid communication errors the density of solids should be given with a note like "including pore volume" or "without pore volume." This can be accomplished by how the system boundaries are defined, and can be calculated as follows:

$$\rho = \frac{m_S}{V_S} \tag{2.8}$$

where

m_S	mass of solid material in kg
V_S	volume of solid material in m^3
ρ	density of solid in $kg \cdot m^{-3}$

To measure the density of a solid particle often simply means to measure its volume, because its mass is known upon weighing. To get the volume of the solid sample without its open pores, a pycnometer technique with an appropriate liquid can be used. The liquid must not alter or dissolve the sample. For this purpose, a sequence of weighings is conducted as indicated in Figure 2.14. After weighing the empty pycnometer m_0 the pycnometer is weighed with the sample m_P. Then the pycnometer is filled up to a designated mark with an appropriate reference liquid of known density and weighed again $m_{P,F}$. Finally, the pycnometer is weighed when filled to the same mark with only the reference liquid m_F [4]:

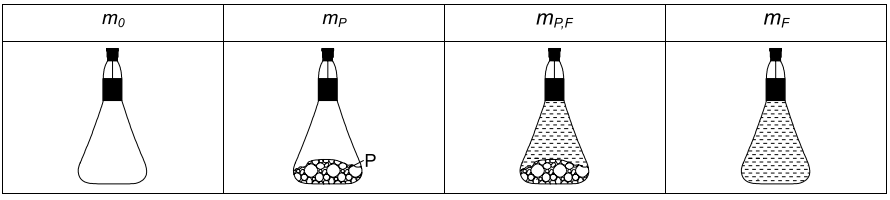

Figure 2.14. Pycnometer measurement of the density of a solid granular material, e.g. a powder

The density of the solid material then is

$$\rho_S = \frac{m_S}{V_S} \tag{2.8}$$

$$m_S = m_P - m_0 \tag{2.64}$$

$$V_S = V_0 - V_F \tag{2.65}$$

$$V_F = \frac{m_{P,F} - m_P}{\rho_F} \tag{2.66}$$

$$\rho_S = \frac{m_P - m_0}{V_0 - \dfrac{m_{P,F} - m_P}{\rho_F}} \tag{2.67}$$

$$\rho_S = \frac{m_P - m_0}{\dfrac{m_F}{\rho_F} - \dfrac{m_{P,F} - m_P}{\rho_F}} \tag{2.68}$$

$$\rho_S = \rho_F \frac{m_P - m_0}{m_F - m_{P,F} + m_P} \tag{2.69}$$

$$d = \frac{\rho_S}{\rho_F} \tag{2.70}$$

$$d = \frac{m_P - m_0}{m_F - m_{P,F} + m_P} \tag{2.71}$$

where

m_0	mass of empty pycnometer in kg
m_S	mass of sample in kg
m_P	mass of pycnometer with sample in kg
$m_{P,F}$	mass of pycnometer with sample and filled with reference liquid in kg
m_F	mass of pycnometer with reference liquid only in kg
V_0	volume of pycnometer in m^3
V_S	volume of sample in m^3
V_F	volume of reference liquid filled in pycnometer in m^3
ρ_S	density of solid in $kg \cdot m^{-3}$
ρ_F	density of reference liquid in $kg \cdot m^{-3}$

For precision measurements the true mass instead of apparent mass (see Section 2.1) should be used. In that case the true density of the reference liquid should also be used.

Bulk Density

Powders and bulk goods contain hollow spaces or voids filled with gas, normally air. The density of that type of bulk material, including the void spaces, is called bulk density. Using equation (2.8) the bulk density can be calculated by weighing a sample of the bulk material and measurement of its volume.

The volume of the whole bulk material must be taken "as is." To measure this volume, the sample material can be poured into a beaker or cylinder up to a known volumetric mark. Different technique in filling the beaker or cylinder may lead to different distributions of solid particles and hollow spaces. So, to get repeatable results the technique of filling has to be standardized.

To overcome problems with repeatable filling technique, the bulk material can be tapped before reading of the volume. By tapping the material, the solid particles will "settle" into the most stable situation they can reach. The void spaces will get smaller as the solid particles settle step by step into a spatial situation where the bulk density will reach a maximum. The time needed to reach this maximum depends on tapping speed and tapping amplitude. There are laboratory devices available which perform a chosen number of tappings in a continuous motion. Depending on the sample properties, sometimes 10, 100, 1000 or more tappings may be appropriate to reach maximum bulk density.

Figure 2.15 shows an example of a device which can be used to measure bulk density and tapped bulk density subsequently. First the bulk material is filled into a 1000 cm^3 cylinder until it is overflowing under repeatable technique conditions. Then with aid of a flat spatula, the excess overflow of sample material is scraped away from the top of the cylinder to leave the sample perfectly level at the top, and the 1000 cm^3 sample is weighed to get the bulk density.

Now a cylindrical extension overring is slipped onto the 1000 cm^3 cylinder and more sample material is filled in. The cylinder is mounted on the tapping device and moved for a fixed number of tappings. In German testing standards (DIN EN 1237 in [101]) a number of 2500 with a frequency of 250 s^{-1} is specified.

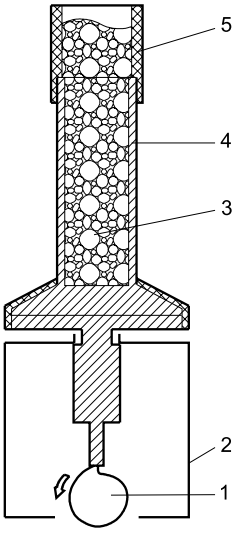

Figure 2.15. Device for tapping of bulk goods: **1:** rotating cam, **2:** housing, **3:** powder sample, **4:** cylinder, **5:** overring

Table 2.7. Characterization of powder flowability by HAUSNER ratio [141]

HAUSNER ratio	powder flowability
1.0–1.1	free flowing
1.1–1.25	medium flowing
1.25–1.4	difficult flowing
> 1.4	very difficult or nonflowing

After this the sample material is adjusted to 1000 cm^3 again and weighed. The tapped bulk density should be recorded with the parameters of its measurement.

The difference between bulk density and maximum tapped bulk density provides information about the ability of the bulk material to be compressed by gravity or pressure. Powders can be characterized for this property by the HAUSNERratio, which is the quotient of tapped bulk density over untapped bulk density (see Table 2.7).

Porosity

Also the volume of the hollow void space (pores) can be calculated. The ratio of the volume of the void space (pores) and the total volume of the bulk is called porosity ε:

$$\varepsilon = \frac{V_H}{V_B} \tag{2.72}$$

$$\varepsilon = \frac{V_B - V_S}{V_B} = 1 - \frac{V_S}{V_B} \tag{2.73}$$

because $m_B \approx m_S = m$

$$\varepsilon = 1 - \frac{V_S \cdot m}{m \cdot V_B} \tag{2.74}$$

so

$$\varepsilon = 1 - \frac{\rho_B}{\rho_S} \tag{2.75}$$

With ε as the relative volume of the hollow pore space, and α as the relative volume of the solid particle space it is evident that:

$$\alpha + \varepsilon = 1 \tag{2.76}$$

where

V_B	total volume bulk in m^3
V_H	volume of hollow space in bulk in m^3
V_S	volume of solid material in bulk in m^3
ρ_B	density of bulk in $kg \cdot m^{-3}$
ρ_S	density of solid in $kg \cdot m^{-3}$
m_B	mass of bulk in kg
m_S	mass of solid in kg

ε porosity of bulk
α relative volume of solids in bulk

The porosity of an unconsolidated mass of bulk agricultural materials such as silage, straw and hay is a very important physical property that is needed in air flow and heat flow processes, as well as other applications. Measuring the solid volume of the particles in these types of materials can be very difficult. They are not suitable for being in contact with liquids used with pycnometer methods. For these types of materials, their natural porosity can determined directly with the use of a simple apparatus called porosity tanks. In this apparatus, two tanks of equal volume that can be closed air-tight are connected by a manifold of tubing with shut-off valves and a manometer as shown in Figure 2.16.

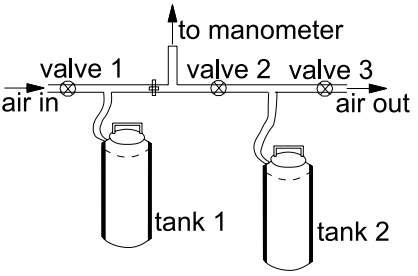

Figure 2.16. Porosity tanks (from [133])

Tank 2 is filled with sample material and sealed. Valves 2 and 3 are closed, and compressed air is brought into tank 1. When a suitable manometer displacement is achieved, valve 1 is also closed, and the pressure in tank 1 p_1 is read and recorded from the manometer. Then, valve 2 is quickly opened, and the new lower equilibrium pressure in the system p_3 is measured and recorded from the manometer. From the perfect gas law at constant temperature, the mass of air added to the system when tank 1 was initially pressurized m can be expressed as:

$$m = \frac{p_1 \cdot V_1}{R_S \cdot T_1} \tag{2.77}$$

After valve 2 is opened, this same mass becomes distributed between the empty volume of tank 1 m_1 and the available hollow pore spaces in tank 2 m_2 containing the sample. Then, by conservation of mass:

$$m = m_1 + m_2 \tag{2.78}$$

$$\frac{p_1 \cdot V_1}{R_S \cdot T_1} = \frac{p_3 \cdot V_1}{R_S \cdot T_1} + \frac{p_3 \cdot V_2}{R_S \cdot T_1} \tag{2.79}$$

and

$$\varepsilon = \frac{V_2}{V_1} = \frac{p_1 - p_3}{p_3} \tag{2.80}$$

where

ε	porosity of bulk
p	pressure in Pa
V	volume in m^3
m	mass in kg
T	temperature in K
R_S	specific gas constant in $J \cdot K^{-1} \cdot kg^{-1}$

2.4 Applications

alcohol concentration of drinks, pycnometer	[7]
alcohol concentration of drinks, hydrometer	[8]
solids in sugar syrups	[9]
solids in milk	[10]
milk, density by hydrometer	[11]
relative density of fruit and vegetable juices	[12]
relative density of beer wort	[13]
relative density of fruit and vegetable juices	[14]
animal and vegetable fats and oils: determination of conventional mass per volume ("liter weight in air")	[15]
specific gravity of water and brine	[16]
density and specific gravity of viscous materials by BINGHAM pycnometer	[17]
density and specific gravity of viscous materials by LIPKIN bicapillary pycnometer	[18]
density, specific gravity and absorption of fine aggregate	[19]
density, specific gravity and absorption of coarse aggregate	[20]
specific gravity of soil solids by water pycnometer	[21]
specific gravity, apparent, of liquid industrial chemicals	[22]
specific gravity of pigments	[23]

Literature

1. CIPM, Comite Internationale des Poid et Mesures (1979) PTB-Mitt 89:271–280
2. Ludwig H (ed) (1999) Advances in High Pressure Bioscience and Biotechnology, Springer, Berlin
3. EU comission (ed) (1995) EG-Verordnung No 97/95 of Jan 17 1995, Amtsblatt Jan 24 1995, available online http://europa.eu.int/eur-lex/hu/dd/docs/1999/31999R2718-HU.doc
4. DIN ISO 8130-3 (2005) Determination of density by liquid displacement pycnometer, in [101]
5. DIN ISO 3507 (2002) Laboratory glassware – Pycnometers, in [101]
6. DIN 12807 (1975) Laboratory glassware, Bingham pycnometer, in [101]
7. AOAC method 930.17, in [104]
8. AOAC method 9503, in [104]

9. AOAC method 932.14 B, in [104]
10. AOAC method 925.22, in [104]
11. LFGB method L01.00-28 (1988) Untersuchung von Lebensmitteln; Aräometrische Bestimmung der Dichte von Milch, in [100]
12. LFGB method L31.00-1 (1997) Bestimmung der relativen Dichte von Frucht- und Gemüsesäften, in [100]
13. LFGB method L36.00-3 (1994) Untersuchung von Lebensmitteln; Bestimmung der relativen Dichte d 20/20 von Würze und Bier, in [100]
14. DIN EN 1131 (1994) Fruit and vegetable juices – Determination of the relative density; in [101]
15. ISO 6883 (2006) Animal and vegetable fats and oils – Determination of conventional mass per volume ('litre weight in air'), in [101]
16. ASTM D 1429-03 Standard Test Methods for Specific Gravity of Water and Brine, in [132]
17. ASTM D 1480-02e Standard Test Method for Density and Relative Density (Specific Gravity) of Viscous Materials by Bingham Pycnometer, in [132]
18. ASTM D 1481-02 Standard Test Method for Density and Relative Density (Specific Gravity) of Viscous Materials by Lipkin Bicapillary Pycnometer, in [132]
19. ASTM C128-04a Standard Test Method for Density, Relative Density (Specific Gravity), and Absorption of Fine Aggregate, in [132]
20. ASTM C127-04 Standard Test Method for Density, Relative Density (Specific Gravity), and Absorption of Coarse Aggregate, in [132]
21. ASTM D854-06 Standard Test Methods for Specific Gravity of Soil Solids by Water Pycnometer, in [132]
22. ASTM D891-95 (2004) Standard Test Methods for Specific Gravity, Apparent, of Liquid Industrial Chemicals, in [132]
23. ASTM D153-84 (2003) Standard Test Methods for Specific Gravity of Pigments, in [132]
24. Patazca E, Koutchma T, Balasubramaniam VM (2007) Quasi-adiabatic temperature increase during high pressure processing of selected foods. J Food Engineering 80:199–205

3 Geometric Properties: Size and Shape

Geometric properties are those that can be derived from the geometry of a solid body or particle. They are very important as a means by which the size and shape of an irregular shaped particle can be easily quantified. This is true whether the particle is treated as an individual solid body, or as one that is representative of many particles in a disperse system. Material systems that consist of particles surrounded by a continuous medium are known as disperse systems. The particles form the disperse phase, and the surrounding medium is the continuous phase. The size of the particles can vary from the magnitude of 10^{-1} m (grapefruit, melons, potatoes) to 10^{-6} m (emulsions), and down to 10^{-8} m (colloids and nanoparticles). Particles can be solid, liquid or gaseous. Six different classes of disperse systems are known (Table 3.1).

Table 3.1. Classes of disperse systems

disperse phase	continuous phase	disperse system	example
solid	gaseous	powders, dust, bulk good	starch powder, soy beans, corn kernels
solid	liquid	suspension	aqueous starch suspension, ketchup, cocoa drink, liquid chocolate (molten)
liquid	liquid	emulsion	mayonnaise, milk, salad dressing
liquid	gaseous	aerosol	fog/mist, spray coatings
gaseous	liquid	foam	whipped cream, ice cream, beaten egg whites
gaseous	solid	solid foam	marshmallows, bread, angel food cake

Disperse systems can be characterized by specifying the size and form (or shape) of their particles. For example let us imagine a disperse system consisting of sugar particles (crystals) in air (a bowl of sugar). Depending on size and shape of the sugar particles we can distinguish numerous different products with different physical properties like porosity, bulk density, and flow properties (Table 3.2).

In Figure 3.1 an overview is given on magnitudes of particles sizes which occur in food engineering. In this illustration it can be seen that the size of

Table 3.2. Sucrose in air: examples in the class of solid–gaseous disperse systems

English	German
Rock candy sugar crystals	Kandiszucker
Dark brown sugar	Brauner Zucker
Light brown sugar	Teezucker
Refined (white) table sugar	Haushaltszucker
Confectioners' sugar (powdered sugar)	Puderzucker
Cotton candy	Zuckerwatte

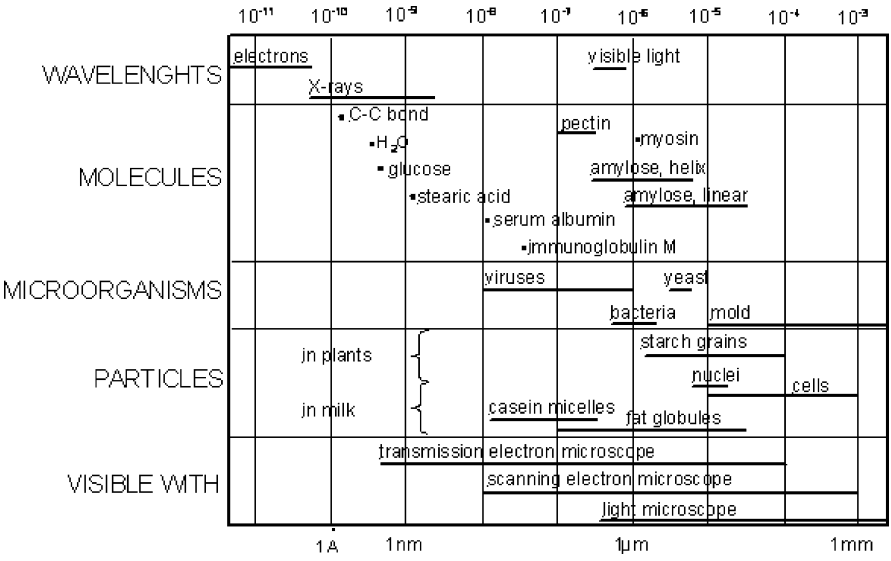

Figure 3.1. Magnitudes of particle sizes and comparison to other lengths

particles, microorganisms and molecules can be compared to the wavelength of electromagnetic radiation.

Particle size and shape are of decisive influence in governing the physical properties of the disperse system. For example, flow properties (see Section 4.3), bulk density, porosity, stability of foams and emulsions depend on it. The interfacial surface area of the bulk materials (sometimes referred to as the "specific surface area") can be thought of as the total surface area exposed to the hollow spaces in between the particles in the disperse system. The specific surface area will depend on particle size and shape, and will affect the kinetics of sorption, dissolution or reactions that may take place involving the disperse system.

For a general definition of particle size there is no need to specify the various classes of disperse systems or to make any distinction between solid particles, liquid droplets or gaseous bubbles. On the other hand, especially in

the case of nonspherical particles, the method or technique by which particle size is measured may influence the end result. Let us imagine an irregular shaped particle like a kidney bean. If we were to attempt to draw its shape on a plane surface like a sheet of drawing paper, it is evident that the particle shape and size we draw will depend on the direction from which we observe the particle. This same situation is true when trying to describe the shape of the many irregular-shaped bodies of materials found among food and agricultural products. Figure 3.2 shows examples of charts prepared in an attempt to describe the shapes of apples, peaches and potatoes in some type of standard way. In addition, not all the beans in a box of kidney beans, nor all the apples in an apple bin, nor all the peaches in a basket of peaches, nor all the potatoes in a sack of potatoes will have the same shape and size. This is the reason why particle size and shape must be dealt with in terms of mathematical distributions. This chapter is about measurement of particle size and shape, as well as particle size and shape distributions in disperse systems, and how these distributions can be quantified and understood.

First we will focus on different definitions for the size of an individual particle. Particle size distributions will be treated in Section 3.2.

3.1 Particle Size

Particles with a regular shape like cubes, rectangular blocks, cylinders or spheres can be characterized by their linear dimensions (lengths) along their principal axes. For example, the size of a cube can be given by specifying the length of any one side, the size of a rectangular block can be given by specifying its three orthogonal (mutually perpendicular) dimensions (length, width and height), the size of a cylinder by its length and diameter, and the size of a sphere by its diameter. Also, the volume and surface area of such solid bodies with regular geometries can be easily calculated by well known mathematical equations that will give volume and surface area as a function of these basic linear dimensions. Normally, a Cartesian system of coordinates is used for this purpose, and one axis is identified as the symmetric axis of the particle. Another way to characterize particle size is to use the volume or the surface area of the particle. So-called equivalent particle sizes are hypothetical dimensions that could be assigned to a model particle with the same volume or surface area. For example, it is often common practice to assign an "equivalent diameter" to an irregular-shaped particle. This would be the diameter of a perfect sphere having the precise same property, e.g. the same volume as the irregular shaped particle (see Section 3.1.2).

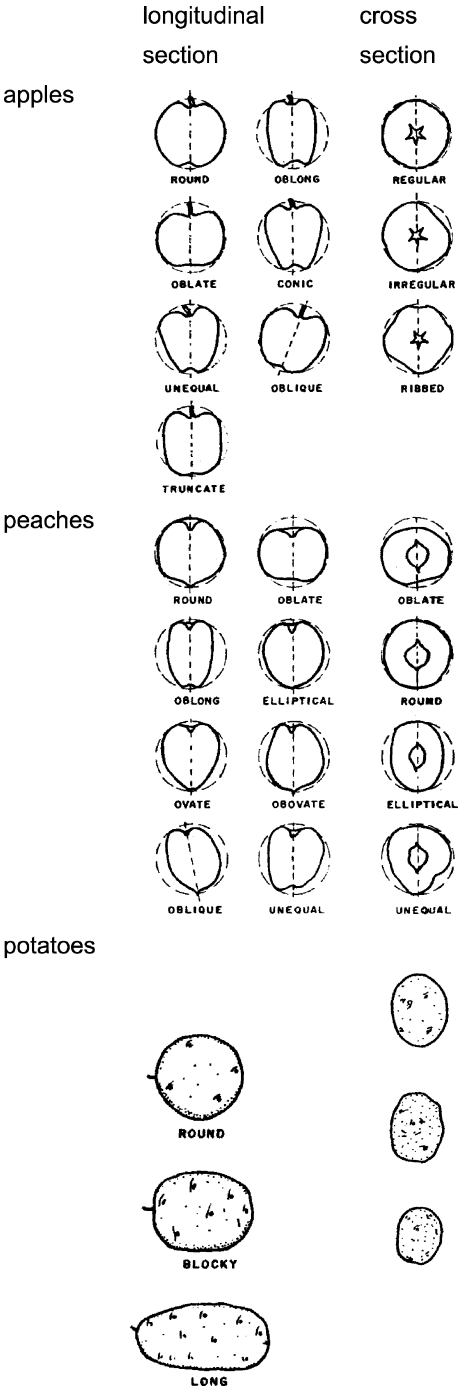

Figure 3.2. Example of charted standards for describing shape of fruits and vegetables (from Mohsenin [133])

3.1.1
Sizing by Image Analysis

When we look at a particle through a microscope we can only see the projection ("shadow") of the particle on a two-dimensional flat plane that is perpendicular to the direction of view through the microscope. When we place a micrometer scale near the particle on the microscope, we can estimate the size of the particle in only two mutually perpendicular dimensions on the same plane (directions x and y). In that case the directions x and y are perpendicular to each other on the same plane, and could represent the length and width of the particle. But, we would not know the height or thickness, which would be the third dimension in the direction of observation z. Therefore, both directions (x and y) are mutually perpendicular to the direction of observation z. In order to measure the particle thickness in the z-direction, the particle would have to be rotated by 90° so that the two-dimensional plane that could be seen would contain the mutually perpendicular directions of (x and z or y and z). Figure 3.3 illustrates these main particle diameters with the example of a kidney bean. Figure 3.4 gives support in understanding how a particle has a maximum area of projection (upper picture), a minimum area of projection (lower picture) and a case in between.

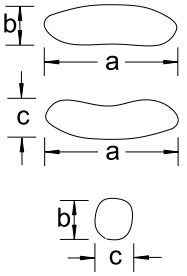

Figure 3.3. Major diameter a, minor diameter c and intermediate diameter b of a particle (kidney bean) can be identified from different projections of the particle (see also Figure 3.4).

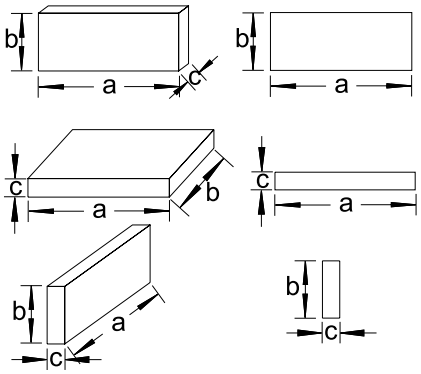

Figure 3.4. Different projection areas of a parallelepipedon allow us to identify the major diameter a, minor diameter c and intermediate diameter b

An average of these three mutually perpendicular dimensions of length a, width b and thickness c, as defined here can often be used to specify the average size of the particle using a single characteristic diameter. This can be an arithmetic mean diameter $\frac{a+b+c}{3}$, or a geometric mean diameter $(a \cdot b \cdot c)^{\frac{1}{3}}$. To avoid basic errors, the length to be measured or used to calculate sizes should be specified carefully. Table 3.3 shows some examples of other characteristic

Table 3.3. Some characteristic diameters of particles (examples)

	definition from Figure 3.5	symbol
FERET diameter	height of projected area (top to bottom)	x_{Fe}
MARTIN diameter	diameter which cuts projected area into equal area parts (but may be different shape)	x_{MA}
major diameter	diameter of smallest circumference	a

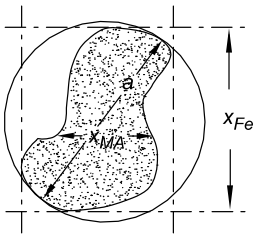

Figure 3.5. Characteristic length of particles (examples). The FERET diameter gives overall height from top to bottom. The MARTIN diameter cuts the projected area into equal area parts. The major diameter a is the very longest diameter completely inside the projected area stretching across opposite ends of the projected area

diameters, which can be used to express particle size, and Figure 3.5 gives the definition of these diameters.

Investigating a number of particles will show that whatever characteristic diameter is used to specify the size of a particle, the actual size of the individual particles will vary to a certain extent within the population of particles. Only in an ideal or theoretical situation will particles all have the same diameters. Many real particles in nature, such as soy beans and oranges, can often be assumed to be characterized by an ideal shape, such as a perfect sphere. Whether or not the error which is introduced by this assumption is significant depends on the application and precision needed to solve the engineering problem of interest. To have greater certainty about the true dimensions and shapes of the particles within a collection of particles a large number of particles should be examined and measured and quantified with the use of appropriate statistic procedures.

3.1.2 Equivalent Diameters

An equivalent diameter of an irregular shaped particle is the diameter of a hypothetical ideal geometric body, such as a perfect sphere, having the same specified properties as the real particle. Depending upon on these specified properties, e.g. geometric property or physical property, there are different definitions for equivalent diameter. Some of them will be introduced in the following subsections.

3.1.3 Geometric Equivalent Diameters

For any irregular shaped particle there exists an hypothetical spherical particle which has the same volume. The diameter of this hypothetical sphere is an equivalent diameter for the real particle and called the diameter of volume-equivalent sphere. This is perhaps the most frequently used type of equivalent diameter for most engineering applications.

In the same manner alternative equivalent diameters may be chosen to be the diameter of sphere having the surface area as the real particle, or the diameter of a perfect circle enclosing the area as the projected area of the real particle, or diameter of a perfect circle having a circumference equal to the perimeter of the projected area of the real particle. Table 3.4 gives an overview of these geometric equivalent diameters.

Table 3.4. Geometric equivalent diameters

diameter of	formula	to be measured is the:
volume equivalent sphere	$d_V = \sqrt[3]{\frac{6 \cdot V}{\pi}}$	volume V
surface area equivalent sphere	$d_A = \sqrt{\frac{A}{\pi}}$	surface area A
projected area equivalent circle	$d_P = \sqrt{\frac{4 \cdot S}{\pi}}$	projected area S
perimeter circumference equivalent circle	$d_{Pe} = \frac{U}{\pi}$	perimeter U of projection area

A particle like a cube or a sphere has the same diameter independent of the direction of observation or direction of measurement. This class of particles is said to have a isotropic shape. "Isotropic" means "being the same in all spatial directions." If particles are anisotropic (nonisotropic) like bricks, cylinders or needles, an additional problem of experimental measurement arises: For example, if they are suspended in a liquid they will be oriented randomly, so measurement of a large number of particles will yield a truly representative average of their dimensions over all axes. However, if the same type of particles were sprinkled on a flat surface or plate for observation with a microscope or camera, their orientation would not be completely randomized. Needles for example would all tend to lie down on the flat surface, and would not stand upright. So, in case of particles with anisotropic shape, the technique of measurement should be chosen carefully and accurately reported or documented to avoid the possibility that observations and measurements from image analysis could be misinterpreted.

3.1.4 Physical Equivalent Diameters

For any irregular shaped particle there also exists a hypothetical spherical particle which has the same physical behavior in a given process situation, such as having the same terminal velocity of free fall in a given fluid (velocity of sedimentation in a liquid, see also falling sphere viscosimeter, p. 171). This type of equivalent diameter is called a physical equivalent diameter. Other examples of physical equivalent diameters are listed in Table 3.5.

Table 3.5. Physical equivalent diameters

diameter of	formula	to be measured is the:
sphere with same terminal velocity of free fall in a fluid	$d_{ST} = \sqrt{\frac{18 \cdot \eta}{\Delta\rho \cdot g}} \cdot c$ (after STOKES) $d_N = 0.33 \frac{\rho_F}{\Delta\rho \cdot g} \cdot c^2$ (after NEWTON)	velocity of sedimentation
sphere with same light scatter property as real particle	see Section 3.3.3	light scattering

where

η	dynamic viscosity of fluid in Pa · s
g	gravitational acceleration in m · s^{-2}
c	terminal velocity of free fall in m · s^{-1}
ρ_F	density of fluid in kg · m^{-3}
ρ_S	density of particle in kg · m^{-3}
	$\Delta\rho = \rho_S - \rho_F$

3.1.5 Specific Surface Area

Specific surface area is another geometric quantity that can be used to characterize the size of individual particles, or to quantify the amount of internal surface area surrounding the hollow pore spaces within a disperse system, such as with bulk granular materials like agricultural grain in a bin, sugar crystals in a bowl, and powder in a box. The precise definition of specific surface area is slightly different for each of these two different applications. Therefore, each application will be treated separately in the following subsections.

3.1.5.1 Specific Surface of Individual Particles

The specific surface of an individual particle can be based on either volume or mass of the particle. Table 3.6 gives the definitions mathematically.

Table 3.6. Specific surface of particles

name	formula	SI unit
specific surface based on volume	$A_V = \frac{A}{V}$	m^{-1}
specific surface based on mass	$A_m = \frac{A}{m}$	$m^2 \cdot kg^{-1}$

With the density of the particle known ρ_S the terms can be converted from one to the other:

$$A_V = \rho_S \cdot A_m \tag{3.1}$$

where

A_V	specific surface based on volume in m^{-1}
A_m	specific surface based on mass in $m^2 \cdot kg^{-1}$
A	surface area of all particles of the sample in m^2
V	volume of all particles of the sample in m^3
m	mass of all particles of the sample in kg
ρ_S	density of particle in $kg \cdot m^{-3}$

Whereas the specific surface based on mass is dependent on the density of the material of which the particle is made, the specific surface based on volume is a geometric quantity solely, and is independent of any information about the particle material. By sorption measurement, i.e. by measuring the ability of the particle material to adsorb a reference material at its surface, the specific surface based on mass can be obtained (see Section 1.2.5).

3.1.5.2 Specific Surface Area in Bulk Materials

In bulk materials made up of disperse systems, the specific surface area is defined as the total surface area covering the inner surface of all the hollow pore spaces within the porous bulk material per unit of bulk volume or unit of bulk mass of the bulk material. When the individual particles are rounded bodies of near sphere-like shape, we can assume the particles touch each other at only one point, which occupies no area. In this situation, the surface area covering the inner surface of all the hollow pore spaces can be assumed to be the same as the sum of the outer surface area of all the particles within the specified unit of volume or mass of the bulk material.

The specific surface area in bulk granular materials can also be thought of as the total inner surface area exposed to a gas or fluid flowing through the porous material. In fact, specific surface is an important property that governs the degree of permeability (ease of fluid flow through pores) of a porous bulk material. For example, measurement of gas flow rate and pressure drop through

a powder sample enables calculation of the gas permeability of the powder, and in turn, the specific surface area per unit of bulk volume if porosity of the powder is known. This method of gas permeability is most useful to estimate the specific surface area in a sample of bulk material like agricultural grains and silage, ground meals, food powders and powdered ingredients.

A more commonly used method for estimating the specific surface area within a bulk material or disperse system is to first estimate the specific surface of representative individual particles on the basis of their mass ($m^2 \cdot kg^{-1}$), and multiply by the bulk density of the bulk material ($kg \cdot m^{-3}$). The result will be specific surface area of the bulk material ($m^2 \cdot m^{-3}$).

For particles with irregular shape the specific surface area can be estimated using equivalent diameters for the individual particles:

$$A_V = \frac{A}{V} \tag{3.2}$$

using equivalent diameters from Table 3.4 it is

$$A = \pi \cdot d_A^2 \tag{3.3}$$

$$V = \frac{\pi}{6} \cdot d_V^3 \tag{3.4}$$

and so

$$A_V = \frac{\pi \cdot d_A^2}{\frac{\pi}{6} \cdot d_V^3} = \frac{6 \cdot d_A^2}{d_V^3} \tag{3.5}$$

If precise equivalent diameters are not available, the assumption can be made that they can be approximated by assuming the particles have the shape of spheres. Then with $d_A = d_V$ the calculation is simplified to:

$$A_V = \frac{6}{d} \tag{3.6}$$

Example 3.1. Specific surface area of powdered sugar
Assuming sugar powder consists of uniform spherical particles with a diameter of $d = 10$ µm with equation (3.6) we have

$$A_V = \frac{6}{d} = \frac{6}{10 \cdot 10^{-6}\ \mathrm{m}} = 6 \cdot 10^5\ \mathrm{m}^{-1}$$

when the particle density is $\rho_S = 1500\ \mathrm{kg} \cdot \mathrm{m}^{-3}$ then with equation (3.1)

$$A_m = \frac{A_V}{\rho_S} = \frac{6 \cdot 10^5\ \mathrm{m}^{-1}}{1.5 \cdot 10^3\ \mathrm{kg} \cdot \mathrm{m}^{-3}} = 400\ \mathrm{m}^2 \cdot \mathrm{kg}^{-1}$$

This is the specific surface of individual sugar crystal particles in the powder. To determine the specific surface area of the powdered sugar as a bulk material (disperse system), we would multiply the solid particle specific surface by the bulk density of powdered sugar of e.g. $\rho_B = 700\ \mathrm{kg} \cdot \mathrm{m}^{-3}$ the result would be

$$A_m = \frac{A_V}{\rho_S} = \frac{6 \cdot 10^5\ \mathrm{m}^{-1}}{7 \cdot 10^2\ \mathrm{kg} \cdot \mathrm{m}^{-3}} \approx 860\ \mathrm{m}^2 \cdot \mathrm{kg}^{-1}$$

3.1.6
Particle Shape and Size for Crystals

Some examples of varying shape and size of agricultural products have been shown in Figure 3.6. The quantities of size and shape can be quality parameters for fruits and vegetables, as well as for grains and all kind of powders. Many food powders are made up of particles that are individual crystals, such as sugars and salts. These small crystals possess various geometric forms and shapes, depending on their chemical structure and method of crystallization. When describing crystalline materials, an important distinction must be made between shape and form of a crystal. The form is a consequence of the solid state structure of the material. For example, a crystal may have an octahedral, tetrahedral or pyramidal form. Let us take as an example a crystal with a pyramidal form like in Figure 3.6, on the right: There are three geometric dimensions called *a*, *b*, *c* which describe the size of the pyramid. A pyramid can be a tall narrow pyramid or a short broad pyramid, based on the relative values of these geometric dimensions. A very tall pyramid looks like a needle and a very short pyramid can look like a nearly flat plate that is slightly thicker at the center than at the edges. Thus, both pyramids have the same form of a pyramid. But, they are of different shape; one is tall and the other short. This is what crystal shape means. The crystal shape can be influenced by processing. So for our example the shape of the crystal may depend on crystallization solute, temperature and ingredients. These may dictate whether our pyramid comes out nearly flat or needle like. When the solid state lattice is governed by the chemical composition of a solid material, then the form given to the crystal (pyramidal or octahedral, etc.) from the lattice is fixed and is independent of processing. On the other hand there are many solids which may occur in different solid states i.e. different lattices and therefore different forms. With good understanding and control of crystallization processes, the solid state can be controlled such that the crystal form derived from the lattice structure can also be a function of process parameters [2].

So the overall form and shape of crystalline particles is a consequence of different factors like chemical structure and conditions of crystallization.

Examples where food engineers have to control crystallization are in the solidification of fat products like chocolate and butter, solidification of products rich in sugar, and freezing and hardening of aqueous solutions and suspensions involving formation of ice crystals. Nevertheless, different solid states of

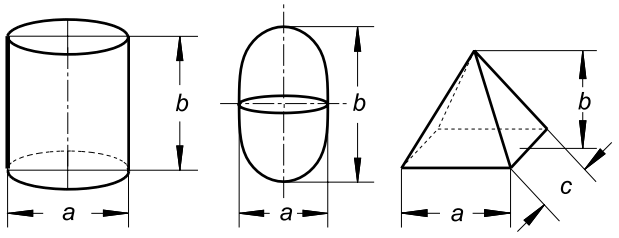

Figure 3.6. Examples of particle form (cylindrical, ellipsoidal, pyramidal)

the same material can have different properties, such as sweetness or solubility (e.g. alpha- and beta-lactose) [16,138–140].

3.1.6.1 Form Factor – Sphericity

For food technologists who use these crystalline products as food ingredients only, there is little need to distinguish between different factors of shape and form. In that case the "overall shape" of all the particles in the bulk ingredient is the quantity needed to characterize the quality of the bulk material. This can be done with the use of descriptive terminology, such as "needle like," "flaky," "caking," or with a mathematical quantity like a "form factor."

A form factor is a dimensionless ratio indicating the similarity of the given particle shape to a perfect sphere. For many applications in food engineering, this factor is called "sphericity," meaning sphere-like. There are different definitions in use for quantifying sphericity or form factor. In general all form factors compare one property of the given particle to that same property in a perfect sphere. Among the simplest definitions are those that quantify sphericity as a dimensionless ratio of any specified equivalent diameter for the particle (arithmetic or geometric mean, or other equivalent diameter from Table 3.4 divided by the particle's major diameter (see Table 3.3). Note that the major diameter of a particle is the same as the diameter of the smallest circumscribing sphere (smallest sphere that can completely surround the particle).

$$\text{Sphericity} = \frac{d_e}{d_c} \tag{3.7}$$

where
d_e any specified equivalent diameter
d_c diameter of smallest circumscribed sphere (particle major diameter)

Other more elegant definitions are given in Table 3.7.

When the definition of a form factor contains the "diameter x," this diameter can be any one of the various equivalent diameters defined earlier in Table 3.4 or Table 3.5. Therefore, it is necessary to specify which equivalent diameter has been used for calculation. Focussing on the Wadell sphericity we see its value ranges from 0 to 1. For spherical particles $\varphi_{Wa} = 1$, for needles $\varphi_{Wa} \to 0$. Like the particle size, the particle shape is not the same for all particles but is distributed.

Roundness. When a particle is observed by optical means, we see the projection of the particle (projected area). To estimate the shape of the particle from that two-dimensional view there are different roundness factors that can be used. For example, one of the most useful definitions for the roundness factor is [133].

$$R = \frac{A_p}{A_c} \tag{3.8}$$

Table 3.7. Definitions of form factors (examples)

name	definition	formula
	$\frac{\text{diameter of a volume-equivalent sphere}}{\text{diameter of area-equivalent particle}}$	$\psi_{V,A} = \frac{d_V}{d_A}$
sphericity after WADELL	$\frac{\text{surface area of a volume-equivalent sphere}}{\text{surface area of particle}}$	$\psi_{Wa} = \frac{\pi \cdot d_V^2}{A} = \frac{\pi \cdot d_V^2}{\pi \cdot d_A^2}$
HEYWOOD factor	$\frac{\text{specific surface area measured}}{\text{specific surface area of a sphere with diameter } x}$	$f = \frac{A_V}{6/x}$
volume form factor	$\frac{\text{volume of particle measured}}{\text{volume of a sphere with diameter } x}$	$k_V = \frac{V}{x^3}$
surface form factor	$\frac{\text{surface of particle measured}}{\text{surface of a sphere with diameter } x}$	$k_A = \frac{A}{x^2}$

Table 3.8. Examples of sphericity [119]

Particle	sphericity after WADELL
sphere	1.000
cylinder	0.874
octahedron	0.846
cylinder	0.832
cube	0.806
tetrahedron	0.670
needle	$\rightarrow 0$
corn kernel	0.655
sucrose crystal	0.848
wheat grain	0.833
oat grain	0.555
soy bean	0.860
potato	0.780

with

R	roundness factor
A_p	largest projected area of particle
A_c	area of smallest circumscribed circle

When particles are observed by optical means (image analysis, microscope, see Figure 3.5) to obtain a two-dimensional image (projected area), the orientation of the particles under observation will result from the natural tendency of the particle to lay in a stable position. Therefore, the roundness factor relies on a "natural rest position" that may present a different projected area from

particle to particle for particles of irregular shape. In these types of situations, roundness should be measured on a large number of samples in order to determine a representative average roundness factor for all the particles in a population sample.

Example 3.2. Equivalent diameter of a sphere with same volume
Calculate the volume equivalent diameter of a hypothetical sphere

(a) for a cube with (edge) length of $a = 0.7$ mm
(b) for a tetrahedral regular shape with an (edge) length of $a = 0.7$ mm
(c) for an octahedral regular shape with an (edge) length of $a = 0.7$ mm

Solution:
General: for a hypothetical sphere the volume is

$$V = \frac{\pi}{6} d_v^3$$

so

$$d_v = \sqrt[3]{\frac{6}{\pi} \cdot V}$$

(a) cube: the volume is $V = a^3$

$$d_v = \sqrt[3]{\frac{6}{\pi} \cdot V} = \sqrt[3]{\frac{6}{\pi} \cdot a^3} = \sqrt[3]{\frac{6}{\pi}} \cdot a$$

$$d_v = \sqrt[3]{\frac{6}{\pi}} \cdot 0.7 \text{ mm} = 1.2407 \cdot 0.7 \text{ mm} = 0.87 \text{ mm}$$

(b) tetrahedron: the volume is $V = \frac{a^3 \cdot \sqrt{2}}{12}$

$$d_v = \sqrt[3]{\frac{6}{\pi} \cdot V} = \sqrt[3]{\frac{6}{\pi} \cdot \frac{a^3 \cdot \sqrt{2}}{12}} = \sqrt[3]{\frac{\sqrt{2}}{2\pi}} \cdot a$$

$$d_v = \sqrt[3]{\frac{\sqrt{2}}{2\pi}} \cdot 0.7 \text{ mm} = 0.6083 \cdot 0.7 \text{ mm} = 0.43 \text{ mm}$$

(c) octahedron: the volume is $V = \frac{a^3 \cdot \sqrt{2}}{3}$

$$d_v = \sqrt[3]{\frac{6}{\pi} \cdot V} = \sqrt[3]{\frac{6}{\pi} \cdot \frac{a^3 \cdot \sqrt{2}}{3}} = \sqrt[3]{\frac{2 \cdot \sqrt{2}}{\pi}} \cdot a$$

$$d_v = \sqrt[3]{\frac{2 \cdot \sqrt{2}}{\pi}} \cdot 0.7 \text{ mm} = 0.9656 \cdot 0.7 \text{ mm} = 0.68 \text{ mm}$$

Example 3.3. Equivalent diameter of sphere with same area
Calculate the surface equivalent diameter of a hypothetical sphere

(a) for a cube with (edge) length of $a = 0.7$ mm
(b) for a tetrahedral regular shape with an (edge) length of $a = 0.7$ mm
(c) for an octahedral regular shape with an (edge) length of $a = 0.7$ mm

Solution:
General: for a hypothetical sphere the surface area is

$$A = \pi \cdot d_A^2$$

so

$$d_A = \sqrt{\frac{A}{\pi}}$$

(a) cube: the surface area is $A = 6 \cdot a^2$

$$d_A = \sqrt{\frac{A}{\pi}} = \sqrt{\frac{6 \cdot a^2}{\pi}} = \sqrt{\frac{6}{\pi}} \cdot a$$

$$d_A = \sqrt{\frac{6}{\pi}} \cdot 0.7 \text{ mm} = 1.382 \cdot 0.7 \text{ mm} = 0.97 \text{ mm}$$

(b) tetrahedron: the surface area is $A = \sqrt{3} \cdot a^2$

$$d_A = \sqrt{\frac{A}{\pi}} = \sqrt{\frac{\sqrt{3} \cdot a^2}{\pi}} = \sqrt{\frac{\sqrt{3}}{\pi}} \cdot a$$

$$d_A = \sqrt{\frac{\sqrt{3}}{\pi}} \cdot 0.7 \text{ mm} = 0.7425 \cdot 0.7 \text{ mm} = 0.52 \text{ mm}$$

(c) octahedron: the surface area is $A = 2\sqrt{3} \cdot a^2$

$$d_A = \sqrt{\frac{A}{\pi}} = \sqrt{\frac{2\sqrt{3} \cdot a^2}{\pi}} = \sqrt{\frac{2 \cdot \sqrt{3}}{\pi}} \cdot a$$

$$d_A = \sqrt{\frac{2 \cdot \sqrt{3}}{\pi}} \cdot 0.7 \text{ mm} = 1.050 \cdot 0.7 \text{ mm} = 0.74 \text{ mm}$$

3.2 Particle Size Distributions

Mathematical distributions play an important role in characterizing the variability of particle size that is needed in designing the processes for many biological materials that are made up of dispersed systems. Quantities of various characteristics of individuals within a population, like the age of individual

persons in a population of people, or the yield of an agricultural crop in different sections of the growing field, or the amount of traffic on the internet, can be expressed by distribution functions and their related statistical parameters. One basis of a mathematical distribution given in the appendix of this book is an example of cars driving with different velocities. Highway patrol officers conducting a survey with a radar "speed gun" are taking a sample of the situation by measuring the velocity of a number of individual cars driving by the survey point. By applying statistics to the measured data, information can be given about the population of cars driving by, their velocities, percentages of different types of vehicles (cars, trucks, vans, those pulling trailers, etc.). This example leads directly to the velocity distribution of atoms or molecules in gases, which is one of the most important distribution functions for many diffusion processes found in nature and in food technology (see Appendix 15.2).

Let us now focus on particle size distributions. For mathematics it is not relevant whether we have a natural product like corn cornels or a manufactured product like powdered sugar or flour. More important is the quantity which is measured to get information about the size of the particles. This quantity can be a length but also an area or a volume. Let us take the example where the length is measured. Because the individual particles can vary widely in size, the length of a large number of particles has to be measured. After these measurements are obtained, the resulting data are sorted into classes and further evaluated (see below). Normally, the results are frequently presented in the form of a diagram, called a particle size diagram. The horizontal axis is used for plotting the different lengths observed for the various particle sizes. The vertical axis is used to plot the information gathered from evaluation of the data. So the vertical axis depends on the type of set (category of characteristic) that was chosen to be measured. For example, this could be the percentage of population of particles measured that fell into different sizes (lengths).

Very often particle sizing is done by sieving, i.e. classifying the size of particles by measuring the quantity that can fall through the openings in a given sieve (screen). A collection of sieves having different size openings (mesh size) would normally be used. The sieves would be stacked upon each other, with largest sieve mesh size at the top, and the smallest at the bottom (Figure 3.7). A pre-weighed sample of bulk particulate material would be placed on the top sieve, and the particles would be allowed to fall through the series of sieves while the entire stack is made to vibrate mechanically over a period of time. Afterward, when the stack of sieves is disassembled, the quantity of particles left on each sieve would consist of only those particles small enough to fall through the openings from the sieve above, but too large to fall through the openings of the sieve on which they rest.

After classifying the size of particles in this way, the quantity of particles on each sieve is weighed to get information about the size distribution of all the particles. In this example, the weight of sample in each size category was the quantity measured in order to get a distribution about particle size, and the quantity under investigation was the size (length). The resulting distribution

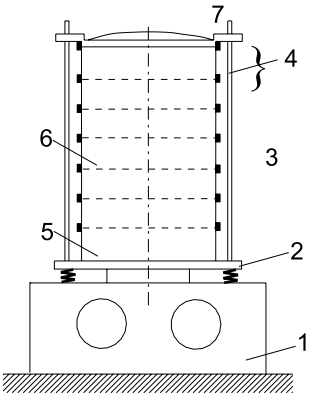

Figure 3.7. Sieving machine. **1:** engine housing, **2:** vibrating plate, **3:** set of sieves (sieve tower), **4:** straps for mounting of sieve tower, **5:** pan, **6:** sieve **7:** cover

curve will have the particle size on the x-axis and a term related to the mass on the y-axis. When the particles are not weighed, but instead are counted, then the scale on the y-axis would be a term related to the number of particles instead of mass.

In order to avoid confusion with different types of size distributions, care should taken in addressing questions like "what is the quantity we want to know about (size)?" and "what is the quantity we intend to measure (weight or number)?" Table 3.9 shows a list of sets (categories of characteristics) which can be used for experimental investigation of particle size distributions. To understand this chapter fully we start with a simple case of sieving, in which the mass is measured to obtain a size distribution.

Table 3.9. List of sets (categories of characteristics) used in quantifying particle size distributions

sets (categories of characteristics)	Index r	usage
number	$r = 0$	very often
length	$r = 1$	very seldom
area	$r = 2$	often
volume	$r = 3$	often
mass	$r = 3^*$	very often

* Mass and volume have the same index because from a mathematical point of view they are different only by a factor called density (constant of proportionality)

3.2.1 Sizing by Sieving

A powder sample has passed through a couple of sieves with different mesh sizes. Part of the sample is remaining on each sieve because the openings were too small for the particles to pass through. Now each sieve is weighed.

After subtracting the empty weight of each respective sieve, the fraction of the sample having particles too large to pass through the sieve is obtained. The particles of that fraction have a size larger than the mesh size of the sieve they were lying on (lower interval limit) and a smaller size than the mesh size of the upper sieve through which they fell (upper interval limit). The interval is

$$\Delta x_i = x_i - x_{i-1} \tag{3.9}$$

$$\overline{x_i} = \frac{x_i + x_{i-1}}{2} \tag{3.10}$$

When a powder sample passes a set of different sieves, fractions of the sample will remain on some, if not each, of the sieves. A fraction is characterized by the sieve mesh size of the upper sieve and the lower sieve. Particles in the fraction are smaller than the mesh width of the upper sieve and larger than the mesh size of the lower sieve. So the size of the particles in that fraction is between the interval limits x_{i-1} and x_i. The fraction can be further characterized by the arithmetic mean of the interval $\overline{x_i}$ and by the interval width Δx_i (see Figure 3.8, and Table 3.10 for the terms). Since the fraction, itself, is a mass fraction, then the set or category of characteristic we are using is mass, or a mass set.

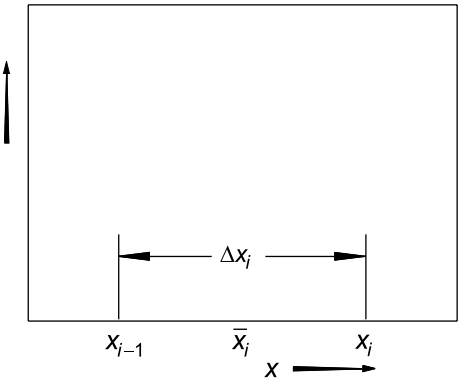

Figure 3.8. Particle sizing: Definition of a category i, arithmetic mean $\overline{x_i}$ and an interval width Δx_i

Table 3.10. Terms to define a set, or characteristic category

x_{i-1}	lower limit interval (mesh width of underlying sieve)
x_i	upper limit interval (mesh width of upper sieve)
Δx_i	interval width
$\overline{x_i}$	arithmetic mean of interval
i	identity of any given interval (usually defined by upper limit)

Now the particle size distribution diagram can be drawn. The horizontal axis is the axis of particle size (a length axis). On the vertical axis is, in case of sieve analysis, the relative mass fraction of the powder sample:

$$Q_3(x_i) = \frac{\text{mass fraction } (x_{\min} \cdots x_i)}{\text{total mass } (x_{\min} \cdots x_{\max})} \tag{3.11}$$

According to Table 3.9, in case of sieve analysis, the index of Q_r is 3. On the vertical axis, Q_3 can be replaced by its derivative with respect to length, x, called q_3. It is:

$$q_r = \frac{\mathrm{d}Q_r}{\mathrm{d}x} \tag{3.12}$$

so with

$$r = 3 \tag{3.13}$$

$$q_3 = \frac{\mathrm{d}Q_3}{\mathrm{d}x} \tag{3.14}$$

in the case of sieves with intervals Δx_i

$$q_3(x_i) = \frac{\Delta Q_3(x_i)}{\Delta x_i} \tag{3.15}$$

with

$$\Delta Q_3(x_i) = Q_3(x_i) - Q_3(x_{i-1}) \tag{3.16}$$

and

$$\Delta x_i = x_i - x_{i-1} \tag{3.9}$$

Example 3.4. Evaluation of a sieve analysis
A powder sample was placed on the top of a set of eight sieves, and sieved for 2 minutes. By weighing the quantity of sample on each sieve, the distribution of mass fractions on the sieves could be obtained. From these data of mass fractions, the diagram showing particle size distribution of the sample can be constructed. Following the numbers in Table 3.11, starting with sieve 1, i.e. $i = 1$:

Table 3.11. Evaluation of a sieve analysis (example). The illustration on the far left column represents each of the respective sieves (size category)

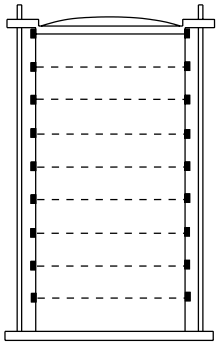

i	mesh width x_i/µm	Δx_i/µm	m_i/g	$\frac{m_i}{m}$	$Q_{3,i}$	$q_{3,i}$/µm^{-1}
8	500	100	0.6	0.006	1.000	$0.6 \cdot 10^{-4}$
7	400	85	2.2	0.022	0.994	$2.6 \cdot 10^{-4}$
6	315	115	12.2	0.122	0.972	$10.6 \cdot 10^{-4}$
5	200	75	34.8	0.348	0.850	$46.4 \cdot 10^{-4}$
4	125	25	17.0	0.170	0.502	$68.0 \cdot 10^{-4}$
3	100	37	25.2	0.252	0.333	$68.1 \cdot 10^{-4}$
2	63	13	4.9	0.049	0.080	$37.7 \cdot 10^{-4}$
1	50	50	3.1	0.031	0.031	$6.2 \cdot 10^{-4}$
	0				0.000	

m_i	mass fraction in category i in kg
$\frac{m_i}{m}$	relative mass fraction in category i
$m_i = \sum_{i=1}^{i} m_i$	sum of mass fractions with size $x < x_i$ "sum particles passing through"
$m = \sum_{i=1}^{k} m_i$	total mass of sample in kg
$Q_3(x_i) = \sum_{i=1}^{i} \frac{m_i}{m}$	"ratio of sum of mass fractions passing through over total mass" "relative pass through fraction" (dimensionless)
$q_{3,i} = \frac{\frac{m_i}{m}}{\Delta x_i}$	"relative pass through fraction" related to interval width (discretized derivative function of Q_3)
indices	
i	index of category, a sieve category is specified by the width of the upper interval limit
k	total number of categories

Figure 3.9 shows the size distribution diagram of Q_3 and q_3 versus particle size x. When a set of eight sieves is used, the resulting diagram consists of eight vertical bars. We call that type diagram a histogram. A larger number of categories would result in a larger number of bars. An infinite number of categories would result in a smooth curve, as indicated in Figure 3.9. Most laboratory instruments designed for measurement of particle size distributions come with computer software, which calculates smooth curves for better presentation and comparison. The food engineer should always be aware of how many data sets upon which the reported result is based.

As shown, a particle size distribution function can be calculated from a set of mass fractions obtained by weighing the sample fraction captured on each sieve. There are a few other ways for obtaining a particle size distribution like that. Recall from Table 3.9, instead of a mass fraction, a fraction of volume, surface area, length or number can be measured to obtain a distribution function. Very often the number is the quantity of measurement. The relative contribution ("relative amount") in a general form is

$$Q_r(x_i) = \frac{\text{part of the set } (x_{\min} \cdots x_i)}{\text{total set } (x_{\min} \cdots x_{\max})} \tag{3.17}$$

and its derivative

$$q_r(x_i) = \frac{\text{part of set } (x_{i-1} \cdots x_i)}{\text{total set } (x_{\min} \cdots x_{\max}) \cdot \text{interval width}} \tag{3.18}$$

or

$$q_r(x_i) = \frac{\text{relative part of set } (x_{i-1} \cdots x_i)}{\Delta x_i} \tag{3.19}$$

Then, the particle size distribution curve is constructed by $Q_r(x)$ or $q_r(x)$ versus size x. The shape of these curves is the same as that shown in Figure 3.9.

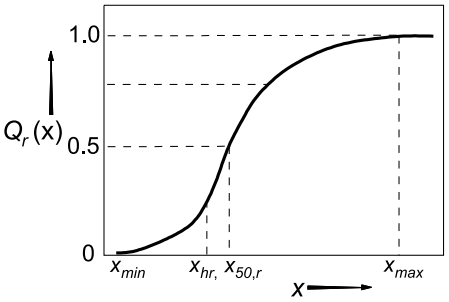

Summation distribution function showing accumulation of "pass through" fraction as a function of sieve size ("accumulating pass through diagram")

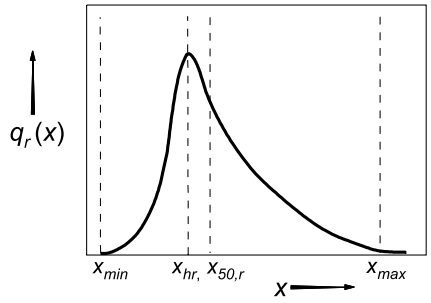

Derivative function of upper curve

$$q_r(x) = \frac{dQ_r(x)}{dx}$$

Showing "pass through" fraction in each size category (smooth curve histogram)

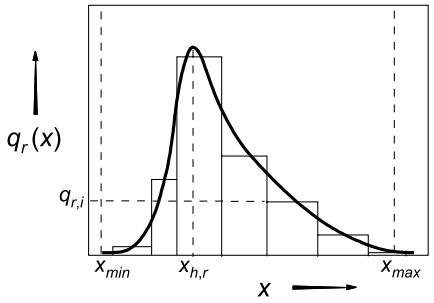

Discretized derivative function, showing "pass through" fraction in each discrete size category, (as classic bar-graph histogram)

Figure 3.9. Particle size distribution curves. In case of a sieve analysis, $Q_3(x)$ or $q_3(x)$ is plotted versus size x

By definition, $Q_r(x)$ranges from 0 to 1. Mathematically, the integration of the function $q_r(x)$ for all particle sizes x yields unity (1) or 100%:

$$Q_r\,(x_{\max}) = \int_{x_{\min}}^{x_{\max}} q_r(x) \cdot \mathrm{d}x = 1 \tag{3.20}$$

Consider now, a particle size distribution which is obtained by a counting method. Imagine we separate a bulk material into different categories of size. Then we count the particles in each category instead of weighing. In that case, $r = 0$ and equations (3.17)–(3.19) are valid for obtaining $Q_0(x)$ and $q_0(x)$, and the distribution diagrams might have a shape like that shown in Figure 3.9.

Example 3.5. Comparison of simple size distributions obtained by weighing and counting

Table 3.12. A 100 g powder sample was sieved, and the fractions are weighed

i	x_i/mm	Δx_i/mm	$\overline{x_i}$/mm	m_i/g	$\frac{m_i}{m}$	$Q_{3,i}$	$q_{3,i}$/mm^{-1}
	0					0	
1	2	2	1	40	0.40	0.40	0.20
2	4	2	3	50	0.50	0.90	0.25
3	6	2	5	10	0.10	1.00	0.05

Results show that 90% of the mass of the particles has a size below 3 mm.

Table 3.13. The same sample sieved and the particles in the fractions are counted

i	x_i/mm	Δx_i/mm	$\overline{x_i}$/mm	N_i	$\frac{N_i}{N}$	$Q_{0,i}$	$q_{0,i}$/mm^{-1}
	0					0	
1	2	2	1	300	0.30	0.30	0.15
2	4	2	3	550	0.55	0.85	0.28
3	6	2	5	150	0.15	1.00	0.075

Results show that 85% of the (number of) particles have a size below 3 mm.

Question: How much of the sample has a particle size below 3 mm?
Answer: 90% of the powder mass, and 85% of all particles (in number).

Example 3.5 shows that a different result will occur depending on whether the particle size distribution was measured by weighing or by counting. Fortunately, there are mathematical tools for easily transforming, e.g. a $Q_0(x)$ function into a $Q_3(x)$ function. When $Q_0(x)$is plotted versus any quantity, the distribution often is called a probability distribution.

Particle sizing instrumentation often is based on weighing ($r = 3$) or counting. Light scattering experiments are based on volume, such as in the measurement of sedimentation in a fluid ($r = 3$) (experimental; see Section 3.3).

The principles learned in this section are valid not only for size distribution. With these same principles the distributions of many other characteristics of a population of individual entities can be obtained, such as form factor distributions, velocity distributions, age distributions. Not to be confused with the different types of sets (categories of characteristics) that can be measured, different types of diagrams, and the large number of quantities which must underlie the obtaining of valid distributions, here are some rules to be followed:

Table 3.14. Rules for preparing a distribution function

do	this	example
put on the x-axis	the quantity which is distributed	size
find out r	what was measured?	answer: weight of fractions so ($r = 3$)
put on the y-axis	Q_r or q_r	Q_3
name the distribution	after the quantity on the x-axis	size distribution

Quantification of Distribution Functions

The simplest way of reading a distribution diagram and to communicate information about a sample distribution is to use statistical quantities that can be used to quantify the distribution of a characteristic in a population, like median, modal, average particle size, specific surface area, or equivalent diameter based on specific surface area (SAUTER diameter). Each of these is described in greater detail in the following subsections:

3.2.2 Median

The median value of a distributed characteristic in a population set is the middle value of the range of values for that characteristic within that set. The median can be determined by listing or sequencing the values of the characteristic into an increasing order (from smallest to largest). Then, the value in the middle of the sequence is the median. So the median cuts the population into two equal parts. Because of this, the median is often given the mathematical symbol x_{50}. If the number of values n in the sequence is an even number, then two values will be at the middle of the sequence. In that case, the median is the average of these two values. Table 3.15 shows the definition for the median in mathematical terms:

To calculate a median, there is no need for knowledge about the type of distribution. Compared to e.g. the arithmetic mean, another advantage of the median is that it is robust against singular extreme values. Example 3.8 demonstrates this.

Table 3.15. Definition of median

n	definition of median
n = odd number	$x_{50,r} = x_{\frac{n+1}{2}}$
n = even number	$x_{50,r} = \left(x_{\frac{n}{2}} + x_{\frac{n}{2}+1}\right)/2$

Example 3.6. Median in a sequence having an odd number of values

48 51 55 60 66 75 87

The median is 60.

Example 3.7. Median in a sequence having an even number of values

48 51 55 60 66 75 76 87

The median is 63 (average between 60 and 66).

Example 3.8. Median in a sequence of values having an extreme at one end

48 51 55 60 66 75 76 187

The median is 63, which is more representative of the population than if an arithmetic average were to be used because of the extreme singular value at the end of the sequence.

From a diagram like in Figure 3.9, the median can be read by finding the 50% percentile, and reading the related value on the x-axis. A median has to carry information from what type of set it was taken ($r = 1,2$ or 3). The median of a sieve analysis ($r = 3$) would be written as: $x_{50,3}$

Example 3.9. Interpretation of a median
The median of a sieve analysis is $x_{50,3} = 75$ µm. That means 50% have a particle size smaller than 75 µm. So, 50% of the mass of the sample will pass a sieve with a mesh width of 75 µm. It does not mean that 50% of all the particles (of the number of particles) are smaller than 75 µm.

3.2.3 Modal Value

The modal value $x_{h,r}$ characterizes the maximum of the $q_r(x)$ function. It can be thought of as the maximum in a frequency distribution function. If the distribution is a $q_0(x)$ function, then the maximum indicates the particle size which occurred most frequently (in the case of number of particles counted,

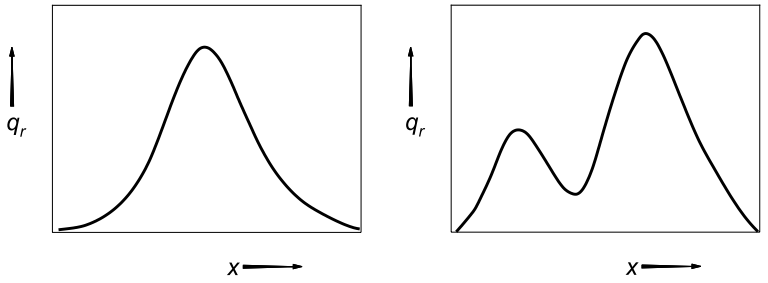

Figure 3.10. Examples of distribution curves: mono-modal (left), bi-modal (right)

with $r = 0$). In the case of the $q_3(x)$ function, the maximum indicates the particle size which contributes most to the mass of the sample (in the case where the particle samples were weighed, with $r = 3$). The modal value can be obtained mathematically by calculating the derivative of the $Q(x)$ function, and then finding the point of zero slope. If the distribution is presented as a histogram in the form of a bar graph, then the highest bar indicates the modal value. Distribution curves $Q(x)$ sometimes have more than one maximum (see Figure 3.10). In that case it means there are two or more particle sizes which have the most significant contribution to the mass of the sample set measured. In Figure 3.11 the difference between the modal value and median is illustrated.

3.2.4 Average Particle Size – Integral Mean

An alternative characteristic value that can be used to quantify a distribution function is the average, or arithmetic mean. To obtain the average diameter in a population of particles with different diameters, all the individual particle sizes that were measured are added and the resulting sum divided by the number of added values. Recall that the median and modal value do not carry any information about each of the values measured. In contrast, it is important to note that the average value depends heavily on the value of each of the individual measurements, and when a measured value occurs n times, it will contribute to the average n times. So an average can be calculated by multiplying each value with a factor which accounts for the frequency of contribution of it. This is often called a "weighing factor" that is assigned to each of the individual contributions. In this case, the average value is sometimes called a "weighted average."

To understand the mathematical approach for obtaining such a weighted average, we will refer back to our previous sieve analysis again:

For a given average particle size (arithmetic mean of particles in a given size category):

$$\overline{x_i} = \frac{x_i + x_{i-1}}{2} \tag{3.10}$$

we have a fraction, i.e. a mass fraction

$$\frac{m_i}{m} = \Delta Q_{3,i} \tag{3.21}$$

The contribution of $\overline{x_i}$ to the average is

$$\overline{x_i} \cdot \Delta Q_{3,i} \tag{3.22}$$

so for all particle categories,

$$\overline{x_3} = \sum_{i=1}^{k} \overline{x_i} \cdot \Delta Q_{3,i} \tag{3.23}$$

Because of

$$\Delta Q_3 = q_3 \cdot \Delta x \tag{3.24}$$

this is

$$\overline{x_3} = \sum_{i=1}^{k} \overline{x_i} \cdot q_{3,i} \cdot \Delta x_i \tag{3.25}$$

This result is the weighted average particle size derived from a $q_3(x)$ function. It is the sum of all size values measured $\overline{x_i}$ multiplied with their related "weighing factors" (relative contribution) $q_3 \cdot \Delta x$.

As we further diminish the size range of each category from the extended sieve categories Δx to infinitely small intervals dx, we can express the summation as an integral:

$$\overline{x_3} = \int_{x_{\min}}^{x_{\max}} \overline{x_i} \cdot q_{3,i} \cdot \mathrm{d}x \tag{3.26}$$

This is the true weighted average of the particle size distribution of our sample. The index 3 in $\overline{x_3}$ indicates that we are still in the example of our sieve analysis ($r = 3$). In a general form the weighted average (integral mean) is:

with a general fraction

$$\frac{\mu_i}{\mu} = \Delta Q_{r,i} \tag{3.27}$$

the contribution of $\overline{x_i}$ to the average is

$$\overline{x_i} \cdot \Delta Q_{r,i} \tag{3.28}$$

So, for all particle classes it is

$$\overline{x_r} = \sum_{i=1}^{k} \overline{x_i} \cdot \Delta Q_{r,i} \tag{3.29}$$

because of

$$\Delta Q_r = q_r \cdot \Delta x \tag{3.30}$$

that is

$$\overline{x_r} = \sum_{i=1}^{k} \overline{x_i} \cdot q_{r,i} \cdot \Delta x_i \tag{3.31}$$

with $\Delta x \to 0$

$$\overline{x_r} = \int_{x_{\min}}^{x_{\max}} \overline{x_i} \cdot q_{r,i} \cdot \mathrm{d}x \tag{3.32}$$

or more generally

$$\overline{x_r} = \int_{x_{\min}}^{x_{\max}} x \cdot q_r \cdot \mathrm{d}x \tag{3.33}$$

This is the general definition of an average calculated from a distribution function $q_r(x)$.

Referring to Figure 3.9, we can understand the step $\Delta x \rightarrow dx$ as progressing to more and more ever smaller intervals. This process can be envisioned by beginning with a bar-graph histogram with only three or four relatively wide bars. Then, imagine that these few wide bars are further subdivided into a greater number of narrower bars to show the distributions over a greater number of size categories with each of narrower range. Eventually, we can produce a histogram with thousands of bars, and ultimately we see the smooth curve of $q(x)$ instead of discrete steps.

Some particle sizing software provides automatic calculation and conversion of different characteristic values used to quantify particle size distributions (mean, median, modal, etc.). So, let us look at what can be done starting with an average particle size (arithmetic mean). Let us start with a $q_0(x)$ distribution. So the type of set (or population) is "number of particles:"

Equation (3.32) now is:

$$\overline{x_0} = \int_{x_{\min}}^{x_{\max}} x \cdot q_0(x) \cdot \mathrm{d}x \tag{3.34}$$

That is the "normal" arithmetic mean of the particle size, meaning the particle length which was measured. Often it is written with the notation $\overline{x} = \overline{x_0}$.

Suppose for a given task, we do not need the arithmetic mean of the length, but the mean of the length squared (representing area) or cubed (representing volume), instead. Then, we can use:

$$\overline{x_0^2} = \int_{x_{\min}}^{x_{\max}} x^2 \cdot q_0(x) \cdot \mathrm{d}x \tag{3.35}$$

and

$$\overline{x_0^3} = \int_{x_{\min}}^{x_{\max}} x^3 \cdot q_0(x) \cdot \mathrm{d}x \tag{3.36}$$

and also

$$\overline{x_0^4} = \int_{x_{\min}}^{x_{\max}} x^4 \cdot q_0(x) \cdot \mathrm{d}x \tag{3.37}$$

How do we interpret such average quantities?

Let us take (3.36). The equation provides the average of all x cubed. All x cubed are summed after multiplying each with its appropriate weighing factor to reflect the relative importance of contribution, called $q(x)$. Assume this information about relevance was achieved by a particle counting technique ($r = 0$). So the contribution here is related to the number of occurrences.

Recall the following:

$$Q_0(x_{\max}) = \int_{x_{\min}}^{x_{\max}} q_0(x) \cdot \mathrm{d}x = 1 \tag{3.38}$$

The same rules can be applied for a q_1 distribution ($r = 1$):

Then, we have:

$$\overline{x_1} = \int_{x_{\min}}^{x_{\max}} x \cdot q_1(x) \cdot \mathrm{d}x \tag{3.39}$$

$$\overline{x_1^2} = \int_{x_{\min}}^{x_{\max}} x^2 \cdot q_1(x) \cdot \mathrm{d}x \tag{3.40}$$

$$\overline{x_1^3} = \int_{x_{\min}}^{x_{\max}} x^3 \cdot q_1(x) \cdot \mathrm{d}x \tag{3.41}$$

and for $r = 2$:

$$\overline{x_2} = \int_{x_{\min}}^{x_{\max}} x \cdot q_2(x) \cdot \mathrm{d}x \tag{3.42}$$

$$\overline{x_2^2} = \int_{x_{\min}}^{x_{\max}} x^2 \cdot q_2(x) \cdot \mathrm{d}x \tag{3.43}$$

$$\overline{x_2^3} = \int_{x_{\min}}^{x_{\max}} x^3 \cdot q_2(x) \cdot \mathrm{d}x \tag{3.44}$$

and for $r = 3$:

$$\overline{x_3} = \int_{x_{\min}}^{x_{\max}} x \cdot q_3(x) \cdot \mathrm{d}x \tag{3.45}$$

$$\overline{x_3^2} = \int_{x_{\min}}^{x_{\max}} x^2 \cdot q_3(x) \cdot \mathrm{d}x \tag{3.46}$$

$$\overline{x_3^3} = \int_{x_{\min}}^{x_{\max}} x^3 \cdot q_3(x) \cdot \mathrm{d}x \tag{3.47}$$

These types of averages are called weighted averages, and they are mathematically named the integral mean. In general, an integral mean can be defined mathematically as:

$$\overline{x_r^k} = \int_{x_{\min}}^{x_{\max}} x^k \cdot q_r(x) \cdot \mathrm{d}x \tag{3.48}$$

with

k	power of particle size x
r	index of set used (see Table 3.9)

In statistics, these averages are called statistical moments M.

$$M_{k,r} = \overline{x_r^k} \tag{3.49}$$

In using this nomenclature, the averages from equations (3.38)–(3.47) are:

for $r = 0$

$$M_{1,0} = \overline{x_0} = \int_{x_{\min}}^{x_{\max}} x \cdot q_0(x) \cdot \mathrm{d}x \tag{3.50}$$

$$M_{2,0} = \overline{x_0^2} = \int_{x_{\min}}^{x_{\max}} x^2 \cdot q_0(x) \cdot \mathrm{d}x \tag{3.51}$$

$$M_{3,0} = \overline{x_0^3} = \int_{x_{\min}}^{x_{\max}} x^3 \cdot q_0(x) \cdot \mathrm{d}x \tag{3.52}$$

$$M_{4,0} = \overline{x_0^4} = \int_{x_{\min}}^{x_{\max}} x^4 \cdot q_0(x) \cdot \mathrm{d}x \tag{3.53}$$

for $r = 1$

$$M_{1,1} = \overline{x_1} = \int_{x_{\min}}^{x_{\max}} x \cdot q_1(x) \cdot \mathrm{d}x \tag{3.54}$$

$$M_{2,1} = \overline{x_1^2} = \int_{x_{\min}}^{x_{\max}} x^2 \cdot q_1(x) \cdot \mathrm{d}x \tag{3.55}$$

Table 3.16. Nomenclature of characteristic particle sizes

k	r	$d_{k,r}$	with statistical moments
1	0	$d_{1,0}$	$\frac{M_{1,0}}{M_{0,0}}$
2	0	$d_{2,0}$	$\frac{M_{2,0}}{M_{0,0}}$
3	0	$d_{3,0}$	$\frac{M_{3,0}}{M_{0,0}}$
2	1	$d_{2,1}$	$\frac{M_{2,0}}{M_{1,0}}$
3	1	$d_{3,1}$	$\frac{M_{3,0}}{M_{1,0}}$
3	2	$d_{3,2}$	$\frac{M_{3,0}}{M_{2,0}}$
4	3	$d_{4,3}$	$\frac{M_{4,0}}{M_{3,0}}$

$$M_{3,1} = \overline{x_1^3} = \int_{x_{\min}}^{x_{\max}} x^3 \cdot q_1(x) \cdot \mathrm{d}x \tag{3.56}$$

for $r = 2$

$$M_{1,2} = \overline{x_2} = \int_{x_{\min}}^{x_{\max}} x \cdot q_2(x) \cdot \mathrm{d}x \tag{3.57}$$

$$M_{2,2} = \overline{x_2^2} = \int_{x_{\min}}^{x_{\max}} x^2 \cdot q_2(x) \cdot \mathrm{d}x \tag{3.58}$$

$$M_{3,2} = \overline{x_2^3} = \int_{x_{\min}}^{x_{\max}} x^3 \cdot q_2(x) \cdot \mathrm{d}x \tag{3.59}$$

for $r = 3$

$$M_{1,3} = \overline{x_3} = \int_{x_{\min}}^{x_{\max}} x \cdot q_3(x) \cdot \mathrm{d}x \tag{3.60}$$

$$M_{2,3} = \overline{x_3^2} = \int_{x_{\min}}^{x_{\max}} x^2 \cdot q_3(x) \cdot \mathrm{d}x \tag{3.61}$$

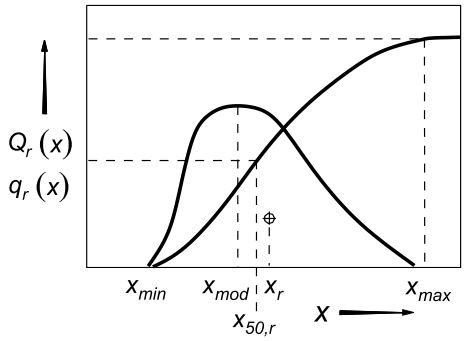

Figure 3.11. Median value $x_{50,r}$, modal value x_{mod} and average x_r (integral mean) of the $q_r(x)$ curve [1]

$$M_{3,3} = \overline{x_3^3} = \int_{x_{\min}}^{x_{\max}} x^3 \cdot q_3(x) \cdot dx \tag{3.62}$$

Statistical moments can be mathematically converted from one into another. For example in the case of the q_0 function, the conversion is:

$$M_{k,r} = \int_{x_{\min}}^{x_{\max}} x^k \cdot q_r(x) \cdot dx = \overline{x_r^k} = \frac{M_{k+r,0}}{M_{r,0}} \tag{3.63}$$

Table 3.16 shows the nomenclature used for characteristic particle sizes, and how they are formed with the help of statistical moments.

Figure 3.11 shows the difference graphically between average (integral mean value) x_r, modal value x_{mod} and median value x_{50} in a population distribution.

3.2.5 Specific Surface Distribution

Recall, the ratio of surface area of a particle to its volume is called specific surface. It is:

$$A_V = \frac{A}{V} = \frac{6}{x} \cdot f \tag{3.64}$$

where

A_V	specific surface in m^{-1}
f	HEYWOOD factor
A	particle surface in m^2
V	particle volume in m^3
x	particle size in m

So, for a sample consisting of these particles, we have:

$$A_V = \frac{A_{total}}{V_{total}} = \frac{\sum_{i=1}^{k} A_i}{V_{total}} = \frac{\sum_{i=1}^{k} \frac{A_i}{V_i} \cdot V_i}{V_{total}} = \sum_{i=1}^{k} \frac{A_i}{V_i} \cdot \frac{V_i}{V_{total}} \tag{3.65}$$

which means

$$A_V = \sum_{i=1}^{k} \frac{A_i}{V_i} \cdot \Delta Q_{3,i} = \sum_{i=1}^{k} \frac{6 \cdot f}{\overline{x_i}} \cdot \Delta Q_{3,i} = 6 \cdot f \cdot \sum_{i=1}^{k} \frac{\Delta Q_{3,i}}{\overline{x_i}} \tag{3.66}$$

With $\Delta x \to 0$, this is

$$A_V = 6 \cdot f \cdot \int_{x_{\min}}^{x_{\max}} \frac{1}{x} \cdot q_3(x) \cdot \mathrm{d}x \tag{3.67}$$

With equation (3.66) the calculation of the specific surface area is possible directly from a sieve analysis. When a q_3 function is available, then equation (3.67) is the one to choose.

In case of $r = 0$ it is

$$A_V = 6 \cdot f \frac{\overline{x^2}}{\overline{x^3}} = 6 \cdot f \cdot \frac{\sum_{i=1}^{k} \overline{x_i}^2 \cdot \Delta Q_{0,i}}{\sum_{i=1}^{k} \overline{x_i}^3 \cdot \Delta Q_{0,i}} \tag{3.68}$$

With $\Delta x \to 0$ this is

$$A_V = 6 \cdot f \cdot \frac{\int_{x_{\min}}^{x_{\max}} x^2 \cdot q_0(x) \cdot \mathrm{d}x}{\int_{x_{\min}}^{x_{\max}} x^3 \cdot q_0(x) \cdot \mathrm{d}x} \tag{3.69}$$

Using statistic moments then only

$$A_V = 6 \cdot f \cdot \frac{M_{2,0}}{M_{3,0}} \tag{3.70}$$

3.2.6 Sauter Diameter

The so-called Sauter diameter d_{32} is another equivalent diameter. It is the diameter of a hypothetical sphere with the same specific surface as the irregular shaped particle. So it is:

$$d_{3,2} = \frac{1}{f} \cdot \frac{M_{3,0}}{M_{2,0}} \tag{3.71}$$

or

$$d_{3,2} = \frac{\overline{x^3}}{\overline{x^2}} \cdot \frac{1}{f} = \frac{6}{A_V} \tag{3.72}$$

Example 3.10. Calculation and comparison of characteristic particle sizes
Taking the sieve analysis from Table 3.11:

median	$x_{50,3} = 113\ \mu m$
modal value	$x_{h,3} = 110\ \mu m$
average particle size	$\overline{x_3} = \sum_{i=1}^{8} \overline{x_i} \cdot \Delta Q_{3,i} = 145\ \mu m$
specific surface (with $f = 1.0$)	$A_V = 6 \cdot f \cdot \sum_{i=1}^{8} \frac{\Delta Q_{3,i}}{\overline{x_i}} = 56432.8\ m^{-1}$
Sauter diameter	$d_{3,2} = \frac{6}{A_V} = 106\ \mu m$

3.2.7 Characteristics of Distributions

For many process engineering applications, it is important to know "what is the mean" and "how broad" is the distribution. Options used to statistically quantify these characteristics about distributions are statistical parameters, such as the "norm" of a distribution and the standard deviation from the norm. For every day work in engineering it is useful to have linear functions instead of nonlinear curves that require more complicated mathematical equations. Particle size distributions can be transformed into linear functions by using appropriate transformation model functions. In the following subsections we will learn about some options to represent complete distribution functions by two parameters only.

GGS Distribution

The function after Gates, Gaudin and Schuhmann is a power-law function. By plotting values on logarithmic paper, the distribution function appears as a straight line which can be easily quantified by a slope and an intercept:

for $x \leq x_{max}$ it is

$$Q_r(x) = \left(\frac{x}{x_{max}}\right)^m \tag{3.73}$$

so

$$\lg Q_r(x) = m \cdot \lg x - m \cdot \lg x_{max} \tag{3.74}$$

When a particle size distribution function can be fitted with a GGS distribution then two parameters are sufficient to represent the total curve. These are the

slope m, representing the width of the original distribution and x_{max} which locates the point of the curve where $Q_r(x) = 1$.

Log Normal Distribution

$$q_r(x) = \frac{1}{\sigma \cdot \sqrt{2\pi}} \cdot \exp\left(-\frac{1}{2}\left(\frac{x - \overline{x}}{\sigma}\right)^2\right) \tag{3.75}$$

with the median $x_{50,r}$ taken for $\overline{x}, \sigma$ as standard deviation of x and

$$c = \frac{x - \overline{x}}{\sigma} \tag{3.76}$$

it is

$$q_r(c) = \frac{1}{\sqrt{2\pi}} \cdot e^{-\frac{c^2}{2}} \tag{3.77}$$

Using special grid paper a log-normal distribution appears as a straight line in the diagram. Also a particle size distribution can be plotted as a straight line which is characterized by its median $x_{50,r}$ and the standard deviation σ of the distribution.

RRSB Distribution

The RRSB distribution (after Rosin, Rammler, Sperling and Benett) is a two-parameter exponential function

$$1 - Q_r(x) = \exp\left(-\frac{x}{x'}\right)^n \tag{3.78}$$

with

$$R_r(x) = 1 - Q_r(x) \tag{3.79}$$

Then

$$\lg\left(\lg\frac{1}{R_r}\right) = n \cdot \lg x - n \cdot \lg x' + \lg(\lg e) = n \cdot \lg x + d \tag{3.80}$$

where d is a constant.

Using special grid paper (RRSB net) our particle size distribution appears as a straight line in the diagram which can be characterized by x' and the slope n only.

There is no guarantee that an experimental particle size distribution can be represented with one of the models mentioned. Whether a model can be used or choosing what model will best fit the data depends on the food sample properties that result from the process of its preparation, e.g. milling process or crystallization process. For more details about working with distribution functions see [1] or [17].

3.3 Measuring Particle Size by Other Techniques

Particle size measurement can be performed with optical, electrical, weighing or other techniques. In the following sections the principles of these techniques are described. Before a particle size measurement can be made, a representative sample needs to be taken. Because powders and bulk materials can show separation effects or particle breakage into nonrepresentative fragments (particle attrition), it is necessary to carefully arrange the conditions of sampling. Sometimes it is useful to take samples at different locations within the bulk material, or at different times from the same location, and to mix the sample prior to analysis. On the other hand there are devices for automatic dividing of a large sample into a certain number of smaller samples without changing the particle size distribution. For details, see [1].

3.3.1 Weighing Technique

The use of gravity to measure the amount of particles is the most commonly used technique for powders and bulk materials. Although the technique is widely used in laboratories, for on-line sensing during the manufacturing process on the factory floor, other techniques have to be chosen. We have already learned how sieving can be used to divide the sample into mass fractions of different size ranges. The particle amount in each fraction is measured by weighing. So particle sizing by sieving is not a measurement of particle dimensions but a gravimetric measurement of the fractions obtained elsewhere. Normally, particles are divided into size categories by sieving, but other techniques, such as light scattering, and air flow separation (air classification) can be used as an alternative to sieves for the same purpose.

In case of using sieves, the mesh width is taken to describe the particle size. The arithmetic mean between the mesh widths of two sieves is taken for the average particle size in that size category (class).

$$\overline{x_i} = \frac{x_i + x_{i-1}}{2} \tag{3.10}$$

In case of nonisometric particles, the mesh width can be a rough estimate of particle size only. Particles with different diameters in different directions will pass a given sieve to a certain extent depending on sieving conditions that can induce particle orientation. Furthermore there are different types of sieves available. For example, in the USA, there are sieves designed to comply with US standards (e.g. Tyler Sieves), and in the EU there are sieves designed to comply with EU or other standards. There are woven screen sieves or perforated plate sieves. Perforated plate sieves can have orifices with square, rectangular, round or other shapes. Because of this feature, the type of sieves used for particle size measurement should be noted and reported with the results from a sieve analysis.

Performing a sieve analysis with a device as shown in Figure 3.7 consists of putting a defined (pre-weighed) amount of sample on the top of the set of sieves. By starting the sieve machine to induce mechanical vibration to the sieves, the sieves will vibrate at set frequency and amplitude of vibration for a fixed period of time. The vibrating movement often is a vertical reciprocation (up and down vibration) with adjustable amplitude and frequency. It can also be a horizontal movement (by eccentric rotation), or any combination of both types. The movement of the sieves provides each particle multiple chances for passing through an orifice. This vibrating motion also has a mixing effect and helps to avoid clogging of the sieves. To enhance these effects, in additional to the sieve movement, sieving tools like ceramic balls or cubes of rubber can be added to the powder sample on each sieve. In any case, disintegration of the particles (particle attrition) has to be avoided. For difficult sample materials that have a tendency for clogging, there are sieve machines available that make use of air impingement as a sieving tool.

After operation of the sieving machine, the sieve tower is disassembled and the sieves are weighed to get the weights of the fractions. For evaluation of such weights, see Table 3.11 and Figure 3.9.

For very small particles, there are sieves available for use with suspending solvents. As an additional sieving tool, ultrasonic vibration can be used.

3.3.2 Sedimentation and Aerodynamic Classification with Fluids

Sedimentation in liquids and aerodynamic classification with gases (usually air) can also be used to separate particles into classes or categories. Both of these techniques are based on Stokes' law involving the terminal velocity of a particle in free fall through the fluid. When a particle is allowed to fall freely through a fluid under the acceleration of gravity, the increasing relative velocity of the particle through the fluid will increase drag force (caused by friction at the particle–fluid surface) at an exponential rate (quadratic). Stokes' law (equation (3.81)) states that terminal velocity is reached during free fall when the drag force on a particle acting upward becomes equal to the gravitational force on the particle (particle weight) acting downward. At that moment, the particle comes into static equilibrium, and velocity ceases to increase, having reached "terminal" velocity. The force of friction after Stokes (drag force) is

$$F_R = 6\pi \cdot r \cdot \eta \cdot v \tag{3.81}$$

The gravitational force (weight of body) is

$$F_G = (\rho_K - \rho_F) \cdot V_K \cdot g \tag{3.82}$$

At equilibrium we have steady state velocity (terminal velocity)

$$v = \frac{(\rho_K - \rho_F) \cdot V_K \cdot g}{6\pi \cdot r \cdot \eta} \tag{3.83}$$

with the volume of a sphere

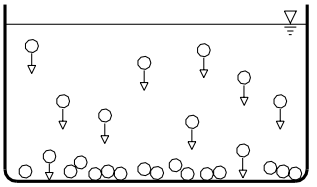

Figure 3.12. Sedimentation of spherical particles in a fluid

$$V = \frac{4}{3}\,\pi \cdot r^3 \tag{3.84}$$

Then

$$v = \frac{2 \cdot g \cdot r^2 \cdot (\rho_K - \rho_F)}{9 \cdot \eta} \tag{3.85}$$

or with

$$d = 2 \cdot r \tag{3.86}$$

$$v = \frac{g \cdot d^2 \cdot (\rho_K - \rho_F)}{18 \cdot \eta} \tag{3.87}$$

where

F_G	weight force in N
F_R	drag force in N
r	radius of spherical particle in m
d	diameter of spherical particle in m
V	volume of spherical particle in m^3
g	gravitational acceleration in $m \cdot s^{-2}$
v	particle velocity in $m \cdot s^{-1}$
ρ_K	density of particle in $kg \cdot m^{-3}$
ρ_F	density of fluid in $kg \cdot m^{-3}$
η	dynamic viscosity of fluid in $Pa \cdot s$

From equation (3.87) it can be seen that from the steady state velocity v of the particles we get information about their diameter d. This is the principle of separation by sedimentation and aerodynamic particle classification.

Sedimentation

Sedimentation is the process of allowing particles initially suspended near the surface of a liquid to fall freely to the bottom, forming a layer of sediment (sedimentation). Note that sedimentation relies on the influence of gravity, and is only possible when the particles have solid density greater than the suspending liquid. It can be seen from Stokes' law that the velocity of free fall (terminal velocity) will largely depend upon particle diameter (equation (3.87)). Therefore, when a sample of particles having different sizes (different diameters) is placed on the surface of a liquid at the top of a tall container, the particles will fall to the bottom at different velocities, depending on their diameters.

The largest size particles will reach the bottom first, followed by those slightly smaller, and so on.

For sedimentation separation in liquids the sample of particles is placed into an appropriate liquid (having less density than the particle solid density, and having no sorption or chemical reactions at the particle/liquid surface) contained in a relatively tall vessel (to allow sufficient time for free fall). After the specified time for free fall, a sample of the sediment layer is analyzed, e.g. by optical or gravimetric measurement. In this case the particle size measured is the equivalent diameter for sedimentation (see Table 3.5).

Air Classification

Separation by air classification is commonly used in the process industries to separate particles having different terminal velocities (hence, particle size diameters) in air. The scientific principle is the same as sedimentation (based on STOKES' law), but works backwards from sedimentation. Instead of allowing particles to free fall in still air, the mixture of particles is placed to rest upon a perforated screen surface. Then, air is blown upward from beneath the perforated screen at a controlled velocity. As soon as the velocity exceeds the terminal velocity of the smallest size particles, the drag force acting upward will exceed the weight of the particles, and they will become airborne, rising upward to be captured by an appropriate particle collection system. Samples of these particles can then be taken for analysis to measure particle size. When higher air flow velocities are used, then larger size particles will become airborne, and so on. In the oil seed crushing and grain processing industries, air classification is widely used to automatically separate the light weight (low density) hulls, husks and shells from the relatively higher density seeds, grains and kernels. In this way, the seeds continue down-stream to the oil extraction or other process operations free of contamination from the unwanted shells or hulls.

3.3.3 Optical Techniques

Microscopic techniques, with manual or automatic image analysis and light scattering are methods for optical measurement of particle size.

Light scattering often is performed with monochromatic laser light. The particles are passed along the light beam, which causes scattering by reflection, refraction and diffraction as illustrated in Figure 3.13. Following the theory of MIE, the angle of diffraction is related to the size of a particle. So, the particle size can be determined by measuring the angle of diffraction. The MIE theory assumes the particles have a spherical shape, and does not take into account for particle with other shapes. This is the reason why light-scattering experiments with nonspherical particles will give only a light-scattering equivalent diameter, i.e. the diameter of a spherical particle with the same light scattering property. Most light scattering instruments provide particle size distributions

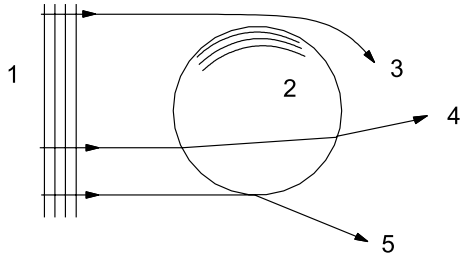

Figure 3.13. Scattering of light (**1**) at a particle (**2**) by diffraction (**3**), refraction (**4**) and reflection (**5**)

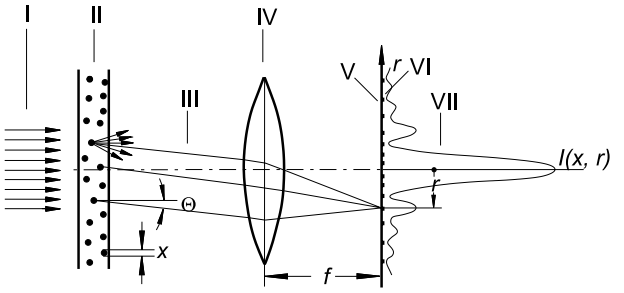

Figure 3.14. Principle of laser scattering: I laser, II sample particles, III scattered light, IV lens, V focus surface, VI light detector, VII distribution of light intensity I (schematic)

based on the particle volume (i.e. $Q_3(x)$ function), and computer software for use in making transformations to other types of distributions, e.g. $Q_0(x)$.

An important advantage of light scattering is the speed of the method. Because the light intensity distribution can be measured multiple times during one second, the results, including related statistical parameters, can be obtained within seconds. Furthermore, the sample particles can be measured while they are in motion. There is no need to have the sample particles in a fixed position. So, flow cells can be mounted in the path of the light beam with sample particles flowing through it. The particles can be suspended in appropriate liquids or in air. Another advantage of light scattering is the very small particle size (10^{-7} to 10^{-3} m), which can be measured. Limits of the technique are the wavelength used and the concentration of particles. If the concentration is too high, multiple scattering occurs. For measurement of highly concentrated emulsions by acoustics see Section 12.3 and [1].

3.3.4 Electrical Techniques

Electrical techniques are also available for particle size determination. In these techniques, the particles are suspended in a liquid which contains dissolved electrolytes, and pumped through a capillary tube (see Figure 3.15). Each time a particle passes through the capillary tube, the electric impedance (see Section 8.2) of the capillary changes. This change in impedance is related to the volume occupied by the particle (volumetric size) in the capillary. These changes

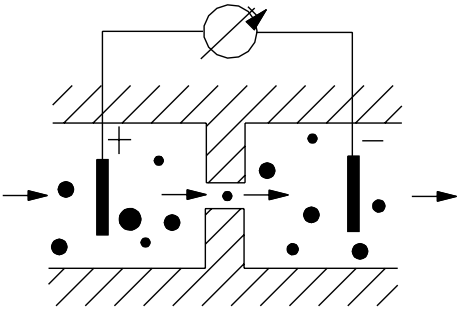

Figure 3.15. Electrical counting of particles with different sizes through a capillary tube (schematic)

in impedance are classified by their magnitude, and automatically counted. Instruments based on this principle provide $Q_0(x)$distributions. To cover a wide range of particle sizes capillaries with different diameters are used.

3.3.5 Other Techniques

Another possibility for estimating particle size is to measure the specific surface of a powder by e.g. gas adsorption. Once a monolayer is formed (see Section 1.2) using the BET theory the surface area of the solid can be calculated. For powders, gaseous nitrogen at 77 K is normally used. A further possibility is measuring the flow resistance of a powder sample against a gas (or air) after BLAINE [4]. Acoustic techniques are based on measuring the acoustic impedance of a sample.

Table 3.17. Comparison of particle sizing techniques

technique	normally provides a distribution with	applications
sieving	$r = 3$ (mass)	powder, bulk materials
sedimentation, and air classification	$r = 3$ (mass)	powder, bulk materials
light scattering	$r = 3$ (volume)	powder, bulk materials emulsions
gas adsorption	$r = 2$ (area)	power
electrical counting	$r = 0$ (number)	powder
microscopy, image analysis	$r = 0$ (number)	powder, bulk materials emulsions, foams
acoustic impedance	$r = 3$ (volume)	emulsions

User Notes

A median can be calculated from different types of distributions. To account for this, the abbreviations in Table 3.18 are usual.

Table 3.18. Nomenclature of different medians

formula	median of a distribution based on
$x_{50,3}$	volume ($r = 3$)
$x_{50,2}$	area ($r = 2$)
$x_{50,1}$	length ($r = 1$)
$x_{50,0}$	number ($r = 0$)

Table 3.19. Where to apply what diameter from distribution functions [109]

diameter	this integral mean is based on ...	so, it is useful in characterization of, e.g.
$d_{3,1}$	...length	flow through pores of membranes
$d_{3,2}$	...area	surface adsorption of droplets
$d_{4,3}$	...volume	creaming of emulsions due to buoyancy

Table 3.20. Common sets of sieves and their sizes [109]

DIN 4188 (mm)	ASTM E11-70 (mesh)	ASTM E161-70 (mesh)	BS 410:1969 (µm)	Tyler (mesh)
0.022		22		
0.032		32		
	400	38	38	400
0.045	325	45	45	325
0.063	230	63	63	250
0.09	170	90	90	170
0.125	120	125	125	115
0.18	80		180	80
0.25	60		250	60
0.355	45		355	42
0.5	35		500	32
0.71	25		710	24
1	18		1000	16
1.18	16		1180	14
1.4	14		1400	12
2	10		2000	9
2.8	7		2800	7
4	5		4000	5
5.6	3.5″		5600	3.5

Table 3.21. US standard sieve numbers and their related sizes

	nominal sieve opening	
Sieve No.	in mm	in inch
4	4.76	0.187
6	3.36	0.132
8	2.38	0.0937
12	1.68	0.0661
16	1.19	0.0469
20	0.841	0.0331
30	0.595	0.0234
40	0.420	0.0165
50	0.297	0.0117
70	0.210	0.0083
100	0.149	0.0059
140	0.105	0.0041
200	0.074	0.0029
270	0.053	0.0021
pan		

3.4 Applications

chocolate: particle size and quality	[10,11]
peanut butter: particle size and quality	[12]
fibers of grain: particle size and sorption	[13]
organoleptic testing: particle size and creaminess	[14]
apple powder: particle size and functional properties	[15]
separation of hulls from seeds in grain processing	[117]
separation of cream from skim in milk processing	[109]
sizing of protein nanofibers	[18]

Literature

1. Stieß M, Ripperger S (2007) Mechanische Verfahrenstechnik. Springer, Heidelberg
2. Hartel RW (2001) Crystallization in foods. Aspen Publishers, Gaithersburg
3. Baltes W (Hrsg.) (1995) Schnellmethoden zur Beurteilung von Lebensmitteln und ihren Rohstoffen. Behr's, Hamburg
4. Allen T (1997) Particle Size Measurement. Chapman and Hall, New York
5. Coupland JN, McClements D (2001) Droplet size determination in food emulsions: comparison of ultrasonic and light scattering methods. J Food Engineering 50:117–120
6. Javanaud C, Gladwell NR, Gouldby SJ, Hibberd DJ, Thomas A, Robins MM (1991) Experimental and theoretical values of the ultrasonic properties of dispersions: effect of particle state and size distribution. Ultrasonics 29:331–337
7. McClements DJ, Povey MJW, Jury M, Betsanis E (1990) Ultrasonic characterization of a food emulsion. Ultrasonics 28:266–272
8. Povey MJW, McClements DJ (1988) Ultrasonics in food engineering, Part I: introduction and experimental methods. J Food Engineering 8:217–245
9. Babick F, Ripperger S (2002) Schallspektroskopische Bestimmung von Partikelgrößenverteilungen submikroner Emulsionen. Filtrieren und Separieren 16, 6:311–313
10. Ziegler G, Mongia G, Hollender R (2001) The role of particle size distribution of suspended solids in defining the sensory properties of milk chocolate. Intern J Food Properties 4:353
11. Windhab EJ, Attaie H, Breitschuh B, Braun P (2003) The functionality of milk powder and its relationship to chocolate mass processing, in particular the effect of milk powder manufacturing and composition on the physical properties of chocolate masses. Intern J Food Science & Technology 38:325–335
12. Santos BL, Resurreccion AVA (1989) Effect of particle size on the quality of peanut pastes. J Food Quality 12:87–97
13. Strange ED, Onwulata CI (2002) Effect of particle size on the water sorption properties of cereal fibers. J Food Quality 25:63–73
14. Kilcast D, Clegg S (2002) Sensory perception of creaminess and its relationship with food structure. Food Quality and Preference 13 (7/8):609–623
15. Grover SS, Chauhan GS, Masoodi FA (2003) Effect of particle size on surface properties of apple pomace. Intern J Food Properties 6:1–7
16. Figura LO (1993) Physical modification of lactose and its thermoanalytical identification. Thermochim. Acta 222:187–194

17. Schubert Heinrich (2002) Handbuch der Mechanischen Verfahrenstechnik. Wiley-VCH, Weinheim
18. Zeeuw EA. van der, Sagis LMC, Koper GJM, Mann EK, Haarmans MT, Bedeaux D (1996) The suitability of scanning angle reflectometry for colloidal particle sizing. Chemical Physics 105: 1646

4 Rheological Properties

Rheology is the branch of physics in which we study the way in which materials deform or flow in response to applied forces or stresses. The material properties that govern the specific way in which these deformation or flow behaviors occur are called rheological properties. The Greek philosopher and scholar, HERACLIT (550–480 BC) once said "*πάντα ῥεῖ*" ("everything flows"). In the context of physics, "flow" can be defined as continuous deformation over time, and it can be said that *all* materials can flow. Therefore the ability to flow is not only possessed by gases and liquids, but also by solids to a varying degree. Indeed, we all know examples of solids which are capable of continuous deformation over time (flow), like asphalt on a road surface after long term usage. It is also evident that temperature can have a strong influence on the ability of materials to flow. For example, the asphalt road surface will deform at a faster rate when carrying traffic during time periods of elevated temperatures.

In this chapter, the rheology of both solids and liquids will be studied, but in the context of being at opposite ends of a continuum (continuous spectrum) of rheological behavior exhibited by matter in different forms. Because liquids and gases are the forms in which matter can flow most easily, the flow of liquids and gases will be covered in greater depth. After an introduction of ideal rheological behavior in solids and liquids, nonideal behavior is treated, and concepts like viscoelasticity will be discussed. At the end of the chapter, texture measurement and quantification in food will be discussed as an important practical application of rheology of solids to food technology.

4.1 Elastic Properties

When a solid body at rest on an immovable surface is loaded with a weight (in this case, a force acting downward) it will respond with a deformation that can be characterized by a reduction in its initial height dimension. However, a solid body will deform in different ways depending upon how the force is acting upon it. Therefore, it is important to distinguish between the three different ways in which a solid body can be stressed (can have forces acting upon it): In the first instance, like in the example with the weight on the body, a body can be stressed under "axial loading" in an uniaxial direction (force acting normal to the surface upon which it is applied, causing a normal stress).

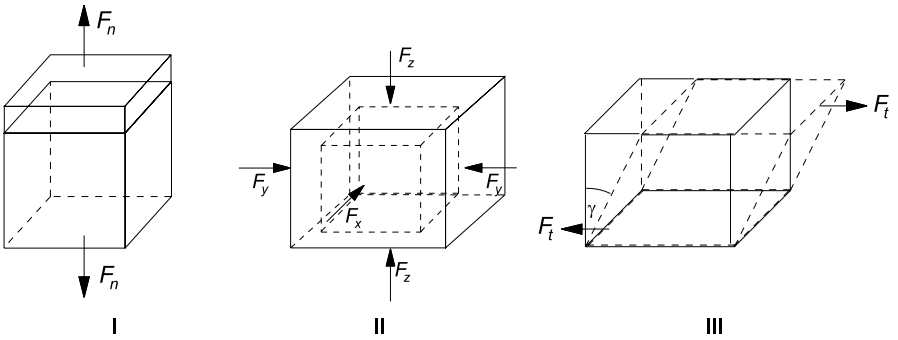

Figure 4.1. Types of loading with force *F*. I uniaxial, II bulk compression, III shear

Secondly, a body can be pressed upon from all directions, like when subjected to an underwater hydrostatic pressure or pressurized in a pressure chamber. This is called bulk compression loading, and results in a volume change in the solid body. In the third instance, a body can be loaded with a shear stress (when the force is acting parallel to the plane surface on which it is applied). Under a shear stress, the responding deformation is in the form of a bending or twisting of the body. Figure 4.1 illustrates these different types of loading which will be discussed further.

4.1.1 Uniaxial Stress

As explained earlier, an uniaxial stress is caused by a force pushing or pulling the body in a direction perpendicular to the surface of the solid body upon which the force is acting. Pushing would cause a compressive stress on the body, resulting in an uniaxial "compression" deformation, in which the initial length of the sample would decrease (become shorter) in the direction of the applied force. Pulling would cause a tensile stress (tension) on the body, resulting in an uniaxial "extension" deformation, in which the initial length of the sample would increase (become longer) in the direction of the applied force. Mathematically, these opposite directions of uniaxial compression or tension would simply be assigned as positive (extension) or negative (compression) directions along the same uniaxial path.

It is important to realize that, in addition to the inherent rheological properties of a material, the amount of deformation observed in a sample of material in response to a given applied force will also depend on the geometric size and shape of the sample. For example, under the same applied force, a tall slender sample will exhibit a much greater deformation than a short flat sample of the same material. Therefore observations of force and deformation will only reveal rheological behavior of the sample, but not the material out of which the sample is made. In order to have these observations reflect true rheological behavior of the material from which the sample is made, it is necessary to elim-

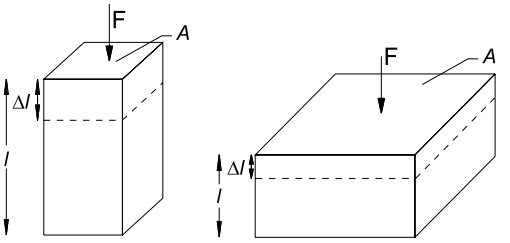

Figure 4.2. Differences in shape and size will result in different deformation in response to the same applied force, even though samples are of the same material

inate the interference caused by sample size and shape. This is accomplished by converting the applied force into stress, and the responding deformation into strain. The stress is obtained when we divide the applied force by the area of the surface over which it is applied. The strain is obtained when we divide the measured deformation (compression or extension) by the initial length of the sample in the direction of the applied force. When these transformations are made, the resulting strain that is observed in response to an applied stress will be the same for any sample of a given material, regardless of size or shape of the sample. These transformations are described mathematically below, and illustrated in Figure 4.2.

The quotient of force over area is called stress, with units of force over area ($N \cdot m^{-2} = Pa$)

$$\sigma = \frac{F}{A} \tag{4.1}$$

The relative change in length is called strain ε:

$$\varepsilon = \frac{\Delta l}{l} \tag{4.2}$$

where

F	force in N
A	area in m^2
σ	stress in $N \cdot m^{-2}$
Δl	deformation in m
l	initial length in m
ε	strain

Therefore, as stress increases on a sample of a given material, it will cause the responding strain to increase, as well. The relationship between stress and strain is one of the most fundamental rheological behaviors to be studied in solid materials. This relationship can be studied and analyzed mathematically when a simple graph is constructed on which the stress is plotted on the vertical axis with corresponding strain plotted on the horizontal axis, as shown in Figure 4.3. This type of graph is called a stress–strain diagram. When a material exhibits a linear relationship between increasing stress and strain, it is said to be a classic elastic material that follows Hooke's law. According to Hooke's law, the change in strain in response to increasing stress can be approximated by a linear function that will appear as a straight line through the origin on a

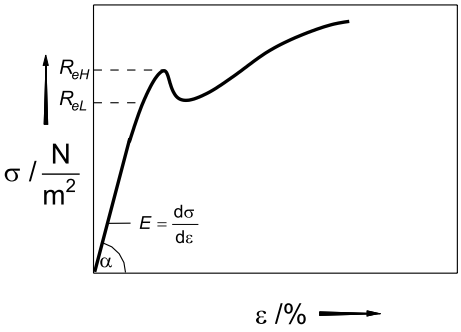

Figure 4.3. Stress–strain diagram of a material with a distinct yield stress R_{eH}

stress–strain diagram. Figure 4.3 shows such a linear relationship beginning at the origin, but only up to a certain point on the diagram. Within the range of values over which the stress–strain relationship is linear, the slope of the straight line can be mathematically expressed as the ratio of stress over strain.

This ratio of stress over strain is known as the modulus of elasticity E, and must not be confused with the elasticity or degree of elasticity of a material. Elasticity can only be measured when a load–unload test is performed. In such a test, the sample is loaded to a given stress causing a corresponding strain. Then, the sample is unloaded by releasing the stress back to zero, and the degree to which the strain recovers is observed. In the case of an elastic deformation, the strain is completely reversible, and fully recovers. That means when the stress is taken away, the strain (deformation) goes back to zero.

When such a test is repeated with the application of higher and higher stresses, an elastic limit is reached beyond which the strain no longer fully recovers. This means that after taking away the stress, part of the strain (deformation) will remain as a permanent "set." This unrecovered strain is called a plastic deformation (see Section 4.3.9).

Many of the most important rheological properties of solid materials can be extracted from a graph on which stress is plotted along the vertical axis, and strain is plotted along the horizontal axis. These are called stress–strain diagrams, like that shown in Figure 4.3. Examining this figure more closely, we can see that the straight line coming from the origin (0,0) indicates that HOOKE's law is valid in the linear region of the graph. The point at which the graph begins to deviate from a straight line is called the proportional limit (R_{eL}). Stresses beyond this point lead to nonlinear deformation (starting with R_{eL}). At the point R_{eH}, the solid begins to flow or yield, but only temporarily, since the stress is able to increase once again with increasing strain up to a maximum level on the diagram. At the yield point, the strain is able to continue increasing with little or no increasing stress. If the stress were to be released at this point, the sample would keep its deformation as a permanent set (it was deformed by flowing, and is therefore a nonelastic or plastic deformation). At a certain point, the strain reaches a limit beyond which the sample can no longer sustain its original structure, and rupture or breakage occurs. That is the

point in Figure 4.3 where the curve ends. However, for most solids, this point occurs at the very maximum stress value reached during testing. In any case, the maximum stress value reached is called the maximum strength of the material, and the stress at which rupture occurs is called the rupture strength. Again, for most solid materials, maximum strength and rupture strength are often the same. Note the conventional use of terminology here, in that, whenever we refer to a specific stress where something happens (yield stress, maximum stress, rupture stress, etc.), we call it a "strength."

Many food and biological materials will give only a smooth curve on a stress–strain diagram that may still begin as a straight line, but will only gradually bend away from linearity such that no distinct yield point can be seen (mathematically, the stress–strain curve is monotone), as shown in Figure 4.4. In this case, it is difficult to determine at what point the material will make the transition from elastic to plastic behavior. In this type of situation, a special technique called the 0.2% strain limit can help. This technique proposes a technical limit of elasticity that is used to specify the stress at which the permanent strain reaches a value of 0.2%. Figure 4.4 shows the use of this technique as an example:

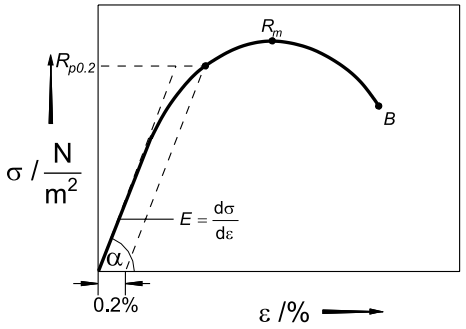

Figure 4.4. Stress–strain diagram of a material with a smooth profile showing no distinct yield point. $R_{p0.2}$ is the technical limit of elasticity for the 0.2 strain limit technique. The slope of the straight line portion gives the modulus of elasticity E for the material. The highest point on the curve (R_m) gives the maximum strength of the material. B is the rupture point (rupture strength)

4.1.2 Young's Modulus

Recall the three different ways in which a solid body can be stressed (can have forces acting upon it, see Figure 4.1): In the first instance, like in the example with the weight on the body, a body can be stressed under "axial loading" in an uniaxial direction (force acting normal to the surface upon which it is applied, causing a normal stress) Secondly, a body can be pressed upon from

all directions, like when subjected to an underwater hydrostatic pressure or pressurized in a pressure chamber. This is called bulk compression loading, and results in a volume change in the solid body. In the third instance, a body can be loaded with a shear stress (when the force is acting parallel to the plane surface on which it is applied). Under a shear stress, the responding deformation is in the form of a bending or twisting of the body.

All three of these types of stress application can be studied with stress–strain diagrams like those shown in Figure 4.3 and Figure 4.4, and all three may show a linear region of elastic behavior from which the slope will give a value for modulus of elasticity. However, the value of this modulus will be different for the same material, depending upon which of the three ways the sample was stressed. When the modulus of elasticity is obtained from axial loading tests, it is called YOUNG's modulus E. When it is obtained from bulk compression tests, it is called the "bulk" modulus K, and when obtained from shear tests, it is called the "shear" modulus G. Each of these three moduli are fundamental rheological properties of a solid material. But, each modulus will have a different value for the same material. However, all three can be mathematically related to each other through a related rheological property called POISSON's ratio. YOUNG's modulus will be discussed in this subsection, followed by discussions of the other two moduli and POISSON's ratio in subsequent subsections.

Recall that ideal elastic behavior is characterized by a straight line through the origin on a stress–strain diagram, and can be mathematically expressed by HOOKE's law:

$$\sigma = E \cdot \varepsilon \tag{4.3}$$

E is a material property named the modulus of elasticity. When the stress and strain result from axial loading conditions, this modulus is called YOUNG's modulus, and given the symbol (E). YOUNG's modulus gives an indication of easily a material can be stretched or contracted, and is sometimes referred to as "stiffness." Experimentally, E is obtained from the slope of the stress–strain curve (see Figure 4.4):

$$E = \frac{\mathrm{d}\sigma}{\mathrm{d}\varepsilon} = \tan\alpha \tag{4.4}$$

If instead of stress and strain, the quantities of force and extension are used, HOOKE's law is expressed as:

$$\frac{F}{A} = F \cdot \frac{\Delta l}{l} \tag{4.5}$$

$$F = \frac{E \cdot A}{l} \cdot \Delta l \tag{4.6}$$

$$F = D \cdot \Delta l \tag{4.7}$$

with

σ	stress in $\mathrm{N} \cdot \mathrm{m}^{-2}$
E	modulus of elasticity in Pa
ε	strain

F force in N
A area in m^2
Δl extension in m
l initial length of solid in m
D HOOKE's constant in $N \cdot m^{-1}$

In addition to the modulus of elasticity, stress–strain diagrams like those in Figure 4.3 or Figure 4.4 can be used to obtain many other rheological terms such as those listed in Table 4.1.

Table 4.1. Terms for interpretation of σ-ε diagrams

description		characteristic feature	
		σ	ε
elastic range	$\frac{d\sigma}{d\varepsilon} = const$		strain is completely reversible
nonelastic range	$\frac{d\sigma}{d\varepsilon} \neq const$		strain is not completely reversible
	$\frac{d\sigma}{d\varepsilon} = 0$	yield stress (flow starts)	strain continues without increasing stress
maximum of curve	$\sigma = \max$	maximum strength of material	strain at maximum stress
technical limit plasticity	$\varepsilon = 0.2\,\%$	stress for 0.2 % strain permanent strain	strain goes to 0.2 % permanent
rupture (breakage)	σ shows sudden drop	stress at rupture	strain at the point of rupture

The magnitude of some YOUNG's modulus values E are listed in Table 4.2.

Table 4.2. Values of YOUNG's modulus of elasticity, examples [115]

material	$E/N \cdot m^{-2}$
ice	$9.9 \cdot 10^9$
stainless steel	$195 \cdot 10^9$
aluminum	$72 \cdot 10^9$
rubber	$8 \cdot 10^5$
dry spaghetti	$3 \cdot 10^9$
apple, raw	$0.6 \ldots 1.4 \cdot 10^7$
gelatine (gel)	$2 \cdot 10^5$
banana	$0.8 \ldots 3 \cdot 10^6$

4.1.3 Bulk Modulus

As an alternative to axial stress, a body can also be pressed upon from all directions, like when subjected to an underwater hydrostatic pressure or pressurized in a pressure chamber. This is called bulk compression loading, and results in a volume change in the solid body (see Figure 4.1). When a body is compressed from all directions, this causes a decrease of the body dimensions in x-, y- and z-directions in a CARTESian system of coordinates. This is called a bulk compression. There is also an elastic range of compression and a nonelastic range. A normal rule of convention is to let positive stress be considered pressure, which causes a reduction in dimensions from all directions, resulting in a reduction in volume of the sample. In contrast, negative stress would be called expansion, and causes an increase in dimensions in all directions, resulting in an increase in volume. This is called volume dilatation, and can happen when a sample is placed under vacuum, or is suddenly released from high pressure to a lower pressure (expansion).

An elastic compression is a volume decrease in a solid caused by decreasing the distance between the molecules within the molecular structure of the material. Once the applied pressure is released back to zero, the initial molecular distances and the initial volume of the body are restored. HOOKE's law would again apply:

$$-\frac{\mathrm{d}V}{V} = \kappa \cdot \mathrm{d}p \tag{2.18}$$

$$\kappa = -\frac{1}{V}\,\frac{\mathrm{d}V}{\mathrm{d}p} \tag{2.18}$$

$$K = -V\frac{\mathrm{d}p}{\mathrm{d}V} \tag{4.8}$$

where

V	volume in m^3
p	pressure in Pa
K	bulk modulus in Pa
κ	compressibility in Pa^{-1}

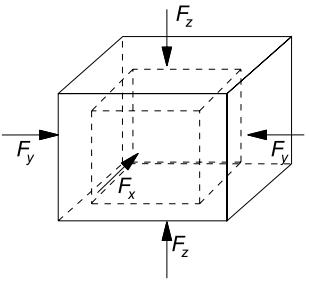

Figure 4.5. Bulk compression

The bulk modulus K characterizes how a material can withstand an elastic compression, and is sometimes referred to as "firmness" of a material.

Normally gases can be compressed easily (see Section 2.3.2), liquids less so, and solids need much higher loads (like in high pressure processing) to show changes in volume. Whereas gases and normal liquids show an isotropic K modulus, solids may have different values in different spatial directions. Such a material property is called an anisotropic material. A bulk modulus for an anisotropic material can be expressed as a tensor with 9 components:

$$K = \begin{pmatrix} K_{xx} & K_{xy} & K_{xz} \\ K_{yx} & K_{yy} & K_{yz} \\ K_{zx} & K_{zy} & K_{zz} \end{pmatrix} \tag{4.9}$$

For isotropic solids and normal fluids the modulus is simply:

$$K = K_{ij} \tag{4.10}$$

and

$$\kappa = \frac{1}{K} \tag{4.11}$$

A pressure has the same value in all three directions. So normally, the reduction in the dimensions of a solid is the same in all three directions. If a material has an anisotropic bulk modulus, the reduction in dimensions can be different in each of the three directions. The consequence is a change in the shape, as shown in Figure 4.6. In high pressure processing of foods, phenomena like this should be considered.

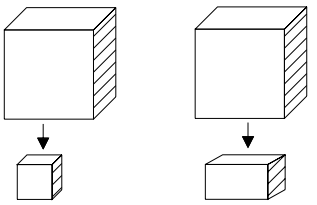

Figure 4.6. Compression of an anisotropic solid. An isotropic material shows the same reduction in length in all directions (left). An anisotropic material (right) does not, and shows a change in shape.

Table 4.3. Values of bulk modulus K, examples [115]

material	K/N · m^{-2}
ice	$10 \cdot 10^9$
stainless steel	$170 \cdot 10^9$
dough	$1.4 \cdot 10^6$
rubber	$1.9 \cdot 10^7$
glass	$3.8 \cdot 10^9$

4.1.4 Shear Modulus

When a force F_t is acting parallel to a surface, the resulting stress is called a shear stress. The type of loading is called shear. The resulting deformation is a shear deformation. The shear deformation is not an axial change in length, but a rotational change (torsion or twisting). For this reason, it can be expressed as an angle of deformation.

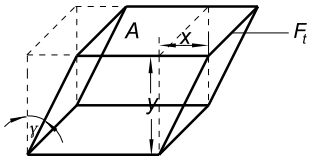

Figure 4.7. Shear stress on a body because of a tangential force F_t causing angular rotational strain

The quotient of tangential force F_t and area A is called the shear stress τ. The angle of deformation γ is called shear deformation, and tangent of that angle is shear strain. In the elastic range of the material, the elongation x (see Figure 4.7) with respect to the sample height y is the ratio $\frac{x}{y}$, which is $\tan \gamma$. This is the shear strain, and is a linear function of the shear stress in the elastic region:

With

$$\tau = \frac{F_t}{A} \tag{4.12}$$

in case of elasticity it is:

$$\tau = G \cdot \tan \gamma \tag{4.13}$$

With small deformations it can be approximated:

$$\tan \gamma = \gamma \tag{4.14}$$

so

$$\tau = G \cdot \gamma \tag{4.15}$$

Solids with ideal elastic behavior show a linear relationship between shear stress and shear strain. The material property G in equation (4.15) is called the shear modulus G, and gives an indication of how easily the material will bend or twist in response to an applied shear stress. This is sometimes called "rigidity" in common terminology. Thus, the common terms "stiffness," "firmness" and "rigidity" can be related to the YOUNG's, bulk and shear modulus, respectively.

Just as with the bulk elastic modulus, the shear modulus for an anisotropic material can be written as a tensor. For isotropic materials G is not dependent on the spatial direction.

F_t tangential force in N
A area in m^2
τ shear stress in $N \cdot m^{-2}$
G shear modulus in $N \cdot m^{-2}$
γ angle of deformation in rad

Example 4.1. A rubber eraser (length 20 mm) with a cubic shape is loaded with a tangential force of 10 N as shown in Figure 4.7. With a shear modulus of the material of $0.2 \cdot 10^6$ Pa calculate the angle of deformation and the elongation x.

Solution:

$$\tau = \frac{F}{A} = \frac{10\,\text{N}}{2 \cdot 2 \cdot 10^{-4}\,\text{m}^2} = 25000\,\text{Pa}$$

$$\gamma = \frac{\tau}{G} = \frac{25000\,\text{Pa}}{0.2 \cdot 10^6\,\text{Pa}} = 0.125$$

$$x = \gamma \cdot y = 0.125 \cdot 20\,\text{mm} = 2.5\,\text{mm}$$

4.1.5 Poisson's Ratio and Transverse Strain

Let us return to the case of axial loading. When a sample of material is subjected to a normal stress pushing downward, it will show an elastic decrease in length Δl. At the same time, however, it must also show an increase in thickness Δd, that will appear as a "bulge" along the sides of the sample. This is because the volume of the sample cannot change under simple axial loading. Thus, if the dimension in one direction (height) must decrease because of the applied stress, then dimensions in the transverse direction (thickness) must increase. The relative change in thickness $\frac{\Delta d}{d}$ is called "transverse strain" and is dependent on the axial strain. The ratio of transverse strain to axial strain produces a proportionality factor called Poisson's ratio μ. These terms are defined mathematically below:

$$\varepsilon_q = \frac{\Delta d}{d} \tag{4.16}$$

$$\varepsilon = \frac{\Delta l}{l} \tag{4.2}$$

$$\varepsilon_q = -\mu \cdot \varepsilon \tag{4.17}$$

Poisson's ratio:

$$\mu = -\frac{\text{transfer strain}}{\text{axial strain}} \tag{4.18}$$

where

d	thickness in m
Δd	change in thickness in m
l	length in m
Δl	change in length in m
ε	axial strain
ε_q	transverse strain
μ	POISSON's ratio

Table 4.4. POISSON's ratio for different materials, examples [115]

material	μ
cheddar cheese	0.5
potato issue	0.49
rubber	0.49
apple tissue	0.37
apple	0.21–0.34
copper	0.33
steel	0.30
glass	0.24
cork	0

Table 4.5. Special cases for POISSON's ratio

case	K	E	G	μ
A	large	small	small	$\mu = 0.5$
B	small	large	large	$\mu = 0$

Table 4.6. Calculations of moduli

case A	case B
$\mu = 0.5$	$\mu = 0$
$G = \frac{E}{2(1+\mu)} = \frac{E}{3}$	$G = \frac{E}{2} = \frac{3}{2} K$
$K = \frac{E}{3(1-2\mu)} = \infty$	$K = \frac{E}{3(1-2\mu)} = \frac{E}{3}$
$E = 3 \cdot G$	$E = 3 \cdot K$

POISSON's ratio μ provides a key link between the YOUNG's E, shear (G) and bulk (K) modulus. If POISSON's ratio for a material is known, along with just one of the three moduli, then the other two moduli for that material can be calculated, as shown by the mathematical relationships listed below in equations (4.19)–(4.21). POISSON's ratio can take on values only within the range, $0 \leq \mu \leq 0.5$. Table 4.5 shows the extreme cases in which these values are reached. When stiffness and rigidity (E and G moduli) is very low compared to firmness (K modulus), then case A applies. On the other hand case B applies when a solid material has a low K modulus (low firmness, high compressibility) and very large stiffness and rigidity (large E and G). Table 4.6 shows the relationship between moduli for those cases.

In reality, Poisson's ratio μ lies between these extreme values for most materials. It can be calculated from [116]:

$$G = \frac{E}{2(1+\mu)} = \frac{3E \cdot K}{9K - E} = \frac{3K(1-2\mu)}{2(1+\mu)} \tag{4.19}$$

$$K = \frac{E}{3(1-2\mu)} = \frac{E \cdot G}{9G - 3E} = G\left[\frac{2(1+\mu)}{3(1+2\mu)}\right] \tag{4.20}$$

$$E = \frac{9G \cdot K}{3K + G} = 2G(1+\mu) = 3K(1-2\mu) \tag{4.21}$$

$$\mu = \frac{E - 2G}{2G} = \frac{1 - \frac{E}{3K}}{2} = \frac{3K - 2G}{2(3K+G)} \tag{4.22}$$

4.2 Rheological Models

Rheological models consisting of mechanical elements like springs and dashpots can be used to explain and interpret the rheological behavior of viscoelastic materials. The model is intended to behave qualitatively in a manner similar to that of the actual material. If the mechanical behavior can be expressed in terms of force–deformation or stress–strain and time, the results can lead to a mathematical equation. These equations can be used to explain, and in some cases predict the behavior of the material in response to various loading conditions. Thus, such models can be quite useful.

Most rheological models are intended to show ideal behavior. The basic models most often used are those intended for ideal rigid, ideal viscous, ideal elastic and ideal plastic behavior. Figure 4.8 and Table 4.7 give an overview of the names and symbols used for these models.

These basic mechanical elements can be further assembled into various combinations to produce more sophisticated mechanical models capable of

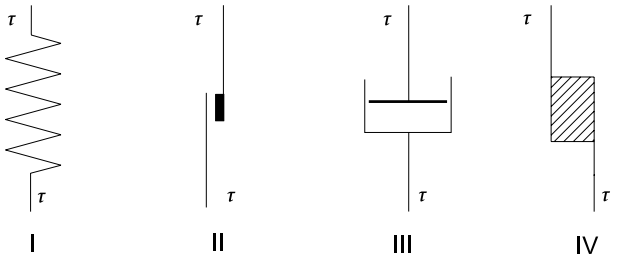

Figure 4.8. Symbols of mechanical elements used for basic rheological models. I Hookean element (spring), II breakage (rupture) element, III Newtonian element (dashpot), IV St.Venant element.

Table 4.7. Basic rheological models

name of model	rheological property	application
Pascal	ideal frictionless flow	fluids
Newton	ideal viscous flow	fluids
St. Venant	ideal plastic deformation	solids
Hooke	ideal elastic deformation	solids
Euklid	ideal inelastic (stiff, rigid)	solids

simulating more complicated rheological behaviors, such as the models listed in Table 4.8.

It is interesting to note that the Hookean spring and the Newtonian dashpot are the mechanical elements used most often in these rheological models. Note that they are the sole mechanical elements in the first two rheological models listed in Table 4.8. For example when used alone, the spring is a mechanical model representing ideal (Hookean) elastic behavior in solids. If we apply a force to the spring, it will extend a distance directly proportional to the applied force, with the constant of proportionality (modulus of elasticity) being represented by the spring constant. If we remove the applied force, the spring extension will fully recover. Likewise, the dashpot alone serves as a model for ideal viscous behavior exhibited by liquids. If we apply a constant force to the dashpot, it will extend continuously, representing flow, at a speed directly proportional to the applied force. A greater force will cause it to extend at a faster rate. The constant of proportionality between applied force and extension rate represents the viscosity of a liquid, and is called the viscosity of the viscous element (similar to spring constant for elasticity).

Near the bottom of Table 4.8 are two more complicated models called the Maxwell model and the Kelvin model. Note that both these models consist only of spring and dashpot. In the Maxwell model both elements are combined in series, while in the Kelvin model they are combined in parallel. The Maxwell model is used to simulate stress relaxation in solid materials. This is a time-dependent rheological behavior characterized by the observation of stress decreasing over time in a sample subjected to a constant applied strain. The Kelvin model is used to simulate strain retardation (creep) in solid materials. This is also a time-dependent rheological behavior, but is characterized by the observation of strain increasing over time in a sample subjected to a constant applied stress. Application of the Kelvin and Maxwell models to creep and stress relaxation will be discussed more extensively in the section on texture measurement later in this chapter (see Section 4.6.1). The goal is to find the model which is best suited to describe the rheological behavior of the actual material of interest under conditions appropriate to the intended application. Examples of various such models are given in Table 4.8.

Use of the Maxwell and Kelvin models in describing stress relaxation and creep behavior will be discussed later in Sections 4.6.1 and 4.6.2.

Table 4.8. Combinations of mechanical elements to form basic rheological models

element name	element symbol	same with breakage element
Hooke	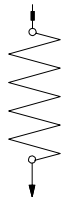	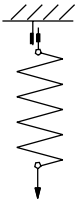
Newton	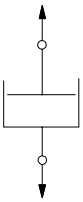	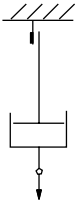
St.Venant	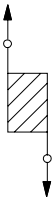	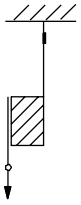
Pascal	ideal flow without friction	
Euclid	ideal inelastic (rigid)	
Maxwell	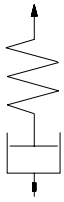	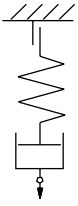
Prandtl	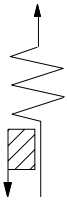	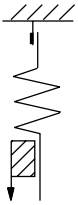
Kelvin	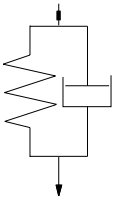	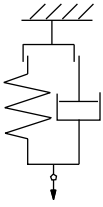

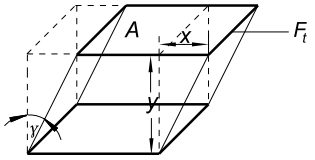

Figure 4.9. Viscous behavior: In response to a shear stress, the deformation γ continues to increase indefinitely, exhibiting the phenomenon of flow

4.3 Viscous Behavior – Flow

Unlike solids, liquids cannot support their own weight, and are incapable of holding any shape. They must be contained in a vessel or surface depression. Otherwise, they will flow under the shear stress caused by their own weight. Therefore, the way in which liquids deform to an applied stress is to flow (continuous deformation). Recall when a shear stress causes a reversible angular deformation γ on a solid, we call it an elastic shear deformation. When instead, a shear stress causes a continuously increasing strain γ i.e. a constant $\dot{\gamma}$, we call this flow. Flow is not elastic behavior, but is viscous behavior.

Figure 4.9 appears the same as Figure 4.7 presented earlier to illustrate elastic shear on a solid. However, the same figure can also be used to illustrate ideal viscous behavior in a liquid. We only need to imagine that the upper surface with area A is a flat plate resting on top of a sample of liquid film having thickness y. When we pull on the flat plate with force F, we will be applying a shear stress to the liquid, and the liquid film will allow the plate to move in the direction of the force at a constant velocity dictated by the viscosity of the liquid. If we pull with greater force (increasing shear stress), the plate will move faster at a higher constant velocity. Therefore, not only do liquids respond to an applied stress by flowing, they respond to changes in stress by changes in the speed by which they flow (flow rate).

Just as ideal elastic behavior of a solid material is a linear relationship between shear stress and shear strain governed by the shear modulus of elasticity G, ideal viscous behavior is a linear relationship between shear stress and the rate of shear strain, governed by the viscosity of the liquid. The rate of shear strain is the shear rate $\mathrm{d}y/\mathrm{d}t$. These relationships are expressed mathematically below.

Ideal elastic behavior in solid:

$$\tau = G \cdot \gamma \tag{4.15}$$

Ideal viscous behavior in liquid:

$$\tau = \eta \cdot \dot{\gamma} \tag{4.23}$$

where

F_t	tangential force in N
A	area in m^2
τ	shear stress in $N \cdot m^{-2}$
G	shear modulus in $N \cdot m^{-2}$

γ angle of deformation in rad
$\dot{\gamma}$ shear rate in s^{-1}
η viscosity in $N \cdot m^{-2} \cdot s$

Atoms and molecules in solids have stronger binding forces between them than in liquids or gases. Because of this, solids normally tend to show elastic behavior, whereas liquids and gases show viscous behavior. This is not a matter of molecular binding forces alone, but also of the competition between binding energy attracting molecules close together, and thermal energy driving molecules further apart. With rising temperature, the thermal energy can override the binding energy and a solid (elastic) changes into a liquid (viscous).

On the other hand a solid can be brought to flow without raising the temperature by applying sufficiently high stress that the yield stress can be exceeded. For example, this can be done with a material like steel. Once the yield stress is exceeded, the steel will flow and the material will show permanent deformation. This is precisely what the blacksmith is doing when he strikes a hammer blow to a piece of steel.

4.3.1 Shear Rate

It seems that one of the more difficult concepts to be grasped in the study of liquid rheology is a physical conceptualization of what is meant by rate of shear or shear rate. To help meet this objective, we will refer once again to Figure 4.9. Basically, the continuing change of the shear angle γ deformation over time is called shear rate $\dot{\gamma}$. The SI unit is s^{-1}.

$$\dot{\gamma} = \frac{d\gamma}{dt} \tag{4.24}$$

A more general way to look at the continuing shear angle deformation, is to view the deformation as the increasing angle caused the circular rotation of a radius on a fixed circle, as shown in Figure 4.10. The same deformation can be described by an angle γ or by a distance along the perimeter ds:

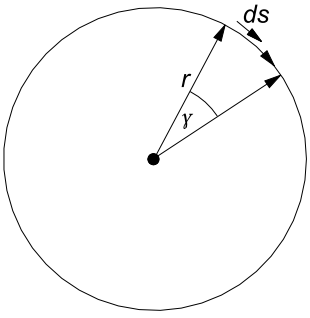

Figure 4.10. Angular deformation γ and lateral (tangential) deformation ds

Mathematically, these can be expressed as follows:

$$\tan \gamma = \frac{\mathrm{d}s}{r} \tag{4.25}$$

for small angles the approximation is valid

$$\tan \gamma = \gamma \tag{4.26}$$

so

$$\gamma = \frac{\mathrm{d}s}{r} \tag{4.27}$$

and

$$\frac{\mathrm{d}\gamma}{\mathrm{d}t} = \frac{\mathrm{d}s}{\mathrm{d}t \cdot r} \tag{4.28}$$

Using the tangential velocity (see Figure 4.10)

$$v = \frac{\mathrm{d}s}{\mathrm{d}t} \tag{4.29}$$

the shear rate is

$$\dot{\gamma} = \frac{v}{r} \tag{4.30}$$

So the shear rate is the quotient of the tangential velocity and the radius of the rotational movement. So the shear rate is the same as the angular velocity of the rotation.

Looking at Figure 4.9 again, the shear rate can be recognized as the quotient of the velocity of the upper plate and the distance to the (nonmoving) base plate, with:

$$\tan \gamma = \frac{\mathrm{d}x}{y} \tag{4.31}$$

and with equation (4.26) the shear rate is

$$\dot{\gamma} = \frac{\mathrm{d}x}{y \cdot \mathrm{d}t} = \frac{v_x}{y} \tag{4.32}$$

When then lower base plate in Figure 4.9 is no longer fixed, but allowed to move freely, then the more general definition of the shear rate has to be applied:

$$\dot{\gamma} = \frac{\mathrm{d}v_x}{\mathrm{d}y} \tag{4.33}$$

or

$$\dot{\gamma} = \frac{\mathrm{d}v}{\mathrm{d}r} \tag{4.34}$$

with

$$\dot{\gamma} = \frac{\Delta v_x}{\Delta y} = \frac{v_{x2} - v_{x1}}{y_2 - y_1} \tag{4.35}$$

Table 4.9. Terms used for the shear rate

$\dot{\gamma}/s^{-1}$
shear rate
rate of shear
shear velocity gradient
rotational velocity
angular velocity

Table 4.10. Terms for the shear angle

γ/rad
shear angle
shear
shear deformation
angular deformation

It is possible to calculate the shear rate between two moving plates. First of all, if the plates move together in the same direction at the same velocity, there is no relative difference in velocity, and the shear rate is zero. When the lower base plate is fixed (not moving), then equation (4.33) would apply:

$$\dot{\gamma} = \frac{dv_x}{dy} \approx \frac{\Delta v_x}{\Delta y} = \frac{v_2 - v_1}{y_2 - y_1} = \frac{v_2 - 0}{y_2 - 0} = \frac{v}{y} \tag{4.36}$$

Imagine if in Figure 4.9 the upper plate were a round flat disk instead of a rectangular flat plate. Then a torque could be applied to induce a shear stress that would cause the circular plate to rotate upon the liquid film of thickness y, instead of moving (sliding) in a linear direction. Now, we can look at Figure 4.10 to help us recognize that the description of the shear rate in equations (4.33) and (4.36) are the same. In the case of the rectangular model in Figure 4.9, the finite element with would become a part of r. The SI unit in either case is s^{-1}. For example, from equation (4.33), we have , which algebraically reduces to s^{-1}.

Example 4.2. Understanding shear rate during painting
Using the symbols of Figure 4.9:

(a) Assume a paint brush is moving at a velocity $v = 0.5\ m \cdot s^{-1}$ with each stroke, and is leaving a paint film of 2 mm thickness. Then, we have:
$y = 2$ mm, and the shear rate is $\dot{\gamma} = \frac{dv}{dy} = 250\ s^{-1}$.

(b) Assume a paint brush stroke velocity is changed to $v = 1\ m \cdot s^{-1}$, and is leaving a paint film of $d = 0.2$mm thickness. Then, we have:
$y = 0.2$ mm, and the shear rate is $\dot{\gamma} = \frac{dv}{dy} = 5000\ s^{-1}$.

Example 4.3. Shear rate during roller drum process
Using the symbols of Figure 4.10:

(a) Assume a roller drum process produces a film layer with a thickness of $y = 100$ µm with a roll of radius $r = 50$ cm and 20 RPM. Then, the tangential velocity of the roll is:

$$v = \omega \cdot r = \frac{20 \cdot 2\pi}{60\ s} \cdot 0.5\ m \approx 1\ m \cdot s^{-1}$$

Table 4.11. Magnitudes and examples of shear rates

process	shear rate $\dot{\gamma}/\mathrm{s}^{-1}$	example
sedimentation of small solid particles	$10^{-6} \ldots 10^{-4}$	fruit juice, medical suspensions
sedimentation of larger solid particles	$10^{-4} \ldots 10^{-1}$	paint pigment, ceramic suspensions, spice particles in dressing
flow caused by surface tension	$10^{-2} \ldots 10^{-1}$	dessert toppings, paint film, coatings,
flow caused by gravity	$10^{-1} \ldots 10^{1}$	pouring out of containers, flow of paint, dripping off excess coating
extrusion processing	$10^{0} \ldots 10^{3}$	snacks, cereals, tooth paste, noodles, pet food, polymers
roller drum processing	$10^{1} \ldots 10^{2}$	rolling of dough
pouring	$10^{1} \ldots 10^{2}$	out of bottles, food, cosmetics
dipping	$10^{1} \ldots 10^{2}$	dipping of confectionary in chocolate
chewing / swallowing	$10^{1} \ldots 10^{2}$	food, feed, pharmaceutical products
flow through pipe	$10^{0} \ldots 10^{3}$	pumping of liquds
stirring / mixing	$10^{1} \ldots 10^{3}$	liquids
painting, brushing	$10^{2} \ldots 10^{4}$	paint, lip gloss, nail polish, spreads
surface smearing	$10^{2} \ldots 10^{4}$	skin creams, salves, bath gels, hand lotion
spraying (aerosols)	$10^{3} \ldots 10^{6}$	spray drying, spray painting, fuel injection
wet milling	$10^{3} \ldots 10^{5}$	grain processing, food suspensions, mustard
roller (pressing)	$10^{4} \ldots 10^{6}$	printing of newspapers, lithography,
homogenization (high pressure nozzle)	$10^{5} \ldots 10^{6}$	fluid milk, soft-scrub scouring creams
lubrication	$10^{3} \ldots 10^{7}$	motor oil, machine oil, axle grease
calandering	$10^{3} \ldots 10^{7}$	polymer films, rubber sheeting

and the shear rate is:

$$\dot{\gamma} = \frac{\mathrm{d}v}{\mathrm{d}y} = \frac{1\,\mathrm{m}\cdot\mathrm{s}^{-1}}{10^{-4}\,\mathrm{m}} = 10000\,\mathrm{s}^{-1}$$

(b) Assume we change the conditions in the previous example to a thickness of $y = 25$ µm with a roll of radius $r = 25$ cm and 100 RPM. Then, the tangential velocity of the roll is

$$v = \omega \cdot r = \frac{100 \cdot 2\pi}{60\,\mathrm{s}} \cdot 0.25\,\mathrm{m} = 2.6\,\mathrm{m}\cdot\mathrm{s}^{-1}$$

So, the shear rate is

$$\dot{\gamma} = \frac{\mathrm{d}v}{\mathrm{d}y} = \frac{2.6\,\mathrm{m}\cdot\mathrm{s}^{-1}}{25\cdot 10^{-6}\,\mathrm{m}} \approx 10^{5}\mathrm{s}^{-1}$$

Example 4.4. Shear rate for liquid flow in a pipe or tube
During laminar flow of an incompressible, ideal viscous fluid in pipe, the shear stress is given by $\tau_W = \frac{r \cdot \Delta p}{2l}$ and the shear rate $\dot{\gamma}_W = \frac{4 \cdot \dot{V}}{\pi \cdot r^2}$. In a tube with a radius of 10 cm and at a flow rate of 6000 l/min, the shear rate between fluid and wall of the tube is:

$$\dot{\gamma}_W = \frac{4 \cdot \dot{V}}{\pi \cdot r^3} = \frac{4 \cdot 6000 \cdot 10^{-3} \mathrm{m}^3}{60\,\mathrm{s} \cdot \pi \cdot (0.1\,\mathrm{m})^3} = 127\,\mathrm{s}^{-1}$$

Example 4.5. Shear rate during sedimentation
According to Stokes law, for Reynolds number < 1 and without interactions between particles and fluid, the terminal velocity of a particle falling through a fluid can be given by:

$$v = \frac{d^2 \cdot g}{18 \cdot \eta}(\rho_K - \rho_{fl}).$$

For sand particles with $d = 0.5$ µm in water, there is a difference between fluid and particle density of:

$$\rho_K - \rho_{fl} = 1500\,\mathrm{kg} \cdot \mathrm{m}^{-3} - 1000\,\mathrm{kg} \cdot \mathrm{m}^{-3} = 500\,\mathrm{kg} \cdot \mathrm{m}^{-3}.$$

With the dynamic viscosity of water of about $\eta = 1$ mPa · s, there will be a terminal velocity of:

$$v = \frac{(5 \cdot 10^{-7}\,\mathrm{m})^2 \cdot 9.81\,\mathrm{m} \cdot \mathrm{s}^{-2}}{18 \cdot 10^{-3}\,\mathrm{N} \cdot \mathrm{m}^{-2} \cdot \mathrm{s}} \cdot 500\,\mathrm{kg} \cdot \mathrm{m}^{-3} = 6.8 \cdot 10^{-8}\,\mathrm{m} \cdot \mathrm{s}^{-1}$$

So, the shear rate is:

$$\dot{\gamma} = \frac{\mathrm{d}v}{\mathrm{d}y} \approx \frac{6{,}8 \cdot 10^{-8}\,\mathrm{m}}{5 \cdot 10^{-7}\,\mathrm{s} \cdot \mathrm{m}} \approx 0.1\,\mathrm{s}^{-1}$$

4.3.2 Newtonian Flow Behavior

When there is a linear relationship between shear stress and resulting shear rate, the flow behavior is called ideal viscous or Newtonian. Fluids with that behavior are named Newtonian fluids. In the same sense, equation (4.23) is the classic mathematical equation that describes Newtonian flow behavior. It is the equation of a straight line passing through the origin.

$$\tau = \eta \cdot \dot{\gamma} \tag{4.23}$$

In a diagram of shear stress versus shear rate the slope of this straight line gives the dynamic viscosity η, which remains constant for all shear rates (see Figure 4.11).

$$\eta = \frac{\mathrm{d}\tau}{\mathrm{d}\dot{\gamma}} \tag{4.37}$$

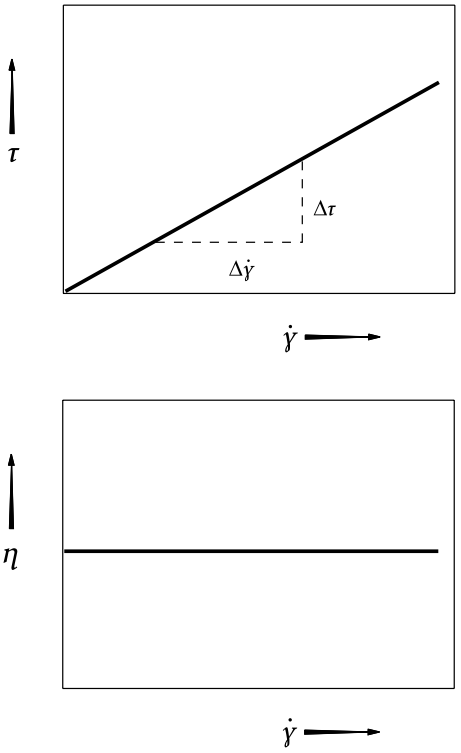

Figure 4.11. Flow behavior curve (upper diagram) and viscosity curve (lower diagram) of a NEWTONian fluid. The slope η of the upper curve is constant for all shear rates.

or

$$\eta = \frac{\Delta\tau}{\Delta\dot{\gamma}} \tag{4.38}$$

Examples of common NEWTONian fluids are listed in Table 4.12:

Table 4.12. NEWTONian fluids, examples

material	$\eta_{20\,^\circ C}$/mPa · s
carbon dioxide	0.0148
nitrogen	0.0177
water	1.002
ethanol	1.20
milk	2
olive oil	84
glycerol	1490

Sometimes the kinematic viscosity ν is used instead of the dynamic viscosity η. The transformation simply is:

$$\nu = \frac{\eta}{\rho} \tag{4.39}$$

where

η	dynamic viscosity in $\mathrm{Pa \cdot s}$
ν	kinematic viscosity in $\mathrm{m^2 \cdot s^{-1}}$
ρ	density of fluid in $\mathrm{kg \cdot m^{-3}}$
ϕ	fluidity (flowability) in $\mathrm{Pa^{-1} \cdot s^{-1}}$

The inverse quantity of the dynamic viscosity is called fluidity:

$$\phi = \frac{1}{\eta} \tag{4.40}$$

The SI units for dynamic viscosity are $\mathrm{N \cdot m^{-2} \cdot s}$, which reduces to $\mathrm{Pa \cdot s}$. Water at room temperature has a dynamic viscosity of about $\eta = 1\ \mathrm{mPa \cdot s}$. With a density of about $1000\ \mathrm{kg \cdot m^{-3}}$, the kinematic viscosity is about $\nu = 10^{-6}\ \mathrm{m^2 \cdot s^{-1}}$. For conversion, see Table 4.13.

Table 4.13. Conversion of older viscosity units

dynamic viscosity	kinematic viscosity
Poise (P)	Stokes (St)
Poiseuille (Pl)	
$1\ \mathrm{P} = 1\ \mathrm{dyn \cdot s \cdot cm^{-2}} = \frac{10^{-5}\ \mathrm{N \cdot s}}{10^{-4}\ \mathrm{m^2}} = 10^{-1}\ \mathrm{Pa \cdot s}$	$1\ \mathrm{St} = 1\ \mathrm{cm^2 \cdot s^{-1}} = 10^{-4}\ \mathrm{m^2 \cdot s^{-1}}$ $1\ \mathrm{St} = 10^{-6}\ \mathrm{m^2 \cdot s^{-1}}$
$1\ \mathrm{cP} = 10^{-2}\ \mathrm{P} = 10^{-3}\ \mathrm{Pa \cdot s} = 1\mathrm{mPa \cdot s}$	
$1\mathrm{Pa \cdot s} = 1\ \mathrm{Pl}$	
value of water $\eta = 1$ cP	value of water $\eta = 1$ cSt

In the case of Newtonian fluids the slope of the straight line on the shear stress versus shear rate diagram is constant (see Figure 4.11). This means the dynamic viscosity, which is the derivative of shear stress with respect to shear rate, $\eta = \frac{\mathrm{d}\tau}{\mathrm{d}\dot{\gamma}}$ must also be a constant, and will be the same for all shear rates. So, in the case of Newtonian fluids, a single value for η is sufficient to describe the flow behavior for all shear rates. It is a "universal" viscosity for all situations of laminar flow in which the material is used.

This is not the case for most biological materials and foods: For many of these materials, the viscosity is not the same at different shear rates. We call this non-Newtonian behavior.

4.3.3 Non-Newtonian Flow Behavior

If there is no linear relationship between shear stress τ and shear rate $\dot{\gamma}$ or if the flow behavior curve does not pass through the origin (0,0) on the shear

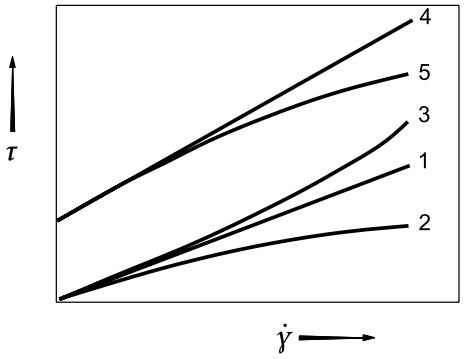

Figure 4.12. Flow behavior curves. **1:** NEWTONian, **2:** pseudoplastic (shear thinning), **3:** dilatant (shear thickening), **4:** BINGHAM plastic (linear with yield stress), **5:** HERSCHEL–BULKLEY or mixed plastic (pseudoplastic with yield stress)

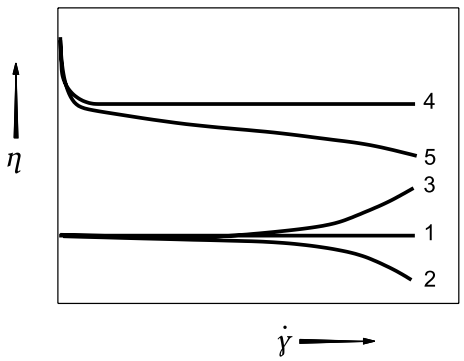

Figure 4.13. Viscosity curves **1:** NEWTONian, **2:** pseudoplastic, **3:** dilatant, **4:** BINGHAM plastic, **5:** HERSCHEL–BULKLEY

stress–shear rate diagram, we call this non-NEWTONian flow behavior. The flow behavior of non-NEWTONian fluids depends on the stress conditions to which the fluids are subjected. Some typical flow behavior curves are summarized in Figure 4.12.

4.3.4 Comparison of Newtonian with Non-Newtonian Fluids

NEWTONian fluids have the same viscosity at low shear rates as at high shear rates. In contrast, non-NEWTONian fluids do not have a constant viscosity with respect to shear rate. Their viscosity will depend on stress conditions (shear rate), and often also on time. Figure 4.14 is a viscosity versus shear rate diagram on which viscosity curves for two different non-NEWTONian fluids are shown, along with the horizontal straight line representing the constant viscosity of a NEWTONian fluid. At low values of shear rate $\dot{\gamma}_1$, the viscosity of fluid 3 is higher than that of fluid 2. However, as shear rate increases to a higher value $\dot{\gamma}_2$, now the viscosity of fluid 3 is lower than that of fluid 2. The viscosity of fluid 1 is the same over all shear rates.

This example shows that for non-NEWTONian fluids, it is not sufficient to provide one single value of viscosity to describe the flow behavior. Instead, it

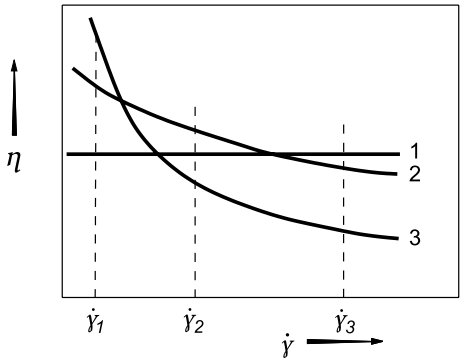

Figure 4.14. NEWTONian fluid (1), and non-NEWTONian fluids (2,3) in comparison

is necessary to say "viscosity at shear rate *zzz*." It would be far more useful, however, to provide the total flow behavior curve or viscosity curve. There are ways to specify a total flow behavior curve with numerical values for the constant parameters in the mathematical equations describing the flow behavior curves (see later in the chapter).

For a very small interval in the range of shear rates of interest, a nonlinear flow curve may be approximated by a linear function. That means a non-NEWTONian fluid can be treated approximately as a NEWTONian fluid within a small interval of shear rates. Whether an approximation is acceptable depends on many factors like the type of material, the nature of question being asked, and the intended use of the result.

4.3.5 Pseudoplastic Flow Behavior

Pseudoplastic flow behavior occurs when we observe shear stress increasing at a diminishing rate with increasing shear rate. On a shear stress–shear rate diagram, the flow behavior curve has a convex profile in which the tangential slope is decreasing with increasing shear rate. This means the viscosity is decreasing with increasing shear rate. Sometimes this observation is referred to as "shear-thinning" behavior. Figure 4.12 and Figure 4.13 show examples of the flow behavior curve and viscosity curve for a pseudoplastic fluid.

It is characteristic of pseudoplastic fluids that the increasing flow resistance (shear stress) seems to decrease when the fluid is subjected to higher shear rates. This behavior is assumed to be caused by decreasing molecular interactions within the molecular structure of the fluid during flow. In the case of flowing macromolecules, the additional effects of unfolding and reorientation of molecules may be occurring. When these effects are completely reversible, we call this "true" pseudoplasticity. This means that if we first increase shear rate to a given value, and then decrease it back again, the viscosity will be fully restored to the same value as before.

Sometimes the effect of shear-thinning is not completely reversible. This can be explained by a permanent loss of structure in the material under inves-

Table 4.14. True and apparent pseudoplasticity

pseudoplasticity	true	apparent
behavior	reversible	irreversible
example	aqueous xanthan solution	yogurt

tigation (e.g. yogurt shows this effect). In that case we have no "true" pseudoplasticity, but an apparent pseudoplasticity. Table 4.14 shows some examples.

4.3.6 Thixotropic Flow Behavior

Thixotropic flow behavior is observed when shear stress or viscosity decreases over time at a constant shear rate. The reason for the decreasing viscosity (or shear stress) is assumed to be caused by a decrease in the intermolecular interactions within the molecular structure of the material. When shear rate stops, the original structure is restored, as well as the initial viscosity. This is called "true" thixotropicity. If the viscosity is not restored because of irreversible structure breakdown, the behavior is called apparent thixotropicity. Many of us have experienced thixotropicity when stirring paint. When first beginning to stir the paint, a great effort is needed (shear stress) to get the paint moving at a given rate of stirring. But as time goes on, it seems that less and less effort is needed to maintain the rate of stirring, because the viscosity is decreasing over time at constant shear rate. This is thixotropicity.

4.3.7 Dilatant Flow Behavior

Dilatant flow behavior occurs when we observe shear stress increasing at an increasing rate with increasing shear rate. On a shear stress–shear rate diagram, the flow behavior curve has a concave profile in which the tangential slope is increasing with increasing shear rate. This means the viscosity is also increasing with increasing shear rate. Sometimes this observation is referred to as "shear-thickening" behavior. This flow behavior is seen in highly concentrated suspensions. Figure 4.12 and Figure 4.13 show examples of the flow behavior curve and viscosity curve for a dilatant fluid.

It is assumed that under increasing shear rate the liquid between the solid particles is squeezed out and the friction between the particles increases. This increasing friction accounts for the increasing shear stress and increasing viscosity experienced as shear rate increases. Also, the squeezing causes a dilatation (an increase in volume) of the suspension, and therefore the phenomenon is called dilatant flow behavior. When these effects are completely reversible, we call this "true" dilatancy. This means that if we first increase shear rate to a given value, and then decrease it back again, the viscosity will be fully restored to the same value as before. Sometimes the effect of shear-thickening is not completely reversible. This can be explained by a permanent damage to the

molecular structure in the material under investigation. In that case we have no "true" dilatancy, but an apparent dilatancy.

4.3.8 Rheopectic Flow Behavior

Rheopectic flow behavior is observed when shear stress or viscosity increases over time at a constant shear rate. The reason for the increasing viscosity (or shear stress) is also assumed to stem from the intermolecular interactions causing friction to increase with time at constant shear rate within the molecular structure of the material. When shear rate stops, the original structure is restored, as well as the initial viscosity. This is called "true" rheopecticity. If the viscosity is not restored because of irreversible structure damage, the behavior is called apparent rheopecticity.

When observing what appears to be rheopectic behavior, it is important that we interpret correctly what we observe. For example, when whipping liquid heavy cream into whipped cream, we observe the need for more and more effort to maintain the same whipping speed (viscosity increasing over time at constant shear rate). This would appear to be rheopectic behavior. But, that is not the case here. In whipping cream, we start out with a liquid of relatively low viscosity that becomes transformed into a soft-solid foam as a result of incorporating air into the cream producing a gas–liquid emulsion. We now have a totally new material with different rheological properties, and not a liquid with rheopectic behavior.

4.3.9 Plastic Flow Behavior

When a solid material keeps its deformation as a permanent set after taking away the shear stress, we call that plastic deformation. Liquids will demonstrate plastic behavior when they will not begin to flow until a minimum shear stress is exceeded that allows them to yield and begin to flow. This initial stress that must be overcome before the liquid will yield to begin flow is called the yield stress. So, the yield stress is the minimum shear stress needed to get the material flowing, and it is a characteristic of plastic flow behavior. An example is steel which can be deformed if the shear stress from a hammer blow exceeds this value. Another example is butter, which looks like a solid, but can be deformed, and keeps its deformation as a permanent set. When a solid body is loaded with a shear stress below its yield stress, it can be deformed elastically, but will not flow.

In a flow behavior curve on a shear stress–shear rate diagram, the yield stress can be easily found as the intercept on the stress axis at zero shear rate (see Figure 4.12). Because the viscosity (Figure 4.13) mathematically is the derivative of the flow behavior curve, the yield stress on the viscosity curve appears to originate as an indefinitely high viscosity. This can be interpreted as a nonflowing solid, which must have infinite viscosity.

Reasons for plasticity in liquids also stem from strong intermolecular interactions between the molecules within the molecular structure of the material. The stronger are these interactions, the higher the yield stress.

As with many other properties, the yield stress also depends on temperature. For example butter kept cold in the refrigerator will have a much higher yield stress than if the butter were left out at room temperature. This is the reason why the blacksmith prefers to work with hot steel in order to get more yield (deformation) with each hammer blow.

In the preparation of certain foods, it is important to achieve a needed yield stress. For example, whipped cream must have a sufficiently high yield stress in order to hold its shape as a decorative dessert topping. If the yield stress is too low, it will begin to flow and lose its shape, and we cannot use it for a dessert topping.

From a scientifically pure standpoint, all materials have a yield stress, but it is sometimes so low that we do not notice it, such as with water or air. Therefore, for practical reasons, we define plastic materials as those with a measurable (observable) yield stress. Normally this is defined as having a yield stress of such magnitude that they do not flow by themselves, meaning they will not flow under the force of their own weight in response to gravity.

Example 4.6. An ice cream bar shall be dipped into molten chocolate to get a chocolate coating of 2 mm thickness. To what temperature should the molten chocolate be heated in order that it will leave this coating thickness? Assume density of chocolate is 1235 $\mathrm{kg \cdot m^{-3}}$.

Temp. in °C	yield stress in Pa
37.5	32
38.0	28
38.5	25
39.0	22
39.5	19

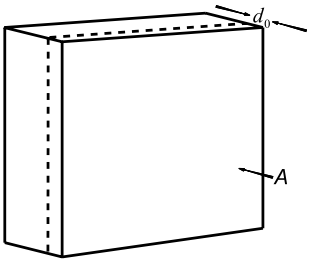

Figure 4.15. Chocolate coating with thickness d_0

Looking at Figure 4.15 the weight force of the chocolate layer with the thickness d is

$$F_G = m \cdot g = \rho \cdot A \cdot d \cdot g$$

The final coating thickness will be left on the bar when the weight force of the coating acting downward is equal to the shear force caused by the yield stress acting upward. So, the shear stress caused by this layer is set equal to weight stress:

$$\tau = \frac{F_G}{A} = \frac{m \cdot g}{A} = \frac{\rho \cdot A \cdot d \cdot g}{A} = \rho \cdot d \cdot g$$

To have the desired thickness d_0, the excess molten chocolate must stop flowing at yield stress τ_0

$$\tau_0 = \rho \cdot d_0 \cdot g$$

$$\tau_0 = 1235\,\text{kg} \cdot \text{m}^{-3} \cdot 2 \cdot 10^{-3}\,\text{m} \cdot 9.81\,\text{m} \cdot \text{s}^{-2} = 24\,\text{Pa}$$

Using the data given, we get a temperature of 38.4 °C, which we should choose for the molten chocolate to achieve this 2 mm coating.

Here

τ_0	yield stress in Pa
A	area in m^2
d	thickness in m
ρ	density in $kg \cdot m^{-3}$
g	gravitational acceleration in $m \cdot s^{-2}$
F_G	weight force in N
m	mass in kg

4.3.10 Overview: Non-Newtonian Flow Behavior

In all cases of non-NEWTONian flow, the flow behavior curve on a shear stress–shear rate diagram is not a straight line through the origin (see Figure 4.11). Because only a NEWTONian fluid has a viscosity which is constant over time, we call those cases of non-NEWTONian fluids, in which the flow properties (especially viscosity and yield stress) are dependent on time, time-dependent behaviors. These behaviors are clearly evident in thixotropicity and rheopecticity. Figure 4.16 shows a schematic of non-NEWTONian flow behavior.

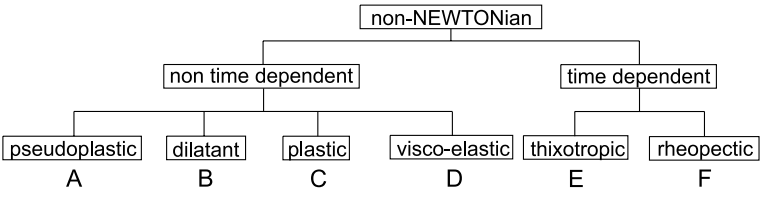

Figure 4.16. Non-NEWTONian flow behavior, schematic of behavior categories and their terminology. Examples are: A: paint, tomato paste, B: crystallized honey, C: whipped eggwhite, solid butter, lipstick, D: wheat dough, E: ketchup

Materials which show plastic flow are also non-NEWTONian materials, even when the viscosity is not dependent on shear stress and time. Flow behavior like this is called BINGHAM plastic flow, and the material is called a BINGHAM plastic fluid (see Figure 4.11).

Table 4.15. Glossary of flow behavior terms

NEWTONian	the flow curve is a straight line through the origin
non-NEWTONian	the flow curve is not a straight line through the origin
pseudoplastic	viscosity decreases with increasing shear rate (shear thinning)
dilatant	viscosity increases with increasing shear rate (shear thickening)
plastic	the fluid has a yield stress
thixotropic	viscosity decreases over time at constant shear rate
rheopectic	viscosity increases over time at constant shear rate

Real materials normally have a more complicated flow behavior which can be explained with various mixtures of the different ideal behaviors described up to here. Sometimes approximations can help, like treating the BINGHAM plastic fluid as a NEWTONian fluid once the initial yield stress has been discounted.

For many food science and engineering applications, it is convenient to transform complicated flow behavior curves and viscosity curves into mathematical equations with constant parameters. Then only a few numbers (parameters) are sufficient to represent and to specify the complete curves. For this purpose, model functions have to be derived, and tested and challenged to be sure of their validity.

4.3.11 Model Functions

Rheological model functions are nothing more than the mathematical equations derived to describe the various flow behavior curves on shear stress–shear rate diagrams. First we will focus on model functions for fluids without yield stress. Then, we will address fluids with yield stress.

Pseudoplastic fluids are assumed to have an initial viscosity at the origin $\eta(\dot{\gamma} = 0) = \eta_0$ which then decreases with increasing shear rate. The decrease is assumed to be the consequence of (reversible) loss of structure/network in the material (in the German language pseudoplastic is called *strukturviskos* because of this interpretation). When the molecular structure/network in the fluid has reached a steady state (where the intermolecular forces acting to build the structure/network and those acting to break it down by shear are in equilibrium) no further decrease of viscosity is observed. This viscosity is called equilibrium viscosity $\eta(\dot{\gamma} = \infty) = \eta_\infty$. Figure 4.17 shows a typical profile for a flow curve of this type. The viscosity curve (which is the derivative of the flow behavior curve) can also be constructed, and is given in Figure 4.18. In this type of pseudoplastic material, the viscosity is changing from η_0 to η_∞ with increasing shear rate. For a mathematical description of these sigmoid shaped curves, a number of model functions have been developed.

In general, most of these functions require two or three parameters. These parameters are constants in the model function, whose numerical values make

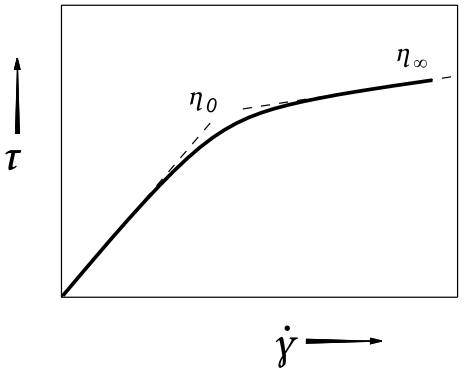

Figure 4.17. Flow behavior curve during structure loss in a pseudoplastic fluid (schematic)

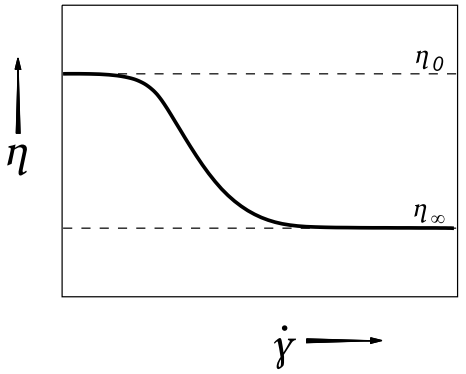

Figure 4.18. Viscosity curve during structure loss in a pseudoplastic fluid (schematic)

the function specific for a given material. Therefore, in order to use these model functions, these parameters have to be known. Normally, model parameters are measured experimentally, or they be obtained from other investigators working on the same material, who report their findings in the scientific literature. Table 4.16 lists some model functions like these. There are cases where a model function takes on the same form as that of a simpler more easily recognized model function, like NEWTON's law. In other words, these model functions can be thought as more or less sophisticated modifications of basic functions like which describes NEWTONian flow behavior.

A classic question posed by investigators working on rheology of fluids is, "Which model is the right one for my material and/ or application?" The answer will depend on factors like: for what purpose is the viscosity needed? In what range of shear rates will the work be done? How precise must the data be? These models differ in their ability for preciseness or "goodness of fit" in approximating experimental data. For example, the model functions after FERRY, STEINER–STEIGER–ORY, DE HAVEN, OSTWALD–DE-WAELE, ELLIS I, and SISKO are valid only in the region $\eta < \eta_\infty$ where the fluid structure is not completely broken down.

Table 4.16. Model functions for fluids without yield stress, examples

name	model function for flow behavior curve	model function for viscosity curve	
Newton	$\tau = \eta \cdot \dot{\gamma}$	$\eta = \frac{\tau}{\dot{\gamma}}$	τ shear stress in Pa η viscosity in Pa · s $\dot{\gamma}$ shear rate in s^{-1}
Ferry	$\tau = \frac{\eta_0}{1 + C \cdot \tau} \cdot \dot{\gamma}$	$\eta_s = \frac{\eta_0}{1 + C \cdot \tau}$	C constant in Pa^{-1} η_0 initial viscosity in Pa · s (for $C = 0 \Rightarrow$ Newton)
Steiner–Steiger–Ory	$\tau = \frac{1}{C + A \cdot \tau^2} \cdot \dot{\gamma}$	$\eta_s = \frac{1}{C + A \cdot \tau^2}$	$C = \frac{1}{\eta_0}$ constant in $(Pa \cdot s)^{-1}$ A constant in Pa^{-1} η_0 initial viscosity in Pa · s
De Haven	$\tau = \frac{\eta_0}{1 + C \cdot \tau^n} \cdot \dot{\gamma}$	$\eta_s = \frac{\eta_0}{1 + C \cdot \tau^n}$	C constant in Pa^{-n} η flow behavior index (for $n = 1 \Rightarrow$ Ferry)
Ostwald–de-Waele (Power law)	$\tau = K_{OW} \cdot \dot{\gamma}^n$	$\eta_s = K_{OW} \cdot \dot{\gamma}^{n-1}$	K_{OW} consistency coefficient in $(Pa \cdot s)^n$ n flow behavior index (for $n = 1 \Rightarrow$ Newton)
Sisko	$\eta_s = \eta_\infty + b \cdot \dot{\gamma}^{n-1}$	$\tau = \eta_\infty \cdot \dot{\gamma} + b \cdot \dot{\gamma}^n$	b constant in $(Pa \cdot s)^n$ η_∞ equilibrium viscosity in Pa · s
Ellis I	$\eta_s = \eta_0 + K \cdot \dot{\gamma}^{n-1}$	$\tau = \left(\eta_0 + K \cdot \dot{\gamma}^{n-1}\right) \dot{\gamma}$	η_0 initial viscosity in Pa · s K constant in $Pa \cdot s^n$
Ellis II	$\eta_s = \frac{\eta_0}{1 + \left(\frac{\tau}{\tau_{1/2}}\right)^{A-1}}$	$\tau = \frac{\eta_0}{\left(1 + \frac{\tau}{\tau_{1/2}}\right)^{A-1}} \cdot \dot{\gamma}$	η_0 initial viscosity in Pa · s A constant $\tau_{1/2} = \frac{\tau(\eta_\infty) - \tau(\eta_0)}{2}$ η_∞ equilibrium viscosity in Pa · s
Peek–McLean–Williamson	$\eta_s = \left(\frac{\eta_0 - \eta_\infty}{1 + \frac{\tau}{\tau_m}}\right) + \eta_\infty$	$\tau = \left(\eta_\infty + \frac{\eta_0 - \eta_\infty}{1 + \frac{\tau}{\tau_m}}\right) \dot{\gamma}$	$\tau_m = \tau\left(\frac{\eta_0 + \eta_\infty}{2}\right)$
Reiner–Philliphoff	$\eta_s = \left(\frac{\eta_0 - \eta_\infty}{1 + \left(\frac{\tau}{\tau_m}\right)^2}\right) + \eta_\infty$	$\tau = \left(\eta_\infty + \frac{\eta_0 - \eta_\infty}{1 + \left(\frac{\tau}{\tau_m}\right)^2}\right) \dot{\gamma}$	
Reiner		$\tau = \frac{\eta_\infty}{1 - \frac{\eta_0 - \eta_\infty}{\eta_0} \cdot e^{-\frac{\tau^2}{\kappa}}} \cdot \dot{\gamma}$	$\kappa = \frac{\varphi_\infty - \varphi_0}{\frac{d\varphi}{d(\tau^2)}}$ coefficient of pseudoplasticity $\varphi = \frac{1}{\eta}$ fluidity

For synthetic polymers (but not those in the form of dispersions or gels), the models after Carreau, Cross, Ellis–Sisko, Phillips–Deutsch, Reiner–Phillippoff, Krieger–Dougherty are recommended [2].

4.3.12 Ostwald–de-Waele Law

A very useful and not to complicated model function is the power-law equation after Ostwald–de-Waele:

$$\tau = K_{OW} \cdot \dot{\gamma}^{n} \tag{4.41}$$

where

K_{OW}	consistency coefficient in Pa · s^n
$\dot{\gamma}$	shear rate in s^{-1}
τ	shear stress in Pa
n	flow behavior index

The factor K_{OW} is called the consistency coefficient. The flow behavior index n indicates the deviation of the flow curve from a straight line, i.e. from NEWTONian behavior. For NEWTONian behavior (a linear curve) it is $n = 1$. This model function is most useful in describing simple pseudoplastic and dilatant flow behaviors. When the flow behavior index is less than unity ($n < 1$) the function describes a pseudoplastic flow behavior curve (convex profile). When the flow behavior index is greater than unity ($n > 1$) the function describes a dilatant flow behavior curve (concave profile). For NEWTONian fluids, the flow behavior index becomes 1, and the consistency coefficient becomes the viscosity. In other words, for NEWTONian fluids $n = 1$ and $K_{OW} = \eta$.

The quotient $\frac{d\tau}{d\dot{\gamma}}$ of the flow behavior curve gives the apparent viscosity η_s of the material.

$$\eta_s = \frac{\text{shear stress}}{\text{shear rate}} = \frac{\tau}{\dot{\gamma}} \tag{4.42}$$

It is important to have a clear understanding of the distinction between "apparent" and "true" viscosity. All laboratory instruments can obtain an instantaneous reading of the quotient of shear stress over shear rate $\frac{d\tau}{d\dot{\gamma}}$, and report it as a reading of "viscosity." However, if the instrument gives a different reading at a different shear rate, then we know this cannot be true viscosity because the material is exhibiting non-NEWTONian flow behavior. Remember, only NEWTONian fluids can have "true" viscosity because it remains constant over all stress conditions, and is a fundamental rheological property describing the flow behavior of the material. An instantaneous measurement of $\frac{d\tau}{d\dot{\gamma}}$ on a non-NEWTONian fluid simply gives us a momentary value of a variable quantity, which cannot be used as a rheological property. Therefore, whenever $\frac{d\tau}{d\dot{\gamma}}$ is reported for a non-NEWTONian fluid, it must be called "apparent" viscosity.

To calculate the apparent viscosity η_s in the case of OSTWALD–DE-WAELE flow, the logarithm of the flow behavior function is taken. This produces an algebraic equation of a straight line in which the slope is the flow behavior index n, and $\log K_{OW}$ is the intercept. To obtain these parameters, the flow curve is plotted using logarithmic scales. So we have a linear curve with the slope n:

$$\lg \tau = \lg K_{OW} + n \cdot \lg \dot{\gamma} \tag{4.43}$$

We get K_{OW} by substitution in the equation where shear rate is $\dot{\gamma} = 1\ \text{s}^{-1}$.

$$\lg K_{OW} = \lg \tau - n \cdot \lg \cdot \dot{\gamma} \tag{4.44}$$

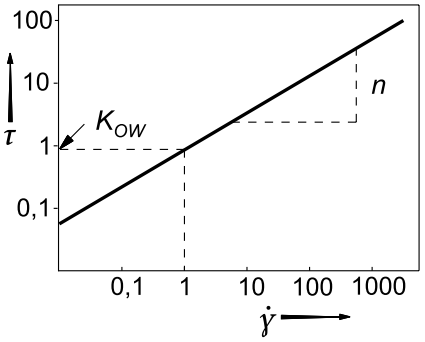

Figure 4.19. Constructing a log–log plot of an Ostwald–De-Waele flow behavior curve

and looking at $\dot{\gamma} = 1\ \mathrm{s}^{-1}$, we have:

$$\lg K_{OW} = \lg \tau \tag{4.45}$$

The evaluation can be done quickly with the help of log–log graph paper to eliminate the need to calculate logarithms, as shown in Figure 4.19.

So, the apparent viscosity is a variable whose value depends on shear rate:

$$\eta_s = \frac{\tau}{\dot{\gamma}} = \frac{K_{OW} \cdot \dot{\gamma}^n}{\dot{\gamma}} = K_{OW} \cdot \dot{\gamma}^{n-1} \tag{4.46}$$

Using equation (4.46) we can calculate the apparent viscosity of our fluid for each shear rate. We only need to know two numerical values for the constant parameters, that are n and K_{OW}, for our material. Table 4.17 shows some examples of these parameters for different food materials.

Table 4.17. Flow behavior indices and consistency coefficients, examples

material	ϑ/°C	K_{OW}/Pa · s^n	n	source
custard	80	7.24	0.36	[115]
gravy	80	2.88	0.39	[115]
tomato juice 12.8% (m/m) dm	32	2.0	0.43	[117]
tomato sauce 25.0% (m/m) dm	32	12.9	0.4	[117]
tomato paste 30.0% (m/m) dm	32	18.7	0.4	[117]
UF concentrate (protein concentrate from cheese whey or whole milk) 1–99% (m/m)	5–50	20–16000	1.13–0.17	[115]
xanthan solution 1% (m/m) in water	N/A	10	0.18	[115]
xanthan solution 0.5% (m/m) in water	N/A	3	0.24	[109]
xanthan solution 0.25% (m/m) in water	N/A	0.4	0.35	[109]
xanthan solution 0.125% (m/m) in water	N/A	0.14	0.5	[109]
pure water	20	0.001	1	[106]

4.3.13 Model Functions for Plastic Fluids

The models best suited to describe plastic flow behavior (those with a yield stress) are the Bingham, Casson, Heinz, Herschel–Bulkley, Schulmann–Haroske–Reher, Tscheuschner and Windhab models (see Table 4.18 and Table 4.19).

In the use of models like these, the model parameters are often given special names. For example, the parameter τ_0 in the Bingham model is given the name Bingham yield stress, and the parameter η of this model is named

Table 4.18. Model functions for plastic fluids, examples

			with $\tau_0 = 0$:
Bingham	$\tau = \tau_0 + \eta \cdot \dot{\gamma}$	τ_0 Bingham yield stress in Pa η Bingham viscosity in Pa · s (plastic viscosity)	$\tau = \eta \cdot \dot{\gamma}$ Newton
Casson	$\tau^{\frac{1}{2}} = \tau_0^{\frac{1}{2}} + (\eta \cdot \dot{\gamma})^{\frac{1}{2}}$	τ_0 Casson yield stress in Pa η Casson viscosity in Pa · s	$\tau = \eta \cdot \dot{\gamma}$ Newton
Heinz	$\tau^{\frac{2}{3}} = \tau_0^{\frac{2}{3}} + (\eta \cdot \dot{\gamma})^{\frac{2}{3}}$	τ_0 Heinz yield stress in Pa η Heinz viscosity in Pa · s	$\tau = \eta \cdot \dot{\gamma}$ Newton
Casson (general)	$\tau^{\frac{1}{n}} = \tau_0^{\frac{1}{n}} + (\eta \cdot \dot{\gamma})^{\frac{1}{n}}$	τ_0 Casson yield stress in Pa η Casson viscosity in Pa · s	$\tau = \eta \cdot \dot{\gamma}$ Newton for $n = 1 \Rightarrow$ Bingham $n = 2 \Rightarrow$ Casson $n = \frac{3}{2} \Rightarrow$ Heinz
Herschel–Bulkley	$\tau = \tau_0 + K \cdot \dot{\gamma}^n$	τ_0 yield stress in Pa K consistency coefficient in Pa · s η flow behavior index	$\tau = K \cdot \dot{\gamma}^n$ Ostwald–de-Waele
Schulmann–Haroske–Reher	$\tau^{\frac{1}{n}} = \tau_0^{\frac{1}{n}} + (K \cdot \dot{\gamma})^{\frac{1}{m}}$	τ_0 yield stress in Pa K consistency coefficient in Pa · s m, n, k constants	$\tau = K' \cdot \dot{\gamma}^k$ Ostwald–de-Waele

Table 4.19. Model functions after Tscheuschner and after Windhab

Tscheuschner	$\tau = \tau_0 + \eta_\infty \cdot \gamma + \eta_{Str1} \cdot \frac{\dot{\gamma}}{\dot{\gamma}_r^n}$	τ_0 yield stress in Pa η_∞ final viscosity in Pa · s $\dot{\gamma}_{Str1} = 1\mathrm{s}^{-1}$ $\dot{\gamma}_r = \frac{\dot{\gamma}}{\dot{\gamma}_{Str1}}$ $\eta_{Str1} = \eta(\dot{\gamma}_{Str1})$
Windhab	$\tau = \tau_0 + \eta_\infty \cdot \dot{\gamma} + (\tau_1 - \tau_0) \cdot \left(1 - e^{-\frac{\dot{\gamma}}{\dot{\gamma}^*}}\right)$	$\dot{\gamma}^* = \dot{\gamma}(\tau^*)$ $\tau^* = \tau_0 + (\tau_1 - \tau_0) \cdot \left(1 - \frac{1}{e}\right)$ τ_1 extrapolated yield stress in Pa

the BINGHAM viscosity. By use of this naming convention, we know to which model the parameter belongs. Otherwise, the parameters per se, would not give any indication as to what model they belonged.

In many of these models that describe flow behavior with a yield stress, the viscosity term η sometimes is called plastic viscosity, and the parameter K often is called consistency coefficient.

For very small yield stress τ_0 the approximation $\tau_0 = 0$ leads to simpler model function (see Table 4.18). So, for $\tau_0 = 0$ the models after BINGHAM, CASSON, and HEINZ, transform into the basic NEWTONian model. In the same way, the models after HERSCHEL–BULKLEY and SCHULMANN–HAROSKE–REHER, for the case where $\tau_0 = 0$ would transform into the OSTWALD–DE-WAELE model.

CASSON's model (the general CASSON's model) represents stronger dependency on the flow behavior index n than other models like BINGHAM, CASSON or HEINZ. In the case of no yield stress, where $\tau_0 = 0$, CASSON's general model will transform into the basic NEWTONian model. The models after BINGHAM, CASSON and HEINZ can be seen as special cases of the CASSON's general model. In the same way, the OSTWALD–DE-WAELE model obviously is a special case of the HERSCHEL–BULKLEY model.

The model function after SCHULMANN–HAROSKE–REHER is a power law function like OSTWALD–DE-WAELE, but with 4 parameters instead of two. Table 4.18 gives an overview of these model functions.

The models after TSCHEUSCHNER and after WINDHAB require using additional parameters (η_{str1} and τ_1) in order to reach a better fit between experimental data and the mathematical curve. For molten chocolate the International Office of Cocoa, Chocolate and Sugar Confectionery (IOCCC) recommended in 1973 CASSON's model for shear rates from 5 to 60 s^{-1}. However, since the year 2000, the WINDHAB model has been recommended for shear rates in the range $\dot{\gamma} = 2 \ldots 50\ s^{-1}$ at $\varphi = 40\,^{\circ}C$:

$$\tau = \tau_0 + \eta_\infty \cdot \dot{\gamma} + (\tau_1 - \tau_0) \cdot \left(1 - e^{-\frac{\dot{\gamma}}{\dot{\gamma}^*}}\right) \tag{4.47}$$

where

$\dot{\gamma}$	shear rate in s^{-1}
τ	shear stress in Pa
η_∞	equilibrium viscosity in Pa · s
$\dot{\gamma}^*$	constant in s^{-1}
τ_1	constant in Pa

The WINDHAB model is often used to describe the flow behavior of liquid chocolate. This model assumes that when liquid chocolate is put under shear, there is a change in structure of the molten chocolate. This can be observed by noting a change (decrease) in viscosity from an initial value (structure of no shear) to a steady state value. Here, the ordering forces ("building structure") and disordering forces ("breaking down structure") are in equilibrium, and the chocolate shows an equilibrium viscosity. When the shear stress is increased further, an equilibrium viscosity is reached which no longer decreases any fur-

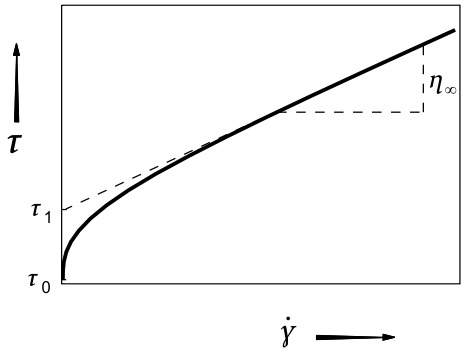

Figure 4.20. Determining the extrapolated yield stress τ_1 for the WINDHAB model

ther, and a final viscosity η_∞ is reached. In the region of this final viscosity η_∞, there is a straight line with a constant slope in the flow curve. This straight line can be extrapolated back to the point of zero shear rate in order to find the intercept. This intercept would give the parameter τ_1 which is a hypothetical yield stress (see Figure 4.20).

In order to find the point on the curve where the final viscosity η_∞ is reached, the WINDHAB model uses a second parameter $\tau^* = \tau(\dot{\gamma}^*)$ indicating that the shear-induced loss of structure is at a maximum when $\dot{\gamma} = \dot{\gamma}^*$ is reached. For shear rates higher than $\dot{\gamma}^*$ the material behaves like a plastic fluid [2], and the BINGHAM equation in Table 4.18 would apply.

$$\tau = \tau_0 + \eta_\infty \cdot \dot{\gamma} + (\tau_1 - \tau_0)\left(1 - \frac{1}{e}\right) \tag{4.48}$$

so

$$\tau = \tau_0 + \eta_\infty \cdot \dot{\gamma} + (\tau_1 - \tau_0) \cdot 0.632 = \tau^* \tag{4.49}$$

It can be seen that the point $(\tau^*, \dot{\gamma}^*)$ is a mathematical point where the difference $(\tau_1 - \tau_0)$ reaches $\left(1 - \frac{1}{e}\right) = 63.2\%$.

4.4 Temperature Dependency of Viscosity

Viscosity of fluids is a consequence of the molecular interactions that take place within the molecular structure of the material. From the study of molecular thermodynamics, we learn that temperature has a direct effect on molecular motion. As temperature increases, molecular motion takes place at a faster rate (molecules move with greater velocity). Therefore, viscosity must also depend on temperature.

When liquids are flowing, there is on-going competition between the forces of molecular attraction causing molecules to come closer together, and those of molecular motion (controlled by temperature) causing molecules to move apart from each other. Therefore, for each temperature, there is a new state of

equilibrium between these forces. The result is that viscosity will decrease with increasing temperature, if no other reactions or transformations are involved (like starch gelatinization). The inverse quantity of viscosity (fluidity) will therefore increase with increasing temperature.

For materials with low viscosity, the temperature dependency can be described mathematically with an ARRHENIUS type of equation:

$$\eta = A \cdot e^{\frac{B}{T}} = A \cdot e^{\frac{E_0}{RT}} \tag{4.50}$$

or

$$\ln \frac{\eta}{\eta_r} = \frac{E_a}{R} \left(\frac{1}{T} - \frac{1}{T_r} \right) \tag{4.51}$$

where

η	dynamic viscosity in Pa · s at T
η_r	dynamic viscosity in Pa · s at T_r
T	temperature in K
T_r	reference temperature in K
E_a	activation energy in J · mol^{-1}
R	universal gas constant in J · K^{-1} · mol^{-1}
A, B, C	constants

On a semi-log graph of viscosity versus inverse absolute temperature will produce a straight line with slope m.

$$m = \frac{E_a}{R} \tag{4.52}$$

In the classic ARRHENIUS equation, the quantity E_A is called activation energy. In the case of viscosity there is no real physical meaning for this quantity because there is no need for "activation" to reach a lower viscosity. Moreover, in food systems where the molar mass is frequently unknown, it would be difficult to measure any molecular activation energy. So, for practical purposes, the slope m is used as a material-specific parameter to transform a viscosity from one temperature (reference temp) to another temperature:

$$\ln \eta = \ln \eta_r + m \cdot \left(\frac{1}{T} - \frac{1}{T_r} \right) \tag{4.53}$$

Recall that the ARRHENIUS concept is an idealized model, and real materials must be tested to see if their behavior can be approximated sufficiently well by this model. In any case, experience has shown that the fit is always better as the difference between the two temperatures T and T_r remains reasonably small.

Example 4.7. Olive oil in the country of growth (at 30 °C) has a viscosity of 58 mPa · s. Estimate the viscosity in a Canadian plant at 18 °C.

ϑ in °C	η in mPa · s
20	86.5
25	71.3
30	58.0

From a $\ln \eta$ versus $\frac{1}{T}$ plot of these data we get a slope (see equation (4.52)) of $\frac{E_A}{R} = 3551.1$ K. Using equation (4.53) yields

$$\ln \eta = \ln 58 + 3551.1\,\mathrm{K} \cdot \left(\frac{1}{291.15\,\mathrm{K}} - \frac{1}{303.15\,\mathrm{K}} \right)$$

$$\ln \eta = 4.06 + 0.483 = 4.543$$

$$\eta = 94\,\mathrm{mPa} \cdot \mathrm{s}$$

Another way to bring the temperature dependency of a liquid into a mathematical function is the use of the VOGEL equation:

$$\ln \eta = \frac{B}{T + C} + A \tag{4.54}$$

or

$$\ln \frac{\eta}{\eta_\mathrm{r}} = B \left(\frac{1}{T + C} - \frac{1}{T_r + C} \right) \tag{4.55}$$

Besides this three-parameter equation, there are over 100 other empirical equations that can be used to estimate values of viscosity at different temperatures (see, e.g. [15]).

4.5 Measurement of Rheological Properties

There is any number of different types of laboratory instrumentation by which to measure rheological properties of materials. Perhaps the most commonly used type of instruments for studying the rheology of liquids are rotational viscometers (or rheometers). They will be described first in this section. Other types of instruments, based on different principles like capillary types and falling sphere type, will be described later.

4.5.1 Rotational Rheometers

All rotational devices consist of a rotating body (rotor) and a nonmoving body (stator). The liquid sample is always placed between the rotor and stator, which causes the sample to experience shear during operation of the instrument. Within the broad category of rotational instruments, the coaxial cylinder system is perhaps most widely used. It consists of a smaller cylinder (bob) within a slightly larger cylinder (cup), such that an annular gap is left between the two cylinders, into which the liquid sample is placed. When the cup is fixed and the bob is rotated, this is called a SEARLE-type coaxial cylinder system. When the cup is rotated around a fixed bob, this is called a COUETTE-type coaxial cylinder system. Figure 4.21 illustrates these two different principles. In Figure 4.22 a SEARLE-type lab rheometer is shown.

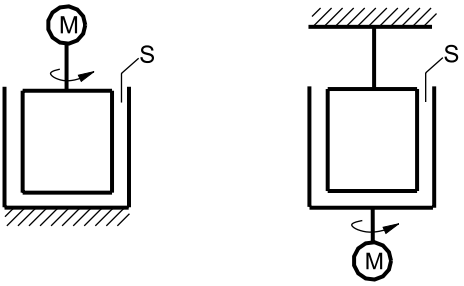

Figure 4.21. Coaxial cylinder systems after SEARLE (left) and COUETTE (right)

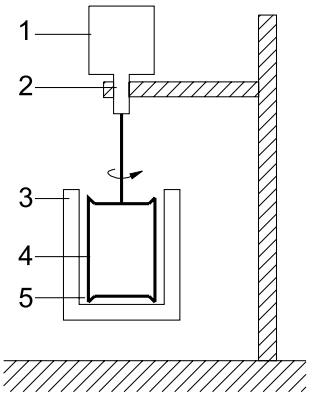

Figure 4.22. Rotational rheometer, SEARLE-type. **1:** motor, **2:** torque meter, **3:** temperature controlled cylindrical beaker, **4:** rotating cylinder (bob), **5:** annular space for liquid sample

These instruments are designed in such a way that it is possible to subject the liquid sample to controlled known conditions of shear stress and shear rate. From the known geometry of the cup and bob, as well as the drive mechanism causing rotation, the torque (force) needed to cause rotation can be converted into shear stress, and resulting speed of rotation can be converted into shear rate. The instrument can be operated over a range of shear rates to produce a set of shear stress–shear rate data points from which a shear stress–shear rate diagram can be constructed. The main advantages of the coaxial cylinder system are a well defined annular space for known geometry of the sample, and ease of filling with sample. For rheometer operation standards see, e.g. [7–9].

Another type of rotational rheometer is based on cone–plate or plate–plate geometry. In a cone-and-plate rheometer, a very shallow cone (conical plate) rotates above a fixed (nonmoving) flat plate, as shown in Figure 4.23. The primary advantage of the cone-and-plate rheometer is that it will function well with highly viscous materials (emulsion, paste, whipped cream), which would otherwise not flow easily into the narrow cylindrical annular space of a coaxial rotational rheometer. These rheometers also deliver the same shear rate all over the shear surface as shown in development of equation (4.91) on p. 163.

In a plate-and-plate rheometer, a flat plate rotates above a fixed (nonmoving) flat plate, as shown in Figure 4.24. These rheometers are also recommended

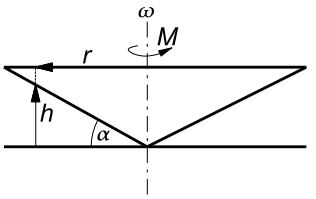

Figure 4.23. Cone–plate geometry

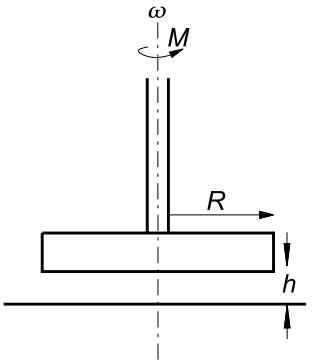

Figure 4.24. Plate–plate geometry

for highly viscous materials (emulsion, paste, whipped cream) which would otherwise not flow easily into the narrow cylindrical annular space of a coaxial rotational rheometer. The plate-and-plate rheometer is particularly useful for suspensions that have relatively large particles (e.g. 50 microns) such that a cone-and-plate would be too narrow for them.

With the Mooney–Ewart geometry, shown in Figure 4.25, an attempt is made to combine the advantages of a coaxial cylindrical system and a cone-and-plate system.

Normally, rotational rheometers allow an independent choice of geometry, as well as the opportunity to vary the speed of the rotor, and by this the shear rate applied to the sample. By electronic measurement of the torque needed to achieve a given angular velocity, the shear stress can be measured. From the rotational speed and the geometry, the shear rate can be calculated, from the torque and the geometry the shear stress can also be calculated. A plot of shear stress over shear rate gives the flow curve, as described previously (Figure 4.11).

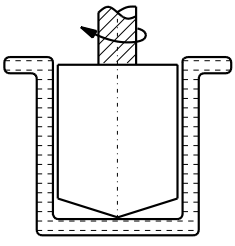

Figure 4.25. Money–Ewart geometry

Modern instruments allow a choice between controlled shear rate mode (CSR) and controlled shear stress mode (CSS). In the CSR mode, the shear rate is programmed and presented to the sample, and the resulting shear stress is measured. In the CSS mode, the shear stress is programmed and presented to the sample, and the resulting shear rate is measured.

Many instruments also allow a means of operation to perform measurements in an oscillating mode. Under an oscillating mode of operation, the rotor reverses direction periodically at a programmed frequency, meaning it rotates back and forth, first clockwise, then counter-clockwise, performing a swinging movement with the sample. This mode of operation is recommended for materials with viscous, as well as elastic properties.

Cylindrical System Geometry

When using coaxial cylindrical rheometers, it is necessary to know the general relationships between the parameters of the rotating cylinder and the rheological quantities of shear stress and shear rate. First let us calculate the shear stress when a cylinder is rotated as shown like in Figure 4.26: With the measured torque M and the area A, the following can be computed:

$$A = 2 \cdot \pi \cdot r \cdot h \tag{4.56}$$

with

$$M = r \cdot F \tag{4.57}$$

Then

$$\tau = \frac{F}{A} = \frac{M}{2 \cdot \pi \cdot r^2 \cdot h} \tag{4.58}$$

Thus, shear stress is calculated as a function of measured torque and bob geometry.

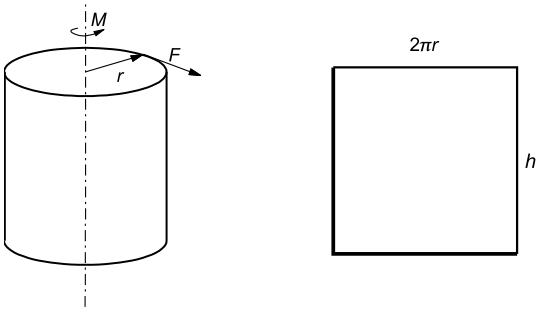

Figure 4.26. Torque M on a rotating cylinder with surface area $2\pi \cdot r \cdot h$ (right)

With

$\dot{\gamma}$	shear rate in s^{-1}
τ	shear stress in Pa
A	area of cylinder surface in m^2
F	tangential force in N
M	torque in Nm

r radius of cylinder in m
h height of cylinder in m
v tangential velocity in $\mathrm{m} \cdot \mathrm{s}^{-1}$
ω rotational velocity in s^{-1}
η viscosity in $\mathrm{Pa} \cdot \mathrm{s}$

the shear rate within the annular sample space is:

$$\frac{\mathrm{d}v}{\mathrm{d}r} = \frac{\mathrm{d}}{\mathrm{d}r}(\omega \cdot r) = \frac{\mathrm{d}\omega}{\mathrm{d}r} \cdot r \tag{4.59}$$

$$\dot{\gamma} = -\frac{\mathrm{d}v}{\mathrm{d}r} = -\frac{\mathrm{d}\omega}{\mathrm{d}r} \cdot r \tag{4.60}$$

That means, at a constant speed of rotation ω, the shear rate $\dot{\gamma}$ depends on the distance r:

From equation (4.58) we know

$$r = \left(\frac{M}{2 \cdot \pi \cdot h}\right)^{1/2} \cdot \tau^{-1/2} \tag{4.61}$$

so,

$$\frac{\mathrm{d}r}{\mathrm{d}\tau} = \left(\frac{M}{2 \cdot \pi \cdot h}\right)^{1/2} \cdot \left(-\frac{1}{2}\right) \cdot \tau^{-3/2} \tag{4.62}$$

With (4.58) it can be said that

$$\frac{\mathrm{d}r}{\mathrm{d}\tau} = \left(\frac{\tau \cdot 2 \cdot \pi \cdot r^2 \cdot h}{2 \cdot \pi \cdot h}\right)^{1/2} \cdot \left(-\frac{1}{2}\right) \cdot \tau^{3/2} \tag{4.63}$$

so

$$\frac{\mathrm{d}r}{\mathrm{d}\tau} = -\frac{r}{2\tau} \tag{4.64}$$

and

$$\frac{\mathrm{d}r}{r} = \frac{\mathrm{d}\tau}{2\tau} \tag{4.65}$$

From (4.60) it follows that, for the $\omega(r)$ function:

$$\mathrm{d}\omega = -\frac{\mathrm{d}r}{r} \cdot f(\tau) = \frac{\mathrm{d}\tau}{2\tau} \cdot f(\tau) \tag{4.66}$$

Integration over the thickness of the annular shear space gives:

$$\int_{\omega_i=\Omega}^{\omega_a=0} \mathrm{d}\omega = \frac{1}{2} \int_{\tau_i}^{\tau_a} f(\tau) \cdot \frac{\mathrm{d}\tau}{\tau} \tag{4.67}$$

$$\Omega = -\frac{1}{2} \int_{\tau_i}^{\tau_a} f(\tau) \cdot \frac{\mathrm{d}\tau}{\tau} \tag{4.68}$$

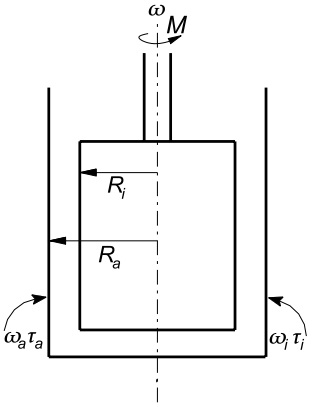

Figure 4.27. Inner cylinder (bob) rotating with torque M in a fixed outer cylinder (cup)

where

τ	shear stress in Pa
R	radius of cylinder in m
ω	angular velocity in s^{-1}
Ω	angular velocity of inner cylinder in s^{-1}
index i	inner cylinder (bob)
index a	outer cylinder (cup)

This is the general function between angular velocity Ω of the inner cylinder (bob) and the resulting shear rate in a SEARLE-type rheometer. The equation can be solved only by substituting the behavior of the fluid $f(\tau)$. To do this we first choose a NEWTONian fluid. After that it will be shown how the equation also works with a OSTWALD–DE-WAELE fluid.

For a Newtonian Fluid

The expression for flow behavior in a NEWTONian fluid:

$$\dot{\gamma} = f(\tau) = \frac{\tau}{\eta} \tag{4.69}$$

So, equation (4.68) becomes:

$$\Omega = -\frac{1}{2}\int_{\tau_i}^{\tau_a} f(\tau)\,\frac{\mathrm{d}\tau}{\tau} = -\frac{1}{2}\int_{\tau_i}^{\tau_a} \frac{\tau}{\eta}\cdot\frac{\mathrm{d}\tau}{\tau} = -\frac{1}{2\eta}\int_{\tau_i}^{\tau_a} \mathrm{d}\tau \tag{4.70}$$

which means:

$$\Omega = \frac{1}{2\eta}\,(\tau_i - \tau_a) \tag{4.71}$$

and with (4.58) we get a term called MARGULES's equation:

$$\Omega = \frac{M}{4\cdot\pi\cdot h\cdot\eta}\left(\frac{1}{R_i^2} - \frac{1}{R_a^2}\right) \tag{4.72}$$

MARGULES' equation provides the relationship between angular velocity Ω of the rotor and the resulting torque M (angular moment) when a NEWTONian fluid with viscosity η is in the annular space between R_i and R_a (see Figure 4.27). It can also be seen that there is linear relationship.

For an Ostwald–De-Waele Fluid

Here in this case, instead of (4.69), we have to introduce the following:

$$\dot{\gamma} = f(\tau) = \left(\frac{\tau}{K_{OW}}\right)^{1/n} \tag{4.73}$$

$$\Omega = -\frac{1}{2}\int_{\tau_i}^{\tau_a} f(\tau)\,\frac{d\tau}{\tau} = -\frac{1}{2}\int_{\tau_i}^{\tau_a}\left(\frac{\tau}{K_{OW}}\right)^{1/n}\frac{d\tau}{\tau} \tag{4.74}$$

So, the rotational speed is:

$$\Omega = \frac{n}{2\cdot {K_{OW}}^{1/n}}\left(\tau_i^{1/n} - \tau_a^{1/n}\right) \tag{4.75}$$

Putting in (4.58) yields

$$\Omega = \frac{n}{2\cdot {K_{OW}}^{1/n}}\left(\left(\frac{M}{2\cdot\pi\cdot h\cdot R_i^2}\right)^{1/n} - \left(\frac{M}{2\cdot\pi\cdot h\cdot R_a^2}\right)^{1/n}\right) \tag{4.76}$$

and therefore:

$$\Omega = \frac{n}{2\cdot {K_{OW}}^{1/n}}\left(\frac{M}{2\cdot\pi\cdot h\cdot R_i^2}\right)^{1/n}\cdot\left(1 - \left(\frac{R_i}{R_a}\right)^{2/n}\right) \tag{4.77}$$

It can be seen that here we have no linear relationship between Ω and angular moment M. The flow behavior index has a decisive role in this relationship. To make further progress we must use an approximation called the "simple shear approximation":

For a small annular space between the cylinders, i.e. $(R_a - R_i) \ll R$ we can treat the system as though the liquid sample were held between two flat surfaces instead of curved cylindrical surfaces. In other words, we are using the plate-and-plate model as described before (see Figure 4.10):

With (4.36) we have:

$$\dot{\gamma}_i = \frac{\Omega\cdot R_i}{R_a - R_i} \tag{4.78}$$

With the abbreviation:

$$\delta = \frac{R_a}{R_i} \tag{4.79}$$

that is

$$\dot{\gamma}_i = \frac{\Omega}{\delta - 1} \tag{4.80}$$

For calculation of shear stress, we use the average between inner and outer radius:

$$\tau = \frac{1}{2}(\tau_a - \tau_i) \tag{4.81}$$

with (4.58) that is

$$\tau = \frac{1}{2}\left(\frac{M}{2 \cdot \pi \cdot h \cdot R_a^2} - \frac{M}{2 \cdot \pi \cdot h \cdot R_i^2}\right) \tag{4.82}$$

so,

$$\tau = \frac{M}{4 \cdot \pi \cdot h}\left(\frac{1 + \delta^2}{R_a^2}\right) \tag{4.83}$$

From this equation, and a measured M, we can derive the shear stress applied to the sample. However, note that the approximation of "simple shear" is valid only for a small annular space. In standard DIN 53019 and ISO 3219, it is recommended that this space be no greater than $\delta = 1.0847$, or it should be at least $\delta \leq 1.2$. Also, another important point that must be made is that all the calculations presented here are valid only under the assumptions that we have laminar flow in the annular cylinder space. Otherwise, errors caused by effects like vortex forming, wall slip etc, that can occur outside the laminar flow regime will have to be addressed [1].

Cone-and-Plate Geometry

Cone-and-plate systems consist of a shallow conical plate which rotates above a fixed flat plate (see Figure 4.23). The shear rate for a sample held in this geometry is:

$$\dot{\gamma} = \frac{\mathrm{d}v}{\mathrm{d}h} \tag{4.84}$$

with

$$v = \omega \cdot r \tag{4.85}$$

and

$$\tan \alpha = \frac{\mathrm{d}h}{\mathrm{d}r} \tag{4.86}$$

Then:

$$\dot{\gamma} = \frac{\omega \cdot dr}{\tan \alpha \cdot dr} = \frac{\omega}{\tan \alpha} \tag{4.87}$$

and with Ω

$$\dot{\gamma} = \frac{\Omega}{\tan \alpha} \tag{4.88}$$

So, the angular moment on the cone is:

$$M = r \cdot F = r \cdot \tau \cdot A \tag{4.89}$$

i.e.

$$M = \int r \cdot \tau \cdot \mathrm{d}A = \int_0^R r \cdot \tau \cdot 2 \cdot \pi \cdot r \cdot \mathrm{d}r = \left| \frac{1}{3} r^3 \cdot 2 \cdot \pi \cdot \tau \right|_0^R = \frac{2}{3} \cdot \pi \cdot R^3 \cdot \tau \tag{4.90}$$

so, we have the shear stress:

$$\tau = \frac{3}{2} \cdot \frac{M}{\pi \cdot R^3} \tag{4.91}$$

We see the shear rate is not dependent on the distance r. This is the most important advantage of a cone-and-plate geometry compared to other geometries, such as cylindrical geometry. So, all parts of the sample experience the same shear stress. There is no average shear stress to be calculated.

If we have an Ostwald–de-Waele fluid in a cone-and-plate rheometer, then (4.41) applies:

$$\frac{3 \cdot M}{2 \cdot \pi \cdot R^3} = K_{OW} \left(\frac{\Omega}{\tan \alpha} \right)^n \tag{4.92}$$

So, a log–log plot of measured M versus angular velocity of the cone Ω provides the flow behavior index n.

In practice, very flat cones are used ($\alpha = 0 \cdots 5^\circ$). Then, the following approximation can be used (see Figure 4.23):

$$\tan \alpha \cong \alpha \tag{4.93}$$

So, the shear rate is simply

$$\dot{\gamma} = \frac{\Omega}{\alpha} \tag{4.94}$$

Plate-and-Plate Geometry

In a plate-and-plate geometry, a round plate rotates above a fixed (nonmoving) plate (see Figure 4.24). The distance between the plates can be adjusted and provides space for the sample. The shear rate here is:

$$\dot{\gamma} = \frac{\mathrm{d}v}{\mathrm{d}h} = \frac{d(\omega \cdot r)}{dh} \tag{4.95}$$

At the outer edge of the rotating plate, this is:

$$\dot{\gamma} = \frac{\omega \cdot R}{h} \tag{4.96}$$

so,

$$\dot{\gamma} = \frac{\Omega \cdot R}{h} \tag{4.97}$$

For the angular moment we can say:

$$M = \int r \cdot \tau \cdot \mathrm{d}A = \int_0^R r \cdot \tau \cdot 2 \cdot \pi \cdot r \cdot \mathrm{d}r = \int_0^R 2 \cdot \pi \cdot r^2 \cdot \tau \cdot \mathrm{d}r \tag{4.98}$$

with

$$r^2 = \left(\frac{\dot{\gamma} \cdot h}{\Omega}\right)^2 \tag{4.99}$$

respectively

$$\mathrm{d}r = \frac{h}{\Omega}\mathrm{d}\dot{\gamma} \tag{4.100}$$

is

$$M = \int_{\dot{\gamma}=0}^{\dot{\gamma}_R} 2 \cdot \pi \cdot \frac{\dot{\gamma}^2 \cdot h^3}{\Omega^3} \cdot \tau \cdot \mathrm{d}\dot{\gamma} \tag{4.101}$$

so,

$$\frac{M}{2 \cdot \pi \cdot R^3} = \frac{1}{(\dot{\gamma}_R)^3} \int_0^{\dot{\gamma}_R} \dot{\gamma}^2 \cdot \tau \cdot \mathrm{d}\dot{\gamma} \tag{4.102}$$

By replacing τ with $f(\dot{\gamma})$ we have

$$\frac{M}{2 \cdot \pi \cdot R^3} = \frac{1}{(\dot{\gamma}_R)^3} \int_0^{\dot{\gamma}_R} \dot{\gamma}^2 \cdot f(\dot{\gamma}) \cdot \mathrm{d}\dot{\gamma} \tag{4.103}$$

By differentiating this equation with respect to $\mathrm{d}\dot{\gamma}_R$, and use of rule of Leibnitz (for the right side of the equation):

$$\dot{\gamma}_R^3 \frac{\mathrm{d}\left(\frac{M}{2 \cdot \pi \cdot R^3}\right)}{\mathrm{d}\dot{\gamma}_R} + \left(\frac{M}{2 \cdot \pi \cdot R^3}\right) \cdot 3 \cdot \dot{\gamma}_R^2 = \dot{\gamma}_R^2 \cdot f(\dot{\gamma}_R) \tag{4.104}$$

For the shear stress at the outer edge we get

$$\tau = f(\dot{\gamma}_R) \tag{4.105}$$

$$\tau = \frac{3M}{2 \cdot \pi \cdot R^3} + \dot{\gamma}_R \frac{\mathrm{d}\left(\frac{M}{2 \cdot \pi \cdot R^3}\right)}{\mathrm{d}\dot{\gamma}_R} \tag{4.106}$$

respectively

$$\tau = \frac{M}{2 \cdot \pi \cdot R^3}\left(3 + \frac{\mathrm{d}\ln M}{\mathrm{d}\ln \dot{\gamma}_R}\right) \tag{4.107}$$

With a Newtonian fluid, this means:

$$\tau = \eta \cdot \dot{\gamma} = \eta \cdot \frac{\Omega \cdot r}{h} \tag{4.108}$$

so

$$M = \int_0^R 2 \cdot \pi \cdot r^3 \cdot \eta \cdot \frac{\Omega}{h} \mathrm{d}r \tag{4.109}$$

$$M = \frac{\pi \cdot \eta \cdot \Omega}{2 \cdot h} \cdot R^4 \tag{4.110}$$

With

$$\dot{\gamma} = \frac{\Omega \cdot R}{h} \tag{4.111}$$

this is simplified to

$$M = \frac{\pi}{2} \cdot \eta \cdot \dot{\gamma} \cdot R^3 \tag{4.112}$$

which means:

$$M = \frac{\pi}{2} \cdot R^3 \cdot \tau \tag{4.113}$$

respectively

$$\tau = \frac{2 \cdot M}{\pi \cdot R^3} \tag{4.114}$$

Because of equation (4.23), this becomes:

$$\frac{2 \cdot M}{\pi \cdot R^3} = \eta \cdot \frac{\Omega \cdot R}{h} \tag{4.115}$$

respectively

$$\eta = \frac{2 \cdot M \cdot h}{\pi \cdot R^4 \cdot \Omega} \tag{4.116}$$

For an Ostwald–de-Waele fluid, it is analogous:

$$\frac{M(3+n)}{2 \cdot \pi \cdot R^3} = K_{OW} \cdot \left(\frac{\Omega \cdot R}{h} \right)^n \tag{4.117}$$

Comparison of Cone-and-Plate System with Plate-and-Plate System

With a cone-and-plate system, the shear rate is the same all over the sample. But, the space width (gap) in which shear occurs is very small for part of the sample.

With a plate-and-plate system, the shear rate is not the same all over the sample. But, the space width h (the gap) is larger and adjustable.

So, for disperse systems like pastes or emulsions with larger particle sizes, the cone-and-plate geometry might be too small for the particles. To overcome this disadvantage, there are truncated cones available. In these truncated cones, the peak of the cone is removed, and particles cannot be damaged by this if the resulting gap is sufficiently large, such as 50 µm. As a rule of thumb, disperse systems with particle sizes up to up to 10 µm can be measured without damage to particles if particle size is no greater than 20% of gap width ($\leq \frac{1}{5}$ gap).

Example 4.8. Calculations with the cone-and-plate geometry
With a cone-and-plate viscometer ($R = 25$ mm, $\alpha = 1^\circ$) at 16.7 RPM and an angular moment of $M = 10\,\text{mN} \cdot \text{m}$ was measured. Calculate the viscosity of the sample.

First we calculate the shear rate:

$$\omega = 2 \cdot \pi \cdot n$$

$$\omega = 2 \cdot \pi \cdot \frac{16.7}{60\,\text{s}} = 1.748\,\text{s}^{-1}$$

$$\dot{\gamma} = \frac{\omega}{\tan \alpha}$$

$$\dot{\gamma} \approx \frac{\omega}{\alpha}$$

$$\dot{\gamma} = \frac{2 \cdot \pi \cdot \frac{16.7}{60\,\text{s}}}{1/360 \cdot 2\pi}$$

$$\dot{\gamma} = \frac{16.7 \cdot 360}{60\,\text{s}}$$

$$\dot{\gamma} = 6 \cdot 16.7\,\text{s}^{-1}$$

$$\dot{\gamma} = 100\,\text{s}^{-1}$$

Second we calculate the shear stress:

$$\tau = \frac{3 \cdot M}{2 \cdot \pi \cdot R^3}$$

$$\tau = \frac{3 \cdot 10 \cdot 10^{-3}\,\text{N} \cdot \text{m}}{2 \cdot \pi \cdot (0.025\,\text{m})^3}$$

$$\tau = \frac{3 \cdot 10^{-3}}{2 \cdot \pi \cdot 2.5^3 \cdot 10^{-6}}\text{Pa}$$

$$\tau = \frac{30 \cdot 10^3}{2 \cdot \pi \cdot 2.5^3}\text{Pa}$$

$$\tau = 305.6\,\text{Pa}$$

Now, we calculate the viscosity:

$$\eta = \frac{\tau}{\dot{\gamma}}$$

$$\eta = \frac{305.6\,\text{Pa}}{100\,\text{s}^{-1}}$$

$$\eta = 3.056\,\text{Pa} \cdot \text{s}$$

Example 4.9. Calculations with plate-and-plate geometry
There is a plate-and-plate system with $H = 1$ mm, $R = 37.5$ mm. Calculate the deformation angle of the sample when the upper plate is rotated by 0.15°.

First we draw a sketch:

The plate is seen from above. The angle seen is α. This shall be 0.15°.

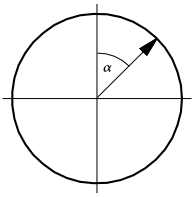

Angle α causes a deformation γ in the sample between the plates.

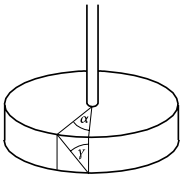

Figure 4.28. Sketch of relationship between sample deformation γ and angle of rotation α.

So, we can calculate:

$$\dot{\gamma} = \frac{\omega \cdot R}{H}$$

$$\gamma = \frac{\varphi \cdot R}{H}$$

$$\gamma = \frac{\frac{0.15}{360} \cdot 2 \cdot \pi \cdot 37.5\,\text{mm}}{1\,\text{mm}}$$

$$\gamma = 0.1 = 10\,\%$$

Example 4.10. Calculation of the viscosity from a plate-and-plate measurement
With a plate-and-plate system ($n = 30$ RPM, $R = 25$ mm, $H = 1$ mm), the moment was measured as $M = 10$ mN · m. Calculate the viscosity of the sample.

First we calculate the shear stress:

$$\tau = \frac{2 \cdot M}{\pi \cdot R^3}$$

$$\tau = \frac{2 \cdot 10 \cdot 10^{-3}\,\mathrm{N \cdot m}}{\pi \cdot (0.025\,\mathrm{m})^3} = 407\,\mathrm{Pa}$$

Second we calculate the shear rate:

$$\dot{\gamma} = \omega \cdot \frac{R}{H}$$

$$\dot{\gamma} = \frac{2 \cdot \pi \cdot n \cdot R}{H}$$

$$\dot{\gamma} = \frac{2 \cdot \pi \cdot \frac{30}{60\,\mathrm{s}} \cdot 0.025}{0.001}$$

$$\dot{\gamma} = 78.5\,\mathrm{s}^{-1}$$

Then the viscosity is:

$$\eta = \frac{\tau}{\dot{\gamma}}$$

$$\eta = \frac{407\,\mathrm{Pa}}{78.5\,\mathrm{s}^{-1}}$$

$$\eta = 5.2\,\mathrm{Pa \cdot s}$$

4.5.2 Measuring Instruments Based on Other Principles

Other types of instruments, based on different principles like capillary tubes and falling sphere type, will be described here, beginning first with capillary tube viscometers.

Capillary Tube Viscometers

In many ways, a capillary tube viscometer may be considered the very simplest of all types of viscometers. It consists simply of short length of tube through which the liquid sample must flow with pressure ports at each end of length through which measurements are to be made. The only requirements are that the tube must be of known length between pressure ports and known diameter (inside dimensions). In addition, it is necessary to be able to measure the pressure difference between the two pressure ports while the sample flows through the tube, and be able to measure flow rate of sample through the tube. The principle of operation is on the basis of the Hagen–Poiseuille law from fluid mechanics. When a liquid sample is flowing through the tube, the frictional forces along the inside tube wall surface causing the pressure drop along the tube length between pressure ports can be related to the shear stress acting on the sample, and the resulting flow rate can be related to the

corresponding shear rate. When the liquid sample is forced to flow at a faster rate (increased shear rate), the measured pressure drop across the ports will be higher (increased shear stress). As always, these relationships only apply when flow through the tube is strictly laminar. These relationships can be described mathematically as follows:

Liquid flow through a capillary tube:

with the force from a pressure

$$F_p = \sigma \cdot A = \Delta p \cdot \pi \cdot r^2 \tag{4.118}$$

and the force of friction

$$F_t = \tau \cdot A \tag{4.12}$$

with the shear stress being

$$\tau = \eta \cdot \dot{\gamma} \tag{4.23}$$

with (4.30) the shear stress is

$$\tau = -\eta \cdot \frac{\mathrm{d}v}{\mathrm{d}r} \tag{4.119}$$

The negative sign is because we have decreasing v with increasing r in a tube.

In equilibrium we have

$$F_P = F_t \tag{4.120}$$

i.e.

$$\Delta p \cdot \pi \cdot r^2 = -\eta \cdot 2\pi \cdot r \cdot l \cdot \frac{\mathrm{d}v}{\mathrm{d}r} \tag{4.121}$$

which means

$$r \cdot \mathrm{d}r = -\frac{2\eta \cdot l}{\Delta p} \cdot \mathrm{d}v \tag{4.122}$$

Integration over r

$$\int_{r=r}^{r=R} r \cdot \mathrm{d}r = -\frac{2\eta \cdot l}{\Delta p} \cdot \int_{v=v(r)}^{v=0} \mathrm{d}v \tag{4.123}$$

provides

$$\frac{1}{2}(R^2 - r^2) = +\frac{2\eta \cdot l}{\Delta p} \cdot v(r) \tag{4.124}$$

since we have a parabolic velocity profile

$$v(r) = \frac{\Delta p}{4\eta \cdot l} \cdot (R^2 - r^2) \tag{4.125}$$

or

$$v(r) = \frac{\Delta p \cdot R^2}{4\eta \cdot l} \cdot \left(1 - \left(\frac{r}{R}\right)^2\right) \tag{4.125}$$

from continuity of mass:

$$\mathrm{d}\dot{V} = v(r) \cdot \mathrm{d}A \tag{4.126}$$

written as

$$\mathrm{d}\dot{V} = v(r) \cdot 2\pi r \cdot \mathrm{d}r \tag{4.127}$$

we get the flow rate

$$\dot{V} = \int_{r=0}^{r=R} \frac{\Delta p \cdot R^2}{4\eta \cdot l} \cdot \left(1 - \left(\frac{r}{R}\right)^2\right) \cdot 2\pi \cdot r \cdot \mathrm{d}r \tag{4.128}$$

or

$$\dot{V} = \int_{r=0}^{r=R} \frac{\Delta p \cdot \pi \cdot R^2}{2\eta \cdot l} \cdot \left(1 - \left(\frac{r}{R}\right)^2\right) \cdot r \cdot \mathrm{d}r \tag{4.129}$$

and the same as

$$\dot{V} = \frac{\Delta p \cdot \pi \cdot R^2}{2\eta \cdot l} \cdot \int_0^R \left(1 - \frac{r^2}{R^2}\right) \cdot r \cdot \mathrm{d}r = \frac{\Delta p \cdot \pi \cdot R^2}{2\eta \cdot l} \cdot \int_0^R \left(r - \frac{r^3}{R^2}\right) \cdot \mathrm{d}r \tag{4.130}$$

Performing the integration

$$\dot{V} = \frac{\Delta p \cdot \pi \cdot R^2}{2\eta \cdot l} \cdot \left|\frac{1}{2}r^2 - \frac{1}{4}\,\frac{r^4}{R^2}\right|_0^R = \frac{\Delta p \cdot \pi \cdot R^2}{2\eta \cdot l} \cdot \left[\frac{1}{2}R^2 - 0 - \frac{1}{4}\,\frac{R^4}{R^2} + 0\right] \tag{4.131}$$

provides

$$\dot{V} = \frac{\Delta p \cdot \pi \cdot R^2}{2\eta \cdot l} \cdot \frac{1}{4}R^2 \tag{4.132}$$

which is called Hagen–Poiseuille's law:

$$\dot{V} = \frac{\Delta p \cdot \pi \cdot R^4}{8\eta \cdot l} \tag{4.133}$$

This is the basis of capillary tube viscometers. Capillary viscosimeter are available in different designs, e.g. after Ubbelohde [46], Cannon-Fenske [47], Ostwald [48,49]. For operation standards, see, e.g. [50,51].

Here

τ	shear stress in Pa
σ	axial stress in Pa
F	force in N
A	area in m^2
η	dynamic viscosity of fluid in $\mathrm{Pa} \cdot \mathrm{s}$
r	radius in m
R	radius of capillary tube in m
l	length of capillary tube in m

v flow velocity in $m \cdot s^{-1}$
$\dot{V}$ volumetric flow rate in $m^3 \cdot s^{-1}$
Δp pressure drop in Pa

Falling Sphere Viscometer

In a falling sphere viscometer, the objective is to measure the terminal velocity of a falling sphere through the liquid sample under study. The scientific principle behind this method is STOKES' law, which states that when a body is allowed to fall freely through a fluid, the increasing velocity will quickly reach a terminal value when the increasing drag force acting upward on the body becomes equal the weight force of the body acting downward. At this point, the falling body comes into static equilibrium, and velocity of free fall ceases to increase, and remains constant at a terminal value (terminal velocity). Since the drag force responsible for this terminal velocity is a function of the fluid viscosity, it is possible to relate the measured velocity of free fall to the viscosity of the fluid sample through which the body falls.

When a body is in free fall through a fluid under laminar flow, equations (3.81)–(3.87) apply. Measuring the velocity of a falling sphere we can calculate the viscosity. From (3.87) can be formed:

$$\eta = \frac{g \cdot d^2(\rho_K - \rho_F)}{18 \cdot v} \tag{4.134}$$

where
η dynamic viscosity of fluid in $Pa \cdot s$
d diameter of spherical particle in m
g gravitational acceleration in $m \cdot s^{-2}$
v particle velocity in $m \cdot s^{-1}$
ρ_K density of particle in $kg \cdot m^{-3}$
ρ_F density of fluid in $kg \cdot m^{-3}$

The falling sphere method is only applicable for determining the viscosity of NEWTONian fluids, since there is no means for adjustment to change shear rate. In most traditional techniques for the use of this method, the falling bodies are usually spheres made of glass, metal or plastic. The HÖPPLER type falling ball viscosimeter is described in [52].

4.5.3 Funnel Flow from Beaker or Cup

Funnel flow from a small beaker or cup is a very simple method for checking viscosity or related flow behavior of a fluid (as well as powders). It consists of a beaker or cup with a funnel outlet at the bottom. The cup is filled with a liquid sample to a designated level, and then the time required for the sample to drain out through the funnel at the bottom is measured by stop watch, as shown in Figure 4.29. This drain time relates to shear rate and the fixed

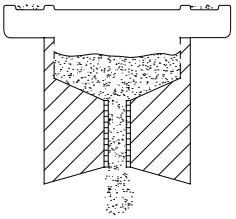

Figure 4.29. Funnel flow device with defined specified tube flow dimensions for calibration of kinematic viscosity as a function of flow time

elevation head of liquid sample in the cup relates to shear stress. Therefore, if the liquid maintains a constant viscosity the drain time will be same every time a check is made. If a change in drain time is detected, then the viscosity has changed. When it is necessary to know the viscosity, a calibration chart of kinematic viscosity versus drain time can be developed so long as the funnel is made of a precisely defined tube section of specified length and diameter, as shown in the figure.

However, most often in industry, no attempt is made to convert these measurements into viscosity (shear stress or shear rate). It is strictly used mostly as an indicator of viscosity for quality control purposes. The technician simply needs to confirm that the time measured to drain the sample agrees with the given specification of drain time for that product. In this type of design, the sample cup with funnel bottom is suspended from a long handle. When a measurement is needed, the technician submerges the sample cup into the liquid, and begins the stop watch at the moment the cup is lifted above the surface. In this way, the quantity of sample is fixed and always the same each time a test is performed. No time is devoted to measuring sample quantities, or judging meniscus levels.

Laboratory instruments for measuring viscosity based on this principle have been developed (Engler, Shell, Ford, Zahn and Redwood). Also, standards for beakers or cups to be used for this method are specified in published standards (BS, DIN, and ASTM). Each different standard will often have its own units based on the type of beaker or cup. For example, there are old units like Engler, Redwood-seconds, and Sayboldt-seconds.

Specifications for beakers that are to be used for determining precise values of viscosity can be found in [53,54]. The flow cup after DIN ISO 2431 has a 20 mm long capillary tube so the shear rate can be calculated using Hagen–Poiseuille's law.

One disadvantage of this funnel flow cup method is that the sample level decreases in the cup while draining. This means the elevation head or hydrostatic pressure that is driving the flow rate is decreasing during the time of a test. Therefore, shear stress is not constant over the time of the experiment, and the method should be used only for Newtonian fluids.

This funnel flow cup method can also be used to characterize flow of powders, by serving as a small-scale hopper in laboratory experiments with powder flow through hoppers [17].

Bostwick Consistometer

The Bostwick consistometer is a somewhat unique instrument used primarily viscosity-related properties of highly viscous liquids like ketchup. In fact, the Bostwick consistometer was developed by scientists working in the tomato processing industry specifically for use with concentrated tomato sauce, tomato puree, tomato paste and ketchup (catsup). In principle, it is a very simple instrument. It consists of an inclined plane and a stop watch. A sample of the viscous liquid is applied at the top of the incline, and the time required for it to flow down to a designated end point near the bottom of the incline is measured. The height of the incline relates to the shear stress applied to the sample, and the time for flow relates to the flow rate or shear rate of the sample. However, no attempt is made to convert these measurements into shear stress or shear rate, since this instrument was not designed for that purpose. It is strictly used as an indicator of viscosity for quality control purposes. The technician simply needs to confirm that the time measured for flow of the sample down the incline agrees with the given specification of flow time for that product.

4.6 Viscoelasticity

Let us focus on soft solid material like a camembert cheese or a marshmallow product. When a material of this type is subjected to a shear stress, it starts to flow very slowly, and will show a slowly increasing deformation γ. If we release the shear stress back to zero again, the deformation will slowly recover to its initial value (see Figure 4.30). An ideal elastic solid material would show an instant deformation γ and instant recovery of that deformation, like the behavior of a Hookean spring. The deformation would follow the rectangular stress profile shown in Figure 4.30. On the other hand, an ideal viscous liquid would flow (continuous deformation), but never recover to its initial zero deformation. Therefore, when we have a material showing both viscous behavior and also elastic behavior, it is called a viscoelastic material [4,5,15].

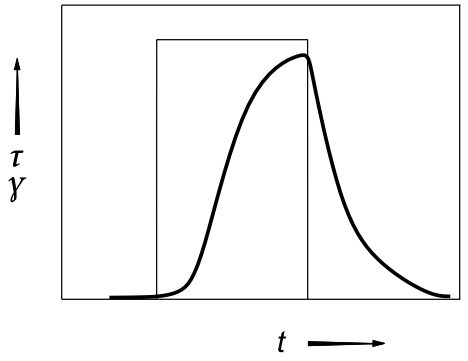

Figure 4.30. Viscoelasticity. In response to a rectangular shear stress signal, a viscoelastic material shows a delayed increase and decrease in the responding deformation.

Recalling the mechanical models used to illustrate ideal rheological behavior (see Section 4.2), we can use a MAXWELL model or a KELVIN model to describe viscoelastic behavior. Both models consist of a spring and dashpot. As explained earlier, the spring represents ideal elastic behavior, and the dashpot represents ideal viscous behavior. The dashpot controls the rate of the elastic behavior, causing it to occur more slowly.

After a shear experiment such as the one shown in Figure 4.30, many real materials may not recover their deformation completely. They may show a permanent deformation, called a set. This behavior occurs because these materials have a yield stress. This causes them to exhibit plastic flow behavior in addition to their elastic and viscous behavior. Sometimes they are called viscoplastic. For terminology and examples see Table 4.20 and Figure 4.31.

If we also consider the rheological behavior of rupture (break down of structure) in a sample of material, then the number of options mixed cases increases further.

Recalling the first few sentences in the introduction to this chapter on rheological properties about the asphalt on the road surface which is solid (elastic) but can show flow behavior (viscous), we should now call this material a viscoelastic material. Let us assume we would obtain data about the rate at which deformation would occur on the road surface by two photographs only:

Table 4.20. Spectrum of rheological terminology for fluids, solids and soft solids

ideal materials:	solid	fluids
name of scientific discipline:	rheology of solids	rheology
main properties:	elasticity, plasticity	viscosity
real materials:	mixed – depending on composition	
real properties:	mixed, e.g. viscoelastic, viscoplastic	

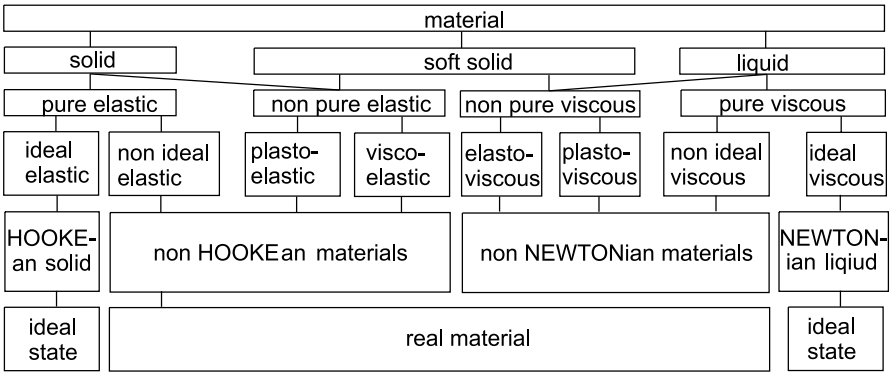

Figure 4.31. Schematic of ideal and nonideal rheological behavior of materials

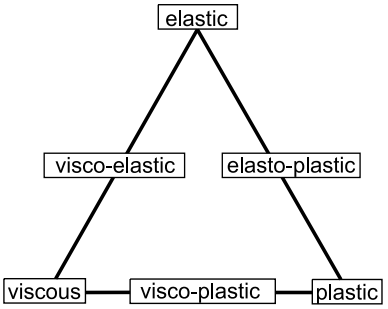

Figure 4.32. Real rheological behavior is found mostly is between these ideal cases

Photo 1 was taken when the road was newly paved, and photo 2 was taken at a later time.

Case 1: Time period between photos 1 and 2 is one day.
Case 2: Time period between photos 1 and 2 is five years.

In case 1, the road will appear to have the same shape in both photos. This observation would lead us to believe that no deformation occurred, and we would assume the asphalt material is a solid. In case 2, the shape of the road will appear noticeably different between photos 1 and 2. Then, we would have to assume the asphalt is a flowing material, like a fluid.

This example illustrates that the time taken between experimental observations of a material may influence the result. This is especially true for viscoelastic materials. To characterize the ratio of flow time and observation interval time, Reiner introduced Deborah's number *De*:

$$De = \frac{\text{characteristic time period of material}}{\text{time period of observation}} \tag{4.135}$$

Deborah's number is the ratio of a characteristic time period for flow of the material and the time period of experimental observation (e.g. one day or five years). The relaxation time constant for a viscoelastic material (see Section 4.6.1) can be used for this characteristic time period of the material.

A predominantly viscous material will have a very short relaxation time. So, Deborah's number *De* will have a low value. Whereas, a predominantly elastic material like glass will have a very long relaxation time, and the Deborah's number *De* will have a high value. Therefore, a large *De* number indicates the material is more elastic than viscous, and a small *De* number indicate the material is more viscous than elastic.

Let us look at the asphalt road surface again. Asphalt under normal climatic conditions will flow very slowly. So, only when we make observations over long periods of time, like 10 years will we observe some flow. *De* is low. If we are not patient enough, and look at the road and look again only 1 hour later, we cannot observe flow. *De* is high. So, high values for Deborah's number indicate predominantly elastic behavior, small values indicate predominantly viscous behavior (Table 4.21 gives the extreme cases). But, recall that a real material is

Table 4.21. DEBORAH's number of ideal materials

ideal elastic material	ideal viscous material
$De = \infty$	$De = 0$

not truly elastic or viscous, but simply "looks like" it is elastic or viscous (or more or less viscoelastic) depending on the type of experiment that is conducted (observation period). Taking this into account we can understand that solids like glaciers, windows glass and also mountains can show flow properties. DEBORAH's number is named after the clairvoyant, DEBORAH, mentioned in Judges 5,5 (The Bible), which says "The mountains flow before the Lord" [1]. HERACLIT's "$\pi\acute{\alpha}\nu\tau\alpha\ \acute{\rho}\varepsilon\tilde{\imath}$" ("everything flows") also fits here perfectly.

4.6.1 Stress Relaxation

Recall that when we conduct a simple stress response test a sudden constant deformation is applied to the sample and the stress necessary for that deformation is measured and recorded. In Figure 4.33 typical stress curves are shown from such a test. An ideal elastic material will respond with a constant stress. An ideal viscous material (free flowing) will respond with a constant zero stress. However, a viscoelastic material will show a decreasing stress over time in the form of an exponential decay. As mentioned earlier, this type of behavior is called stress relaxation. The rate of decrease will depend on the sample material i.e. on the elastic and viscous parts of the sample. To characterize the stress relaxation of the material the relaxation curve can be approximated by an exponential decay (equation (4.141)), and the time constant for this equation can be calculated as follows [10].

With

$$\sigma = \sigma_0 \cdot \mathrm{e}^{-\frac{t}{t_R}} \tag{4.136}$$

when $t = t_R$ then

$$\sigma = \frac{\sigma_0}{\mathrm{e}} \tag{4.137}$$

In other words

$$\sigma = 0.368 \cdot \sigma_0$$

So the relaxation time is that time after which the initial stress has decayed to $\frac{1}{\mathrm{e}} = 36.8\%$.

Here

σ	stress in $\mathrm{N} \cdot \mathrm{m}^{-2}$
σ_0	initial stress in $\mathrm{N} \cdot \mathrm{m}^{-2}$
t	time in s
t_R	relaxation time in s

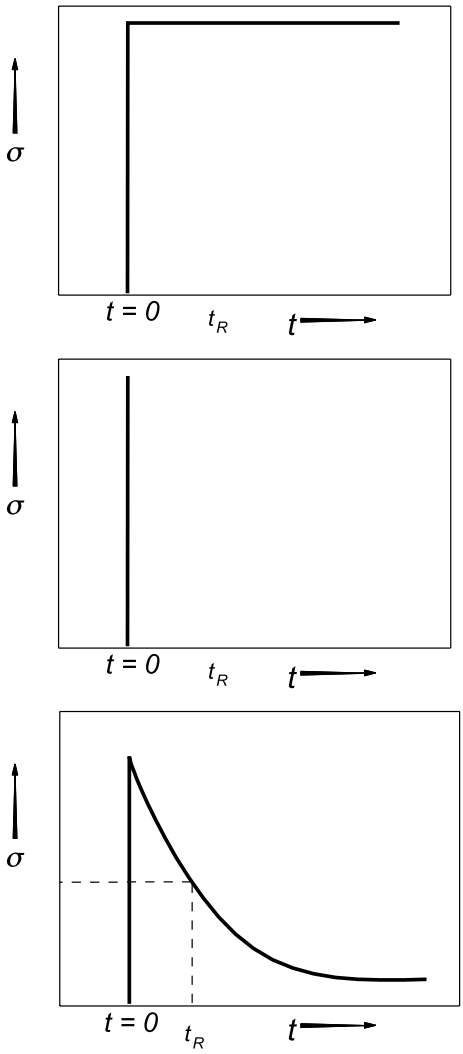

Figure 4.33. Stress response to a sudden constant deformation. Ideal elastic sample (upper picture), ideal viscous sample (middle) and viscoelastic sample (shown at the bottom).

Mathematically, the time constant is the reciprocal of the first order rate constant in a simple first order exponential decay reaction. This means that a semi-log plot of stress over time will produce a straight line with slope equal to the rate constant (when converted from common to natural logarithms). The reciprocal of this rate constant will give the time constant.

To understand viscoelasticity let us imagine a body consisting of molecular elements which are interacting with each other. Strong bonding forces are not released (destroyed) by a mechanical deformation of the body, but they can be elastically deformed on a molecular scale. The energy for elastic deformation of these bindings is recovered when the deformation is released.

On the other hand, weak bonds such as noncovalent bonds like VAN DER WAALS bonds can be opened and closed again later. In this way a permanent deformation (flow) of the material is possible. The opening of the bonds requires energy. After flow has occurred, a new bond of the same type (e.g. VAN DER WAALS) is created, and some bonding energy is released. The bonding energy is not released in the same way it was taken in (mechanical energy) but in the form of bonding heat, instead. So the mechanical energy we had put into the system is not recovered, but is lost in the form of heat. However, any temperature increase caused by this release of heat is normally not perceptible. This conversion of mechanical energy to non-useful heat is called energy dissipation. So, the elastic properties of a material are useful for the purpose of storing and releasing mechanical energy, whereas viscous properties are useful for the purpose of dissipating that energy [6].

Simple Maxwell Model

To illustrate relaxation of a stress we may use the MAXWELL model (see Table 4.8). It consists of a spring and a dashpot to represent the elastic part and the viscous part, respectively (see Figure 4.34). In response to a sudden deformation of the model, the spring will be immediately extended, while the dashpot remains initially motionless. But the extended spring will be applying a steady force on the dashpot in an attempt to recoil. This will cause the dashpot to begin to move in the direction of the spring force at a speed governed by the spring force. As the spring begins to recoil with the moving dashpot, the spring force begins to decrease in accordance with the elastic modulus of the spring (spring constant). As the spring force continues to decrease, the rate at which the dashpot is moving will also decrease, giving rise to the exponential decay

Figure 4.34. MAXWELL model element: spring and dashpot in series.

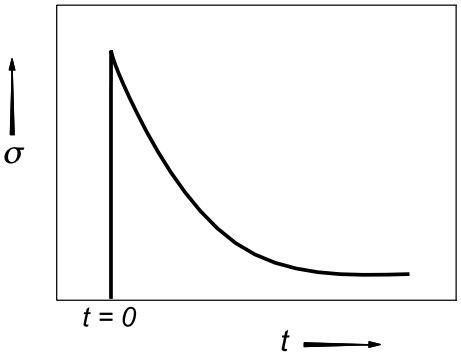

Figure 4.35. Relaxation curve of a MAXWELL model element

rate of the relaxing stress. Figure 4.35 shows the stress versus time curve of produced by this simple MAXWELL model.

The relaxation time constant can be used to characterize the elastic and viscous parts in the behavior of a material. The relaxation time constant of liquids normally is very small. For example, in the case of water it has a magnitude of 10^{-3} s. Solid elastic materials have very large relaxation time constants. Viscoelastic materials have time constants that fall in between, and can have values in the range of $t_R = 10^{-1} \ldots 10^{6}$ s [10].

Problem 4.1. Focus on the MAXWELL element: What will happen when the spring is very weak and the dash pot is very tough, like asphalt? What foods will behave like this?

Problem 4.2. Focus on the MAXWELL element: What will happen when the spring is very strong but the dash pot is very weak, like water? What foods behave like this ?

When we perform a relaxation experiment we have to recall that the time of observation can play a role. Imagine the interior of a soft camembert cheese having a relaxation time constant of $t_R = 2$ h. That means when we deform a camembert cheese sample after two hours the stress will have decayed remarkably, namely to 36.8%. But if we do not observe the stress over the two-hour period and observe for only two seconds instead, we may see no stress decay at all. In that case we would mistakenly call the material "solid, elastic" having no viscous parts in its behavior.

Recalling DEBORAHS number *De* we can use the relaxation time constant to calculate *De* as follows:

$$De = \frac{t_R}{t} \tag{4.138}$$

Large relaxation time constants will give big *De* numbers, which would represent solid or elastic materials with little or nearly no flow. Small relaxation time constants will give small *De* numbers representative of free flowing materials. When *De* is in the magnitude of $10^{-1} \ldots 10^{1}$ we can expect the material to have noticeable viscoelastic properties (Table 4.22).

Table 4.22. Material classification with DEBORAH's number

case	*De* number	material is…
$t > t_R$	$De < 1$	viscous
$t < t_R$	$De > 1$	elastic
$t \approx t_R$	$De \approx 0.1 \cdots 10$	viscoelastic

Stress relaxation tests are tests where stress is recorded over time. There are two choices: Relaxations can provide information about materials with elastic and viscous properties. When a material has mostly viscous properties the flow test is the better choice. Table 4.23 gives an overview.

Table 4.23. Stress test: experimental variations

load	given	recording of	type of test
axial strain	ε	stress over time	relaxations test (Figure 4.35)
shear	γ	shear stress over time	relaxations test (Figure 4.35)
axial strain rate	$\dot{\varepsilon}$	stress over time	flow test (Figure 4.44)
shear rate	$\dot{\gamma}$	shear stress over time	flow test (Figure 4.44)

Generalized Maxwell Model

When a stress relaxation test is performed on many biological materials and the recorded stress over time is plotted on a semi-log graph, we will often observe a nonlinear semi-log curve, which eventually becomes asymptotic to a straight line (or tail) after sufficient time. This means that the behavior cannot be completely described by a single simple exponential decay term, and a more generalized form of the MAXWELL model is needed as shown in Figure 4.36.

The total stress is

$$\sigma = \sigma_1 + \sigma_2 + \sigma_3 + \ldots \sigma_n + \sigma_e \tag{4.139}$$

The generalized MAXWELL model consists of any number n of MAXWELL elements arranged in parallel with each element having its own set of spring constant and time constant. This means that the equation needed to describe the complete behavior will have to consist of a summation series of exponential decay terms, with each term being similar to equation (4.136) but having a different time constant in the exponent and different initial stress as the coefficient (see equation (4.140)). Sometimes the predominant straight line "tail" is observed to be horizontal, meaning that a permanent residual stress remains indefinitely. In this case, one of the terms (the most important for predicting stress after long time) is simply a constant (the residual stress σ_e). The other terms are needed to accurately predict stress at earlier times when the single straight line prediction would be in error. The number of terms required as well as the time constant and initial stress needed in each term can be determined by the method of successive residuals.

$$\sigma(t) = \sigma_{1,0} \cdot e^{-\frac{t}{\tau_1}} + \sigma_{2,0} \cdot e^{-\frac{t}{\tau_2}} + \sigma_{3,0} \cdot e^{-\frac{t}{\tau_3}} + \ldots \sigma_{n,0} \cdot e^{-\frac{t}{\tau_n}} + \sigma_e \tag{4.140}$$

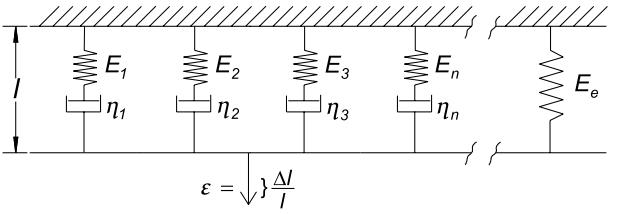

Figure 4.36. Generalized MAXWELL model showing multiple MAXWELL elements arranged in parallel with external spring element representing residual stress

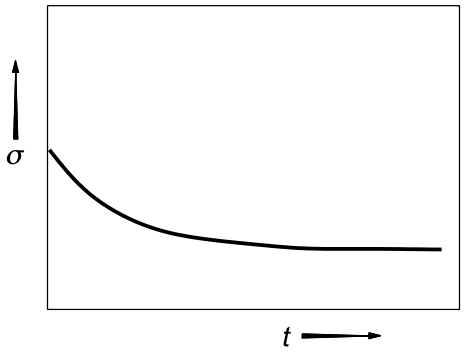

Figure 4.37. Semi-log stress relaxation response curve showing graphical representation of the generalized MAXWELL model

4.6.2 Creep

The corollary to stress relaxation is strain retardation or creep, in which we observe how strain responds over time to a constant applied stress. Modern texture analyzers allow us to put a defined stress on a sample and record of the strain or strain rate over time. This type of test is called a strain response test or a creep test. The experiment can be performed in an axial direction or as a shear motion (see Table 4.24).

Table 4.24. Creep test: experimental variations

load	given	recording of ...
stress	σ	strain ε over time
		strain rate $\dot{\varepsilon}$ over time
shear stress	τ	shear γ over time
		par shear rate $\dot{\gamma}$ over time

Kelvin Model

Just as in the case with stress relaxation, simple creep behavior can be described mathematically by the KELVIN model made up of spring and dashpot in parallel. This is in contrast to MAXWELL model, which consists of spring and dashpot in series. For ease of comparison, both KELVIN and MAXWELL model descriptions of creep and stress relaxation behavior are illustrated side-by-side in Figure 4.38.

When a sudden stress is applied to a sample of material and held constant over time, simple creep behavior is exhibited by the strain beginning to increase rapidly but the rate of increase diminishes over time in the form of an exponential decay. This can be seen in the KELVIN model by noting that the dashpot will control the rate at which the spring can elongate. The initial stress puts maximum force on the dashpot while the spring is fully recoiled

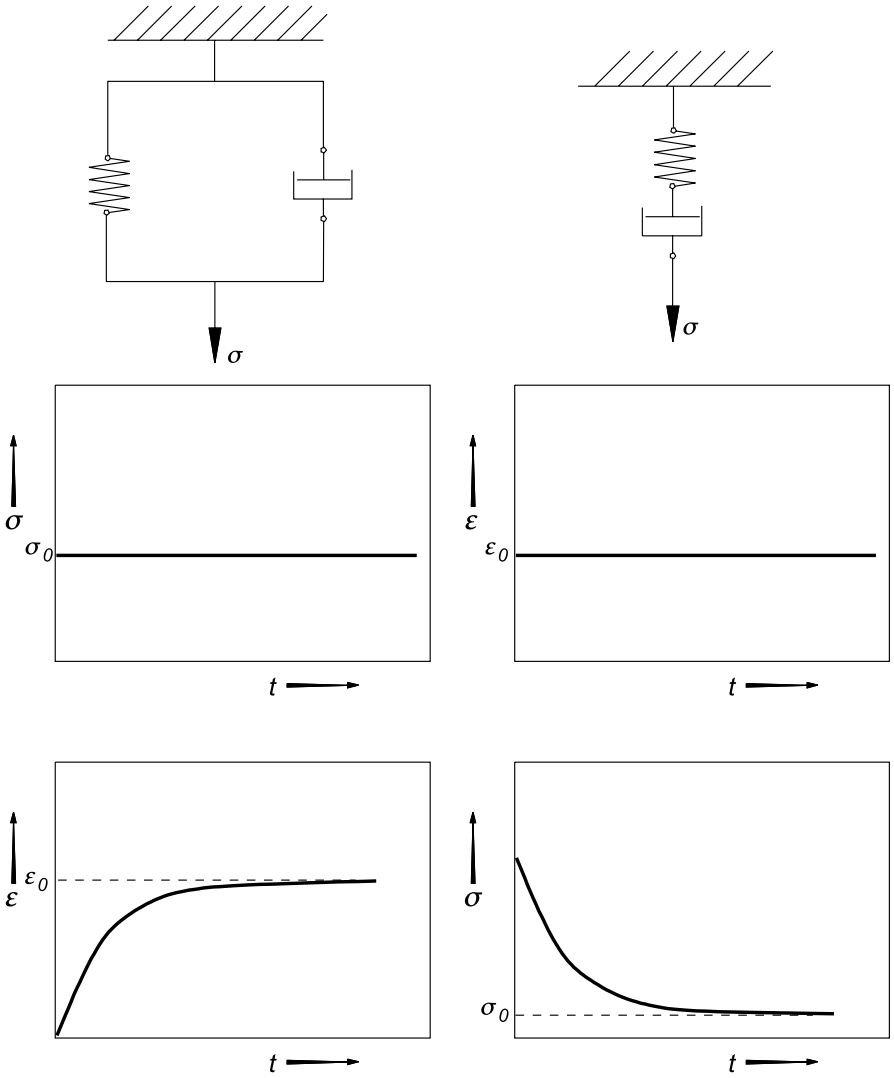

Figure 4.38. KELVIN and MAXWELL models showing creep and stress relaxation. From [133]

(relaxed). Thus, the dashpot will begin to move at maximum speed, allowing the spring to extend along with it. In so doing, the spring begins to take on its share of the applied constant stress with the dashpot being relieved of its share of force. As the force on the dashpot diminishes while being taken up by the spring, the speed of the dashpot likewise diminishes. Thus the rate of strain is retarding exponentially (strain retardation), and is called creep. Again the period of observation time is important. Just as with stress relaxation in soft camembert cheese. If we observe the strain response to an applied stress for just a few seconds with camembert cheeses, we may mistakenly assume the

sample is an elastic solid. However, if we observe the cheese after two days of constant applied stress or load, we will see a broad flat puddle that will clearly reveal the material did flow.

Burger Model

A more realistic creep curve, typical of biological materials, will differ from the simple classical creep described by the KELVIN model in that it will initially show a sudden elastic strain response before beginning the exponential retarding increase that will usually be followed by a perpetual linear increase over time. This type of creep curve and the four-element BURGER model that describes it is shown in Figure 4.39.

The four-element BURGER model consists of the simple KELVIN model sandwiched between an external spring and an external dashpot. The external spring allows the initial elastic deformation to occur in response to the applied stress, while the external dashpot allows for the perpetual linear increase in strain over time so long as the applied stress remains. The mathematical equation for the four-element BURGER model to predict strain as a function of time is given by equation (4.141).

$$\varepsilon(t) = \frac{\sigma_0}{E_0} + \frac{\sigma_0}{E_r} \cdot \left(1 - e^{-\frac{t}{\tau}}\right) + \frac{\sigma_0 \cdot t}{\eta_0} \tag{4.141}$$

where

ε	strain
E_0	YOUNG's modulus of outer spring in Pa
E_r	YOUNG's modulus of inner spring in Pa
t	time in s
τ	relaxation time of inner MAXWELL element in s
σ_0	initial stress in Pa
η_0	viscosity of outer dashpot in Pa · s

In order to determine the numerical values for all of the constants needed in the four-element BURGER model equation, a creep test is performed in which the strain is measured and recorded over time while the applied stress is held constant for a period of time, and then suddenly released part way during the test. When the data are plotted on a strain versus time graph, the resulting curve will appear like that shown in Figure 4.40. As response to a sudden applied stress at $t = 0$, the sample shows a sudden (i.e. elastic) deformation that is then followed by further deformation (viscous) that occurs at an exponentially deceasing rate called creep flow. After sudden release of the stress, the elastic deformation is restored but the viscous deformation remains as a permanent set. The behavior of a viscoelastic sample can be characterized by the amount of elastic to viscous deformation.

The constant first term in the creep equation can be obtained from the initial elastic strain directly from part (1) of the graph. The coefficient in the second term can be obtained from parts (3) and (4) of the graph as the

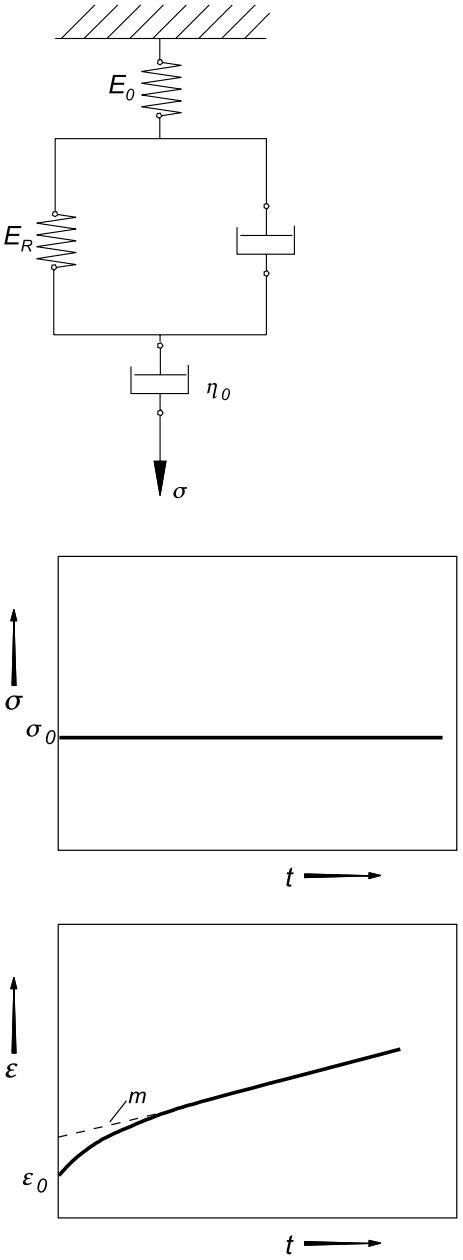

Figure 4.39. Top: Four-element BURGER model explaining complex creep behavior, middle: step function curve showing fixed applied stress, bottom: creep curve showing strain as function of time in response to constant applied stress. From [133]

vertical distance (strain) between the end of the elastic recovery (3) and the horizontal permanent set (4). The exponent needed in the second term is the retardation time constant. This can be obtained by constructing a semi-log plot of the retarding exponential approach between the end of the elastic recovery

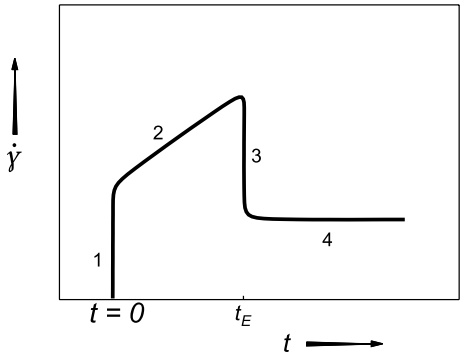

Figure 4.40. Creep test: **1:** elastic deformation, **2:** creep flow, **3:** recovery of initial elastic deformation, **4:** permanent deformation (set)

(3) and the horizontal permanent set (4). This semi-log plot will result in a straight line whose slope will give the time constant. Finally, the coefficient needed in the last term can be found as the slope of the straight line incline in part (2) of the graph. It can also be obtained from the permanent set in part (4) of the graph and the time at which the load was removed (the permanent set was equal to the distance travelled by the external dashpot up to the time of unloading).

4.6.3 Oscillation Testing

Modern rotational viscometers can be operated in a oscillating mode instead of a rotational mode. With an oscillating mode, both viscous and elastic properties of a material can be measured simultaneously. When the amplitude of the oscillation is appropriately chosen so as not to be too high, the sample material can be subjected to an oscillating shear stress without breakage of any molecular structure within the sample.

In the case of a sinusoidal oscillation, the deformation is:

$$\gamma = \gamma_0 \sin \omega t \tag{4.142}$$

So, the shear rate is:

$$\dot{\gamma} = \gamma_0 \cdot \omega \cdot \cos \omega t = \dot{\gamma}_0 \cos \omega t \tag{4.143}$$

$$\dot{\gamma} = \dot{\gamma}_0 \sin(\omega t + 90^\circ) \tag{4.144}$$

This means that, in the case of a sinusoidal function being applied to the deformation of the sample, we will have a cosine function for the resulting shear rate. This means the shear rate function follows the deformation function with a phase shift of 90°. Recalling the difference between an elastic material and a viscous material, we know an elastic material will show a shear stress which is proportional to the shear deformation (strain), and a viscous material will show a shear stress which is proportional to the shear rate. Referring to Section 4.1 it was:

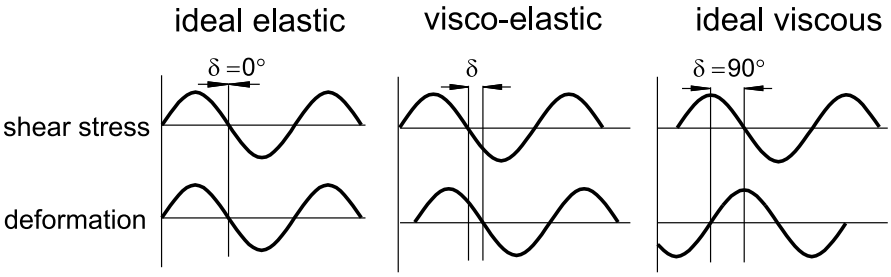

Figure 4.41. Phase shift during an oscillating shear load

For elastic behavior:

$$\tau = G \cdot \gamma \tag{4.15}$$

For ideal viscous behavior:

$$\tau = \eta \cdot \dot{\gamma} \tag{4.23}$$

So, we can say that for an ideal viscous material, the shear stress is following the shear deformation with a phase shift of 90°, whereas an elastic material would have a phase shift of 0°. Real materials will have a phase shift between 0 and 90°. In Figure 4.41 this is illustrated schematically.

Therefore, the measurement of the phase shift δ (see Figure 4.42) between an oscillating excitement and the oscillating response of a material becomes a simple technique by which to characterize materials which are elastic and viscous at the same time (viscoelastic).

There is a mathematical way to describe these behavioral properties with only one quantity. These types of mathematical quantities are called complex numbers, frequently used in the study of electricity and electronics. By using the complex shear modulus, we can characterize both the viscous and the elastic properties of a material by measuring the phase shift δ only.

With the shear modulus from Section 4.1.4, we can write the complex shear modulus:

$$G^* = G' + G'' \tag{4.145}$$

with G' for the elastic component, and G'' for the viscous component. In Table 4.25, additional terms for these components are listed. In Appendix 15.3, the basis of calculus for complex numbers is summarized.

Table 4.25. Terms explaining the complex shear modulus

complex shear modulus	=	"real" shear modulus	+	"imaginary" shear modulus
		storage modulus		loss modulus
		elastic component		viscous component
G^*	=	G'	+	G''

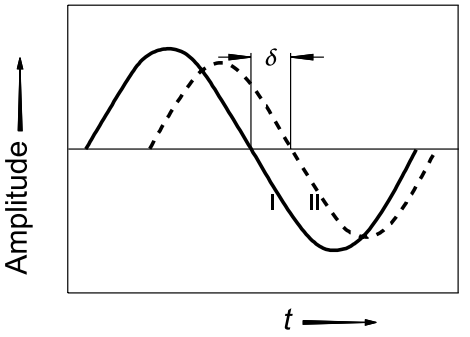

Figure 4.42. Phase shift between deformation γ (I) and shear stress τ (II)

The phase shift then simply is

$$\tan\delta = \frac{G''}{G'} \tag{4.146}$$

To understand the concept of a complex shear modulus, let us focus again on ideal materials. A material with ideal elastic properties (Hookean body, see Section 4.2) would have a viscous component of $G'' = 0$. So the complex shear modulus would be the same as we learned before: $G^* = G' + 0 = G$. Experimentally, we would recognize this case as phase shift $\delta = 0$.

A material with ideal viscous properties (Newtonian body see 4.2) has no elastic component, so $G' = 0$. Therefore, $\tan\delta = \frac{G''}{G'} = \infty$, i.e. $\delta = 90^\circ$. So, here the elastic component is zero and the complex shear modulus consists only of the viscous component, $G' = 0 + G''$.

Again, real materials lie between Hookean and Newtonian materials, and present a phase shift in the range $0 < \delta < 90^\circ$.

Sometimes it is more useful to work with a complex viscosity instead of complex shear modulus. Then it is:

$$\eta^* = \eta' + \eta'' \tag{4.147}$$

The complex viscosity also has two components: The real component characterizes the viscous property and the imaginary component characterizes the elastic component. So here $\delta = 0$ means $\eta^* = \eta' + 0$ i.e. ideal viscous and $\delta = 90^\circ$ means $\eta^* = 0 + \eta''$ i.e. ideal elastic.

Table 4.26. Complex viscosity terms

complex viscosity	=	"real" viscosity	+	"imaginary" viscosity (which is elasticity)
η	=	η'	+	η''

For the phase shift:

$$\tan\delta = \frac{\eta''}{\eta'} \tag{4.148}$$

Referring to equation (4.96) and Figure 4.10 for the relationship between shear strain and shear rate, we can say:

$$\dot{\gamma} = \omega \cdot \gamma \tag{4.149}$$

so the elastic component is

$$G' = \omega \cdot \eta'' \tag{4.150}$$

and the viscous component is

$$G'' = \omega \cdot \eta' \tag{4.151}$$

Besides the shear modulus, there is another quantity to characterize the rheological behavior called compliance J, which is simply the inverse or reciprocal of rigidity (shear modulus). Table 4.27 shows the comparison.

All three quantities can be used as complex numbers, in Figure 4.43 the complementary behavior of J and G and their dependency on phase shift δ is illustrated.

Table 4.27. Comparison of important rheological quantities

$\frac{\tau}{\dot{\gamma}} = \eta$	viscosity
$\frac{\tau}{\gamma} = G$	shear modulus
$\frac{\gamma}{\tau} = J$	compliance

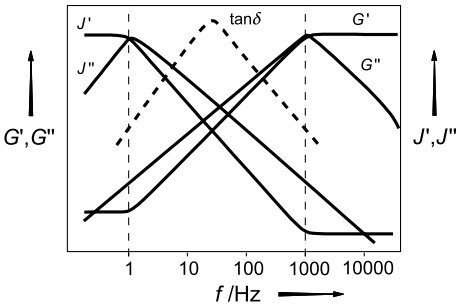

Figure 4.43. Oscillation testing of a viscoelastic material (schematic)

The oscillation test is useful for simultaneous measuring of elastic and viscous properties. Using complex quantities, the material can be characterized very simply by using the phase shift angle only. When an oscillation test of a material is studied under different frequencies ω this is called a frequency sweep. This type of testing allows us to obtain elastic and viscous properties as a function of the frequency with which the material is tested. An overview for

applications in food science and engineering is presented in [42], for standards see [43–45].

Besides rotational rheometers that operate in an oscillation mode, there are instruments available which perform oscillation in an uniaxial or linear direction. They are called dynamic mechanical analysis (DMA) instruments. These types of instruments are closely related to texture testers (which normally do not oscillate).

It is also important to note that all the instrumentation and methodology described up to this point has been based upon the assumption that temperature was always maintained constant and known. Certain types of experiments have been devised specifically for the purpose studying the effect increasing temperature on rheological behavior of materials. Some of these are described in a later chapter (see thermal analysis, Chapter 7).

4.7 Rheology and Texture of Solid Foods

This section will focus on the rheological behavior of what we consider to be primarily solid food materials. We learned earlier that some food and/or biological materials exhibit both solid (elastic) and fluid (viscous) behavior at the same time (i.e. viscoelastic). However, many food materials will behave predominantly as though they were only solid. This simply means they have a very high Deborah's number (*De*), and the solid behavior is the only behavior visible to the consumer. In this section we will introduce both rheological tests that help us understand the scientific principles underlying the behaviors we observe; as well as texture tests, which are more empirical in nature, but help us more easily compare and qualify differences in observed behaviors.

4.7.1 Rheological Tests

Stress Response Test

In this type of test we record the stress over time in response to a constant applied strain. In order to conduct such a test, a given deformation (strain) is applied to the sample and the responding force (stress) is measured and observed over time. Let us assume once again axial deformation and axial stress (it will be the same with shear testing, but most texture testing instruments are commonly used in the axial loading mode). When the sample is a purely elastic solid with no viscous behavior, the response will be an instantaneous stress to a fixed level that remains constant over time. However, when the sample is not purely elastic and exhibits some viscous behavior (able to flow), the initial stress will not remain constant but will decrease (relax) over time at a decreasing rate in the form of an exponential decay. This behavior is known as stress relaxation, and is exhibited by viscoelastic materials, such as soft cheeses

like camembert cheese. The decay of stress over time is exponential, and allows us to calculate the relaxation time constant of the material (see 4.6.1 below).

A stress response test can be carried out easily on sophisticated universal testing machines with electronic load cells. The crosshead is brought down on the sample to apply a fixed predetermined deformation, and the load cell senses the initial stress as well as the exponential decay in stress over time as a smooth curve on a chart recording or stress–time data file. With more free flowing materials on less sophisticated instruments, it is difficult to show any noticeable stress in response to a constant deformation. To be able to measure a stress in these situations, we must apply a continuously increasing deformation to the sample. This is called a flow test, and is described in the following section.

Flow Test

For relatively free flowing materials it is more appropriate to use a flow test instead of a stress response test. In a flow test under axial loading, the deformation is not applied instantaneously, but is gradually increased at a constant rate $\dot{\varepsilon} = \frac{d\varepsilon}{dt}$, and the responding stress is recorded. In Figure 4.44 typical flow test curves are shown. After reaching the yield stress the sample shows constant stress over time for a given rate of axial deformation.

The applied strain rates $\dot{\varepsilon}_1, \dot{\varepsilon}_2, \dot{\varepsilon}_3$ are different rates of deformation, and can represent such different loading characteristics as cutting, biting, and pressing. Note that the yield stress measured (Figure 4.44) can depend on the deformation rate.

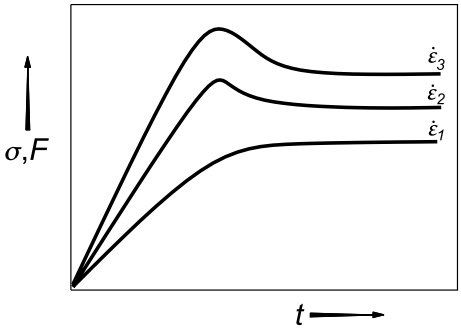

Figure 4.44. Flow test with a viscoelastic material. After reaching the yield stress at a constant rate of axial deformation or strain $\dot{\varepsilon}$ the sample shows a constant stress indicating flow. Measuring the force F instead of a stress σ give a similar diagram.

Breakage or Rupture Tests

If the strain on a sample becomes too large the sample will break. The stress where this occurs can be taken to characterize the maximum strength of the material. Sometimes the breakage of a food is directly related to its quality such

as in the case of crackers or cookies. It is very seldom the case that materials behave like an ideal elastic solid, which suddenly break upon increasing stress. Often before breakage, nonideal behavior such as creep is observed. This nonideal behavior before breakage can make a rupture test more difficult than expected. Therefore, the rate at which stress or strain is applied (stress ramp or strain ramp) can influence the point of breakage or rupture (see Figure 4.49).

Breakage tests can be performed with either axial loading or shear loading, but we will focus on axial loading in this section only. Under axial loading there are only two directions of movement: We can push (compress) the sample until it breaks or we can pull (extend) the sample until breakage occurs (see, e.g. [10]). These are called uniaxial compression and extension tests, respectively. These tests are conducted on material testing machines or texture analyzers that enable us to obtain continuous recordings of force and deformation or stress–strain diagrams like that shown in Figure 4.45.

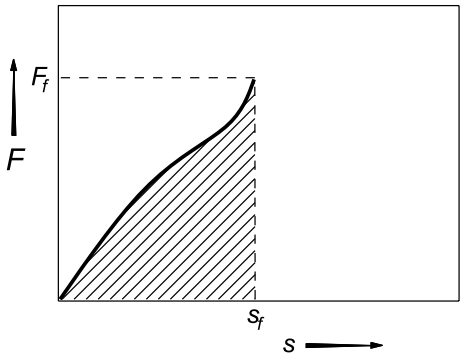

Figure 4.45. Uniaxial compression until breakage of the sample. Stress strain diagram or force length diagram (both have a similar shape). The area below the curve indicates the mechanical energy applied.

We can extract several important material properties from the force–deformation curve shown in Figure 4.45. Note first of all that the raw data are usually provided in terms of force (from the load cell) and deformation (distance of crosshead movement). These are easily converted later to stress and strain from the geometry and dimensions of the sample tested in order to produce a stress–strain diagram. Both diagrams will appear the same and have the same shape, but the scales and units will be different. The important distinction is that force–deformation data give properties that pertain only to the size and shape of sample tested, while stress–strain data give properties that pertain to the material out of which the sample was made (independent of size and shape of sample).

Among the various properties that can be extracted from such diagrams are the following:

- Stiffness: The initial slope of the force–deformation curve can reported as the stiffness of the sample.
- Modulus of elasticity: When the slope is taken from the stress–strain diagram, it can be reported as the modulus of elasticity of the material.
- Rupture point: The force or deformation (or stress or strain) at which the sample breaks (often maximum point on the curve).
- Rupture strength: Stress at which rupture occurs (strength of the material).
- Work energy to breakage or rupture: This is the product of force and deformation under the curve, and represents the work energy absorbed by the sample.
- Toughness of material: Area under the stress–strain diagram up to the point of rupture, expressed in units of work energy per cubic unit of volume of material.

Other properties important to texture measurement can only be obtained from load–unload tests conducted far below the stress and strain levels that might cause rupture. Data from these tests will provide information about the elasticity of a material (ability to recover deformation upon unloading, and its resilience (ability to recover deformation energy upon unloading). Results from one of these types of tests are shown in Figure 4.46.

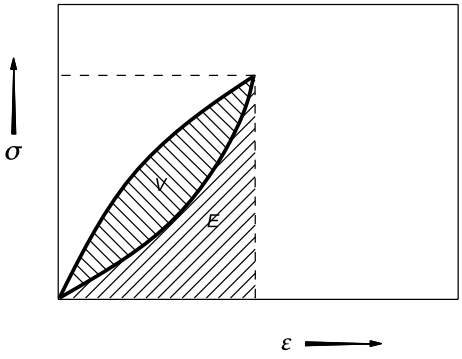

Figure 4.46. Load–unload stress–strain diagram of a material. V is the energy dissipated, E is the resilience

Again, it is important to remember that the rate of loading and unloading may affect the resulting shape of the curves. Therefore, tests should be repeated using different speeds of loading in order to observe differences in results if they exist.

When we make a texture test we may want to set the instrument to a defined strain rate $\dot{\varepsilon} = \frac{\mathrm{d}L}{\mathrm{d}t}$, e.g. 2 millimeters per minute.

So the strain rate based on the initial length L_0 is constant throughout the experiment:

$$\dot{\varepsilon} = \frac{1}{L_0} \cdot \frac{\mathrm{d}L}{\mathrm{d}t} \tag{4.152}$$

This is called strain rate based on Cauchy strain.

From the point of view within the sample, the continued strain occurring during the experiment will appear to the sample as a strain rate of:

$$\dot{\varepsilon} = \frac{1}{L(t)} \cdot \frac{\mathrm{d}L}{\mathrm{d}t} \tag{4.153}$$

with L changing over time

$$L(t) = L_0 - \frac{\mathrm{d}L}{\mathrm{d}t} \cdot t \tag{4.154}$$

The strain then is

$$\dot{\varepsilon} = \frac{1}{L_0 - \frac{\mathrm{d}L}{\mathrm{d}t} \cdot t} \cdot \frac{\mathrm{d}L}{\mathrm{d}t} \tag{4.155}$$

so

$$\dot{\varepsilon} = \frac{1}{L_0 \cdot \frac{\mathrm{d}t}{\mathrm{d}L} - t} \tag{4.156}$$

This is called strain rate based on Hencky strain.

We can see the strain rates based on Cauchy strain and Hencky strain are not the same, and the difference increases with time.

After the experiment we can calculate the strain applied to the sample:

Cauchy strain:

$$\varepsilon = \frac{1}{L_0} \int \frac{\mathrm{d}L}{\mathrm{d}t} \cdot \mathrm{d}t \tag{4.157}$$

$$\varepsilon = \frac{\Delta L}{L_0} \tag{4.158}$$

Hencky strain:

$$\varepsilon = \int_{L_0}^{L} \frac{\mathrm{d}L}{L(t)} \tag{4.159}$$

$$\varepsilon = \ln \frac{L(t)}{L_0} \tag{4.160}$$

For a small strain, Cauchy strain and Hencky strain are approximately the same. For larger extensions or axial compressions there is a noticeable difference, and Hencky's strain should be used (Peleg [11]).

If our instrument does not allow a Hencky strain rate, we should choose small rates of $\frac{\mathrm{d}L}{\mathrm{d}t}$. Then we can approximate the strain rate to be nearly the Cauchy strain rate, and to be constant over time.

With

$$\frac{L_0}{\frac{\mathrm{d}L}{\mathrm{d}t}} \gg t \tag{4.161}$$

we have

$$\dot{\varepsilon} \approx \frac{1}{L_0} \cdot \frac{\mathrm{d}L}{\mathrm{d}t} = \text{const.} \tag{4.162}$$

Sample Geometry

Let us assume we want to measure YOUNG's modulus of a sample with initial length $L_0 = 1$ cm. The linear elastic range of the material ends at a strain of 5%. So the range of movement of our movable testing tool (crosshead) may not exceed the maximum value of $\Delta L = \varepsilon \cdot L_0 = 5\% \cdot 1\text{ cm} = 5 \cdot 10^{-4}$ m. That means our sample must be prepared in a manner that has no "geometric errors" in the magnitude of 10^{-4}m. The term "geometric errors" means the sample is uneven or has nonparallel opposing faces, etc.

When we excessively large strain, the cross-sectional area of the sample can change remarkably, as follows:

$$A(t) = A_0 \cdot \frac{L_0}{L_0 - \Delta L} \tag{4.163}$$

In the case of uniaxial compression experiments and large strains, a lubricant between the sample and platform and crosshead can be helpful to avoid errors caused by friction. For these reasons, uniaxial compression samples with low length to width ratio are most often chosen, because they have the advantage of producing only a small change in A.

When samples are tested under uniaxial tension (pulled instead of pushed), the mounting of the sample becomes more important. Technical materials like synthetic polymers can be prepared in geometrical shapes which are needed for mechanical testing instruments. In texture analysis of food materials, this is often not possible. The type of test and also the type of sample mounting is a consequence of the size and shape of the food material. For example, a strand of spaghetti in an uniaxial extension test will need a totally different mounting from that needed for a cookie or a cracker. If breakage of the sample occurs at the place where the sample was mounted, this can indicate the sample was damaged by the mounting and an alternative method of mounting should be adopted.

Results from an uniaxial extension test on a sample of packaging material are shown in Figure 4.47. These results show stress at breakage σ_f, and maximum strength $\sigma_{\max}$ of the material e.g. for packaging materials or joints in food packages.

Such tests are also very useful for measuring the force needed to open a food package (flexible pouch, paper board boxes, sealed beakers, unscrew jars or bottles). These features are a very important convenience factor for the

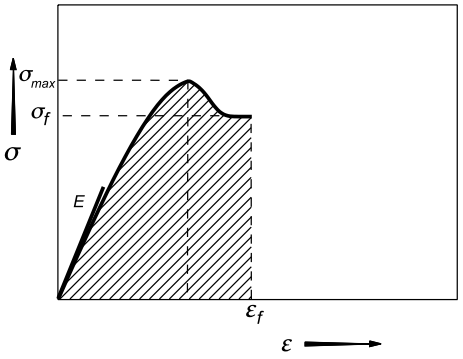

Figure 4.47. Uniaxial extension test until breakage of the sample

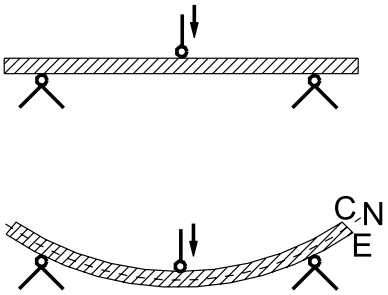

Figure 4.48. Three point test. N neutral axis, C compression axis, E strained axis

consumer. In order to conduct such tests with samples of such unique configuration and geometry, a host of specialized sample holders may be needed, such as shown in Figure 4.48 [12] for samples which are long (large length to width ratio).

The shape of the sample holder can be designed in many ways. Imagine the moving tool in Figure 4.48 being a sharp knife or a steel sphere; then the experiments would be different. Clearly, there are many different possibilities for sample holders that are constantly being developed as needed based upon what information is needed to describe quality as the consumer perceives it and to try to do it better or less expensively than with sensory panels. Examples of the types of questions to ask and types of answers given in a set of guidelines on an approach to design an empirical test are given in the table below:

Table 4.28. Guidelines for empirical tests

question	example of answer
what properties of the material are to be described?	hardness
what physical quantity is assumed to be helpful for this?	breaking stress
what type of load is best used to get a response of this physical quantity?	uniaxial compression
what must be controlled for this test ?	strain rate
are there other experimental parameters to be controlled?	air humidity in the room

Uniaxial strains can also be applied to a sample in an oscillating manner. Instruments doing this are called DMA instrumentation (dynamic mechanical analysis). DMA instruments are similar (in operation and evaluation) to oscillating rheometers, but they are operated in an axial motion instead of a shear motion. Frequency and amplitude of the loading can be controlled. Advantages are speed and smaller sample size [14].

4.7.2 Texture Tests

The term texture stems from the Latin word "textura" for tissue or woven material (textile). According to the Oxford English Dictionary (1989), texture is used for description of the "constitution, structure or substance of anything with regard to its constituents, or formative elements."

In food technology applications, the term 'texture' is used to describe quality attributes of food materials having to do with sensory response to touching or feeling the food material, such as being hard or soft or brittle or crispy. As such, texture can have many different meanings and interpretations. Table 4.29 lists examples of terms that are frequently used to describe the texture of foods.

Table 4.29. Terms used for describing texture of food

hard
soft
stiff
rubbery / gummy
pasty
spreadable
short
crumbly
brittle
tough
sticky
slippery
creamy

Texture of a food material is a matter of organoleptic (sensory) description of the tactile quality attributes of a food. According to ISO 5492, food texture is "all the mechanical, geometrical and surface attributes of a product perceptible by mechanical, tactile and where appropriate visual and auditory receptors" [10].

Therefore, the term "texture" covers organoleptic, sensorial, mechanical and geometric properties of a food. Organoleptic and sensorial sensations can be translated into mechanical, acoustic and visual phenomena. Mechanical characteristics (all that we can "feel") can be divided into tactile and

kinaesthetic characteristics. Tactile characteristics are those feelings experienced during passive touching of the food with fingers, tongue and mouth. Kinaesthetic characteristics are those feelings experienced during breakage and rupture of the material, such as biting, chewing and swallowing. Acoustic phenomena involve the sound and noise that is generated during breakage, biting, chewing, and swallowing. Normally, the acoustic phenomena are complementary to the overall mechanical impressions experienced when biting and chewing on a food material (the experience would be incomplete without the expected accompanying sound). Visual phenomena cover all that can be seen with the eye when unassisted by instrumentation.

According to Escher [18], a description of the total sensory quality of a food must address the following three domains:

- color
- flavor
- texture.

With color being an optical property that can be measured, and flavor being all that belongs to smell and taste, we can try to formulate what texture must be in accordance with Escher's three domains for describing total sensory quality. Therefore, texture must include the following:

- all that can be sensed by tongue and mouth-feel except flavor
- all that can be sensed by eye except color
- all that can be sensed by touch, and
- all that can be sensed by ear.

The advantage of a definition like this is that flavor and color do not belong to texture, and have to be measured separately from texture tests. Table 4.30 shows some examples.

Table 4.30. Texture of food, examples

food	texture terms
cucumber	firm, crisp
steak	tender, juicy, not tough, not chewy
liver	smooth, not hard, not fibrous
apple	crisp, firm, juicy, not soft, not dry, not starchy
ice cream	smooth, creamy, not icy, not gritty
cooky (bakery)	crisp, crunchy, not soft
bread	soft, doughy, hard, crusty
margarine	spreads easily

Textural attributes can also be related to mechanical properties that can be measured and quantified, such as those shown in Table 4.31.

In the field of food technology there has been a never ending quest to find methods for measuring and quantifying the phenomena of texture by the use of instruments instead of reliance on the human judgement and uncertainty

Table 4.31. Relations between texture term and physical properties

texture term	physical property
hard–soft – …	stiffness, modulus of elasticity
elastic, rubbery	elasticity
paste like, plastic, bendable, flowable, dough-like …	flow behavior, viscosity, viscoelasticity
short, crumbly, crunchy, crispy…	breaking or rupture behavior
smeary, creamy, gel like, spreadable	flow behavior, yield stress
grainy, gritty, sand like, icy	particle size and shape and conformity
pulp-like, fibrous	particle shape

of sensory panels. Much of the basics related to texture measurement by the use of materials testing with instruments were published by [5,10,133]. Some of the important principles of instrumental texture testing are described in the following sections.

Test Principles

Test principles can be different depending on the question of interest. For example, a test designed to measure for breakage cannot be the same test as for creaminess or smoothness. Therefore, test principles need to be sorted out by the type of load that must be brought to the sample based on an understanding of the physical characteristics involved and the question to be answered or the intended application of the results. Table 4.32 gives examples of the type of loading appropriate for different test principles.

Table 4.32. Test principles sorted by type of loading

loading	symbol	to be recorded e.g.
axial stress	σ	$\varepsilon, \dot{\varepsilon}$
axial strain	ε	σ
shear stress	τ	$\gamma, \dot{\gamma}$
shear	γ	τ
force	F	s
length	s	F
strain rate	$\dot{s}$	F
shear rate	$\dot{\gamma}$	τ

We can also distinguish between static tests and dynamic tests. In a static test the load is constant over time. In dynamic tests the load can be varied over time such as in a linear ramp or periodic sinusoidal cycling. With periodical variation these tests can also be called oscillation tests (see Section 4.6.3).

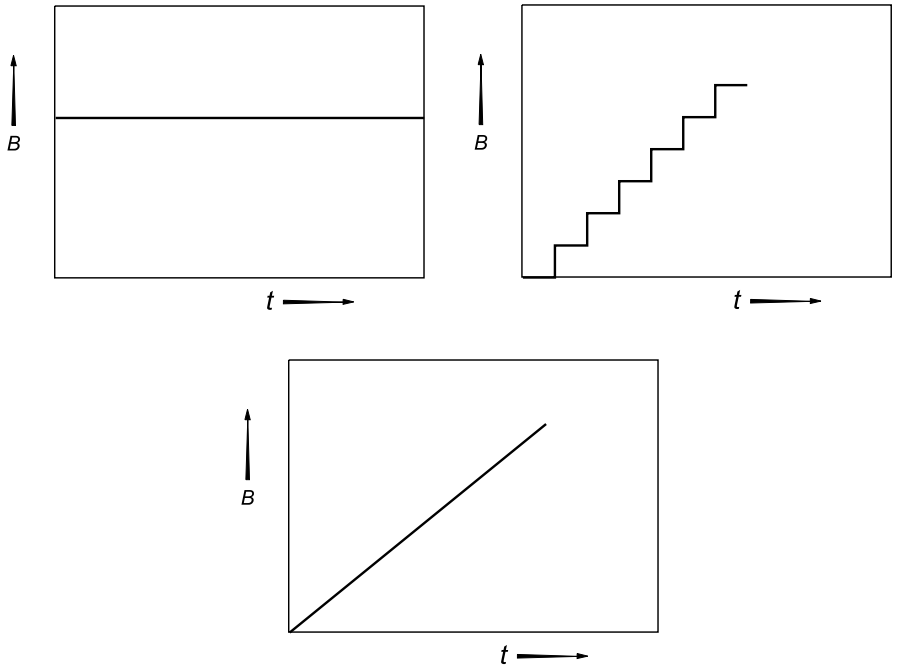

Figure 4.49. Types of tests: Static (upper left diagram) and dynamic (lower diagram) loading of a sample. The stepwise test is in the upper right middle diagram.

Table 4.33. Characteristics of static and dynamic tests

term	typical
static testing	load is constant over time
dynamic testing	load is varied over time
steady state	measured quantity is constant over time
transient state	measured quantity is changing over time

In a "step-wise test," the load is changed over time step-wise fashion, taking on a different value at different time intervals. This type of test can be understood to lie partway between static and the dynamic tests. When there are longer periods of waiting between each step the test can be thought of as a number of consecutive static tests. When the waiting periods are very short (let say approaching zero) we have a dynamic test (Figure 4.49 and Table 4.33).

There is no rule that static testing provides information about an equilibrium state only and dynamic testing about nonequilibrium states. Imagine relaxation of a sample (see Figure 4.30). In that case, the applied strain is constant, but the sample is not yet in equilibrium. Whether a sample is in equilibrium or not is most often a matter of time. So, depending on the type of sample material, we can have very slow step-wise testing (i.e. dynamic) made

up of hundreds of consecutive equilibrium measurements. We saw examples of these types of behaviors when we discussed stress relaxation and strain retardation (creep) in Section 4.6.

Let us consider a simple axial loading test in which we apply a static axial stress onto the sample. Recall that we can apply either axial stress or shear stress, depending on how the sample is loaded. First we will focus on axial stress and strain. A simple elastic material will respond with a one time static deformation. A simple viscous material will respond with a continuous deformation over time that we call flow. Table 4.34 gives an overview.

Table 4.34. Options of response to a stress

static axial stress to a sample can cause...	elastic response	viscous response
i.e.	static strain	dynamic strain, flow
in ideal case	$\sigma = E \cdot \varepsilon$	$\sigma = \eta_E \cdot \dot{\varepsilon}$

where

σ	axial stress in Pa
E	YOUNG's modulus in Pa
ε	strain
$\dot{\varepsilon}$	strain rate in s^{-1}
η_E	viscosity in Pa · s

Experiments of this type with uniaxial strain can be performed easily. In Figure 4.50 the principle of a testing device is shown. It consists of a movable crosshead which allows tools like plates or knifes to move up and down against the sample. A load cell to measure force and a device to record the movement of the crosshead allows the device to produce force versus deformation (length) data from which we can derive stress–strain diagrams.

Various types of testing tools can be mounted on the crosshead depending on what type of experiment is planned to be performed. These various testing

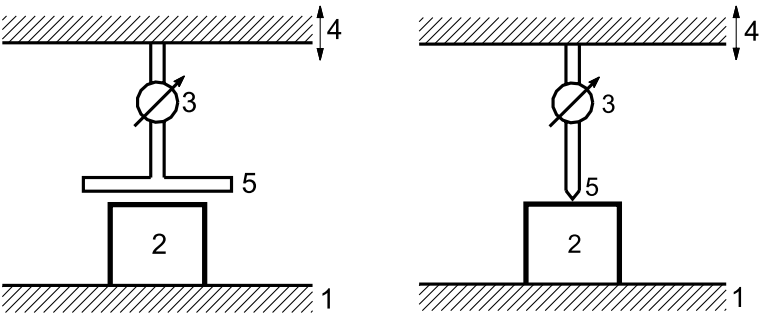

Figure 4.50. Compression test between parallel plates (left). Penetration test or cutting test (right). **1:** platform or workbench,, **2:** sample, **3:** load cell (force meter), **4:** movable crosshead, **5:** individual testing tool

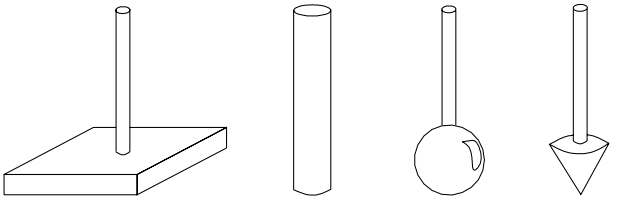

Figure 4.51. Types of testing tools, examples

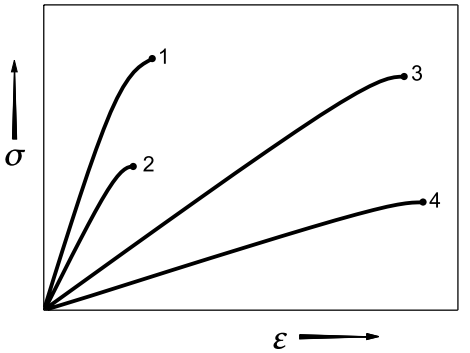

Figure 4.52. Simple stress–strain curves: **1:** hard strong, **2:** hard weak, **3:** soft strong, **4:** soft weak

Table 4.35. Physical meaning of types of curves shown in Figure 4.52

No	type	*E*-modulus	stress a breakage
1	hard strong	large	high
2	hard weak	large	low
3	soft strong	small	high
4	soft weak	small	low

tools may be rectangular or circular flat plates, or protruding bodies with cylindrical, conical or spherical shapes.

All these tools are available with different sizes and shapes (angle), see Figure 4.51. Figure 4.52 gives an illustration of stress–strain curves which can be obtained using a given testing tool, and Table 4.35 lists the types of curves and their physical meaning.

Materials with less ideal behavior can show more complicated stress strain curves. Some examples are shown in Figure 4.53.

Up to this point we have described instrumental testing methods that allow us to study the deformation response of solid materials to applied forces by analysis of stress–strain diagrams. These have been examples of rheological testing methods, based upon scientific principles of physics. However, the rheological behavior of food material is normally perceived as "texture." Characterizing the texture of food by describing and quantifying some type of a texture profile is often understood to involve organoleptic testing (tasting, biting, chewing, etc.). Over the years, a host of various laboratory instruments have been introduced for the purpose of simulating these organoleptic sensa-

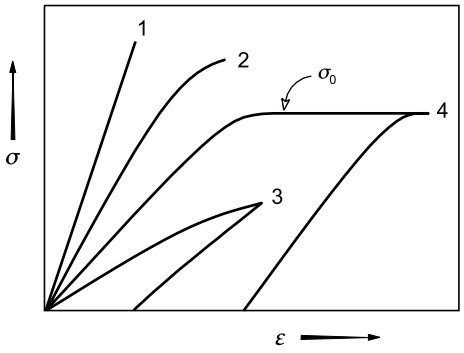

Figure 4.53. Stress strain curves: **1:** ideal elastic, **2:** nonlinear elastic, **3:** nonlinear elastic plastic, **4:** plastic. σ_0 is the yield stress

tions in order to have the possibility for an instrumental method of texture profiling. Some of these are described in the following subsection.

Texture Profile Analysis

Instrumental texture profile analysis (TPA) involves the use of instruments in such a way that a sample can be subjected to a program of repeated loading and unloading over a specified number of time cycles. The objective of such testing is to simulate or imitate the repeated biting or chewing of a food, or the cutting and slicing in an industrial manufacturing process. Instead of pushing or pulling with flat plates or clamps, respectively, the samples are often loaded with sharp blades, or multiple blades or spherical indenters and the like. Figure 4.50 illustrates the use of a testing tool which is driven in and out of the sample at the same speed repeatedly for several times. In this type of test the sample is subjected to a predetermined known series of deformation–time cycles, and the responding force–time (or stress–time) function is measured and recorded.

With the help of appropriate mathematical algorithms, a number of textural terms can be quantified, such as hardness, cohesiveness, springiness, chewiness, gumminess, resilience or fracturability.

Results from such tests are usually compared with results from organoleptic tests carried out by trained sensory test panelists. These panelists are trained persons who use their human sensory perception to detect differences in textural characteristics. The development of instrumental TPA and related test methods with associated computer software is nearly always confirmed or validated by comparison with the performance of trained sensory test panels, and with the purpose of achieving the same level of performance at higher speed and reliability [16].

4.8 Applications

spaghetti: mechanical properties, relaxation test	[19]
alginate gel: stress strain behavior and viscoelasticity	[20]
mustard: yield stress, complex viscosity, thixotropicity	[21]
whey protein concentrate: flow properties	[22]
ketchup: hydrocolloids and flow behavior	[23]
ketchup: BOSTWICK consistometer	[24]
fish: fracture stress and glass transition temperature	[25]
fat: viscoelastic properties	[26]
fruit and vegetable puree products: rheological properties	[27]
mayonnaise: rheological characterization with HERSCHEL–BULKLEY model, viscoelasticity, slippage problems	[28,29]
chocolate drinks: rheological and optical properties	[30]
starch honey systems: dynamical rheological properties	[31]
O/W emulsion: storage modulus and loss modulus	[32]
cheddar cheese: stress relaxation characteristics	[33]
whey protein gel: penetrometric measurement	[34]
apple: POISSON's ratio, *E*-modulus and vicoelasticity	[35,36]
chocolate: texture, storage, polymorphs	[37,38]
cracker snacks: MAXWELL body	[39]
fruits: on-line texture sensing	[40]
powders: flow properties, nonflow problems	[41]
butter: hardness test	[13,55]
wheat flour: rheological properties using farinograph, extensograph, valorigraph, alveograph device	[56–59]
meat-based baby food: dynamic rheology and thermal analysis	[60]
microcrystalline wax: measurement of viscosity	[61]
fresh carrots under high pressure: texture study by microstructural and biochemical approach	[62]

Literature

1. Steffe JF (1996) Rheological Methods in Food Process Engineering, 2nd edN. Freeman Press, East Lansing
2. Mezger Th (2000) Das Rheologie-Handbuch, Vincentz-Verlag, Hannover
3. Wijk RA de, Terpstra MEJ, Janssen AM, Prinz JF(2006) Perceived creaminess of semi-solid foods. Trends in Food Science and Technology 17: 412 –422.
4. Rao MA, (1999) Rheology of Fluids and Semisolid Foods: Principles and Applications. Kluwer Academic, Dordrecht 1999
5. Lucas PW, Prinz JF, Agrawal KR, Bruce IC (2002) Food physics and oral physiology. Food Quality and Preference 13:203–213
6. Ferry JD (1980) Viscoelastic Properties of Polymers. Wiley New York
7. DIN 53019 (2004) Viscosimetry – Measurement of viscosities and flow curves by means of rotation viscometers – Part 1–2, in [101]

8. ASTM D2196 Standard Test Methods for Rheological Properties of Non-Newtonian Materials by Rotational (Brookfield type) Viscometer, in [132]
9. DIN EN ISO 2884 (2006) Paints and varnishes – Determination of viscosity using rotary viscometers – Part 1–2, in [101]
10. Rosenthal AJ (1999) Food Texture, Perception and Measurement. Aspen Publishers, Gaithersburg, p. 89
11. Peleg M, Bagley EB (1982) Physical Properties of Foods. AVI Publishing, Westport
12. van Vliet T, Luyten H (1995) Fracture mechanics of solid foods, in Dickison E (ed) New Physicochemical Techniques for the Characterization of Complex Food Systems. Blackie, Glasgow, pp. 157–176
13. Walstra P (ed.) (1980) Evaluation of the firmness of butter. Int. Dairy Federation Document, Brussels 135:4–11
14. Meyvis TKL, Stubbe BG, Van Steenbergen MJ, Hennink WE, De Smedt SC, Demeester J (2002) A comparison between the use of dynamic mechanical analysis and oscillatory shear rheometry for the characterisation of hydrogels. Intern J Pharmaceutics 244:163–168
15. Kulicke WM (1986) Fließverhalten von Stoffen und Stoffgemischen. Hüthig & Wepf, Basel
16. Bourne MC Food (2002) Texture and Viscosity: Concept and Measurement. Academic Press, San Diego
17. Teunou E, Fitzpatrick JJ, Synnott EC (1999) Characterisation of food powder flowability. J Food Engineering 39:31–37
18. Escher F (1993) in: Jowitt R, Escher F, Hallström B, Meffert HFTh, Spiess WEL, Vos G (1983) Physical Properties of Food. Applied Science Publishers, Barking
19. Cuq B, Gonçalves F, Mas JF, Vareille L, Abecassis J (2003) Effects of moisture content and temperature of spaghetti on their mechanical properties. J Food Engineering 59:51–60
20. Mancini M, Moresi M, Rancini R (1999) Mechanical properties of alginate gels: empirical characterisation. J Food Engineering 39:369–378
21. Juszczak L, Witczak M, Fortuna T, Banys A (2004) Rheological properties of commercial mustards. J Food Engineering 61:209–217.
22. Resch JJ, Daubert CR (2002) Rheological and physicochemical properties of derivatized whey protein concentrate powders. Intern J of Food Properties 5:419
23. Gujral HS, Sharma A, Singh N (2002) Effect of hydrocolloids, storage temperature, and duration on the consistency of tomato ketchup. Intern J of Food Properties 5:179
24. Haley TA, Smith RS (2003) Evaluation of in-line absorption photometry to predict consistency of concentrated tomato products. Lebensmittel Wissenschaft und Technologie 36:159–164
25. Watanabe H, Qi Tang Cun, Toru Suzuki, Mihori T (1996) Fracture stress of fish meat and the glass transition. J Food Engineering 29:317–327
26. Shellhammer TH, Rumsey TR, Krochta JM (1997) Viscoelastic properties of edible lipids. J Food Engineering 33:305–320
27. Krokida M, Maroulis Z, Saravacos G (2001) Rheological properties of fluid fruit and vegetable puree products: compilation of literature data. Intern J of Food Properties 4:179
28. Ma L, Barbosa-Cánovas GV (1995) Rheological characterization of mayonnaise. Part I: Slippage at different oil and xanthan gum concentrations. J Food Engineering 25:397–408
29. Ma L, Barbosa-Cánovas GV (1995) Rheological characterization of mayonnaise. part II: flow and viscoelastic properties at different oil and xanthan gum concentrations. J Food Engineering 25:409–425

30. Mario Yanes LD, Costell E (2002) Rheological and optical properties of commercial chocolate milk beverages. J Food Engineering 51:229–234
31. Sopade PA, Halley PJ, Junming LL (2004) Gelatinization of starch in mixtures of sugars. I. Dynamic rheological properties and behaviors of starch–honey systems. J Food Engineering, 61:439–448
32. Rose Ch (1999) Stabilitätsbeurteilung von O/W-Cremes auf Basis der wasserhaltigen hydrophilen Salbe DAB 1996. Dissertation, Technische Universität Braunschweig
33. Venugopal V, Muthukumarappan K (2001) Stress relaxation characteristics of cheddar cheese. Intern J Food Properties 4:469
34. Kessler HG (1996) Technologische Beeinflussung funktioneller Eigenschaften von Molkenproteinen zur Gestaltung von Prozessen und Produkten. Proc. 54. Diskussionstagung FEI, Bonn p. 18–41
35. Grotte M, Duprat F, Piétri E, Loonis D (2002) Young's modulus, Poisson's ratio, and Lame's coefficients of golden delicious apple. Intern J Food Properties 5:333
36. Lewicki PP, Lukaszuk A (2000) Effect of osmotic dewatering on rheological properties of apple subjected to convective drying. J Food Engineering 45:119–126
37. Schantz B, Linke L (2001) Messmethoden für Erstarrung und Kontraktion. Zucker- und Süßwarenwirtschaft 54(12):15–17
38. Ali A, Selamat J, Che Man YB, Suria AM (2001) Effect of storage temperature on texture, polymorphic structure, bloom formation and sensory attributes of filled dark chocolate. Food Chemistry 72:491–497
39. Kim MH, Okos MR (1999) Some physical, mechanical, and transport properties of crackers related to the checking phenomenon. J Food Engineering 40:189–198
40. García-Ramos FJ, Ortiz-Cañavate J, Ruiz-Altisent M, Díez J, Flores L, Homer I, Chávez JM (2003) Development and implementation of an on-line impact sensor for firmness sensing of fruits. J Food Engineering 58:53–57
41. Adhikari B, Howes T, Bhandari B, Truong V (2001) Stickiness in foods: a review of mechanisms and test methods. Int J Food Properties 4:1
42. Gunasekaran S, Ak MM (2000) Dynamic oscillatory shear testing of foods – selected applications. Trends in Food Science and Technology 11:115–127
43. ASTM D7271 Standard Test Method for Viscoelastic Properties of Paste Ink Vehicle Using an Oscillatory Rheometer, in [132]
44. DIN EN 14770 (2006) Bitumen and bituminous binders – Determination of complex shear modulus and phase angle – Dynamic Shear Rheometer, in [101]
45. ISO 6721-10 (1999) Plastics – Determination of dynamic mechanical properties – Part 10: Complex shear viscosity using a parallel-plate oscillatory rheometer, in [101]
46. DIN 51562 (1999) Viscometry – Measurement of kinematic viscosity by means of the Ubbelohde viscometer, in [101]
47. DIN 51336 (1977) Testing of mineral oil hydrocarbons; measurement of kinematic viscosity by means of the Cannon–Fenske viscometer, in [101]
48. ISO 3105 (1994) Glass capillary kinematic viscometers – Specifications and operating instructions, in [101]
49. ASTM D 446 (2006) Standard Specifications and Operating Instructions for Glass Capillary Kinematic Viscometers, in [132]
50. ASTM D445 Standard Test Method for Kinematic Viscosity of Transparent and Opaque Liquids (and Calculation of Dynamic Viscosity), in [132]
51. ISO 1628 (1999) Plastics – Determination of the viscosity of polymers in dilute solution using capillary viscometers, in [101]
52. DIN EN ISO 12058 (2002) Plastics – Determination of viscosity using a falling-ball viscometer, in [101]

53. DIN EN ISO 2431 (1996) Paints and varnishes – Determination of flow time by use of flow cups, in [101]
54. ASTM D 5125 (1997) Standard Test Method for Viscosity of Paints and Related Materials by ISO Flow Cup, in [132]
55. DIN 10331 (1996) Determination of the hardness of butter, in [101]
56. ISO 5530-1 (1997) Wheat flour – Physical characteristics of doughs – Part 1: Determination of water absorption and rheological properties using a farinograph, see [101]
57. ISO 5530-2 (1997) Wheat flour – Physical characteristics of doughs – Part 2: Determination of rheological properties using an extensograph, see [101]
58. ISO 5530-3 (1988) Wheat flour; physical characteristics of doughs; part 3: determination of water absorption and rheological properties using a valorigraph, see [101]
59. BS ISO 5530-4 (2002) Wheat flour (Triticum aestivum L.) – Physical characteristics of doughs – Determination of rheological properties using an alveograph, see [101
60. Jasim Ahmed and Hosahalli S. Ramaswamy (2007) Dynamic rheology and thermal transitions in meat-based strained baby foods. J Food Engineering 78:1274–1284
61. LFGB method L57.12.15-1, micrcrystalline waxes – measurement of viscosity, in [100]
62. Ximenita I. Trejo Araya, Hendrickx M, Verlinden BE, Van Buggenhout S, Smale NJ, Stewart C, Mawson AJ (2007) Understanding texture changes of high pressure processed fresh carrots: A microstructural and biochemical approach. J Food Engineering 80:873–884

5 Interfacial Phenomena

Interfacial phenomena are behaviors that occur at the interface or boundary surface between a suspended particle and the continuous phase material in which it is suspended. For this reason, interfacial phenomena are almost always associated with disperse systems. Recall from Chapter 3 that disperse systems consist of discrete particle phases surrounded by a continuous phase medium. The particles can be in the solid, liquid or gaseous phase; and the continuous phase medium can also be solid, liquid or gas. Thus, disperse systems can exist in any one of nine different combinations of particle phase and continuous phase. Some examples of cases where interfaces can be formed are given in Table 5.1.

The key feature of any disperse system is that the two phases cannot be soluble (or miscible) with each other. They must be immiscible, meaning they are incapable of dissolving in each other to form a solution. For example, if we dissolve a small amount of salt or sugar crystals in a glass of water, the crystals disappear, and we have a clear (miscible) solution. The same would be true of mixing alcohol in water. Although two different substances are being mixed together in these examples, the resulting mixtures remain as single phase systems (miscible solutions). They do not have two separate phases. Thus, no interface is formed, and no interfacial phenomena occur.

On the other hand, if we try to mix salad oil (or any oil) in a glass of water, the oil will not mix or dissolve in the water. The oil will separate into small droplets (particle phase) that remain suspended and visible in the continuous water phase. This is an example of a two-phase disperse system. In this type of system, an interface exists between the surface of each droplet (particle phase) and the surrounding liquid (continuous phase) in contact with the particle surface. The various reactions and behaviors that can take place at these types of interfaces are the phenomena to be studied in this chapter.

Table 5.1. Examples of cases where interfaces are formed (based on three aggregate states)

fluid–fluid interfaces		solid–fluid/solid interfaces	
liquid–gas	e.g. beer – CO_2	solid–gaseous	e.g. powders, grains (in air)
liquid–liquid	e.g. water–oil	solid–liquid	e.g. sugar–oil
gas–liquid	e.g. whipped cream, foam on beer	solid–solid	e.g. glass–plastic (acrylics)

When either one of the phases in a two-phase disperse system is a solid (solid–gas, solid–liquid, solid–solid), the interfaces at the boundary surfaces between particle phase and continuous phase are considered to be rigid interfaces (nonflexible). Rigid interfaces of this type were discussed earlier in the chapters on water activity and geometrical properties about size and shape of disperse systems. In this chapter, we will focus on interfaces between only fluids (gas–liquid), in which the boundary surface between particle phase and continuous phase involves flexible interfaces (nonrigid). These are called fluid interfaces.

Molecules within the interior of the particle or continuous phase material are surrounded by a microenvironment made up of similar neighboring molecules with similar properties. This is different from the microenvironment surrounding molecules on the particle surface at an interface between the two material phases, where their neighbors may be different molecules with different properties. For this reason, molecules at an interface will have different properties from those within the interior material of either phase, such as vapor pressure. Sometimes the region at the interface is called the interfacial phase [1]. Recall from Chapter 1 on water activity, that when water vapor molecules are adsorbed onto a solid food surface, the water molecules accumulating at the solid/liquid interface are in a liquid state, but they do not behave like normal liquid water because they are bound at the interface. In this example, the interface (and the situation of molecular binding at the interface) plays an important role in governing the physical properties of the solid material [2].

More dramatic examples of how interfacial phenomena affect physical properties of materials are when bipolar molecules of surfactants and emulsifiers are adsorbed on interfaces. They can totally change the behavior of the two-phase material to which they are added, such as when soap or detergent (surfactant) is added to suspended particles in water to get a permanent miscible disperse gas and liquid system (foam), or when an emulsifier like lecithin is added to an oil and water disperse system to get a permanent miscible emulsion (mayonnaise). These complex situations occurring at the interface between the surfaces of both phases can be characterized by the forces involved in interfacial tension, more commonly called "surface tension" in the cases of solid–gas and liquid–gas interfaces.

5.1 Interfacial Surface Tension

Figure 5.1 illustrates the different microenvironments surrounding molecules on the surface at an interface, and those deep within the interior of a material. A molecule *M* in the interior of the material has neighbors all of the same nature. So, forces of attraction and repulsion are the same in all directions, and the net force acting on the molecule is zero. However, a molecule at the interface will be surrounded by different neighboring molecules at the surface with lesser

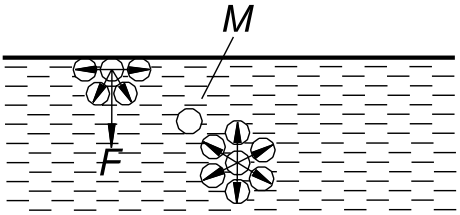

Figure 5.1. Intermolecular forces at an interface. A molecule M is driven inward away from the interface by the resultant intermolecular force F (surface tension)

attracting forces, like gases. In this case, the net force will not be zero, but will be in the direction into the interior of the phase of interest. Therefore, in order to attract a molecule from the interior to an interface at the surface, this net force acting inward needs to be overcome. As a consequence, the molecules at the interface have a higher energy level than molecules within the interior of the material.

This is the reason why altering conditions at an interface (or a surface) requires input of work or energy, such as in making foams or emulsions. This is also the reason why materials try to minimize the available surface area at their interfaces (minimize the energy required). Liquid droplets take the form of an enclosed volume with minimal surface area (spherical shape). Solids cannot do this, so they are not always in a spherical shape. In that case we characterize their shape with form factors (see Section 3.1.6), which are normally not needed for liquids. Although the interfacial energy requirement is a minimum for spherical droplets, sometimes liquid droplets are not spherical because of other forces acting them, such as falling rain drops are not spheres because of gravimetric weight, drag, and inertia forces acting on them simultaneously.

Recall that in order to attract a molecule from the interior to an interface at the surface, the net force acting inward (surface tension) needs to be overcome. This is illustrated as work energy in Figure 5.2. In order to create an additional segment of interface $\mathrm{d}A = s \cdot \mathrm{d}b$, we have to move the piston rod against this force F by distance $\mathrm{d}b$. This is an element of work energy (force multiplied by distance, or $\mathrm{d}E = F \cdot \mathrm{d}B$). The energy divided by the newly created area dA is called specific interfacial energy σ (specific with respect to a unit of area, not mass).

Thus:

$$\sigma = \lim_{\Delta A \to 0} \frac{\Delta E}{\Delta A} = \frac{\mathrm{d}E}{\mathrm{d}A} \tag{5.1}$$

$$\sigma = \frac{F \cdot \mathrm{d}b}{s \cdot \mathrm{d}b} = \frac{F}{s} \tag{5.2}$$

where

F	interfacial force in N
A	area in m^2
σ	specific interface energy in $\mathrm{N} \cdot \mathrm{m}^{-1}$
$\mathrm{d}b$	length in m
s	width in m

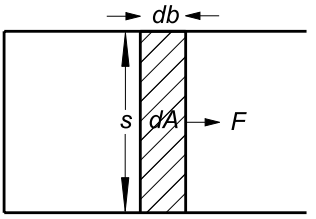

Figure 5.2. Creating an element of interface dA

The SI units are: $\frac{\mathrm{J}}{\mathrm{m}^2} = \frac{\mathrm{N} \cdot \mathrm{m}}{\mathrm{m}^2} = \frac{\mathrm{N}}{\mathrm{m}}$

The specific interfacial energy σ is also called interfacial stress in the case of surface tension with gases, and is not to be confused with the type of stress (axial or shear) discussed in the chapter on rheology.

So in the engineering design of systems or methods to produce or enlarge an interfacial area, the energy needed can be calculated by:

$$\mathrm{d}E = \sigma \cdot \mathrm{d}A \tag{5.3}$$

or

$$\Delta E = \sigma \cdot \Delta A \tag{5.4}$$

It is evident that lowering the specific interfacial energy σ would decrease the total energy needed to achieve the new system with the larger interfacial area, and it will be more stable [1,2].

5.1.1 Curved (Convex / Concave) Interfaces

When a beaker is overfilled with water, a curved interface is formed at the top surface, and the water reaches a slightly higher level than the rim of the beaker. It looks as though an invisible thin skin would retain the water at the top of the beaker. The reason for this "skin" is what we call "surface tension," and is a result of the interfacial energy discussed previously. This phenomenon is also the reason why the molecules in the inner volume are exposed to a slight pressure which would not be there without that "skin." This pressure is called capillary pressure.

Assume we wish to slightly enlarge a small liquid droplet (increase its volume), as shown in Figure 5.3. An incremental amount of work energy is needed by applying pressure to increase V by dV. This incremental work can be expressed as $\mathrm{d}W = -p \cdot \mathrm{d}V$. Since increasing the volume requires work to flow out of the system, it must be mathematically negative. This type of work is called volume work. To make the volume larger we have to overcome the capillary pressure p_σ at the interface.

Thus:

$$\mathrm{d}W_P = -p_\sigma \cdot \mathrm{d}V \tag{5.5}$$

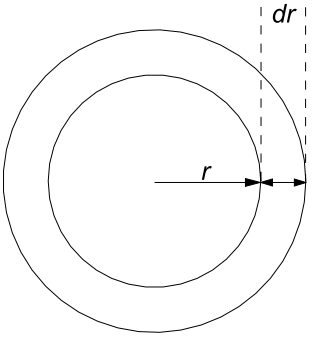

Figure 5.3. Volume increase of a liquid droplet (needs energy because of surface tension)

where

W_P	volume work in N · m
W_σ	interfacial work in N · m
p_σ	capillary pressure in N · m^{-2}
V	volume in m^3

Considering $\frac{\mathrm{d}V}{\mathrm{d}r}$ for a sphere, and taking the volume $V = \frac{3}{4}\pi \cdot r^3$ of a sphere:

$$\frac{\mathrm{d}V}{\mathrm{d}r} = \frac{\mathrm{d}d}{\mathrm{d}dr} \cdot \left(\frac{4}{3}\pi \cdot r^3\right) = 4\pi \cdot r^2 \tag{5.6}$$

so

$$\mathrm{d}W_P = -p_\sigma \cdot 4\pi \cdot r^2 \cdot \mathrm{d}r \tag{5.7}$$

A larger interface results from increasing the radius of the droplet. The work needed for this enlargement is interfacial work $\mathrm{d}W_\sigma$.

With reference to equation (5.3):

$$\mathrm{d}W_\sigma = \sigma \cdot \mathrm{d}A \tag{5.8}$$

For a sphere with $A = 4\pi \cdot r^2$:

$$\frac{\mathrm{d}A}{\mathrm{d}r} = \frac{\mathrm{d}}{\mathrm{d}r} \cdot \left(4\pi \cdot r^2\right) = 8\pi \cdot r \tag{5.9}$$

so

$$\mathrm{d}W_\sigma = \sigma \cdot 8\pi \cdot r \cdot \mathrm{d}r \tag{5.10}$$

Applying the law of energy conservation:

$$\mathrm{d}W_\sigma + \mathrm{d}W_P = 0 \tag{5.11}$$

respectively,

$$\mathrm{d}W_\sigma = -\mathrm{d}W_P$$

so, from equations (5.7) and (5.10) follows

$$\sigma_{12} \cdot 8\pi \cdot r \cdot \mathrm{d}r = p_\sigma \cdot 4\pi \cdot r^2 \cdot \mathrm{d}r \tag{5.12}$$

which means

$$p_\sigma = \frac{2\sigma_{12}}{r} \tag{5.13}$$

This is called the capillary pressure after LAPLACE. It is also called "pressure because of curvature." The radius r is the radius of curvature, and is influenced by the capillary pressure.The surrounding pressure outside the droplet "p_σ" is an over pressure. The LAPLACE equation gives the pressure difference between inside and outside the droplet.

When there is a convex shaped interface on one phase (1) with a radius of curvature r_1 then the pressure difference between this one phase and the surrounding phase (2) is:

$$p_1 - p_2 = \frac{2\sigma_{12}}{r_1} = p_\sigma \tag{5.14}$$

where

σ_{12}	surface tension (between phase 1 and phase 2) in $\mathrm{N \cdot m^{-1}}$
r_1	radius of curvature (phase 1) in m
p_1	absolute pressure in phase 1 (droplet) in Pa
p_2	absolute pressure in phase 2 (surrounding) in Pa
p_σ	"over" pressure (= capillary pressure) of phase 1 in Pa

From equation (5.14) it can be seen that the smaller the radius the higher is the capillary pressure.

When the radius r is very high, the curvature of the interface is very low. For $r = \infty$, the interface is flat. For flat interfaces, LAPLACE's equation gives: $p_1 - p_2 = p_\sigma = 0$ meaning there is no difference in pressure when the interface has no curvature.

The curvature of an interface can be convex or concave. LAPLACE's equation is valid for both types:

The interface of an overfilled glass beaker is convex; so, $r > 0$. The pressure in the liquid volume is higher than the pressure outside in the surrounding air. The higher this pressure, the smaller will be r. When an interface has a concave curvature, this is indicated by a negative value of r. LAPLACE's equation gives: $p_1 - p_2 < 0$. That means the pressure in the phase with the concave interface is lower than the pressure in the surrounding phase. We often see this when measuring a liquid level in a graduated cylinder. The liquid surface at the interface is concave. Now we see the origin of equation (1.1) in Chapter 1 which we used to calculate the water vapor pressure above a capillary filled with water. In a dispersed system of water air, an air bubble in water is an example of a concave surface with respect to the water phase. However, a water droplet in air is an example of a convex surface with respect to the water phase. Table 5.2 shows a systematic approach.

Problem 5.1. There are two droplets of different particle size having different capillary pressures. When they touch each other, the different pressures will start to equilibrate. What will happen?

Table 5.2. Capillary pressure at interfaces of different curvature

Interface curvature	curvature is…	curvature is…	no curvature
curvature (of phase1)	concave	convex	flat
	phase 2	phase2	phase 2
looks like (schematic)			
	phase 1	phase 1	phase 1
radius of curvature r_1 is…	$r_1 < 0$	$r_1 > 0$	$r_1 = \infty$
$p_1 - p_2 = \frac{2\sigma_{12}}{r_1}$	< 0	> 0	0
in words: in phase 1 there is …	lower pressure than in phase 2	higher pressure than in phase 2	same pressure than in phase 2
examples:	a bubble of gas (air) (phase 2) in water (phase 1). Water (phase 1) –air (phase 2) interface in a capillary	a droplet of water (phase 1) in air (phase 2)	flat water–air surface

a) the bigger droplet will decrease in size
b) the smaller droplet will decrease in size
c) both droplets are going to have the same size

For a spherical interface, the radius of curvature r is the same in the x- and y-direction of that interface. Nonspherical interfaces have different radii in the x– and y-direction. LAPLACE's equation is also valid for these interfaces, and then should be used as:

$$p_\sigma = \sigma \cdot \left(\frac{1}{r_x} + \frac{1}{r_y} \right) \tag{5.15}$$

With $r_x = r_y = r$ (sphere) we have again equation (5.13).

5.1.2 Temperature Dependency

Temperature has a significant effect on surface tension (specific interfacial energy). Interfacial energy will decrease with increasing temperature, and will

decrease to zero when a critical temperature is reached at which there is no longer any interface between liquid and gas phases.

A linear mathematical function (model) was developed by Eötvös for predicting the decrease of interfacial energy as a function of temperature for temperature ranges far beyond the critical temperature [1]. However, for this purpose, interfacial energy was based on the amount of substance (in moles), and was not the specific interfacial energy (divided by area) defined earlier.

Let's assume for a moment that a liquid consists of cubic molecules with length l. Then, the volume of 1 mole of liquid can be expressed as:

$$V_m = N_A \cdot l^3 \tag{5.16}$$

One of these cubic molecules at an interface would need the space:

$$l^2 = \left(\frac{V_m}{N_A}\right)^{\frac{2}{3}} \tag{5.17}$$

so, 1 mole of the substance would need an interfacial area of:

$$A_m = N_A \cdot l^2 = {N_A}^{\frac{1}{3}} \cdot {V_m}^{\frac{2}{3}} \tag{5.18}$$

so, the interfacial energy can be calculated:

$$\sigma_m = \sigma \cdot A_m = \sigma \cdot {N_A}^{\frac{1}{3}} \cdot {V_m}^{\frac{2}{3}} \tag{5.19}$$

with the volume of a mole of these molecules,

$$V_m = \frac{M}{\rho} \tag{5.20}$$

then

$$\sigma_m = \sigma \cdot {N_A}^{\frac{1}{3}} \left(\frac{M}{\rho}\right)^{\frac{2}{3}} \tag{5.21}$$

For this quantity, Eötvös found a linear temperature dependency:

$$\sigma_m = k_E \cdot (T_C - T_\theta - T) \tag{5.22}$$

Substituting (5.19) for the volume into (5.20):

$$\sigma \cdot {N_A}^{\frac{1}{3}} \cdot M^{\frac{2}{3}} \cdot \rho^{-\frac{2}{3}} = k_E \cdot (T_C - T_\theta - T) \tag{5.23}$$

and so

$$\sigma = {N_A}^{-\frac{1}{3}} \cdot M^{-\frac{2}{3}} \cdot \rho^{+\frac{2}{3}} \cdot k_E \cdot (T_C - T_\theta - T) \tag{5.24}$$

This is the equation after Ramsey and Shield [115] for the temperature dependency of surface tension. For materials like water which have an abnormally high tendency for molecular association, a specific factor χ is introduced:

$$\sigma = {N_A}^{-\frac{1}{3}} \cdot \left(M \cdot \chi\right)^{-\frac{2}{3}} \cdot \rho^{+\frac{2}{3}} \cdot k_E \cdot (T_C - T_\theta - T) \tag{5.25}$$

where

k_E	Eötvös constant
T	absolute temperature in K
T_C	critical temperature in K
T_θ	material constant in K
N_A	Avogadro's constant
V_m	volume of a mole in $m^3 \cdot mol^{-1}$
ρ	density in $kg \cdot m^{-3}$
σ	surface tension in $N \cdot m^{-1}$
M	molar mass in $kg \cdot mol^{-1}$
χ	molecular association factor

Figure 5.4 illustrates the linear relationship between surface tension and temperature after equation (5.25).

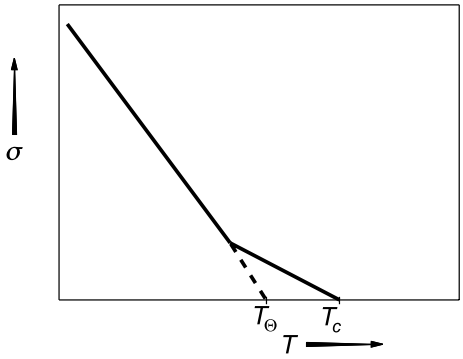

Figure 5.4. Temperature dependency of surface tension after Eötvös resp. after Ramsey and Shield

Example 5.1. Surface tension of water–air at 20 °C
Using equation (5.25) with the following data:

	for H_2O
k_E	$7.5\ J \cdot K^{-1}\ mol^{-1}$ (at 20 °C)
T_C	647.15 K
T_θ	6 K
N_A	$6.023 \cdot 10^{23}\ mol^{-1}$
ρ	$1000\ kg \cdot m^{-3}$ (at 20 °C)
M	$18 \cdot 10^{-3}\ kg \cdot\ mol^{-1}$
χ	0.47

gives:

$$\sigma = \frac{\left(1000\,kg \cdot m^{-3}\right)^{\frac{2}{3}} \cdot 7.5\,N \cdot m \cdot K^{-1} \cdot mol^{-1}}{\left(6.023 \cdot 10^{23}\,mol^{-1}\right)^{\frac{1}{3}} \cdot \left(0.47 \cdot 18 \cdot 10^{3}\,kg \cdot mol^{-1}\right)^{\frac{2}{3}}} \cdot (647.15\,K - 6\,K - T/K)$$

This can be simplified to:

$$\sigma = 0.2133 \frac{\text{mN}}{\text{m}} \cdot (368 - \vartheta/^\circ\text{C}) \tag{5.26}$$

So, for 20 °C we get $\sigma = 74.2\,\text{mN} \cdot \text{m}^{-1}$.

Another way is to measure values of surface tension for different temperatures, and then find a mathematical function to fit this relationship. Two approaches of this type are the following equations: equation (5.27) is a simple linear regression (from [106]). Equation (5.28) is a polynomial regression recommended by the International Association for the Properties of Steam [108].

$$\sigma/\text{mN} \cdot \text{m}^{-1} = 76.056 - 0.1675 \cdot \vartheta/^\circ\text{C} \tag{5.27}$$

$$\sigma = B \cdot \left(\frac{T_C - T}{T_C}\right)^{\mu} \cdot \left(1 + b \cdot \left(\frac{T_C - T}{T_C}\right)\right) \tag{5.28}$$

For water:

$$B = 235.8 \cdot 10^{-3}\text{N} \cdot \text{m}^{-1}$$
$$b = 0.625$$
$$\mu = 1.256$$
$$T_C = 647.15\,\text{K}$$

A comparison of the predicted values calculated from these equations with measured experimental data is shown in Table 5.3.

A comparison of experimentally measured data with calculated values shows that equation (5.28) performs best by delivering the best "goodness of fit." It can also be seen that the simple linear regression in equation (5.27) provides predicted values with smaller differences than those predicted by equation (5.26). So we see that the mathematical polynomial fitting provides better predicted values than equation (5.26). However, equation (5.26) is the one which was derived from a theoretical basis. It was developed by considering the simple geometric space needed on a molecular scale. A factor "association

Table 5.3. Surface tension of water: Comparison of measured data with calculated values.

	measured [106]	calculated by (5.26)		calculated by (5.27)		calculated by (5.28)	
$\vartheta/^\circ$C	σ_{exp}/mN · m^{-1}	σ_{cal}/mN · m^{-1}	difference	σ_{cal}/mN · m^{-1}	difference	σ_{cal}/mN · m^{-1}	difference
0.01	75.65	78.50	3.8%	76.05	0.5%	75.65	–0.001%
10	74.22	76.37	2.9%	74.38	0.2%	74.22	0.006%
20	72.74	74.24	2.1%	72.71	0.0%	72.74	0.000%
30	71.20	72.11	1.3%	71.03	–0.2%	71.20	–0.003%
40	69.60	69.97	0.5%	69.36	–0.4%	69.60	0.001%
50	67.95	67.84	–0.2%	67.68	–0.4%	67.95	–0.002%
60	66.24	65.71	–0.8%	66.01	–0.4%	66.24	0.005%
70	64.49	63.57	–1.4%	64.33	–0.2%	64.49	–0.006%
80	62.68	61.44	–2.0%	62.66	0.0%	62.68	–0.003%
90	60.82	59.30	–2.5%	60.98	0.3%	60.82	0.003%
100	58.92	57.17	–3.0%	59.31	0.7%	58.92	–0.004%

constant" was introduced, but no consideration was given to the fact that the factor is dependent on temperature. Moreover, the density was also considered independent of temperature. So, there are opportunities to further improve the "goodness of fit" of (5.26).

These models provide an impression of what options are available for engineering purposes in process simulation. We can obtain experimental data and develop mathematical equations to model these data. We can start with fundamental equations derived from a theoretical basis, and then improve the precision ("goodness of fit") with appropriate mathematical regression analysis. Recall all these options are approximations. The approximations have different "grades of goodness." Even the experimental data carry a given uncertainty because of experimental errors. Often, more complicated equations are needed for improved precision. The choice we make will depend on the question to be answered. For a rough estimate, a simple linear regression equation may suffice, and the more complicated equations are unnecessary. On the other hand, if we make computer simulations for process development, there is no problem for the computer to use the best (even the most complicated) equation in order to obtain results with the greatest precision.

Decisions of these types involve determining what level of precision is needed, what level of computational power is readily available, what time limitations are imposed, what will be the economic impact of lack of precision, etc.

5.1.3 Concentration Dependency

Concentration dependency is important in substances which tend to adsorb at their interfaces. This adsorption significantly influences the surface tension, and for this reason these substances are called "interfacially active" substances. The most common of these substances are emulsifiers and surfactants. An emulsifier is an amphiphilic (bipolar) molecule that will strongly adsorb to an interface between water and air or between water and oil. An amphiphilic molecule is bipolar because one end of the molecule is attracted to one phase in the dispersion, and the opposite end is attracted to the other phase. Thus, these molecules have both lyophilic ("loving or attracting the solvent") and lyophobic ("fearing or rejecting the solvent") properties. In the specific case of water molecules, they are called hydrophilic and hydrophobic properties.

In the case of emulsifiers, this adsorption can lead to a dramatic reduction in the surface tension, even when very small amounts are used. This is because the molecules will reorient themselves within the interfacial layer to reach the lowest energy level possible. This reduces the interfacial energy and thus, the surface tension. Adsorption of additional emulsifier molecules at the interface further decreases the surface tension until all available spaces for these molecules at the interface are occupied. At this point, any further addition of emulsifier molecules will cause them to associate forming micelles. This creates an interface within the system leading to a lower energy state in which

interactions with "unfriendly" parts of the molecules are minimized. This association is governed by the size and geometry of the polar groups in the newly formed micelle. There are spherical micelles (see Figure 5.7) and inverse spherical micelles. But, there are also other types like lamellar and hexagonal types [3,136], which are not discussed in any detail here.

So, adsorption of an emulsifier or surfactant leads to a decrease in surface tension with increasing concentration of emulsifier or surfactant until a critical point is reached when micelles begin to form. Then there will be no further decrease in surface tension with further increase in concentration. This critical point in concentration is called the critical micelle formation concentration (cmc). The relation between the surface tension and the emulsifier concentration in the aqueous phase is well known, and is shown graphically, along with the critical micelle formation concentration (cmc) zone in Figure 5.5.

The same graph with $\sigma - c$ curve is shown with a series of beakers beneath it in Figure 5.6. The beakers beneath the graph indicate the situation at the interface at the different stages of concentration.

Assuming that surfactants form a monolayer between two immiscible phases the amount of surfactant needed (the monolayer concentration) can be calculated using the adsorption models we learned about in Section 1.2, e.g. the FREUNDLICH or LANGMUIR model (see Section 1.2.3) [136].

SZYSZKOWSKI's equation allows the calculation of the interfacial surface tension as a function of surfactant concentration [22]:

$$\sigma_0 - \sigma = a \cdot \ln\left(1 + \frac{c}{b}\right) \tag{5.29}$$

where

σ	surface tension in $N \cdot m^{-1}$
σ_0	surface tension at $c = 0$
c	concentration of surfactant in $kg \cdot m^{-3}$
b	material specific constant in $m^3 \cdot kg^{-1}$
a	material specific constant in $N \cdot m^{-1}$

In contrast to the addition of emulsifiers which leads to decreased surface tension, there are materials which increase the surface tension when added to

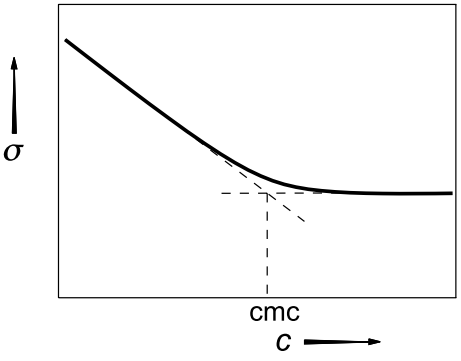

Figure 5.5. Surface tension as function of emulsifier concentration

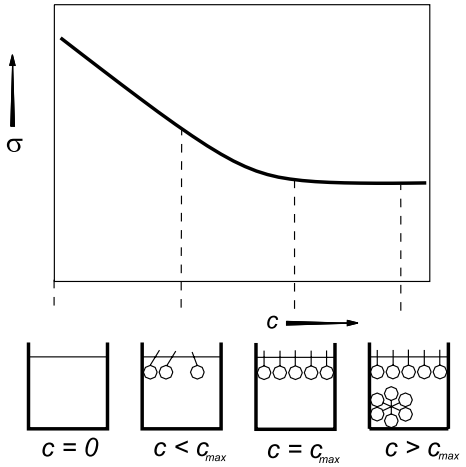

Figure 5.6. After reaching the monolayer at the critical concentration point, cmc, the surface tension remains constant with increasing concentration.

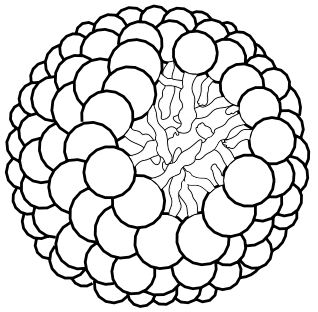

Figure 5.7. Spherical micelle (schematic). The lyophobic parts (drawn as lines) of the molecules are inside the micelle, covered from the surrounding solvent by the lyophilic parts (drawn as balls) of the molecules.

a dispersed system. In the case of aqueous systems these are strong electrolytes (inorganic salts) and hydroxyl compounds like carbohydrates [2]. The increase in surface tension comes about because of strong interaction between these substances and the solvent. This interaction is called negative adsorption or depletion and is a form of hydration which prevents these molecules from adsorption at the interface, and keeps them well within the interior of the continuous phase volume. Strong depletion can lead to forming an interface between two different aqueous phases [16].

5.1.4 Liquid–Liquid–Gas Systems

The shape of a liquid droplet dispersed within another liquid in a three-phase system is determined by the interfacial tensions between the phases. Such a droplet is shown in Figure 5.8. The droplet consists of phase 3, and is dispersed at the interface between phases 2 and 1. In this situation, three interfacial tensions are acting on the droplet, σ_{12}, σ_{13} and σ_{23}, which are causing the shape of the droplet not be a sphere.

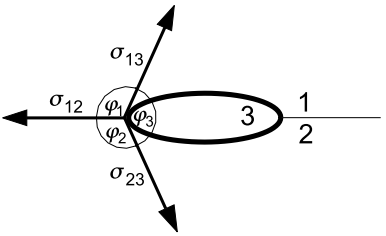

Figure 5.8. Interfacial tensions at the point where three phases are in contact. For example, phase1 is a gas, phase 2 is liquid A, and phase 3 is liquid B.

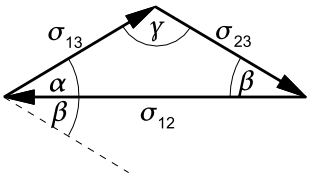

Figure 5.9. Addition of vectors in Figure 5.8

The values of the vectors σ_{12}, σ_{13} and σ_{23} are governed by the substances of which phases 1, 2, 3 are made, but the direction of each vector is a matter of static equilibrium. The equilibrium is reached when tension σ_{12} at the point of contact has the same value as the resulting vector resolved from addition of σ_{13} and σ_{23}. That means that the resulting contact angle φ_3 can have only one possible value, as shown in Figure 5.9.

With the help of the cosine function for an obtuse angle:

$$c^2 = a^2 + b^2 - 2a \cdot b \cdot \cos\gamma \tag{5.30}$$

according to Figure 5.9 we can write

$${\sigma_{12}}^2 = {\sigma_{13}}^2 + {\sigma_{23}}^2 - 2\sigma_{13} \cdot \sigma_{23} \cdot \cos\gamma \tag{5.31}$$

because of

$$\alpha + \beta = \varphi_3 \tag{5.32}$$

and

$$\gamma + \varphi_3 = 180^\circ \tag{5.33}$$

or

$$\gamma = 180^\circ - \varphi_3 \tag{5.34}$$

then

$$\cos\gamma = -\cos\varphi_3 \tag{5.35}$$

and therefore

$${\sigma_{12}}^2 = {\sigma_{13}}^2 + {\sigma_{23}}^2 - 2\sigma_{13} \cdot \sigma_{23} \cdot \cos\varphi_3 \tag{5.36}$$

so

$$\cos\varphi_3 = \frac{{\sigma_{12}}^2 - ({\sigma_{13}}^2 + {\sigma_{23}}^2)}{2 \cdot \sigma_{13} \cdot \sigma_{23}} \tag{5.37}$$

Table 5.4. Typical cases of contact angles on a liquid underlying phase

case	φ_3	$\cos\varphi_3$	shape of phase 3	example
I	≈ 0	is ≈ 1	film on phase 2	gasoline on water
II	$0^\circ - 90^\circ$	is positive and $\ll 1$	lens on phase 2	olive oil on water
III	$90^\circ - 180^\circ$	is negative	sphere on phase 2	water on silicone oil

For equation (5.37) we want to distinguish three cases: contact angle φ_3 above 90°, below 90° or equal to zero. In Table 5.4 the consequences for these three cases are listed.

Let us focus on the droplet behavior from an energetic point of view: In case I, formation of a film, an increased adhesion between phases 2 and 3 takes place. Adhesion energy is released. In cases II and III, formation a lens or sphere, instead of adhesion now cohesion of phase 3 is taking place. Cohesion energy is released. The difference between adhesion energy and cohesion energy characterizes the ability of the system to form a film on the underlying phase and is called spreading pressure. This pressure characterizes the tendency for forming a film on the underlying phase. When a small amount of this liquid is dropped on the underlying phase, the liquid spreads along the interface forming a thin film. The thickness of this film can be decreased down as far as the monolayer thickness. The spreading pressure also drives the spreading rate when surfactant molecules spread onto newly generated interfaces e.g. during foaming or emulsifying processes [136].

5.1.5 Solid–Liquid–Gas systems

When a liquid droplet forms onto a solid interface, the shape of the droplet is governed by the interfacial tensions of the phases in contact (see Figure 5.10).

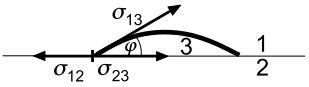

Figure 5.10. Interfacial tensions at the point of contact between three phases with phase 2 being solid. For example, phase 3 is a liquid and phase 1 is a gas.

We can derive the following from Figure 5.10:

In equilibrium we have

$$\sigma_{12} = \sigma_{23} + \sigma_{13} \cdot \cos\varphi_3 \tag{5.38}$$

This is called Young's equation.

With the abbreviation $\varphi \equiv \varphi_3$, this means

$$\cos\varphi = \frac{\sigma_{12} - \sigma_{23}}{\sigma_{13}} \tag{5.39}$$

Table 5.5. Typical cases of contact angles on a solid underlying phase

case		$\cos\varphi$	φ	consequence
I	$\sigma_{12} - \sigma_{23} \geq \sigma_{13}$	$\cos\varphi \geq 1$	$= 0$	complete wetting, phase 3 forms a film on a solid surface
II	$0 > \sigma_{12} - \sigma_{23} < \sigma_{13}$	$0 > \cos\varphi > -1$	$90^\circ > \varphi > 180^\circ$	partial wetting, phase 3 forms flat wet spots on solid surface
III	$0 < \sigma_{12} - \sigma_{23} < \sigma_{13}$	$0 < \cos\varphi < 1$	$90^\circ > \varphi > 0^\circ$	no wetting, phase 3 forms droplets on a solid surface

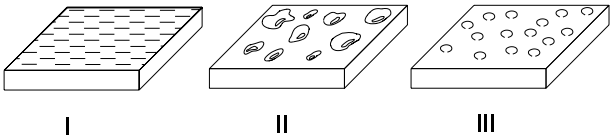

Figure 5.11. A liquid on a solid interface: I: complete wetting (film forming), II: partial wetting, III: no wetting

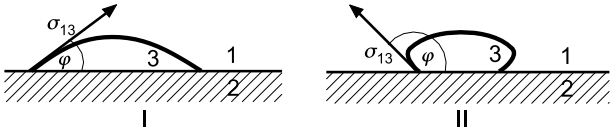

Figure 5.12. Contact angle φ below 90° (left), and above 90° (right)

Let us again focus on three cases where the contact angle φ is above or below 90° or equal to zero. In Table 5.5 these cases and their consequences are listed. In Figure 5.11 and Figure 5.12 the different behaviors are illustrated.

5.1.6 Kinetics of Interfacial Phenomena

The effect of decreasing the interfacial tension by adsorption of polar (amphiphilic) molecules at the interface is an equilibrium state. Until the equilibrium is reached these molecules must do the following:

- (eventually) detach from a micelle
- find their way to the interface (diffusion)
- adjust to the proper orientation in order to adsorb
- find available space at the interface for adsorption.

For engineering processes like formation of bubbles (foaming) and forming of droplets (emulsifying), it is important to have information about the kinetics of these steps (speed or rate in which they occur) [4,15]. The kinetics of interfacial adsorption can be studied by measurement of interfacial tension over time, as discussed in the following subsection.

5.1.7
Adsorption Kinetics at Solid Interfaces

When molecules from a liquid phase are going to become adsorbed onto a solid interface, they must undergo the same procedural steps listed above. Let us imagine macromolecules like proteins which are to be adsorbed onto a solid. They must first undergo diffusion to the interface before they can be adsorbed. Then they have to adjust to the right spatial orientation, and then they must find an available space on the interface. Because of the bonding forces between such a macromolecule and the solid surface, the adsorption isotherm (see Section 1.2) often has the form of the LANGMUIR isotherm, which has the typical profile for adsorption at the monolayer, with maximum interfacial concentration (see Table 1.4). The kinetics of processes like this can also be studied by interfacial tension measurement over time. The opposite case, in which desorption of macromolecules from the interface into the volume of the liquid occurs, is called depletion. It can be identified by an increase of interfacial tension over time.

5.2
Measurement

5.2.1
Measuring Interfacial Tension

One of the methods used for measurement of interfacial (surface) tension is known as the bow wire method. Figure 5.13 shows a schematic of how this method is applied. A piece of wire of length l is lifted for a distance dh out of a liquid interface. This causes the interfacial surface area to increase by $\mathrm{d}A = 2 \cdot l \cdot \mathrm{d}h$. The force F necessary for lifting the wire is measured and used to calculate the surface tension.

An alternative is the "ring method" after DU NOUY. In this method, a ring made of platinum wire is used. Like in Figure 5.13 the wire ring is lifted a distance dh, resulting in the interfacial area increasing by $\mathrm{d}A = 2 \cdot l \cdot \mathrm{d}h$ with the circumference of the ring. Measuring F and using equation (5.2) the following expressions can be derived:

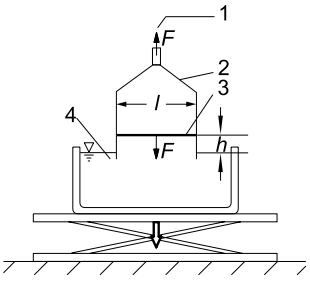

Figure 5.13. Schematic for measuring surface tension with the bow wire. **1**: forcemeter, **2**: bow wire, **3**: horizontal piece of wire, **4**: liquid sample

$$\sigma = \frac{\mathrm{d}E}{\mathrm{d}A} = \frac{F \cdot \mathrm{d}h}{2 \cdot l \cdot \mathrm{d}h} = \frac{F}{2 \cdot \pi \cdot d} \tag{5.40}$$

Another possibility is using a vertical plate instead of a wire ring or straight wire. In Figure 5.14 the so-called WILHELMY plate is shown. The interfacial force on a plate like this is:

$$F = \sigma \cdot 2 \cdot l \cdot \cos\varphi \tag{5.41}$$

where

σ	surface tension in $\mathrm{N \cdot m^{-1}}$
F	force in N
E	interface energy in $\mathrm{N \cdot m}$
A	interface area in $\mathrm{m^2}$
l	length in m
h	height in m
d	diameter in m

The wire ring and vertical plate techniques after DE NOUY and WILHELMY are often used to measure the surface tension of aqueous solutions. However, they can also be used to measure the interfacial tension between two liquids. Then, in that case, the effects from buoyancy and wetting properties have to be taken into account. In equation (5.40) it was assumed that the liquid in Figure 5.13 was wetting the ring or the plate in an ideal manner, i.e. the contact angle $\varphi = 0$ (see Figure 5.14). For interfaces between water and hydrophilic solids this approximation is mostly valid.

Another method of approach for measuring interfacial tension is to use capillary pressure. When a glass capillary tube is dipped vertically into a beaker with water, water will flow up the capillary tube to a certain height forming a concave meniscus at the air–water interface (Figure 5.15).

The height depends on the capillary diameter, interfacial tension and contact angle between liquid and solid material. The evaluation is based on LAPLACE's equation. Recall in a liquid with a concave interface, there is lower pressure compared to the phase behind the interface (in this case, air). The lower pressure sucks the liquids into the capillary until the equilibrium vertical height is reached. The equilibrium is reached when the pressure on both sides of the meniscus (interface with curvature in Table 5.2 is the same. That

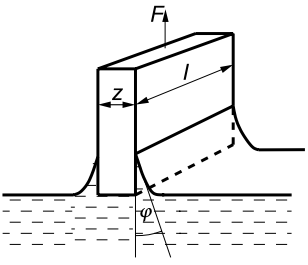

Figure 5.14. WILHELMY plate

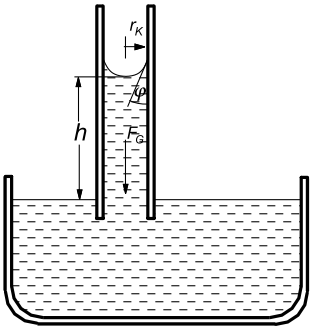

Figure 5.15. Capillary action (rise in liquid level in capillary tube) to evaluate interfacial tension

occurs when the hydrostatic pressure of the water in the capillary (below the interface) reaches the capillary pressure.

To calculate the capillary rise, we first calculate the specific interfacial energy to raise the liquid in the capillary:

$$\mathrm{d}E = F_A \cdot \cos\varphi \cdot \mathrm{d}h \tag{5.42}$$

With the wetted area in the capillary

$$\mathrm{d}A = 2\pi \cdot r_K \cdot \mathrm{d}h \tag{5.43}$$

the specific interfacial energy is:

$$\sigma = \frac{\mathrm{d}E}{\mathrm{d}A} = \frac{F \cdot \mathrm{d}h}{2 \cdot \pi \cdot r_K \cdot \mathrm{d}h} = \frac{F_A \cdot \cos\varphi}{2\pi \cdot r_K} \tag{5.44}$$

With the interfacial force acting on the liquid

$$F = 2\pi \cdot r_K \cdot \sigma \tag{5.45}$$

and its vertical component is

$$F_A = F \cdot \cos\varphi = 2\pi \cdot r_K \cdot \sigma \cdot \cos\varphi \tag{5.46}$$

The contact angle φ in Figure 5.15 between the wall of the capillary and the liquid interface – sometimes called the wetting angle – depends of the materials used. Materials with ideal wetting properties have zero contact angle ($\varphi = 0$). In that case, $\cos\varphi = 1$, and there is no influence on the calculated value in equation (5.51).

The weight force of the liquid in the capillary is

$$F_G = \pi \cdot r_K^2 \cdot h \cdot g \cdot \Delta\rho \tag{5.47}$$

In case of a liquid–air surface, it is

$$\Delta\rho = \left(\rho_{Fluid} - \rho_{air}\right) \approx \rho_{Fluid} \tag{5.48}$$

so

$$F_G = \pi \cdot r_K^2 \cdot h \cdot g \cdot \rho_{Fluid} \tag{5.49}$$

At equilibrium, this force is equal to that in (5.46)

$$\pi \cdot r_K^2 \cdot h \cdot g \cdot \rho_{Fluid} = 2\pi \cdot r_K \cdot \sigma \cdot \cos\varphi \tag{5.50}$$

and, therefore

$$\sigma = \frac{h \cdot r_K \cdot g \cdot \rho_{Fluid}}{2 \cdot \cos\varphi} \tag{5.51}$$

with the ideal case $\varphi = 0$ i.e. $\cos\varphi = 1$

$$\sigma = \frac{h \cdot r_K \cdot g \cdot \rho_{Fluid}}{2} \tag{5.52}$$

where

σ	interfacial tension in $N \cdot m^{-1}$
F_A	interfacial force in N
F_G	weight force in N
E	specific interfacial energy in $N \cdot m^{-1}$
A	interface area in m^2
r_K	capillary radius in m
f	correction factor for droplet radius
h	height in m
g	acceleration of gravity in $m \cdot s^{-2}$
ρ_{Fluid}	density of fluid in $kg \cdot m^{-3}$
φ	contact angle
m	mass of a droplet in kg
V	volume of a droplet in m^3

There are further possibilities for measuring the interfacial tension based on capillary action. The general principle is to measure geometric quantities like diameter, radius or volume of droplets or bubbles, and calculate σ by applying Laplace's equation.

A simple technique is to form droplets with a pipette of given orifice. By measuring the volume of the droplets, the interfacial tension can be calculated. This type of drop forming pipette is called a stalagmometer, Figure 5.16 shows an example. An easy way of working with a stalagmometer is to drop a known volume, count the number of drops and calculate the average volume of one drop. Another way is to drip a fixed number of drops, e.g. 20 into a beaker on a balance and measure the average mass of a drop.

The evaluation of interfacial tension is based on the equilibrium of weight force of a drop and force of adhesion to the capillary: With the weight force $m \cdot g$ of a drop and the adhesion force $2\pi \cdot r_K \cdot f \cdot \sigma$ in equilibrium it is

$$m \cdot g = 2\pi \cdot r_K \cdot f \cdot \sigma \tag{5.53}$$

called Tate's law and so

$$\sigma = \frac{m \cdot g}{2\pi \cdot r_K \cdot f} \tag{5.54}$$

in case the drop volume was measured:

$$\sigma = \frac{\rho \cdot V \cdot g}{2\pi \cdot r_K \cdot f} \tag{5.55}$$

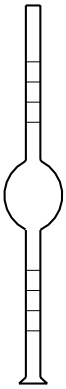

Figure 5.16. Stalagmometer

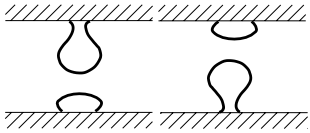

Figure 5.17. Pendant drop/bubble and sessile drop/bubble (schematic)

When drops are formed out of a small capillary, the droplet radius is larger than the capillary radius. A correction factor f (which is available from tables) is introduced to take account for this.

Other techniques based on this principle also compare gravitational force with adhesive force. They are called the pendant drop method and sessile drop method (see Figure 5.17). It is important to note that LAPLACE's equation is valid for both convex and concave interfaces. So, instead of a sessile or pendant drop, these experiments can be performed with a sessile bubble or a pendant bubble. In case of bubbles (see bubble point tensiometer in Figure 5.18) the buoyancy force has to be taken as gravitational force. By reading the pressure p in the capillary and using equation (5.15) we can get the surface tension between gas and liquid of interest.

When a drop is rotated, its shape is changed until centrifugal forces and interfacial forces are in equilibrium. The microscopic observation of a rotating drop to measure the interfacial tension is called the spinning drop method (Figure 5.19). Because of temperature dependency (recall Section 5.1.2) all measurements of these types must be carried out under good temperature control.

Example 5.2. A liquid in a glass capillary of 1 mm diameter rises to a height of 28 mm. What is the surface tension of the liquid?

Using equation (5.51) and assuming contact angle to be zero and it is:

$$\sigma = \frac{10^3\,\mathrm{kg}\cdot\mathrm{m}^{-3}\cdot 28\cdot 10^{-3}\,\mathrm{m}\cdot 9.81\,\mathrm{m}\cdot\mathrm{s}^{-2}\cdot 0.5\cdot 10^{-3}\,\mathrm{m}}{2} = 68.7\,\mathrm{mN}\cdot\mathrm{m}^{-1}$$

Example 5.3. We have a liquid with surface tension of 70 $\mathrm{mN}\cdot\mathrm{m}^{-1}$. To what height can we expect it to rise in a capillary with a diameter of $D = 0.5$ mm?

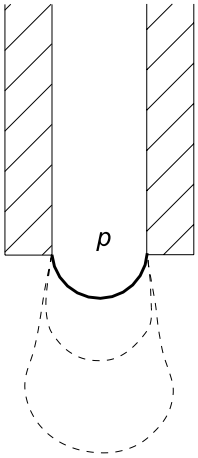

Figure 5.18. Bubble point tensiometer (schematic). At the orifice of a glass capillary a bubble is formed

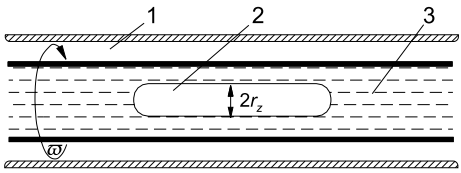

Figure 5.19. Schematic of spinning drop method. **1**: heating jacket around rotating tube, **2**: drop, **3**: liquid in rotating tube

Using equation (5.51) and assuming the contact angle to be zero then

$$h = \frac{2 \cdot \sigma}{r_K \cdot \rho \cdot g}$$

so

$$h \approx \frac{4 \cdot 70 \cdot 10^{-3}\mathrm{N \cdot m^{-1}}}{D/\mathrm{m} \cdot 10^3\,\mathrm{kg \cdot m^{-3}} \cdot 10\,\mathrm{m \cdot s^{-2}}} = \frac{280 \cdot 10^{-4}\,\mathrm{m}}{D/\mathrm{m}}$$

$$h \approx \frac{28\mathrm{mm}}{D/\mathrm{mm}}$$

In this way, we can create a table listing the height to which a liquid will rise in capillaries of different diameter:

D / mm	h / mm
0.5	56
1	28
2	14
5	5.6
10	2.8

5.2.2 Measuring Contact Angle

Measuring the contact angle with use of YOUNG's equation (5.39) can provide information about interfacial tension and wetting ability, and can also give information about kinetics of interfacial effects. Contact angle measurement is normally performed by optical means. With the help of an optical instrument, along with appropriate image processing software, the shape of a single droplet can be analyzed and evaluated. This is called drop shape analysis (DSA).

The contact angle can also be approximated with the WILHELMY method. The interfacial force on the WILHELMY vertical plate depends on the contact angle, φ, and so it can be calculated. Sometimes, the WILHELMY plate is moved in and out of the liquid to measure the contact angles for "wetting" and "unwetting," which may be different. Then, the readings have to be corrected for buoyancy effects. This is called the dynamic WILHELMY technique [5].

When the contact angle between a liquid and a porous solid (or powder particles) has to be measured, it can be performed with the technique after WASHBURN. In this technique, the powder is placed in a glass tube with a filter at the bottom, all of which hangs from a balance. By dipping the filter bottom into the liquid of interest, the powder begins to become wetted. By recording the weight gain of the powder (moisture uptake), the wetting progress can be studied over time. The WASHBURN method also includes plotting the square of the weight gain versus time, which normally appears as a straight line. From the slope of this line, the contact angle can be calculated [14], as follows:

$$t = \frac{\eta}{C \cdot \rho^2 \cdot \sigma \cdot \cos\varphi} \cdot m^2 \tag{5.56}$$

where

t	time after contact in s
σ	interfacial tension in $\mathrm{N} \cdot \mathrm{m}^{-1}$
C	constant of solid sample
η	viscosity in $\mathrm{Pa} \cdot \mathrm{s}$
ρ	density of fluid in $\mathrm{kg} \cdot \mathrm{m}^{-3}$
φ	contact angle
m	mass of liquid adsorbed in kg

5.2.3 Dynamic Measurement

In order to study the kinetics of interfacial effects, measurements have to be performed over time [6, 7]. Dynamic interfacial tension measurements are based on the principle of generating a "fresh" interface area, and observe how the surface tension changes over time on the way to reaching equilibrium. In order to study liquid–liquid interfaces, small droplets are formed through a narrow orifice at a given rate. When the gravitational force of a droplet exceeds the interfacial force, it detaches from the orifice. The time period between

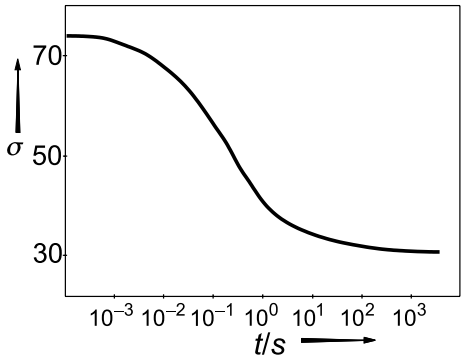

Figure 5.20. Tension versus surface age (schematic)

"birth" of a droplet and its detachment (lifetime) is identical to the age of the interfacial area. The interfacial tension of a droplet with a given interfacial age can be calculated as shown in equation (5.55) for a stalagmometer. By increasing the droplet formation rate, different ages can be scanned, and interfacial tension can be plotted versus lifetime of the interface. This method can be used to study how fast an emulsifier or surfactant can act in decreasing the surface tension of a system. For fast processes like emulsification or homogenization, fast interfacial kinetics are desirable. If a surfactant or emulsifier is too slow, new droplets are not stabilized fast enough, and the desired quality of emulsion or dispersion cannot be achieved in spite of good equipment performance. Other techniques are the overflowing cylinder technique [6,18] and dynamic bubble pressure method [17,19] and the drop volume method [20] which allows for time resolved measurement of interfacial tensions [21,22].

Also, similar to surface tension, the contact angle (e.g. of a droplet on a surface) can be measured and recorded over time to study the kinetics of wetting processes.

5.3 Applications

ice cream: foam stability and interface properties	[8–10]
chocolate: emulsifiers and physical properties of chocolate	[11]
whey protein: foam stability and interface properties	[12]
emulsions: adhesion on packaging materials and equipment surfaces	[13]
membrane emulsification: effects of interfacial tension	[7,15]
interfacial properties of water / water emulsions	[16]
wine tears: forming by interfacial tension gradient	[136]
liquid films: MARANGONI effect enhances film stability	[136]
foam stability: milk protein surfactant system	[23,26]
proteins adsorbed at O/W interfaces: dynamic measurement	[24]
galactomannans: emulsification activity	[25]

Literature

1. Brezesinski G, Mögel, HJ (1993) Grenzflächen und Kolloide. Spektrum Akademischer Verlag, Berlin
2. Brash JL, Wojciechowski PW (eds) (1996) Interfacial Phenomena and Bioproducts Marcel Dekker, New York
3. Martin AN, Swarbrick J, Cammarata A (1983) Physical Pharmacy. Lea & Febinger, Philadelphia
4. Karbstein H (1994) Untersuchungen zum Herstellen und Stabilisieren von Öl in Wasser Emulsionen. Dissertation, University Karlsruhe Germany
5. Sadhal SS (1996) Transport Phenomena With Drops and Bubbles, Springer New York
6. Bergink-Martens DJM (1993) Interface dilation, the overflowing cylinder technique. Dissertation, Agricultural University Wageningen
7. Muschiolik G (2000) Produkte der Zukunft auf der Basis von Öl- in Wasser- Emulsionen. Proc. 58. Discussion meeting FEI, Bonn, Germany, p. 60–86
8. Goff HD (1988) The role of chemical emulsifiers and dairy proteins in fat destabilization during the manufacture of ice cream. Dissertation, Cornell University, Ithaca
9. Rohenkohl H (2003) Influence of recipe parameters on fat- and gas-phase-structure in ice cream. Proc. FIL-IDF - 2^{nd} Intern. Symp. Ice Cream, Thessaloniki, Greece
10. Chang Y, Hartel RW (2002) Stability of air cells in ice cream during hardening and storage. J Food Engineering 55:59–70
11. Schantz B, Linke L, Rohm H (2003) Effects of different emulsifiers on rheological and physical properties of chocolate. Proc. 3^{rd} Intern. Symp. Food Rheology and Structure
12. Nylander T, Hamraoui A, Paulsson M (1999) Interfacial properties of whey proteins at air/water and oil/water interfaces studied by dynamic drop tensiometry, ellipsometry and spreading kinetics. Int J Food Sci Tech 34:573–585
13. Michalski MC, Desobry S, Babak V, Hardy J (1999) Adhesion of food emulsions to packaging and equipment surfaces. Colloids and Surfaces A: Physicochemical and Engineering Aspects 149:107–121
14. Washburn EW (1921) The dynamics of capillary flow. Physical Review 17: 374–382
15. Graaf S van der (2006) Membrane emulsification: droplet formation and effects of interfacial tension. Dissertation, University of Wageningen, Netherlands
16. Scholten E (2006) Interfacial properties of water-in-water emulsions and their effect on dynamical behavior. Dissertation, University of Wageningen, Netherlands
17. Otis DR, Ingenito EP, Kamm RD, Johnson M (1994) Dynamic surface tension of surfactant TA: experiments and theory. J Appl Physiol 77: 2681–2688
18. Joos P, Fainerman VB, Loglio G, Lucasses-Reynders EH, Miller R, Pterov P (1999) Dynamic Surface Phenomena. V.S.P. Intl Science, Utrecht Netherlands
19. Fainerman VB, Miller R, Joos P (1994) The measurement of dynamic surface tension by the maximum bubble pressure method. J Colloid & Polymer Sci 272: 731–739
20. Miller R, Hofmann A, Hartmann R, Halbig A, Schano KH (2000) Measuring dynamic surface and interfacial tensions. Advanced Materials 4: 370–374
21. Rosen MJ (2004) Surfactants and Interfacial Phenomena. Wiley-VCH, Weinheim
22. Vogler EA (1989) A simple mathematical model of time-dependent interfacial tension. J Colloid & Interface Sci 133:228–236
23. Rouimi S, Schorsch C, Valentini AC, Vaslin S (2005) Foam stability and interfacial properties of milk protein–surfactant systems. Food Hydrocolloids 19: 467–478
24. Beverung CJ, Radke CJ, Blanch HW (1999) Protein adsorption at the oil–water interface: characterization of adsorption kinetics by dynamic interfacial tension measurements. Biophysical Chemistry 81:59–80

25. Garti N, Reichmann, D (1994) Surface properties and emulsification activity of galactomannans. Food Hydrocolloids 22:155–173
26. Damodaran S, (2005) Protein stabilization of emulsions and foams. J Food Science 70:R45

6 Permeability

Permeability is a property of porous materials that quantifies the relative ease with which a transporting substance can pass through the material. For example, the air permeability of grain stored in a grain bin will help engineers to determine how much air pressure will be needed to make air flow through the grain at a required flow rate in designing a grain drying process. Similarly, the hydraulic permeability of a granular or powdered material in a packed column will help determine the pumping energy required to make water flow through the column at a given flow rate. In the food industry, permeability of packaging materials to such transporting substances as water vapor and oxygen is extremely important in the design of packages capable of protecting food quality [1–5]. In order to solve problems of permeability through packaging materials, we need to understand some basic principles of mass transport phenomena across a permeable barrier (permeation). Depending on the specific nature of the system, some of these phenomena will include the geometry of the system, but some will not, and depend only on the material properties. At the beginning of this chapter, we will look at mass transport through a solid packaging material. At the end of the chapter we will learn that there are common principles applicable to other transport processes like transport of heat and electricity through solids, which are also based on diffusion.

6.1 Steady State Diffusion in Solids

Let us begin the section looking at an example of a packaging film: Consider a polymer packaging film that is wrapped around a food product to avoid loss of a gaseous flavor and aroma from the food. In this application, the film separates a small enclosed space containing a high concentration (high potential) of that flavor compound from the surrounding ambient environment in which the concentration of that compound is very low (low potential). The mass transfer of flavor compound through the film depends on

- how permeable is the film (material property)
- how large is the difference in potential (concentration gradient)
- how thick is the film (geometric property)

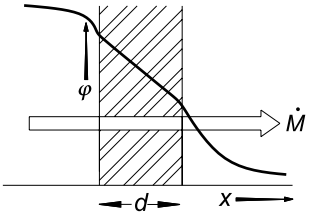

Figure 6.1. Curve of potential (driving force) along the axis of a solid film of thickness d, caused by gradient of the concentration resulting in a transport rate $\dot{M}$

- how large is the area of the film exposed to the environment (geometric property)

The quotient $\frac{d\varphi}{dx}$ in Figure 6.1 is called the gradient of potential. If this gradient is constant over time we will expect a steady state transport rate. Quantification of the transporting substance M can be in terms of the number of flavor molecules, their mass, volume, or moles. For general purposes, we will refer to the quantity of this transporting substance by the term "set." So, before we know whether we should measure the mass or the volume of the escaping flavor (set), let us deal with a general transport rate $\frac{dM}{dt} = \dot{M}$. The surface area across which transfer can occur is called A. The quotient of $\dot{M}$ and A is called transport rate density. This is the same as flow rate per unit area in mass transport across a permeable barrier, and is referred to as "flux." When steady state is reached and maintained, this transport rate density (flux) is proportional to the gradient of potential. We can write:

$$-\frac{1}{A} \cdot \frac{dM}{dt} = K \cdot \frac{d\varphi}{dx} \tag{6.1}$$

In words:

$-$ transport rate density = coefficient · gradient of potential

or:

$$-\frac{\text{amount of set}}{\text{area} \cdot \text{time}} = \text{coefficient} \cdot \text{gradient of potential}$$

where

A	area
M	amount of set
t	time
φ	potential
x	length
K	coefficient

Equation (6.1) is called the general transport equation. When the potential is decreasing over x like in Figure 6.1, we have a negative gradient. Therefore, the negative sign is applied to equation (6.1) in order to represent a positive transfer density.

The transporting substance or set M is a general quantity representing the amount of material which is transported along the gradient. Let us assume we

measure the amount of permeating flavor compound in terms of mass. Then, would be a mass transfer rate density with SI units of $\mathrm{kg} \cdot \mathrm{m}^{-2} \cdot \mathrm{s}^{-1}$. Let us further assume we measure the potential in terms of pressure. Then our gradient will be a pressure gradient. The pressure in this case is the partial pressure of the flavor compound inside the package with respect to the concentration outside the package. The transport equation will then take on the following form:

$$-\frac{\text{mass}}{\text{area} \cdot \text{time}} = K \cdot \text{gradient of partial pressure}$$

In mathematical terms:

$$-\frac{1}{A} \cdot \frac{\mathrm{d}m}{\mathrm{d}t} = P \cdot \frac{\mathrm{d}p}{\mathrm{d}x} \tag{6.2}$$

where

A	area in m^2
m	mass in kg
t	time in s
p	partial pressure in Pa
x	length in m
P	permeability coefficient in $\mathrm{kg} \cdot \mathrm{s}^{-1} \cdot \mathrm{m}^{-1} \cdot \mathrm{Pa}^{-1}$

The coefficient P in equation (6.2) is called permeability coefficient. Its units depend (among other things) on the partial pressure units used. The SI units for P are: $\mathrm{kg} \cdot \mathrm{s}^{-1} \cdot \mathrm{m}^{-1} \cdot \mathrm{Pa}^{-1}$. In Example 6.1 the conversion to other units is shown.

If volume is chosen to monitor permeation of our flavor compound instead of mass, then equation (6.1) will take on the form:

$$-\frac{\text{volume}}{\text{area} \cdot \text{time}} = K \cdot \text{gradient of partial pressure}$$

In mathematical terms

$$-\frac{1}{A} \cdot \frac{\mathrm{d}V}{\mathrm{d}t} = P \cdot \frac{\mathrm{d}p}{\mathrm{d}x} \tag{6.3}$$

where

A	area in m^2
V	volume in m^3
t	time in s
p	partial pressure in Pa
x	length in m
P	permeability coefficient in $\mathrm{m}^2 \cdot \mathrm{s}^{-1} \cdot \mathrm{Pa}^{-1}$

The coefficient P in equation (6.3) is also called permeability coefficient, and its units also depend on the partial pressure units used. The SI units for P are: $\mathrm{m}^3 \cdot \mathrm{s}^{-1} \cdot \mathrm{m}^{-2} \cdot \mathrm{Pa}^{-1} \cdot \mathrm{m} = \cdot \mathrm{m}^2 \cdot \mathrm{s}^{-1} \cdot \mathrm{Pa}^{-1}$. In Example 6.1, the use of other units is shown. When we use volume instead of mass we have to remember that the temperature has a large influence (see Section 2.3.1). Because of this, it is useful

Table 6.1. Expressions of concentration (examples)

	in SI units	in non-SI units
molarity	$\mathrm{mol \cdot m^{-3}}$	$\mathrm{mol \cdot l^{-1}}$
mass concentration	$\mathrm{kg \cdot m^{-3}}$	$\mathrm{g \cdot cm^{-3}}$
mass fraction	$\mathrm{kg \cdot kg^{-1}}$	%, ‰, ppm, ppb
volume fraction	$\mathrm{m^3 \cdot m^{-3}}$	%, ‰, ppm, ppb
substance amount fraction (mole fraction)	$\mathrm{mol^3 \cdot mol^{-1}}$	%, ‰, ppm, ppb
molality	$\mathrm{mol \cdot kg^{-1}}$	

to work with standard conditions for gas volume (hypothetical gas volume our sample would have at standard conditions of temperature and pressure). For gases these standard conditions are 0 °C and 101.3 kPa (atmospheric pressure at sea level). This standard volume is designated volume at STP [12].

Remember that we can choose other quantities to characterize the potential instead of the partial pressure. For example, we can use a concentration gradient. Because there are many ways to express a concentration (see Table 6.1), numerous expressions for the permeability coefficient P with different units will arise.

Instead of mass or volume, we can quantify the permeating flavor compound (transporting substance) in moles, i.e. in terms of substance. In that case it would be convenient to use a gradient of a concentration c on a mole basis. Then we have

$$-\frac{\text{amount of substance}}{\text{area} \cdot \text{time}} = K \cdot \text{concentration gradient}$$

so

$$\frac{1}{A} \cdot \frac{\mathrm{d}n}{\mathrm{d}t} = D \cdot \frac{\mathrm{d}c}{\mathrm{d}x} \tag{6.4}$$

Then, equation (6.4) is a special case of the general transport equation (6.2), and is called Fick's law. The coefficient in equation (6.4) is named coefficient of diffusion D. The physical units for D depend on the concentration units used. In the case where $[c] = \mathrm{mol \cdot m^{-3}}$, D has the simple units of $[D] = \mathrm{m^2 \cdot s^{-1}}$. Use of other units for concentration will result in other units for D.

Here

A	area in $\mathrm{m^2}$
n	amount of substance in mol
t	time in s
c	concentration in $\mathrm{mol \cdot m^{-3}}$
x	length in m
D	coefficient of diffusion in $\mathrm{m^2 \cdot s^{-1}}$

From the above study of flavor compound molecules permeating through a packaging film, we can see that there are numerous ways in which to express and to approach the same problem. In Table 6.2 and Table 6.3 an overview of

Table 6.2. Terms used in different transport processes

transport rate based on	$\dot{M}$ in equation (6.1) is called	SI unit of $\dot{M}$
mass	mass transport rate	$kg \cdot s^{-1}$
volume	volume transport rate density (flux)	$m^3 \cdot s^{-1}$
amount of substance (moles)	molar transport rate density	$mol \cdot s^{-1}$

Table 6.3. Cases of equation (6.1) and related terms

type of transport rate density	along gradient of …	then the coefficient is …
mass …	concentration in $kg \cdot m^{-3}$	coefficient of diffusion in $m^2 \cdot s^{-1}$
volume …	concentration in $m^3 \cdot m^{-3}$	coefficient of diffusion in $m^2 \cdot s^{-1}$
substance (moles) …	concentration in $mol \cdot m^{-3}$	coefficient of diffusion in $m^2 \cdot s^{-1}$
mass…	partial pressure in Pa	coefficient of permeability in $kg \cdot s^{-1} \cdot m^{-1} \cdot Pa^{-1}$
volume…	partial pressure in Pa	coefficient of permeability in $m^2 \cdot s^{-1} \cdot Pa^{-1}$
substance (moles) …	partial pressure in Pa	coefficient of permeability in $mol \cdot s^{-1} \cdot m^{-1} \cdot Pa^{-1}$

some of these expressions is given. In Table 6.5 some recommendations are made which give useful expressions for special cases of water vapor permeation.

6.2 Conductivity, Conductance and Resistance

The coefficient K of the general transport equation has the function of a specific conductivity. 'Specific' in this sense means the conductivity is specific for the material in which the transport is observed. The specific conductivity (like any specific coefficient) does not depend on the length and width of the system or the intersectional area A. So it is independent of the system geometry. Alternatively, we can work with a quantity that includes the geometry i.e. the surface area A across which permeation occurs and the length d. This is called conductance G. Writing equation (6.1) with the film thickness d we have:

$$-\frac{1}{A}\dot{M} = K \cdot \frac{\Delta\varphi}{d} \tag{6.5}$$

With

$$G = K \cdot \frac{A}{d} \tag{6.6}$$

this is

$$-\dot{M} = G \cdot \Delta\varphi \tag{6.7}$$

In words

– transport rate = conductance · difference in potential

The reciprocal of the conductance G is called resistance R.

$$G = \frac{1}{R} \tag{6.8}$$

where

M	transport rate
K	coefficient
A	area
d	thickness
φ	potential
G	conductance
R	resistance

The parameters of conductance G and its inverse, the resistance R, contain information about the sample geometry (length and width with respect to area A). The specific conductivity K and its inverse, specific resistivity, do not depend on geometry. These are material properties, only. Therefore, we use the specific conductivity and resistivity when quantifying the permeability of a material, such as a polymer packaging film to a given transporting substance. In contrast, we would use the conductance and resistance when quantifying the permeability of a specific package or packaging system with specified area and thickness of its protective polymer film.

6.3 Transport Through Solid Multilayers

When we need to study transport processes through a solid barrier which consists of two or more layers of different materials, the concept of added resistances can make our job very easy. Let us refer back to our flavor compound and packaging film example. In this case, we will assume we have a packaging material consisting of three different layers of materials. Packaging materials are often designed to serve as a barrier against various types of contamination from outside the package, as well as to prevent escape of desirable compounds from inside the package. Therefore, different materials may be needed in combination in order to meet each of these different objectives. For example a composite packaging material may need to serve as a barrier against light, oxygen, water vapor, etc. But, it must also serve to act as a marketing and sales display or handling tool [22,24].

Let us focus again on calculation of the flavor compound permeation through such a composite packaging material. First we have to take into account the make up of the three-layered material. Figure 6.2 illustrates the two principle ways in which a three-layered barrier material can offer resistance to mass transport (permeability). When the permeating flavor molecules have

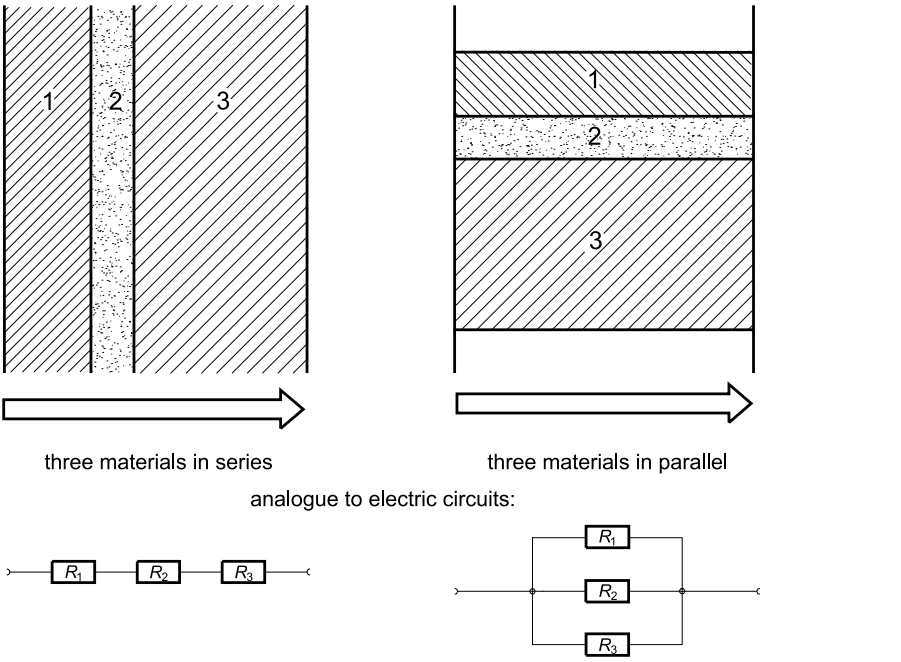

Figure 6.2. Diffusion through three layers of material seen as transport through resistances in series (left) or in parallel (right)

only one path such that they must travel through all three layers in series (one after the other), we can say the flavor molecules have to pass three resistances in series (Figure 6.2, left). When the three layers are oriented in the direction parallel to the path of the transporting molecules, the flavor molecules can travel on three different paths. In this parallel situation, they will do so according to the permeation resistances of the different paths. In this case, we can say the flavor molecules have to pass three resistances in parallel (Figure 6.2, right). These two resistance situations are completely analogous to the study of electric circuits with resistors in series or in parallel.

In the case of resistances in series, the total equivalent resistance is found by simply adding:

$$R_{total} = \sum_{i=1}^{n} R_i \tag{6.9}$$

In the case of resistances in parallel, the total equivalent resistance determined by taking the reciprocal of the sum of the reciprocal resistances:

$$\frac{1}{R_{total}} = \sum_{i=1}^{n} \frac{1}{R_i} \tag{6.10}$$

This is identical to:

$$\frac{1}{R_{total}} = \sum_{i=1}^{n} G_i = G_{total} \tag{6.11}$$

This general principle works for calculating mass transport, volume transport, or substance (mole) transport. At the end of the chapter we will see that it also works for transfer of heat or electricity.

Packaging films with multiple layers that act as resistances in series of the type shown on the left side in Figure 6.2, are very common in food packaging, where one layer may be needed to match the barrier properties against flavor permeation, and another thin layer of a costly high resistance material may be needed against oxygen permeation, which may need to be mounted on a thick layer of a bulk polymer in order to provide the mechanical strength needed of the package (see Section 4.7.1, with maximum breaking stress of a polymer). Further layers with barrier properties against other substances, or to meet label printing requirements can be further added. From the viewpoint of permeability, multilayer films are to be treated like resistances in series. On the other hand, when a food package consists of different parts, such as a jar and cap, then permeation can happen along two paths, i.e. through the wall of the jar and through the material of the cap. In that case, the total permeate resistance must be calculated by equation (6.10) for the case of resistances in parallel. The electric circuit analogy concept of added resistances shows its usefulness here, especially in more complicated cases where materials are combined in parallel and in series at the same time. Recall that the overall resistance and/or conductance of such complex packaging systems must take into account the geometry of the component parts and materials in addition to the material properties. These geometric properties would include the thickness d and the area A of the part of interest, such as the film or the cap.

In cases where parts of the multilayer material have the same area A or the same thickness d, the calculation can be further simplified. For the case of resistances in series only:

Sum of resistances in series:

$$R_{total} = \sum R_i \tag{6.9}$$

Because of (6.6) and (6.8)

$$R = \frac{d}{A} \cdot \frac{1}{K} \tag{6.12}$$

Therefore

$$R_{total} = \sum_i \frac{d_i}{A_i} \cdot \frac{1}{K_i} \tag{6.13}$$

If $A_1 = A_2 = A_3 = A$ and $d_1 = d_2 = d_3 = d$ we can write

$$R_{total} = \frac{d}{A} \sum_i \frac{1}{K_i} \tag{6.14}$$

If $A_1 = A_2 = A_3 = A$ only we can write

$$R_{total} = \frac{1}{A} \sum_i \frac{d_i}{K_i} \tag{6.15}$$

When we have multilayer films then normally the permeation area of all the films is the same, but the thickness of the layers will be different. So, equation (6.15) applies.

6.4 Food Packaging Considerations

When we deal with food packaging technology, we are looking for packaging systems which enhance shelf life of food. In other words, the packaging goal is to retain the quality of a food as much as possible during the time period between release and time of use. When we look more deeply into reaction kinetics and keeping quality, we recognize that the packaging objective often is to slow down specific deterioration reaction rates, but we cannot bring them to zero [23]. So, with a planned schedule of food production, storage and shipping time, we have to design food processes and packaging systems capable of delivering the food to the consumer with the level of acceptable quality expected by the consumer.

Depending on the type of food product, decreasing deterioration reaction rates by packaging can be reached in some of the following ways as examples:

- keep out light
- suppress uptake of gaseous substances (water vapor, oxygen, off flavors)
- suppress loss of gaseous substances (flavor compounds, water vapor, oxygen, nitrogen, carbon dioxide).

Again, depending on the type of food product, we can define critical parameters inside the package which must be controlled in order to have good quality, such as water activity or oxygen concentration. With these critical parameters under control, we can specify the permeability needed by the package. For example, by choosing appropriate material and thickness, the permeation of water vapor or oxygen through the package can be controlled. Specification of permeability is only part of the design of a package. Additional factors that must be considered include mechanical, economical, marketing and regulatory requirements.

Let us focus next on the calculation of permeation for packaging materials, and let us start with a packaging film like that shown in Figure 6.3.

When we calculate the permeation of water vapor, we often use a transport rate based on mass instead of a volume base (see Table 6.2). With the assumption of steady state, then we have:

$$-\frac{1}{A} \cdot \frac{\mathrm{d}m}{\mathrm{d}t} = P \cdot \frac{\Delta p}{d} \tag{6.2}$$

and the coefficient of permeability is

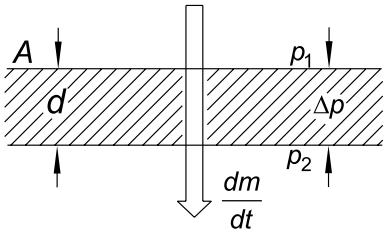

Figure 6.3. Permeation through a film (schematic)

$$P = \left| \frac{\dot{m} \cdot d}{A \cdot \Delta p} \right| \tag{6.16}$$

where

A	area in m^2
m	mass in kg
t	time in s
p	partial pressure in Pa
d	thickness of film in m
P	coefficient of permeability in $kg \cdot s^{-1} \cdot Pa^{-1} \cdot m^{-1}$

When we have to calculate the permeation of a gas like oxygen, nitrogen, or carbon dioxide, we often prefer to specify the transport rate based on volume instead of mass (see Table 6.2). With the assumption of steady state, then we have:

$$-\frac{1}{A} \cdot \frac{\mathrm{d}V}{\mathrm{d}t} = P \cdot \frac{\Delta p}{d} \tag{6.3}$$

$$P = \left| \frac{\dot{V} \cdot d}{A \cdot \Delta p} \right| \tag{6.17}$$

where

V	volume in m^3
P	coefficient of permeability in $m^2 \cdot s^{-1} \cdot Pa^{-1}$

We can also use a transport rate based on substance (moles), which often is preferred in chemical considerations:

$$-\frac{1}{A} \cdot \frac{\mathrm{d}n}{\mathrm{d}t} = P \cdot \frac{\Delta p}{d} \tag{6.4}$$

$$P = \left| \frac{\dot{n} \cdot d}{A \cdot \Delta p} \right| \tag{6.18}$$

where

n	amount of substance in mol
P	coefficient of permeability in $mol \cdot s^{-1} \cdot m^{-1} \cdot Pa^{-1}$

Whether we choose mass, volume or mole base, depends most often on the measuring technique used. So, water vapor uptake often is measured by gravity,

i.e. on a mass basis, whereas other gases are not weighed but measured as gas concentrations in form of a volume fraction, as an example.

In all cases steady state can be assumed only when (besides temperature) the driving force, i.e. the gradient of the partial pressure, is constant over time. This assumption (p_1, p_2 = constant) is an approximation we have to check for each individual case.

Example 6.1. Calculate the coefficient of permeability of a polymer film bag
A closed film bag consists of a film with an area of 14 cm^2 and a thickness of 20 µm. The bag is stored in a room at 25 °C under air at 102.0 kPa. Initially the closed film bag was free of oxygen, but after 20 hours in the bag, an oxygen level of 0.2 cm^3 O_2 was detected. Calculate the coefficient of permeability for the entire bag.

Solution
First, let us calculate the *STP* gas volume. We assume the oxygen behaves like an ideal gas (equation (2.10)):

$$\frac{p_1 V_v}{T_1} = \frac{p_2 V_2}{T_2}$$

so

$$V_{STP}^{O_2} = \frac{p_2 V_2 \cdot T_{STP}}{T_2 \cdot p_{STP}} = V_2 \cdot \frac{T_{STP}}{T_2} \cdot \frac{p_2}{p_{STP}} = 0.2\,\mathrm{cm}^3 \cdot \frac{273.15}{298.15} \cdot \frac{102.0}{101.3}$$

that is

$$V_{STP}^{O_2} = 0.184\,\mathrm{cm}^3(STP) = 1.84 \cdot 10^{-7}\,\mathrm{m}^3(STP)$$

Second, let us calculate the partial pressure difference. Outside of the bag we have air with an oxygen concentration of 20.9% (V/V). So the oxygen partial pressure outside is:

$$p_{outside}^{O_2} = p_{total} \cdot x_{O_2} = 102.0\,\mathrm{kPa} \cdot 0.209 = 21.318\,\mathrm{kPa}$$

Assuming the oxygen partial pressure inside is constant at zero, the difference is

$$\Delta p = p_2 - p_1 = 0\,\mathrm{Pa} - 21.318\,\mathrm{kPa} = -21.318\,\mathrm{kPa}$$

Now we can calculate the coefficient of permeability using equation (6.17):

$$P = \left| \frac{1.84 \cdot 10^{-7}\,\mathrm{m}^3(STP) \cdot 20 \cdot 10^{-6}\,\mathrm{m}}{14 \cdot 10^{-4}\,\mathrm{m}^2 \cdot (-21.318\,\mathrm{kPa}) \cdot 20 \cdot 3600\,\mathrm{s}} \right| = \frac{1.71 \cdot 10^{-18}\mathrm{m}^3(STP) \cdot \mathrm{m}}{\mathrm{m}^2 \cdot \mathrm{Pa} \cdot \mathrm{s}}$$

So,

$$P = 1.49 \cdot 10^{-4} \frac{\mathrm{cm}^3(STP) \cdot \mathrm{cm}}{\mathrm{cm}^2 \cdot \mathrm{bar} \cdot \mathrm{d}}$$

If we could tolerate less precision, we could estimate the coefficient of permeability a little more easily as follows:

$$P \approx \left| \frac{0.2\,\mathrm{cm}^3 \cdot \frac{1}{500}\,\mathrm{cm}}{14\,\mathrm{cm}^2 \cdot \frac{1}{5}\,\mathrm{bar} \cdot \mathrm{d}} \right| = \frac{0.2}{14 \cdot 100} \frac{\mathrm{cm}^2}{\mathrm{bar} \cdot \mathrm{d}} = 1.4 \cdot 10^{-4} \frac{\mathrm{cm}^2}{\mathrm{bar} \cdot \mathrm{d}}$$

Now let us consider a two-layer packaging film like in Figure 6.4. More than one layer of film is used in order to combine desirable properties of both materials, e.g. mechanical properties and gas barrier properties. Sometimes for quality reasons food is packaged under modified atmosphere. Depending on the type of food, a modified atmosphere can consist of an oxygen-free mixture of nitrogen and carbon dioxide, but sometimes may consist of mixtures with high oxygen concentrations. Recalling that each material has different barrier properties for different types of gas, we have to calculate the coefficients of permeability for each gas separately.

Example 6.2. Calculate the coefficient of permeability for CO_2 transfer across a two-layer film like in Figure 6.4. Material 1 has a thickness of 40 µm and a $P_1^{CO_2} = 2 \cdot 10^5\ \mathrm{cm}^3 \cdot \mu\mathrm{m} \cdot \mathrm{m}^{-2} \cdot \mathrm{bar}$. Material 2 has a thickness of 10 µm and a $P_2^{CO_2} = 5.65\ \mathrm{cm}^3 \cdot \mu\mathrm{m} \cdot \mathrm{m}^{-2} \cdot \mathrm{bar}$.

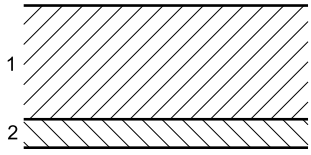

Figure 6.4. Two layer packaging film (schematic)

Recalling Section 6.3, we can treat the problem like a combination of resistances in series. So, with equation (6.14), we have the following:

$$R_{total} = \frac{1}{A} \sum_i \frac{d_i}{K_i} = \frac{1}{A} \sum_i \frac{d_i}{P_i}$$

and

$$R_{total} = \frac{1}{A} \cdot \frac{d_{total}}{P_{total}}$$

so

$$P_{total} = \frac{d_{total}}{A} \cdot (R_{total})^{-1}$$

Now with equation (6.14)

$$P_{total} = \frac{d_{total}}{A} \cdot \left(\frac{1}{A} \sum_i \frac{d_i}{P_i} \right)^{-1} = \frac{d_{total}}{\sum_i \frac{d_i}{P_i}}$$

so

$$P_{total} = \frac{d_{total}}{\sum_i \frac{d_i}{P_i}} = \frac{d_1 + d_2}{\frac{d_1}{P_1} + \frac{d_1}{P_2}} = \frac{(40 + 10)\,\mu m}{\left(\frac{40}{2 \cdot 10^5} + \frac{10}{5.65}\right)\frac{m^2 \cdot bar}{cm^3}}$$

that is

$$P_{total} = \frac{(40 + 10)\,\mu m \cdot cm^3}{1.77\,m^2 \cdot bar} = 28.2\,cm^3 \cdot \mu m \cdot m^{-2} \cdot bar^{-1}$$

When we compare P_{total} to P_1,

$$\frac{P_{total}}{P_1} = \frac{28.2}{2 \cdot 10^5} = 1.4 \cdot 10^{-4} = \frac{1}{7000}$$

We see that the CO_2 permeability of the composite film is significantly lower than that of the single material (by a factor of 7000).

6.5 Molecular Transport in Permeation

In order to obtain a better understanding of transport phenomena across a permeable barrier (permeation) it is important to study what is happening on a molecular scale. Permeation takes place through a process involving a number of consecutive steps. In order for a molecule to permeate through a solid, it must go through the following necessary steps:

- transport of the molecule to the solid interface
- adsorption of the molecule on interface of the solid (see Section 1.2 on sorption)
- dissolution of the molecule into the solid
- diffusion of the molecule in the direction of the driving force (counter-current to the partial pressure gradient)
- dissolution of the molecule onto the surface at the other side of the solid interface
- desorption of the molecule from this opposite interface surface
- transport away from this interface surface

Note that these multiple steps involve the phenomena of both solubility, as well as diffusion. Therefore, information about the solubility S of the molecules in the solid barrier material is needed, as well as the coefficient of diffusion D of the permeating molecule in the solid. In this case, the overall coefficient of permeability is the product of diffusion coefficient D and solubility S:

$$P = D \cdot S \tag{6.19}$$

For small pressures, the solubility is given by Henry's law which represents a linear relationship between partial pressure and the concentration of the dissolved gas:

$$S = \frac{c}{p} \tag{6.20}$$

where

P	coefficient of permeability in $m^2 \cdot s^{-1} \cdot Pa^{-1}$
D	coefficient of diffusion in $m^2 \cdot s^{-1}$
S	solubility in $\frac{m^3(STP)}{m^3 \cdot Pa}$
c	concentration of dissolved gas in $\frac{m^3(STP)}{m^3}$
p	partial pressure in Pa

From equation (6.19), it can be seen that the coefficient of permeability for a packaging film against an "invading" gaseous molecule can be decreased by choosing a material with a low solubility for that gas. For example polyolefin materials have a lower solubility for water than polyamide polymers. Therefore polyolefin films are preferred to be used as a barrier against water vapor rather than polyamide films.

6.6 Temperature Dependency

Diffusion and solubility both depend upon temperature. The temperature dependency for both of these can be approximated by the Arrhenius relationship [3], i.e.

$$S = S_0 \cdot e^{\frac{\Delta_{sol}H}{RT}} \tag{6.21}$$

and

$$D = D_0 \cdot e^{\frac{E_D}{RT}} \tag{6.22}$$

and, because of (6.19), also:

$$P = P_0 \cdot e^{-\frac{E_P}{RT}} \tag{6.23}$$

whereas,

$$E_P = E_D + \Delta_{sol}H \tag{6.24}$$

where

E_p	activation energy for permeation in $J \cdot mol^{-1}$
E_D	activation energy for diffusion in $J \cdot mol^{-1}$
$\Delta_{sol}H$	dissolution enthalpy in $J \cdot mol^{-1}$
R	universal gas constant

Plotting the logarithm of permeability versus the inverse absolute temperature, we get a straight line (Figure 6.5). The activation energy for permeation, in $J \cdot mol^{-1}$, can be calculated. from the slope this line.

$$\ln \frac{P(T_2)}{P(T_1)} = -\frac{E_P}{R}\left(\frac{1}{T_2} - \frac{1}{T_1}\right) \tag{6.25}$$

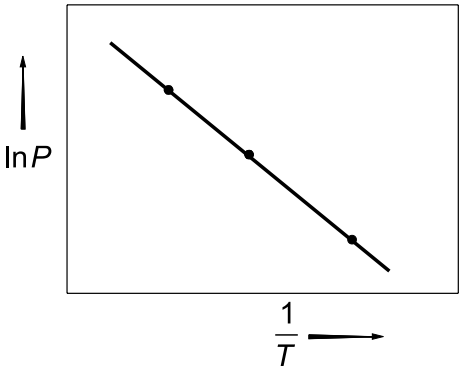

Figure 6.5. Arrhenius plot of permeability at different absolute temperatures (reciprocal)

with the slope m in Figure 6.5

$$E_P = m \cdot R \tag{6.26}$$

Therefore, in order to calculate the permeability of a material at a certain temperature, we need data for activation energy E_P. Often for a special material, those data are not available from literature. In that case, it is necessary to perform experiments at different temperature in order to construct an ARRHENIUS plot from which to estimate E_P.

6.7 Measurement of Permeability

Now, we have a clear understanding of the importance for knowing the permeability of a permeable barrier material like a packaging film to a transporting substance. Therefore, it is important to know how permeability can be measured in the laboratory. Measurements can be made with either pieces of a packaging material or with a complete package. Polymer films and composite materials are the type of barrier materials which are of most interest in food packaging for measurement of permeability because they posses some degree of permeability to most gaseous substances. In contrast, impervious packaging materials like glass and metal (glass jars and metal cans) have no permeability at all, and are not subject to measurement of permeability. However, sometimes the influence of caps, seals and other accessories may be of interest when permeability of the entire sealed container is in question [4,5].

To measure permeability, the partial pressure on both sides of the material sample or sealed package has to be controlled. It is also desirable to have steady state permeation, because analysis of the data is much simpler than from a transient state. Therefore, to assure steady state mass transfer conditions, we only have to keep partial pressures on both sides constant. Then, the amount of gas permeating through the barrier material is measured and recorded over time.

Table 6.4. Standard climatic conditions, examples

climate code	after	φ / %r.h.	T/°C
23/50	[24]	23	50
20/65	[24]	65	20
27/65	[24]	65	27
C	[14]	75	25
E	[14]	85	20
D	[14]	85	23
A	[14]	90	25
B	[14]	90	38

Measuring water permeability of a package can be performed easily by placing a water-absorbent (desiccant, see Section 1.2.9) in the sealed package. The desiccant will maintain a controlled constant near zero partial pressure of water vapor in the sealed package. Meanwhile, the pressure of the humid atmosphere outside the sealed package must be adjusted to the desired constant value, and controlled constant at this value, thus assuring steady state conditions. Under these conditions a constant pressure gradient is established. All water vapor which reaches the inside of the package will be absorbed into the desiccant over time. So, by recording the increasing weight of the desiccant over time, we can measure the water vapor transport rate. This can be accomplished by simply weighing the entire sealed package with desiccant in it, hour by hour, to record the weight gain.

To adjust the water vapor pressure $p_D^{H_2O}$ outside of the package, there are different possibilities. In climate-controlled chambers, the desired water vapor pressure is established by adjusting and controlling (and measuring) the relative humidity in the chamber. This is normally accomplished by humidification and dehumidification systems which cause evaporation or condensation of water on surfaces at controlled temperature. These systems are a normal part of the control systems in climate-control chambers. Another possibility is to place a humidity standard in a closed chamber. Saturated electrolyte solutions are often used for this purpose [13–15,17,18] (see Table 1.12). For better comparison of results, sometimes standardized climatic conditions are used in testing of permeability. Table 6.4 shows some examples of standard climates.

Standards for testing water vapor transmission are available from metrological institutions (see e.g. [19–21]. A procedure given in [18] (see Figure 6.6) works as follows: A circular sample of film to be analyzed is used to seal the mouth of a glass jar having diameter of 90 mm containing a desiccant within the jar. The desiccant-equipped jar is placed in a chamber with adjusted to a standard climate control set for climate "C" from Table 6.4. From time to time the weight of the jar is recorded and plotted versus time. This is done until there is a linear m–t curve with at least three points. From the slope $\frac{\Delta m}{\Delta t}$ of

the line drawn through the plotted data points and the area of the sample, the water vapor permeability is calculated:

$$WVP = \frac{1}{A}\frac{\Delta m}{\Delta t} \tag{6.27}$$

The unit of WVP is e.g. $g \cdot m^{-2} \cdot d^{-1}$. The climate conditions and the thickness of the sample must also be recorded and reported with the calculated result. The desiccant can be silica with a particle size between 1.5 mm and 2 mm or a $CaCl_2$ granulate.

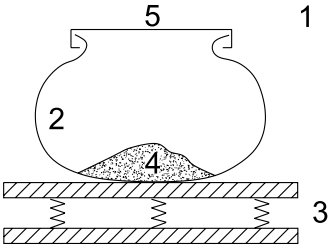

Figure 6.6. Gravimetric measurement of the water vapor permeability of a film (schematic). **1:** chamber with standard climate, **2:** jar, **3:** balance, **4:** absorbent (desiccant), **5:** film sample

Example 6.3. Gravimetric measurement of water vapor permeability of a food wrap film

An experiment as described in the section above was performed at 25 °C with a climate of 25 °C and 66% r.h. in a chamber with an opening width of 25.5 mm. Calculate the water vapor permeability in $g \cdot m^{-2} \cdot d^{-1}$.

plot

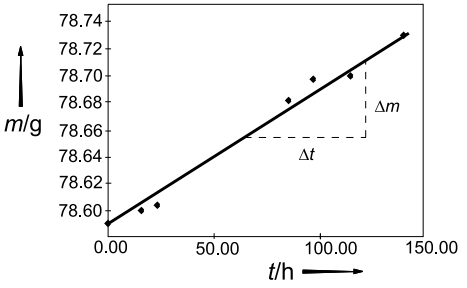

raw data

time stamp	*t*/h	*m*/g
05.10.00 15:56	0.000	78.5908
06.10.00 08:10	16.233	78.6063
06.10.00 15:20	23.400	78.6155
09.10.00 08:45	88.817	78.6841
09.10.00 16:25	96.483	78.6928
10.10.00 08:25	112.483	78.7092
11.10.00 11:15	139.317	78.7370

Figure 6.7. Mass versus time plot during water vapor permeation

From the slope in Figure 6.7 we get

$$\frac{\Delta m}{\Delta t} = 3 \cdot 10^{-10}\,kg \cdot s^{-1}$$

So, with $A = \pi \cdot r^2 = \pi \cdot (12.75\,\text{mm})^2 = 5.1 \cdot 10^{-4}\,\text{m}^2$

$$WVP = \frac{1}{A}\frac{\Delta m}{\Delta t} = \frac{1}{5.1 \cdot 10^{-4}\,\text{m}^2} \cdot 3 \cdot 10^{-7}\,\text{g} \cdot \text{s}^{-1} = 50.8\,\text{g} \cdot \text{d}^{-1} \cdot \text{m}^{-2}$$

Example 6.4. Knowing the thickness of the film to be 10 µm, calculate the water vapor permeability in the form of equation (6.27).
First we have to calculate the water vapor partial pressures:

With $p = \varphi \cdot p_s$ we get

$$p_s\ (25\,^\circ\text{C}) = 3.166\,\text{kPa}$$

We have outside:

$$p = 0.66 \cdot 3.1666\,\text{kPa} = 2.090\,\text{kPa}$$

with the value inside of:

$$p = 0 \cdot 3.1666\,\text{kPa} = 0\,\text{Pa}$$

The difference remains:

$$\Delta p = 2089.6\,\text{Pa} - 0\,\text{Pa} = 2.090\,\text{kPa}$$

so with

$$P = \frac{\Delta m}{\Delta t} \cdot \frac{d}{A \cdot \Delta p}$$

the coefficient is

$$P = 3 \cdot 10^{-10}\,\text{kg} \cdot \text{s}^{-1} \frac{10 \cdot 10^{-6}\,\text{m}}{\pi\left(12.75 \cdot 10^{-3}\right)^2\,\text{m}^2 \cdot 2090\,\text{Pa}}$$

i.e.

$$P = 2.8 \cdot 10^{-15}\,\text{kg} \cdot \text{m} \cdot \text{m}^{-2} \cdot \text{s}^{-1} \cdot \text{Pa}^{-1}$$

There are some alternative ways to express this same result.

Table 6.5 suggests what expression is best to use for what purpose or situation.

Table 6.5. Different ways to express water vapor transmission rates

case	formula		in case of Example 6.3
A	based on the mass flow rate, only	$\frac{\Delta m}{\Delta t} =$	$\dot{m} = 3 \cdot 10^{-10}\,\text{kg} \cdot \text{s}^{-1} = 26\,\text{mg} \cdot \text{d}^{-1}$
B	taking into account the area also ("flux")	$\frac{1}{A} \cdot \frac{\Delta m}{\Delta t} =$	$50.8\,\text{g} \cdot \text{d}^{-1} \cdot \text{m}^{-2} = 5.1\,\text{mg} \cdot \text{d}^{-1} \cdot \text{cm}^{-2}$
C	taking into account the thickness also	$\frac{1}{A} \cdot \frac{\Delta m}{\Delta t} \cdot d =$	$50.8\,\text{mg} \cdot \text{d}^{-1} \cdot \mu\text{m} \cdot \text{cm}^{-2}$
D	taking into account the pressure also	$\frac{1}{A} \cdot \frac{\Delta m}{\Delta t} \cdot \frac{d}{\Delta p} =$	$2.8 \cdot 10^{-15}\,\text{kg} \cdot \text{s}^{-1} \cdot \text{m} \cdot \text{m}^{-2} \cdot \text{Pa}^{-1}$ or $2.4\,\text{g} \cdot \text{d}^{-1} \cdot \text{cm}^{-2} \cdot \mu\text{m} \cdot \text{bar}^{-1}$

6.8 Analogous Transport Phenomena (Heat and Electricity)

The general transport equation is not limited to mass transfer only. It can also be used for heat transfer and transfer of electricity under steady state conditions.

Recall our equation (6.1) from the beginning of the chapter:

$$-\frac{1}{A}\cdot\frac{\mathrm{d}M}{\mathrm{d}t} = K\cdot\frac{\mathrm{d}\varphi}{\mathrm{d}x} \tag{6.1}$$

It can also be used with

$$-\frac{\text{amount of heat}}{\text{area}\cdot\text{time}} = \text{coefficient}\cdot\text{gradient of potential}$$

with the temperature representing the potential, so

– heat flow density = coeffcient · gradient of temperature

or

$$-\frac{1}{A}\cdot\frac{\mathrm{d}Q}{\mathrm{d}t} = \lambda\cdot\frac{\mathrm{d}T}{\mathrm{d}x} \tag{6.28}$$

In this case the equation is called Fourier's law (the first of Fourier's laws), and the coefficient is simply the thermal conductivity of the material across which the heat transfers.

Here

A	area
Q	heat
t	time
φ	potential
T	temperature
U	voltage
x	length
K	coefficient
λ	thermal conductivity
κ	electrical conductivity

Equation (6.1) can also be written as:

$$-\frac{\text{amount of electricity}}{\text{area}\cdot\text{time}} = \text{coefficient}\cdot\text{gradient of potential}$$

with the voltage being the potential, so

– electric current density = coefficient · gradient of voltage

or

$$-\frac{1}{A}\cdot\frac{\mathrm{d}Q_C}{\mathrm{d}t} = \kappa\cdot\frac{\mathrm{d}U}{\mathrm{d}x} \tag{6.29}$$

Table 6.6. Types of transport phenomena

type of transport rate density	along gradient of …	then the coefficient is …
mass …	concentration, in $kg \cdot m^{-3}$	coefficient of diffusion in $m^2 \cdot s^{-1}$
volume …	concentration, in $m^3 \cdot m^{-3}$	coefficient of diffusion in $m^2 \cdot s^{-1}$
substance (moles) …	concentration, in $mol \cdot m^{-3}$	coefficient of diffusion in $m^2 \cdot s^{-1}$
mass …	partial pressure	coefficient of permeability in $kg \cdot s^{-1} \cdot m^{-1} \cdot Pa^{-1}$
volume …	partial pressure	coefficient of permeability in $m^2 \cdot s^{-1} \cdot Pa^{-1}$
substance (moles) …	partial pressure	coefficient of permeability in $mol \cdot s^{-1} \cdot m^{-1} \cdot Pa^{-1}$
heat …	temperature	thermal conductivity in $W \cdot K^{-1} \cdot m^{-1}$
electricity…	voltage	electrical conductivity in $S \cdot m^{-1}$

In this case, the equation is called OHM's law, and the coefficient consists of the specific electrical conductivity (reciprocal of electrical resistance). So Table 6.3 obviously was not complete and should be as shown in Table 6.6.

Depending on the type of transport phenomena we investigate, there are different terms for the transport coefficient and its derived quantities. Table 6.7 gives a comprehensive overview.

6.9 Applications

pizza: mass transfer during baking [6]
apple: influence of water vapor diffusion coefficient on drying [7]
strawberries: role of diffusion coefficient on osmotic drying [8]
shelf life prediction: influence of water activity on permeability of a film [9]
Mass transfer coefficients: collection of literature data [10]
lactose crystallization: role of diffusion coefficient [11]
whey-protein-coated plastic films as oxygen barrier [25]
cellophane films: water vapor permeability [26]
high pressure: permeation of aroma compounds through plastic films [27]
aluminum oxynitride films: nanodefects influencing gas barrier properties [28]
horticultural packaging: mathematical modeling of water vapor transport [29]

Table 6.7. Terms of different usages of the general transport equation

transport phenomena	transport equation	R is called	$\frac{1}{R} = G$	$\frac{1}{R} = K \cdot \frac{A}{d}$	K is called	$\frac{1}{K}$ is called
substance amount/mol	$\dot{n} = \frac{1}{R} \cdot \Delta c$ (Fick´s law)	resistance of diffusion in $s \cdot m^{-3}$	conductance of diffusion in $m^3 \cdot s^{-1}$	$\frac{1}{R} = D \cdot \frac{A}{d}$	coefficient of diffusion in $m^2 \cdot s^{-1}$	diffusion resistivity in $s \cdot m^{-2}$
mass/kg	$\dot{m} = \frac{1}{R} \cdot \Delta p$ (permeation of gases)	resistance of permeation in $Pa \cdot s \cdot kg^{-1}$	conductance of permeation in $kg \cdot s^{-1} \cdot Pa^{-1}$	$\frac{1}{R} = P \cdot \frac{A}{d}$	coefficient of permeation in $kg \cdot m \cdot s^{-1} \cdot m^{-2} \cdot Pa^{-1}$	permeation resistivity in $Pa \cdot s \cdot m \cdot kg^{-1}$
charge/C	$I = \frac{1}{R} \cdot U$ (Ohm's law)	electric resistance in Ω	electrical conductance in S	$\frac{1}{R} = \kappa \cdot \frac{A}{d}$	specific electric conductivity in $S \cdot m^{-1}$	electric resistivity in $\Omega \cdot m^{-1}$
heat/J	$\dot{Q} = \frac{1}{R} \cdot \Delta T$ (Fourier's law)	thermal resistance in $K \cdot W^{-1}$	thermal conductance of in $W \cdot K^{-1}$	$\frac{1}{R} = \lambda \cdot \frac{A}{d}$	specific thermal conductivity in $W \cdot K^{-1} \cdot m^{-1}$	heat resistivity in $K \cdot m \cdot W^{-1}$
			Geometry-dependent quantities		Non-geometry-dependent quantities	

Literature

1. DIN 55405 (2006) Packaging – Terminology – Terms and definitions, in [101]
2. Henyon DK(ed) (1991) Food Packaging Technology. American Society of Testing and Materials (ASTM), West Conshohocken, PA
3. Piringer OG, Baner AL (2007) Plastic Packaging Materials for Food. Wiley-VCH, Weinheim
4. Robertson GL (1993) Food Packaging. Marcel Dekker, New York
5. Bureau G, Multon JL (eds.) (2003) Food Packaging Technology. Wiley-VCH, Weinheim
6. Dumas C, Mittal GS (2002) Heat and mass transfer properties of pizza during baking. Intern J Food Properties 5:161
7. Funebo T, Ahrne L, Prothon F, Kidman S, Langton M, Skjoldebrand C (2002) Microwave and convective dehydration of ethanol treated and frozen apple - physical properties and drying kinetics. Int J Food Sci Tech 37:603–614
8. Fernando M, Spiess WEL (2003) Mass transfer in strawberry tissue during osmotic treatment. J Food Sci 68:1347–1364
9. Del Nobile MA, Buonocore GG, Limbo S, Fava P (2003) Shelf life prediction of cereal-based dry feeds packed in moisture sensitive films. J Food Sci 68: 1292–1300
10. Krokida M, Zogzas N, Maroulis, Z (2001) Mass transfer coefficient in food processing: compilation of literature data. Intern J Food Properties 4:373
11. Visser RA (1983) Crystal growth kinetics of alpha lactose hydrate. Dissertation, Catholic University Nijmwegen
12. DIN 1343 (1990) Reference conditions, normal conditions, normal volume; concepts and values, in [101]
13. ASTM E104-02 Standard practice for maintaining constant relative humidity by means of aqueous solutions, in [132]
14. DIN 50014 (1985) Climates and their technical application; standard atmospheres, or ISO 554 (1976) Standard atmospheres for conditioning and/or testing; Specifications, both in [101]
15. ISO 554 (1976) Standard atmospheres for conditioning and/or testing; Specifications, in [101]
16. BS EN 20187 (1993) Paper, board and pulps - Standard atmosphere for conditioning and testing and procedure for monitoring the atmosphere and conditioning of samples, in [101]
17. ASTM D5032-97 (2003) Standard Practice for Maintaining Constant Relative humidity by Means of Aqueous Glycerin Solutions, in [132]
18. DIN 50008-1 (1981) Atmospheres and their technical application; Standard atmospheres over aqueous solutions; Saturated salt solutions, glycerol solutions, in [101]
19. DIN 53122-1 (2001) Testing of plastics and elastomer films, paper, board and other sheet materials - Determination of water vapour transmission – Part 1: Gravimetric method, in [101]
20. ASTM E96/E96M-05 (2004) Standard Test Methods for water vapour transmission of Materials, in [132]
21. ASTM E 398 (2003) Standard Test Method for Water Vapor Transmission Rate of Sheet Materials Using Dynamic Relative Humidity Measurement, in [132]
22. Paine FA, Paine HY (1995) Handbook of Food Packaging. Aspen Publishers Gaithersburg
23. Mc Elhatton A,Marshall RJ(eds) (2006) Food Safety - A Practical and Case Study Approach, Springer Heidelberg
24. Bernd S, (2003) Lexikon der Verpackungstechnik. Behr´s, Hamburg

25. Seok-In Hong, Krochta JM (2006) Oxygen barrier performance of whey-protein-coated plastic films as affected by temperature, relative humidity, base film and protein type. J Food Engineering 77:739–745
26. Del Nobile MA, Fava P, Piergiovanni L (2002) Water transport properties of cellophane flexible films intended for food packaging applications. J Food Engineering 53:295–300
27. Götz J, Weisser H (2002) Permeation of aroma compounds through plastic films under high pressure: in-situ measuring method. Innovative Food Science & Emerging Technologies 3:25–31
28. Erlat AG, Henry BM, Ingram JJ, Mountain DB, McGuigan, A, Howson RP, Grovenor CRM, Briggs GAD, Tsukahara Y (2001) Characterisation of aluminium oxynitride gas barrier films. Thin Solid Films 388:78–86
29. Tanner DJ, Cleland AC, Robertson TR (2002) A generalised mathematical modelling methodology for design of horticultural food packages exposed to refrigerated conditions: Part 3, mass transfer modelling and testing. Intern J Refrigeration 25:54–65

7 Thermal Properties

Most of the food processing operations used to prolong the shelf life of foods involve heating foods to temperatures capable of inactivating microbial and enzymatic activity. These heat treatments are based on controlled heat transfer that depends upon thermal properties of the food materials. In order to increase the internal temperature of a food product, heat must first be transferred to the outer surface of the food, and then transmitted through the food material in order to reach the center of the food product. This is an example of heat transfer. In Section 7.6 heat transfer is described in more detail. When heat is added to a material (heating), the temperature of that material will increase so long as it is not undergoing a change in phase. The extent of temperature rise is governed by the heat capacity of the material (see Section 7.4). When heat is removed from a material (cooling), and transferred to a surrounding heat exchange medium at a lower temperature, the temperature of the material will decrease. Figure 7.1 illustrates these different directions of heat flow. In food processing, thermal process operations are very important for food safety. Some examples of thermal process operations are listed in Table 7.1.

In this chapter we want to focus on thermal properties of foods, such as heat capacity, temperature and enthalpy of phase transition points (melting, freezing, glass transition, chemical reactions, evaporation, etc.), as well as the

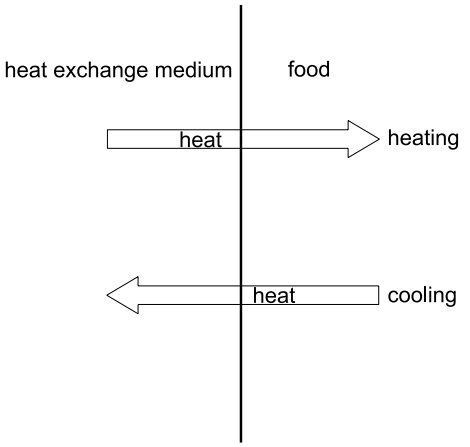

Figure 7.1. Heat transfer across the interface of a food

Table 7.1. Thermal process operations important in food engineering:

operation	purpose	food examples	heat exchange medium	temperature range
pasteurization/ sterilization	inactivation of pathogenic microorganisms for increasing shelf life.	meat, fish, soup, vegetables, fruit, cream	electricity, hot water, steam (direct or indirect steam)	63–135 °C
– batch	canned solids and liquids	milk, cream, custard, desserts, soup, fruit, juice, beer, egg		
– continuous flow / liquids (UHT/HTST)	long-life aseptic packaging	long-life milk, cream, fruit juices		
evaporation	removal of water, production of liquid concentrate	milk, fruit and vegetables, coffee, cheese whey	steam	40–100 °C
dehydration	removal of water, production of dried material with low water activity	milk, potato, vegetables, fruit, meat, fish	hot air, steam, hot water, electricity	150–250 °C
frying	reactions (proteins, carbohydrates), evaporation of water	French fries, potatoes, doughnuts	hot oil	100–150 °C
cooking/baking	reactions (proteins, carbohydrates), evaporation of water	catering operations, bread, meat pies, cakes	steam, hot air, microwaves	100–200 °C
chilling/freezing	reducing spoilage reactions, microbial activity	dairy products, meat, fish, fruit, vegetables, frozen desserts	cold air, refrigerants, cryogenic fluids (liquid nitrogen)	10–0 °C (−18)–(−30) °C (−100)–(−200) °C

caloric value of foods. We will also introduce some methods and techniques for measuring some of these thermal properties.

7.1 Temperature

The temperature of a system is an indication of the kinetic energy exhibited by the molecular motion taking place within the constituent substances of the system. This kinetic energy increases with increasing temperature (molecules move about at greater speed). The mathematical product of absolute temperature T and BOLTZMANN's constant k is called the thermal energy E of a system.

$$E = k \cdot T \tag{7.1}$$

where

E	energy in J
k	BOLTZMANN's constant in $\mathrm{J \cdot K^{-1}}$
T	temperature in K

On a molecular scale, the thermal energy is the kinetic energy of the molecules moving about within a system. Recall the ideal gas where there velocity distribution of the gas atoms is a function of the temperature (see Appendix 15.2 about distribution functions). On a macroscopic scale, the thermal energy of a system can be expressed by the temperature of the system. So, a high system temperature indicates the molecules have high kinetic energy. At a hypothetical zero temperature, the molecules will be completely at rest with no kinetic energy. This is the lower limit (zero point) of the absolute temperature scale (thermodynamic temperature scale). It has no upper limit. The temperature unit chosen for this scale is 1 K (KELVIN), which is defined as $\frac{1}{273.16}$ of the triple point temperature of water. This triple point is the same at any point in the world, and is called a fixed point of the thermodynamic temperature scale. Figure 15.8 illustrates the triple point of water as a point in the state diagram that can be exactly defined by the temperature and pressure at which the three phases of water are coexisting.

Because of historic reasons, there are other temperature scales (°C, °F, °R) having other units and fixed points. For example, the CELSIUS scale is based on the fixed points for the temperatures at which water will freeze (freezing point) and boil (boiling point) at standard atmospheric pressure. The temperature difference between those fixed points was defined to be 100 degrees. In a similar manner the FAHRENHEIT scale was based on two fixed points that could be recognized at the time. Zero on the FAHRENHEIT scale ($-17.8\,^{\circ}\mathrm{C} = 0\,^{\circ}\mathrm{F}$) was the lowest temperature that could reached at that time, and the high point of the scale ($100\,^{\circ}\mathrm{F}$) was set at what was believed to be body blood temperature of a healthy person ($37\,^{\circ}\mathrm{C} = 100\,^{\circ}\mathrm{F}$). The temperature difference between those fixed points was defined to be 100 degrees. Likewise, there exists an absolute temperature scale based on each degree being the same as a FAHRENHEIT

Table 7.2. Some fixed points for temperature, and related scales

	absolute zero	boiling temperature of N_2	freezing temperature of H_2O	triple point of H_2O	temperature of human body blood	boiling temperature of H_2O	temperature scale name
T/K	0	77.4	273.15	273.16	310.15	373.15	KELVIN
ϑ/°C	–273.15	–195.8	0.0	0.01	37	100.0	CELSIUS
ϑ/°F	–459.67	–320.4	32.0	32.02	100	212.0	FAHRENHEIT
ϑ/°R	0	139.3	491.67	491.69	560	672	RANKINE

degree. This is called the RANKINE temperature scale (R), and is a counterpart to the KELVIN temperature scale, but in FAHRENHEIT degree units (instead of CELSIUS degree units). Table 7.2 shows an overview. Table 15.17 in the Appendix allows the conversion temperatures between these different scales.

For industrial use, there is an international temperature scale called ITS-90 (international temperature scale of 1990). It is based on fixed points in the range between 0.7 K and 2500 K, which can be reproduced by many laboratories. In Table 7.3 there are some fixed points of ITS-90 shown, which are of interest for food engineers. The number of fixed points and their values are adjusted occasionally by international conventions between the national metrological institutes (list of them see Table 2.2).

Table 7.3. Some fixed points of the international temperature scale, ITS-90, which are in the temperature range of food processes

equilibrium state	ϑ/°C after ITS-90
triple point of water	0.01
melting point of Gallium	29.7646
melting point of Indium	156.5985

7.2 Heat and Enthalpy

Heat is a form of energy. Energy exists in many forms (heat, light, work, chemical, e.g. in fuel, electricity, etc.), and often changes from one form into another, such as heat into work, chemical (fuel combustion) into heat, etc. (see Table 7.4). Energy per se, however, can neither be created nor destroyed. This is known as the first law of thermodynamics, and is often used by engineers as the rule of energy conservation in carrying out energy balance calculations on a system.

When energy is transformed from one form to another, we have to take into account the efficiency of this transformation. Except for heat, all forms of

Table 7.4. Different forms of energy

energy form	example: energy in …
mechanic energy	a loaded spring (potential energy) a moving body (kinetic energy)
electrical energy	electric power networks
light energy	light of sun, light from incandescent bulb
chemical energy	vegetable oil, mineral oil, potato starch, fuel
nuclear energy	nucleus of atom emitting radioactivity
heat energy	cooking/heating stove, home heating system

energy can be converted to each other with 100% efficiency in theory. However, this is not true in reality where we have efficiencies below 100%. In the case of heat, the conversion to other energy forms can be 100% displacement only when absolute zero temperature is reached. Because of the third law of thermodynamics, this is considered to be impossible. So as a consequence, heat cannot be converted to other forms of energy with efficiency of 100%. Therefore, heat as a form of energy, has some special character.

The internal energy U of a thermodynamic system exists in the forms of both heat and work. Therefore, two transformations are possible for internal energy. Transfer of heat Q and/or transfer of work W'. So, we can express internal energy in the following way:

$$\mathrm{d}U = \mathrm{d}Q + \mathrm{d}W' \tag{7.2}$$

In a thermodynamic system, we treat work only in the form of displacement work W (force–displacement, or pressure–volume). We assume that other forms of work like electric, magnetic, elastic and frictional are not involved.

$$\mathrm{d}U = \mathrm{d}Q + \mathrm{d}W \tag{7.3}$$

With the definition of displacement work:

$$\mathrm{d}W = -p \cdot \mathrm{d}V \tag{7.4}$$

we have

$$\mathrm{d}U = \mathrm{d}Q - p \cdot \mathrm{d}V \tag{7.5}$$

or

$$\mathrm{d}Q = \mathrm{d}U + p \cdot \mathrm{d}V \tag{7.6}$$

where

U	internal energy in J
Q	heat in J
p	pressure in Pa
W'	work in J
W	displacement work in J
V	volume in m^3
H	enthalpy in J

The negative sign in equation (7.4) takes into account that negative displacement $\mathrm{d}V$ represents energy uptake of a system, and has to be counted as a positive contribution (and vice versa).

The term enthalpy H now is used for the sum of internal energy and the product pV:

$$H = U + p \cdot V \tag{7.7}$$

So, for a change in enthalpy, we have:

$$\mathrm{d}H = \mathrm{d}U + p \cdot \mathrm{d}V + V \cdot \mathrm{d}p \tag{7.8}$$

If we consider only cases where the pressure is constant ($\mathrm{d}p = 0$), then we have:

$$\mathrm{d}H = \mathrm{d}U + p \cdot \mathrm{d}V \tag{7.9}$$

Together with equation (7.6), this means:

$$\mathrm{d}H = \mathrm{d}Q \tag{7.10}$$

This means that the amount of heat $\mathrm{d}Q$ which occurs during an isobaric (constant pressure) process is the same as the change in enthalpy of the system. So, when we investigate material properties in a laboratory under constant (e.g. normally atmospheric) pressure, we talk about enthalpy instead of energy of a system.

So the difference between the change in the internal energy $\mathrm{d}U$ of a system and the change in its enthalpy $\mathrm{d}H$ lies in the work, and with the approximations above, specifically in the displacement work $\mathrm{d}W = -p\mathrm{d}V$. If in an isobaric process, there is no displacement or it is nearly zero, then the displacement work plays no role in the system, and the distinction between internal energy and enthalpy is no longer important. The values of $\mathrm{d}H$ and $\mathrm{d}U$ are the same (see Table 7.5).

When heat is transferred into or out of a system, normally the temperature rises or falls, respectively. This type of heat is called sensible heat because we can "sense" the warming or cooling effect by change in temperature. But there are also cases where we can transfer heat into or out of a system, but the temperature stays constant. This happens during boiling of water as it changes phase from liquid into gas (water vapor) or during freezing water into ice as it changes phase from liquid to solid. This type of heat is called latent heat. Latent heat is connected with phase transitions in the materials. Before going into details about phase transitions, it will be helpful to recall some of the basic principles from thermodynamics in the next section.

Table 7.5. Heat $\mathrm{d}Q$ transferred to/from a system (isobaric cases)

general process	$\mathrm{d}Q = \mathrm{d}U + p \cdot \mathrm{d}V + V \cdot \mathrm{d}p$	$\mathrm{d}Q = \mathrm{d}H$
isobaric process with displacement work	$\mathrm{d}Q = \mathrm{d}U + p \cdot \mathrm{d}V + 0$	$\mathrm{d}Q = \mathrm{d}H$
isobaric process with displacement work being zero	$\mathrm{d}Q = \mathrm{d}U + 0 + 0$	$\mathrm{d}Q = \mathrm{d}H = \mathrm{d}U$

7.3 Thermodynamics – Basic Principles

Thermodynamics is the body of science in which we study the way in which substances are affected by heat, either when being heated or cooled, and especially when heat addition or removal causes a phase change. It is no surprise therefore, that thermodynamics is an essential topic that must be well understood by most engineers, and especially food engineers. Normally, entire textbooks are devoted solely to a basic primer in thermodynamics. Since thermodynamics is not the main topic of this book, only a brief discussion of basic principles will be presented in order to appreciate the importance of thermal properties.

Measuring thermal properties of materials requires that we conduct experiments to cause thermal effects to occur, and record the results of these effects. Most often temperature or quantity of heat are measured and monitored. Observing the temperature dependency (like the pressure dependency) of a physical quantity is a common way to study the energetic behavior of a material on a molecular scale.

7.3.1 Laws of Thermodynamics

In the previous section, we just learned that the law of energy conservation stems directly from thermodynamics, and is called the first law of thermodynamics (equation (7.6)). Recall this equation was derived with the assumption that no work other than displacement work would occur.

$$\mathrm{d}U = \mathrm{d}Q - p \cdot \mathrm{d}V \tag{7.6}$$

If we have a system which is thermally insulated so that no heat can cross the system boundary ($\mathrm{d}Q = 0$), we call the system adiabatic (= isentropic). When an adiabatic system shows no displacement work ($\mathrm{d}V = 0$), then the internal energy of the system is constant ($\mathrm{d}U = 0$).

When heat $\mathrm{d}Q$ is entering or departing a system at a temperature T, the quotient of heat divided by temperature is called change in entropy S of the system:

$$\mathrm{d}S \equiv \frac{\mathrm{d}Q_{rev}}{T} \tag{7.11}$$

This definition is valid for a closed system and a completely reversible process. When the process of interest is partly or completely irreversible then we have:

$$\mathrm{d}S > \frac{\mathrm{d}Q}{T} \tag{7.12}$$

Equation (7.12) is an expression of the second law of thermodynamics, stating that if a system is not in equilibrium the entropy S tends to increase and to reach a maximum.

When we take into consideration reversible processes and reversible displacement work only, the combination of equations (7.6) and (7.11) provides:

$$dU = T \cdot dS - p \cdot dV \tag{7.13}$$

That means that the internal energy of a closed system can be changed only by changing the entropy S or the volume V.

In thermodynamics there is another "energy term" that is sometimes useful: It is GIBBS' enthalpy G. This is the difference of enthalpy H and product of temperature T and entropy S.

$$G = H - T \cdot S \tag{7.14}$$

With equation (7.7)

$$G = U + p \cdot V - T \cdot S \tag{7.15}$$

any change in GIBBS' enthalpy is

$$dG = dU + p \cdot dV + V \cdot dp - S \cdot dT - T \cdot dS \tag{7.16}$$

Then, with equations (7.6) and (7.11) this becomes:

$$dG = V \cdot dp - T \cdot dS \tag{7.17}$$

When we consider an equilibrium situation, such as water vapor above a surface of liquid water at a given temperature, with $dQ = T \cdot dS = 0$:

$$dG = V \cdot dp \tag{7.18}$$

or

$$\frac{dG}{dp} = V \tag{7.19}$$

If we treat water vapor under the given conditions like an ideal gas, we get:

$$\frac{dG}{dp} = \frac{R \cdot T}{p} \tag{7.20}$$

or

$$dG = R \cdot T \cdot d\ln p \tag{7.21}$$

Because water vapor is not an ideal gas, we can adjust the water vapor properties to account for its nonideal behavior by using the fugacity f of the vapor, instead of the pressure p.

$$dG = R \cdot T \cdot d\ln f \tag{7.22}$$

This shows that GIBBS' energy of a simple system can be calculated by measuring the vapor pressure i.e. the fugacity f, only.

The dimensionless relative fugacity is called the activity of the chemical compound. In the case of water, we recognize this quantity as water activity (Chapter 1):

$$a_W = \frac{f}{f_0} \tag{7.23}$$

When Gibbs' enthalpy is dependent on a chemical compound, the partial derivative of dG over dn is called chemical potential μ.

$$\mu_i \equiv \left(\frac{\delta G}{\delta n_i}\right)_{S,p,n_{j(j\neq i)}} \tag{7.24}$$

The chemical potential indicates the ability of a component to undergo a reaction. In terms of our example of water vapor, the chemical potential indicates the ability of water to act as part of a chemical reaction. We see now, that what we learned about water activity being an indicator of bound or available water in order to support various reactions has a sound thermodynamic basis. It tells us, that if we want to know the ability of water to undergo reactions (i.e. want to know the chemical potential), then we should measure water vapor pressure p (more exactly the fugacity f). That is what we do in measuring the water activity. The water activity is nothing more than a relative measure of the chemical potential of water.

$$\mathrm{d}\mu = R \cdot T \cdot \mathrm{d}\ln f \tag{7.25}$$

with equation (7.8)

$$\mathrm{d}\mu = \text{function}\,(a_W)$$

where

G	Gibbs energy in J
n	substance in mol
f	fugacity in Pa
μ	chemical potential in J · mol^{-1}
S	entropy in J · K^{-1}
a_W	water activity

7.4 Heat Capacity

The heat capacity of a material is a thermal property that indicates the ability of the material to hold and store heat. It can be quantified by specifying the amount of heat that is needed to raise the temperature by a specified amount. Mathematically, it is the quotient of heat divided by temperature:

$$C = \frac{\mathrm{d}Q}{\mathrm{d}T} \tag{7.26}$$

respectively,

$$C = \frac{\Delta Q}{\Delta T} \tag{7.27}$$

When heat capacity is defined only in this way, it will also depend upon the mass of the material sample, and serves as a property only of the specific sample size measured. For this reason, we normally measure and report the heat capacity on the basis of a common unit of mass. When we do this, we call it the specific heat capacity. Sometimes this property is called specific heat of the material but this should be avoided because $\mathrm{d}Q/\mathrm{d}m = q$ is specific heat.

$$c = \frac{C}{m} \tag{7.28}$$

$$c = \frac{1}{m} \cdot \frac{\mathrm{d}Q}{\mathrm{d}T} = \frac{\mathrm{d}q}{\mathrm{d}T} \tag{7.29}$$

In order to help better understand heat capacity, let us assume we wish to determine how much heat is needed to raise the temperature of one liter of water at 21 °C up to 23 °C (by 2 K). When we do this, we measure the heat required to be 8.36 kJ.

When heat is added to a system like this (liter of water), the water molecules experience an increase in their kinetic energy. They move in both rotational and translational motion at faster rates. If we insert our finger (or a thermometer) into this liter of water, we can sense this increased thermal energy level by a warming sensation on our finger, and a rise in the temperature scale on the thermometer. Therefore, we use temperature as a measure of increased thermal energy. In this case, the temperature increase was $\Delta T = 2$ K.

Table 7.6. Heat capacity terms

p = const.		V = const.	
$C_p = \frac{\mathrm{d}H}{\mathrm{d}T}$	(7.30)	$C_V = \frac{\mathrm{d}U}{\mathrm{d}T}$	(7.31)
$c_p = \frac{1}{m} \cdot \frac{\mathrm{d}H}{\mathrm{d}T}$	(7.32)	$c_V = \frac{1}{m} \cdot \frac{\mathrm{d}U}{\mathrm{d}T}$	(7.33)
$c_p = \frac{\mathrm{d}h}{\mathrm{d}T}$	(7.34)	$c_V = \frac{\mathrm{d}u}{\mathrm{d}T}$	(7.35)

where

C	heat capacity in $\mathrm{J} \cdot \mathrm{K}^{-1}$
c	specific heat capacity in $\mathrm{J} \cdot \mathrm{kg}^{-1} \cdot \mathrm{K}^{-1}$
Q	heat in J
q	specific heat in $\mathrm{J} \cdot \mathrm{kg}^{-1}$
T	temperature in K
m	mass in kg
H	enthalpy in J
h	specific enthalpy in $\mathrm{J} \cdot \mathrm{kg}^{-1}$
U	internal energy in J
u	specific internal energy in $\mathrm{J} \cdot \mathrm{kg}^{-1}$

Example 7.1. Calculating the specific heat capacity of water
With the values from above, and equation (7.29) we get

$$c_p = \frac{1}{m} \cdot \frac{\Delta Q}{\Delta T}$$

$$c_p = \frac{8.36\,\mathrm{kJ}}{1\,\mathrm{kg} \cdot 2\,\mathrm{K}}$$

$$c_p = 4.18\,\mathrm{kJ} \cdot \mathrm{kg}^{-1} \cdot \mathrm{K}^{-1}$$

Often in thermodynamics it is necessary to distinguish between internal energy terms in which displacement work is present or not present. When there is no displacement work, the volume of the system remains constant (V = const., $\mathrm{d}Q = \mathrm{d}U$), and the subscript V is used with the heat capacity term. When displacement is present, then the pressure of the system remains constant (p = const., $\mathrm{d}Q = \mathrm{d}H$), and the subscript p is used with the heat capacity term (see Table 7.6).

7.4.1 Ideal Gases and Ideal Solids

For ideal gases and solids, the movement of molecules in response to thermal energy can be predicted from theory. Therefore, the heat capacity of such ideal substances can also be predicted from theory. In an ideal gas, the molecules are free to have translational motion in the three directions of three-dimensional space (back and forth, side-to-side, and up and down). Thus we say, they have three degrees of freedom for translational motion, $f = 3$.

In addition to translational motion, molecules are also free to have rotational motion. Gas molecules consisting of only two atoms, such as nitrogen N_2, are bonded linearly. This makes them look like a rigid body which can rotate about two axes. This gives them two more additional degrees of freedom. Thus, they have a total of five degrees of freedom, $f = 5$.

In the case of solids, the molecules are fixed in place, and can have no translational or rotational motion. Therefore, they have no translational or rotational degrees of freedom. However, they are free to oscillate in three directions. Thus, they have six degrees of freedom in response to thermal energy. Table 7.7 lists the degrees of freedom for atoms or molecules in some simple ideal systems.

Table 7.7. Degrees of freedom for atoms and molecules in simple, ideal systems

	translational	rotational	oscillatory	total
one atom gas	3	–	–	$f = 3$
two-atom gas molecule	3	2	0	$f = 5$
molecules in a solid	–	–	6	$f = 6$

With the kinetic energy of an ideal gas equal to its thermal energy:

$$\frac{1}{2}m \cdot \bar{v}^2 = \frac{f}{2}k \cdot T \tag{7.36}$$

$$E = \frac{f}{2}k \cdot T \tag{7.37}$$

The internal energy U for $\overline{N}$ particles (atoms or molecules) is:

$$U = \bar{N} \cdot \frac{f}{2}k \cdot T \tag{7.38}$$

with $R = k \cdot N_A$ we get

$$U = \frac{\bar{N}}{N_A} \cdot \frac{f}{2}k \cdot N_A \cdot T = n \cdot \frac{f}{2}R \cdot T \tag{7.39}$$

$$U = n \cdot M \cdot \frac{f}{2} \cdot \frac{R}{M} \cdot T = m \cdot \frac{f}{2}R_s \cdot T \tag{7.40}$$

With

$$C_V = \frac{\mathrm{d}U}{\mathrm{d}T} \tag{7.31}$$

we get

$$C_V = m \cdot \frac{f}{2}R_s \tag{7.41}$$

respectively,

$$c_V = \frac{f}{2}R_s \tag{7.42}$$

In the isobaric case we get

$$C_p = \frac{\mathrm{d}Q}{\mathrm{d}T} = \frac{\mathrm{d}H}{\mathrm{d}T} = \frac{\mathrm{d}U}{\mathrm{d}T} + \frac{p\mathrm{d}V}{\mathrm{d}T} = \frac{\mathrm{d}U}{\mathrm{d}T} + \frac{m \cdot R_s \cdot \mathrm{d}T}{\mathrm{d}T} \tag{7.43}$$

so we see

$$C_p = C_V + m \cdot R_s \tag{7.44}$$

or

$$c_p = c_V + R_s \tag{7.45}$$

where

k	Boltzmann's constant
N_A	Avogadro's constant
m	mass in kg
v	velocity in $\mathrm{m \cdot s^{-1}}$
$\overline{N}$	number of particles
U	internal energy in J
M	molecular mass in $\mathrm{kg \cdot mol^{-1}}$
R	universal gas constant in $\mathrm{J \cdot K^{-1} \cdot mol^{-1}}$
R_s	specific gas constant in $\mathrm{J \cdot K^{-1} \cdot kg^{-1}}$
f	degrees of freedom

p pressure in Pa
V volume in m^3
C_p heat capacity (p = constant) in $J \cdot K^{-1}$
C_V heat capacity (V = constant) in $J \cdot K^{-1}$
c_p specific heat capacity (p = constant) in $J \cdot kg^{-1} \cdot K^{-1}$
c_V specific heat capacity (V = constant) in $J \cdot kg^{-1} \cdot K^{-1}$

In the case of solids without very high pressure, we have the following:

$$c_p \approx c_V \tag{7.46}$$

with $f = 6$, we have:

$$c_p \approx 3R_s \tag{7.47}$$

Equation (7.47) is the rule of DULONG–PETIT for the heat capacity of solids. Table 7.8 illustrates how theoretical values based on thermodynamic considerations and experimental data for heat capacity fit.

Table 7.8. Theoretical and experimental values of specific heat capacity of selected systems

substance	f	R_s/kJ · kg^{-1} · K^{-1}	c_p (theory)/kJ · kg^{-1} · K^{-1}	c_p (exp.)/kJ · kg^{-1} · K^{-1}	from:
He	3	2.078	5.195	5.23	[106]
N_2	5	0.297	1.039	1.03	[106]
air	5	0.287	1.0045	1.005	[106]
Pb	6	0.0401	0.1203	0.129	[106]

There are also many solid materials which, at room temperature do not follow the rule of DULONG–PETIT for calculating the heat capacity. In this case the method described in the following paragraph is recommended.

7.4.2 Heat Capacity of Real Solids

With known heat capacities of the ingredients and assuming that heat capacity is additive we can calculate the heat capacity of a material by equation (7.48). Table 7.9 lists the specific heat capacity of various food constituents.

Table 7.9. Some data for specific heat capacities of food constituents [116]

	c_p/kJ · kg^{-1} · K^{-1}		c_p/kJ · kg^{-1} · K^{-1}
water	≈ 4.2	ash (minerals)	≈ 0.8
carbohydrates	≈ 1.4	ice	≈ 2.1
proteins	≈ 1.6	nonfat solids (from animal)	$\approx 1.34 \cdots 1.68$
fats	≈ 1.7	nonfat solids (from plants)	≈ 1.21

$$c_p = \sum_i x_i \cdot c_{p,i} \tag{7.48}$$

with

$$x_i = \frac{m_i}{m} \tag{7.49}$$

$$m = \sum_i m_i \tag{7.50}$$

where

c_p	specific heat capacity in $J \cdot K^{-1} \cdot kg^{-1}$
x_i	mass fraction of component i
$c_{p,i}$	specific heat capacity of component i in $J \cdot K^{-1} \cdot kg^{-1}$
m_i	mass of component i in kg
m	total mass in kg

Example 7.2. Estimation of heat capacity for foods
The composition of a food product is given as follows:

	mass fraction x_i/% (m/m)
water	84
fat	12
protein	3
minerals	1

The specific heat capacity can be estimated as follows:

$$c_p/\text{kJ} \cdot \text{kg}^{-1} \cdot \text{K}^{-1} = \sum 0.84 \cdot 4.2 + 0.12 \cdot 1.7 + 0.03 \cdot 1.6 + 0.01 \cdot 0.8$$

$$c_p = 3.8\ \text{kJ} \cdot \text{kg}^{-1} \cdot \text{K}^{-1}$$

Knowing the basic terms of thermodynamics, let us now examine a classification of phase transitions based on these terms.

7.5 Classification of Phase Transitions

When we look at a simple phase transition, such as when a substance undergoes freezing from a liquid to a solid phase, then we normally see significant changes in enthalpy, entropy and volume. When we start in the liquid phase toward transition to the solid phase, we will observe these changes at the phase transition point, which is a point on the p–T diagram (phase diagram) of the material. The chemical potential of both phases are equal at the transition point, but the enthalpies and entropies of the different phases (solid and liquid) are different.

In other situations we can observe phase transitions where a solid is melting to become a viscous liquid without sudden change in enthalpy. This type of

phase transition is called a glass transition, and is observed when we deal with noncrystalline materials. For example formulations with solid carbohydrates like confectionery or powders can exhibit glass transitions.

According to Ehrenfest [1] phase transitions are called first order ($n = 1$) phase transitions when the first derivative of Gibbs' enthalpy over temperature has a discontinuity (a "jump" in the curve). In the same manner, a phase transition is of second order ($n = 2$) when the discontinuity appears in the curve for the second derivative of Gibbs' enthalpy over temperature.

Let us consider a simple example of a liquid–solid phase transition upon cooling of a material. Then, the thermal effect observed during this transition will be the release of the difference in the enthalpy of the two phases (liquid phase and the solid phase), $\Delta_{trs}G_m$:

$$\Delta_{trs}G_m = G''_m - G'_m = 0 \tag{7.51}$$

So, the partial derivate over temperature is:

$$\left(\frac{\partial \Delta_{trs}G_m}{\partial T}\right) = \left(\frac{\partial G''_m}{\partial T}\right)_p - \left(\frac{\partial G'_m}{\partial T}\right)_p = -S''_m + S'_m = -\Delta_{trs}S_m \tag{7.52}$$

With equations (7.8) and (7.13) and $\mathrm{d}p = 0$ the change in enthalpy H is:

$$\Delta_{trs}H_m = T \cdot \Delta_{trs}S_m \tag{7.53}$$

This means that the first derivative of Gibbs enthalpy is represented by $\Delta_{trs}S$ or $\Delta_{trs}H$. Recalling equation (7.30), we know C_p is the derivative of H over T, so it is the second derivative of G over temperature. Having this in mind, let us now look at the graphs in Figure 7.2. Let us imagine moving along on a curve in the diagram from higher to lower temperature (in the direction from liquid to a solid state). In the upper left figure, we see the G–T graphs of the liquid phase (2) and the solid phase (1), which meet at the transition temperature. Upon decreasing the temperature, the system will normally change from curve 1 to curve 2 to reach a low energy state. Plotting the derivative of these curves, we get the H–T curve immediately below (middle left), which has a distinct discontinuity ("jump") at the transition temperature. This is a first order phase transition.

Let us now look at the graphs for second order transitions shown on the right side of Figure 7.2. In the upper right graph, we can see that, at the transition temperature, the G–T curve of phase 2 and phase 1 do not intersect, but are tangent to each other, and simply touch at a point of tangency. Upon decreasing the temperature, we will enter the transition from phase 2 to 1. The first derivative is shown in the graph immediately below (middle right). In this case, the first derivative curve, which is H, simply changes direction abruptly at the transition point, but shows no discontinuity or "jump." The second derivative (bottom right) does show such a discontinuity "jump": This transition is a second order phase transition. A glass transition is a typical example of a second order phase transition. In a thermal analysis experiment, these orders of transition can be identified by having a "jump" in the heat capacity $C_{p,m}$, but not in the enthalpy ΔH_m.

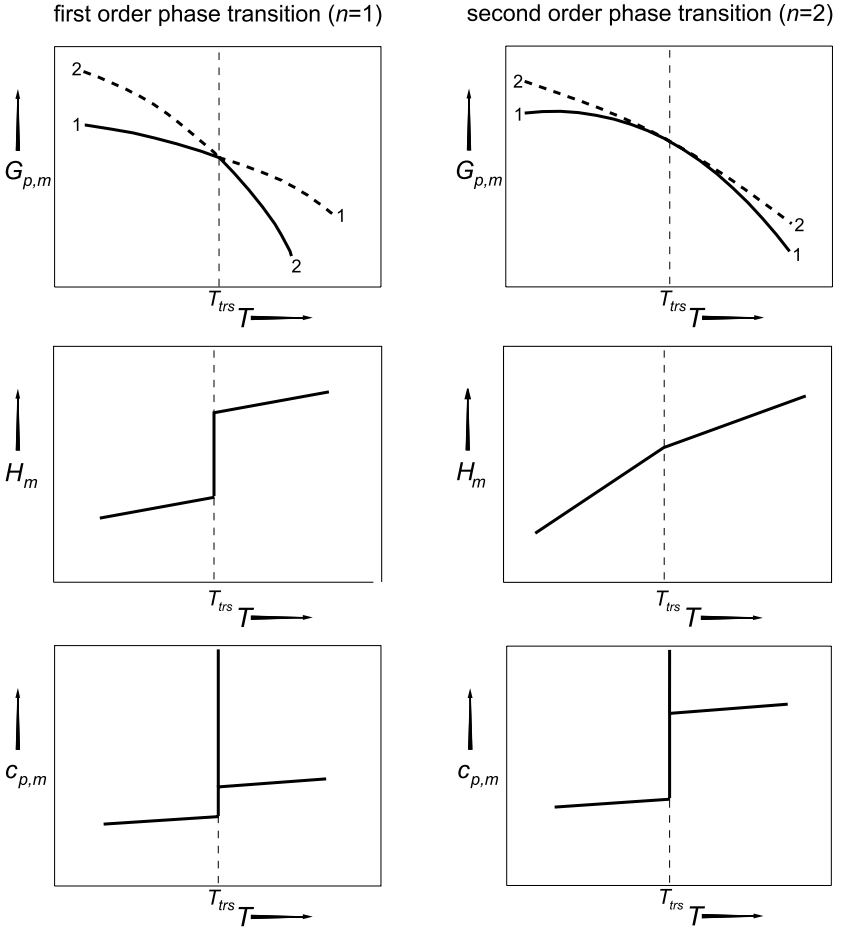

Figure 7.2. Classification of phase transitions after EHRENFEST

	first order phase transition ($n = 1$)	second order phase transition ($n = 2$)
	$\left(\frac{\partial^n G'_m}{\partial T^n}\right)_p \neq \left(\frac{\partial^n G''_m}{\partial T^n}\right)_p$	
	$\Delta_{trs} G = 0$	
$\left(\frac{\partial \Delta_{trs} G_m}{\partial T}\right)_p = -\Delta_{trs} S_m$	$\neq 0$	$= 0$
$\left(\frac{\partial^2 \Delta_{trs} G_m}{\partial T^2}\right)_p = -\frac{\Delta_{trs} C_{p,m}}{T}$	$\neq 0$	$\neq 0$

A more detailed application and critical discussion of Ehrenfest's classification can be found, e.g. in [2,3]. For completeness, we should also mention that Ehrenfest's classification of phase transitions works equally well with the derivative of Gibbs' enthalpy over pressure, instead of temperature: In that case, we have:

	first order phase transition ($n = 1$)	second order phase transition ($n = 2$)
	$\left(\frac{\partial^n G'_m}{\partial p^n}\right)_T \neq \left(\frac{\partial^n G''_m}{\partial p^n}\right)_T$	
	$\Delta_{trs} G = 0$	
and as first derivative $\left(\frac{\partial \Delta_{trs} G_m}{\partial p}\right) = \left(\frac{\partial G''_m}{\partial p}\right)_T - \left(\frac{\partial G''_m}{\partial p}\right)_T$	$\neq 0$	$= 0$
$= V''_m - V'_m = \Delta_{trs} V_m$		
and as second derivative $\left(\frac{\partial^2 \Delta_{trs} G_m}{\partial p^2}\right)_T = -V_m \cdot \Delta_{trs} \kappa$	$\neq 0$	$\neq 0$

Here

C	heat capacity in $\mathrm{J \cdot kg^{-1} \cdot K^{-1}}$
Q	heat in J
T	temperature in K
p	pressure in Pa
H	enthalpy in J
U	internal energy in J
G	Gibbs' enthalpy in J
S	entropy in $\mathrm{J \cdot K^{-1}}$
V	volume in $\mathrm{m^3}$

with indices

trs	transition
m	molar
n	order

With these excursions into the thermodynamics of phase transitions, which are not simply freezing/melting or evaporating/condensing, we want to leave this section and return to thermal properties. We might keep in mind that glass transitions, as well as some solid–solid transitions are related to the quality and the stability of the food substance in which they occur. There are two approaches through which to obtain data for constructing phase diagrams: One approach is by scanning the temperature (thermal analysis) and observing the related quantities that result from the scan. The other approach is to study materials under an isothermal pressure scan.

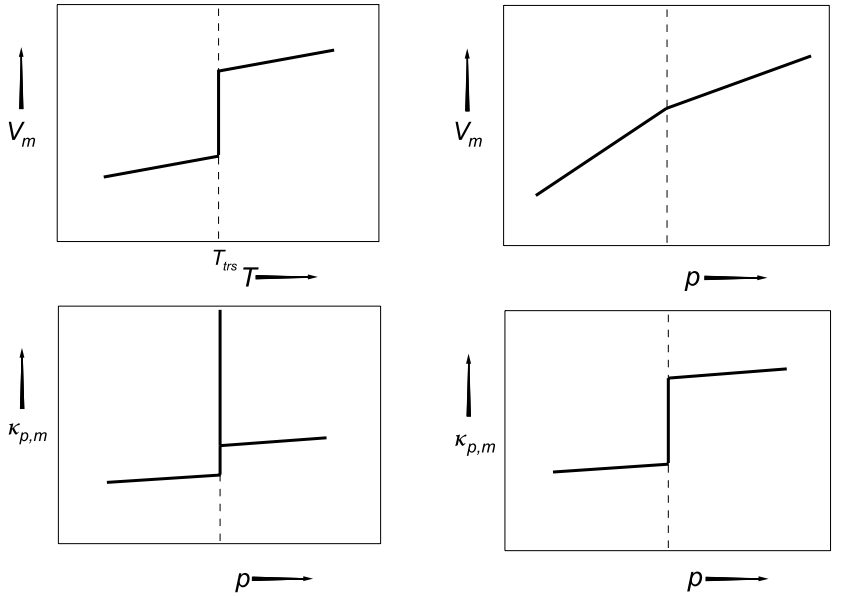

Figure 7.3. Alternative classification of phase transitions after EHRENFEST

7.6 Heat Transfer in Food

Spontaneous heat transfer always takes place from a region of higher temperature to a surrounding region of lower temperature. There are four mechanisms by which heat can transfer: radiation, conduction, convection, and phase transitions. In Table 7.10 they are listed and described briefly. In this section and those that follow, we will discuss each of these mechanisms and the thermal properties that are needed in each case.

Table 7.10. Mechanisms of heat transfer

mechanism	description	example
heat radiation	electromagnetic radiation with wavelengths from 1 µm to 1 mm	broiling, grilling, infrared heat lamps
heat conduction	transport of heat by excited molecules "bumping" against each other	solid being heated at one end, warming opposite end
heat convection	transport of heat being carried by a flowing fluid	flowing hot water or air in central home heating system
phase transitions	uptake/release of latent heat	condensing of water vapor

7.6.1 Heat Radiation

Heat radiation is electromagnetic radiation with frequencies below that of visible light. It is also called infrared radiation. All bodies with a temperature above 0 K emit heat by radiation. As with all heat transfer mechanisms, heat will flow from the body at higher temperature to the one at lower temperature. However, there is no need for the bodies to contact each other, nor is there any need for any substance to exist between the two bodies. Therefore, heat radiation can occur in a perfect vacuum and over great distances. For example, this is how we receive heat from the sun. In order for heat radiation to occur, the bodies must simply be able to "see" each other. The Stefan–Boltzmann law allows us to calculate the heat flow under radiation:

$$\dot{Q} = A \cdot \varepsilon \cdot \sigma \cdot T^4 \tag{7.54}$$

where

ε	emissivity of a body
σ	Stefan–Boltzmann constant
T	thermodynamic temperature of the body in K
A	area which is emitting or absorbing radiation in m^2

When we have two bodies of different temperatures T_1 and T_2, each one is emitting heat radiation according to Stefan–Boltzmann's law, and at the same time they are receiving radiation from the other body. So there is a net heat flow of:

$$\Delta\dot{Q} = A \cdot C_{12} \cdot (T_2^4 - T_1^4) \tag{7.55}$$

where

$\Delta\dot{Q}$	heat flow from/to body 1 to/from body 2 in $J \cdot s^{-1}$
A	area emitting radiation in m^2
T_1	temperature of body 1 in K
T_2	temperature of body 2 in K
C_{12}	radiation exchange factor in $W \cdot K^{-4} \cdot m^{-2}$
ε_1	emissivity of body 1
ε_2	emissivity of body 1

The heat radiation exchange factor C_{12} is a quantity combining the emissivities of the bodies as well as their geometries (shape factors) and the relative surface absorptivities of the bodies. If, for example, we have two parallel plates with identical geometry and surface absorptivity emitting / absorbing heat radiation, then the heat radiation exchange factor would consist of the following expression, C_{12} [119]:

$$c_{12} = \frac{\sigma}{\frac{1}{\varepsilon_1} + \frac{1}{\varepsilon_2} - 1} \tag{7.56}$$

Table 7.11. Values for emissivitiy ε (absorptivities α) of some material surfaces at room temperature, examples

surface	ε
chromium, polished	0.058
aluminum, polished	0.095
copper, polished	0.03
copper, oxidized	0.76
iron sheet, rusty	0.685
iron sheet, tin plated	0.083
concrete, rough	0.94
paint, white	0.925
paint, (flat black)	0.97
glass	0.88
brick, red	0.93
wall (plaster board)	0.93
ice, rough surface	0.985
water	0.90

Emissivity

The emissivity of a material gives an indication of its ability to emit electromagnetic radiation (in this case, heat radiation). A corollary property is absorptivity, which indicates the ability of a material to absorb heat radiation. When a material is in thermal equilibrium, we can assume that its emissivity and absorptivity are equal. This is known as KIRCHHOFF's law of thermal radiation.

An ideal black body is defined as a body having maximum absorptivity, with a value for absorptivity of $\varepsilon = 1$. An ideal reflective body is incapable of absorbing any heat radiation, and has a value for absorptivity of $\varepsilon = 0$. All real bodies are known as "grey bodies," and have values for absorptivity between zero and one.

If we know the emissivity ε of a material body and its surface temperature, we can calculate the energy lost from the body caused by radiation heat transfer. Likewise, if we do not know the temperature but can measure the quantity of radiant heat energy emitted, we can calculate the surface temperature of the body. This is the principle for measuring surface temperatures by infrared thermometry (IR thermometers, sometimes called pyrometers) [72].

7.6.2 Conduction Heat Transfer

Heat transfer by conduction was first mentioned in Section 6.8 as an example of other diffusion-like transport phenomena that can be described with the same type of mathematical equation as that used to describe molecular diffusion through a material substance.

When we first approach the study of heat conduction, it is important to make a distinction between heat conduction under steady state conditions (temperatures remain constant at any point over time while heat is flowing) and unsteady state, or transient, conditions (temperatures at any point change over time while heat is flowing). In this section, we will limit our study to steady state heat conduction. This is the situation encountered most frequently in food processing involving the heating and cooling of liquid food products through heat exchangers and holding tubes. These heating and cooling systems operate under steady state conditions because product and heat exchange medium temperatures at the entrance and exit of these systems remain constant over time while conduction heat transfers at a steady (constant) rate. Most heat exchangers used in food processing operations are either a plate-type (made up of flat plates) or tubular type (made up of cylindrical tubes). In a plate heat exchanger, liquid product flows through a narrow space between two parallel stainless steel plates. On the other side of these plates, a heat exchange medium at a different temperature is flowing (e.g. hot water or condensing steam). This situation causes heat to flow from the high temperature side to the low temperature side causing the temperature of the cool incoming product to rise as it exchanges heat with the hot heat exchange medium fluid on the other side. In a tubular heat exchanger, the product flows through a narrow cylindrical tube to exchange heat with a fluid heat exchange medium on the other side of the tubular wall. For this reason, we will first consider heat conduction across a flat plate "wall" barrier. Then, we will consider heat conduction across a cylindrical "wall" barrier.

Heat transfer through a material can occur in all three directions (dimensions) of space. However, in heat exchanger applications, the temperature gradient across the thin stainless steel wall drives the heat transfer predominantly in the one direction crossing the wall, and there is little or no temperature gradient (potential) causing heat to travel along the metal wall material in either of the other two directions. Therefore, we can limit our analysis of heat conduction to the most simple case of one dimensional steady state heat conduction across a flat plate wall.

One-Dimensional Steady-State Heat Conduction Across a Flat Plate

Let us consider heat travelling across a solid flat plate by conduction like in Figure 7.4, we can express the quantity of heat flow by Fourier's first law:

$$\frac{\dot{Q}}{A} = -\lambda \cdot \frac{\mathrm{d}T}{\mathrm{d}x} \tag{6.28}$$

With the symbols of Figure 7.4:

$$\frac{\dot{Q}}{A} = \lambda \cdot \frac{T_0 - T_1}{\delta} \tag{7.57}$$

so

$$\dot{Q} = A \cdot \lambda \cdot \frac{T_0 - T_1}{\delta} \tag{7.58}$$

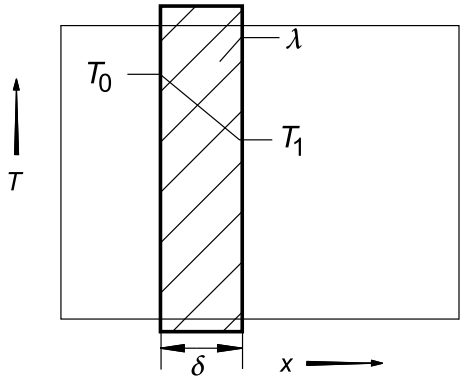

Figure 7.4. Temperature profile across a solid flat plate

Table 7.12. Sign of temperature gradient and resulting heat flow in Figure 7.4

case	temperature gradient	description
$x > 0$ $T_1 > T_0$	positive	T is increasing with increasing x
$x > 0$ $T_1 < T_0$	negative	T is decreasing with increasing x

$\frac{dT}{dx}$ temperature gradient in $K \cdot m^{-1}$
λ heat conductivity in $W \cdot K^{-1} \cdot m^{-1}$
$\dot{Q}$ heat flow in W
$\frac{\dot{Q}}{A}$ heat flow density in $W \cdot m^{-2}$

The negative sign in FOURIER's law is necessary in order to have a positive heat flow in response to a negative temperature gradient. This is because heat will only flow from high to low temperature, which is "down hill," or having a negative slope. Table 7.12 shows the type of responding heat flow to positive and negative temperature gradients.

The heat transferred can be calculated by integration over time: Because of

$$\dot{Q} = \frac{dQ}{dt} \tag{7.59}$$

or

$$dQ = -A \cdot \lambda \cdot \frac{T_1 - T_0}{\delta} \cdot dt \tag{7.60}$$

we have

$$Q = \int_{t=0}^{t} A \cdot \frac{\lambda}{\delta} \cdot (T_0 - T_1) \cdot dt \tag{7.61}$$

Three-Dimensional Steady State Heat Conduction

In the most general case when temperature gradients exist in all three dimensions of space, heat will transfer through a material in all three directions. In this situation, FOURIER's law must be expressed in the form of a partial differential equation to include terms for the temperature change in each of the three directions x, y, z:

$$\frac{\dot{Q}}{A} = -\lambda \left(\frac{\partial T}{\partial x}, \frac{\partial T}{\partial y}, \frac{\partial T}{\partial z} \right) \tag{7.62}$$

i.e.

$$\frac{\dot{Q}}{A} = -\lambda \cdot \left(\frac{\partial}{\partial x}, \frac{\partial}{\partial y}, \frac{\partial}{\partial z} \right) T = -\lambda \cdot \text{grad}\, T \tag{7.63}$$

or with the abbreviation

$$\nabla T = grad\, T = \left(\frac{\partial}{\partial x}, \frac{\partial}{\partial y}, \frac{\partial}{\partial z} \right) T \tag{7.64}$$

briefly

$$\frac{\dot{Q}}{A} = -\lambda \cdot \nabla T \tag{7.65}$$

where ∇ is called the nabla or dell operator in matrix algebra.

One-Dimensional Steady-State Heat Conduction Across Multiple Layers

Figure 7.5 illustrates the case of conduction heat transfer occurring across a flat wall that is made up of several layers of different materials, with each material having a different thermal conductivity λ and different layer thickness δ.

In this case, the mathematical expression for the quantity of heat flow can be derived as follows. Because the heat flowing through all three layers is the same:

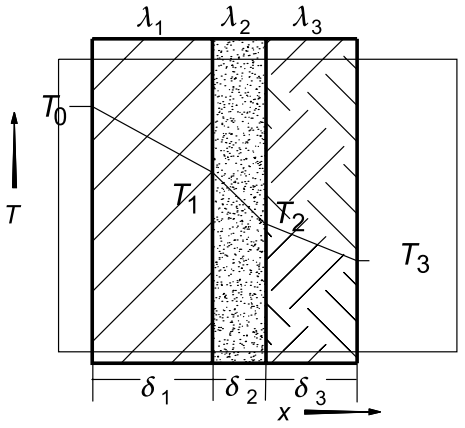

Figure 7.5. Temperature profile across a multilayer solid flat wall

$$\dot{Q}_1 = \dot{Q}_2 = \dot{Q}_3 \tag{7.66}$$

$$\frac{\dot{Q}_1}{A} = \frac{\dot{Q}_2}{A} = \frac{\dot{Q}_3}{A} \tag{7.67}$$

$$\frac{\dot{Q}_1}{A} = -\lambda_1 \cdot \frac{T_1 - T_0}{\delta_1} \tag{7.68}$$

with

$$T_0 - T_1 = \frac{\dot{Q}_1}{A} \cdot \frac{\delta_1}{\lambda_1} \tag{7.69}$$

and

$$\frac{\dot{Q}_2}{A} = -\lambda_2 \cdot \frac{T_2 - T_1}{\delta_2} \tag{7.70}$$

with

$$T_1 - T_2 = \frac{\dot{Q}_2}{A} \cdot \frac{\delta_2}{\lambda_2} \tag{7.71}$$

and

$$\frac{\dot{Q}_3}{A} = -\lambda_3 \cdot \frac{T_3 - T_2}{\delta_3} \tag{7.72}$$

with

$$T_2 - T_3 = \frac{\dot{Q}_3}{A} \cdot \frac{\delta_3}{\lambda_3} \tag{7.73}$$

By adding the temperature differences from equations (7.69), (7.71) and (7.73) we get the total temperature difference:

$$T_0 - T_3 = \frac{\dot{Q}}{A} \cdot \left(\frac{\delta_1}{\lambda_1} + \frac{\delta_2}{\lambda_2} + \frac{\delta_3}{\lambda_3} \right) \tag{7.74}$$

So, we get for heat flow density:

$$\frac{\dot{Q}}{A} = \frac{1}{\left(\frac{\delta_1}{\lambda_1} + \frac{\delta_2}{\lambda_2} + \frac{\delta_3}{\lambda_3} \right)} \cdot (T_0 - T_3) \tag{7.75}$$

respectively,

$$\frac{\dot{Q}}{A} = \frac{1}{\left(\frac{\delta_1}{\lambda_1} + \frac{\delta_2}{\lambda_2} + \frac{\delta_3}{\lambda_3} \right)} \cdot \Delta T \tag{7.76}$$

Writing a more general expression for the steady state case with n layers we have:

for the heat flow density

$$\frac{\dot{Q}}{A} = \frac{1}{\sum_{i=1}^{n} \frac{\delta_i}{\lambda_i}} \cdot \Delta T \tag{7.77}$$

for the heat flow

$$\dot{Q} = A \cdot \frac{1}{\sum_{i=1}^{n} \frac{\delta_i}{\lambda_i}} \cdot \Delta T \tag{7.78}$$

for the heat quantity

$$Q = A \cdot \frac{1}{\sum_{i=1}^{n} \frac{\delta_i}{\lambda_i}} \cdot \Delta T \cdot t \tag{7.79}$$

When we have different sizes of areas for each layer, we write equation (7.79)

$$\dot{Q} = \frac{1}{\sum_{i=1}^{n} \frac{\delta_i}{\lambda_i \cdot A_i}} \cdot \Delta T \tag{7.80}$$

A comparison of equation (7.80) with the related expression in Table 6.7 shows, the term in the denominator is equal to the sum of the heat resistances. So, the concept of addition of resistances can also be used here in the case of steady state multilayer conduction of heat. We can write this in a more abbreviated way as follows:

$$\sum_{i=1}^{n} \frac{\delta_i}{\lambda_i \cdot A_i} = \sum_{i=1}^{n} R_i \tag{7.81}$$

where

λ	heat conductivity in $W \cdot K^{-1} \cdot m^{-1}$
δ	thickness in m
$\dot{Q}$	heat flow in W
Q	heat in J
A	area in m^2
R	heat resistance in $K \cdot W \cdot {}^{-1}$
i	layer index
n	total number of layers

One-Dimensional Steady State Conduction Across a Single Layer Cylindrical Wall

Figure 7.6 illustrates the case when heat must transfer across a cylindrical wall, such as when tubular heat exchangers are used. In this case, the same expression for Fourier's law still applies except that the total wall thickness must be expressed as the difference between outer and inner tube radii, and

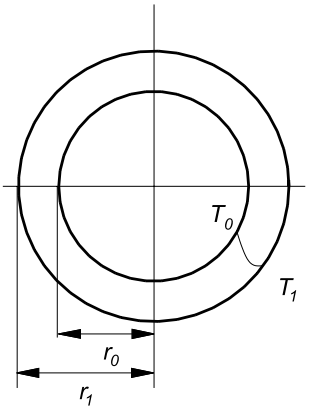

Figure 7.6. Temperature profile across a single-layer cylindrical wall

the incremental distance along the tube wall thickness must be expressed as radius r.

Therefore, in the case of a single-layer cylindrical wall, FOURIER's law can be expressed as follows:

$$\frac{\dot{Q}}{A} = -\lambda \cdot \frac{\mathrm{d}T}{\mathrm{d}r} \tag{7.82}$$

The heat flow is obtained by integration over the cylindrical wall:

$$\mathrm{d}T = -\frac{\dot{Q}}{A \cdot \lambda}\mathrm{d}r = -\frac{\dot{Q}}{2\pi \cdot l \cdot r \cdot \lambda}\mathrm{d}r \tag{7.83}$$

$$\int_{T_0}^{T_1} \mathrm{d}T = -\int_{r_0}^{r_1} \frac{\dot{Q}}{2\pi \cdot l \cdot r \cdot \lambda}\mathrm{d}r = -\frac{\dot{Q}}{2\pi \cdot l \cdot \lambda}\int_{r_0}^{r_1} \frac{\mathrm{d}r}{r} \tag{7.84}$$

$$T_1 - T_0 = -\frac{\dot{Q}}{2\pi \cdot l \cdot \lambda} \ln \frac{r_1}{r_0} \tag{7.85}$$

so

$$\dot{Q} = \frac{2\pi \cdot l}{\ln \dfrac{r_1}{r_0}} \cdot \lambda \cdot (T_0 - T_1) \tag{7.86}$$

An alternative calculation for the heat conducted in Figure 7.6 is to use an average area A_m. The value of A_m can be calculated by use of an average radius r_m. For the simplest case in a thin walled tube, we can use the arithmetic mean between outer and inner diameter for the average radius r_m (see also Example 7.3).

$$r_m = \frac{r_1 + r_0}{2} \tag{7.87}$$

But, let us first calculate a general average radius r_m between r_0 and r_1. Equation (7.82) is going to be:

$$-\frac{\dot{Q}}{A_m} = \frac{\dot{Q}}{2\pi r_m \cdot l} = \frac{\lambda}{(r_1 - r_0)} \cdot (T_1 - T_0) \tag{7.88}$$

For the heat flow, we get:

$$\dot{Q} = \frac{2\pi r_m \cdot l}{(r_1 - r_0)} \cdot \lambda \cdot (T_0 - T_1) \tag{7.89}$$

Comparing this with equation (7.86) provides:

$$2\pi \cdot r_m \cdot l \cdot \frac{\lambda}{r_1 - r_0} \cdot (T_0 - T_1) = \frac{2\pi l}{\ln \frac{r_1}{r_0}} \cdot \lambda (T_0 - T_1) \tag{7.90}$$

so

$$\frac{r_m}{r_1 - r_0} = \frac{1}{\ln \frac{r_1}{r_0}} \tag{7.91}$$

respectively

$$r_m = \frac{r_1 - r_0}{\ln \frac{r_1}{r_0}} \tag{7.92}$$

So, now we have an algorithm to calculate r_m for all type of tubes. This type of average radius r_m is called the logarithmic mean radius. It can be used for all cases of tubes. In case of a thin walled tube, we learned we could use the arithmetic average. But how can we decide what is a thin walled or thick walled tube? Figure 7.7 illustrates that a thin walled tube is a tube with outer radius smaller than twice the inner radius ($r_a < 2r_i$). The opposite case is when the outer radius is greater than twice the inner radius ($r_a > 2r_i$), and we call a tube thick walled. Between both cases we have the case in which the outer radius is precisely twice the inner radius ($r_a = 2r_i$), which presents a borderline situation, and either approach can be used.

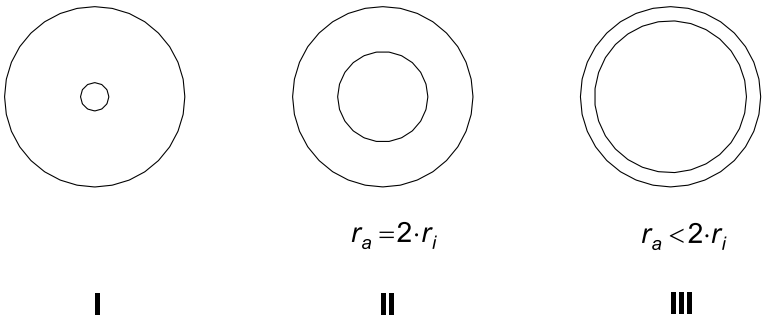

Figure 7.7. Thick walled tube (I) and thin walled tube (III). II is borderline between I and III

Example 7.3. Comparison of logarithmic and arithmetic mean
At this point we have learned that usage of the arithmetic mean is an approximation, and usage of the logarithmic mean is exact. But how big is the error we might get by using the approximation from the arithmetic mean instead of the exact result from the logarithmic mean? Let us compare: We calculate for case II in Figure 7.7:

logarithmic mean	arithmetic mean
$r_m = \dfrac{r_a - r_i}{\ln \dfrac{r_a}{r_i}}$	$r_m = \dfrac{r_a + r_i}{2}$
$r_a = 2r_i$	
$_m = \dfrac{2r_i - r_i}{\ln \dfrac{2r_i}{r_i}}$	$r_m = \dfrac{2r_i + r_i}{2}$
$r_m = \dfrac{r_i}{\ln 2}$	$r_m = \dfrac{3}{2} r_i$
$r_m = 1.44\, r_i$	$r_m = 1.5\, r_i$

Therefore, the relative error is:

$$\frac{\Delta r_m}{r_m} = \frac{1.5\, r_i - 1.44\, r_i}{1.44\, r_i} = \frac{0.06}{1.44} = 4\%$$

So if we use the approximation we get a result which is 4% lower then the exact value.

For the cylindrical, one-dimensional, steady state, single layer case we get:

For the heat flow density

$$\frac{\dot{Q}}{A_m} = \frac{\lambda}{r_a - r_i} \cdot (T_i - T_a) \tag{7.93}$$

For the heat flow

$$\dot{Q} = A_m \cdot \frac{\lambda}{r_a - r_i} \cdot (T_i - T_a) \tag{7.94}$$

For the heat

$$Q = A_m \cdot \frac{\lambda}{r_a - r_i} \cdot (T_i - T_a) \cdot t \tag{7.95}$$

One-Dimensional Steady State Conduction in a Multilayer Cylindrical Wall

Figure 7.8 illustrates the case of conduction heat transfer occurring across a cylindrical wall that is made up of several layers of different materials, with each material having a different thermal conductivity λ and different layer thickness δ. In this case, the general mathematical expression for the quantity of heat flow can be expressed the same as in the case for a flat plate wall (equation (7.77)).

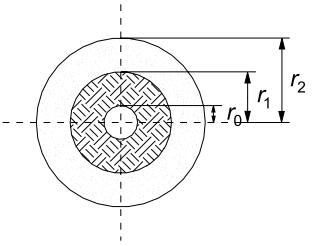

Figure 7.8. Multilayer cylindrical solid wall

Starting with the equation from the flat plate multilayer case,

$$\dot{Q} = \frac{1}{\sum_{i=1}^{n} \frac{\delta_i}{\lambda_i \cdot A_i}} \cdot \Delta T \tag{7.80}$$

The values of the areas A_i depend on the inner and outer radius of each layer. Therefore, they are not the same for all the layers. They have to be added separately. The denominator of equation (7.80) is the sum of all n heat resistances. Again, we have a case in which to use the concept of adding resistances:

$$\sum_{i=1}^{n} \frac{\delta_i}{\lambda_i \cdot A_i} = \sum_{i=1}^{n} R_i \tag{7.81}$$

With equation (7.92) in the form of:

$$r_m = \frac{r_n - r_{n-1}}{\ln \frac{r_n}{r_{n-1}}} \tag{7.96}$$

then

$$\dot{Q} = \frac{1}{\sum \frac{r_n - r_{n-1}}{\lambda_n \cdot 2\pi r_m \cdot l}} \cdot \Delta T = \frac{2\pi l}{\sum \frac{r_n - r_{n-1}}{\lambda_n \cdot r_{m_n}}} \cdot \Delta T \tag{7.97}$$

and the denominator alone is:

$$\sum \frac{(r_n - r_{n-1}) \cdot \ln \frac{r_n}{r_{n-1}}}{\lambda_n \cdot (r_n - r_{n-1})} = \sum \frac{\ln \frac{r_n}{r_{n-1}}}{\lambda_n} \tag{7.98}$$

So, for the heat flow we get:

$$\dot{Q} = \frac{2\pi l}{\sum_{i=1}^{n} \frac{\ln \frac{r_n}{r_{n-1}}}{\lambda_n}} \cdot \Delta T \tag{7.99}$$

Recall that in addition to heat transfer by radiation and conduction, we also have heat transfer by convection and phase transition as alternative mechanisms by which to transfer heat (Table 7.10). So, to calculate heat transfer in general we have more properties and parameters yet to study, which are only mentioned briefly here.

7.6.3
Convection Heat Transfer

Convection heat transfer occurs when heat energy is carried along by a moving fluid in contact with a solid surface. The fluid can be either liquid or gas. For example, we feel warm when we enter a heated room from the cold outdoors because the surface of our body comes in contact with the warm heated air that circulates in the room. Likewise, the air in the room receives heat when it comes in contact with the heated surface of a metal radiator. The inside metal walls of the radiator become heated when hot water flows in contact with the inner surface of these walls. The means by which heat transfers from the flowing hot water to the inside metal surface of the radiator, as well as from the outer metal surface of the radiator to the circulating air in the room is heat transfer by convection.

In the case of convection heat transfer, the fluid experiencing heating or cooling also moves. This movement may be due to the natural buoyancy effect of decreased density with increased temperature (natural convection), or it may be caused artificially by imparting mechanical energy to the fluid, such as with pumps or blowers for liquids and gases, respectively (forced convection).

Determining the rate of heat transfer from convection is complicated because of this fluid motion. When a fluid is flowing over a solid surface, shear stresses occur in the fluid near the surface because of the viscous properties of the fluid. Molecules at the surface try to attach themselves to the surface while neighboring molecules are trying to pass them by within the bulk fluid flow. This causes a velocity profile to develop near the surface. The fluid next to the surface does not move but sticks to it, while neighboring fluid flow is slowed down by the friction of trying to pass the stationery molecules. Therefore, fluid velocity gradually increases with distance away from the surface until the

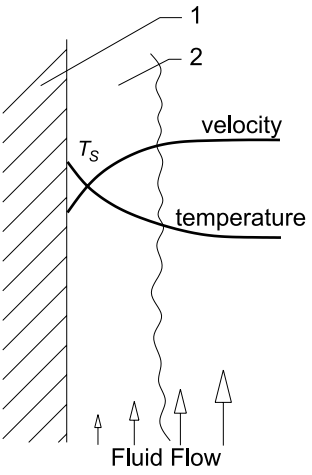

Figure 7.9. Convection heat transfer. Showing boundary layer where velocity and temperature profiles exist near wall surface, **1:** hot wall, **2:** boundary layer

region of bulk fluid flow is reached, where the fluid velocity is all the same at the maximum. This region is known as a boundary layer.

Along with the velocity profile, a temperature profile develops in this boundary layer near the wall. This is because the rate of convective heat transfer from a fluid to a solid surface depends in part on the relative velocity of the fluid in contact with the surface. Since this relative velocity is near zero at the surface because of the sticky viscous effects, transfer of heat is also poor. This means the surface does not readily sense the temperature in the bulk fluid flow, and the temperature will change with distance away from the surface as it moves from surface bulk fluid temperature. Therefore, this invisible boundary layer region near the surface acts as though it were an additional layer of insulating material, adding further resistance to the heat transfer between the fluid and the surface.

Heat Transfer Coefficient

Mathematically, we can account for this convective heat transfer resistance by assuming it represents another layer of material across which heat must transfer in the expression for steady state heat conduction from FOURIER's first law. We can do this by assigning a value for the "thermal conductance" of this invisible boundary layer, which is known as the surface heat transfer coefficient α. Then we could express the simple case of heat transfer across such a boundary layer from a hot surface temperature T_s to a cool bulk fluid temperature T_∞ in the following way:

$$\dot{Q} = \alpha \cdot A \cdot (T_S - T_\infty) \tag{7.100}$$

It is important to note that the heat transfer coefficient is a numerical value that represents the overall "thermal conductance" of the invisible boundary layer. Its value will depend on the combined effects of the physical, thermal and viscous properties of the fluid in contact with the surface, relative velocity of the fluid at the surface, as well as system geometry at the contacting surface, among other things. Therefore, the heat transfer coefficient is not a material property, and cannot be looked up in a handbook. It is a parameter (coefficient) in heat transfer equations that depends on conditions of the process system under study. Normally, it is determined experimentally for heat exchanger systems by running experiments under controlled conditions, where all temperatures, surface areas, material properties and flow rates are known, and the heat transfer coefficient is the only unknown. There are also various approaches for attempting to estimate values for the heat transfer coefficient under different specified sets of heating and cooling conditions and surface contact geometries. These approaches can be found in references devoted more completely to heat transfer and fluid mechanics (e.g. [118]).

Overall Heat Transfer Coefficient

The convective boundary layers are only part of the multilayer systems across which heat must transfer in more realistic heating and cooling situations. Recall

our radiator for heating the room. The air in the room receives heat when it comes in contact with the heated surface of the metal radiator. The inside metal walls of the radiator become heated when hot water flows in contact with the inner surface of these walls. Let us take a close look at just a small section of radiator wall that we could imagine as a flat plate with hot water flowing along the inside surface, and cool room air flowing along the outside surface. In this case, we have a boundary layer on the inside caused by the flowing hot water represented by a heat transfer coefficient α_1. We also have a boundary layer on the outside caused by the flowing cool air represented by a heat transfer coefficient α_2. Let us imagine further that the radiator wall has a layer of rust on the inside and a layer of paint on the outside in addition to the metal core between these rust and paint layers. Each of these material layers would have its own thermal conductivity and thickness. Then we would have a multilayer situation consisting of five layers. This would be a situation similar to that shown earlier in Figure 7.5, but with two additional boundary layers with their respective heat transfer coefficients on each side, as shown in Figure 7.10.

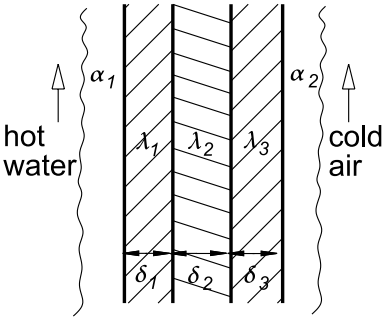

Figure 7.10. Multilayer heat transfer with convection on both sides. Example: Material 2 is steel, 1 is rust and 3 is paint. The overall heat transfer coefficient k is given in equation (7.102) below.

We could also use equation (7.81) to express the heat flow across this three-layer system by adding the two more resistances caused by the boundary layers. Recall that resistance is the reciprocal of conductance (see Section 6.3). Therefore, the thermal resistance of our two boundary layers can be expressed as the reciprocal of their respective heat transfer coefficients $\frac{1}{\alpha_1}$ and $\frac{1}{\alpha_2}$. Likewise, the thermal resistances of each of the material layers (rust, metal, paint) can be expressed as $\frac{\delta_1}{\lambda_1}, \frac{\delta_2}{\lambda_2}, \frac{\delta_3}{\lambda_3}$ respectively. Then, the sum of all five resistances would be:

$$R = \left(\frac{1}{\alpha_1} + \frac{\delta_1}{\lambda_1} + \frac{\delta_2}{\lambda_2} + \frac{\delta_3}{\lambda_3} + \frac{1}{\alpha_2} \right) \tag{7.101}$$

This sum represents the overall equivalent thermal resistance to heat transfer across the five-layer system. Likewise, the reciprocal of this sum would represent the overall equivalent thermal conductance of the system. We call this the overall heat transfer coefficient k:

$$k = \left(\frac{1}{\alpha_1} + \frac{\delta_1}{\lambda_1} + \frac{\delta_2}{\lambda_2} + \frac{\delta_3}{\lambda_3} + \frac{1}{\alpha_2} \right)^{-1} \tag{7.102}$$

In this way, the overall heat transfer coefficient k appears as a single coefficient in the FOURIER heat transfer equation for steady state heat conduction across a barrier:

$$\dot{Q} = k \cdot A \cdot \Delta T \tag{7.103}$$

Process engineers often use this simplified expression with heat transfer calculations involving heat exchangers. Often it is much too difficult to estimate or measure the exact thermal conductivity and thickness of various material layers in a system, especially if they consist of poorly defined rust and scale deposits or fouling layers. It is also difficult to correctly characterize the fluid boundary layers from convective heat transfer in order to estimate convective surface heat transfer coefficients. The overall heat transfer coefficient k takes into account all of these factors. It is most often determined experimentally for heat exchanger systems by running experiments under controlled conditions, where all temperatures, surface areas, and flow rates are known, and the overall heat transfer coefficient k is the only unknown. For more details, see hydrodynamics and process engineering [109,116–121].

7.6.4 Heat Transfer by Phase Transition

We learned earlier from our review of basic thermodynamics that when we look at a simple phase transition, such as when a substance undergoes freezing from a liquid to a solid, or condenses from a vapor to a liquid, then we normally see significant changes in enthalpy, entropy and volume. These are caused by the change of enthalpy ΔH in the form of latent heat of fusion or latent heat of vaporization. These enthalpy changes involve significant quantities of heat transfer to occur in support of the phase change. Because of these significant quantities of latent heat energy transferred during phase change, process engineers prefer to use condensing steam (water vapor) whenever practical as a heat exchange medium in heat exchanger systems.

Example 7.4. When 1 kg of saturated steam at 100 °C condenses onto the cool metal surface of a heat exchanger, it immediately gives up its latent heat of vaporization as the enthalpy changes from the value at saturated vapor ($2676\,\mathrm{kJ \cdot kg^{-1}}$) to that of saturated liquid ($419\,\mathrm{kJ \cdot kg^{-1}}$). This represents a net heat transfer of (at normal pressure) $2257\,\mathrm{kJ \cdot kg^{-1}}$:

So with $\Delta h_{vap} = 2257\,\mathrm{kJ \cdot kg^{-1}}$ we can calculate the latent heat of the steam:

$$|Q_{steam}| = m_{steam} \cdot \Delta h_{vap} = 1\,\mathrm{kg} \cdot 2257\,\mathrm{kJ \cdot kg^{-1}} = 2257\,\mathrm{kJ}$$

If instead, we used 1 kg of liquid hot water at 100 °C as the heat exchange medium, it would probably experience a change in temperature of about 10 °C, and the heat given up would be the sensible heat loss. With $c_p = 4.2\,\mathrm{kJ \cdot kg^{-1} \cdot K^{-1}}$ and $|Q_{water}| = m \cdot c_p \cdot \Delta T$ we would get e.g.

$$|Q_{water}| = 1\,\mathrm{kg} \cdot 4.2\,\mathrm{kJ \cdot kg^{-1} \cdot K^{-1}} \cdot 10\,\mathrm{K} = 42\,\mathrm{kJ}\,.$$

Clearly in the case of condensing water vapor, the amount of heat transferred from the same quantity of steam or water is two orders of magnitude greater for condensing steam (phase transition) than when water is used alone without any phase change.

Q	heat in J
h	specific enthalpy in $J \cdot kg^{-1}$
m	mass in kg
c_p	specific heat capacity in $J \cdot kg^{-1} \cdot K^{-1}$
T	temperature in K

In order to carry out heat transfer calculations involving phase change, it is necessary to know the thermodynamic properties of the material and which phase transition it is undergoing. In the case of condensing steam, we would need the thermodynamic properties of saturated steam. These properties include enthalpy, entropy and specific volume of both saturated liquid and saturated vapor as a function of temperature and pressure. These are material properties, but they depend on temperature and pressure. Therefore, they are normally published in hand books and text books in the form of tables or charts for easy reference. An example of such a steam table can be found in Appendix 15.8.

7.6.5 Thermal Conductivity

In previous sections we described conduction heat transfer through solid materials (across heat exchanger walls), and how we use FOURIER's law to derive mathematical expressions that characterizes conduction heat transfer. You will recall that the thermal conductivity λ was the singular coefficient representing material properties in FOURIER's law. In the case of conduction heat transfer, this material property is called thermal conductivity, and indicates how easily heat will pass through the material. Different materials have different thermal conductivities. This difference helps to explain why a metal spoon gets too hot to hold in your hand when stirring a boiling liquid in a pan, but a wooden spoon of the same size and dimensions does not.

The reason different materials have different thermal conductivities is because they have different chemical and physical compositions. Recall that heat is conducted through solid materials because the increasing kinetic energy imparted to the molecules at the point where the heat is entering the material excites them to oscillate at greater speeds and amplitudes. This excitation is driven by higher electron mobility within the atomic structure of each molecule, and causes the molecules to experience increased "bumping" into neighboring molecules. This molecular "bumping" propagates along the material, and further continues this process of heat transmission (conduction) along the material substance. Therefore, thermal conductivity must depend on both molecular structure at the atomic electron level (the chemical composition), as well as the physical lattice structure by which the molecules are held

in place within the material substance (physical structure). Now, we will look at thermal conductivity in solids, liquids and gases more closely.

Solids

In metal solids, much of the molecular excitation that occurs in response to heat is due to the relatively high mobility of the electrons in metals. Therefore, this electron mobility accounts for the fact that in metals, electron conductivity is the major contributing mechanism for the relatively high thermal conductivity found in metals. The ratio of electric conductivity to thermal conductivity is a linear function of temperature (Wiedemann–Franz law):

$$\frac{\lambda}{\sigma} = L \cdot T \tag{7.104}$$

where

λ	heat conductivity in $W \cdot K^{-1} \cdot m^{-1}$
σ	electric conductivity in $S \cdot m^{-1}$
L	Lorenz coefficient (for metals at room temperature)
T	temperature in K

The relatively high thermal conductivity found in metals is due to the high mobility of electrons in a highly ordered crystalline structure. When we have solid materials without free electrons, then heat is conducted only by the oscillation of the crystalline lattice structure, as explained earlier. Thermal conductivity tends to decrease with decreasing order of crystal structure. For example partly crystalline nonmetallic materials and polymers show decreasing thermal conductivities with decreasing crystallinity [37].

When we compare the thermal conductivity of different metals, we find that silver and copper are among the metals with greatest thermal conductivity. However, in the food industry, we require use of stainless steel in food processing equipment in order to avoid problems with corrosion, oxidation and sanitation, even though stainless steel has slightly lower thermal conductivity than silver or copper.

We should mention that copper is sometimes used in certain food process operations, especially when the rate of heat conduction is very important and is the limiting step in the process. However, when the rate of heat conduction is not a limiting step, stainless steel would be chosen for the reasons given above.

Sometimes foods are heated after first being filled and sealed in packages (packaged foods), such as in the thermal processing of canned foods for long-life shelf stability. In this case, the thermal properties of the packaging material (as well as the thermal and physical properties of the food, itself) will dictate the type of thermal process conditions needed. For example, foods packed in glass jars or flexible or semi-rigid plastic packages will require thermal process conditions different from foods packed in metal cans.

The thermal conductivity of solid foods is largely dependent on the moisture content of the food. Although water often makes up the largest percentage

of the gross composition of most moist solid foods, we must remember that much of this water is tightly bound within the cellular and tissue structure of the food material (see Section 1.2.7), and is not free to flow. Therefore, little or no convective heat transfer will occur, and heat will primarily transfer by solid conduction. For this reason, the moisture content is a predominant variable in empirical equations commonly used for estimating the thermal conductivity of foods.

In simple cases food materials with high moisture content (e.g. juices) have thermal conductivities close to that of pure water. However, some foods may contain atmospheric air as a major component in their physical structure, such as whipped creams and foams, as well as dry bulk granular materials and powders. The thermal conductivity will be governed largely by the amount of air in their composition, causing them to have very low thermal conductivities because of the low thermal conductivity of air. This is why the thermal conductivity of porous materials will depend largely on the porosity of these materials, as well as pore size and type, and pore-size distribution through these materials. In some types of porous materials, the pores are completely closed, while in others the pores are open to each other, as well as to the surrounding atmosphere. In the case of open pores, the relative humidity of the surrounding atmospheric air can greatly affect the thermal conductivity. That is why materials designed to serve as thermal insulation are usually made of polymer foams with closed pores that contain trapped dry gaseous air.

In materials that are anisotropic, the thermal conductivity will be different depending on the direction of heat flow within the material. This is particularly apparent in fibrous materials in which the tissue structure is made up of long thin fibers going only one direction, such as the tissue in muscle meats. As a rule of thumb, the thermal conductivity in meats is normally about 10% greater in the direction along the fibers than in the perpendicular direction across the fibers [115].

Multilayer Solids

For multilayered solid materials, such as those made up of layers of different materials with different thermal conductivities, we can again make use of the concept of adding resistances in series, as we learned earlier in Section 6.8. Remember that resistance is simply the reciprocal or inverse of conductance, whether thermal or electrical. The resistance in terms of heat conduction is called specific heat conduction resistance, and is the same as the inverse of thermal conductivity. If the resistances are in series, we simply can add them. If they were in parallel, we would add the inverse resistances i.e. the conductivities. Table 7.13 illustrates.

When the composition of the multilayer materials is a combination of different components, we can add the thermal conductivity according to their

Table 7.13. Total resistance to heat conduction

in series	in parallel
$R_{total} = \sum_i R_i$	$G_{total} = \sum_i G_i$
$R_{total} = \sum_i \frac{d_i}{A_i} \cdot \frac{1}{\lambda_i}$	$G_{total} = \sum_i \frac{A_i}{d_i} \lambda_i$
	with $A_1 = A_2 = A_3 \ldots$ and $d_1 = d_2 = d_3 \ldots$
$\frac{1}{\lambda_{total}} = \sum_i \frac{1}{\lambda_i}$	$\lambda_{total} = \sum_i \lambda_i$

volume fractions x to calculate the total thermal conductivity. With λ_i and the volume fraction x_i of the material i we have:

in series	in parallel
$\frac{1}{\lambda_{total}} = \sum_i \frac{x_i}{\lambda_i}$	$\lambda_{total} = \sum_i x_i \cdot \lambda_i$

where

λ	specific heat conductivity in $W \cdot K^{-1} \cdot m^{-1}$
$\frac{1}{\lambda}$	specific heat resistivity in $K \cdot m \cdot W^{-1}$
R	heat conduction resistance in $W \cdot K^{-1}$
G	heat conductance $K \cdot W^{-1}$
A	area in m^2
d	thickness in m
x_i	volume fraction

Temperature Dependency of Thermal Conductivity

The thermal conductivity of solid food materials is only mildly dependent on temperature, and increases slightly with increasing temperature. This mild dependency is overshadowed by the effect of gross composition, such as content of water or air. However, at temperatures near the freezing point of water, solid foods with high water content will experience much stronger temperature dependency. The thermal conductivity of water at its freezing point undergoes a dramatic change in value as water undergoes phase transition from liquid into solid ice. Because of the orderly crystalline structure of solid ice, its thermal conductivity is much greater than that of liquid water. Therefore, while water, or food with high water content, is freezing, the thermal conductivity will become a strong function of the ice fraction α present in the water–ice mixture, as shown in Figure 7.11.

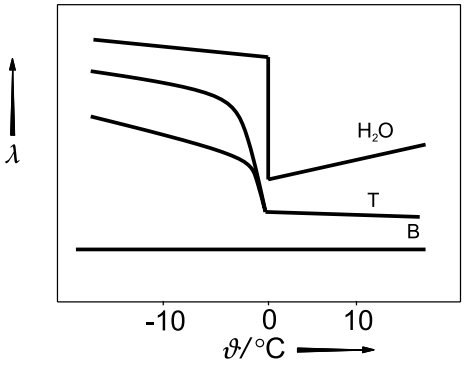

Figure 7.11. Thermal conductivity of water (H_2O), butter (B) and turkey meat (T). T: upper curve indicates λ parallel to fiber, lower curve λ perpendicular to meat fiber [115]

When we simplify the composition of a food product into just two components, water and dry solids, we can estimate a value for its thermal conductivity by the following way:

$$\lambda_{total} = x_{dm} \cdot \lambda_{dm} + x_{H_2O} \cdot (1 - \alpha) \cdot \lambda_{H_2O} + x_{H_2O} \cdot \alpha \cdot \lambda_{ice} \tag{7.105}$$

with

$$x_{H_20} = 1 - x_{dm} \tag{7.106}$$

The parameter α is called ice fraction and can be measured e.g. by DSC (see 7.9.2) or by NMR (see 9.3.2). At temperatures above the freezing point we have $\alpha = 0$ and equation (7.105) simplifies to:

$$\lambda_{total} = x_{dm} \cdot \lambda_{xm} + x_{H_2O} \cdot \lambda_{H_2O} \tag{7.107}$$

where

x_{dm}	mass fraction of dry matter in $kg \cdot kg^{-1}$
x_{H_2O}	mass fraction of water in $kg \cdot kg^{-1}$
α	mass fraction of ice in $kg \cdot kg^{-1}$
λ_{dm}	thermal conductivity of dry matter in $W \cdot K^{-1} \cdot m^{-1}$
λ_{H_2O}	thermal conductivity of water in $W \cdot K^{-1} \cdot m^{-1}$
λ_{ice}	thermal conductivity of ice in $W \cdot K^{-1} \cdot m^{-1}$

Examples of values for thermal conductivity of different foods are given in the Appendix 15.9, along with additional information about references, in which additional data may be found, e.g. [134,141,142].

Liquids

In liquids, heat transfer occurs mostly by convection, the mechanism by which heat is carried along with the flowing fluid. So, it is difficult to measure pure thermal conductivity in liquids. Pure heat conduction can only take place in liquids if they can be completely prevented from flowing in some way, such as when they are formed into a gel. In the case of water, the thermal conductivity of water can be estimated as follows [119]. Further equations can be found in Appendix 15.9.

$$\lambda_{H_2O}/W \cdot K^{-1} \cdot m^{-1} = 0.100 + 0.00166 \cdot T/K \quad (7.108)$$

where
λ_{H_2O} thermal conductivity of water in $W \cdot K^{-1} \cdot m^{-1}$
T temperature in K

Gases

In the case of gases, molecules are not fixed in place, but are free to have translational motion as they become excited with increased kinetic energy from heat input. Therefore, heat conduction in gases evidences itself by the propagation of kinetic energy of the molecules as they "bump" into each other in response to receiving heat energy. This transmission of kinetic energy occurs at a faster rate with increasing velocity of the molecules. Therefore, thermal conductivity in gases increases with increasing temperature, and with decreasing molecular weight of the gas molecule.

This is why we use low molecular weight gases like water vapor and helium for heating and cooling when we want high thermal conductivity, and we use heavier molecular weight gas like xenon for thermal insulation when we want low thermal conductivity.

The thermal conductivity of air at atmospheric pressure in the temperature range 0–500 °C can be estimated from the following empirical expression:

$$\lambda/mW \cdot K^{-1} \cdot m^{-1} = 0.701 + 0.0629 \cdot T/K \quad (7.109)$$

More exact values for air at different relative humidity can be found in reference [105].

Recall that thermal conductivity in gases will increase as molecules are "bumping" against each other with increased kinetic energy. At the same energy level, this "bumping" will occur more frequently when the molecules are located more closely together. Therefore, thermal conductivity in gases will also increase as the mean distance between molecules decreases.

At low pressures or at low concentrations of gas molecules in a given space, the mean distance between molecules can be very large. When such a gas is confined to limited volume of space, such as when held in a closed tank or vessel, this mean distance between molecules may extend beyond the interior space of the enclose tank or vessel. When this occurs, the molecules are forced to be closer together than they would normally be, and pressure develops. As pressure increases the molecules are forced to be closer together. Therefore, in the case of such gases, thermal conductivity will also increase with increasing pressure.

For this reason, the thermal conductivity in a vacuum is very low and essentially nonexistent. That is why thermally insulated bottles are sometimes lined with a glass-enclosed partial vacuum space for very effective thermal insulation. The temperature dependency of thermal conductivity in gases is shown in Figure 7.12. We take advantage of this low thermal conductivity in a vacuum by carrying out certain food processes under vacuum, such as in freeze

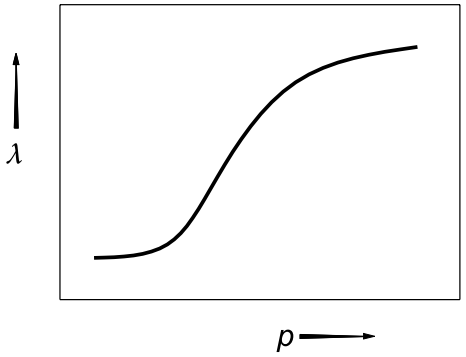

Figure 7.12. Pressure dependency of thermal conductivity of gases (schematic)

drying. The vacuum in the freeze dryer does not permit any heat conduction from the gaseous phase to reach the food product. Similarly to the thermally insulated vacuum bottle, thermally insulated windows are made of two glass window panes just one or two centimeters apart trapping a "dead" space of partial vacuum between them to serve as very effective thermal insulation.

Apparent Heat Conductivity

In systems containing both solids and liquids, heat will transfer by convection as well as conduction (and radiation in some cases). In these types of systems the overall rate of heat transfer is greater than if it were to occur only by pure conduction. If we assume this overall heat transfer is coming only from conduction, then we observe an "apparent" thermal conductivity that is greater than the pure thermal conductivity of any of the component substances in the system.

In the case of dry porous materials with open pores filled with air, like bulk granular materials such as grains and powders, much of the heat transfer will occur by natural convection as the heated air tries to rise through the porous material. Remember that natural convection always occurs in the direction opposite to gravitational acceleration because the temperature-dependent

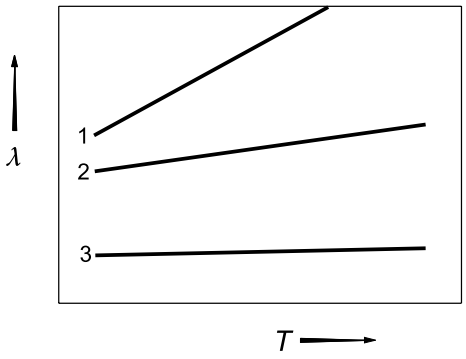

Figure 7.13. Increase of apparent thermal conductivity in a bulk good with increasing temperature gradient: Heat going from bottom to top (1), from top to bottom (2). Thermal conductivity of air, alone, is independent of direction (3).

density of the heated air (or fluid) will decrease with increasing temperature causing the air to rise above the cooler air with greater density. This means that such materials will exhibit anisotropic heat transfer, favoring the direction of natural convection. Therefore, the apparent thermal conductivity of such materials will be anisotropic (Figure 7.13).

7.6.6 Thermal Diffusivity

Recall at the beginning of the chapter, we mentioned the need to distinguish between steady state and unsteady state (transient) heat transfer. In steady state heat conduction, the temperature gradient is constant with time, and we used FOURIER's first law to describe it mathematically (Figure 7.14). In transient (unsteady state) heat conduction, the temperature gradient is not constant and varies as a function of time (Figure 7.15). We can mathematically describe unsteady state heat conduction with FOURIER's second law, equation (7.111). The coefficient a in FOURIER's second law is known as the thermal diffusivity of a material, and it plays a similar role to the thermal conductivity in his first law.

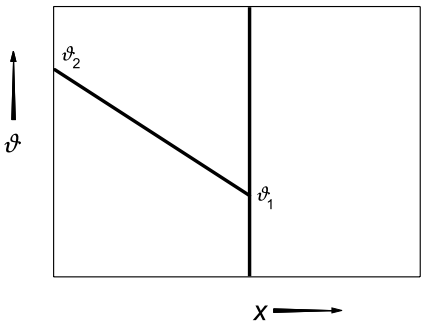

Figure 7.14. Steady state heat conduction: Temperature gradient is constant over time

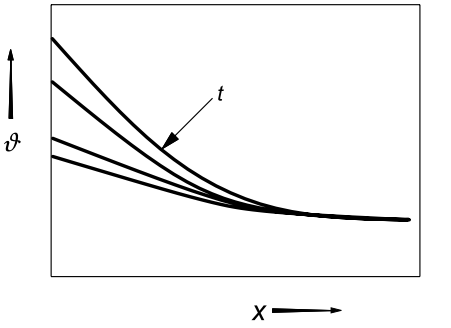

Figure 7.15. Transient heat conduction: Temperature gradient is a function of time

FOURIER's second law for transient heat conduction:

one dimensional:

$$\frac{\mathrm{d}T}{\mathrm{d}t} = a \cdot \frac{\mathrm{d}^2T}{\mathrm{d}x^2} \tag{7.110}$$

three dimensional:

$$\frac{\mathrm{d}T}{\mathrm{d}t} = a \cdot \nabla^2 T \tag{7.111}$$

The thermal diffusivity differs from thermal conductivity because it must also account for the other physical and thermal properties (density and specific heat capacity) that govern the rate of temperature response to a given rate of

heat flow. Therefore, thermal diffusivity is made up of the quotient of thermal conductivity divided by the product of density and specific heat capacity.

$$a = \frac{\lambda}{\rho \cdot c_p} \tag{7.112}$$

where

T	temperature in K
t	time in s
x	length in m
λ	thermal conductivity in $W \cdot K^{-1} \cdot m^{-1}$
ρ	density in $kg \cdot m^{-3}$
c_p	specific heat capacity in $J \cdot K^{-1} \cdot kg^{-1}$
a	thermal diffusivity in $m^2 \cdot s^{-1}$

Magnitude of thermal diffusivity:

Most foods have thermal conductivities in the range of 0.2–0.6 $W \cdot K^{-1} \cdot m^{-1}$ (above 0 °C), and densities from 900–1500 $kg \cdot m^{-3}$ and heat capacities between 1.2–4.2 $kJ \cdot kg^{-1} \cdot K^{-1}$. So, the values of thermal diffusivity according to equation (7.112) can range from $0.02 \cdot 10^{-6}$ to $0.6 \cdot 10^{-6}$ $m^2 \cdot s^{-1}$. Very often we find values in the range $0.1 \cdot 10^{-6}$–$0.6 \cdot 10^{-6}$ $m^2 \cdot s^{-1}$. More exact values can be found by laboratory experiments involving heat penetration tests.

7.7 Measurement of Thermal Properties

7.7.1 Measurement of Thermal Conductivity and Thermal Diffusivity

Thermal conductivity and thermal diffusivity are material properties that govern the rate at which heat will conduct through the material. Both of these properties pertain to conduction heat transfer. Thermal conductivity is the governing property in steady state heat conduction, while thermal diffusivity is the governing property in transient (unsteady-state) heat conduction. Recall that steady state heat conduction occurs in response to a constant temperature gradient that does not change with time. Therefore, measurement techniques used to measure thermal conductivity rely on a constant temperature gradient and constant flow of heat. Techniques for measuring thermal diffusivity are carried out under a transient temperature gradient that usually decreases with time causing flow of heat to also decrease with time.

Steady State Techniques

The primary advantage of measurement under steady state conditions is that experiments can be performed with relatively simple and inexpensive laboratory equipment and straight forward data analysis following Fourier's first

law. The disadvantage is that measurements must be taken under steady state conditions, and it can be very time consuming to reach a controlled steady state condition in many laboratory situations.

A basic type of experiment for measuring thermal conductivity of a material involves arranging a sample of known geometry (area and thickness) so that it will be subjected to heat transfer in only one direction. Once steady state is reached (temperatures at opposite ends of the sample remain constant), it is only necessary to record the constant temperatures and measure the flow of heat. Then, thermal conductivity can be calculated from FOURIER's first law.

The source of heat normally used in these experiments is a simple electric resistance heater in which the heat flow (power) can be determined from the product of measured voltage and current. Temperatures are normally measured by thermocouples or resistance thermometers.

A schematic drawing of the laboratory apparatus used for such an experiment is shown in Figure 7.16. A sample of material of known geometry is sandwiched on both sides of a heat source between the heat source (hot plate) and a heat sink (cold plate), with the edges thermally insulated to prevent any heat transfer in a transverse direction. Details for conducting this experiment are described in [134] or [107].

When we use the type of apparatus shown in Figure 7.16, it is possible to put only the sample material of unknown thermal conductivity on one side of the hot plate, and a reference material sample of known thermal conductivity on the other side of the hot plate. This allows the determination of the thermal conductivity in the sample material on a relative basis to that of the reference material, and eliminates the need to measure heat flow, as shown in Figure 7.17. It is only necessary to measure the steady state temperatures. Then we have:

$$\frac{\lambda_p}{\lambda_R} = \frac{d_p}{d_R} \cdot \frac{\Delta T_R}{\Delta T_p} \tag{7.113}$$

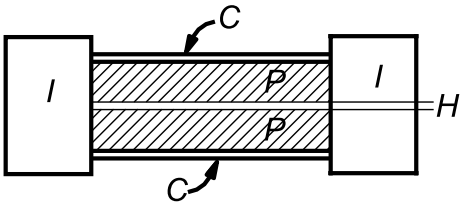

Figure 7.16. Guarded hot plate method: Measurement of thermal conductivity. *P* sample, *C* cooled plate, *H* heater, *I* thermal insulation

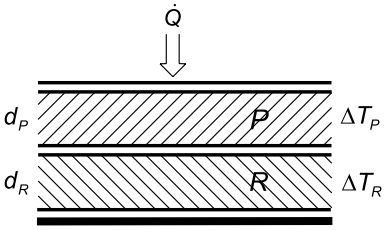

Figure 7.17. Two-plate technique with reference material for measurement of thermal conductivity relative to a reference material. *P* sample material, *R* reference material

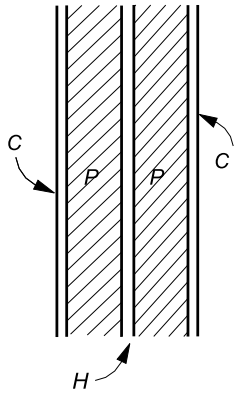

Figure 7.18. Concentric cylinder method for measurement of thermal conductivity of fluid sample materials (schematic). A thin layer of sample *P* is the annular space between heater rod *H* and cooled outer cylindrical jacet *C*

For measurement of thermal conductivity in liquid or fluid samples, a flat plate method is not appropriate, and a concentric cylinder method is used, as shown in Figure 7.18. In this method the heat source is a cylindrical rod as the axis inside a hollow cylindrical tube leaving a narrow annular space in which the fluid sample is held. In order to avoid development of any natural convection, the thickness of the annular space must be kept very small (1–3 mm) depending on fluid viscosity, and the temperature differences must also be small (1–5 K) [134].

These types of measurement techniques require great care that the equipment and apparatus is well thermally insulated to minimize heat losses from the system, as well as heat transfer in unwanted transverse directions. It is also important that temperature sensing probes be insulated and carefully located to ensure that only sample temperatures are being measured, and that these measurements are confounded by inadvertent contact with any part of the apparatus or equipment housing. Descriptions of other measurement methods for thermal conductivity can be found e.g. in [7,8,107].

Quasisteady State Techniques

There are some techniques which are based on FOURIER's second law with the assumption that the heat flow is only approximately constant during the measurement. These are particularly useful when the sample material has very poor (low) thermal conductivity. One of these techniques is the FITCH method. This method consists of a heat source or sink, in the form of an insulated vessel with a copper plate bottom, filled with a constant temperature liquid, and a sink or source in the form of a copper plug insulated on all sides except the one in contact with the sample to be measured (Figure 7.19). The sample is sandwiched between the copper plate at the bottom of the vessel (above the sample) and the insulated copper plug (beneath the sample).

This arrangement causes quasisteady state heat conduction through the sample that can be expressed mathematically with the following simplified equation:

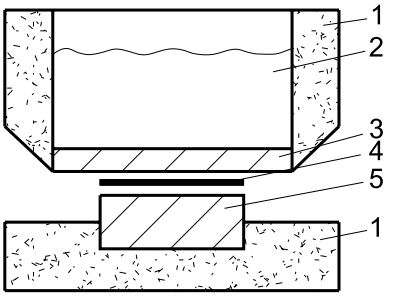

Figure 7.19. FITCH apparatus for measuring thermal conductivity [134]. **1:** insulation, **2:** liquid with temperature T_S, **3:** and **5:** copper block, **4:** sample

$$\frac{A \cdot \lambda \cdot (T - T_S)}{\delta} = m \cdot c_p \cdot \frac{\mathrm{d}T}{\mathrm{d}t} \tag{7.114}$$

with initial conditions at $t = 0, T = T_0$.

The solution of the above with these initial conditions is:

$$\ln \frac{T_0 - T_S}{T - T_S} = \frac{A \cdot \lambda \cdot t}{\delta \cdot m \cdot c_p} \tag{7.115}$$

where

T_0	initial temperature of copper block in K
T	temperature of copper block in K
T_S	temperature of upper vessel in Figure 7.19 in K
t	time in s
m	mass in kg
δ	thickness in m
λ	thermal conductivity in $\mathrm{W \cdot K^{-1} \cdot m^{-1}}$
c_p	specific heat capacity in $\mathrm{J \cdot K^{-1} \cdot kg^{-1}}$
A	area in $\mathrm{m^2}$

The thermal conductivity can be calculated from the slope of the semi-log plot of canonical temperature ratio ($\ln \frac{T_0 - T_S}{T - T_S}$) versus time. This method is valid only if the following assumptions hold:

1. contact resistance is negligible,
2. heat storage (accumulation) in the sample is negligible,
3. transverse heat transfer from the edges of the sample and copper plug is negligible,
4. temperatures of the heat source and sink are constant over time,
5. initial temperature of the sample and copper plug are the same,
6. temperature distribution throughout the copper plug is uniform,
7. sample material is homogeneous, and
8. temperature profile is linear on a semi-log plot for duration of the experiment.

Errors associated from invalidity of any of these assumptions can often be corrected by calibrating the method with a sample of precisely known thermal conductivity, and obtaining a correction factor. To minimize experimental

errors numerous modifications to the FITCH methods have been developed like CENCO–FITCH method, ZURITZ et al.–FITCH method, RAHMAN–FITCH method, which are described and compared in reference [134].

Transient (Unsteady State) Techniques

Unsteady-state or transient heat conduction methods are also used to measure thermal conductivity of a sample material. In transient heat conduction, heat flows into a material and accumulates within the sample over time, causing the internal temperature of the sample to increase with time. Thus, the temperature gradient is not constant, but will diminish over time as an exponential decay. Therefore, the objective of these experimental methods is to obtain a recording of the temperature–time profile experienced within the sample in response to a known heat flow. Data analysis is then carried out based on FOURIER's second law.

An experimental apparatus similar to the concentric cylinder method shown in Figure 7.18 can also be used for this purpose. The sample material is placed in the annular space, and the heat source is the central core rod of length L. At the beginning of the experiment, the temperature of the sample and heat source rod are the same at $t = 0$. When the heater is turned on, heat will begin to flow at a constant rate $\dot{Q}$ established by the constant electric power delivered to the heat source rod. Then, the sample temperature is measured and recorded over time during heating. The thermal conductivity of the sample is obtained from equation (7.116):

$$\lambda = \frac{\dot{Q}}{4\pi \cdot L \cdot (\vartheta_2 - \vartheta_1)} \cdot \ln \frac{t_2}{t_1} \tag{7.116}$$

Another method involves the use of a needle-type heat probe, which serves as a defined heat source [5]. The probe is inserted into the center of the material sample with initial temperature measured and recorded. Then a known quantity of heat flow is emitted from the probe, and the sample temperature is measured and recorded over time in response to this flow of heat (Figure 7.20). A comprehensive description of this heat line source method is presented together with an experimental example on the thermal conductivity of red delicious apple in [135].

When it is necessary to measure thermal diffusivity instead of thermal conductivity, a relatively simple method can be used based on simultaneous

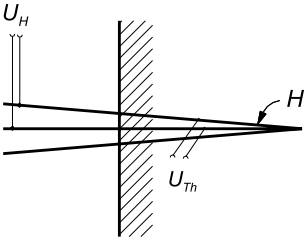

Figure 7.20. Heat probe sensor to measure thermal conductivity (after SWEAT et al [5]), showing needle-type heating element H with electrical voltage potential (U_H) for power to heat source, and voltage potential from thermocouple junction (U_{Th}) for temperature measurement

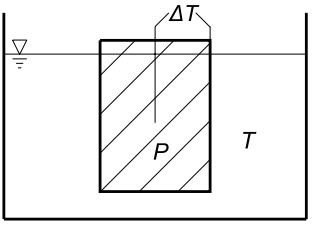

Figure 7.21. Technique for measurement of thermal diffusivity by recording of constant surface temperature and internal core temperature of a sample P which is in a temperature-controlled bath at temperature T

measurement of internal core temperature and external surface temperature while the sample is being heated from the outside. To accomplish this, experiments are designed in such a way, that a known constant temperature (different from the initial sample temperature) is suddenly applied at the outside surface of the sample, while the temperature at the geometric center (cold spot) is measured and recorded over time. This is usually accomplished by immersing the sample (with temperature probe attached) into a heated liquid or fluid held at constant temperature (Figure 7.21). The resulting cold spot temperature profile will still produce a straight line on a semi-log plot when plotted as log of canonical temperature ratio ($\ln \frac{T_0 - T_S}{T - T_S}$) versus time [6].

Thermal diffusivity can also be measured by use of differential scanning calorimetry (DSC), described later in this chapter.

7.8 Caloric Value of Foods

7.8.1 Caloric (Energy) Requirement of the Human Body

Foods contain energy, which is taken up by the body when they are consumed. This energy is used first to sustain basic metabolism of the cells in the body tissues and organs, which is necessary even when the body is at rest (basal metabolism). Next, additional energy is converted into work energy by the muscle tissues of the body in contracting and expanding in order for the body to undergo movement and do work. Finally, more energy is also given off as excess heat from the body after maintaining normal body temperature. This total energy requirement can be calculated from the following energy balance:

$$E_A = E_M + E_N \tag{7.117}$$

where

E_A energy taken up in J
E_M energy metabolized in J
E_N energy which is not metabolized in J
E_B energy excreted with body waste in J

Very little energy is normally excreted with body waste (urine and feces) from a healthy person because these waste materials contain very little protein,

carbohydrates or fat. Also, the carbon dioxide exhaled from breathing contains no combustion energy.

In the case of carbohydrates in our foods, only the digestible part, which can be absorbed from the intestinal track, is taken up as energy by the body. The remainder is called dietary fiber that is made up largely of cellulose fibers, and is excreted with the body waste. We now know that this undigested dietary fiber still plays an important role in sustaining a healthy balance of natural microbial populations in the intestinal track. These cellulose fibers are further broken down by enzymes produced by intestinal microbes to provide important nutrients for sustaining microbial metabolism in the intestines. Therefore, this activity provides an important physiological effect for sustaining good health, but it does not contribute to any remarkable further uptake of energy by the body. So, looking at the energy balance once again, we can say:

$$E_A = E_M + E_B \tag{7.118}$$

In the case of a diet low in dietary fiber,

$$E_A \approx E_M \tag{7.119}$$

The energy required by the human body $\dot{E}$ depends on many factors, such as age, sex, work load, surrounding temperature that may fluctuate strongly during a day. As a rule of thumb, we require approximately 100 W over a 24-hour period as a measure of human power intake. It is remarkable that about 70% of this power is needed just to sustain basal metabolism: in other words, just for "being there," or while sleeping. Only 30% is needed for doing something over shorter periods. Table 7.14 provides some data.

Another rule of thumb for the power required by our body is: The minimum power needed to sustain basal metabolism (being there, doing nothing) is one kcal per hour for each kg body weight we carry.

Table 7.14. Power required by the human body (after HAWTHORN in [115])

$\dot{E}$/W	type of activity
70	none (sitting, sleeping, "being there")
200–300	light work (painting, driving a car)
300–500	medium activity (tennis, bicycling at 16 km·h^{-1})
500–700	heavy activity (swimming, running, rowing a boat)
100	24 h – average

Example 7.5. Minimum power required by human body per day, in SI units
Applying this rule of thumb with a body mass of 65 kg, we get

$$\dot{E} = \frac{1\,\text{kcal}}{\text{h} \cdot \text{kg}} \cdot 65\,\text{kg} = \frac{65000\,\text{cal}}{3600\,\text{s}} = 18\,\text{cal} \cdot \text{s}^{-1} = 75\,\text{J} \cdot \text{s}^{-1} = 75\,\text{W}$$

This is close to the value in the first line of Table 7.14.

Example 7.6. Expressing "1 kcal per hour for each kg body weight" in SI units

$$\dot{E} = \frac{1\,\text{kcal}}{\text{h} \cdot \text{kg}} = \frac{4.18\,\text{kJ}}{\text{h} \cdot \text{kg}} = \frac{24 \cdot 4.18\,\text{kJ}}{\text{d} \cdot \text{kg}} = 100\,\text{kJ} \cdot \text{d}^{-1} \cdot \text{kg}^{-1}$$

$$\dot{E} = 100\,\text{kJ} \cdot \text{d}^{-1} \cdot \text{kg}^{-1}$$

So, we can say the minimum power required for a human body is about 100 kJ per kg body weight per day.

However, the average daily human body power requirement for an active adult male will be greater than this minimum requirement. Studies have shown that the best estimates for the human body power requirements of individual persons are based upon a correlation with the actual body surface area of the person, which also correlates with body mass, as follows:

$$\frac{\dot{E}}{A} = 58.2\,\text{W} \cdot \text{m}^{-2} \tag{7.120}$$

If we assume an average adult male has a body surface area of approximately $A = 1.75\,\text{m}^2$, then we would estimate the daily power requirement as:

$$\dot{E} = 58.2\,\text{W} \cdot \text{m}^{-2} \cdot 1.75\,\text{m}^2 \cong 100\,\text{W} \tag{7.121}$$

We can convert those 100 Watts of daily power requirement into units of energy:

$$E = \dot{E} \cdot t \tag{7.122}$$

$$E = 100\,\text{W} \cdot 24 \cdot 3600\,\text{s} = 8640\,\text{kJ} \tag{7.123}$$

When we convert this value of 8640 kJ into units of calories, we get 2067 kcal. It is more common to use the unit of Calorie (Cal) to represent 1000 calories (1 Cal = 1 kcal). This is why most nutritionists' recommendations for a daily caloric intake are in the range of 2000 ± 500 Calories. The plus or minus 500 Calories is to allow consideration for wide differences in age, sex, health, body size, level and type of activity, etc.

Another approach to estimating daily power requirements is to multiply the minimum power by a "consideration" factor f between 1 and 1.7. Then, with a minimum power of 70 watts as an example, we would get:

$$E = f \cdot 70\,\text{W} \cdot 24 \cdot 3600\,\text{s} = f \cdot 6048\,\text{kJ} = f \cdot 1447\,\text{kcal}$$

Some estimates of the factor f are shown in Table 7.15.

Table 7.15. Factors for estimating average power requirement

activity	f	E/kcal
doing nothing	1.0	1560
office job	1.4	2184
doing sports	1.7	2460

Recall that use of equation (7.120) requires a value for mean body surface area. Human body surface area can be estimated with the following empirical equation from reference [9]:

$$A/\mathrm{m}^2 = (\text{body mass in kg})^{0.5378} \cdot (\text{body height in cm})^{0.3964} \cdot 0.024265 \quad (7.124)$$

7.8.2 Caloric Value of Food

Foods are composed mainly of water, carbohydrate, fat and protein. Since we know how these components are metabolized in the human body (including the energy value from each), it is possible to calculate the energy value contained in any food product, as long as we know its gross composition in terms of fat, protein and carbohydrate. These components are metabolized into energy in the human body by oxidation reactions supported by oxygen obtained from respiration. These oxidation reactions convert the carbon source coming from our food into the carbon dioxide gas that we exhale during respiration.

The specific energy that the human body can obtain from metabolizing each of these macronutrients is called the physiological heat of combustion, or physiological caloric value. They are also known as ATWATER factors [10,11], and are listed in Table 7.16:

Table 7.16. ATWATER factors: Physiological caloric values [110]

ingredient	$e_i/\mathrm{kJ} \cdot \mathrm{g}^{-1}$	$e_i/\mathrm{kcal} \cdot \mathrm{g}^{-1}$
proteins	17	4
carbohydrates	17	4
fats	37	9
alcohol	29	7

With the help of these factors e, we can calculate the energy value contained in any food product, as long as we know its gross composition in terms of fat, protein and carbohydrate. This is done by multiplying the mass of each component in the food product by its respective ATWATER factor, and summing the multiplications. Published data on food composition are available from references like [128,143–145].

$$E = \sum_i m_i \cdot e_i \quad (7.125)$$

where

E	physiological combustion energy in J
e_i	physiological combustion value of ingredient i in $\mathrm{J} \cdot \mathrm{g}^{-1}$
m_i	mass of ingredient in g

Example 7.7. Caloric value of potato
From [128] we can find the composition for 100 g potato:

m/g	
798	water
2.1	protein
0.1	fat
17.7	carbohydrates

So the energy (combustion value) is:

$$E = 2.1\,\mathrm{g} \cdot 17\,\mathrm{kJ} \cdot \mathrm{g}^{-1} + 0.1\,\mathrm{g} \cdot 37\,\mathrm{kJ} \cdot \mathrm{g}^{-1} + 17.7\,\mathrm{g} \cdot 17\,\mathrm{kJ} \cdot \mathrm{g}^{-1}$$

$$E = 340.3\,\mathrm{kJ} = 81.4\,\mathrm{kcal}$$

Sometimes this is written $E = 81.4$ kcal $= 81.4$ Cal.

7.8.3 Measurement of Caloric (Combustion) Values

The caloric value (energy content) of a food sample can be measured experimentally in a laboratory with the use of a combustion calorimeter. The sample is placed in the combustion calorimeter and completely oxidized. The heat evolved from this oxidation reaction causes a rise in temperature that is measured and recorded, from which the caloric value can be calculated. Standard methods for measuring caloric food values with combustion calorimeters can be found in [12,13].

In a combustion calorimeter all the protein, carbohydrate and fat is completely oxidized into NO_2, CO_2 and H_2O. However, the human body has a different need for the nitrogen in the protein, and does not oxidize the nitrogen into NO_2 as does the calorimeter. Therefore, the energy value obtained from the calorimeter is not the same as the energy value taken up by the body, and some adjustment is needed.

Much of the nitrogen coming from proteins in the human body is metabolized in the following way: 80–90% to urea (H_2N–CO–NH_2), 3–5% to ureic acid and $< 1\%$ to creatinine.

We see that the oxidation of nitrogen in our body is low, and the physiologic combustion value, therefore, is considerably lower than that measured in a calorimeter (Table 7.17).

Table 7.17. Comparison of physical and physiological combustion data

ingredient	physical combustion value in kJ · g^{-1}	physiological combustion value in kJ · g^{-1}
fat	38.9	37
carbohydrate	17.2	17
protein	23.4	17
alcohol	30.0	29

Other methods for estimating caloric food values are based on total body calorimetry, or on measurement of oxygen uptake by persons being tested.

In matters of human nutrition, food energy is only one consideration out of many. For example, consulting nutritionists and dieticians will consider many different health and lifestyle factors in recommending diet plans for an individual person.

7.9 Thermal Analysis

The International Confederation for Thermal Analysis and Calorimetry (ICTAC) has defined Thermal Analysis (TA) as a group of techniques that allow us to study the relationship between material properties of a sample and its temperature [19]. Examples of such techniques include thermal gravimetric analysis, thermal mechanical analysis, dielectric thermal analysis, thermometry, etc. Table 7.18 gives a listing of such examples.

If we were to take this definition very strictly, then even the study of flow properties versus temperature (Chapter 4) or measurement of solid-fat index by nuclear magnetic resonance (Section 9.3.2) would also belong to thermal analysis.

The following table helps to sort out the various techniques and the thermal quantity with which they are associated.

Performance of these analytical methods can often be enhanced by coupling different methods of thermal analysis, such as DSC-TG, DSC-TOA, TG-EGA. In the following section, we will focus on TG and DSC.

7.9.1 Thermogravimetry (TG)

A thermogravimetric measuring unit consists mainly of a sensitive weighing balance that is placed within an oven (Figure 7.22). During a temperature–time program in the oven, the weight of the sample is measured and recorded over time.

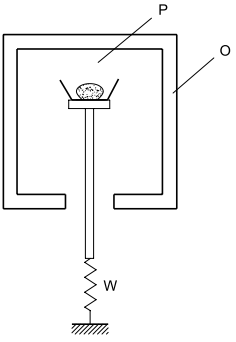

Figure 7.22. Thermogravimetric measuring system (schematic): The sample P is in an oven O. The sample carrier is coupled to a balance W which is outside of the oven [15].

Table 7.18. Examples of techniques used in thermal analysis [15]

property measured	name of technique	abbre-vation	note
mass	thermogravimetry or thermogravimetric analysis	TG TGA	mass of sample is recorded during a given temperature–time program
dimensional and mechanical	dynamic mechanical analysis, thermomechanical analysis, thermodilatometry	DMA TMA TD	deformation or dimensions are measured to get mechanical moduli (storage/loss)
electrical	dielectric thermal analysis	DEA	permittivity/dielectric loss measured
electrical	thermally stimulated current	TSC	
magnetic	thermomagnetometry		often combined with TGA
gas flow	evolved gas analysis	EGA	nature and/or amount of gas/vapor is determined
gas flow	emanation thermal analysis	ETA	trapped radioactive gas within the sample is released and measured
pressure	thermomanometry		evolution of gas is detected by pressure change
pressure	thermobarometry		pressure exerted by a dense sample on the walls of a constant volume cell is studied
optical	thermoptometry	TO	family of techniques in which an optical characteristic or property of a sample is studied
optical	thermoluminescense	TL	emitted light measured
acoustic	thermosonimetry or thermoacoustimetry		techniques where the sound emitted (sonimetry) or absorbed (acoustimetry) by the sample is studied

Table 7.19. Classification of thermal techniques by quantity measured

quantity	technique
heat	calorimetry
temperature	thermometry
temperature difference	differential thermal analysis
heat flow rate	differential scanning calorimetry

The temperature–time program can be a simple linear ramp, but can also be a step-wise increasing temperature function with each step increase consisting of a short isothermal time interval. The program can also be a single step increase to a specified oven temperature held constant over a specified time. This is called an isothermal analysis.

The oven atmosphere can be dry air or just nitrogen. At high temperatures, volatile substances are driven off, and a decrease in sample mass can be observed and measured, as shown in Figure 7.24.

The various reactions that can be studied in this way are listed in Table 7.20. Those most used in food technology are involved in food drying (desorption and evaporation of water). Figure 7.23 shows some typical TG signals for these types of transitions:

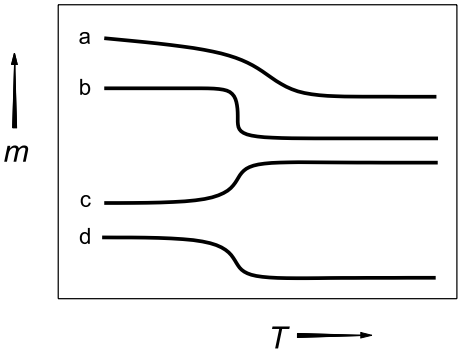

Figure 7.23. TG signals (schematic): (a) evaporation, drying, sublimation; (b) boiling in pan with small hole; (c) sample oxidation; (d) CURIE transition

Table 7.20. Reactions which can be investigated by TG

sample behavior	TG signal on heating
desorption, evaporation (e.g. drying)	mass decrease
sublimation	mass decrease
dissociation into gaseous substances	mass decrease
reaction with gases (e.g. oxidation)	mass increase
CURIE transition of metals	apparent mass change

In food process engineering, drying and oven roasting processes can be studied by thermogravimetric analyses. By observing the moisture loss as a function of temperature over time, the water binding characteristics of the food sample can be studied, as well as the enthalpy of desorption or adsorption (Section 1.2).

We can also use TG to validate the performance of techniques used to measure the moisture content in foods, such as oven drying or infrared balance methods. The use of TG analyses in these applications also allows us to determine at what temperatures and after what times drying is completed, and at what point thermal degradation of the food material will occur.

The output signal from a TG analysis is a smooth curve on a graph of mass versus temperature, called a TG signal, as shown in the upper graph of Figure 7.24. The first derivative of this TG signal curve is the mass flow. When it is plotted versus temperature this is called a DTG plot as shown in the lower graph of Figure 7.24. When we examine the DTG signal curve, we can see that a negative peak will represent a decrease in mass, while a positive peak would represent an increase in mass. The integration of the DTG peak (area within the peak profile) will result in the total mass that was lost or gained during the analysis.

Making a DTG signal plot instead of a TG signal plot, allows us to apply standard mathematical techniques to analyze the important features. For example, we can determine the temperatures at the beginning and end of a

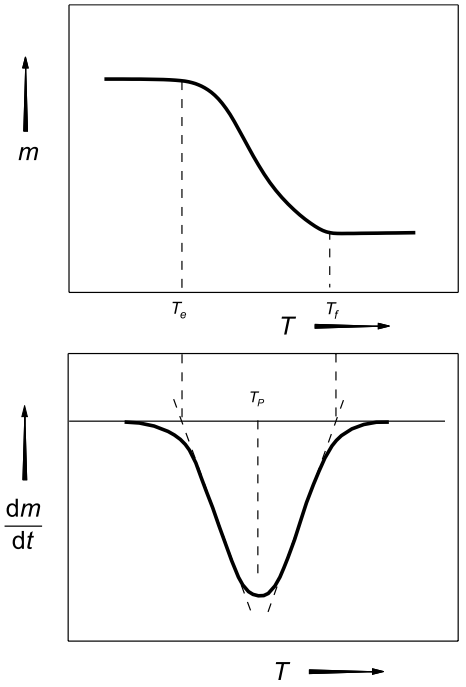

Figure 7.24. TG and DTG signal curves. Beginning T_e and end T_f of the transition can be read out as extrapolated temperatures. T_p is the peak temperature, it is the temperature where the mass flux has its maximum [15]

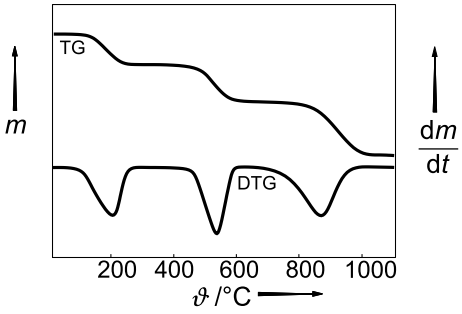

Figure 7.25. TG and DTG plot: thermal degradation of calcium-oxalate-dihydrate: three steps of mass drop due to dehydration and dissociation [15]

given peak, as well as the maximum temperature of each peak, as shown in the lower curve in Figure 7.24. In Figure 7.25 we can see an example of both TG and DTG signal plots from the thermal degradation (roasting) of calcium oxalate dihydrate, showing three steps of mass drop due to dehydration and dissociation.

Another example is shown in Figure 7.26, where we have both TG and DTG signal plots from the thermal degradation of aspartame (artificial sweetener used in many food formulations). In this case, we see a distinct peak occurring in the temperature range between 180 and 200 °C. This is the temperature range normally used in most food baking and roasting processes, and poses a problem with the stability of aspartame during such processes.

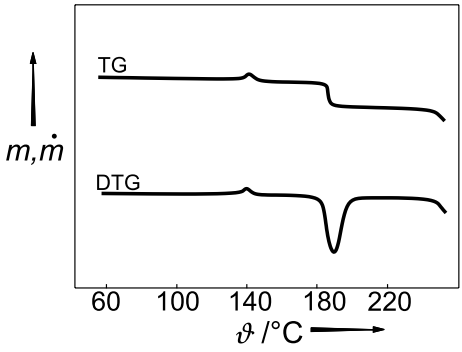

Figure 7.26. TG of aspartame. Note the mass drop on heating above baking temperatures of 180 °C.

In many food ingredients the mass loss during oven roasting processes is not only due to moisture, but many gaseous components, such as CO_2 emissions and volatile flavor and aroma compounds. In order to study such compound losses by thermal analysis, it is necessary to use TG analysis coupled to other appropriate methods of thermal analysis, such as EGA. The roasting of coffee falls into this category, and was examined further by Cammenga et al. [16,17].

Calibration of TG

A thermal gravimetric method must be calibrated first for the weighing system, using methods discussed earlier in Chapter 2. Then, it must be calibrated for the temperature measuring system by using standard materials with defined transition points at known temperatures as well. Standard materials that can be used for this purpose are various hydrates, which give up their water of hydration at exactly known temperatures (see Figure 7.25). Alternatively, materials which exhibit a well-defined CURIE transition can be used as standards. A CURIE transition is when ferromagnetic materials lose their magnetization and therefore lose their magnetic attraction to a magnet. Therefore, if a permanent magnet is placed near to the sample in a thermogravimetric system, the balance will show a signal. When a permanent magnet is mounted in the region just below the sample on the weighing balance, the sample will be attracted to the magnet, and show more than its true weight while initially resting on the balance. Then upon heating, the sample will show a CURIE transition (loss of its magnetic attraction to the magnet). This will be observed as an apparent sudden mass loss by the sample resting on the balance because of the loss of magnetic attraction. This will happen at a specific defined temperature that is precisely known for the standard material, and is called the CURIE temperature.

Consideration must also be given to the precision with which temperature is measured in thermogravimetric analysis. For example, the temperature measuring sensor or probe used in TG analysis is not located within the sample material itself, but in close proximity to the sample. Therefore, the temperatures measured and recorded during a test are not precisely those experienced by the sample material. The difference between displayed and sample temperature will depend on the thermal conductivity and size of the material sample. This difference will increase as thermal conductivity decreases and sample size increases, and will cause large differences that may be problematic with large sample size and low thermal conductivity. Therefore, it is recommended that sample sizes (as well as rate of heating) be as small (or low) as practically possible to minimize this lack of precision in temperature measurement with TG analysis.

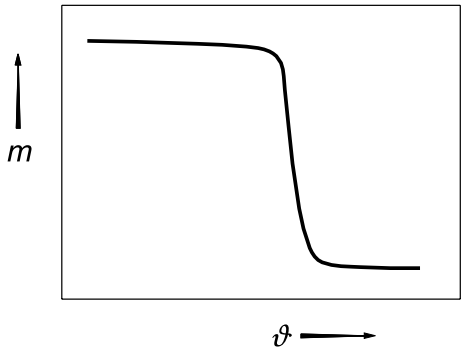

Figure 7.27. TG calibration with a nickel standard. On reaching the CURIE temperature (for nickel $351.4 \pm 4.8\,^{\circ}C$) the magnetic attraction disappears and the mass signal shows a sudden decrease.

Additional information can be obtained from TG analysis by modification of the gaseous atmosphere surrounding the sample in the heating oven chamber. For example by changing the atmosphere from low to high relative humidity in the chamber, we can study first desorption, then adsorption. Or, by changing from aerobic to anaerobic atmosphere, we can study what part of the reaction depends on oxygen. We can also study applications under near vacuum [18]. When extreme levels of accuracy and precision are important, then we must also consider buoyancy effects of the atmospheric gases or fluids surrounding the sample in the heating oven chamber, and the fact that different gases will have different buoyancy effects. In those types of situations, correction factors for these buoyancy effects must be applied (see Section 2.2, weighing and buoyancy effects).

7.9.2 Heat Flow Calorimetry

Heat flow calorimetry is useful for relating temperature and heat flow measurements with heat capacity of a material. Heat flow calorimeters display a heat flow signal by sensing a temperature difference between the sample and a reference material during application of a temperature–time program [19].

The use of a reference material is the key to the relative simplicity of this method. Only the signal representing the difference between sample and reference temperature is needed. Measurement of absolute temperature is not required anywhere. However, initial and boundary test conditions surrounding both sample and reference materials must be identically the same. For this reason, both sample and reference materials are handled like twin sister samples during the complete procedure. For example, the pans used for sample and reference must have exactly the same heat capacity.

Most heat flow calorimeters in modern use today are known as differential scanning calorimeters (DSC). There are two general principles of DSC hardware. First is the temperature difference ΔT-measuring system, and second is the power compensation system.

ΔT-Measuring System

Figure 7.28 shows a schematic diagram of a DSC oven chamber containing both sample and reference materials. On the left side is the sample in a pan and on the right side is the reference material in an identical pan. When the oven is turned on, heat will flow into both pans at a given controlled rate. This will cause the temperature to rise in both sample and reference material in accordance with the thermal properties of each material.

The DSC oven chamber is designed in such a way, that heat transfer by radiation and convection is negligible. Therefore, heat transfers from the oven into both sample and reference material by pure conduction, and we can apply Fourier's first law to calculate the heat flow into the sample material using

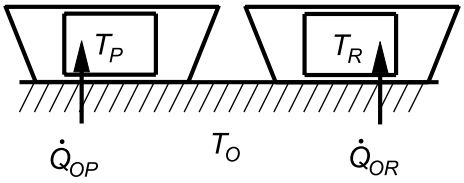

Figure 7.28. DSC oven schematic. T_P sample temperature, T_R reference temperature, T_O oven temperature, $\dot{Q}$ heat flow.

the temperature difference $(T_O - T_P)$ between oven and sample. In the same way, we can calculate the heat flow from the oven to the reference material. Then, we can determine the difference in heat flow between the sample and the reference material by subtracting the heat flow into the reference from the heat flow into the sample:

heat flow into the sample:

$$\dot{Q}_{OP} = k \cdot A \cdot (T_O - T_P) \tag{7.126}$$

heat flow into reference material:

$$\dot{Q}_{OR} = k \cdot A \cdot (T_O - T_R) \tag{7.127}$$

difference:

$$\dot{Q} = \dot{Q}_{OP} - \dot{Q}_{OR} \tag{7.128}$$

so

$$\dot{Q} = k \cdot A \cdot (T_O - T_P - (T_O - T_R)) \tag{7.129}$$

or:

$$\dot{Q} = k \cdot A \cdot (T_R - T_P) \tag{7.130}$$

As a short cut, we can say:

$$\dot{Q} = k \cdot A \cdot \Delta T \tag{7.131}$$

Using the hardware constant:

$$K = k \cdot A \tag{7.132}$$

we get for the heat flow

$$\dot{Q} = K \cdot \Delta T \tag{7.133}$$

where

$\dot{Q}$	heat flow in W
T	temperature in K
ΔT	temperature difference in K
A	area in m^2
k	overall heat transfer coefficient in $W \cdot m^{-2} \cdot K^{-1}$
K	hardware constant in $W \cdot K^{-1}$

Indices:

O	oven
P	sample
R	reference

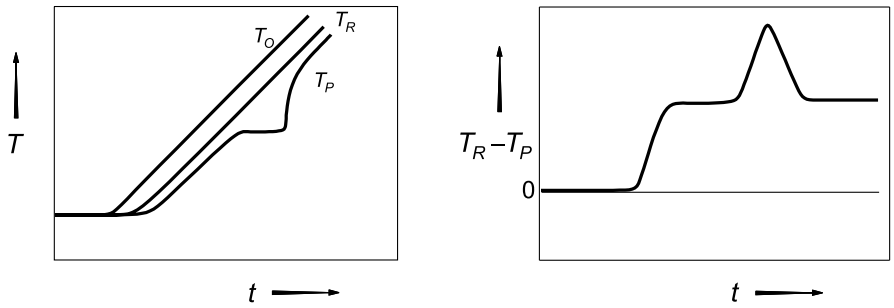

Figure 7.29. $\Delta T = T_r - T_P$ versus time during a DSC run

The temperature–time plots for the oven, sample and reference material are shown in the upper graph of Figure 7.29, while the temperature difference between sample and reference over time (ΔT signal) can be seen on the lower graph in Figure 7.29. As can be seen from equation (7.133) this ΔT signal is proportional to the heat flow into the sample.

We can distinguish two types of hardware systems used in DSC heat flow calorimetry. One system is known as the DSC disk system in which the sample and reference pans are placed upon a disk. The thermocouples used for measuring ΔT are incorporated into the disk, as shown in Figure 7.30.

The other type is a cylindrical system, in which the temperature probes are in the form of cylindrical cups, as shown in Figure 7.31. This type is appropriate for larger volume sample sizes.

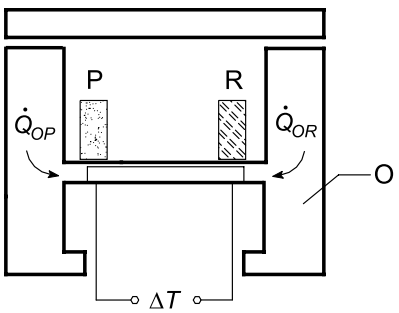

Figure 7.30. DSC disk system [15]

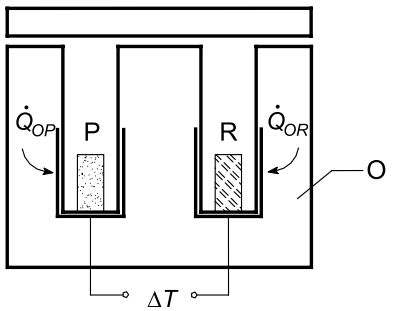

Figure 7.31. DSC cylindrical system [15]

Power Compensation System

Besides the ΔT-measuring system, there are DSC instruments that are based upon the principle of power compensation. The general construction of such a system is illustrated in Figure 7.32. The main characteristic of these systems is the use of small individual heaters beneath each separate pan. These small

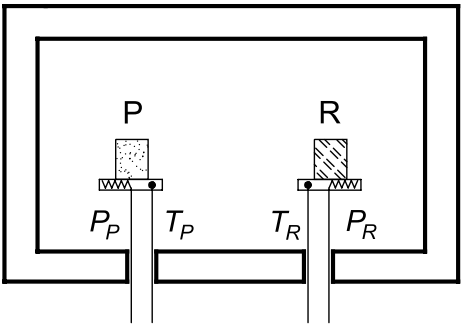

Figure 7.32. Power compensation calorimeter (schematic). T_P sample temperature, P_P heating power for the sample, T_R temperature of reference, P_R heating power for reference [15]

heaters allow independent control of heat flow so that the temperature in both sample pan and reference pan is kept the same, and the difference between them kept at zero all the time. In this case, the power needed to keep this difference at zero is what is measured and recorded during the test.

Evaluation of a DSC Plot

A typical DSC plot is shown in Figure 7.33, in which we see a graph of heat flow plotted against temperature. Such a DSC plot is sometimes called a thermogram. In thermodynamic systems analysis, heat taken up by a system (gain) is considered positive, while heat given up (loss) is considered negative. Likewise with heat flow, in which heat flowing into a system is positive (endothermic), and heat flowing out is negative (exothermic). This same convention is used in thermal analysis and DSC peaks. In cases where different rules of convention are used, the terms "endothermic" or "exothermic" heat flow in the DSC plot must be specified.

The DSC plot shown in Figure 7.33 has a positive peak, meaning we are looking at an endothermic reaction. The figure shows how the quantity of heat delivered can be calculated by integration of heat flow over temperature within the peak (area under the peak), and how the onset temperature is determined by reading the temperature at which the peak begins to develop.

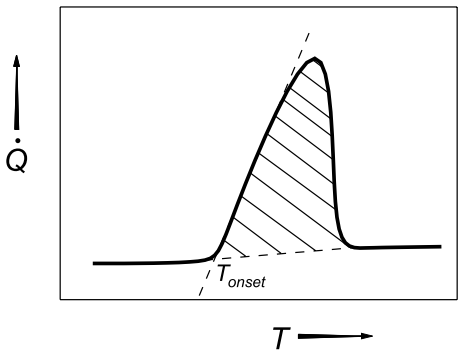

Figure 7.33. Simple endothermic DSC plot. Illustration of onset temperature and area of a DSC peak

To calculate the quantity of heat delivered, the incremental heat flow is expressed as:

$$\mathrm{d}q = c_p \cdot \mathrm{d}T \tag{7.134}$$

and

$$\Delta q = \int_T c_p \cdot \mathrm{d}T \tag{7.135}$$

With the heating rate β

$$\beta = \frac{\mathrm{d}T}{\mathrm{d}t} \tag{7.136}$$

we get:

$$\Delta q = \int_t c_p \cdot \beta \cdot \mathrm{d}t \tag{7.137}$$

When we use equation (7.9) then it is

$$\mathrm{d}h = \mathrm{d}q \tag{7.138}$$

and the integral provides:

$$\Delta h = \int_t c_p \cdot \beta \cdot \mathrm{d}t \tag{7.139}$$

where

c_p	specific heat capacity in $\mathrm{J \cdot kg^{-1} \cdot K^{-1}}$
q	specific heat in $\mathrm{J \cdot kg^{-1}}$
T	temperature in K
t	time in s
β	heating rate in $\mathrm{K^{-1} \cdot min^{-1}}$
h	specific enthalpy in $\mathrm{J \cdot kg^{-1}}$

During a DSC experiment, the temperature of the sample changes over time. From this profile, we can integrate the heat flow over time to obtain the enthalpy that is taken up or given up by the sample.

Process engineers often need to work with thermodynamic properties like heat and enthalpy on the basis of a unit mass of material (mass-specific quantities). These mass-specific quantities are designated by using lower case letters, such as q, c_p, h, instead of upper case letters Q, C_p, H normally used for the global (total) values. Table 7.21 presents a comparison of the total and mass-specific quantities for specific heat, heat, and enthalpy.

When enthalpy change is plotted over temperature for a given system, we obtain a graph similar to that shown in Figure 7.34, below.

Figure 7.34 shows an enthalpy–temperature diagram for ice cream mix, on which the enthalpy is plotted as a function of temperature. Enthalpy is decreasing with decreasing temperature, and we should want to know at what

Table 7.21. Calculation of enthalpy from a DSC peak. Comparison of total and mass-specific nomenclature

total	mass-specific
$C_p = \frac{\mathrm{d}Q}{\mathrm{d}T}$	$c_p = \frac{\mathrm{d}q}{\mathrm{d}T}$
$\mathrm{d}Q = C_p \cdot \mathrm{d}T$	$\mathrm{d}q = c_p \cdot \mathrm{d}T$
with $\beta = \frac{\mathrm{d}T}{\mathrm{d}t}$	
$\mathrm{d}Q = C_p \cdot \beta \cdot \mathrm{d}t$	$\mathrm{d}q = c_p \cdot \beta \cdot \mathrm{d}t$
$Q = \int C_p \cdot \beta \cdot \mathrm{d}t$	$q = \int c_p \cdot \beta \cdot dt$
When $V \cdot dp = 0$ the heat measured is identical to the change of enthalpy of the system	
$\mathrm{d}H = \mathrm{d}Q$	$\mathrm{d}h = \mathrm{d}q$
$\Delta H = \int \mathrm{d}Q$	$\Delta h = \int \mathrm{d}q$
$\Delta H = \int C_p \cdot \beta \cdot \mathrm{d}t$	$\Delta h = \int c_p \cdot \beta \cdot \mathrm{d}t$

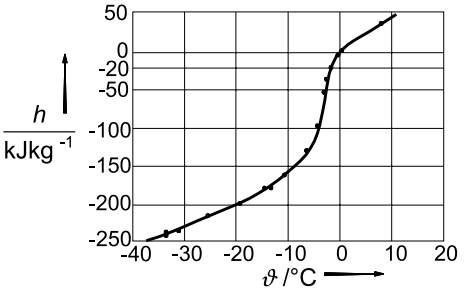

Figure 7.34. Enthalpy of ice cream mix [109]

temperature it will reach zero. We know it is not possible to measure enthalpy at zero absolute temperature. Therefore, it will be useful to designate a reference point where the enthalpy can be considered to be zero for subsequent calculations. For practical reasons, this reference point has been chosen to be at zero degrees on the centigrade temperature scale, $h(0\,^\circ\mathrm{C}) = 0$.

In working with thermodynamics and heat transfer calculations, process engineers need only deal with changes in enthalpy between different states of a system. Therefore, it is not important at what point the zero reference has been chosen. In the following example, we will perform a calculation that will help us recognize that it was not important where we had chosen the enthalpy to be zero.

Example 7.8. Chilling of ice cream mix
How much heat must be drawn out of 500 kg ice mix to chill it from $-5\,^\circ\mathrm{C}$ to $-20\,^\circ\mathrm{C}$?

From Figure 7.34 we read:

$$\Delta h = h_2 - h_1$$
$$\Delta h = h(-20^\circ\mathrm{C}) - h(-5^\circ\mathrm{C})$$
$$\Delta h = -200\,\mathrm{kJ}\cdot\mathrm{kg}^{-1} - \left(-100\,\mathrm{kJ}\cdot\mathrm{kg}^{-1}\right)$$
$$\Delta h = -100\,\mathrm{kJ}\cdot\mathrm{kg}^{-1}$$
$$\Delta H = \Delta h \cdot m$$
$$\Delta H = -100\,\mathrm{kJ}\cdot\mathrm{kg}^{-1}\cdot 500\,\mathrm{kg} = -50\,\mathrm{MJ}$$

So a heat of 50 MJ has to be drawn out of the material sample. The negative sign in the result indicates that this heat leaves the system, it is an exothermic process.

When we integrate completely under the peak in a thermogram like in Figure 7.33, we obtain the heat or enthalpy of the transition that occurred during the thermal analysis, such as the heat of vaporization or the heat of fusion. It is also possible to carry out the integration only part way through the peak, resulting in a partial integration. This partial integration can be quantified as a ratio of the partial integration over the whole integration, as illustrated in Figure 7.35. This ratio will have a value between zero and one. This quantity can be called the turnover of the peak α, and can also be plotted against temperature. This is known as a turnover plot, and is shown in Figure 7.36 for the case of ice cream.

Figure 7.36 gives turnover plots for three different ice cream mixes, with each mix containing different carbohydrate systems. When we look at the diagram at −5 °C, we see that recipe 1 has a 60% turnover at that temperature, while recipe 3 has only 20%, and recipe 2 is in between. Turnover plots can be constructed from any DSC peaks, as well as peaks from other types of analyses. Therefore, they can help us get information about many other types of reactions and transitions that can be studied with thermoanalysis.

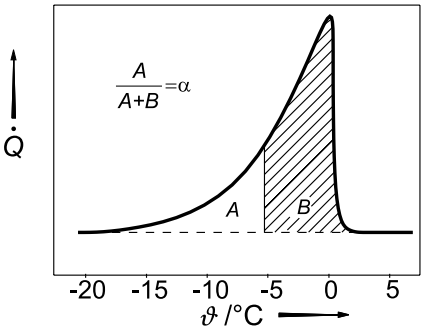

Figure 7.35. Partial integration of a DSC peak

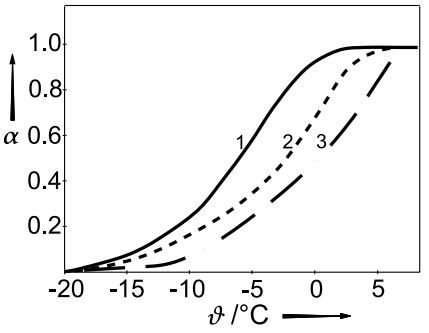

Figure 7.36. DSC turnover plots of the melting transition for different ice cream mix recipes

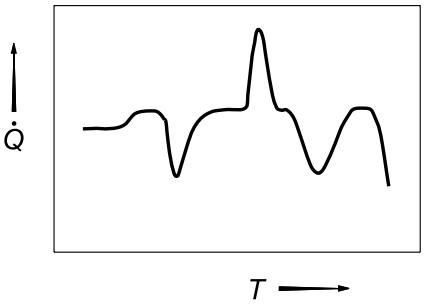

Figure 7.37. Schematic of hypothetical DSC signal options

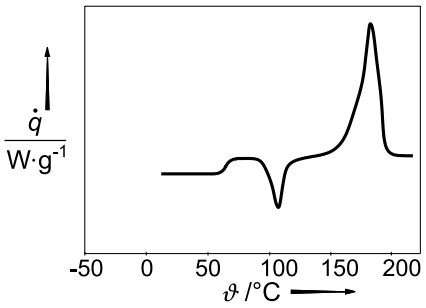

Figure 7.38. DSC plot (thermogram) of PET

Figure 7.37 shows some typical signals which may occur during a DSC run. Looking at the graph from left to right we see a step in the baseline which can indicate a glass transition followed by an exotherm peak which can be the signal of a recrystallization. The following endotherm peak might be due to a melting transition, vaporization, sublimation, or another type of transition.

At high temperatures, many materials will undergo some type of thermal degradation in the form of decomposition or oxidation. This will appear as a strong exothermal signal near the end of the DSC plot with very poor reproducibility. A good introduction to thermal analysis of foods can be found in reference [20].

Figure 7.38 is a DSC plot (thermogram) of a plastic film consisting of poly-ethylene-therephthalate (PET). It is an example of an amorphous plastic material out of which most soft drink bottles are made. In the DSC plot, we see a glass transition with a step in the base line at about 60 °C. Upon further heating, we see an exothermic peak just after 100 °C due to recrystallization of the polymer. Finally, we see an endothermic peak due to the melting of the crystalline structure at about 180 °C. Glass transition is a second order transition (see Section 7.3.1) and can be detected by shifting of the baseline in a thermogram. This is because, at the glass transition temperature, the heat capacity of the material changes dramatically. Glass transitions can occur only with solids that are not crystalline.

There are some applications in which food products are in the form of a solid glass state material. In these types of products, the moisture content has strong influence on the glass transition temperature. A good introduction into this field of phase diagrams and glassy states can be found in references [21,23].

Temperature Modulated DSC

Temperature modulated DSC (MDSC) is based upon the superposition of a periodic cycling temperature program onto a linear temperature–time program. Sometimes this technique is called alternating DSC (ADSC). In Figure 7.39 we show an example of a periodic modulated temperature–time profile superimposed upon a linear ramp temperature–time profile. If the periodic profile is a

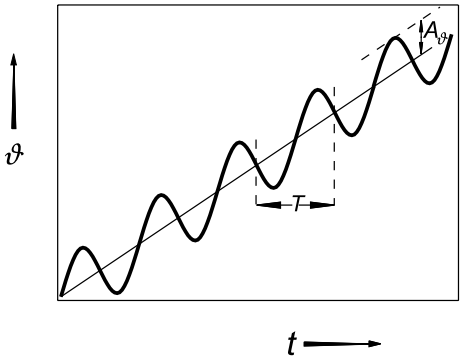

Figure 7.39. Temperature modulated heating rate

sinusoidal function, then we can express the temperature as a function of time as follows:

$$\vartheta = \vartheta_0 + \beta_0 \cdot t + A_\vartheta \cdot \sin(\omega \cdot t) \tag{7.140}$$

The period T of the modulation can be obtained from:

$$\omega = 2\pi \cdot f = \frac{2\pi}{T} \tag{7.141}$$

so

$$T = \frac{2\pi}{\omega} \tag{7.142}$$

The heating rate can be obtained as the derivative of the temperature

$$\beta = \frac{\mathrm{d}\vartheta}{\mathrm{d}t} \tag{7.143}$$

Then, we get:

$$\beta = \beta_0 + A_\vartheta \cdot \omega \cdot \cos(\omega \cdot t) \tag{7.144}$$

The product $A_\vartheta \cdot \omega$ we call the amplitude A_β of the heating rate. So:

$$\beta = \beta_0 + A_\beta \cdot \cos(\omega \cdot t) \tag{7.145}$$

β_0 is the underlying linear heating rate, whereas β is the actual (momentary) heating rate.

Here

ϑ	temperature in °C
ϑ_0	initial temperature in °C
t	time in s
β_0	underlying heating rate in $\mathrm{K \cdot s^{-1}}$
β	actual heating rate in $\mathrm{K \cdot s^{-1}}$
A_ϑ	amplitude of temperature in K
A_β	amplitude of heating rate in $\mathrm{K \cdot s^{-1}}$
ω_f	angular frequency in $\mathrm{s^{-1}}$

f frequency in s^{-1}
T period in s

When the heating rate is modulated, the resulting heat flow is modulated also. Because of

$$C_P = \frac{dQ}{d\vartheta} \tag{7.146}$$

the modulated heat flow is:

$$\dot{Q} = C_p \cdot \frac{d\vartheta}{dt} = C_p \cdot \beta \tag{7.147}$$

When we place a sample into a MDSC instrument and apply a sinusoidal temperature modulation, the system will respond with a sinusoidal modulated heat flow $\dot{Q}$. This heat flow is not proportional to the temperature, but to the first derivative of temperature with respect to time, which is the heating rate $\frac{d\vartheta}{dt} = \beta$. Therefore, heat flow $\dot{Q}$ and heating rate β are said to be "in phase" with each other, and there is zero phase shift between them, $\delta = 0^\circ$.

Zero phase shift represents a behavior in which a sample responds only on the basis of its heat capacity. When there are thermal transitions in the sample this is different from the behavior of a simple heat capacity because then heat can be "consumed" by the sample or dissipated. In such cases the response to temperature modulated analysis in a MDSC will show a phase shift greater than zero. So the value of the phase shift δ provides information about the extent to which a sample takes up heat in a reversing or in a nonreversing mode. Table 7.22 gives an overview of typical phase shifts.

Table 7.22. MDSC: Cases of phase shifts between heating rate and heat flow and reasons for them

phase shift angle δ	heating rate and heat flow are…	the heat flow results from …
$\delta = 0$	… in phase	a heat capacity only
$0^\circ < \delta < 90^\circ$	… shifted by δ	both parts
$\delta = 90^\circ$	… shifted by 90 °	a kinetic part only

When the response of a sample to MDSC differs from ideal heat capacity, it means some type of transition is occurring that requires heat in addition to the heat capacity part. We call this added heat flow for transitions the kinetic part. In general, we can say the modulated heat flow to a sample from MDSC is made up of a part due to the heat capacity of the sample as well as a kinetic part due to transitions.

Therefore, the response signal from a MDSC thermogram can be separated by Fourier analysis into two component heat flow signals. Conversely, when we add these two components with the phase shift δ, we can obtain the total measured signal.

In mathematics, we make use of complex numbers to represent these types of quantities. A complex number contains an imaginary part and a real part

(see Appendix 15.3). So, using complex numbers, we can express the heat flow mathematically as follows:

$$\dot{Q} = C_p \cdot \beta + f(\vartheta, t) \tag{7.148}$$

as a complex quantity:

$$\dot{Q} = \dot{Q}' + i \cdot \dot{Q}'' \tag{7.149}$$

where

$\dot{Q}$	complex heat flow in W
$\dot{Q}'$	real part of complex heat flow in W
$\dot{Q}''$	imaginary part of complex heat flow in W

Recall that we first worked with complex numbers in Chapter 4 on rheology. The real part of the number is the storage part, and the imaginary part is called the loss quantity. In the case of heat flow, the real part $\dot{Q}'$ is that part which can be taken up by the sample with its heat capacity, so the heat can be stored and subsequently released. We call this real part reversible heat flow. The imaginary part, on the other hand, is the heat flow for the kinetic effects that are consumed by the sample. This part is nonreversible, and is lost from the sample. Table 7.23 summarizes these definitions.

Table 7.23. Complex heat flow. Synonymous terms

$\dot{Q}$	$\dot{Q}'$	$\dot{Q}''$
complex quantity	real part	imaginary part
total heat flow	reversing heat flow	nonreversing heat flow
	part from heat capacity of the sample	part from kinetic effects in the sample
	in-phase part ($\delta = 0°$)	out-of-phase part ($\delta = 90°$)

We can now appreciate how MDSC experiments can allow us to distinguish between reversible and nonreversible heat flow. Figure 7.40 is a MDSC thermogram from a partly crystalline carbohydrate sample. We can see that the glass transition can be detected in the reversing signal. Whereas, the recrystallization reaction (exothermic peak), is detectable in the nonreversing signal. The melting signal seems to have both components (reversing and nonreversing). Note that this type of information cannot be derived from conventional DSC analysis.

In the same way, we can think of the heat capacity of a sample as being a complex quantity made up of a real part and an imaginary part. The terms used for this purpose are listed in Table 7.24.

$$C_p = \frac{\dot{Q}}{\beta} \tag{7.150}$$

$$C_p = C_p' + i \cdot C_p'' \tag{7.151}$$

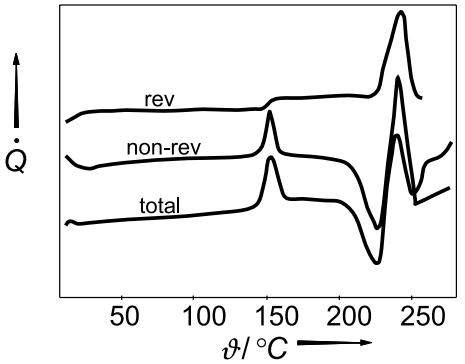

Figure 7.40. MDSC plot of a semicrystalline carbohydrate. The glass transition can be seen in the reversing signal (rev). The classic DSC signal (total) does not show the glass transition because it is hidden by another thermal event [24]

Table 7.24. Complex heat capacity terms

C_p	C_p'	C_p''
complex quantity	real part	imaginary part
	in-phase part ($\delta = 0°$)	out-of-phase part ($\delta = 90°$)

where

C_p complex heat capacity in $J \cdot K^{-1}$
C_p' real part of heat capacity in $J \cdot K^{-1}$
C_p'' imaginary part of heat capacity in $J \cdot K^{-1}$

With the phase shift δ known it is possible to calculate the parts of that complex heat capacity:

real part:

$$C_p' = |C_p| \cdot \cos \delta \tag{7.152}$$

imaginary part:

$$C_p'' = |C_p| \cdot \sin \delta \tag{7.153}$$

Experimental Conditions for MDSC Experiments

Recall that in carrying out a DSC experiment, only certain experimental conditions and parameters are subject to being controlled by the operator of the instrument. These include heating rates, oven atmospheres, types of pans used, sample size, etc. We also learned that very small sample sizes are always recommended for best results. However, the size of the sample must be sufficiently large so that the limited sensitivity of the instrument and of the sample weighing balance will not introduce any significant error.

When we advance to Modulated DSC (MDSC), we also introduce frequency and amplitude of the oscillations as additional control variables. If the frequency is set at zero, then we have no modulations at all, and the experiment reverts to a classic DSC analysis. If the frequency is set too high, the hardware system may be incapable of reversing the direction of heat flow at such a high

speed. Therefore, it is always necessary to perform a series of preliminary experiments for the purpose of determining the most appropriate frequencies and amplitudes to be used in order to meet the intended objectives of the MDSC analysis. For details refer to reference [25,61].

7.10 Applications

Temperature Sensing

remote temperature sensing in logistics of frozen goods	method L00.00-5 in [100]
liquid crystals as temperature probes for food between 30 °C and 115 °C	[24]
Wireless temperature sensing system for monitoring pig meat	[26]
freezing point temperature of milk as a measure of quality	[28] method L01.00-29 in [100] method 961.07 in [104]
temperature indicator for food and frozen food	[29–31]

Thermal Conductivity and Diffusivity

thermal diffusivity measurement using a simple one-dimensional FOURIER cylindrical solution	[33]
thermal diffusivity of amylose, amylopectin and starch: photoacoustic measurement	[34]
thermal diffusivity of foamed food gels	[35]
thermal diffusivity of granular food	[36]
thermal diffusivity measurement during high-pressure treatment	[37]
thermal diffusivity and conductivity of crystalline polymers	[38]
pet food: thermal diffusivity measurement	[39]
thermal conductivity of frozen dough	[40]
shrimp: thermal conductivity and heat capacity	[41]
ice cream: modeling of thermal properties	[32,42]
influence of moisture to heat conductivity of food	[43]

Thermal Analysis

meat: thermophysical properties by DSC	[44]
cheddar cheese: modeling thermal properties	[45]
meat and dough: prediction of thermal properties during freezing and thawing	[46]
frozen wheat dough: phase transitions by thermal analysis	[47]
glassy state and invertase stability in amorphous dried matrices of trehalose, maltodextrin	[48]
glass transition and enthalpy relaxation of amorphous lactose glass	[49]

anhydrous lactose: a study with DSC and TXRD	[50]
effect of phase transitions on release of *n*-propanol entrapped in carbohydrate glasses	[51]
water plastication effects in amorphous carbohydrates	[52]
chicken meat: desorption isotherms and glass transition temperature	[53]
strawberries: water sorption isotherms and glass transition	[54]
color of strawberries: effect by modification glass transition temperature	[71]
bacterial spores: glass formation and dormancy	[55]
texture testing instrumentation for glass transitions of food powders	[56]
DSC under pressure up to 200 MPa	[57]
Simultaneous DSC and DTG for determination of sorption isotherms and enthalpies	[58]
solid–solid transitions reactions: DSC and X-ray scattering	[59]
purity of solids: measurement by DSC	[60]
caffein adsoption process: investigation by TG	[61]
coffee roasting process: investigation by TG	[16,17]
dynamic thermal treatments in process engineering: kinetic parameter estimation and model development	[63,64]
frozen food: modeling heat and mass transfer	[72]
lactose, freeze dried: influence of salt on crystallization behavior	[74,75]

Standards

thermal analysis; differential thermal analysis	[65]
testing of plastics and elastomers by DSC	[66]
glass transition temperature of rubber by DSC	[67]
glass transition temperatures by DSC	[68]
glass transition temperatures by DMTA	[69]
enthalpies of fusion and crystallization of polymers by DSC	[70]

Literature

1. Ehrenfest P (1933) Phase changes classified according to singularities of the thermodynamic potential. Proc Acad Sci Amsterdam 36:153
2. Jankea W, Johnston DA, Kennac R (2006) Properties of higher-order phase transitions. Nuclear Physics B 736:319–328
3. Gutzow I, Petroff B (2004) The glass transition in terms of Landau's phenomenological approach. J of Non-Crystalline Solids 345–346:528–536
4. Rao MA, Rizvi SSH (1995) Engineering Properties of Foods. Marcel Dekker, New York
5. Sweat (1974) in: Jowitt R, Escher F, Kent M, McKenna B, Roques M (1987) Physical Properties of Food –2. Elsevier Applied Science, New York
6. Dickersen (1965) in: Jowitt R, Escher F, Kent M, McKenna B, Roques M (1987) Physical Properties of Food –2. Elsevier Applied Science, New York

7. Spiess WEL, Walz E, Nesvadba P, Morley M, van Haneghem IA, Salmon D (2001)Thermal conductivity of food materials at elevated temperatures. ECTP European Conference on Thermophysical Properties No15, Würzburg, Germany (05/09/1999) vol 33:631–723
8. Nesvadba P (1982) A new transient method for the measurement of temperature dependent thermal diffusivity. J Phys D: Appl Phys 15:725–738
9. Haycock GB, Schwartz GJ, Wisotsky DH (1978) Geometric method for measuring body surface area: A height–weight formula validated in infants, children and adults. J Pediatr 93:62–66
10. Atwater WO, Benedict FG (1902) An experimental inquiry regarding the nutritive value of alcohol. Government Printing Office, Washington DC
11. Atwater WO, Woods CD (1898) The chemical composition of American food materials. US Office of Experiment Stations, Experiment Stations Bulletin 28
12. DIN 51900 (2003) Testing of solid and liquid fuels – Determination of the gross calorific value by the bomb calorimeter and calculation of the net calorific value, in [110]
13. ASTM D6446-01(2006) Standard test method for estimation of net heat of combustion (specific energy) of aviation fuels. in [132]
14. Höhne G, Hemminger W, Flammersheim HJ (2003) Differential Scanning Calorimetry. Springer Heidelberg
15. Hemminger W, Cammenga HK (1989) Methoden der thermischen Analyse, Springer Verlag, Heidelberg
16. Fischer C, Cammenga HK, (2001) When are coffee beans just right? Development of physico-chemical properties during roasting. Proc IXX Int Conf on Coffee Science ASIC (Association Scientifique Internationale du Café) Trieste/Italia
17. Cammenga HK (2004) Thermochemistry of the roasting of coffee beans for optimal modelling, and conduct of coffee roasting. Proc XX Int Conf on Coffee Science ASIC (Association Scientifique Internationale du Café) Bangalore /India
18. Wiedemann HG (1970) in: Vacuum Microbalance Techniques. Vol. 7, 217–229 (C.H. Massen, H.J. van Beckum, eds.) Plenum Press, New York
19. Hemminger W, Höhne G (1984) Calorimetry – Fundamentals and Practise, Verlag Chemie, Weinheim
20. Harwalker VR, Ma CY (1990) Thermal Analysis of Foods. Elsevier Applied Science, New York
21. Slade L, Levine H (1995) Water and the glass transition – dependence of the glass transition on composition and chemical structure: special implications for flour functionality in cookie baking. J Food Engineering 24:431–509
22. Roos YH (1995) Phase transitions in foods. Academic Press, San Diego
23. Roos YH (1995) Characterization of food polymers using state diagrams. J Food Engineering 24:339–360
24. Figura LO (2003) Thermoanalytische Charakterisierung teilkristalliner Trehalose, in: Kunze, W(ed) Anwenderseminar Thermische Analyse in der pharmazeutischen Industrie und der Lebensmitteltechnologie, Würzburger Tage 2003, Reuters, Alzenau, p 125–137
25. Schick C, Merzlyakov M (2000) Optimization of experimental parameters in TMDSC: The influence of non-linear and non-stationary thermal response. J Therm Anal Calorimetry 61:649–657
26. Frisby J, Raftery D, Kerry JP, Diamond D (2005) Development of an autonomous, wireless pH and temperature sensing system for monitoring pig meat quality. Meat Science 70:329–336
27. Balasubramaniam VM, Sastry SK (1995) Use of liquid crystals as temperature sensors in food processing research. J Food Engineering 26:219–230

28. Ping Chen, Xiao Dong Chen, Free KW (1996) Measurement and data interpretation of the freezing point depression of milks. J Food Engineering 30:239–253
29. Aust P (1996) Frozen food temperature abuse indicator. Trends in Food Science and Technology 7:175
30. Fanni J, Ramet JP (1996) Time–temperature indicator. Trends in Food Science and Technology 7:67–68
31. Trintignac F (1997) Time–temperature monitor. Trends in Food Science and Technology 8:208
32. Tavman S, Tavman IH (1999) Measurement of thermal conductivity of dairy products. J Food Engineering 41:109–114
33. Baïri A, Laraqi N, García de María JM (2007) Determination of thermal diffusivity of foods using 1D Fourier cylindrical solution. J Food Engineering 78:669–675
34. Rodríguez P, de la Cruz GG (2003) Photoacoustic measurements of thermal diffusivity of amylose, amylopectin and starch. J Food Engineering 58:205–209
35. Takaharu Sakiyama, Masanori Akutsu, Osato Miyawaki, Toshimasa Yano (1999) Effective thermal diffusivity of food gels impregnated with air bubbles. J Food Engineering 39:323–328
36. Tavman S, Tavman IH, Evcin S (1997) Measurement of thermal diffusivity of granular food materials. Internl Comm Heat and Mass Transfer 24:945–953
37. Kubásek M, Houška M, Landfeld A, Strohalm J, Kamarád J, Žitný R (2006) Thermal diffusivity estimation of the olive oil during its high-pressure treatment J Food Engineering 74:2006
38. Choy CL, Ong EL, Chen FC (2003) Thermal diffusivity and conductivity of crystalline polymers. J Applied Polymer Science 26:2325–2335
39. Kee WL, Ma S, Wilson DI (2002) Thermal diffusivity measurements of petfood. Int J Food Properties 5:145
40. Kumcuoglu S, Tavman S, Tavman ICH, Nesvadba N (2007) Thermal conductivity measurements of a traditional fermented dough in the frozen state. J Food Engineering 78: 1079–1082
41. Karunakar B, Sushanta KM, Bandyopadhyay S (1998) Specific heat and thermal conductivity of shrimp meat. J Food Engineering 37:345–351
42. Cogné C, Andrieu J, Laurent P, Besson A, Nocquet J (2003) Experimental data and modelling of thermal properties of ice creams. J Food Engineering 58:331–341
43. Maroulis ZB, Saravacos GD, Krokida, MK, Panagiotou NM (2002) Thermal conductivity prediction for foodstuffs: effect of moisture content and temperature. Intern J Food Properties 5:23
44. Tocci AM, Mascheroni RH (1998) Characteristics of differential scanning calorimetry determination of thermophysical properties of meats. Lebensmittel-Wissenschaft-und-Technologie 31:418–426
45. Marschoun L, Muthukumarappan K, Gunasekaran S (2001) Thermal properties of cheddar cheese: experimental and modeling. Int J Food Properties 4:383
46. Lind I (1991) The measurement and prediction of thermal properties of food during freezing and thawing – a review with particular reference to meat and dough. J Food Engineering; 13: 285–319
47. Laaksonen TJ (2001) Effects of ingredients on phase and state transitions of frozen wheat doughs. Dissertation, University of Helsinki
48. Schebor C, del Pilar Buera M, Chirife J (1996) Glassy state in relation to the thermal inactivation of the enzyme invertase in amorphous dried matrices of trehalose, maltodextrin and pvp. J Food Engineering 30:269–282

49. Kamrul Haque, Kiyoshi Kawai, Toru Suzuki (2006) Glass transition and enthalpy relaxation of amorphous lactose glass. Carbohydrate Research 341:1884–1889
50. Figura LO, Epple W (1994) Anhydrous lactose: a study with DSC and TXRD. J Therm Anal 41:45–53
51. Levi G, Karel M (1995) The effect of phase transitions on release of n-propanol entrapped in carbohydrate glasses. J Food Engineering 24:1–13
52. Biliaderis CG, Lazaridou A, Mavropoulos A, Barbayiannis N (2002) Water plasticization effects on crystallization behavior of lactose in a co-lyophilized amorphous polysaccharide matrix and its relevance to the glass transition. International J Food Properties 5:463
53. Delgado AE, Sun DW (2002) Desorption isotherms and glass transition temperature for chicken meat. J of Food Engineering 55:1–8
54. Moraga G, Martínez-Navarrete N, Chiralt A (2004) Water sorption isotherms and glass transition in strawberries: influence of pre-treatment. J Food Engineering 62:315–321
55. Ablett S, Darke AH, Lillford PJ, Martin DR (1999) Glass formation and dormancy in bacterial spores. Int J Food Sci Tech 34:59–69
56. Boonyai P, Howes T, Bhandari B (2007) Instrumentation and testing of a thermal mechanical compression test for glass–rubber transition analysis of food powders. J Food Engineering 78:1333–1342
57. Masberg St (1999) Differentialkalorimetrie (DSC) und Differenzthermoanalyse (DTA) bei hohen Drücken. Dissertation, Universität Bochum, Germany
58. Ferrasse JH, Lecomte D (2004) Simultaneous heat-flow differential calorimetry and thermogravimetry for fast determination of sorption isotherms and heat of sorption in environmental or food engineering. Chem Eng Sci 59:1365–1376
59. Epple M (1992) Untersuchung von Festkörperreaktionen und fest-fest-Phasenumwandlungen mit zeit- und temperaturaufgelöster Röntgendiffraktometrie. Dissertation, Technische Universität Braunschweig, Germany
60. Sarge St (1988) Dynamische Kalorimetrie zur Bestimmung der Reinheit organischer und anorganischer Substanzen sowie der Energetik und Kinetik elementorganischer Umlagerungsreaktionen. Dissertation, Technische Universität Braunschweig, Germany
61. Gabel P (1988) Charakterisierung von Adsorbentien für einen Einsatz in der Kaffeeindustrie. Dissertation, Technische Universität Braunschweig, Germany
62. Figura LO (2004) Lebensmittelphysik. Springer Berlin
63. Welt BA, Teixeira, AA, Balaban MO, Smerage, GH, Sage DS (1997) Iterative method for kinetic parameter estimation from dynamic thermal treatments J Food Science 62:8
64. Teixeira AA, Balaban MO, Germer SPM, Sadahira MS, Teixeira-Neto RO, Vitali AA (1999) Heat transfer model performance in simulation of process deviations. J Food Science 64:488
65. DIN 51007 (1994) Thermal analysis; differential thermal analysis; principles, in [101
66. DIN 53765 (1994) Testing of plastics and elastomeres; thermal analysis; DSC-method, in [101]
67. BS ISO 22768 (2006) Determination of the glass transition temperature by differential scanning calorimetry (DSC), in [101]
68. E1356-03 Standard Test Method for Assignment of the glass transition temperatures by Differential Scanning Calorimetry, in [132]
69. E1640-04 Standard Test Method for Assignment of the glass transition temperature by Dynamic Mechanical Analysis, in [132]
70. D3418-03 Standard Test Method for Transition Temperatures and Enthalpies of Fusion and Crystallization of Polymers by Differential Scanning Calorimetry, in [132]

71. Torreggiani D, Forni E, Guercilena I, Maestrelli A, Bertolo, G, Archer P, Kennedy CJ, Bone S, Blond G, Contreras-Lopez E, Champion D (1999) Modification of glass transition temperature through carbohydrates additions: effect upon colour and anthocyanin pigment stability in frozen strawberry juices. Food Research International 32:441–446
72. Pham QT(2006) Modelling heat and mass transfer in frozen foods: a review. Intern J Refrigeration 29:876–888
73. Nesvadba P (1985) Measurements of total emissivity of chilled and frozen foods. High Temp. – High Press. 17:219–224
74. Elmonsef Omar AM, Roos,YH (2007) Glass transition and crystallization behavior of freeze-dried lactose–salt mixtures. LWT – Food Science and Technology 40:536–543
75. Elmonsef Omar AM, Roos YH (2007) Water sorption and time-dependent crystallization behavior of freeze-dried lactose–salt mixtures. LWT – Food Science and Technology 40:520–528

8 Electrical Properties

In this chapter we will study some of the electrical properties of foods, such as electrical conductivity, impedance and capacitance, along with the reasons we need to know these properties and their relationships, and why they are important in certain food process situations. In subsequent chapters, we will study magnetic properties (Chapter 9), and then electromagnetic properties (Chapter 10).

8.1 Conductivity

The property of electrical conductivity has to do with how easily an electric current can be transmitted through a material. Food materials that contain positively charged or negatively charged electrolytes, or charged molecules or macromolecules, are capable of transmitting an electric current. Positively charged ions are called cations, and negatively charged ions are called anions. In order to transmit electric current, it is necessary to have "carriers" for the charged ions present in the food material, and that these carriers are mobile. Some of the factors influencing the efficacy of these charged ion carriers in foods are listed in Table 8.1.

In general, we can say that if there are charged ions with mobile carriers present within a sample of food material, then if we apply a voltage potential across the food sample, an electric current will flow through the sample, as part of an electric circuit (Figure 8.1). The strength of this electric current will be governed by the electrical resistance R of the food sample. The electrical resistance impedes the flow of electric current through the sample. The reciprocal of resistance is conductance G. Therefore, the less resistance in an electric circuit, the more conductance it has. There exists a linear relationship between voltage, current and resistance within an electric circuit that is known as Ohm's law:

Table 8.1. Factors influencing the electrical conductivity of foods

influencing factor	e.g.
concentration of charge carriers	salinity, formulation
charge and number of charge carriers	single charged, or twice charged ions
mobility of charge carriers	aggregate state, molar mass, type of bonding

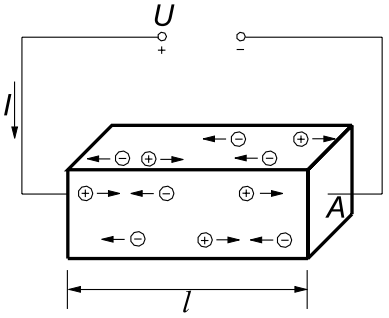

Figure 8.1. Food with electric current passing through (schematic)

$$I = \frac{1}{R} \cdot U \tag{8.1}$$

or

$$I = G \cdot U \tag{8.2}$$

where

U	electric voltage in V
I	electric current in A
R	electric resistance in Ω
G	electric conductance in S
A	area for current in m^2
l	length in m

In order to be independent of sample and circuit geometry in performing certain types of calculations, we need to introduce these properties as properties of the material (not the sample). Therefore, we must use the specific electric resistivity ρ and its reciprocal, the specific conductivity κ. The specific conductivity κ is dependent only on the composition of the material (phase of state, moisture content, chemical composition, etc.), and not on sample size or shape. It can be expressed as follows:

$$R = \rho \cdot \frac{l}{A} \tag{8.3}$$

or

$$\kappa = \frac{1}{\rho} \tag{8.4}$$

where

ρ	specific electric resistivity in $\Omega \cdot m$
κ	specific electric conductivity in $S \cdot m^{-1}$

Units for resistance and conductance:

$1\,V \cdot A^{-1} = 1\,\Omega$ (Ohm)
$1\,\Omega^{-1} = 1\,S$ (Siemens)

Examples of specific electrical resistivity for some food materials are given in Table 8.2.

Table 8.2. Specific electric resistivity of some food material (examples)

material	ϑ/°C	$\rho/\Omega \cdot \mathrm{m}$	from:
KCl solution 0.01 M	25	7.08	[106]
KCl solution 0.1 M	25	0.78	[106]
KCl solution 1 M	25	0.09	[106]
milk 1.5% fat	20	0.57	[1]
orange juice	20	0.44	[1]
apple juice	20	0.29	[1]
wheat beer	20	0.20	[1]
tap water	20	0.06	[1]
tomato juice	20	1.5	[1]
sauerkraut brine	20	2.1	[1]

In some cases, materials may possess an anisotropic structure. This means that the electrical properties of these materials will depend on direction or the orientation in space with which the sample material presents itself in the presence of an electric field (voltage potential).

8.1.1 Temperature Dependency of Electrical Conductivity

We learned earlier in Section 4.4 that the viscosity of many liquid foods is temperature dependent, and will usually decrease with increasing temperature. This decrease in viscosity will enhance the mobility of charged ion carriers, enabling them to move about more freely. In the case of weak electrolytes, we need to take into account the fact that the degree of disassociation will also increase with increased mobility under decreasing viscosity caused by increasing temperature. For many liquid foods, the temperature dependency of electrical conductivity can be approximated by the following linear function (see also Figure 8.2) [1]:

$$\kappa = \kappa_0 \, (1 + b_0 \cdot \Delta T) \tag{8.5}$$

where

κ	electric conductivity in $\mathrm{S} \cdot \mathrm{m}^{-1}$
κ_0	electric conductivity at a reference temperature in $\mathrm{S} \cdot \mathrm{m}^{-1}$
b_0	temperature coefficient in K^{-1}
ϑ_R	reference temperature in °C
ϑ	temperature in °C
	$\Delta T = \vartheta - \vartheta_R$

This linear relationship was first proposed by Reitler [1] for a number of different food materials. Some food liquids do not follow this linear relationship or the temperature range of linearity is limited. For example, if normal tap water is heated to about 100 °C, carbon dioxide is released from the water

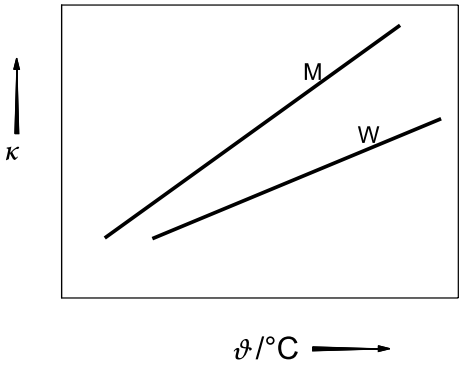

Figure 8.2. Milk (M) and wheat beer (W) have a nearly linear temperature dependency for electric conductivity [1].

and the water actually loses carbonate ions upon increasing temperature, and its electrical conductivity cannot follow this linear relationship. We will now move our focus away from food liquids, and discuss electrical properties of plant and animal materials.

8.1.2 Solid Foods of Plant Origin

Most fresh fruits and vegetables are high in water content, but normally have very poor electrical conductivity because much of the water is held immobile, trapped within the cells and the intercellular spaces within the tissue structure of these plant materials. However, whenever this cell structure is broken by such mechanisms as thermal heating, mechanical crushing, or enzymatic activity, the water containing charged ions is free to flow about serving as a mobile carrier for these charged ions, and the electrical conductivity can increase significantly. This is illustrated in Figure 8.3 for the case of banana puree compared with solid pieces of banana, as an example. Therefore, we can often expect electrical conductivity to increase in fruit and vegetable products during such processing operations as milling, squeezing, crushing, and mashing.

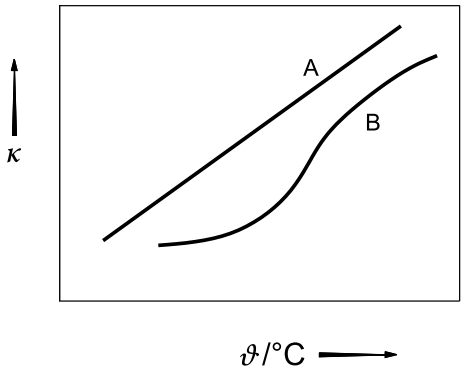

Figure 8.3. Temperature dependency of electric conductivity in banana (A, puree and B, pieces) [1]

8.1.3
Solid Foods of Animal Origin

In fresh meat, the same situation exists as in fresh fruits and vegetables. Although fresh meat is also high in water content (ca. 75% m/m), much of the water is held immobile, trapped within the cells and the intercellular spaces within the meat tissue, and cannot contribute any electrical conductivity. Once this cellular structure is broken down by such processing operations as cutting, grinding, and mincing, then the water containing charged ions is free to flow about serving as a mobile carrier for these charged ions, and the electrical conductivity can increase significantly. This breakdown cellular structure can also occur in nature. When an animal is in a post mortem state, microbial and enzyme activity (autolysis) will break down the cellular tissue structure causing increased electrical conductivity.

In the case of meat, the temperature coefficient in equation (8.5) for the temperature range (20–60 °C) is $b = 0.022\ \mathrm{K}^{-1}$ [1]. Above 60 °C, the linear relationship no longer seems to be valid, and collagen proteolysis has been proposed to be one of the reasons for that [109]. Meat muscle also shows an anisotropic electric conductivity. This should not be surprising when we take note that meat muscle tissue has a type of laminar structure, made up of layers all going in one direction. We are often taught to cut meat "across the grain" in order to have clean-cut slices. Otherwise, the meat will shear along the irregular tissue layers. This laminar structure will clearly cause conductive properties to depend upon direction relative to these tissue layers.

8.1.4
Electrolyte Solutions

The electrical conductivity of an electrolyte solution is often characterized by an equivalent conductivity, defined as the quotient of specific electrical conductivity over electrolyte concentration.

$$\Lambda = \frac{\kappa}{\nu \cdot c} \tag{8.6}$$

where

Λ	equivalent conductivity in $\mathrm{S} \cdot \mathrm{m}^2 \cdot \mathrm{mol}^{-1}$
κ	electric conductivity in $\mathrm{S} \cdot \mathrm{m}^{-1}$
c	electrolyte concentration in $\mathrm{mol} \cdot \mathrm{m}^{-3}$
ν	equivalent number of ions

The concept of equivalent conductivity arises from the study of physical chemistry. It provides a means by which we can compare electrolyte solutions containing the same concentration of charged ion carriers, although made of different substances, but can exhibit different equivalent electrical conductivity. For example, if we compare an aqueous solution of sodium chloride with one of acetic acid of equal concentration, they will have different equivalent

Table 8.3. Equivalent number of electrolytes for different systems, examples

electrolyte system	$(z \cdot n)_{cation}$	$= (z \cdot n)_{anion}$	$= \nu$
$Al_2(SO_4)_3 \rightarrow 2\ Al^{3+} + 3\ SO_4^{2-}$	$2 \cdot 3$	$3 \cdot 2$	$= 6$
$H_3PO_4 \rightarrow 3H^+ + PO_4^{3-}$	$3 \cdot 1$	$1 \cdot 3$	$= 3$
$NaCl \rightarrow Na^+ + Cl^-$	$1 \cdot 1$	$1 \cdot 1$	$= 1$
$CaCl_2 \rightarrow Ca^{2+} + 2\ Cl^-$	$1 \cdot 2$	$2 \cdot 1$	$= 2$

electrical conductivity. This means that there must be a difference in the degree of mobility or dissociation of the ions in the two electrolyte solutions.

Referring back to the definition of equivalent electrical conductivity in equation (8.6), the equivalent number of ions ν is the product of the stoichiometric factor z of either a cation or anion of a dissociating electrolyte and its charge number n. Some examples are given in Table 8.3.

If we dissolve 1 mol $Al_2(SO_4)_3$ in a liter of water, we have six times the number of charge carriers as with 1 mol of NaCl. So, in terms of electrical conductivity, we can say a 1 M $Al_2(SO_4)_3$ solution is equivalent to a 6 M NaCl solution.

With increasing electrolyte concentration, the degree of dissociation of electrolytes decreases, as illustrated in Figure 8.4. For strong electrolytes, KOHLRAUSCH found that there is a linear relationship between equivalent electrical conductivity and the square root of the concentration. This is called KOHLRAUSCH's square root law:

$$\Lambda = \Lambda_0 - a\sqrt{c} \tag{8.7}$$

where

Λ	equivalent conductivity in $S \cdot m^2 \cdot mol^{-1}$
Λ_0	equivalent conductivity at $c \rightarrow 0$ in $S \cdot m^2 \cdot mol^{-1}$
c	concentration
a	constant

Figure 8.4 shows that the concentration dependency of equivalent electrical conductivity for strong electrolytes, like sodium chloride, will give a straight line (linear relationship) on a graph of equivalent conductivity versus square

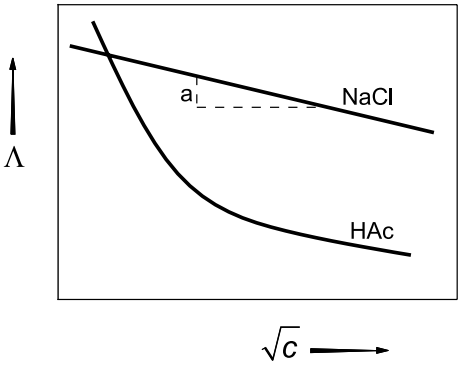

Figure 8.4. Concentration dependency of equivalent conductivity. Strong electrolyte (upper curve, NaCl) and weak electrolyte (lower curve, acetic acid)

Table 8.4. Values of equivalent conductivity for some ions [2]

ion	λ_0/S · cm^2 · mol^{-1}	
	temperature	
	25 °C	18 °C
H^+	349.6	315.0
Na^+	50.1	43.5
NH_4^+	73.5	64.0
$\frac{1}{2}\,Mg^{2+}$	50.3	45.0
$\frac{1}{2}\,Ca^{2+}$	59.0	56.0
OH^-	199.1	174.0
Cl^-	76.4	65.5
NO_3^-	71.5	61.7
CH_3COO^-	40.9	34.5
CO_3^{2-}	138.6	121.0

root of concentration, and thus they follow KOHLRAUSCH's square root law. However, weak electrolytes, such as acetic acid, do not give a straight line on this type of graph, and they do not follow KOHLRAUSCH's square root law.

The extrapolation of the straight line curve to $c = 0$ will intercept the vertical axis at a value of equivalent electrical conductivity designated Λ_0. This is the equivalent conductivity of an electrolyte at an extreme dilution, in which the concentration approaches zero where intermolecular interactions disappear. Values for Λ_0 can be taken from tables that allow estimation of the equivalent conductivity for mixtures of electrolyte solutions:

$$\Lambda_0 = \sum_i \lambda_{0,i}\,(\text{anions}) + \sum_j \lambda_{0,j}\,(\text{cations}) \tag{8.8}$$

where

Λ_0 equivalent conductivity of electrolyte in S · m^2 · mol^{-1}

λ_0 equivalent conductivity of ion S · m^2 · mol^{-1}

Whenever we take values of λ_0 from tables, we have to be careful to avoid confusion. For example, the equivalent conductivity of the calcium ion can be given as $\lambda_0 = (\frac{1}{2}\,Ca^{2+}) = 59$ S · cm^2 · mol^{-1}, or $\lambda_0(Ca^{2+}) = 118$ S · cm^2 · mol^{-1}. In the first case the value is for a hypothetical half of a calcium ion ($\frac{1}{2}\,Ca^{2+}$ion), and is for use in the following equation:

$$\lambda_0 = \left(\frac{1}{n}\cdot\lambda_0\right)_{\text{cation}} + \left(\frac{1}{n}\cdot\lambda_0\right)_{\text{anion}} \tag{8.9}$$

Example 8.1. Electric conductivity of an aqueous solution of $CaCl_2$, 0.5% (m/m)
Because of the dissociation $CaCl_2 \rightarrow Ca^{2+} + 2\,Cl^-$, the equivalent number is $\nu = 2$.

With the molar mass $M(CaCl_2) = 111\,g \cdot mol^{-1}$, we get a concentration of:

$$c = \frac{5\,g}{1000\,g} \approx \frac{5\,g}{1\,l} = \frac{5\,g}{\frac{111\,g \cdot mol^{-1}}{1\,l}} = 0.045\,mol \cdot l^{-1} = 4.5 \cdot 10^{-5}\,mol \cdot cm^{-3}$$

So, the equivalent conductivity of 25 °C is:

$$\Lambda_0 = \lambda_{0,Ca} + \lambda_{0,Cl}$$
$$\Lambda_0 = 59.0\,S \cdot cm^2 \cdot mol^{-1} + 76.4\,S \cdot cm^2 \cdot mol^{-1} = 135.4\,S \cdot cm^2 \cdot mol^{-1}$$

With use of equations (8.6) and without use of KOHLRAUSCH's square root law, we get

$$\kappa = \Lambda_0 \cdot c \cdot \nu = 135.4\,S \cdot cm^2 \cdot mol^{-1} \cdot 4.5 \cdot 10^{-5}\,mol \cdot cm^{-3} \cdot 2 = 1.2\,S \cdot m^{-1}$$

Example 8.2. Find the electric conductivity of an aqueous solution (25 °C) consisting of 0.3% (m/m) $CaCl_2$ and 0.1% (m/m) NaCl.

We have:

$$\nu\,(CaCl_2) = 2$$
$$M\,(CaCl_2) = 111\,g \cdot mol^{-1}$$
$$\nu\,(NaCl) = 1$$
$$M\,(NaCl) = 58.4\,g \cdot mol^{-1}$$

The concentration can be calculated as:

$$c\,(CaCl_2) = \frac{3\,g}{1000\,g} \approx \frac{3\,g}{1\,l} = \frac{3\,g}{\frac{111\,g \cdot mol^{-1}}{1\,l}} = 0.027\frac{mol}{l} = 2.7 \cdot 10^{-5}\,\frac{mol}{cm^3}$$

$$c\,(NaCl) = \frac{1\,g}{1000\,g} \approx \frac{1\,g}{1\,l} = \frac{1\,g}{\frac{58.4\,g \cdot mol^{-1}}{1\,l}} = 0.017\frac{mol}{l} = 1.7 \cdot 10^{-5}\,\frac{mol}{cm^3}$$

So, the equivalent conductivities are:

$$\Lambda_0(NaCl) = \lambda_{Na^+} + \lambda_{Cl^-} = (50.1 + 76.4)\,S \cdot cm^2 \cdot mol^{-1} = 126.5\,S \cdot cm^2 \cdot mol^{-1}$$
$$\Lambda_0(CaCl_2) = \lambda_{Ca^{2+}} + \lambda_{Cl^-} = (59.0 + 76.4)\,S \cdot cm^2 \cdot mol^{-1} = 135.4\,S \cdot cm^2 \cdot mol^{-1}$$

Now, we use KOHLRAUSCH's square root law: $\Lambda = \Lambda_0 - a\sqrt{c}$:

With: $a(NaCl) \approx a(CaCl_2) = 80\,S \cdot cm^2 \cdot mol^{\frac{1}{2}} \cdot l^{-\frac{1}{2}}$

We get:

$$\Lambda(NaCl) = \left(126.5 - 80 \cdot \sqrt{0.017}\right)\,S \cdot cm^2 \cdot mol^{-1} = 116.1\,S \cdot cm^2 \cdot mol^{-1}$$
$$\Lambda(CaCl_2) = \left(135.4 - 80 \cdot \sqrt{0.027}\right)\,S \cdot cm^2 \cdot mol^{-1} = 122.3\,S \cdot cm^2 \cdot mol^{-1}$$

At last, we calculate the specific electric conductivity by use of equation (8.6):

$$\kappa = \Lambda \cdot \nu \cdot c = (\Lambda \cdot \nu \cdot c)_{\mathrm{NaCl}} + (\Lambda \cdot \nu \cdot c)_{\mathrm{CaCl_2}}$$
$$= (116.1 \cdot 1 \cdot 1.7 \cdot 10^{-5} + 122.3 \cdot 2 \cdot 2.7 \cdot 10^{-5})\,\mathrm{S \cdot cm^{-1}}$$
$$\kappa = 858\,\mathrm{mS \cdot m^{-1}}$$

To get a rough estimation, we could leave out KOHLRAUSCH's law by assuming: $a = 0$ (i.e. $\Lambda = \Lambda_0$). Then, we get: $\kappa = 946\ \mathrm{mS \cdot m^{-1}}$, producing an error of approximately 10%.

Frequency Dependency

Dissociated ions moving freely about in an aqueous electrolyte solution are always surrounded by other ions nearby of opposite charge. Consider a solution of potassium chloride (KCl). Positively charged potassium ions (K^+) will be surrounded by negatively charged chloride ions (Cl^-). When placed within an electric field, the positively charged potassium ion will experience force acting upon it in an opposite direction to the force acting upon all the negatively charged chloride ions surrounding it.

In the absence of an electric field, each positively charged ion together with its surrounding negatively charged ions forms a sphere-like grouping within the electrolyte solution. When placed within an electric field, the positively charged ions are pulled in one direction, and the negatively charged ions are pulled in the opposite direction. This causes a deformation in the shape of the initial spherical grouping. This phenomena was demonstrated by DEBYE–HÜCKEL–ONSAGER, and illustrated in Figure 8.5. The deformation causes a drag force on the central ion. This drag force effect is called the catophoretic effect [2].

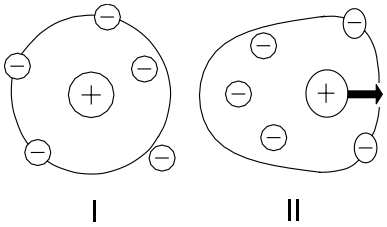

Figure 8.5. Catophoretic effect: I initial state, II response to electric field

In addition to the ions, themselves, within an ion grouping, each grouping also has a surrounding cloud of solvent molecules (mostly water), as illustrated in Figure 8.6. When an ion now starts to travel in response to forces established by an electric field, this cloud consisting of solvent molecules causes an additional drag force. This is called the electrophoretic effect. This effect is used in molecular analysis with laboratory procedures called electrophoresis: Molecules with different drag forces due to the electrophoretic effect can be separated by their different travelling velocities in an electric field. A common application is the investigation of proteins with different sizes, different side groups or different stearic states. To enhance the effect of different electrophoretic mobility, the molecules of interest are brought into a gel, which then

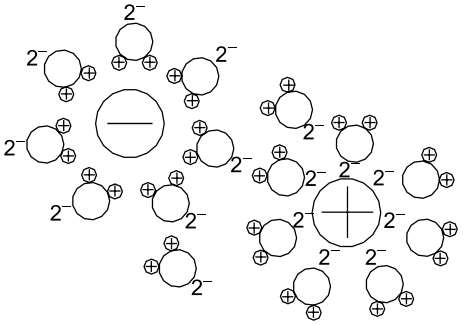

Figure 8.6. Ions with surrounding water molecules – hydrated ions

is exposed then to an electric field (gel electrophoresis). If an electrophoretic analysis is sensitive to molecular size only, we have to make the analysis "blind" to the fact that molecules carry an electric charge and are charged differently. This can be done by adding an ionic surfactant. Often, sodium dodecyl sulphate (SDS) is used for this purpose. It links itself to the charged sites, and thus compensates for ionic effects. When SDS is used on polyacrylamide gel, this technique is called SDS PAGE (SDS polyacrylamide gel electrophoresis).

When we consider the conductivity of an electrolyte solution that is placed within an oscillating electric field, in which the applied voltage is reversing periodically (not static), we observe that the deformation of the initial spherical ion grouping changes in a periodic reversal with the frequency of the outer field electric. When this is happening, the drag forces decrease with increasing frequency and the electric conductivity of a solution seems to increase. This is called the Debye–Falkenhagen effect.

Temperature Dependency of Equivalent Conductivity

Both the electrophoretic and the catophoretic effects depend on the viscosity of the electrolyte solution. We learned earlier that the viscosity of many liquid foods is temperature dependent (see Section 4.4), and will usually decrease with increasing temperature. This decrease in viscosity will lower drag forces, and thus decrease both effects with increasing temperature. Therefore, the equivalent conductivity of an aqueous electrolyte solution will increase with increasing temperature, just as in the case with electrical conductivity. In order to describe this behavior, we need to introduce a temperature coefficient for the equivalent conductivity:

$$k = \frac{1}{\Lambda} \cdot \frac{\mathrm{d}\Lambda}{\mathrm{d}T} \tag{8.10}$$

where

k	temperature coefficient in K^{-1}
Λ	equivalent conductivity in $\mathrm{S} \cdot \mathrm{m}^2 \cdot \mathrm{mol}^{-1}$
T	Temperature in K

Some values of k for different substances are listed in Table 8.5.

Table 8.5. Examples of temperature coefficients for equivalent electric conductivity at room temperature [2]

	k/K^{-1}
strong acids	0.016
strong bases (chemical base)	0.019
salts	0.022
water	0.058

Example 8.3. Change in conductivity of water on raising the temperature from 20 °C to 21 °C

$$\frac{\Delta\Lambda}{\Lambda} = k \cdot \Delta T$$

$$\frac{\Delta\Lambda}{\Lambda} = 0.058\,\mathrm{K}^{-1} \cdot 1\,\mathrm{K} = 0.058 = 5.8\%$$

This example illustrates the significant effect that temperature has on the equivalent electrical conductivity. Therefore, it is imperative that laboratory measurements of electrical conductivity be carried out under conditions of precise temperature control, with the controlled temperature clearly and prominently recorded and reported with the results of the measurement. Measurements made without control or reporting of the temperature are of little value.

8.2 Measurement of Electrical Conductivity

The measurement of electrical conductivity in a liquid solution is normally carried out by immersion of a measuring cell into the solution. The measuring cell consists, in principle, of two electrodes, fabricated in the shape of plates or cylinders. It is also very useful to have a temperature probe in the cell near the electrodes in order to have precise measurement and recording of the temperature during the measurement, as discussed earlier.

The measuring cell is designed in such a way that what is measured is the electrical resistance R, or its reciprocal, the electrical conductance G, of the liquid existing between the two electrodes. Then, from equations (8.3) and (8.4), and having the cell constant b, we have:

$$\kappa = \frac{1}{\rho} = \frac{1}{R} \cdot \frac{A}{l} \tag{8.11}$$

with:

$$b = \frac{l}{A} \tag{8.12}$$

$$\kappa = \frac{1}{R} \cdot \frac{1}{b} \tag{8.13}$$

In order to determine the value for the cell constant b, a calibration has to be performed by conducting experiments with different standard solutions having known, but different, electrical conductivity.

The cell constant is taken from the slope of the $\kappa - R$ plot. Standard materials often used are KCl solutions (see Table 8.6). Hand held instruments often are used with a fast one-point calibration.

Table 8.6. Values of specific conductivity of aqueous solutions of KCl

	$\kappa/\mathrm{S \cdot m^{-1}}$		
$c/\mathrm{mol \cdot dm^{-3}}$	18 °C	20 °C	25 °C
0.1	1.119	1.167	1.288
0.01	0.1225	0.1278	0.1413

As mentioned previously, during all these measurements, temperature must be precisely measured, controlled, recorded and reported. Most laboratory commercial instruments for measurement of electrical conductivity are equipped with a means for automatically adjusting or correcting for different temperature as a normal part of the instrument hardware. An example of this is the internal use of the temperature coefficient in equation (8.10). The capability for such automatic correction for temperature is a very useful feature. For example, a measurement of electrical conductivity taken at a temperature of 21 °C can be corrected to report what the conductivity would be at 25 °C. Of course, in order to do this, the instrument must be programmed with the correct value of temperature coefficient to use. Most instruments allow the operator to enter this value as an input for operation of the instrument. For most dissolved salt solutions, a temperature coefficient of $k = 0.022\ \mathrm{K^{-1}}$ is used (see Table 8.5).

In order to minimize the undesirable interference caused by the catophoretic and electrophoretic effects that develop in a static electric field, conductivity measurements are usually carried out in the presence of a dynamic oscillating field, in which the voltage potential reverses periodically at a regular frequency. This also helps to prolong the lifetime of the electrodes. The frequencies normally used for this purpose are in the range 1–500 kHz. The response in an electric circuit to such periodic reversal in voltage is an alternating current that changes direction periodically in response to the voltage. Likewise, the ions in an electrolyte solution will attempt to move in such an oscillating way. The resistance to this type of oscillating movement in the presence of a periodic alternating electric field is called impedance Z (see also Appendix 15.3 on complex numbers).

$$Z = \sqrt{X_R^2 + X_I^2 + X_C^2} \tag{8.14}$$

with

$$X_R = R \tag{8.15}$$

$$X_I = 2\pi \cdot f \cdot I \tag{8.16}$$

$$X_C = \frac{1}{2\pi \cdot f \cdot C} \tag{8.17}$$

where

Z	electric impedance in Ω
X_R	resistor's impedance in Ω
X_I	inductor's impedance in Ω
X_C	capacitor's impedance in Ω
f	frequency in Hz
C	capacitance in F
I	inductance in H

As can be seen from equation (8.14) for small inductor's impedance and small capacitor's impedance, the electric impedance of the measuring cell is about the same as the resistor's impedance of the cell (this is what we know as Ohmic resistance). Because there is little inductance in a measuring cell, the inductor impedance is naturally very low. However, capacitor impedance is deliberately minimized by design of the measuring cell to have maximum capacitance. This is done by first designing the electrode plates to have large exposed surface area in contact with the solution, and then electroplating the electrodes with a coating of platinum. This electroplated platinum coating appears as a thin black film on the electrodes, which is very delicate and not very stable. In order to have greater durability and robustness, electrodes need to be fabricated from noncoated platinum which limits the degree of capacitance.

The classic design of most conductivity measuring cells consists of flat plate platinum electrodes in a glass body. Alternative designs are available in which the electrodes are encased in plastic bodies instead of glass, or cylindrical electrodes are used rather than flat plate electrodes. More robust types make use of inductive cells based on Hall's effect, instead of flat plate electrodes. Results from measurement of electrical conductivity κ with such cells for various liquids are given in Table 8.7.

Table 8.7. Values of electric conductivities

	κ range
pure water	0.1 μS · cm^{-1}
demineralized water	0.1–10 μS · cm^{-1}
tap water (drinking water)	100–1000 μS · cm^{-1}
waste water	1–10 mS · cm^{-1}
sea water	1–100 mS · cm^{-1}
aqueous salt solutions	10–500 mS · cm^{-1}
concentrated acids and bases	100–1000 mS · cm^{-1}

An application for the measurement of electrical conductivity in foods is in the analytical laboratory testing of fats and oils for their stability against oxidation (oxidative rancidity). This is known as the oil stability index (OSI), and is used in food quality testing laboratories. In performing these analyses, the fat or oil samples are deliberately caused to oxidize. The time required to carry out these analyses is reduced by heating the samples to temperatures in the range (100–130 °C) in order to accelerate the rate of oxidation.

The test is carried out by contacting the hot oil with the oxygen present in air bubbles passing through the hot oil sample. If oxidation reactions take place, the products of these reactions will be adsorbed by the air bubbles, and carried out of the sample to be collected within the head space air for analysis. Products of the oxidation reaction are typically short-chain fatty acids, which can readily dissolve in water. The air bubbles carrying these fatty acids are contacted with rinse water producing an aqueous solution of fatty acids with electrical conductivity proportional to fatty acid concentration. It is only necessary to measure electrical conductivity of the rinse water solution over time to determine stability of the original oil sample to oxidation.

The presence of fatty acids in the aqueous solution causes an immediate increase in electrical conductivity to a significant level. The time required for the electrical conductivity to reach some designated level is a reflection of how stable (or unstable) the sample was to oxidation. This time value is reported as the oil stability index (OSI). Results from OSI analyses are frequently relied upon to confirm the efficacy of antioxidants added to an ingredient formulation, or a new oxygen barrier packaging film, etc. [3,4].

8.3 Capacitance and Inductance

In addition to electrical resistance and impedance, electrical capacitance and inductance are also important electrical properties of foods. The electrical capacity (capacitance) of a material is governed by its permittivity, which is a consequence of its electric polarization.

These quantities can play an important role in process engineering (e.g. microwave heating or inductive heating), or on-line sensing for quality control of materials and processes (see Chapter 14). On-line sensing can be based on monitoring the electrical capacitance of a material. For example, the electrical capacitance of humid air is a function of its moisture content. So, by measuring the capacitance we have a signal which is related to the humidity of an atmosphere. Another example is to monitor the capacitance of a device which is partly filled with a liquid. Then the measured capacitance becomes an indicator for the filling height.

Example 8.4. Metering filling height using electrical capacity
The capacitance of a simple plate capacitor like that shown in Figure 8.7 is:

$$C = \varepsilon \cdot \varepsilon_0 \cdot \frac{a^2}{d} \tag{8.18}$$

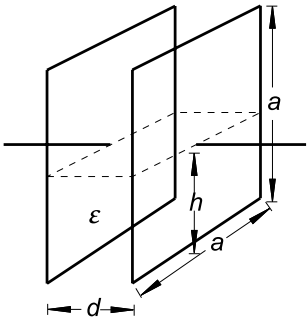

Figure 8.7. Partly filled plate capacitor

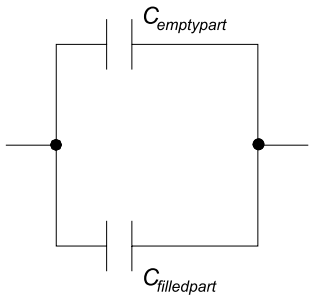

Figure 8.8. Two capacitors in parallel

where

C	capacitance in F
ε	permittivity
ε_0	electric field constant in $\mathrm{C} \cdot \mathrm{V}^{-1} \cdot \mathrm{m}^{-1}$
a	length of plate in m
h	filling height in m
d	distance between plates in m
χ	electric susceptibility

When the plate capacitor is partly filled with a material, we can treat the device like two smaller capacitors – one empty and one completely filled (Figure 8.8).

The total capacity is calculated by

$$C_{total} = C_{filled\ part} + C_{empty\ part} \tag{8.19}$$

with ε_V as permittivity of the filling material

$$C_{filled\ part} = \varepsilon_V \cdot \varepsilon_0 \cdot \frac{a \cdot h}{d} \tag{8.20}$$

$$C_{empty\ part} = \varepsilon_{empty} \cdot \varepsilon_0 \cdot \frac{(a-h) \cdot a}{d} \tag{8.21}$$

So with $\varepsilon_{empty} = \varepsilon_{air} \approx 1$

$$C_{total} = \frac{\varepsilon_0 \cdot a}{d} \cdot (\varepsilon_V \cdot h + (a-h)) \tag{8.22}$$

i.e.

$$C_{total} = \frac{\varepsilon_0 \cdot a}{d} \cdot (h \cdot (\varepsilon_V - 1) + a) \tag{8.23}$$

or

$$C_{total} = \frac{\varepsilon_0 \cdot a}{d} \cdot (a + h \cdot \chi) \tag{8.24}$$

$$C_{total} = C_{empty} + \frac{\varepsilon_0 \cdot a \cdot \chi}{d} \cdot h \tag{8.25}$$

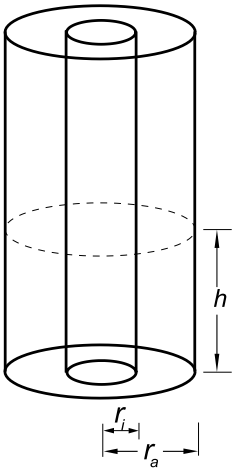

Figure 8.9. Partly filled cylindrical capacitor

The last equation shows that the capacitance is a linear function of the filling height h. So, we have a filling height monitor. When a cylindrical capacitor like the one shown in Figure 8.9 is used, we have:

$$C = \frac{2\pi \cdot \varepsilon_0 \cdot \varepsilon \cdot l}{\ln \frac{r_a}{r_i}} \tag{8.26}$$

The total capacitance is again:

$$C_{total} = C_{filled\ part} + C_{empty\ part} \tag{8.27}$$

with

$$C_{filled\ part} = \frac{2\pi \cdot \varepsilon_0}{\ln \frac{r_a}{r_i}} \varepsilon \cdot h \tag{8.28}$$

$$C_{empty\ part} = \frac{2\pi \cdot \varepsilon_0}{\ln \frac{r_a}{r_i}} (l - h) \tag{8.29}$$

i.e.

$$C_{total} = \frac{2\pi \cdot \varepsilon_0}{\ln \frac{r_a}{r_i}} \varepsilon \cdot h + \frac{2\pi \cdot \varepsilon_0}{\ln \frac{r_a}{r_i}} (l - h) \tag{8.30}$$

$$C_{total} = \frac{2\pi \cdot \varepsilon_0}{\ln \frac{r_a}{r_i}} \cdot (\varepsilon \cdot h + (l - h)) \tag{8.31}$$

$$C_{total} = \frac{2\pi \cdot \varepsilon_0}{\ln \frac{r_a}{r_i}} \cdot (h(\varepsilon - 1) + l) = \frac{2\pi \cdot \varepsilon_0}{\ln \frac{r_a}{r_i}} \cdot (h \cdot \chi + l) \tag{8.32}$$

$$C_{total} = \frac{2\pi \cdot \varepsilon_0 \cdot l}{\ln \frac{r_a}{r_i}} + \frac{2\pi \cdot \varepsilon_0 \cdot \chi}{\ln \frac{r_a}{r_i}} \cdot h \tag{8.33}$$

$$C_{total} = C_{empty} + \frac{2\pi \cdot \varepsilon_0 \cdot \chi}{\ln \frac{r_a}{r_i}} \cdot h \tag{8.34}$$

Again, the total capacitance is a linear function of the filling height.

8.4 Applications

Recall that the measurement of electrical properties of food can be used to get information about food composition and quality. In addition there are some food processes which are based on electrical effects. An electric current which flows through a food material will cause a temperature rise in the material. The temperature rise is due to energy dissipation by the electric resistance of the food. So knowledge of the design of the electric conductivity or resistivity is essential for his type of heating operation, which is called Ohmic heating. Ohmic heating has several advantages. For example, there is no need for double walled heated vessels and no fouling on heated surfaces. Because the heat is produced inside the food, convective heat transfer is not the most important or the single heat transport mechanism. On the other hand high voltage electric pulses can damage cells and cause higher permeability of cell walls. In cases where cells of agricultural products have to be extracted, e.g. in making fruit juices or extracting sugar from beets this electric pulse treatment can increase the extraction efficacy. Electric pulse treatment sometimes is abbreviated PEF (pulsed electric fields) or HELP treatment (high electric field pulses). Some references for these physical proccesses are given here:

Ohmic heating of foods – influence of electric conductivity	[5,6]
Ohmic heating of solid liquid food mixtures	[7]
effect of ohmic heating on cell membranes	[8]
starch gelatinization by Ohmic heating	[9]
strawberry products: ohmic heating effects	[10]
simulation and MRI mapping of ohmic heating in solid liquid food mixtures	[11]
pulsed electric field treatment: comparative evaluation of membrane permeabilization by freezing and by electric treatment	[12]
pulsed electric field treatment: effect of temperature	[13]
pulsed electric field treatment: inactivation of *E. coli* and *L. innocua*	[14]
pulsed electric field treatment: impact of air bubbles	[15]
fish quality measurement using electrical properties	[16,17]
apple juice: detection of yeasts by conductivity measurement	[18]
microbial growth: monitoring using capacitance measurements	[19]

microbial growth: monitoring using impedance measurement	[20]
salmonella growth: monitoring using impedance measurement	[21]
fat: oxidation stability estimation by monitoring the electrical conductivity of a stripping solution (washing column)	[3]
electrostatic atomization of emulsions: impact of electric conductivity	[22]
grain: moisture estimation by electrical conductivity measurement	[110]
honey: moisture estimation by electrical conductivity measurement	method L40.00-5 in [100]
milk: modeling electrical conductivity	[23]
orange juice–milk drink: pulsed electric fields inactivation of *Lactobacillus plantarum*	[24]

Literature

1. Reitler W (1990) Konduktive Erwärmung von Nahrungsmitteln. Dissertation, Technical University Munich
2. Atkins P, de Paula J (2006) Physical Chemistry. Oxford University Press
3. Farooq A, Bhanger MI, Kazi TG (2003) Relationship between rancimat and active oxygen method values at varying temperatures for several oils and fats. J Am Oil Chemists Soc 80:151–155
4. Allam SSM, Mohamed HMA (2002) Thermal stability of some commercial natural and synthetic antioxidants and their mixtures. J Food Lipids 9:277–293
5. Sastry SK, Barach JT (2000) Ohmic and inductive heating. J Food Sci 65:42–46
6. de Alwis AAP, Fryer PJ (1992) Operability of the ohmic heating process: Electrical conductivity effects. J Food Engineering 15:21–48
7. Fryer PJ, de Alwis AAP, Koury E, Stapley AGF, Zhang L (1993) Ohmic processing of solid–liquid mixtures: Heat generation and convection effects. J Food Engineering 18:101–125
8. Kulshrestha SA, Sastry SK (2006) Low-frequency dielectric changes in cellular food material from ohmic heating: Effect of end point temperature. Innovative Food Science & Emerging Technologies 7:257–262
9. Wang WC, Sastry SK (1997) Starch gelatinization in ohmic heating. J Food Engineering 34: 225–242
10. Castro I, Teixeira JA, Salengke S, Sastry SK, Vicente AA (2004) Ohmic heating of strawberry products: electrical conductivity measurements and ascorbic acid degradation kinetics. Innovative Food Science & Emerging Technologies 5:27–36
11. Ye X, Ruan R, Chen P, Doona C (2004) Simulation and verification of ohmic heating in static heater using MRI temperature mapping. Lebensmittel-Wissenschaft und-Technologie 37:49–58
12. Knorr D, Ade-Omowaye BIO, Taiwo KA, Eshtiaghi NM, Angersbach A (2003) Comparative evaluation of the effects of pulsed electric field and freezing on cell membrane permeabilisation and mass transfer during dehydration of red bell peppers. Innovative Food Science & Emerging Technologies 4:177–188

13. Lebovka NI, Praporscic I, Ghnimi, Vorobiev E (2005) Temperature enhanced electroporation under the pulsed electric field treatment of food tissue. J Food Engineering 69:177–184
14. Dutreux N, Notermans S, Wijtzes T, Góngora-Nieto MM, Barbosa-Cánovas GV, Swanson BG (2000) Pulsed electric fields inactivation of attached and free-living *Escherichia coli* and *Listeria innocua* under several conditions. Intern J Food Microbiology 54:91–98
15. Góngora-Nieto MM, Pedrow PD, Swanson BG, Barbosa-Cánovas GV (2003) Impact of air bubbles in a dielectric liquid when subjected to high field strengths. Innovative Food Science & Emerging Technologies 4:57–67
16. Olafsdottir G et al (2004) Multisensor for fish quality determination. Trends in Food Science & Technology 15:86–93
17. Oehlenschlaeger J (2005) The Intellectron Fischtester VI – an almost forgotten but powerfool tool for freshness and spoilage determination of fish at the inspection level. in: Ryder J, Ababouch L. (eds): Fifth World Fish Inspection and Quality Control Congress, FAO Fisheries Proceedings No. 1: 116–122
18. Deak T, Beuchat LR (1993) Evaluation of the indirect conductance method for the detection of yeasts in laboratory media and apple juice. Food Microbiology 10, 3:255–262
19. Noble PA (1999) Hypothetical model for monitoring microbial growth by using capacitance measurements – a minireview. J Microbiological Methods 37:45–49
20. DIN 10115 (1999) Fundamentals for detection and determination of microorganisms in foodstuffs with impedance-method, in [101]
21. DIN 10120 (2001) Analysis of foodstuffs – Detection of Salmonella with impedance-method, in [101]
22. Abu-Ali J, Barringer SA (2005) Method for electrostatic atomization of emulsions in an EHD system. J Electrostatics 63:361–369
23. Therdthai N, Zhou W (2002) Hybrid neural modeling of the electrical conductivity property of recombined milk. Intern J Food Properties 5:49–61
24. Sampedro F, Rivas A, Rodrigo A, Martínez A, Rodrigo M (2007) Pulsed electric fields inactivation of *Lactobacillus plantarum* in an orange juice–milk based beverage: Effect of process parameters. J Food Engineering 80: 931–938

9 Magnetic Properties

When a material is brought into a magnetic field, it becomes magnetically polarized. We can think of materials being made up of small sub microscopic particles like polar molecules that act as tiny magnets. When brought into the presence of a magnetic field, they will orient themselves in order to become aligned with the polarity of the magnetic field.

The material property that quantifies the extent to which a material is capable of becoming magnetically polarized when placed in a magnetic field is called magnetic permeability. Materials with high magnetic permeability will develop strong levels of magnetic polarization in response to an external magnetic field, whereas materials with low magnetic permeability will polarize to a much lesser extent, if at all.

When we consider the atomic basis for magnetic polarization, we need to distinguish between paramagnetism and diamagnetism.

Paramagnetism occurs in materials which have an atomic angular momentum, which mostly is the case when there are unpaired electrons. These types of atoms are said to have a magnetic momentum, and are responsible for the magnetic behavior of paramagnetic materials. Diamagnetism occurs in materials made up of atoms with paired electron spins. These types of atoms are said to have no magnetic momentum, and are responsible for poor magnetic polarization in diamagnetic materials.

9.1 Materials

9.1.1 Paramagnetism

An example of a paramagnetic material is aluminum. The electron configuration of aluminum is $1s^2 2s^2 2p^6 3s^2 3p^1$, and is shown in Figure 9.1. The aluminum atom has an unpaired electron, which gives it permanent magnetic momentum. This type of paramagetism is called Langevin paramagnetism and is most often the reason for materials being paramagnetic. Other contributions to the paramagnetic behavior can be given by excited conduction electrons in metals (Pauli paramagnetism) or by atoms out of their normal energy level (van-Vleck paramagnetism).

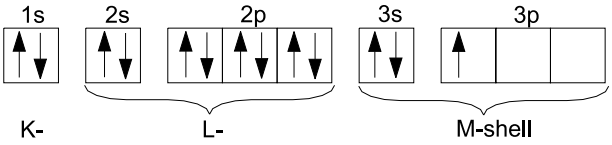

Figure 9.1. Electron configuration of aluminum

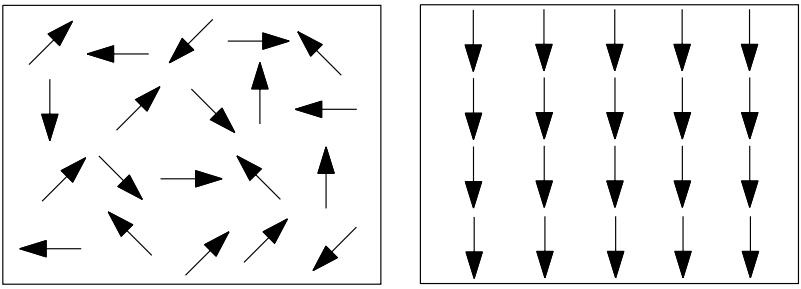

Figure 9.2. Aluminum without outer magnetic field (left). aluminum in an outer magnetic field is magnetically polarized (right)

The addition of different contributions to the atomic angular momentum can affect the paramagnetic behavior of a material. For simplification we can consider matter like this consisting of tiny elemental magnets which can be oriented in response to an external magnetic field (see Figure 9.2).

Recall that when a paramagnetic material is brought into a magnetic field, the polarized atoms will orient themselves to become aligned with the polarity of the magnetic field. In so doing, the strength of the magnetic field (flux) is amplified by this aligned orientation. This is called magnetic field amplification by a paramagnetic material.

In paramagnetic materials, the ability of the atoms to orient themselves in response to an external magnetic field diminishes with increasing temperature, until a temperature is reached at which the atoms no longer respond, and paramagnetism is lost. This is known as the Curie effect, and the critical temperature at which magnetism ceases is known as the Curie temperature. Applications of the Curie effect and temperature to thermal analysis were discussed in Section 7.9.1.

9.1.2 Ferromagnetism

Ferrous materials like iron (Latin *ferrum*) contain microscopic regions within them in which the elemental polarized atoms are already aligned in a fixed orientation. These are called Weiss regions. However, each Weiss region may have all its atoms oriented in a direction that is different from that in other regions, such that the direction of orientation is randomly distributed among all the Weiss regions throughout the ferrous material. When such a material is brought into a magnetic field, those Weiss regions with atoms already oriented

in the correct direction to be in alignment with the polarity of the magnetic field will grow in size, while the others will diminish and ultimately disappear.

For this reason, ferrous materials develop a very strong magnetic polarization in response to an external magnetic field, which is much stronger than paramagnetic materials. This behavior is called ferromagnetism.

However, just as with paramagnetic materials, this ferromagnetic ability to develop strong magnetic polarity in response to an external magnetic field diminishes with increasing temperature until a critical temperature is reached at which the magnetism is lost. Thus, ferromagnetic materials experience the same Curie effect and Curie temperature discussed earlier with paramagnetism.

9.1.3 Diamagnetism

Recall that diamagnetic materials are made up of atoms with paired electron spins, and have no magnetic momentum. These types of materials will develop no magnetic polarization when brought into a magnetic field, and are totally unresponsive to an external magnetic field. In addition to being unresponsive to a magnetic field, these materials have also been found to have a slight adverse effect on the magnetic field by weakening the field near the outer regions of the diamagnetic material. This effect can be explained by induction. When such materials are brought into the presence of a magnetic field, atomic currents are induced near the surface of the material. According to Lenz's law, these induced atomic currents will flow in a direction which causes a weakening of the intruding field.

This is what we call the diamagnetic effect. However, this effect is not limited to only diamagnetic materials. All materials possess this diamagnetic effect, including ferromagnetic and paramagnetic materials. It is not observed in these other materials because it is a very slight effect, that is overshadowed by the stronger magnetic polarization of these other materials.

We can summarize up to this point by defining diamagnetic materials as those which possess no paramagnetism or ferromagnetism. We can also conclude that the diametric effect occurs at the sub atomic level in a material, and not at the molecular level. Therefore, it is immune to Brownian molecular motion, and does not depend on temperature.

Normally, the magnetic moments of nonpaired electron spins are parallel to each other. But, some materials show antiparallel orientation. When that happens, these opposite magnetic moments compensate for each other and cancel each other out so that no magnetic polarization develops. In this case, the material only seems to be diamagnetic or apparently diamagnetic. This is what we call antiferromagnetism. Mostly oxides of iron, manganese and chromium show this behavior.

Again, there exists a critical temperature, similar to the Curie temperature, at which this antiferromagnetic behavior disappears and changes to paramagnetic behavior. This transition temperature is called the Néel temperature.

Table 9.1. Comparison of diamagnetic, paramagnetic and ferromagnetic materials

	diamagnetic	paramagnetic	ferromagnetic
permant dipoles present	no	yes	yes and readily ordered
electronenspins are	paired	unpaired	unpaired
materials amplify field	no	yes	yes, strongly
materials have diamagnetic effect	yes	yes	yes
examples	lead, copper, water, nitrogen, hydrogen	aluminum, platinum, oxygen	iron, cobalt, nickel

When we have materials that show antiparallelism in their electron spins, but the electron spins are not of equal strength, then they do not completely compensate for each other, and some residual magnetism is evident. This behavior is called ferrimagnetism, and the materials which exhibit it are called ferrites.

9.2 Magnetization

Similar to describing an electrical field, we need two quantities by which to describe a magnetic field, the field strength H and the flux density B. The flux density is also sometimes called the magnetic induction B. The relationship between these is:

$$\vec{B} = \mu \cdot \mu_0 \cdot \vec{H} \tag{9.1}$$

where

B	magnetic flux density in $\mathrm{V \cdot s \cdot m^{-2}}$
H	magnetic field in $\mathrm{A \cdot m^{-1}}$
μ_0	magnetic field constant
μ	magnetic permeability
J	magnetization in $\mathrm{V \cdot s \cdot m^{-2}}$

The flux density of a magnetic field within a given space will depend on the nature of the material matter occupying the space, and will be a minimum when no matter is present (i.e. in a vacuum). When we measure the flux density in a vacuum B_0, and then with a sample material B, we can determine the magnetic permeability μ of the sample material by taking the ratio of flux density with sample over flux density in vacuum. With matter equation (9.1) is

$$B = \mu \cdot \mu_0 \cdot H \tag{9.2}$$

without matter

$$B_0 = \mu_0 \cdot H \tag{9.3}$$

Comparing, gives:

$$B = \mu \cdot B_0 \tag{9.4}$$

and

$$\mu = \frac{B}{B_0} \tag{9.5}$$

Therefore, the magnetic permeability is a measure of the field amplification ability of materials. For a vacuum, the magnetic permeability is 1.

The difference in flux density between a material and a vacuum $B - B_0$ is called the magnetization J of the material:

$$J = \Delta B = B - B_0 \tag{9.6}$$

$$J = \mu \cdot \mu_0 \cdot H - \mu_0 \cdot H \tag{9.7}$$

$$J = (\mu - 1)\, \mu_0 \cdot H \tag{9.8}$$

with

$$\chi = \mu - 1 \tag{9.9}$$

and

$$J = \chi \cdot \mu_0 \cdot H \tag{9.10}$$

The property χ is called magnetic susceptibility, and is also a measure of the magnetization of a material and its ability for field amplification. Table 9.2 shows the range of values for magnetic permeability and susceptibility of materials with different magnetisms.

Table 9.2. Magnetic permeability and susceptibility of materials with different magnetism

diamagnetic material	paramagnetic material	ferromagnetic material
$\mu < 1$	$\mu > 1$	$\mu \gg 1$
$\chi < 0$	$\chi > 0$	$\chi \gg 0$

Table 9.3 and Table 9.4 show further data for magnetic permeability and susceptibility of materials [106].

Table 9.3. Magnetic permeability of various materials, order of magnitude

Material	μ
vacuum	1
air	≈ 1
water 20 °C	0.999991
common steel	≈ 100

Table 9.4. Magnetic susceptibility of various materials (at room temperature)

material	χ
copper	$-9.65 \cdot 10^{-6}$
water	$-9.03 \cdot 10^{-6}$
nitrogen	$-8.60 \cdot 10^{-9}$
oxogen (g)	$1.86 \cdot 10^{-6}$
oxygen (l)	$3.62 \cdot 10^{-3}$
aluminum	$2.08 \cdot 10^{-5}$
common steel	$50 \cdots 500$
ferritic materials	$10 \cdots 1000$
special Fe–Ni alloys	$6000 \cdots 70000$

Hysteresis in Magnetization

When a ferromagnetic material is placed within a magnetic field, its level of magnetization will depend on the strength of the external magnetic field. As the field strength H is increased the magnetization will also increase, but at a retarding rate as it approaches an upper saturation limit (Figure 9.3). When the field strength is decreased the level of magnetization will follow a different path, and remain at higher levels for a given field strength in response to decreasing field strength than when responding to increasing field strength. This type of behavior is known as hysteresis. The amount of magnetization retained upon release of the magnetic field is known as remanent magnetization.

As a consequence of this behavior, the magnetic permeability of a material is not a constant, but will depend on the magnetic history of the material. Figure 9.3 shows the hysteresis curve of a ferromagnetic material. The point at which the curve intersects the magnetic field strength axis (H-axis) gives the coercive field strength. This coercive field strength is the field strength required to bring the remaining magnetization in the material (remanent magnetization) back to zero.

Materials with high levels of remanent magnetization tend to retain their magnetism. These types of materials are most useful in such commercial products as magnetic memory tapes (audio and video cassettes and diskettes), and as permanent magnets in electric motors and generators.

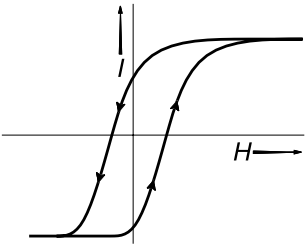

Figure 9.3. Hysteresis behavior in a ferromagnetic material

Table 9.5. Comparison of magnetic materials

	magnetic soft material	magnetic hard material
coercive field strength	low	high
change of magnetization	easy	hard
magnetization	not very durable	durable
application in	transformers, write–read heads	permanent magnets, e.g. in loudspeakers, magnetic tapes

On the other hand materials with low levels of remanent magnetization tend to change their magnetism. They are good, e.g. for write–read devices for magnetic memory materials. Table 9.5 summarizes and gives some examples.

The source used for a magnetic field can be a permanent magnetic material (magnet), or it can be an electromagnet which acts like a magnet only when energized by an electric current, which can be switched on and off. Our planet Earth also has a magnetic field, but its strength is very small when compared to the strength of magnetic fields from magnets used in commercial industry. The flux density of Earth's magnetic field is only about 10^{-4} T (Tesla), whereas strong permanent magnets can have up to 1 T, and magnetic pulses in scientific instruments and technical equipment can reach up to 100 T.

What is commonly known about magnets is that their magnetic fields are capable of exerting attractive and repulsive forces on nearby bodies made of ferromagnetic materials. These same forces are also capable of exciting electrons and inducing flow of electric current (movement of electric charge) in electric circuits. That is why magnets (permanent or electromagnets) are a key component in such machinery as electric motors and generators, linear motors and accelerators, and magnetic trains. Magnets can be used like clamps for holding down metal parts to keep them from moving when being worked upon in a machine shop. They are also used in sorting metals for recycling, as well as sorting out metal food containers from other packaging materials. Tin-coated steel cans are ferromagnetic, and aluminum cans are paramagnetic. Therefore, both types of metal containers lend themselves to separation by magnetic fields.

When electrically charged particles are moving at a velocity v in a magnetic field with field strength B, they will be subjected to a force acting on them called the LORENTZ force F_L. The LORENTZ force will increase with increasing velocity, charge and field strength, and will act in the direction that is mutually perpendicular to both the velocity of the moving particle and the magnetic field. The LORENTZ force acting on a charged particle moving in a magnetic field can be expressed as follows:

$$|F_L| = Q \cdot v \cdot B \cdot \sin \angle \left(\vec{v}; \vec{B}\right) \tag{9.11}$$

where

F_L	LORENTZ's force in N	v	velocity in $\mathrm{m \cdot s^{-1}}$
Q	electric charge in C	B	magnetic flux density in $\mathrm{V \cdot s \cdot m^{-2}}$

The LORENTZ force is the reason why charged particles cannot travel in a straight line when passing through a magnetic field. The LORENTZ forces will "push" them in a direction perpendicular to that of their initial travel direction, so that charged particles will move along a curved path instead of a straight path.

9.2.1 Applications for Magnetic Field Forces

Magnetic field forces, and particularly LORENTZ forces, are used widely in many electronic devices such as magnetic lenses in electron microscopes and scanning electron microscopes and transmitting electron microscopes. They are also used for generating electron beams in television and computer monitors, as well as in cyclotrons and synchrotrons that are used in medical diagnostics. Another application of magnetic fields is metal detection in food processing operations. When food products are being prepared for filling and packaging, the manufacturer must be certain that no chance of contamination with metal fragments has occurred during the processing operations in the factory. For this purpose the food material will pass along a magnetic detector on the conveyor belt, that will trigger an alarm and actuate a divert ejection of the contaminated product from the filling line. Detection of metals in foods is based on induction within the food material. The food product passes through the high frequency magnetic field emitted by the transmitter. A receiver senses and records the induction of that field. By so doing, it can sense and record changes in the signal caused by metal objects passing through the field. Changes in this signal will occur when metal fragments pass through the field because of eddy currents which are induced into the metal. This signal change will be greater with greater particle size and greater electric conductivity. Therefore, materials which are nonconducting (insulators) cannot give a signal (see also Section 14.3.3). However nonmetal contaminations can be detected with other techniques such as thermographic imaging or X-ray imaging.

A basic application is in the measurement of magnetic field strength by use of a HALL sensing probe, described schematically in Figure 9.4. Sensors for measuring the position of a machine part or the strength of an electric current are often based on the use of HALL probes.

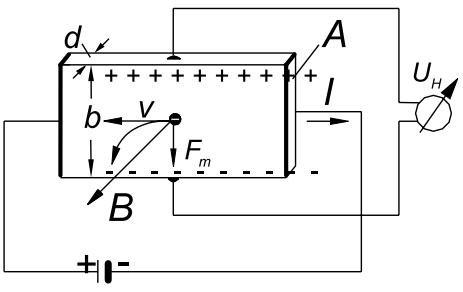

Figure 9.4. HALL sensing probe for measuring magnetic field strength (schematic)

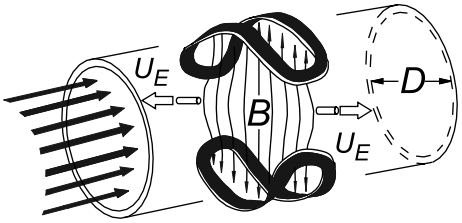

Figure 9.5. Magnetic inductive flow sensor (schematic). Perpendicular to the velocity v of charged particles and perpendicular to the magnetic field B HALL's voltage U_E can be read

An analytical application based on the paramagnetism of atoms is electron spin resonance (ESR) spectroscopy or electron paramagnetic resonance (EPR). It can be used to detect radicals in materials as evidence of prior treatment with ionizing radiation (see Section 13.4.3).

Another food technology application for magnetic fields is in the measurement of liquid flow rates by use of magnetic inductive flow meters (MID). These MID flow meters work on the principle of the LORENTZ forces. These forces act on the electric charges passing through the magnetic field. The charge carriers sense the perpendicular forces acting on them, causing them to change direction which is detected as the HALL voltage. A schematic of such an MID probe is shown in Figure 9.5. Thus, the HALL voltage depends on the velocity of the charge carriers, which in turn, can be directly related to flow rate of the liquid through the detector. These MID flow meters offer the advantage that they operate without any obstruction to the fluid flow, which is often very important in food processing. Because these MID probes are based on magnetic field forces, they can only work on liquids that carry electrically charged particles. This is often not a problem with most aqueous food liquids since the lower limit of electrical conductivity needed to receive a useful signal can be obtained with normal tap water, alone.

Other applications of magnetic fields as detection devices are sensors capable of measuring such quantities as length, thickness, angles, distance and acceleration. Examples are listed in Table 9.6. For more details, see [114].

A technological application of induction is conductive heating. Here an alternating electric field from a sender causes induction in a metal body like the bottom of a vessel or the wall of pipeline. Due to induction in the metal eddy currents will flow and cause OHMIC heating of the metal. As a consequence the metal can be used as a heating device. This principle is used in conductive heating systems [1].

inductive heating compared to OHMIC heating	[2,3]
foreign matter detection: magnetic, optic, electric techniques	[4,5]
magnets for control of pigable process equipment	[6,7]
inactivation of microorganisms: influence of magnetic fields	[8]

Table 9.6. Other technical applications of magnetic fields, examples

magnetic field force on magnetic materials	LORENTZ force on charge carriers	electric induction
electric motor/generator	monitors (BRAUN tube)	eddy current technique
low friction bearing	electron microscope	(measurement of thickness,
magnetic train	(magnetic lenses)	distance etc.)
magnetic clamp holders	HALL sensor (measuring field	metal detectors
magnetic field sensitive	strength, electric current,	induction kitchen stove
resistor (GAUSS's effect)	distance etc.)	
for measurement of field,	cyclotron	
distance, angle,	synchrotron	
revolutions, etc.)	mass spectrometer	
sorting of metals	magnetic inductive flow	
magnetic fluids	meter (MID)	

9.3 Magnetic Resonance

Spectroscopic techniques based on different precession states of magnetic moments are called magnetic resonance techniques. In this section we want to focus on nuclear magnetic resonance (NMR). Some electron spin resonance (ESR) applications will be treated shortly in Section 13.4.3 on radioactivity.

Near the beginning of this chapter we learned some reasons for atoms having a magnetic momentum. Also a reason for having an atomic magnetic moment is when a nuclei has an odd number of protons or an odd atomic mass number (that is the sum of protons and neutrons). In a very simple way we can imagine an atom with a magnetic moment as a rotating sphere containing the core particles. Because of the rotation, the sphere has a magnetic north and a south pole (Figure 9.6).

For example, the nuclei in atoms of ^{1}H, ^{13}C, ^{19}F or ^{31}P have a magnetic moment, while ^{12}C, which consists of six neutrons and six protons, has zero magnetic moment and cannot be analyzed by NMR as summarized in Table 9.7.

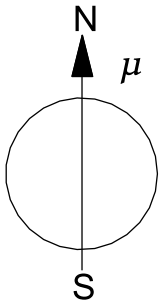

Figure 9.6. Simple model of an atom with magnetic moment: rotating nucleus having a magnetic moment μ, i.e. a magnetic dipole with north N and south S poles

Table 9.7. Atomic nuclei with and without magnetic moment

number of protons	mass number l	named	magnetic moment	example
odd	odd	odd–odd nucleus	yes	^{19}F
even	odd	even–odd nucleus	yes	^{13}C
odd	even	odd–even nucleus	yes	^{1}H
even	even	even–even nucleus	no	^{12}C

Let us now try to understand exactly what magnetic resonance is. Recall when an atom absorbs energy, such as light energy, this energy is used to bring an electron into a higher state of energy. This must be a step-wise function because we learn from quantum mechanics that only specific energy states are possible for electrons spinning around a nucleus. Therefore, only distinct amounts of energy can be used for this purpose.

In the same way, a nucleus can absorb energy but only for distinct energetic states. For example, the spin of the nucleus can have two directions so there are only two states possible. When no external magnetic field is present, these two states have nearly the same energy level (energetic state). On the other hand when there is a magnetic field present, the energetic difference ΔE between these states is higher (Figure 9.7). We might imagine that it is more difficult to change directions in a strong magnetic field than in weak field or in a zero field.

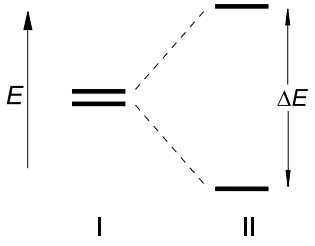

Figure 9.7. Energetic states of atomic nucleus spin. In a magnetic field (II) the energy difference ΔE between energy states is higher than without a magnetic field (I)

This is a simple model. More complex models are based on the idea that a vector μ is performing a precession movement with a characteristic frequency around the vector B. This frequency is called LARMOR's frequency.

For example, when we switch on a radio signal, the nuclei can absorb energy from the radio field if the energy can be matched to the quantum mechanic options of the nucleus. Matching means the nucleus has to be able to absorb these energy quantities, i.e. the frequency. When the frequency of transmitter and receiver are matched, we call this resonance. The resonance frequency depends mostly on the magnetic moment, as shown in equation (9.12):

$$h \cdot f = 2 \cdot \mu \cdot B \tag{9.12}$$

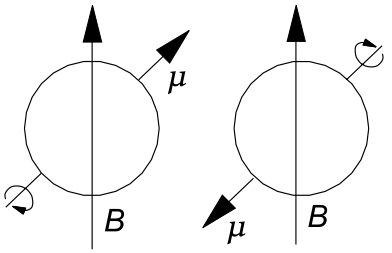

Figure 9.8. Different orientations of magnetic moment μ in relation to magnetic field B having an energetic difference of ΔE

where

h	PLANCK's constant in $J \cdot s$
f	frequency in s^{-1}
μ	magnetic moment in $C \cdot m$
B	magnetic flux density in $V \cdot s \cdot m^{-2}$

However, the exact resonance frequency depends somewhat on the physical and chemical composition of the atomic space surrounding the nucleus. This influence is known as chemical shift of the resonance frequency. The electron clouds of an atom, as well as those of neighboring atoms and their atomic bonding, also further influence the resonance frequency slightly. These combined influences cause there to be a measurable difference in resonant frequencies between, e.g. small and large atoms and, e.g. their types of bonding to other atoms. For example, we can use detection of resonance frequency to distinguish between the hydrogen nucleus in a C–H bonding versus an O–H bonding. Nuclear magnetic resonance (NMR) spectroscopy is based upon the ability to make this type of distinction.

NMR techniques are used to measure the resonance frequencies (absorption frequencies) of atomic nuclei. This gives us information, not only about the atom, but also about the state of chemical bonding in the neighborhood of the atom. In this way, NMR spectra can help us to identify chemical groups and side groups, as well as their chemical state.

For a better understanding of NMR spectroscopy, we can recall what we have learned about light absorption from physics, and make a comparison with

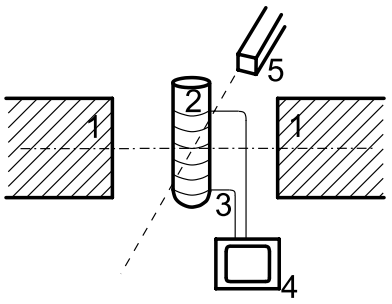

Figure 9.9. Schematic of an NMR spectrometer. **1:** magnet, **2:** sample holder, **3:** receiver coil, **4:** computer, **5:** radio wave transmitter

Table 9.8. Comparison of NMR spectroscopy with visible light

	atom absorption spectroscopy	light spectroscopy	NMR spectroscopy
excitation of …	electrons in atoms	electrons in atoms	atomic nuclei in magnetic field
excitation by …	high temperature	light	radio waves
we have quantized energetic states of the …	electrons	electrons	atomic nuclei
measurement of resonance frequency	no	yes	yes (historic only)
measurement of absorption	yes	yes	yes
analysis on the emission of …	light with typical frequency	light with typical frequency	radio waves with typical frequency
information in emission signal is about…	electron cloud of atom	electron cloud of atom	surrounding of atomic nucleus
we get information about	what type of atom	what molecules, what bonds	molecular structure and bonds

NMR spectroscopy. Table 9.8 lists some examples of this comparison, showing cases where there is commonality and cases where there are differences.

An NMR spectrometer mainly consists of a sample holder that allows placement of the sample into a magnetic field, and subjected to radio frequency waves coming from an external transmitter. A receiving coil wound around the sample holder collects the response signal from the sample. Figure 9.9 provides a schematic illustration of an NMR spectrometer.

NMR Variations

Among the variations in NMR technology are pulse NMR techniques (pulse NMR) and continuous wave NMR techniques (CW-NMR). In pulse NMR techniques, the radio frequency waves are transmitted intermittently in pulses of short time duration, whereas in continuous wave NMR techniques the radio frequency waves are transmitted continuously.

There are two approaches to find the resonance frequency in a CW-NMR spectrometer. One approach, called a field sweep, is to slowly sweep the magnetic field strength. The other approach, called a frequency sweep, is to slowly sweep the radio wave frequency under a constant magnetic field strength. The continuous wave technique is similar to slowly rotating the tuning control knob on an old radio. When we do this, we are sweeping across a band of frequencies until we find a match that brings us a signal (resonance frequency). Just as

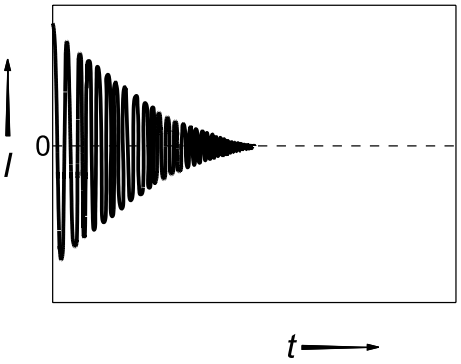

Figure 9.10. The relaxation signal from pulse NMR spectroscopy is called free induction decay (FID) (schematic)

with the disappearance of the rotating knob for tuning radios, continuous wave techniques in NMR are rarely in use today. Instead, nearly all NMR spectrometers work by use of pulse techniques. Pulse NMR spectrometers make use of a strong magnet that generates a magnetic field with constant field strength. When a material sample is subjected to this magnetic field, the atomic nuclei in the material sample receive short electromagnetic pulses of approximately 10 ms in duration. The direction of the radio wave field is then turned by 90 ° in the direction of the magnetic field. Then, the atomic nuclei absorb only those frequencies which match (resonant frequencies), and thereby take up energy. As soon as each radio wave pulse has ended, the atomic nuclei begin to lose the energy they had taken up, and they are said to "relax." Relaxation of the atomic nuclei is accomplished by emission of the radio waves that are received by the receiver coil shown earlier in Figure 9.9. The signal obtained from the receiver coil is transmitted to a computer for further analysis, this signal is called free induction decay (FID), and is shown in Figure 9.10.

Before proceeding to discuss applications to food technology, it is important to understand the distinction between high-resolution NMR (HR-NMR) and low-resolution NMR (LR-NMR).

High resolution machines have a high magnetic field strength produced by a super conductor electromagnet that must be cooled by use of helium. Machines of this type are very expensive, and require a great deal of laboratory

Table 9.9. Terms and differences between high resolution and low resolution NMR

	low resolution	high resolution
NMR provides	FID	FID
FOURIER transformation	not performed	performed to get frequencies of FID
analysis of ...	FID shape	intensity of single frequencies
terms also used:	time domain NMR or wide line NMR	frequency domain NMR

facility space. Low resolution machines are available as bench top instruments that can be easily accommodated by most laboratories, and are relatively inexpensive. These are the type most widely used in food technology laboratories, and are found principally in the fats and oils industry. Terms and differences between high resolution and low resolution NMR are summarized in Table 9.9.

9.3.1 High-Resolution NMR

The primary objective in high resolution NMR is to obtain the chemical shift of the sample, as we discussed earlier. In high resolution NMR, we try to find out at what frequencies the free induction decay signal will resonate. This is done mathematically by using FOURIER's transformation. As shown in Figure 9.11, with the help of the Fourier transformation we can determine what resonant frequencies and at what intensity they occur in the sample. The FOURIER transformation allows us to transform the FID diagram shown at the top of the figure into a spectrum of intensity decay over frequency range shown in the middle graph. Normally, with such spectra the intensity is shown as a function of the chemical shift, rather than as a function of the frequency range, as shown in the bottom graph.

Often a relative resonant frequency is used in NMR analysis, rather than the resonant frequency, alone. The relative resonant frequency is the difference between the resonant frequency in the test sample and a resonant frequency used as a reference standard. This difference is sometimes called a frequency shift, as well as a chemical shift. More sophisticated equipment can bring this information into image analysis techniques. These NMR imaging techniques can – like in medical diagnostics – be used for quality inspection of biological materials and food [9].

9.3.2 Low-Resolution NMR

In low resolution NMR, the FID signal is analyzed with respect to the shape or profile of the signal spectrum, and not with respect to the frequencies involved. From the curve's shape we can obtain information about the relaxation behavior of the sample and can quantify it by a characteristic relaxation time.

When we consider what factors would most likely influence the shape of the FID signal profile, we discover two components. The first one would be the spin–lattice relaxation (relaxation time constant T_1), and the second would be the spin–spin relaxation time constant (T_2) of the atomic nuclei under investigation.

To help us better understand this type of analysis, we will consider first only protons (^{1}H atomic nuclei) in the atomic nucleus. This is what is called ^{1}H NMR or ^{1}H low resolution NMR. Protons, which are ^{1}H atomic nuclei, relax at different rates depending on the physical-chemical make-up of their

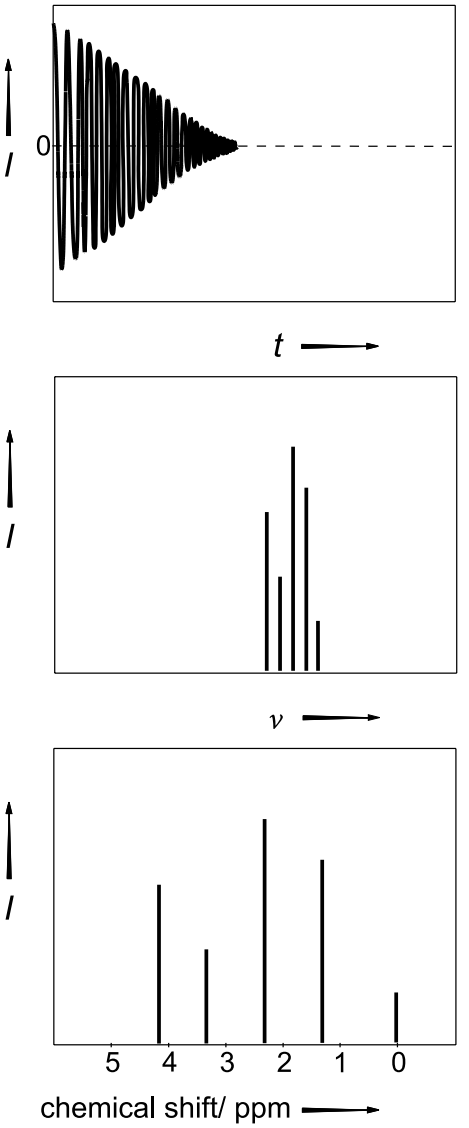

Figure 9.11. HR-NMR: By FOURIER transformation of the free induction decay (upper picture) we get the intensities of the resonance frequencies (picture in the middle) of a sample. Often the frequency shift related to a standard is used is such spectra (picture at the bottom)

immediate surroundings. Protons in a solid phase relax more quickly than those in a liquid phase, so we can say they have greater damping in solids than in liquids. Because of the physical/chemical effects mentioned earlier, protons in substances with different physical/chemical properties will show different levels of damping, even though the different substances are in the same liquid or solid state. For example, protons in water will relax more rapidly than those in oil. On the other hand, the intensity of the signal received is proportional to the number of protons involved. For these reasons, LR-NMR can be used to

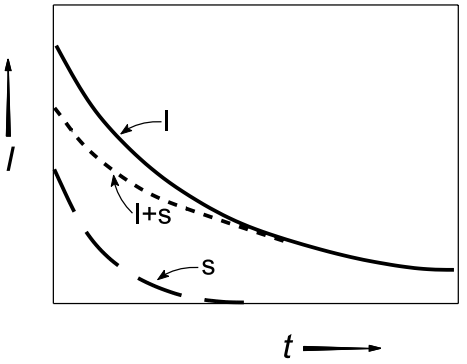

Figure 9.12. Solid (s) and liquid phase (l) show different relaxation behavior. The measured FID (l + s) is the result of addition of both parts

analyze fat and moisture content in food samples, as well as the solid-to-liquid ratio in a food sample. Consider the example in Figure 9.12, showing the FID signal from a sample that might be a fat containing protons in both a liquid and solid phase, e.g. butter or margarine at room temperature. The measured free induction decay (FID) signal seen on the upper curve in the figure reflects the combined relaxation behavior of protons in both the liquid and solid phases of the sample. If we can separate this signal into the two separate relaxation curves for protons in liquid and solid, respectively, we can obtain the solid curve (s) and liquid curve (l) in the figure, from which the solid and liquid contents of the sample can be determined. This is done by a mathematical reconstruction of the measured FID signal into the two components for each phase (solid and liquid) of which it is composed. This can be done for aqueous systems as well as fat systems. In the case of aqueous systems the sample would be a mixture of liquid phase and ice and the solid fraction would be called the frozen fraction α as discussed in Section 7.9.2.

An alternative method for separating the FID signal into the component liquid and solid parts of the sample is to alternate the NMR pulses between pulses of different time duration and direction. For example, after the first 90° pulse and short delay, a second pulse is sent into the sample with twice the duration time and at an angle of 180°. The FID signal resulting from this second pulse is called the spin echo, and is caused mostly by the protons in the nuclei with the longer relaxation time constant [10].

There are other possibilities for using ^{1}H-low-resolution NMR in food analysis. For example, instead of analyzing the FID signal profile (evaluation of relaxation), the intensities or spin echoes can be analyzed. The intensity of a signal correlates with the protons involved. So, by appropriate sample preparation, we can get information about the composition of a sample, such as moisture content or percent solids. Only limited information can be obtained from analysis of intensities, alone. However, this is often sufficient for comparing the composition of samples to check for consistent quality in food processing operations [11].

9.4 Applications

Although the theory behind low resolution NMR can be quite complex, the operation of laboratory LR-NMR equipment can be very easy. We simply place a sample into the instrument, and we have a result in seconds. Often this is used for measurement of the solid fat content (SFC) or solid fat index (SFI) in food samples. For standardized methods see [12–14]. It can also be used to determine water content in food and feed, fat content in confectionery products and emulsions, and water and fat in oil seeds or milk powders as well as in monitoring and control of freezing processes [10, 15, 34, 35]. There may also be future applications in the use of NMR with magnetic resonance imaging (MRI), in which whole products can be analyzed. With MRI technology, spatial as well as temporal spectra are produced and analyzed for structure, composition and quality of food samples. Calibration of instruments for related properties like density, viscosity, water activity and physical texture may also be possible [10, 11]. With on-line NMR equipment, process control and inspection of raw materials and products in connection with industrial food processing operations is also possible.

milk products: Applications of NMR spectroscopy	[16]
fats: measurement of solid fat content of fats and oils (Solid Fat Content, SFC)	[12–14]
fats: authenticity and quality by HR-NMR	[17]
apple: characterization of osmotic dried fruits by NMR and DSC	[18]
online NMR checking: avocado, cherry pits	[19]
fish: water binding, water activity, glass transition by pulse NMR	[20]
inulin and fructose: degree of polymerization by NMR	[21]
frozen gels: modeling thermo-physical properties with NMR data	[22]
collagen: investigation of denaturing by NMR and DSC	[23]
modified starch: hydroxypropyl content by NMR	[34]
oilseed residues: water and oil contents by pulsed NMR	[32]

Magnetic resonance imaging (MRI)

potatoes: water distribution and texture of cooked products	[24]
rice: on-line water content during cooking by NMR	[25]
noodles: NMR imaging during drying process	[26]
meat: muscle characterization, water binding, freezing by NMR	[27–29]
microwaving: 3-D temperature distribution by NMR imaging	[30]
hydration of snack foods, pasta, butter beans by NMR imaging	[31]

Literature

1. Paraskevopoulos PN, Rudnev V, Loveless D, Cook R, Black M (2003) Handbook of Induction Heating. Marcel Dekker, New York
2. Sastry Sudhir K, Barach JT (2000) Ohmic and inductive heating. J Food Science 65:42–46
3. Rosenbauer G (1996) Systemmodell der induktiven Erwärmung fließfähiger Nahrungsmittel. Dissertation Technical University Munich
4. Graves M, Smith A, Batchelor B (1998) Approaches to foreign body detection in foods. Trends in Food Science and Technology 9:21–27
5. Bradford M (1999) Reducing risk of metal contamination in the food processing industry. Leatherhead Food RA Food Industry Journal 2:162–173
6. Weissenbach MJ (1998) Pigging – about new ways of scraping pipes and product economy. Fruit Processing 8:319–326
7. Hiltscher G (1999) Molchtechnik. Wiley-VCH, Weinheim
8. Usha Rani Pothakamury, Barbosa-Canovas GV, Swanson BG (1993) Magnetic-field inactivation of microorganisms and generation of biological changes. Food technology 47:85–93
9. Mc Carthy MJ, Mc Carthy KL (1996) Applications of magnetic resonance imaging to food research. Magn. Resonance Imaging 14:799–802
10. Ruan RR, Chen PL (2001) Nuclear magnetic resonance techniques and their application in food quality analysis, in: Gunaseharan (ed) Nondestructive Food Evaluation: Techniques to Analyze Properties and Quality. Marcel Dekker, New York
11. Belton PS, Delgadillo I, Gil AM, Webb GA (eds.) (1995) Magnetic Resonance in Food Science. Royal Society of Chemistry, London
12. ISO 8292 (1991) Animal and vegetable fats and oils; determination of solid fat content; pulsed nuclear magnetic resonance method, in [101]
13. AOCS method Cd 16-81 (1999) Solid Fat Content (SFC) by Low-Resolution Nuclear Magnetic Resonance – The Indirect Method, in [112]
14. AOCS method Cd 16b-93 (1999) Solid Fat Content (SFC) by Low-Resolution Nuclear Magnetic Resonance – The Direct Method, in [112]
15. Martinez I, Aursand M, Erikson U, Singstad TE, Veliyulin E, van der Zwaag C (2003) Destructive and non-destructive analytical techniques for authentication and composition analyses of foodstuffs. Trends in Food Science and Technology 14:489–498
16. Belloque J, Ramos M (1999) Application of NMR spectroscopy to milk and dairy products. Trends in Food Science and Technology 10:313–320
17. Hidalgo FJ, Zamora R (2003) Edible oil analysis by high-resolution nuclear magnetic resonance spectroscopy: recent advances and future perspectives. Trends in Food Science and Technology 14:499–506
18. Cornillon P (2000) Characterization of osmotic dehydrated apple by NMR and DSC. Lebensmittel-Wissenschaft und –Technologie 33:261–267
19. Kim SM, Chen P, McCarthy MJ, Zion B (1999) Fruit internal quality evaluation using online nuclear magnetic resonance sensors. J Agricultural Engineering Research 74:293–301
20. Ronaldo NMP, Guilherme AMR (2003) Nuclear magnetic resonance and water activity in measuring the water mobility in pintado (Pseudoplatystoma corruscans) fish. J Food Engineering 58:59–66
21. de Gennaro S, Birch GG, Parke SA, Stancher B (2000) Studies on the physicochemical properties of inulin and inulin oligomers. Food Chemistry 68:179–183
22. Cornillon P, Andrieu J, Duplan JC, Laurent M (1995) Use of nuclear magnetic resonance to model thermophysical properties of frozen and unfrozen model food gels. J Food Engineering 25:1–19

23. Rochdi A, Foucat L, Renou JP (2000) NMR and DSC studies during thermal denaturation of collagen. Food Chemistry 69:295–299
24. Thybo AK, Szczypinski PM, Karlsson AH, Dønstrup S, Stødkilde-Jørgensen HS, Andersen HJ (2004) Prediction of sensory texture quality attributes of cooked potatoes by NMR-imaging (MRI) of raw potatoes in combination with different image analysis methods, J Food Engineering 61:91–100
25. Takeuchi S, Fukuoka M, Gomi Y, Maeda M, Watanabe H (1997) An application of magnetic resonance imaging to the real time measurement of the change of moisture profile in a rice grain during boiling. Journal of Food Engineering 33:181–192
26. Hills, BP, Godward J, Wright KM (1997) Fast radial NMR microimaging studies of pasta drying. J Food Engineering 33:321–335
27. Evans SD, Nott KP, Kshirsagar AA, Hall LD (1998) The effect of freezing and thawing on the magnetic resonance imaging parameters of water in beef, lamb and pork meat. Int J Food Sci. Tech. 33:317–328
28. Laurent W, Bonny JM, Renou JP (2000) Muscle characterisation by NMR imaging and spectroscopic techniques. Food Chemistry 69:419–426
29. Renou JP, Foucat L, Bonny JM (2003) Magnetic resonance imaging studies of water interactions in meat. Food Chemistry 82:35–39
30. Nott KP, Hall LD (2001) Three-dimensional MRI mapping of minimum temperatures achieved in microwave and conventional food processing. Int J Food Sci Tech 36:243–252
31. Duce SL, Hall LD (1995) Visualization of the hydration of food by nuclear magnetic resonance imaging. J Food Engineering 26:251–257
32. DIN EN ISO 10565 (1998) Oilseeds – Simultaneous determination of oil and water contents – Method using pulsed nuclear magnetic resonance spectrometry, in [101]
33. ASTM E 386 (1990) Standard Practice for Data Presentation Relating to High-Resolution Nuclear Magnetic Resonance (NMR) Spectroscopy, in [132]
34. DIN EN ISO 11543 (2002) Modified starch – Determination of hydroxypropyl content – Method using proton nuclear magnetic resonance (NMR) spectrometry, in [101]
35. ISO 10632 (2000) Oilseed residues – Simultaneous determination of oil and water contents – Method using pulsed nuclear magnetic resonance spectroscopy, in [101]

10 Electromagnetic Properties

Electromagnetic properties are those properties which govern the rate at which a material will respond to absorption or emission of electromagnetic radiations. Examples of electromagnetic radiations with which we might be familiar are radio waves, microwaves, ultraviolet rays, infrared rays and visible light rays, among others.

Because of the relative importance of visible light in food technology, optical properties of foods will be treated in a separate chapter, which will also include properties important in near-infrared spectroscopy and colorimetery. In this chapter, we will focus mainly on microwaves as a form of electromagnetic radiation.

Knowledge of the electromagnetic properties in foods is important because food materials possess polar molecules that will respond to microwave radiation. When foods are placed into a microwave field in which microwaves are emitted at special frequencies, polar molecules can become electrically polarized, and can absorb microwave energy [1]. Now, we will discuss electric polarization more completely in the following subsection.

10.1 Electric Polarization

As stated earlier, materials that possess polar molecules will respond to an electric field such as microwave radiation because these polar molecules will become polarized in the presence of such an electrical field. First, we must distinguish between molecules that are permanent electric dipoles like water (H_2O) from those that are temporary dipoles like hydrocarbons. When permanent dipoles are brought into the presence of an electric field, they will orient themselves to become aligned with the direction of the electric field. This is called orientation polarization.

Temporary dipoles are not normally polar molecules, but they can be deformed under the influence of an electric field. This causes them to acquire dipoles and become temporarily polarized, so they will also orient themselves to become aligned with the direction of the electric field. However, they will immediately lose their polarization as soon as the electric field disappears when switched off.

Polarization of both permanent and temporary dipoles depends on the strength of the external electrical field. Both together contribute to the overall polarization P of a volume V of material by the following expression:

$$P = \frac{p}{V} \tag{10.1}$$

where
P polarization in $\mathrm{C \cdot m^{-2}}$
p dipole moment in $\mathrm{C \cdot m}$
V volume in $\mathrm{m^3}$

The degree of polarization exhibited by a material when in the presence of an electric field can be quantified by comparing it with the degree of polarization exhibited by an empty space (vacuum) in that same electric field. Let us now consider an electric displacement field D:

$$D = \varepsilon \cdot \varepsilon_0 \cdot E \tag{10.2}$$

in a vacuum

$$D_0 = 1 \cdot \varepsilon_0 \cdot E \tag{10.3}$$

so, the difference is:

$$D - D_0 = \varepsilon \cdot \varepsilon_0 \cdot E - \varepsilon_0 \cdot E = \varepsilon_0 \cdot E(\varepsilon - 1) = P \tag{10.4}$$

The polarization is

$$P = (\varepsilon - 1)\varepsilon_0 \cdot E \tag{10.5}$$

and with

$$\chi = (\varepsilon - 1) \tag{10.6}$$

we have

$$P = \chi \cdot \varepsilon_0 \cdot E \tag{10.7}$$

where
D electric displacement field in $\mathrm{C \cdot m^{-2}}$
E electric field in $\mathrm{V \cdot m^{-1}}$
ε_0 electric field constant in $\mathrm{C \cdot V^{-1} \cdot m^{-1}}$
ε relative permittivity
χ electric susceptibility

The relative permittivity ε and also the susceptibility χ are measures for the polarization potential of a material.

The greater the polarization potential of a material the more energy it can absorb from an electric field. When the direction of the electric field alternates periodically at a given frequency, then the dipoles also alternate their orientation to follow the alternating direction of the electric field at the same frequency. Thus, the direction of polarization in the material alternates with the alternating electric field.

This continuously changing orientation is not completely elastic. A significant part of the absorbed energy is lost in the form of heat that is generated from the work of friction as the dipoles try to reverse their direction of orientation at high frequencies. This heat is absorbed by the material, and results in an increase in the temperature of the material. This is why foods become heated when placed in a microwave oven.

The polarization potential of a material α_{total} can be calculated as the sum of the polarization potential of the temporary (induced) and permanent dipoles α_{ind} and $\alpha_{permanent}$, respectively.

$$\alpha_{total} = \left(\alpha_{ind} + \alpha_{permanent}\right) \tag{10.8}$$

So, we can say the polarization is:

$$P = N \cdot \alpha_{total} \cdot E \tag{10.9}$$

The orientation of permanent dipoles, such as water (H_2O) molecules, when placed into an external electric field, is impeded by the thermal movement of the molecules. The increasing temperature causes the permanent polarization to decrease. This decrease in permanent polarization potential as a function of temperature can be estimated as follows:

$$\alpha_{permanent} = \frac{\mu^2}{3kT} \tag{10.10}$$

With this:

$$P = N\left(\alpha_{ind} + \frac{\mu^2}{3kT}\right) \cdot E \tag{10.11}$$

where

P	polarization in $C \cdot m^{-2}$
N	particle concentration in m^{-3}
α_{ind}	induced polarization potential in $C^2 \cdot m^2 \cdot J^{-1}$
μ	molecular dipole moment in $C \cdot m$
k	Boltzmann's constant
T	temperature in K
E	electric field in $V \cdot m^{-1}$
ε_0	electric field constant in $C \cdot V^{-1} \cdot m^{-1}$

Data for the induced polarization potential α_{ind} of different molecules are listed in literature. Often instead of α_{ind} the so-called polarization volume α' is listed. It is:

$$\alpha' = \frac{\alpha_{ind}}{4\pi \cdot \varepsilon_0} \tag{10.12}$$

Also, values for the permanent dipole moment μ for different molecules are available from referenced literature. A few examples are given in Table 10.1. Sometimes the dipole moment μ is expressed in units of Debyes (D), instead of the SI units of $C \cdot m$. A Debye is $D = 3.3 \cdot 10^{-30}$ $C \cdot m$.

Table 10.1. Dipole moments and polarization potential of some simple molecules [113]

	μ/C · m	μ/D	α_{ind}/C² · m² · J⁻¹	α'/cm³
H_2	0	0	$9.11 \cdot 10^{-41}$	$8.19 \cdot 10^{-25}$
N_2	0	0	$1.97 \cdot 10^{-41}$	$1.77 \cdot 10^{-24}$
CO_2	0	0	$2.93 \cdot 10^{-40}$	$2.63 \cdot 10^{-24}$
H_2O	$6.17 \cdot 10^{-30}$	1.85	$1.65 \cdot 10^{-40}$	$1.48 \cdot 10^{-24}$
C_2H_5OH	$5.64 \cdot 10^{-30}$	1.69	–	–
CH_3OH	$5.70 \cdot 10^{-30}$	1.71	$3.59 \cdot 10^{-40}$	$3.23 \cdot 10^{-24}$

The Clausius–Mosotti–Debye equation (10.13) describes the relationship between relative permittivity ε and polarization potential α. It can be used to express the polarization potential of a material:

$$\frac{\varepsilon - 1}{\varepsilon + 2} = \frac{N}{3 \cdot \varepsilon_0} \left(\alpha_{ind} + \frac{\mu^2}{3kT} \right) \tag{10.13}$$

We can also write as

$$\frac{\varepsilon - 1}{\varepsilon + 2} \cdot \frac{3}{4\pi} = N \cdot \frac{1}{4\pi\varepsilon_0} \left(\alpha_{ind} + \frac{\mu^2}{3kT} \right) \tag{10.13}$$

by use of (10.8), we get:

$$\frac{\varepsilon - 1}{\varepsilon + 2} \cdot \frac{3}{4\pi} = N \cdot \frac{1}{4\pi\varepsilon_0} \cdot \alpha_{total} \tag{10.14}$$

this is:

$$\frac{\varepsilon - 1}{\varepsilon + 2} \cdot \frac{3}{4\pi} = N \cdot \alpha'_{total} = \varphi_N \tag{10.15}$$

The quantity φ_N is dimensionless, and represents the polarization potential caused by a particle concentration N. The molar polarization potential can be calculated by:

$$\varphi_n = \varphi_N \cdot \frac{M}{\rho} \tag{10.16}$$

Using (10.15) this provides

$$\varphi_N = \frac{M}{\rho} \cdot \frac{3}{4\pi} \cdot \frac{\varepsilon - 1}{\varepsilon + 2} \tag{10.17}$$

with the particle concentration

$$N = \frac{\rho \cdot N_A}{M} \tag{10.18}$$

Then, molar polarization potential is:

$$\varphi_n = \frac{N_A}{4\pi\varepsilon_0} \left(\alpha_{ind} + \frac{\mu^2}{3kT} \right) \tag{10.19}$$

The molar polarization potential φ_n can be understood as polarization potential caused by the particles on one mole of substance. The unit of φ_n is $\mathrm{m}^3 \cdot \mathrm{mol}^{-1}$. Particle concentration can be divided by the inverse density $\frac{1}{\rho}$ of the material to obtain the inverse mass:

$$N \cdot \frac{1}{\rho} = \frac{N_A}{M} = \frac{1}{m} \tag{10.20}$$

Applying this to φ_N in equation (10.15), we obtain the mass specific polarization potential

$$\varphi_m = \varphi_n \cdot \frac{1}{\rho} = \frac{1}{m} \cdot \frac{1}{4\pi\varepsilon_0} \cdot \left(\alpha_{ind} + \frac{\mu^2}{3kT}\right) \tag{10.21}$$

Thus, φ_n can be understood to be the polarization potential caused by the particles in a mass m of the sample. The SI unit is $\mathrm{m}^3 \cdot \mathrm{kg}^{-1}$.

Using (10.15) yields the simple relation:

$$\varphi_m = \frac{3}{4\pi \cdot \rho} \cdot \frac{\varepsilon - 1}{\varepsilon + 2} \tag{10.22}$$

where

φ_N	volume-based polarization potential in $\mathrm{m}^3 \cdot \mathrm{m}^{-3}$
φ_n	mole-based polarization potential in $\mathrm{m}^3 \cdot \mathrm{mol}^{-1}$
φ_m	mass-based polarization potential in $\mathrm{m}^3 \cdot \mathrm{kg}^{-1}$
M	molar mass in $\mathrm{kg} \cdot \mathrm{mol}^{-1}$
ρ	density in $\mathrm{kg} \cdot \mathrm{m}^{-3}$
N_A	Avogadro's constant

10.1.1 Temperature Dependency

From equations (10.21) and (10.23) we can derive the following expression which indicates the temperature dependency of the polarization potential and the permittivity of a material:

$$\varphi_m = \frac{3}{4\pi\rho} \cdot \frac{\varepsilon - 1}{\varepsilon + 2} = \frac{1}{4\pi\varepsilon_0 m}\left(\alpha_{ind} + \frac{\mu^2}{3kT}\right) \tag{10.23}$$

When we measure the relative permittivity ε of a material at different temperatures, we can calculate the mass-based polarization potential φ_m according to equation (10.21) and plot it versus $\frac{1}{T}$. Then we are able to obtain the permanent dipole moment μ and the induced polarization potential α_{ind} of the material. As shown in Figure 10.1, the intercept a and the slope b provides us with the following expressions from equation (10.23):

$$a = \frac{\alpha_{ind}}{4\pi\varepsilon_0 m}, \qquad \text{and} \qquad b = \frac{\mu^2}{12\pi\varepsilon_0 m \cdot k}.$$

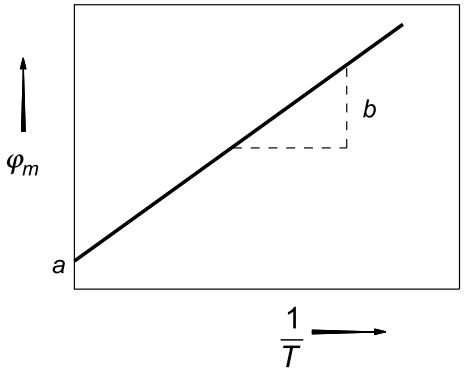

Figure 10.1. Temperature dependency of polarization potential

If we wish to characterize the polarization potential of a food by this experimental procedure, we only have to know the density of the material (see Section 2.3). In cases where the molar mass M or at least the average molar mass $\overline{M}$ is known, we would prefer to use equation (10.19). Then it is:

$$\varphi_n = \frac{M}{\rho} \cdot \frac{3}{4\pi} \cdot \frac{\varepsilon - 1}{\varepsilon + 2} = \frac{N_A}{4\pi\varepsilon_0} \left(\alpha_{ind} + \frac{\mu^2}{3kT} \right) \tag{10.24}$$

and, the intercept and slope in the φ_n versus $\frac{1}{T}$ plot are:

$$a = \frac{N_A \cdot \alpha_{ind}}{4\pi \cdot \varepsilon_0}; \qquad b = \frac{N_A \cdot \mu^2}{12\pi \cdot \varepsilon_0 \cdot k}.$$

We can see that the polarization potential as well as the permittivity of a material decrease with rising temperature. Although this effect is comparably small, it must be taken into account when we plan to heat food by high frequency electric fields or microwaves [2,3].

10.1.2 Frequency Dependency

When molecules absorb energy they can use it to move in different ways, such as translation, oscillation and rotation. In this section we will focus on rotation. The rotation of a molecule in a liquid needs about 10^{-12} s. So, when an electric field is changing with a frequency above of 10^{12} Hz, it becomes difficult for the molecule to follow the rapid reversals in field direction. When the frequency is further increased over 10^{12} Hz, the permanent dipoles like H_2O molecules cannot follow the reversals any longer. That is the reason why the polarization of the permanent dipoles, as well as the total polarization (see equation (10.8)) drops off at higher frequencies. Figure 10.2 illustrates the decrease of α_{total} when the electromagnetic radiation frequencies change from radio frequencies and microwaves to infrared (IR) frequencies. Notice in Figure 10.2 that the contribution of induced dipoles α_{ind} to α_{total} remains

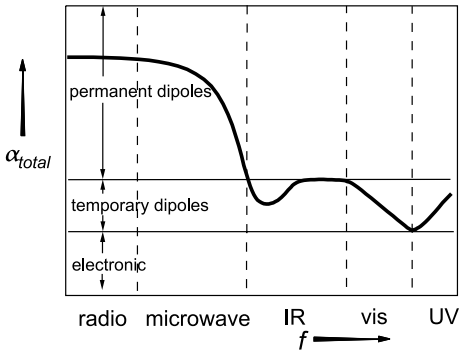

Figure 10.2. Frequency dependency of the electric polarization potential [113]

constant until we reach IR frequencies. When we raise the frequency even further, then α_{ind} as well as α_{total} decrease further.

When discussing the possibility of the electromagnetic radiation frequencies changing from radio frequencies and microwaves to infrared (IR) frequencies, it is helpful to become familiar with the overall spectrum of electromagnetic radiation frequencies and wavelengths. Moving from relatively low frequencies and long wavelengths to higher frequencies and shorter wavelengths, this spectrum includes radio waves, microwaves, ultraviolet rays, visible light, infrared radiation, and ionizing radiations, including X-rays, and gamma rays. Table 10.2 gives an overview of the electromagnetic radiation spectrum, and helps provide orientation as into what range of frequencies and wavelengths each type of electromagnetic radiation can be found.

At optical frequencies (visible light), polarization of dipoles does not play a role any longer. All absorption (all contribution to polarization of a material) is due to electrons in the material which are located in the chemical bonds and electron clouds of atoms. For example, X-rays or gamma rays can only be absorbed by inner electrons of the atoms because of their frequency. When the polarization potential of a material is examined at e.g. visible light frequencies, there is no contribution from permanent dipoles. Instead, we obtain the following from equation (10.19):

$$\varphi_n = \frac{N_A}{4\pi\varepsilon_0}\alpha_{ind} \tag{10.25}$$

With equation (10.17) and MAXWELL's equation:

$$\varepsilon = n^2 \tag{10.26}$$

and we get a relation between polarization potential and refraction index n:

$$\varphi_n = \frac{N_A}{4\pi\varepsilon_0} \cdot \alpha_{ind} = \frac{M}{\rho} \cdot \frac{3}{4\pi} \cdot \frac{n^2 - 1}{n^2 + 2} \tag{10.27}$$

Using equation (10.27) we have the opportunity to obtain the polarization potential of a material by measurement of the refraction index (for measurement of refraction see Section 11.1).

Table 10.2. Electromagnetic spectrum

frequency in Hz	name	wavelength in vacuum in m	objects in the size of wavelength
$3 \cdot 10^{24}$		10^{-16}	
$3 \cdot 10^{23}$		10^{-15}	atomic nucleus
$3 \cdot 10^{22}$	γ-rays	10^{-14}	
$3 \cdot 10^{21}$		10^{-13}	
$3 \cdot 10^{20}$	X-rays	10^{-12}	
$3 \cdot 10^{19}$		10^{-11}	
$3 \cdot 10^{18}$		10^{-10}	electron orbit in an atom
$3 \cdot 10^{17}$		10^{-9}	
$3 \cdot 10^{16}$	ultraviolet	10^{-8}	
$3 \cdot 10^{15}$		10^{-7}	viruses
$3 \cdot 10^{14}$	light	10^{-6}	bacteria
$3 \cdot 10^{13}$	infrared	10^{-5}	
$3 \cdot 10^{12}$		10^{-4}	
$3 \cdot 10^{11}$	millimeter waves (EHF)	10^{-3}	
$3 \cdot 10^{10}$	microwaves	10^{-2}	
$3 \cdot 10^{9}$	ultra high frequencies (UHF)	10^{-1}	
$3 \cdot 10^{8}$	very high frequencies (VHF)	10^{0}	
$3 \cdot 10^{7}$	short waves, radio waves	10^{1}	house
$3 \cdot 10^{6}$	medium waves	10^{2}	skyscraper
$3 \cdot 10^{5}$	long waves	10^{3}	
$3 \cdot 10^{4}$		10^{4}	Mount Everest
$3 \cdot 10^{3}$	very long waves	10^{5}	
$3 \cdot 10^{2}$		10^{6}	
$3 \cdot 10^{1}$		10^{7}	Earth's diameter
$3 \cdot 10^{0}$		10^{8}	

So, up to this point we have learned that polarization potential and permittivity of a material are not constants but depend on temperature and frequency. So, we can understand now why, e.g. water has (at room temperature) a relative permittivity of about $\varepsilon \approx 80$ when we process it with microwaves, but a relative permittivity of only about $\varepsilon \approx 2$ when we expose it to visible light.

10.2 Microwaves

Electromagnetic waves with frequencies between 300 MHz and 300 GHz are called microwaves. Because microwaves are used in navigation and telecommunications (air traffic, satellites etc.) there are official rules on which frequencies can be used for what purpose. Most countries allow the frequencies of (915 ± 13) MHz and (2450 ± 50) MHz for industrial, scientific and medical purposes [14].

The following expression gives the fundamental relationship between wave speed, wavelength and frequency for microwave radiation:

$$c = \lambda \cdot f \tag{10.28}$$

where

c	wave speed in $\mathrm{m} \cdot \mathrm{s}^{-1}$
λ	wavelength in m
f	frequency in Hz

Example 10.1. Calculate the wavelengths of microwaves at the two frequencies mentioned above.

$$\lambda_{915} = \frac{2.99 \cdot 10^8 \,\mathrm{m} \cdot \mathrm{s}^{-1}}{915 \cdot 10^6 \,\mathrm{s}^{-1}} = 32.7 \,\mathrm{cm}$$

$$\lambda_{2450} = \frac{2.99 \cdot 10^8 \,\mathrm{m} \cdot \mathrm{s}^{-1}}{2450 \cdot 10^6 \,\mathrm{s}^{-1}} = 12.2 \,\mathrm{cm}$$

Essentially the same laws apply for microwaves as for other forms of electromagnetic radiation, such as visible light. For example, just as with visible light, microwaves can be transmitted, absorbed, reflected and refracted. When microwaves pass from one material substance into another, they cross an interface between media with different physical properties such as density. Then, just as when light passes from air into water, the microwaves change direction at such an interface.

With the help of metal deflectors and reflectors, microwaves can be turned around and guided to be either focused or scattered as needed. Some materials can readily absorb microwaves. We say such materials have a high degree of absorption and at the same time a low degree of transmission.

Other materials like glass, ceramics and plastic polymers exhibit essentially no absorptivity of microwaves because the polarization potential of these materials is very low at the range of frequencies permitted for use of microwaves in foods. At the same time, we would say these materials have a high degree of transmission. They are essentially transparent to microwave radiation.

The degree of absorption of a material to microwave energy depends on whether it has electric dipoles capable of receiving the transmitted frequencies. These dipoles would act like little antennae that would receive the transmitted frequencies and absorb energy from the transmitted microwaves.

The degree of absorption can be quantified from the relative permittivity of the material. Recall from equation (10.2) discussed earlier in this chapter, that the relative permittivity is the ratio of the electric displacement field in the material D over that in a vacuum D_{vacuum}.

According to (10.2) the relative permittivity is:

$$\varepsilon = \frac{D}{D_{vacuum}} \tag{10.29}$$

where

D	electric displacement field in $\mathrm{C} \cdot \mathrm{m}^{-2}$
D_{vacuum}	electric displacement field in vacuum in $\mathrm{C} \cdot \mathrm{m}^{-2}$

ε_0 electric field constant in $C \cdot V^{-1} \cdot m^{-1}$
ε relative permittivity of material
$\varepsilon \cdot \varepsilon_0$ permittivity of material

A material with high polarization potential has a high number of permanent dipoles and has a high relative permittivity, whereas a vacuum has the very lowest polarization potential with a relative permittivity of $\varepsilon = 1$. In order to calculate how much microwave energy will be absorbed by a material we have to know its relative permittivity. This value will depend on temperature and frequency.

10.2.1 Conversion of Microwaves into Heat

Recall that when the electric dipoles in a material try to orient themselves with the alternating direction of the microwave field, they rotate back and forth rapidly or oscillate in their attempt to respond to the frequency of the alternating field direction. This continuous oscillation is not completely elastic. A significant part of the absorbed energy is lost in the form of heat that is generated from the work of friction (kinetic energy is converted to thermal energy) as the dipoles try to reverse their direction of orientation at high frequencies. This heat is absorbed by the surrounding material, and results in an increase in the temperature of the material. This is why foods become heated when placed in a microwave oven.

Oscillations that are hypothetically ideal would be completely elastic. That means there would be no loss of energy, and the quantum of energy transmitted to the oscillations would sustain the oscillations indefinitely. However, real oscillations are always inelastic; they experience a loss of energy that causes them to become damped, and they diminish over time. The degree of damping is a measure of the extent to which the material will be heated by the absorption of microwaves.

Therefore, the electromagnetic property of permittivity, which governs the microwave energy absorbed by the dipoles, has an elastic component that makes them oscillate and an inelastic component that causes damping. A physical property of this type that has two components can be expressed mathematically as a complex number having a real part and an imaginary part (see also Appendix 15.3 on complex numbers). It would be written as:

$$\varepsilon^* = \varepsilon' + i \cdot \varepsilon'' \tag{10.30}$$

where
ε^* complex relative permittivity
ε' real relative permittivity
ε'' imaginary relative permittivity
i imaginary unit ($i = \sqrt{-1}$)

In equation (10.30), we have the relative permittivity expressed as a complex number consisting of the sum of a real part and an imaginary part. The real

Table 10.3. Terms in using the complex permittivity

ε'	ε''
real part of relative permittivity	imaginary part of relative permittivity
elastic component	inelastic component
in-phase component	out-of-phase component

part of the number represents the elastic component (storage of energy), and the imaginary part represents the inelastic component (loss of energy). Other terms for these real and imaginary components are given in Table 10.3.

When we want to calculate the power needed for heating a food by microwaves, it is the imaginary part of the relative permittivity that we need (ε''), because it governs the quantity of energy loss that causes heating to occur. The imaginary part of the relative permittivity ε'' is called loss factor or the dissipation factor. There is also a name for the ratio of the imaginary part ε'' over the real part ε', which is called the loss tangent. The angle δ in the loss tangent is known as the loss angle [115]:

$$\frac{\varepsilon''}{\varepsilon'} = \tan\delta \tag{10.31}$$

Therefore, in order to characterize the materials ability to absorb microwaves, we can specify any of these parameters (loss or dissipation factor, loss tangent or loss angle). When the loss or dissipation factor ε'' is known, we can calculate the dissipated microwave power in a material using the following expression from reference [15]:

$$P_D = k \cdot E^2 \cdot f \cdot \varepsilon'' \tag{10.32}$$

where

P_D	dissipated power in W
E	electric field in $\mathrm{V} \cdot \mathrm{m}^{-1}$
k	constant ($55.61 \cdot 10^{-14}\ \mathrm{C} \cdot \mathrm{m}^2 \cdot \mathrm{V}^{-1}$)
f	frequency in Hz
ε''	dissipation factor

From equation (10.32), we can see that the electric field strength E has a quadratic influence on the microwave heating effect. In the case where E and f are constant, we see that the material property (loss factor ε'') is the decisive quantity.

10.2.2 Penetration Depth of Microwaves

When microwaves penetrate into a material, they are absorbed by the dipoles within the material. This continual absorption causes them to become weaker and weaker as they attempt to penetrate further into the material. The degree to which microwaves are absorbed by a material is called the attenuation of

the microwaves in that material. The higher the degree of absorption, the higher is the attenuation of the microwaves. In materials with a high degree of absorption the microwaves lose most of their energy after penetrating only a few centimeters into the material. This means that inner regions further to the interior of the material will receive microwaves of less intensity than regions closer to the surface.

The distance d after which the microwave power is absorbed to a level of $\frac{1}{e}$ of its initial value, is called the penetration depth z of the microwave energy. The remaining power at any depth distance can be calculated by

$$P = P_0 \cdot e^{-\frac{z}{d}} \tag{10.33}$$

According to reference [16] we can calculate penetration depth as follows:

$$z = \frac{\lambda}{2\pi} \cdot \left[\frac{2}{\varepsilon' \left(\sqrt{1 + \tan^2 \delta} - 1 \right)} \right]^{1/2} \tag{10.34}$$

This means that at a penetration depth of z in the food, the microwave power at that location will have decreased to $\frac{P}{P_0} = \frac{1}{e} = 0.368$. Therefore, it will have decreased to 36.8% of its initial power. The other 63.2% will have been already absorbed by the food material while penetrating up to that depth.

What we have learned at this point is that microwaves have only limited penetrating ability in materials with high absorptivity, but can penetrate more deeply into materials with less absorptivity. Table 10.4 summarizes.

Table 10.4. Penetration depth of microwaves, examples

	degree of reflection	degree of absorption	degree of transmission	penetration depth
metals	high	low	low	low
glass, polymers ceramic	low	low	high	high
water, liquid	low	high	low	low
ice	low	low	high	high

Example 10.2. Microwave penetration depth in potato [17]
What is the penetration depth of microwaves emitted at 2450 MHz in raw potatoes having $\varepsilon' = 64$ and $\varepsilon'' = 15$?

$$\tan \delta = \frac{\varepsilon''}{\varepsilon'} = 0.23$$

$$\lambda = \frac{c}{f} = \frac{2.99 \cdot 10^8}{2450 \cdot 10^6} \text{ m} = 0.1220 \text{ m}$$

$$z = \frac{\lambda}{2\pi} \left[\frac{2}{\varepsilon' \left(\sqrt{1 + \tan^2 \delta} - 1 \right)} \right]^{1/2}$$

$$z = \frac{0.1220\,\mathrm{m}}{2\pi}\left[\frac{2}{64\left(\sqrt{1+0.23^2}-1\right)}\right]^{1/2}$$

$$z = \frac{0.1220\,\mathrm{m}}{2\pi}\cdot 1.094 = 0.0212\,\mathrm{m} = 21.2\,\mathrm{mm}$$

10.2.3 Microwave Heating of Food

There are significant differences between heating foods in microwave ovens and heating foods in conventional baking ovens. With microwave heating, the power input into the food material can be very high. Industrial microwave equipment can deliver power in the range 5–100 kW, to achieve very steep temperature rises with short treatment times. Before using such high power levels with such short treatment times, it is important to determine that the physical, chemical, biochemical, and/or microbiological reactions that are needed for the food treatment are capable of occurring and going to completion during the short high power heat treatment.

Frozen Food

An important application of microwave heating is in thawing frozen foods to accomplish their phase transition from the frozen to the unfrozen state under controlled conditions. In order to do this, it is important to know and understand the dramatic differences in electromagnetic properties of water when it is in the frozen state (ice) than when in the liquid state. Table 10.5 gives values for the dielectric properties of ice and water, as an illustration. For example, the dissipation or loss factor for solid ice has a very low value when compared to that of liquid water.

Table 10.5. Dielectric properties of water [18]

	ε'	ε''	$\tan\delta$
ice	3.2	0.0029	0.0009
water, 25 °C	78	12.48	0.16

These data show us that ice is essentially transparent to microwaves, just as glass is to light. There is practically no absorption of microwave energy by solid ice. When we treat frozen foods with high microwave power levels, the frozen ice crystals will remain cold, while any unfrozen or liquid regions in the food will become very hot very quickly.

Heat damage to food quality in these liquid regions caused by the high power levels can be avoided by modulating the operation of the microwave field. In simple microwave ovens used at home, this is accomplished by intermittent switching on and off of the microwave field. When microwave thawing

is done on a large scale in food processing factories, the microwave field is controlled electronically in response to on-line sensing of food temperature. For this purpose nonmetallic temperature probes bases on fiber optics are used (see Chapter 11).

Shape of the Food

Because of the higher absorption of microwave energy near the surface of a material, sample shapes with sharp corners like rectangular trays will experience a greater heating effect at the corners while the inner regions go unheated. Therefore, the ideal shape of a food product for uniform penetration from all directions would be a perfect sphere. However, even in the case of a sphere, the inner regions near the center would receive much less microwave intensity than regions closer to the surface because of damping.

In reality for marketing reasons we still use relatively flat profile food packages, such as trays, for microwave heating. However, they are designed with a unique radius of curvature at the corners for the purpose of minimizing the effect overheating at sharp corners. Sharp corners and protrusions from the package are always in danger of becoming overheated from microwave heating, and are to be avoided in package design.

Composition of Food

Recall the role of heat capacity as an important thermal property of food materials from Chapter 7. When foods absorb microwave energy, the temperature in regions with low heat capacity will increase much more rapidly than in regions with higher capacity.

Also, the water content in different regions of the food material plays an important role in affecting the dielectric properties of the food material, and will alter the degree of absorption of microwave energy. Materials with high water content have much better absorption of microwave energy than dry materials. However, the greater heat capacity of water limits the rate at which temperature will rise in high water content materials over those with lower water content when treated with the same amount of microwave energy. When the concentration of electrolytes (see Chapter 8) is increased, then the relative permittivity is increased. Therefore, the electrolyte composition of foods is another means by which microwave heating can be controlled [19,20].

Dry, porous foods containing pockets of air show small microwave absorption. Because of their low thermal conductance (see Section 7.6.5) they can act as thermal insulators. In microwave baking, such materials can be used to insulate regions with higher degrees of microwave absorption and prevent them from cooling after heating [21].

10.3 Applications

food structure investigation by permanent electric dipole moment measurement of lactoglobulin fibrils	[4]
food oil sensor based on dielectricity measurements	[5,6]
wheat: moisture content by radiofrequency polarization potential	[7–9]
agricultural products: moisture estimation by measurement of permittivity	[10,110]
coffee: post harvest quality check by permittivity	[11]
water activity measurement based on polarization potential	[12,13]
potato, mashed: dielectric properties	[22]
chicken egg white: dielectric investigation of denaturing	[23]
fish: microwave cooking and quality	[24]
grape juice: dielectric properties, applicability of HELP treatment	[25]
garlic: dielectric properties	[26]
cheese: dielectric properties	[27]
poultry: dielectric detection of added water	[28]
asparagus: microwave pasteurization	[29]
apple dehydrated: dielectric properties	[30]
dielectric measurement of added glaze on frozen food	[31]
water: free and bound water by dielectric measurements	[32]
microwave based moisture sensor	[33]
modeling microwave heating of foods, theory	[34–37]
radar imaging of food for assessing physical properties of food	[38]
meat batter: effect of fat, water and salt on the thermal and dielectric properties	[39]
tomato products: dielectric spectroscopy of osmotically dehydrated products	[40]
intramuscular fat prediction by impedance spectroscopy	[41]
biological cells membrane structure: study using impedance measurement	[42]
medical diagnostics: magnetic induction impedance measurement	[43]
ham: characterization by electrical impedance spectroscopy (EIS)	[44]

Literature

1. 1 McKenna BM, Lyng J, Brunton N, Shirsat N (2006) Advances in radio frequency and ohmic heating of meats. J Food Engineering 77:215–229
2. Wang Y, Wig TD, Tang J, Hallberg LM (2003) Dielectric properties of foods relevant to RF and microwave pasteurization and sterilization. J Food Engineering 57:257–268
3. Ryynänen S (1995) The electromagnetic properties of food materials: a review of the basic principles. Journal of Food Engineering 26:409–429

4. Rogers SS, Venema P, Ploeg JPM, van der Linden E, van der Sagis LMC, Donald AM (2006) Investigating the Permanent Electric Dipole Moment of ß-Lactoglobulin Fibrils, using Transient Electric Birefringence. Biopolymers 82:241–252
5. Gertz C (2000) Chemical and physical parameters as quality indicators of used frying fats. Europ J Lipid Sci Technol 102:566–572
6. Stier RF (2004)Tests to monitor quality of deep-frying fats and oils. Europ J Lipid Sci 106:766–771
7. Berbert PA, Stenning BC (1996) Analysis of density-independent equations for determination of moisture content of wheat in the radiofrequency range. J Agricultural Engineering Research 65:275–286
8. Berbert PA, Stenning BC (1996) On-line moisture content measurement of wheat. J Agricultural Engineering Research 65:287–296
9. Sokhansanj S, Nelson SO (1998) Dependence of dielectric properties of whole-grain wheat on bulk density. J Agricultural Engineering Research 39:173–179
10. Sheen NI, Woodhead IM (1999) An open-ended coaxial probe for broad-band permittivity measurement of agricultural products. J Agricultural Engineering Research 74:193–202
11. Berbert PA, Queiroz DM, Sousa EF, Molina MB, Melo EC, Faroni LRD (2001) postharvest technology: dielectric properties of parchment coffee. J Agricultural Engineering Research 80:65–80
12. Henry F, Costa LC, Serpelloni M (2003) Dielectric method for the determination of a_w. Food Chemistry 82:73–77
13. Clerjon S, Daudin JD, Damez JL (2003) Water activity and dielectric properties of gels in the frequency range 200 MHz–6 GHz. Food Chemistry 82:87–97
14. ITU (ed) (2004) Radio Regulations. International Telecommunication Union, Geneva Switzerland
15. Decareau RV, Peterson RA (1986) Microwave Processing and Engineering. VCH Publ, Deerfield Beach, Florida
16. Hippel von AR (1954) Dielectrics and Wave. MIT Press, Cambridge
17. Mudgett RE (1986) Microwave properties and heating characteristics of foods. Food Tech. 40(6):84–93
18. Schiffman RF (1986) Food product development for microwave processing. Food Technology 40:94–98
19. van der Veen ME, van der Goot AJ, Vriezinga CA, De Meester JWG, Boom RM (2004) On the potential of uneven heating in heterogeneous food media with dielectric heating. J Food Engineering 63:403–412
20. Bows JR (2000) A classification system for microwave heating of food. Int J Food Sci Tech 35:417–430
21. Khraisheh MAM, Cooper TJR, Magee TRA (1997) Microwave and air drying I. Fundamental considerations and assumptions for the simplified thermal calculations of volumetric power absorption. J Food Engineering 33:207–219
22. Regier M, Housova J, Hoke K (2001) Dielectric properties of mashed potatoes. Intern J Food Properties 4:431
23. Lu Y, Fujii M (1998) Dielectric analysis of hen egg white with denaturation and in cool storage. Int J Food Sci Tech 33:393–399
24. Sahin S, Sumnu G (2001) Effects of microwave cooking on fish quality. Intern J Food Properties 4:501
25. García A, Torres JL, Prieto E, De Blas M (2001) Dielectric properties of grape juice at 0.2 and 3 GHz. J Food Engineering 48:203–211

26. Sharma GP, Prasad S (2002) Dielectric properties of garlic (Allium sativum L.) at 2450 MHz as function of temperature and moisture content. J Food Engineering 52:343–348
27. Herve AG, Tang J, Luedecke L, Feng H (1998) Dielectric properties of cottage cheese and surface treatment using microwaves. J Food Engineering 37:389–410
28. Kent M, Anderson D (1996) Dielectric studies of added water in poultry meat and scallops. J Food Engineering 28:239–259
29. Lau MH, Tang J (2002) Pasteurization of pickled asparagus using 915 MHz microwaves. J Food Engineering 51:283–290
30. Feng H, Tang J, Cavalieri RP (2002). Dielectric properties of dehydrated apples as effected by moisture content. Trans ASAE 54:129–135
31. Kent M, Stroud G (1999) A new method for the measurement of added glaze on frozen foods. J Food Engineering 39:313–321
32. Henry F, Gaudillat M, Costa LC, Lakkis F (2003) Free and/or bound water by dielectric measurements. Food Chemistry 82:29–34
33. Hinz T, Menke F, Eggers R, Knöchel R (1996) Development of a Microwave Moisture Sensor for Application in the Food Industry. Lebensmittel-Wissenschaft und-Technologie 29:316–325
34. Hill JM, Marchant TR (1996) Modelling microwave heating. Applied Mathematical Modelling 20:3–15
35. Bows JR, Patrick ML, Janes R, Dibben DC (1999) Microwave phase control heating. Int J Food Sci Tech 34:295–304
36. Decareau RV (1992) Microwave Foods: New Product Development. Food and Nutrition Press, Trumbull, CT
37. Copson DA, Microwave Heating (1975) AVI Publishing, Westport, CT
38. Abdullah MZ, Guan LC, Lim KC, Karim AA (2004) The applications of computer vision system and tomographic radar imaging for assessing physical properties of food. J Food Engineering 61:125–135
39. Lu Zhang, Lyng JG, Brunton NP (2997) The effect of fat, water and salt on the thermal and dielectric properties of meat batter and its temperature following microwave or radio frequency heating. J Food Engineering 80:142–151
40. De los Reyes R, Heredia A, Fito P, De los Reyes E, Andrés A (2007) Dielectric spectroscopy of osmotic solutions and osmotically dehydrated tomato products. J Food Engineering 80:1218–1225
41. Altmann M, Pliquett U (2006) Prediction of intramuscular fat by impedance spectroscopy. Meat Science 72:666–671
42. Angersbach A, Heinz V, Knorr D (2002) Evaluation of Process-Induced Dimensional Changes in the Membrane Structure of Biological Cells Using Impedance Measurement. Biotechnol Prog 18:597–603
43. Igney C, Jäschke S, Pinter R, Waffenschmidt E, Mühlsteff J, Brauers, A, Such O (2006) Planar Magnetic induction impedance Measurement in medicine: Principles and applications, Technische Mitteilungen 99:24
44. Guerrero L, Gobantes I, Oliver MA, Arnau J, Guardia MD, Elvira J, Riu P, Grebol N, Monfort JM (2004) Green hams electrical impedance spectroscopy (EIS) measures and pastiness prediction of dry cured hams. Meat Science 66:289–294

11 Optical Properties

Optical properties of foods are those properties which govern how food materials respond to absorption of electromagnetic radiation in the range of optical wavelengths and frequencies. These include visible light and color, but also transmission, reflection and refraction of visible light. We will also include in this chapter the radiation of light at frequencies and wavelengths outside the range of visible light. These include infrared and near infrared radiation, as well as ultraviolet light radiation.

Although microwaves are also a form of electromagnetic radiation, they have been addressed in a separate section (10.2). Another area of optics not covered in this chapter is microscopy and automatic imaging systems. Imaging is not only based on visible light, but also involves infrared and ultraviolet light, as well as microwaves, radar and X-rays. A good introduction to microscopy and imaging of foods is given in reference [31].

11.1 Refraction

11.1.1 Basics

Recall the speed of light is maximum in a vacuum. The speed of light is much lower when it must travel through a material substance (medium), and the speed will depend on the physical properties of the medium. When a beam of light (electromagnetic waves) crosses the interface between two different media, the different physical properties of these media will cause the light waves to travel at different propagation velocities in each medium. This results in the electromagnetic light beam changing direction when it crosses the interface between the two different media, as shown in Figure 11.1. We call this refraction.

When we consider a light beam like that shown in Figure 11.2, in which the light is passing from medium 1 into medium 2, part of the light "bounces back" (is reflected) at the interface, while the other part is refracted as it enters material 2. According to HUYGEN's principle, all points at the interface are starting points of spherical waves propagating through medium 2. If these waves have a lower propagation speed in medium 2 than they did in medium 1, they will change the direction of the light beam as a consequence.

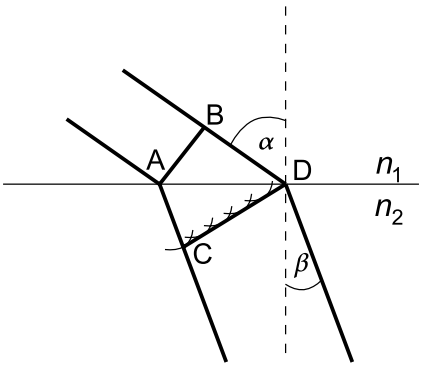

Figure 11.1. Refraction as a consequence of different speeds of wave propagation through different materials

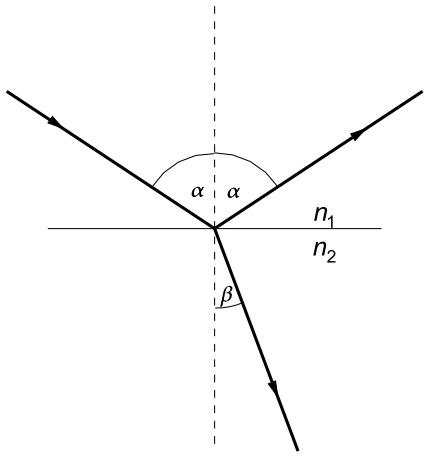

Figure 11.2. Angles of reflection (α) and refraction (β) when light strikes an interface of different materials with refraction indices n_1 and n_2

The refraction angle β in Figure 11.2 can be calculated with Snell's law:

$$\frac{\sin\alpha}{\sin\beta} = \frac{c_1}{c_2} = \frac{\frac{c_0}{n_1}}{\frac{c_0}{n_2}} \tag{11.1}$$

$$\frac{\sin\alpha}{\sin\beta} = \frac{n_2}{n_1} \tag{11.2}$$

As the angle of incidence α increases, so will the refraction angle β increase, according to Snell's law. When $\beta = 90^\circ$, no light will enter the material at all, and all incident light will be reflected. The angle of incidence causing this to happen is called the critical angle of total reflection. It can be used for measurement of refraction indices (see Section 11.1.2).

Snell's law and the simplified definition of the refraction index as ratio of wave propagation speeds is only valid in regular geometric optics in the range of small wavelengths, and in optically transparent media. Recall we learned that the absorptivity, and therefore transparency, of a material depends strongly on frequency (see Section 10.1.2). The effect that the absorptivity, and therefore permittivity and refraction index, has on frequency is called dispersion. So, when we are outside the range of geometric optics, the refraction index has to be replaced with the complex refraction index (see Section 10.1.2).

11.1.2 Measurement of Refraction Index

The refraction index can be determined experimentally from Snell's law by being able to measure the angle of incidence and the angle of refraction in a light beam experiment. From the same experiment is also possible to determine the critical angle of total reflection by finding the angle of incidence at which the angle of refraction goes to 90° [1].

Figure 11.3 shows a schematic diagram of a refractometer based on measurement of the angle of total reflection. By adjusting the angle g of the incoming light (angle of incidence α) until the detector (placed at position 8) gets a signal, the critical incident angle α_G is reached when the outgoing light has an angle of refraction $\beta = 90°$. With n_1 known, we can calculate the following using equation (11.2)

$$\frac{\sin\alpha}{\sin\beta} = \frac{n_2}{n_1} = \frac{\sin\alpha_g}{\sin 90°} \tag{11.3}$$

and so

$$n_2 = n_1 \cdot \sin\alpha_G \tag{11.4}$$

where

c_1	speed of light in material 1 in $m \cdot s^{-1}$
c_2	speed of light in material 2 in $m \cdot s^{-1}$
c_0	speed of light in vacuum in $m \cdot s^{-1}$
n_1	refraction index of material 1
n_2	refraction index of material 2
α	angle of incidence (incoming light)
β	angle of refraction (outgoing light)
α_G	critical angle for total reflection

Because the refraction index n_1 of the refractometer material is known from equation (11.4), we can obtain the refraction index n_2 of the sample very easily. Table 11.1 shows some examples of refraction index data.

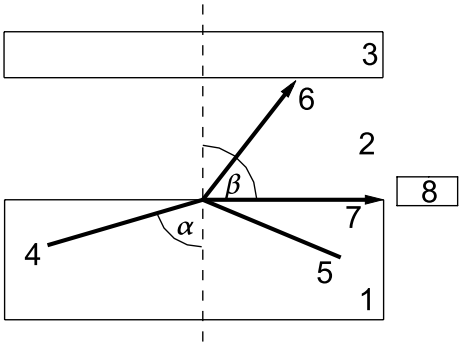

Figure 11.3. Measurement of refraction by total reflection: **1:** window, **2:** sample, **3:** cover, **4:** incoming beam, **5:** reflected beam, **6:** refracted beam, **7:** total reflected beam, **8:** detector

Table 11.1. Refraction indices of some materials

material	refraction index at 20 °C, 10^2 kPa $\lambda = 589$ mm
water	1.333
ethanol	1.362
aqueous sucrose solution, 20% (m/m)	1.364
air	1.0003
quartz glass	1.459
diamond	2.414

Laboratory refractometers are small hand-held instruments that are easy to use. They require only a few drops of a liquid sample, and provide results within just a few seconds. The refraction index can also be measured on-line with flow cells, as well as with in-line refractometers that are commercially available for process control in industrial manufacturing plants [114].

The ability to measure the refraction index easily and quickly with hand-held refractometers is very useful in food technology applications. For example, the sucrose concentration in fruit juices and soft drinks can be related directly to the refraction index of the sample solution. Tables listing sucrose concentration and the corresponding refraction index are available for this purpose, as well as commercially available refractometers already calibrated in units of sucrose concentration. Such tables available for use internationally [130] are included in Appendix 15.6.

Based on tables like this, most refractometers have built in conversions of sucrose concentrations to other units, such as °Bx (degrees Brix). When we use such tables to calibrate our instruments, then we must remember to check the validity of the calibration. For example, the data in the table are given for a certain temperature and wavelength of the refractometer. When we measure food systems containing different sugars (other than sucrose), we should expect some error because the calibration data were based only on binary sucrose–water mixtures.

In spite of the need to check the validity of calibration and other limitations, measuring the refraction index of a food is a very fast tool for checking the quality of raw materials and products. For example, carbohydrates containing liquids such as fruits can be checked without sample preparation.

Recall that all the effects of electromagnetic radiation on food are based on the ability of the food to absorb parts of the radiation. This absorption depends on the molecular receivers in a food material and their polarization potential. With DRUDE's equation, the following expressions can be derived:

$$\varepsilon^* = \varepsilon_0 + N \cdot \alpha^* \tag{11.5}$$

and

$$c_0 = \sqrt{\varepsilon_0 \cdot \mu_0} \tag{11.6}$$

Using MAXWELL's relation,

$$n^* = \sqrt{\varepsilon^* \cdot \mu^*} \tag{11.7}$$

with the assumption $\mu^* = 1$ (see Table 9.3) we get

$$n^* = \sqrt{\varepsilon^*} \tag{11.8}$$

Recall that dispersion is the result of the frequency dependency of the polarization potential of a material (Section 10.1.2). So its permittivity and refraction index will also depend on frequency. The complex refraction index $n^* = \sqrt{\varepsilon^* \cdot \mu^*}$ takes into account that, at different frequencies, we have different parts of absorption, the elastic absorption (real part of ε^*) and the loss or dissipation (imaginary part of ε^*) and also for the relative permeability μ^*. When a material is completely transparent, we can ignore the imaginary part and work only with the real part alone. This is what we do when we use Snell's law (see page 392).

c_0	speed of light in vacuum
ε_0	electric field constant in $C \cdot V^{-1} \cdot m^{-1}$
μ_0	magnetic field constant in $V \cdot s \cdot A^{-1} m^{-1}$
ε	relative permittivity
μ	relative permeability
N	number of resonators in m^{-3}
α^*	complex polarization potential in cm^3
ε^*	complex relative permittivity
n^*	complex refraction index

11.1.3 Applications for Refraction Index

solids in syrup by refraction	[2,8]
solids in tomato paste by refraction	[3]
dissolved solids in fruits and vegetables by refraction	[4–7]
honey: determination of water content by refraction	[9]
animal and vegetable fats and oils: refraction index measurement	[10]
sun flower oil: oleic acid determination by refraction	[11]
butter: reference method for refraction index measurement	[12]
essential oils: determination of refraction index	[13]

11.2 Colorimetry

Color and its measurement (colorimetry) involve organoleptic perception of properties, similar to that involved in Section 4.6 on texture analysis. The different colors we see with visible light are the result of how our eyes perceive electromagnetic radiation at different frequencies and wavelengths. The sensation of color occurs when light rays (electromagnetic radiation) of a certain

frequency and wavelength strike the retina of the human eye. The retina, in turn, transforms this sensation into a nerve signal that is transmitted to our brain, and we perceive color.

Before we can investigate the physical means by which this electromagnetic radiation reaches the eye, we must first take into account how color is perceived. The perception of color depends on many human conditions, such as age, health and visual abilities. The human eye has different receptors for light which have different spectral sensitivities. When we want to describe something we see in terms of alphanumeric figures, we have to look for quantities which allow us to describe in technical terms what the human eye would be sensing. So, let us first recall what is light and what is color.

11.2.1 Light and Color

Visible light is electromagnetic radiation with wavelength between 380 nm and 750 nm. Larger wavelengths belong to infra red radiation (IR) and smaller wavelengths belong to ultraviolet radiation (UV), and are invisible to the human eye. Table 10.2 shows that visible light is only a small part of the total spectrum of electromagnetic waves.

The speed of light is the speed at which the light waves propagate, and can be calculated mathematically as the product of wavelength and frequency.

$$c = \lambda \cdot f \tag{10.28}$$

where

c	speed of wave propagation in $\mathrm{m} \cdot \mathrm{s}^{-1}$
λ	wavelength in m
f	frequency in s^{-1}

The range of wavelengths for visible light can be further subdivided into smaller ranges that are each responsible for the different colors, such as the colors of the rainbow. The wavelength ranges responsible for the primary colors of red, yellow and blue are listed in Table 11.2.

Table 11.2. Rough classification of visible light by color

red:	700 nm – 770 nm
yellow:	570 nm – 590 nm
blue:	400 nm – 475 nm

When light of different wavelengths (different colors) is mixed together, we can produce any other color. This is called additive mixing. On the other hand, filtering can be used to eliminate certain wavelengths in order to produce a different color with those remaining. This is called subtractive mixing [14].

Example 11.1. Color of red wine
When we shine a beam of visible light onto a sample of red wine, the anthocyanins in the wine will absorb only a part of the incident light radiation and convert it into heat. The anthocyanins absorb only wavelengths in the range of 500 nm (green). Therefore, the remaining light that is reflected is missing the green wavelengths, and is perceived as red in our eyes.

Some red wines will also absorb wavelengths of light in the yellow range. When this happens, the remaining light that is reflected is not only red, but a blue–red.

From this example, we have learned that color is a consequence of selective absorption in the visible range of the electromagnetic radiation spectrum. How much energy is absorbed, such as in our red wine example, depends on the concentration of the absorbing ingredients in the sample and the sample thickness. This dependency is described in the Lambert–Beer law [15]:

$$E = k(\lambda) \cdot c \cdot d \tag{11.9}$$

where

E	extinction
k	extinction coefficient
c	concentration
d	thickness of sample in m

When we know the extinction coefficient and sample thickness, we can very easily measure the concentration of the absorbing ingredient in the sample with the use of the Lambert–Beer law. This is the scientific principle behind photometry and spectrometry, and can be used in the same way with light in the infrared and ultraviolet wavelength ranges, as well as with visible light, such as with ultraviolet and infrared spectrometers.

Example 11.2. Red wine in a bottle
Let us now consider red wine contained in a bottle made of green-colored glass. The green solid glass will be absorbing some of the red wavelengths from the incident light because of its green color. The light which reaches the wine is now different than it would be without the green bottle. By filtering out the red wavelengths in this way, some of the quality of the wine can be preserved for a longer time. Color-absorbing packaging materials like this can also be designed to filter out ultraviolet wavelengths, which can be deleterious to quality in many food products.

In the same way, the resulting light that is reflected from the green bottle containing red wine is now different. The green bottle has absorbed the red wavelengths and the red wine has absorbed the green wavelengths. Therefore, the reflected light will be missing both red and green wavelengths, and our eye will perceive a different color for the wine when it is in the bottle from when it is not in the bottle.

Now, let us assume we were to break the empty wine bottle into broken pieces of green glass, and further crush these pieces into smaller and smaller

particles. We would observe the color of these glass particles becoming lighter and lighter as they change from green to light green to nearly white or colorless as the particles become a fine glass powder.

Thus, we have learned that the perception of color is also dependent on particle size. This is the result of what we call light scattering. As the particles become smaller and smaller, the specific surface area of the particle aggregates increases dramatically. This causes more and more of the incident light striking each particle to be fully reflected. Recall that our eye receives only the light that is reflected from an object. When this light contains all the wavelengths in the visible light spectrum, we are receiving the additive mixing of all the colors, which is perceived as white.

Therefore, when we consider the physics of color, it makes a difference whether the body is a radiating body (emitting light) or is a nonradiating body (absorbing light). The color of nonradiating bodies like food materials depends on several factors some of which are listed in Table 11.3.

Table 11.3. Factors influencing the color of a material [16]

factor	parameter
illumination	type of light, illumination angle
transmission	material, particle size
absorption	surface properties, absorptivity
emission	surface properties, absorptivity
reflection	surface properties, absorptivity
observation	observer, observation angle

11.2.2 Physiology of Color Perception

There are two different types of light receptors on the retina of the human eye that are called rods and cones. The rods are sensitive to relative brightness and darkness, while the cones are sensitive to colors. There are three different types of cones, which have pigments that are sensitive to different wavelengths of light. These include wavelengths with absorption maxima of 420 nm (blue), 535 nm (green) and 565 nm (red). Thus, we can simply say that we have cones sensitive to blue, green and red light. By mixing and blending the signals from all three cone sensors, we can perceive all colors made up of added mixtures of light with these wavelengths.

Figure 11.4 shows all colors which can be observed in a so-called color triangle. Here, each place in the diagram is a perception of color defined by x, y coordinates. As we move along the perimeter of the triangle in a clockwise direction, we encounter a system of increasing wavelength. The points on the horseshoe-like curve are the points of maximum brilliance. These are the spectral colors (colors of the rainbow). At the bottom line of the color triangle,

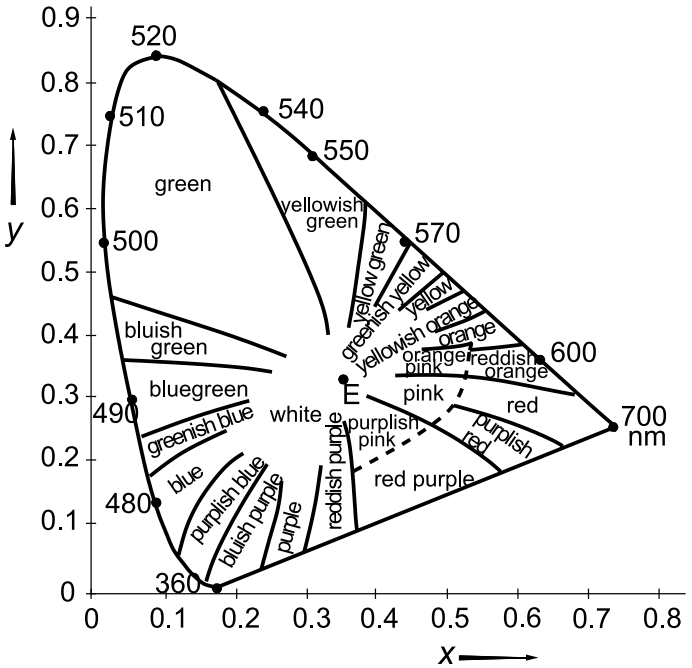

Figure 11.4. Chromaticity diagram. In the triangle are all colors which can be observed. Colors with maximum brilliance are on the horse shoe curve. Point E in the middle is zero brilliance (white)

we have purple colors which are not spectral colors (not components of the rainbow) [17,18].

Moving inward from the outer points of the diagram to the center of the triangle, we come to colors with less brilliance, to pale colors and at last to the point where a color is so pale that it appears white. This is the point of zero brilliance E.

We can represent the mixing of two colors on the color triangle by drawing a straight line from one color to the other in order to see what resulting color is possible. For example, mixing red and green will produce a line going through the region of yellow colors. This illustrates the principle of additive mixing of colors. All lines passing through the point E represent possibilities for reaching a perfect white. Colors which result in white when mixed together are called complementary colors.

11.2.3 Color as a Vector Quantity

A convenient way to describe a color as a quantity is to treat it like a vector with three components. Based on this vector system with three components, we can indicate a color with numbers. For example, we can say color number

80-70-50 after CIE [19, 20] or number 7:3:2 after DIN 6164 [21, 52]. In this way, the communication for describing a color is immune from problems with human perception and subjective judgement. This is important in technical applications [22,23]. Let us now look how this works:

For technical purposes we can describe a color by three attributes;

- hue
- chroma
- brightness

In Table 11.4 the terms are explained and illustrated with examples.

Table 11.4. Terms used in colorimetry

attribute	description	example
hue	region in chromaticity diagram	red–yellow or green–yellow
brightness	degree between darkness and maximum brightness	bright red–yellow or dark red–yellow
chroma	degree of color or colorlessness (brilliance, paleness)	brilliant red–yellow or pale red–yellow

The human eye can distinguish about 200 different hues, 20–25 degrees of chroma and about 500 degrees of brightness. By combination of these we can perceive some millions of different colors [16].

L-a-b System for Color Quantification

One of the first laboratory methods for quantifying colors is the system devised by Munsell. He was an artist and published his Color Notation to have a rational way to describe color in 1905 [24]. In this system, a color is marked by a vector. The vector points to a place in the color space indicating the hue of the color. The length of the vector d indicates the distance from the point of zero color, and quantifies the chroma of the color, while the angle α gives the hue. The vertical axis is scaled for the brightness of the color (see Figure 11.5). So, to describe the color of interest we have to specify α and d of the vector and the value of brightness.

Another presentation of the color vector is made in the Judd–Hunter system [15]. Here, the vector pointing to the place in the color space is indicated with the coordinates a and b. The brightness L again is scaled on the vertical axis (see Figure 11.6). This system often is called the L-a-b system. The a-axis and b-axis are scaled from –100 to +100. So, with the Judd–Hunter system we describe a color with three numbers (L-a-b) which are all between 0 and 100. Using the L-a-b system we see positive values of a represent red, $-a$ for green, $+b$ for yellow, and $-b$ for blue.

When we compare Figure 11.5 with Figure 11.6, we see that they are based on the same idea of specifying a point in the three-dimensional color space, but there are differences in the terms used. So we can calculate α from a and b by the following:

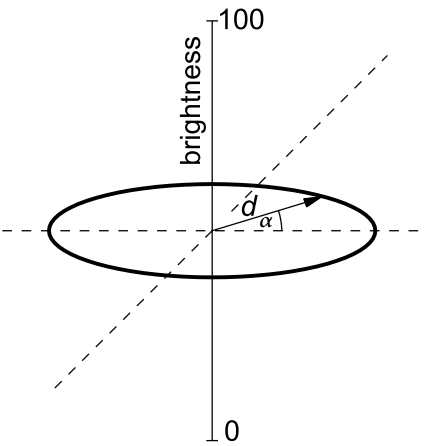

Figure 11.5. Color as a point at the end of a vector. In the MUNSELL system, an arrow (vector) points to a place in the color space. The arrow is described by angle α and length d. The vertical axis represents the brightness scale

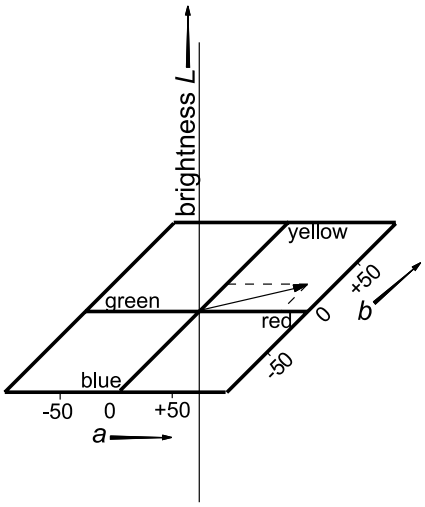

Figure 11.6. Indicating a color in the JUDD–HUNTER system (L-a-b system)

$$\tan\alpha = \frac{b}{a} \tag{11.10}$$

and the chroma d from

$$d = \sqrt{a^2 + b^2} \tag{11.11}$$

When we examine Figure 11.7, we will recognize the quantities a, b and α again. They describe the vector lying in the plane. When we now use the vertical axis

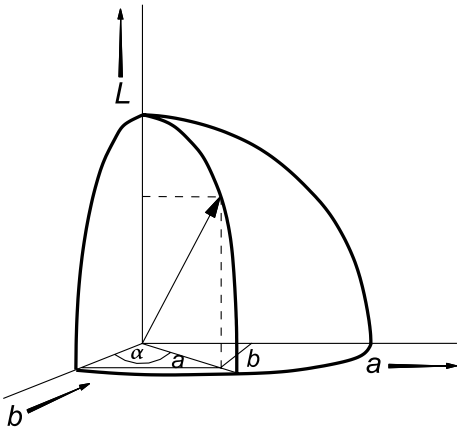

Figure 11.7. Color as a point in a three-dimensional space of polar coordinates

Table 11.5. Characterization of colors by JUDD–HUNTER system

L	a	b	description
0	a	b	black
50	a	b	grey
100	a	b	white, maximum brightness
L	−80	0	green
L	+100	0	red
L	0	−70	blue
L	0	+70	yellow

and let the vector also point to the value for the brightness L, then we can get a three-dimensional vector pointing to our designated color. Now we can understand how both Figure 11.5 and Figure 11.6 illustrate a simplification of a three-dimensional color vector.

In Table 11.5 are some examples of L-a-b number sets with descriptions of the colors they represent.

The JUDD–HUNTER system is widely used, and is often called the L-a-b system. Variations of the name include $L^*a^*b^*$ system and CIELAB system [25]. It should also be understood that all standards for describing colors are based on defined conditions of illumination and observation.

11.2.4 Color Measurement

Color measurements can be performed by visual techniques or a class of spectrometric techniques [26,27]. Classic tri-stimulus colorimeters belong to the class of spectrometric techniques, and try to adopt the function of the human eye [28]. Some product-specific color measurement for food materials are described in [29].

Visual color measurement involves observing a sample without instruments, but under controlled conditions of illumination, along with reference to a set of color standards with which to compare the sample colors observed.

Spectrometric measurements involve measurements of the absorption of specified wavelengths by the sample under controlled defined conditions of illumination.

Tri-stimulus techniques make use of three filters to simulate the function of the three different types of cones in the human eye retina.

Product-specific color measurement techniques include those such as the measurement of the color of brewing malt by the malt beverage industry involving a special EBC (European Brewing Convention) color scale [30], and the measurement of greening in fresh fruits and vegetables in agricultural packing house operations.

Visual Color Measurement

When using visual color measurement techniques, objects can be described as having the same color when they show no observable difference in color under identical conditions of illumination. For this reason, visual techniques involve observing the color of a sample and comparing it against defined color standards under identical conditions of illumination. This is called finding a color match, and falls into the category of organoleptic (sensory) methods of food quality analysis.

Color standards are commercially available in the form of paper board tiles. For liquid samples, colored standard solutions are used as matching fluids. Solutions recommended by the American and European Pharmacopoeae for this purpose, include $CoCl_2$ (rose), $FeCl_3$ (yellow) and $CuSO_4$ (blue). See Appendix 15.10 for more information on these standards.

Tri-Stimulus-Colorimetry

Based on the three types of cones in the retina of the human eye, color measuring instruments have been developed with three filters that function like each of the three types of cones. With these types of instruments, we can measure the intensity of the wavelengths transmitted through each of these filters (Figure 11.8).

The wavelengths transmitted through each filter have been specified as standards [28,52]. In this way, these filters respond with sensitivity in a standard way that is internationally recognized. It is also possible to calculate or convert the readings from a tri-stimulus colorimeter (CIE-*XYZ*-system) into the *L*-*a*-*b* values that are familiar with the HUNTER colorimeter system.

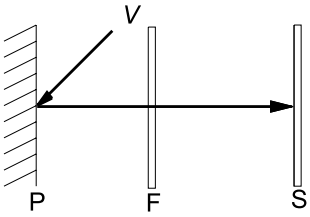

Figure 11.8. Tri-stimulus colorimeter (schematic). Light source V illuminates sample P. Detector S reads the intensity of a frequency given by filter F

11.3 Applications for Color Measurement

poultry color: processing and measurement	[32]
corn farming: color indicating stress like lacking water and nitrogen	[33]
corn: automatic sorting by machine imaging	[34]
pizza: quality checking by computer image analysis	[35]
sugar: color and whiteness as quality parameters	[36]

apple, banana, potato, carrot: Drying process and product color	[37]
color measurement by digital imaging of food surfaces	[38]
computer vision and radar imaging of food for getting physical properties	[39]
poultry: carcass quality by video image analysis	[40]
fruits: detection of surface defects by image analysis	[41]
beer: bubble size distribution by computer vision	[42]
bovine meat: optical texture classification of thin slices	[43]
jam: high pressure effects on color and flow behavior	[44]
tomato colorimeter	[45]
shrimp: visual quality attributes by machine vision	[46]
live goldfish: color measurement by machine vision system	[47]
asparagus: kinetics of color change during thermal processing	[48]
orange fruit products	[49,50]
color measurements using CCD cameras and digital images	[53,54]

11.4 Near infrared (NIR)

11.4.1 Basics

Infrared radiation (IR) is that part of the electromagnetic spectrum with wavelengths in the range from $\lambda = 0.8$–$1000\ \mu m$.

In IR spectroscopy the reciprocal of wavelength is used instead of the wavelength, itself. This reciprocal of the wavelength is called wave number. The SI unit for wave number is m^{-1}, but most often the unit of cm^{-1} is used, instead.

Referring back to speed of light as a function of wavelength and frequency, it can also be expressed as a function of wave number instead of wavelength:

$$c = \lambda \cdot f \tag{10.28}$$

$$\tilde{\nu} = \frac{1}{\lambda} \tag{11.12}$$

where

c	speed of wave propagation in $m \cdot s^{-1}$
λ	wavelength in m
f	frequency in s^{-1}
$\tilde{\nu}$	wave number in m^{-1}

The range of IR wavelengths is further subdivided into the near infrared (NIR), middle infrared (MIR) and far infrared (FIR). These are listed in Table 11.6.

Analysis of the results from IR spectroscopy is accomplished by plotting the infrared absorption in a sample material against frequency. These plots are known as the absorption spectrum of the sample material. However, for reasons

Table 11.6. Sections of IR waves

abbreviation		λ/nm	$\tilde{\nu}$/cm^{-1}
NIR	near IR	800–2500	4000–12500
MIR	middle IR	2500–5000	2000–4000
FIR	far IR	5000–10^6	10–2000

of tradition in IR spectroscopy, most often the wave number is used instead of the frequency. In addition to absorption spectra, transmission spectra can also be obtained and used in IR spectroscopy.

One of the limitations of IR spectroscopy is that it can only be used with materials that contain infrared active molecules. These are molecules capable of absorbing infrared radiation. Recall that in order for a material to respond to any type of electromagnetic radiation (see Section 10.1.2), molecules must possess properties that enable them to become stimulated or excited in some way as they absorb the radiation energy. This response is often governed by the type of bonding that exists between molecules and the atoms within. In the case of IR spectroscopy, this bonding causes molecular groups to respond with a type of oscillation in their bonding behavior that is often called vibration, although the behavior has nothing to do with the type of mechanical vibrations responsible for acoustics.

When we try to understand how the bonding in parts of molecules can oscillate or "vibrate" we can imagine such bonding as flexible links between atoms or molecule groups like elastic bands. Then these bonds would be able to stretch and contract, undergo torsion and twisting, as well as wagging and rocking back and forth. Thus, they could perform different types of periodical movements. Such basic oscillations are called fundamental oscillations of a molecule. In Table 11.7 some fundamental oscillations of the H_2O molecule are listed with their related wave numbers.

Table 11.7. Fundamental oscillations of the H_2O molecule, examples

	name	$\tilde{\nu}$/cm^{-1} (absorption)
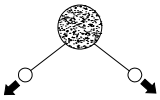	symmetric stretching	3652
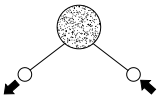	asymmetric stretching	3756
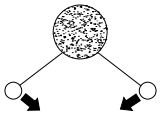	scissoring	1596

Table 11.8. Nomenclature of fundamental oscillations and its overtones

term	frequency	wavelength
fundamental oscillation	f	λ
1. overtone	$2 \cdot f$	$\frac{\lambda}{2}$
2. overtone	$3 \cdot f$	$\frac{\lambda}{3}$

Besides these fundamental oscillations, we can also observe oscillations with twice or triple frequency. Like in acoustics these are called overtones. Table 11.8 shows the nomenclature.

At this point we have looked at only a water molecule as an example with its limited number of absorption frequencies. When we consider larger molecules, they have a much greater number of absorption frequencies. By coupling of different absorption frequencies we can obtain so-called combination absorption bands.

A consequence of all this, infrared spectra often look like a confusing and complicated array of peaks and bands that would appear very difficult to interpret. However, from such spectra trained technicians can obtain such information as the molecular structure, composition and bonding within a material sample.

Table 11.9. Absorption bands (middle MIR) of molecular groups [110], examples

	oscillation	$\tilde{\nu}$/cm^{-1} (absorption)
alkanes	–CH stretching and scissoring	2800–3000
	–CH_2 stretching and scissoring	1420–1470
	–CH_3 stretching and scissoring	1340–1380
alkenes	–CH olefin stretch	3000–3100
alkines	–CH acetylene stretch	3300
aromatic compounds	–CH aromatic stretch	3000–3100
	–C=C– stretch	1600
	–OH stretch	3200–3600
	–OH scissoring	1300–1500
	C–O stretch	1000–1200
ethers	C–O asymmetric stretch	1000–1220
amines	–NH primary and secondary amine stretch	3300–3500
aldehydes, ketones	–C=O stretch	1700–1735
	–OH (dublett)	2700–2850
carboxylic acids	–C=O stretch	1720–1740
amides	–C=O stretch	1640–1670
	–NH stretch	3100–3500
	–NH stretch	1550–1640

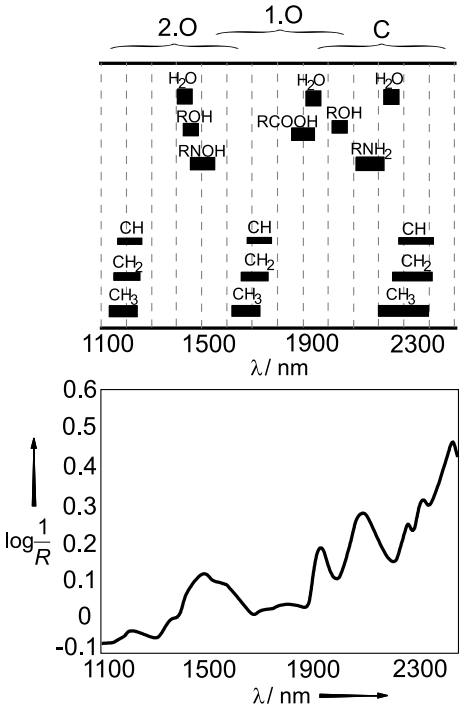

Figure 11.9. Typical absorption bands and their sources [55]

Table 11.9 and Table 11.10 give MIR and NIR absorption bands, respectively, for different molecular groups, and Figure 11.9 helps to illustrate the reading of such bands.

Figure 11.9 illustrates how an IR spectrum is generated by absorption of radiation by different molecular groups. The figure identifies which absorption bands are caused by what molecular group. The region to the far right designated by "C" is the region of fundamental oscillations. The regions designated by 1.O and 2.O indicate first and second overtones. In Table 11.10 we see typical absorption bands exhibited various by food components.

Table 11.10. Absorption band (NIR) of food components [110]

component	oscillation	λ/nm
water	–OH stretch / combination	1920–1950
	–OH stretch	1400–1450
proteins, peptides	–NH deformation	1560–1670
		2080–2220
fats	–CH stretch	2300–2350
	$-CH_2$ and $-CH_3$ stretch	1680–1760
carbohydrates	C–O and O–H stretch / combination	2060–2150

Because NIR spectra are crowded with absorption bands that often overlap, evaluation seems to be very difficult. However, by use of computer software, it is possible to find out such information as the relationship between water content of a sample and the shape of the spectrum. Using software algorithms, NIR instruments can be calibrated for simultaneous analysis of various constituents such as moisture content, protein, fat, and ash in food materials.

Because the shape of the spectra can also be influenced by physical properties like particle size and shape, or bulk density of the sample, calibrations have to be made with appropriate control of these influencing properties. On the other hand, these same influencing properties can also be taken into account as part of the calibration. Then, information about such physical properties as particle size, shape and density can be read simultaneously with information about chemical composition from the same NIR spectrum.

11.4.2 Measuring Techniques

Like other spectrometers, NIR spectrometers consist in principle of a beam generator, a sample holder and a detection system. The location of the detection system depends upon whether we want to detect radiation that was reflected from sample or transmitted by the sample. In order to irradiate the sample with singular (one-by-one) wavelengths at different frequencies, we need monochromatic radiation, which can be achieved by the use of appropriate filters as one of several methods (for appropriate wavelengths see Table 11.10). Filter systems work by placing filters in the path of the beam, and programming which filters to be used and in what sequence.

Another technique involves the use of light emitting diodes (LED), which emit radiation in the near infrared range (NIR-LEDs).

Another possibility for obtaining distinct wavelengths is the use of diffraction grids or acousto-optical filters. Acousto-optical-tunable filters (AOTF) are optical filters whose transmission can be tuned with the help of acoustic oscillations (see Section 12.2). These filters can provide a spectrum of distinct wavelengths very fast and without having moving parts in the instruments.

Table 11.11. Types of NIR spectrometers

spectrometer type	
filter	movable IR filters
tunable filter	optic filters which can be tuned (e.g. acousto-optical)
diodes (IR-LED)	monochromatic IR emitting diodes
grid	movable grid
prism	movable prism
FOURIER transform (FT)	built-in interferometer

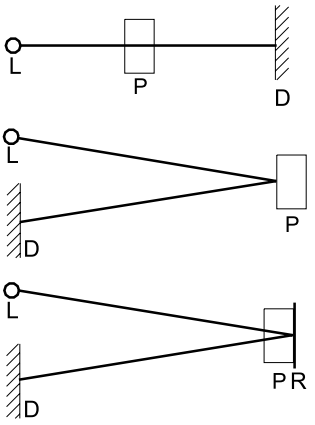

Figure 11.10. Modes of NIR illumination (schematic): sample transmission (upper picture), reflection (middle) and transflection (bottom). Light source L, sample P, detector D, reflector R

FOURIER transform spectrometers (FT spectrometers) work with the help of a built-in MICHELSON interferometer. From the interferogram of the sample that is obtained from these FT spectrometers, the absorption frequencies and their related intensities can be calculated by FOURIER transform analysis. Table 11.11 lists these techniques.

In every case we characterize samples by their near infrared absorption or transmission or reflection. It is only a matter of location of the detection system. Recall that in classic IR spectrometers, we detect only absorption in the sample, whereas in modern NIR spectrometers we detect reflection from the sample. In order to do this, a reflector is placed at the bottom of the sample cup. When radiation is transmitted through the sample it is reflected at the bottom and returns through the sample in a different direction before reaching the detector, as illustrated in Figure 11.10. This type of beam transmission is called transflection.

Often the detector is placed in such a way that it does not receive a singular direct reflection, but the spatial average of all reflections which occur. This can be resolved with the help of an integrating sphere (ULBRICHT's sphere) which collects signals from all directions. In addition, the sample cup can be rotated so that we get an average over time, taking into account that a sample might have nonhomogeneity. An important advantage of using NIR for quality assessment of raw materials, ingredients and products, is that in many cases the sample material can be used "as-is" (no sample preparation), and many different quality and compositional attributes such as concentration of different ingredients can be sensed simultaneously.

Calibration of NIR instruments is accomplished by taking readings of spectra with a large number of samples that have already been analyzed by other means, and whose chemical compositions are precisely known. Then the spectra from each sample are compared with their respective known chemical compositions in order to identify the influences on the spectra. This is nor-

mally done with the help of mathematical algorithms in commercially available computer software.

With calibrated instruments, quality checks can be performed very quickly and are most useful in assisting with automatic process control. As always, it is important to avoid errors in the analysis by carefully checking which factors might influence the spectra besides the components being measured. For example, the range in which the calibration is valid has to be identified. The large potential benefits of NIR spectroscopy as a nondestructive and rapid technique applied increasingly for food quality assessment can be seen in the following list of applications and in references [56,109,110]:

11.5 Applications

water in food by NIR	[57]
frying fat: detection of deterioration	[58]
NIR in dairy industry	[59]
monitoring moisture during heating	[60]
citrus fruits: sugar concentration by NIR	[61]
sorbet: in-line NIR monitoring	[62]
extrusion cooking process: NIR monitoring	[63]
milk: on-line NIR for coagulum setting	[64]
poultry: carcass inspection by multispectral imaging (NIR/vis)	[65]
citrus oils: classification by NIR	[66]
ginseng: water content by NIR	[67]
polymorphism: powder characterization by NIR	[68]
particle size distribution by NIR: microcrystalline cellulose	[69]
sweet potato: composition and quality parameters by NIR	[70]
classification of fish (glycyrrhizia uralensis) by NIR	[71]
sausage: fat, moisture, protein content simultaneous by diode array NIR	[72]
gellan gels: gelling temperature investigation by NIR, rheologic and dielectric properties	[73]
butter and margarine: analytical fingerprinting with spectroscopic techniques	[74]
coffee: identifying arabica, robusta and blends by NIRS	[75]
bacteria: differentiation on the basis of their NIR spectra	[76]
oil content in instant noodles	[77]
NIR as screening tool for GMO in food	[78]
simultaneously color measurement and NIRS on food and agricultural products	[79]
nonfreezable water estimation by NIR	[80]

11.6 Ultraviolet (UV)

11.6.1 Basics

Ultraviolet (UV) light is electromagnetic radiation with a wavelength shorter than that of visible light, but longer than soft X-rays (see Table 10.2) which shows the complete electromagnetic spectrum). It can be subdivided into near UV radiation with wavelengths in the range (380–200 nm), far or vacuum UV (FUV or VUV) with wavelengths in the range (200–10 nm), and extreme UV (EUV or XUV) with wavelengths in the range (1–31 nm).

When considering the effect of UV radiation on human health and the environment, the range of near UV wavelengths is even further subdivided into UVA (UV α, 380–315 nm), also called long wave or "black light;" UVB (UV β, 315–280 nm), also called medium wave; and UVC (UV γ, < 280 nm), also called short wave or "germicidal."

Ultraviolet radiation is often used in connection with visible spectroscopy or photometry (UV/VIS) to determine the existence of fluorescence in a given sample, and it is widely used as a technique in chemistry, for analysis of chemical structure, most notably conjugated systems. Perhaps more importantly, UV radiation has become increasingly used as an effective disinfecting agent in treatment of drinking water and in cold food processing, as discussed further in the following subsections.

11.6.2 Applications

Disinfecting Drinking Water

One important application for UV radiation is in the treatment of drinking water because it acts as a very effective disinfecting agent [81]. Disinfection using UV radiation was historically more commonly used in wastewater treatment applications, but is now finding increased usage in drinking water treatment. It used to be thought that UV disinfection was more effective for bacteria and viruses, which have more exposed genetic material, than for larger pathogens which have outer coatings or that form spore states that shield their DNA from UV light. However, it was recently discovered that ultraviolet radiation can be somewhat effective for treating the microorganism *Cryptosporidium*. These findings resulted in the use of UV radiation as a viable method to treat drinking water. Giardia, in turn, has been shown to be very susceptible to UV-C when the tests were based on infectivity of the organism rather than sole existence. It turns out that protozoa are able to survive high UV-C doses, but are none the less sterilized at low doses, and incapable of reproduction and propagation [82].

Food Processing

As consumer demand for fresh and "fresh like" food products increases, the demand for nonthermal methods of food pasteurization is likewise on the rise. In addition, public awareness regarding the dangers of food-borne illness (food poisoning) is also raising demand for improved food processing methods that assure safety to the consumer with minimum loss in quality. Ultraviolet radiation is used in several food processes to inactivate (destroy) unwanted microorganisms from liquid food products with suitable optical properties (transparent). Among the most common applications today is the use of UV light to pasteurize fruit juices by pumping the juice over a high intensity ultraviolet light source [83,84]. The effectiveness of such a process depends on the UV absorbance of the juice (see Section 11.2.1, Lambert–Beer law).

11.6.3 Further Applications

drinking water: kinetics of UV inactivation of microorganisms	[81]
drinking water: kinetics of *E. coli* inactivation by UV treatment	[85]
drinking water: sequential treatment with UV and ozone	[86]
combined treatment of pulsed light and UV to inactivate microorganisms	[87]
milk: pulsed UV treatment	[88]
fresh eggs: influence of UV treatment on pigmentation	[89]
modeling bacteria inactivation by UV in nutrious media	[90]

Literature

1. ASTM WK7846 (2005) New Guide to Measuring of index of Refraction and Dispersion, in [132]
2. AOAC method 9.32.14 C, in [104]
3. LFGB method L29.11.03-1, in [100]
4. LFGB method L31.00-16, in [100]
5. LFGB method L30.00-2(EG), in [100]
6. AOAC method 976.20, in [104]
7. AOAC method 938.17, in [104]
8. DIN 10304 (1971) Determination of moisture content and dry matter content of glucose syrup; refractive index method, in [101]
9. DIN 10752 (1992) Analysis of honey; determination of water content; refractometric method, in [101]
10. DIN EN ISO 6320 (2000) Animal and vegetable fats and oils – Determination of refractive index, in [101]
11. GOST 28238 (1989) Sunflower. Method for mass fraction determination of oleic acid according to the oil refraction index, in [101]
12. ISO 1739 (2006) Butter; Determination of the refractive index of the fat, in [101]
13. ISO 280 (1998) Essential oils – Determination of refractive index, in [101]

14. Völz HG (2001) Industrial Colour Testing. Wiley-VCH, Weinheim
15. Judd DB, Wyszecki G (1967). Colour in Business, Science, and Industry. Wiley, New York
16. Wyszecki G, Stiles WS (2000). Colour Science – Concepts and Methods, Quantitative Data and Formulae, 2nd edn, Wiley-Interscience, New York.
17. Malacara D (2002) Colour Vision and Colourimetry: Theory and Applications. The International Society for Optical Engineering (*SPIE). SPIE Press,* Bellingham WA
18. Berns RS (ed) (2000) Billmeyer and Saltzman's Principles of Colour Technology. 3rd edn, Wiley-Interscience, New York
19. CIE (1924) Commission Internationale de l'Eclairage Proceedings. Cambridge University Press, Cambridge
20. CIE (1931). Commission Internationale de l'Eclairage Proceedings. Cambridge University Press, Cambridge
21. DIN 6164 (1980) DIN colour chart system, in [101]
22. Gruenwedel DW, Whitaker JR (eds.) (1984) Food analysis I, physical characterization. Marcel Dekker, New York
23. Francis FJ, Clydesdale FM (1975) Food Colourimetry: Theory and Applications. AVI Westport, CT.
24. Munsell AH (1905) A Colour Notation. Munsell Colour Company, Boston MA
25. McLaren K (1976) The development of the CIE 1976 (L*a*b*) uniform colour space and colour-difference formula. J Society of Dyers and Colourists 92:338–341
26. Clydesdale FM (1969). The measurement of colour. Food Technology 23:16–22
27. Hutchings JB (1994) Food Colour and Appearance. Blackie Academic and Professional, London
28. Hunter, R. 5. (1942). Photoelectric Tristimulus Colourimetry with Three Filters. National Bur. Std. Circ. C4 29
29. Clydesdale, FM, Francis FJ (1969) Colourimetry of Foods. J Food Sci 34:349–352
30. EBC (ed) (1998) Analytica-EBC. European Brewery Convention (EBC) (ed), Hans Carl Fachbuchverlag Nürnberg
31. Flint O (1994) Food Microscopy. Bios Scientific, Oxford
32. Froning GW (1995) Colour of poultry meat. Poultry and Avian Biology Reviews 6:83–93
33. Ahmad IS, Reid JF (1996) Evaluation of colour representations for maize images. J Agricultural Engineering Research 63:185–195
34. Liao K, Paulsen MR, Reid J (1994) Real-time detection of colour and surface defects of maize kernels using machine vision. J Agricultural Engineering Research 59:263–271
35. Sun DW (2000) Inspecting pizza topping percentage and distribution by a computer vision method. J Food Engineering 44:245–249
36. LFGB method L39.01.02 in [100]
37. Krokida MK,Maroulis ZB,Saravacos GD (2001) The effect of the method of drying on the colour of dehydrated products. Int J Food Sci Tech 36:53–59
38. Yam KL, Papadakis SE (2004) A simple digital imaging method for measuring and analyzing colour of food surfaces. J Food Engineering 61:137–142
39. Abdullah MZ, Guan LC, Lim KC, Karim AA (2004) The applications of computer vision system and tomographic radar imaging for assessing physical properties of food. J Food Engineering 61:125–135
40. Eger H, Hinz A (1996) Video image analysis of carcass quality. Trends in Food Science and Technology 7:273
41. Davenel A, Guizard C, Labarre T, Sevila F (1988) Automatic detection of surface defects on fruit by using a vision system. J Agricultural Engineering Research 41:1–9
42. Hepworth NJ, Hammond JRM, Varley J (2004) Novel application of computer vision to determine bubble size distributions in beer. J Food Engineering 61:119–124

43. Basset O, Buquet B, Abouelkaram S, Delachartre P, Culioli J (2000) Application of texture image analysis for the classification of bovine meat. Food Chemistry 69:437–445
44. Dervisi P, Lamb J, Zabetakis I (2001) High pressure processing in jam manufacture: effects on textural and colour properties. Food Chemistry 731:85–91
45. Hunter RS, Yeatmen JN (1961) Direct reading tomato colourimeter. J Opt Soc Am 51:552–554
46. Luzuriaga D, Balaban MO, Yeralan S (1997) Analysis of visual quality attributes of white shrimp by machine vision. Journal of Food Science 62:1–7
47. Wallat GK, Chapman FA, Luzuriaga DA, Balaban, MO (2002) Analysis of skin colour development in live goldfish using a colour machine vision system. North American Journal of Aquaculture 64:79–84
48. Lau MH, Tang J, Swanson BG (2000) Kinetics of colour change in asparagus during thermal processing, J Food Engineering 45: 231–236
49. Braddock RJ (2004) The orange fruit and its products, in: The Orange Book, ed. Ulla Ringblom. Tetra Pak Processing Systems AB, Lund, Sweden
50. Braddock RJ (1999) Handbook of Citrus By-Products and Processing Technology. John Wiley, New York
51. DIN 5033 (1979) Colourimetry, in [101]
52. ASTM E1347-03 Standard Test Method for Colour and Colour Difference Measurement by Tristimulus (Filter) colourimetry, in [132]
53. Mendoza F, Dejmek P, Aguilera JM (2006) Calibrated colour measurements of agricultural foods using image analysis. Postharvest Biology and Technology 41:285–295
54. León K, Mery D, Pedreschi F, León J (2006) Colour measurement in L*a*b* units from RGB digital images. Food Research International, 39: 1084–1091
55. Berntsson O (2001) Characterization and application of near infrared reflection spectroscopy for quantitative process analysis of powder mixtures. Diss Kungl Högskolan Stockholm
56. Haiyan Cen and Yong He (2006) Theory and application of near infrared reflectance spectroscopy in determination of food quality. Trends in Food Science & Technology 18: 72–83
57. Büning-Pfaue H (2003) Analysis of water in food by near infrared spectroscopy. Food Chemistry 82:107–115
58. Isengard HD (1999) Analytische Methoden zur Kontrolle des Verderbs von Frittierfetten. Proc. 57. Diskussionstagung FEI, Bonn p. 117–129
59. Wüst E, Rudzik L (2003) The Use of Infrared Spectroscopy in the Dairy Industry. J Molecular Structure 291:661–662
60. Wählby U, and Skjöldebrand C (2001) NIR-measurements of moisture changes in foods. J Food Engineering 47:303–312
61. Miller WM; Zude M (2003). Fusion of physical / colour features with NIR-based sensing to identify brix level of Florida citrus. ASAE Technical paper no 026037
62. Bolliger S, Closs C, Zeng Y, Windhab E (1998) In-line use of near infrared spectroscopy to measure structure parameters of frozen model sorbet. J Food Engineering 38:455–467
63. Guy RCE, Osborne BG, Robert P (1996) The application of near infrared reflectance spectroscopy to measure the degree of processing in extrusion cooking processes. J Food Engineering 27:41–258
64. O'Callaghan DJ, O'Donnell CP, Payne FA (2000) On-line sensing techniques for coagulum setting in renneted milks. J Food Engineering 43:155–165
65. Park B, Chen YR, Huffman RW (1996) Integration of visible/NIR spectroscopy and multispectral imaging for poultry carcass Inspection. J Food Engineering 30:197–207

66. Steuer B, Schulz H, Läger E (2001) Classification and analysis of citrus oils by NIR spectroscopy. Food Chemistry 72:113–117
67. Guixing R, Feng C (1997) Determination of moisture content of ginseng by near infrared reflectance spectroscopy. Food Chemistry 60:433–436
68. Patel AD, Luner PE, Kemper MS (2000) Quantitative analysis of polymorphism binary and multicomponent mixtures by near infrared reflectance spectroscopy, Int J Pharmacy 206:63–74
69. O'Neil AJ, Jee RD, Moffat AC (1999) Measurement of cumulative particle size distribution of microcrystalline cellulose using NIR spectroscopy. Analyst 124:33–36
70. Guoquan Lua, Huahong Huanga, Dapeng Zhang (2006) Prediction of sweetpotato starch physiochemical quality and pasting properties using near-infrared reflectance spectroscopy. Food Chemistry 94:632–639
71. Li Wang F, Lee SC, Wang X (2006) Near-infrared spectroscopy for classification of licorice (Glycyrrhizia uralensis) and prediction of the glycyrrhizic acid (GA) content. LWT – Food Science and Technology 40:83–88
72. Ortiz-Somovilla V, España-España F, Gaitán-Jurado AJ, Pérez-Aparicio J, De Proximate EJ (2007) Analysis of homogenized and minced mass of pork sausages by NIRS. Food Chemistry 101:1031–1040
73. Yiqun Huang, Cavinato AG, Juming Tang, Swanson BG, Mengshi Lin, Rasco BA (2007) Characterization of sol–gel transitions of food hydrocolloids with near infra-red spectroscopy. LWT – Food Science and Technology 40:1018–1026
74. Jaillais B, Morrin V, Downey G (2007) Image processing of outer-product matrices – A new way to classify samples: Examples using visible/NIR/MIR spectral data. Chemometrics and Intelligent Laboratory Systems 86:179–188
75. Esteban-Díez I, González-Sáiz JM, Sáenz-González C, Pizarro C (2007) Coffee varietal differentiation based on near infrared spectroscopy. Talanta 72: 221–229
76. Dubois J, Lewis EN, Fry FS Jr, Calvey EM (2005) Bacterial identification by near-infrared chemical imaging of food-specific cards. Food Microbiology 22:577–583
77. Bin Chen, Xi-guang Fu, Dao-li Lu (2002) Improvement of predicting precision of oil content in instant noodles by using wavelet transforms to treat near-infrared spectroscopy. J Food Engineering 53:373–376
78. Ahmed FE (2002) Detection of genetically modified organisms in foods. Trends in Biotechnology 20: 215–223
79. McCaig TN (2002) Extending the use of visible/near-infrared reflectance spectrophotometers to measure colour of food and agricultural products. Food Research International 35:731–736
80. Jin-hwan Hong, Sakiyo Yamaoka-Koseki, Yoshinobu Tsujii, Kyoden Yasumoto (1997) Applicability of Near-infrared Spectroscopic Method to Unfreezable Water Measurements in Egg White Lysozyme and Soluble Starch. Lebensmittel-Wissenschaft und-Technologie 30:406–410
81. Hijnen WAM, Beerendonk EF, Medema GJ (2006) Inactivation credit of UV radiation for viruses, bacteria and protozoan (oo)cysts in water: A review. Water Research 40:3–22
82. Betancourt WQ, Rose JB (2004) Drinking water treatment processes for removal of Cryptosporidium and Giardia. Veterinary Parasitology 126:219–234
83. Mai Thu Thi Tran, Farid M (2004) Ultraviolet treatment of orange juice. Innovative Food Science & Emerging Technologies 5:495–502
84. Koutchma T, Keller S, Chirtel S, Parisi B (2004) Ultraviolet disinfection of juice products in laminar and turbulent flow reactors. Innovative Food Science & Emerging Technologies 5:179–189

85. Labas MD, Brandi RJ, Martín CA, Cassano AE (2006) Kinetics of bacteria inactivation employing UV radiation under clear water conditions. Chem Eng J 121:135–145
86. Meunier L, Canonica S, von Gunten U (2006) Implications of sequential use of UV and ozone for drinking water quality. Water Research 40: 864–1876
87. Marquenie D, Geeraerd AH, Lammertyn J, Soontjens C, Van Impe JF, Michiels CW, Nicolaï BM (2003) Combinations of pulsed white light and UV-C or mild heat treatment to inactivate conidia of Botrytis cinerea and Monilia fructigena. Intern J Food Microbiology 85:185–196
88. Krishnamurthy K, Demirci A, Irudayaraj JM (2004) Milk pasteurization by pulsed UV-light treatment. ASAE Annual Meeting, American Society of Agricultural and Biological Engineers 2004, paper number 046048
89. Sutly JP, Miles RD, Comer CW, Balaban MO (2001) The influence of UV on pigmentation of brown-shelled eggs. Poult Sci 80:1039
90. Labas MD, Martín CA, Cassano AE (2005) Kinetics of bacteria disinfection with UV radiation in an absorbing and nutritious medium. Chem Eng J 114:87–97

12 Acoustical Properties

Acoustical properties are those that govern how materials respond to sound waves, which are what we perceive as sound. We are all familiar with how a disturbance in a body of water will cause waves to develop and travel along the surface of the water in all directions away from the disturbance. Air is also a fluid and responds to a disturbance in the same way, by creating air waves that travel in all directions away from the disturbance. Just as with waves on the surface of water, these air waves are peaks and valleys of relatively high and low pressure that can be sensed as oscillations of air pressure at a given frequency. When this frequency is in the range between 16 Hz up to about 16,000 Hz (16 kHz) these oscillating air waves are sensed by the human ear as audible sound. Sound with higher frequencies is called ultrasound, and at frequencies above 10^9 Hz it is called hyper sound (Table 12.1).

Table 12.1. Terms used for sound at different frequencies

term	frequency
infra sound	0–16 Hz
audible sound	16 Hz – 16 kHz
ultra sound	20 kHz – 10 GHz
hyper sound	10^9–10^{12} Hz

12.1 Sound

Sound waves are propagated through a material medium in the form of mechanical longitudinal waves. All materials are capable of transmitting sound waves if they have any degree of elasticity (elastic bonds between molecules). This is true of most materials (see YOUNG's modulus of elasticity in Section 4.1). Therefore, sound can be transmitted through gases like air, as well as through liquids and solids.

Sound waves can be generated by a mechanical disturbance, such as when we turn on a machine with moving parts that will make the air vibrate at a given frequency. These air vibrations are the sound waves that travel (propagate) in all directions. If we are standing nearby, these sound waves will strike our

ear drums and cause them to vibrate at the same frequency because of the oscillating air pressure. Our human ear senses the vibrations in our ear drums and transmits these vibrations through the inner ear as nerve signals to our brain. When this happens, we hear sound. This process also means that, in order for sound to occur, there must be a medium of some material substance (gas, liquid, solid) between the source and the receiver (the machine and our ear) in order for sound waves to be generated and transmitted. That is why sound does not exist in a vacuum.

Therefore, sound cannot be transmitted within in a vacuum chamber or in outer space. However, there is technology available that makes it possible to transfer mechanical vibrations from a sending source directly into the inner ear of a person without a substance medium in between.

12.1.1 Speed of Sound

The speed of sound depends on the coupling or bonding strength between the oscillating molecules or atoms within the material medium through which the sound waves are being transmitted. This bonding strength is much greater in solids than in liquids and greater in liquids than in gases where molecules have little interaction. For this reason, sound waves travel much faster in solids than in liquids, and faster in liquids than in gases. A comparison of some data is shown in Table 12.2.

Because this coupling or bonding strength is very weak in gases, the speed of sound through a gaseous medium depends more on how close together the molecules are. The distance between molecules in a gas will depend on its density, which will be a function of pressure and temperature. Therefore, the speed of sound in air depends on its density, which in turn will depend on temperature and pressure, as well as humidity (Table 12.3). To calculate the density of air, refer to Example 2.1.

There are different terms by which we characterize the various features of sound. We will define these here and explain how they are used. First is sound power. This is the quantity of energy flow transmitted by the source of the sound waves. Typical sound power levels for various sound sources are listed in Table 12.4.

Table 12.2. Speed of sound, examples (15 °C, 101.3 kPa [106])

material	$v/\mathrm{m \cdot s^{-1}}$
iron	5170
lead	1250
water	1464
hydrogen	1284
oxygen	316
air	331

Table 12.3. Speed of sound in air, temperature dependency

material	$\vartheta/°\mathrm{C}$	$v/\mathrm{m \cdot s^{-1}}$
dry air	–20	319
dry air	0	331
dry air	20	344
dry air	100	387
water vapor	130	450

Table 12.4. Typical sound power from various sources [106]

	sound power
refrigerator	10^{-7} W
normal talking	10^{-5} W
human voice, maximum	$2 \cdot 10^{-3}$ W
trumpet	0.3 W
auto horn	5 W
75-piece orchestra	70 W
loud speaker at rock concert	$> 10^{2}$ W
siren	$> 10^{3}$ W
rocket engine	10^{6} W

Another term is the particle velocity within each sound wave as it propagates. This is the velocity of each molecule or atom as it oscillates back and forth within the moving wave. This is not the same as the speed of sound or wave speed.

In acoustics, we often refer to relative levels of sound. These levels are generally quantified by taking the logarithms of the ratio of a given sound quantity to a reference quantity. Although different reference quantities can be used, the minimum quantity which a normal human ear can sense is taken as a reference quantity in most cases. These levels have no units, but they are given the name decibel (dB). Table 12.5 shows some definitions of important levels. The definitions and reference quantities are specified in published standards, e.g. [1–3].

Sound intensity is a measure of the amount of sound power per unit area, and can be expressed as the quotient of the incremental sound power dP that is transmitted across an incremental area dA, which is perpendicular to the direction of the energy flow P.

$$I = \frac{\mathrm{d}P}{\mathrm{d}A} \tag{12.1}$$

Another term, sound pressure, quantifies the amplitude of the pressure oscillations, and is given SI units of Pa.

The speed of a pressure signal in a material in general is:

$$c = \sqrt{\frac{K}{\rho}} \tag{12.2}$$

For a gas that can be assumed an ideal gas, we can express the bulk modulus K by:

$$K = \kappa \cdot p \tag{12.3}$$

So, we have:

$$c = \sqrt{\frac{\kappa \cdot p}{\rho}} \tag{12.4}$$

and with:

$$p \cdot V = m \cdot R_s \cdot T \tag{2.10}$$

this is the same as:

$$\rho = \frac{p}{R_S T} \tag{2.10}$$

We obtain

$$c = \sqrt{\frac{\kappa \cdot p}{p} \cdot R_S \cdot T} \tag{12.5}$$

or

$$c = \sqrt{\kappa \cdot R_S \cdot T} \tag{12.6}$$

where

p	pressure in Pa
κ	isentropic exponent
K	bulk modulus in Pa
R_s	specific gas constant in $\mathrm{J \cdot K^{-1} \cdot kg^{-1}}$
m	mass in kg
ρ	density in $\mathrm{kg \cdot m^{-3}}$
T	temperature in K
ϑ	temperature in °C

Example 12.1. Speed of sound in air
According to equation (12.6) for air at 22 °C with $\kappa = 1.4$ and $R_S = 287\,\mathrm{J \cdot kg^{-1} \cdot K^{-1}}$ we get

$$c_L = \sqrt{1.4 \cdot 287\,\mathrm{J \cdot kg^{-1} \cdot K^{-1}} \cdot 295.15\,\mathrm{K}} = \sqrt{118591\,\mathrm{N \cdot m \cdot kg^{-1}}} = 344.3\,\mathrm{m \cdot s^{-1}}$$

As an approximation for the speed of sound in air in the range of −20 °C to 40 °C from published literature, we can use the following rule of thumb: $c_L/\mathrm{m \cdot s^{-1}} = 331.5 + 0.6\,\vartheta/^{\circ}\mathrm{C}$.

Table 12.5 gives definitions and reference quantities for different sound levels.

Table 12.5. Definition and reference quantity of sound levels

sound level (in dB)	definition	reference quantity
sound pressure level	$L_p = 20 \cdot \lg \frac{p}{p_0}$	$p_0 = 2 \cdot 10^{-5}\mathrm{Pa}$
sound velocity level (particle velocity level)	$L_v = 20 \cdot \lg \frac{v}{v_0}$	$v_0 = 5 \cdot 10^{-8}\mathrm{m \cdot s^{-1}}$
sound intensity level	$L_I = 10 \cdot \lg \frac{I}{I_0}$	$I_0 = 10^{-12}\mathrm{W \cdot m^{-2}}$
sound power level	$L_P = 10 \cdot \lg \frac{P}{P_0}$	$P_0 = 10^{-12}\mathrm{W}$

12.1.2 Loudness and Volume

The combination of amplitude (sound pressure) and frequency of a sound wave is what is responsible for what we perceive as loudness of a sound. The sensitivity of the human ear to loudness of a sound is based on the sound pressure and the frequency of the sound. In order to establish a technical measure for loudness, the sound pressure level at a frequency of 1000 Hz is that what we call loudness L_S. Relative loudness is also quantified as a loudness level, and is scaled in phon. So, loudness is:

$$L_S = 20 \cdot \lg \frac{p}{p_0} \text{ phon} \tag{12.7}$$

At a frequency of 1000 Hz the value of the sound pressure level and the loudness are the same. The human ear may be more sensitive at another frequency, such that a lower sound pressure level at that frequency could cause the same perception of loudness. This phenomenon can be illustrated in equal-loudness contours which have been established in international standards for average persons (see, e.g. [4]).

Because the loudness of sound is a matter of human perception, different types of sounds or noises are sensed differently. In order to take these differences into account in measuring loudness, so-called weighing curves have been introduced. For example, the A-weighting curve is used to measure environmental noise and industrial noise, B- and C-curves for louder sounds, and the D-curve for assessing loud aircraft noise [4]. Examples of loudness levels are listed in Table 12.6.

It should be noted that the minimum sound pressure that can be sensed by a human ear (which is used as a reference in calculating the loudness level) also depends on the frequency of the sound waves, as well as the age and health of the person.

Table 12.6. Values of loudness levels [5]

	L_s/phon
detection threshold	0
ticking watch	12
backyard garden	20
normal speech (1 m)	65
heavy traffic (7 m)	80
automobile horn	90
jet aircraft (200 m)	115
pain limit	130

12.1.3 Noise

Up to this point we have learned to understand sound waves as simple oscillations of air pressure with a given frequency, wavelength and speed. When simple sound waves of this type reach our ear, we perceive the sound to be like a tone in music. Several distinct tones being received at the same time together is perceived as what we call a clang. When we receive sound which contains a continuous range of frequencies, it is called noise.

A noise can be typical and expected for a given process, and can be used to analyze or to characterize the process. For example, noises like cracking, crushing, popping, crackling, sizzling, frizzling and detonating can be an expected characteristic for a given process or event. Such noises are time dependent combinations of tones with different intensities.

When we wish to characterize a food material for purposes of consumer perception, we sometimes use terms about the acoustic information provided by taste panelists during taste testing. Imagine if you bite on a crisp or crusty food and try to describe the crispiness: To a great extent, our perception of crispiness is taken from the sound that is made in our mouth. A person without an acoustic sense would not be able to describe food like this. Such a person would have to rely on dental sensations coming from the teeth breaking or crushing the food item. Unfortunately, our dental roots are not very sensitive to such relatively mild forces in crushing foods, they normally start to respond when we bite on a stone or bone.

So, perception of sound can be used as a descriptor of the textural quality of food. For example, the noise we hear when biting may give us information about the freshness of vegetables or about how well cooked they are. In order to develop methods for acoustic characterization of a material, first the process of biting, breaking, chewing, shaking, etc. has to be standardized, and then the resulting noise has to be measured and analyzed for its acoustic spectrum which is a plot of intensity versus frequency.

Excessive noise is that type of noise which is disturbing and can impair our health. Low frequencies enhance the feeling of being disturbed by noise. Permanent high levels of sound pressure can lead to increasing the minimum sound level a person can hear (audibility) at different frequencies and can result in losing the perception of noises at all.

Such dangerously permanent high levels of sound pressure can occur in food processing factories where heavy machinery is operating continuously. These types of industrial situations require hearing protection for the factory workers. This is often accomplished by design of machinery housing, automation to the extent workers are not needed on the factory floor or by having the workers wearing ear protection.

12.2 Ultrasonic Sound

Sound with high frequencies in the range between 20 kHz and 10 GHz is beyond the range of frequencies that can be detected by the human ear, and is called ultrasonic sound or ultrasound. Recall the expression for speed of sound as a function of frequency and wavelength:

$$c = \lambda \cdot f \tag{10.28}$$

where

c	wave speed in $\mathrm{m} \cdot \mathrm{s}^{-1}$
λ	wavelength in m
f	frequency in Hz

When we know the speed of sound in air, water and solids we can calculate the range of wavelengths to be expected in the ultrasonic range of frequencies. For example, the speed of sound in air is about $c = 300\ \mathrm{m} \cdot \mathrm{s}^{-1}$, so we have ultrasonic wavelengths between 33 nm and 1.6 cm. The speed of sound in water is about $c = 1400\ \mathrm{m} \cdot \mathrm{s}^{-1}$, so we have wavelengths between 0.1 µm and 7 cm. In solids the speed of sound is about $c = 4000\ \mathrm{m} \cdot \mathrm{s}^{-1}$ and ultrasonic wavelengths will be between 0.4 µm and 20 cm. These calculations reveal that the shortest ultrasonic waves are in the same range as visible electromagnetic waves (see Table 10.2). So, it is not surprising that ultrasound shows phenomena like refraction, diffraction and reflection, just as light rays. Although ultrasound is not audible to the human ear, it has many useful industrial and technical applications, such as those listed in Table 12.7.

Ultrasound for technical purposes is normally produced with electric oscillators based on the inverse piezoelectric effect which is called magnetostriction. The efficacy of ultrasound applications is largely due to the high accelerations reached by molecules in an ultrasonic field. These accelerations can reach between $10^3 \cdot \mathrm{g}$ and $10^6 \cdot \mathrm{g}$ (multiples of the Earth's gravitational acceleration,

Table 12.7. Technical applications of ultrasonic sound, examples [6]

dispersing
emulsifying
cleaning
degassing
polymerization control
drilling
milling
cutting
welding
material testing
medical diagnostics
ranging (SONAR)

see Section 2.1). When applied to liquids, ultrasonic energy can cause the formation of bursting bubbles called cavitation. These bubbles form small cavities in the fluid which implode shortly after they are formed [6]. These imploding bubbles (cavitation) transfer a high level of local energy to the liquid which may cause particle breakage (emulsifying) or material abrasion (dispersion, dissolution, cleaning, etc.).

Scattering of ultrasonic waves is used in medical diagnostics. The echo of a pulsed signal can be used for imaging inner parts of the human body. Ultrasound waves are not ionizing radiation like X-rays, so little or no shielding is required. In food technology, ultrasound scattering can be used in such applications as for particle sizing and imaging of flow [12–16].

Other applications are based on the measurement of ultrasound wave run times. From these time measurements distances can be measured and translated into filling levels of liquids and bulk goods in containers, or to find fish swarms in the ocean, or to monitor water depth (SONAR). Ultrasound can also be used to measure liquid flow rates through pipes and tubes. For online flow sensors based on ultrasonics see Section 14.3.4.

12.3 Applications

grain: acoustic measurement of moisture	[6]
apple: firmness measurement by acoustics	[7]
Bendix ultrasound viscometer: for NEWTONian fluid up to 50 Pa · s	[8]
particle sizing in emulsions by acoustic spectroscopy	[9]
foam characterization by acoustic impedance	[10]
freezing of food: ultrasonic monitoring	[11]
chicken nuggets: crispiness, texture and moisture by ultrasound analysis	[12]
sol–gel transition of κ-carrageenen and pectin by ultrasound and oscillation rheology	[13]
meat and fish: composition estimation by ultrasound	[14,15]
honey: ultrasound analysis	[16]
foods and drinks: ultrasound characterization	[17]
chocolate: rheological properties by ultrasound scattering technique	[18,19]
particle size measurement by ultrasonic spectroscopy	[20–22]
crispy foods: acoustic emission in texture characterization	[23]
machine operation: monitoring acoustic emission of running machinery	[24,25]
noncontact electromagnetic acoustic transducers for drink can inspection	[26]
ultrasonically assisted polysaccharides extraction from plant material	[27]
plum: ultrasonics fruit quality assessment	[28]

Literature

1. DIN 5493 (1994) Logarithmic quantities and units, in [101]
2. DIN EN 21683 (1994) Acoustics – Preferred reference quantities for acoustic levels, in [101]
3. DIN EN ISO 389 (2000) Acoustics – Reference zero for the calibration of audiometric equipment, in [101]
4. DIN ISO 226 (2006) Acoustics – Normal equal-loudness-level contours, in [101]
5. Crocker M (ed) (1997) Encyclopedia of Acoustics. Wiley VCH, Weinheim
6. Friesen TL, Brusewitz GH, Lowery RL (1988) An acoustic method of measuring moisture content in grain. J Agricultural Engineering Research 39:49–56
7. Duprat F, Grotte M, Pietri E, Loonis D (1997) Impulse Response Method for Measuring the Overall Firmness of Fruit. J Agricultural Engineering Research 66:251–259
8. Laszlo H (1985) Fachlexikon ABC Messtechnik, VEB Fachbuchverlag, Leipzig p. 478
9. Babick F, Ripperger S (2002) Schallspektroskopische Bestimmung von Partikelgrößenverteilungen submikroner Emulsionen. Filtrieren and Separieren 16:311–313
10. Kulmyrzaev A, Cancelliere C, McClements DJ (2000) Characterization of aerated foods using ultrasonic reflectance spectroscopy. J Food Engineering 46:235–241
11. Sigfusson H, Ziegler GR, Coupland JN (2004) Ultrasonic monitoring of food freezing. J Food Engineering 62:263–269
12. Anatoria I, Mallikarjun P, Duncan SE (2003) Correlating objective measurements of crispness of breaded chicken nuggets with sensory crispness. J Food Sci 68:1308–1315
13. Toubal M, Nongaillard B, Radziszewski E, Boulenguer B, Langendorff V (2003) Ultrasonic monitoring of sol–gel transition of natural hydrocolloids. J Food Engineering 58:1–4
14. Simal S, Benedito J, Clemente G, Femenia A, Rosselló C (2003) Ultrasonic determination of the composition of a meat-based product. J Food Engineering 58:253–257
15. Ghaedian R, Coupland JN, Decker EA, McClements DJ (1998) Ultrasonic determination of fish composition. J Food Engineering 35:323–337
16. Kulmyrzaev A, McClements DJ (2000) High frequency dynamic shear rheology of honey. J Food Engineering 45:219–224
17. McClements DJ (1997) Ultrasonic characterization of foods and drinks: principles, methods, and applications. Crit Rev Food Sci Nutr 37:1–46
18. Windhab E, Ouriev B (2003) Novel ultrasound based time averaged flow mapping method for die entry visualization in flow of highly concentrated shear-thinning and shear-thickening suspensions. Meas. Sci. Technol. 14:140–147
19. Windhab E, Ouriev B, Braun P, Birkhofer B (2004) Industrial application of ultrasound based in-line rheometry: From stationary to pulsating pipe flow of chocolate suspension in precrystallization process. Rev. Sci Instrum. 75:3164–3168
20. Goodenough TIJ, Rajendram VS, Meyer S, Pretre D (2005) Development of a multi frequency pulse diagnostic ultrasound device. Ultrasonics 43:165–71
21. Goodenough TIJ, Rajendram VS, Meyer S, Prêtre D (2005) Detection and quantification of insoluble particles by ultrasound spectroscopy. Ultrasonics 43:231–235
22. Meyer S, Berrut S, Goodenough TIJ, RajendramVS, Pinfield VJ, Povey MJW (2006) A comparative study of ultrasound and laser light diffraction techniques for particle size determination in dairy beverages. Meas. Sci. Technol. 17:289–297
23. Luyten JMJG, van Vliet T (2006) Acoustic emission, fracture behavior and morphology of dry crispy foods: a discussion article. J Texture Studies 37:221–240
24. Brown ER, Reuben RL, Neill GD, Steel, JA (1999) Acoustic emission source discrimination using a piezopolymer based sensor. Materials Evaluation 57:515–520

25. Tönshoff HK, Jung M, Männel S, Rietz W (2000) Using acoustic emission signals for monitoring of production processes. Ultrasonics 37:681–686
26. Ho KS, Billson DR, Hutchins DA (2007) Inspection of drinks cans using non-contact electromagnetic acoustic transducers. J Food Eng 80:431–444
27. Jin-wei Li, Shao-dong Ding, Xiao-lin Ding (2007) Optimization of the ultrasonically assisted extraction of polysaccharides from Zizyphus jujuba cv. jinsixiaozao. J Food Engineering 80: 176–183
28. Mizrach A (2004) Assessing plum fruit quality attributes with an ultrasonic method. Food Res Intern 37:627–631

13 Radioactivity

Radioactivity in a material is evident by its ability to emit high energy radiation. Recall a chemical element consists of isotopes which are atoms with the same number in protons but different number in neutrons in the atomic nucleus. Some isotopes have an imbalance between the number of protons and neutrons in the atomic nucleus which puts them in a perpetual state of imbalance "activity," in which they emit high energy particles or radiation. This activity is called radioactivity.

An example is the element carbon with normal atomic mass of 12 ($^{12}_{6}$C) and carbon 13 ($^{13}_{6}$C) with the same atomic number, but higher atomic mass. They are both the same chemical element, carbon, but $^{13}_{6}$C is an unstable isotope, while $^{12}_{6}$C is not. Unstable isotopes are capable of a transformation in which they become "excited" or "active" without external influences, and are able to transmit high-energy radiation. If the isotopes descend from a natural element in nature, this is called natural radioactivity. Whereas, radioactivity induced from isotopes fabricated by nuclear transformations, is called artificial radioactivity.

Natural radioactivity was first discovered in the year 1896 by H.A. Becquerel, during his investigations of Uranium salts, which possess a specific radiation. In our environment more than 40 different natural radioactive isotopes are known, such as ^{14}C and ^{40}K. Isotopes with an atomic number above 83 are essentially always radioactive. The following sections concentrate on natural radioactivity, especially in application to foods.

13.1 Types of Radiation

The emission of particles based on two neutrons and two protons is called α-radiation. During this α-decay, α-particles are emitted, which consist of positive charged particles with a comparatively low velocity and range respectively. If electrons and positrons are also emitted with the decay, the resulting radiation is called β-radiation. These β-particles possess a velocity comparable to the speed of light. In addition they show a high range. A third type of radiation is called γ-radiation, which consists of a quantum of high energy, electromagnetic radiation with frequency above that of the X-rays (see Table 10.2). Radioactive substances, which emit primarily α-radiation, are called

Table 13.1. Types of radioactive radiation

type	description	electric charge	example
α-radiation	emission of slow He nuclei	2+	α (Ra), 4.9 MeV range in air: few cm
β-radiation	emission of fast electrons or positrons	1– or 1+	$\beta(^{40}\mathrm{K})$, 1.4 MeV range in air: few m
γ-radiation	emission of high energy (γ-quanta)	0	wavelength < 10 pm some keV to MeV per quantum range in air: few 100 m
neutron radiation	emission of neutrons	0	

α-radiators. Likewise, those that primarily emit β or γ radiation are called β-radiators and γ-radiators, respectively.

Radiation coming from the nucleus of atoms will generate and energize secondary particles through bombardment while in transit through a radioactive radiation. These secondary particles become likewise charged particles as a result of the bombardment, and become new charge carriers while the initial incident particles disappear (α-particles by transformation into H-atoms, and β-particles by electron capture). Because of this radioactive radiation is called ionizing radiation.

The α-particles have a strong ionizing effect on their nearby surroundings, which hinders their movement and limits their range of action. However, β-particles move with greater energy and generate secondary particles continuously, giving them a longer range of action. The very longest range of action is possessed by the γ-particles, because of their high energy and electromagnetic frequency above that of X-rays. These wide differences in range of action translate into wide differences in the degree to which each type of radiation will be absorbed by a material, as well as by the absorbency of the material to each respective type of radiation. The ranges of action of each of these three types of radiation in air, water, metal or biological substances are summarized in Table 13.1.

13.2 Radioactive Decay

Recall that radioactive materials constantly emit high energy in an attempt to reduce their imbalance between the number of protons and neutrons in their atomic nucleus. Because of this constant emission, the radioactivity of these materials will slowly and gradually decay in strength over time. We have to know the rate of decay in order to predict the radioactivity (radiation intensity) of the isotope. When radioactive materials are to be used as the source of radiation in a controlled process, it is necessary to take into account the rate at which they will decay in order to design the process effectively.

The radioactive transformation of a nucleus proceeds in a spontaneous way, meaning that it takes place without any recognizable external influence. This makes it difficult to calculate the decay for separate individual single atoms. It is only possible to calculate the decay for a large amount of atomic nucleus material with the help of statistical methods. Repeated observations have shown that the decay rate is proportional to the amount of available nucleus. Gradually, the amount of the available nucleus decreases over time, decreasing the intensity of the radioactive radiation with it. This is called radioactive decay. It is not possible to have radioactivity without accompanying decay. Also, the rate of decay is directly related to the intensity of radiation. Radioactive materials with the highest rate of decay are also those which emit radiation with the highest intensity. Recall the decay rate is a function of the amount of nucleus material (number of atoms), and this amount is decreasing over time Therefore, the rate of decay will also be decreasing over time at a slower and slower rate, and can be described mathematically as an exponential decay of the first order:

With a decay rate proportional to the number of atoms N we have:

$$-\frac{\mathrm{d}N}{\mathrm{d}t} = \lambda \cdot N \tag{13.1}$$

with the decay constant

$$\lambda = \frac{-\frac{\mathrm{d}N}{\mathrm{d}t}}{N} \tag{13.2}$$

and the activity of the sample

$$A = -\frac{\mathrm{d}N}{\mathrm{d}t} = N \cdot \lambda \tag{13.3}$$

Calculating the actual number of atoms yields

$$\int_{N_0}^{N} -\frac{\mathrm{d}N}{n} = \lambda \int_{t=0}^{t} \mathrm{d}t \tag{13.4}$$

$$-(\ln N - \ln N_0) = \lambda(t - 0) \tag{13.5}$$

$$\ln \frac{N}{N_0} = \lambda \cdot t \tag{13.6}$$

i.e.

$$N = N_0 \cdot e^{-\lambda \cdot t} \tag{13.7}$$

where

N	number of atoms
N_0	initial number of atoms
A	activity in Bq
λ	decay rate constant in s^{-1}
$T_{1/2}$	half life time in s or d or y

m mass in kg
M molar mass in $kg \cdot mol^{-1}$
N_A Avogadro's number

The activity A is a measure of the radiation intensity (rate of decay at any given moment), and is given the units of Becquerel (Bq), in which $1Bq = 1s^{-1}$. Therefore, an activity of 10^3 Bq stands for 1000 decays per second. Thus, a high level of activity is associated with a high rate of decay. Substances with a low decay rate constant will need much longer time before their radioactivity diminishes to the same degree as a material with higher decay rate constant. In order to easily quantify the decay rate for ease of comparison between materials, as well as for process design calculations, the unit of half-life $T_{1/2}$ has been introduced. This is simply the time needed for the radiation intensity (activity) from a radioactive material to decay to a level of one-half of the initial intensity. Therefore, materials with longer half-lives decay more slowly than those with shorter half-lives. The half-life of materials ranges from seconds to thousands of years.

To reach one-half of the initial number of nuclei

$$N = \frac{N_0}{2} \tag{13.8}$$

The time t is called $T_{1/2}$:

$$-T_{1/2} \cdot \lambda = \ln \frac{N}{N_0} = \ln \frac{1}{2} \tag{13.9}$$

so

$$T_{1/2} = \frac{\ln 2}{\lambda} \tag{13.10}$$

or

$$T_{1/2} = -\ln \frac{1}{2} \cdot \frac{1}{\lambda} \tag{13.10}$$

A quantity derived from activity is the so-called specific activity. It is simply the activity per unit mass of material, and can be expressed as the quotient of the activity A of a substance and its mass m. In the case of a totally pure isotope sample with mass m, which possesses N radioactive nuclei, it is possible to calculate the specific activity a based on the activity A:

$$a = \frac{A}{m} = \frac{\lambda \cdot N}{m} = \frac{\lambda \cdot n \cdot N_A}{n \cdot M} = \lambda \cdot \frac{N_A}{M} \tag{13.11}$$

The specific activity a will have the SI unit of $Bq \cdot kg^{-1}$. In the case of substances which are mixtures of radioactive and nonradioactive isotopes of identical elements, the specific activity of the mixture will be the quotient of the activity and the mass of the whole mixture.

The onset of radioactivity in an isotope (radioactive transformation) brings with it the development of very high energy levels that evolve over long periods of time. For example, the radioactivity from one gram of radium creates an

Table 13.2. Decay constant λ and half life time $T_{1/2}$ of some radioactive materials [1]

Isotope	$T_{1/2}$	λ/s^{-1}
^{40}K	$1.25 \cdot 10^9$ y	$1.8 \cdot 10^{-17}$
^{14}C	5730 y	$3.8 \cdot 10^{-12}$
^{226}Ra	1580 y	$1.4 \cdot 10^{-11}$
^{137}Cs	30 y	$7.3 \cdot 10^{-10}$
^{90}Sr	28.1 y	$7.8 \cdot 10^{-10}$
^{131}I	8.05 d	$1 \cdot 10^{-6}$

energy output of $1.2 \cdot 10^7$ kJ. In comparison, combustion of one gram of carbon creates an energy output of only 32 kJ and referring to combustion energy of food (see Section 7.8.2) we learned that one gram of sugar provides the body of a consumer with 17 kJ.

As explained earlier, the half-life is the time after which half of the initial number of atoms is decayed. Table 13.2 shows some examples.

13.3 Measurement of Ionizing Radiation (α-, β-, γ-)

The evidence and quantitative determination of radioactive radiation is based on the ability for detecting the effects produced by the radiation. Usually this is approached by determining the amount of ions produced with the help of ionization detectors (also: excitation detectors). For differentiating between α-, β- and γ-radiation, it is possible to filter the radiation before entry into the ionization detector. For this purpose, electric and magnetic fields which deflect the charged α-particles and β-particles with the help of COULOMB's force and

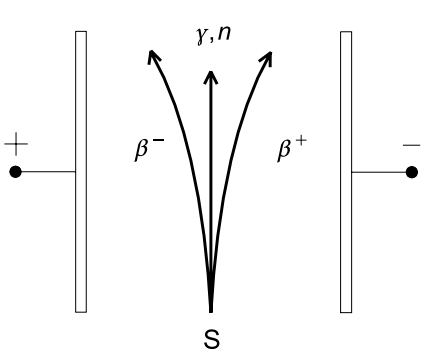

Figure 13.1. Separation of different types of radioactive radiation in an electric field

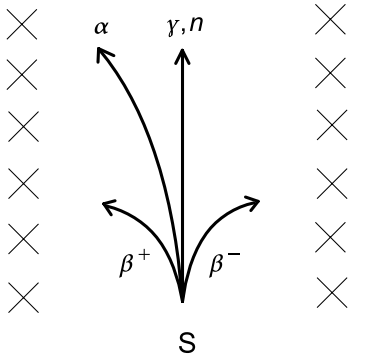

Figure 13.2. Separation of different types of radioactive radiation in a magnetic field. Crosses indicate the backside of a magnetic field vector

LORENTZ's force respectively, are used. But, these fields do not influence gamma radiation (γ-quantum). In the presence of an electric field, it is possible to separate electrons (β^-) and positrons (β^+) from each other, and differentiate them from γ-radiation (see Figure 13.1). In a magnetic field, the LORENTZ force has an effect on charged particles (see Section 9.2.1). Depending on the charge number, sign of the charge, and the velocity of the particles, the particles will deflect in a different way (see Figure 13.2).

Another possibility is selective absorption with appropriate materials. It is possible to block α-radiation for instance with a sheet of cardboard, whereas the differentiation between β- and γ-radiation is only possible with the use of metal sheets of different thickness (depending on the energy of the radiation) across which only the γ-radiation will pass, but the β-radiation will not.

Counter Tube

In a so-called counting gas, such as noble gases (He, Ne, Ar), ions are produced by the passing radiation (primary ionization). Within a strong electric field, these ions generate further ions by impact ionization (secondary ionization). These secondary generated electrons are able to excite further gas atoms and to dissolve photoelectrons out of the wall-material of the counting tube. Because of this effect, an avalanche of electrons develops, which is measurable by a short pulse of electric current. If the electric potential in the counting tube is small enough, the measurable avalanche of electrons is proportional to the amount of primary generated electrons. A counting tube, which works like this, is called a proportional counting tube.

By increasing the electric voltage within the counting tube, a separation of the electrons and positive charged ions takes place because of the different mobility of these two kinds of charge carriers. The remaining positively charged space prevents the production of further avalanches of electrons. As a result, there exists a so-called dead time in the counting tube. This effect can be diminished with the help of a "quenching gas" like ethanol vapor. The quenching gas absorbs ions and photons without generating secondary electrons. Now each ion pair generates an avalanche of electrons, an example of this principle is the GEIGER–MÜLLER counting tube (GEIGER counter).

Semiconductor Detectors

The ions, produced by the radioactive radiation, lead to a countable voltage pulse if they are present in a semiconductor detector. For example, this can be used on transitions in lithium-doped germanium-detectors (for the use on γ-radiation) and lithium-doped silicon detectors (for use on X-ray radiation) and nondoped pure-germanium detectors. It is possible to determine the energy of γ-quantum by the use of semiconductor detectors. As a result of this, it is possible to determine the decay of a nucleus, to count the decays and to get information about the energy spectrum of the radiation (see Figure 13.3). With this spectrum it is possible to draw conclusions about the kind and background

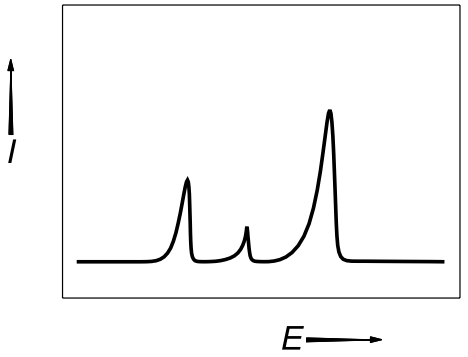

Figure 13.3. Energy spectrum of radioactive radiation (schematic). The intensity is plotted versus the energy of the γ-quanta

of the radiation and as a result of this, about the radiation source [2]. If any radioactive contamination is present in foods, clarification about the kind and source of the radionuclides is an important point.

In so-called excitation detectors, the result of the irradiation from a so-called scintillator is the emission of a light pulse. This light emission is strengthened and counted by a photo-secondary-ion-multiplier. Several types of crystals can be used in scintillators (anthracen for β-radiation, ZnS/Ag for α-radiation, NaI/Tl for γ-radiation), as well as liquids and glasses (e.g. Li-containing glasses for use on slow neutrons). However, the energy resulting from NaI/Tl-scintillation detectors is not as high as that from semiconductor detectors. Liquid scintillator materials can be mixed with the sample and measured in vessels. During this measurement, there is no loss of absorption between the sample and the scintillator. That is why this method is advantageous for low-energy radiation (e.g. ^{14}C).

13.4 Natural Radioactivity

Natural potassium consists mainly of the stable isotopes ^{39}K and ^{41}K, and to a lesser extent of the unstable (radioactive) isotopes ^{40}K, ^{42}K and ^{42}K. In Table 13.3 the natural frequencies with which these particular isotopes occur are listed. Because of the short half-life of the isotopes ^{42}K and ^{42}K, these two isotopes are virtually extinct, and the frequency of their occurrence is listed as 0%.

Table 13.3. Isotopes of Potassium and its half-life $T_{1/2}$

isotope	natural occurrence in %	$T_{1/2}$
K	93.2581	stable
^{40}K	0.0117	$1.25 \cdot 10^9$ a
^{41}K	6.7302	stable
^{42}K	≈ 0	12.36 h
^{43}K	≈ 0	22.3 h

Table 13.4. Natural radio nuclides in the human body and their activities

nuclide	activity in Bq
^{40}K	4500
^{14}C	3800
^{87}Rb	650
^{210}Pb	< 100
^{210}Bi	< 100
^{210}Po	< 100
^{3}H	< 100
^{7}Be	< 100
Rn decay products	< 100
total	$\approx$ 10,000

Because of breathing and food uptake the human body also contains radioactive isotopes, e.g. natural ^{40}K. That is why the human body possesses a specific radioactivity of about 130 Bq $\cdot$ kg^{-1} in an average size person [112]. That means that the human body emits an amount of radioactivity in the magnitude of 10,000 Bq. Table 13.4 compares the contribution of a particular isotope to this amount.

Example 13.1. How much radioactive Potassium is in the human body?
Consider potassium in our body, and calculate how much radioactivity is emitted by 1 gram. Using

$$n = \frac{m}{M} \tag{13.12}$$

with the mean molar mass of potassium of

$$M = 39.1\,\mathrm{g}\cdot\mathrm{mol}^{-1}$$

we can calculate the number of moles to be;

$$n = \frac{1\,\mathrm{g}}{39.1\,\mathrm{g}\cdot\mathrm{mol}^{-1}} = 0.0256\,\mathrm{mol}$$

with

$$N = n \cdot N_A \tag{13.13}$$

We get the number of atoms in 1 g

$$N = 0.0256\,\mathrm{mol}\cdot 6.022\cdot 10^{23}\,\mathrm{atoms}\cdot\mathrm{mol}^{-1} = 1.5\cdot 10^{22}\,\mathrm{atoms}$$

Out of this amount of K-atoms, 0.0117% are ^{40}K-isotopes (Table 13.3), which means:

$$N(^{40}\mathrm{K}) = 0.000117\cdot 1.5\cdot 10^{22} = 1.8\cdot 10^{18}$$

The decay constant of ^{40}K can be calculated by

$$\lambda = \frac{\ln 2}{T_{1/2}}$$

to be

$$\lambda = \frac{\ln 2}{1.25 \cdot 10^9 \text{a}} = 1.76 \cdot 10^{-17}\,\text{s}^{-1}$$

so the activity of 1g of potassium results in:

$$A = \lambda \cdot N \tag{13.3}$$

which means

$$A = 1.76 \cdot 10^{-17}\,\text{s}^{-1} \cdot 1.8 \cdot 10^{18} = 31.7\,\text{s}^{-1}\,.$$

So we can say the radioactivity of natural potassium is caused mainly by isotope ^{40}K. The specific activity is $a = 31.7\,\text{Bq} \cdot \text{g}^{-1}$.

The content of potassium in the human body is influenced by the age, sex and state of nutrition. The average content is around 2 g per kg body weight. A more exact calculation is possible with the help of the following empirical formula:

	K content c in g per kg body weight
men	$c = 2.38658 - (0.00893 \cdot \text{age in years})$
women	$c = 1.9383 - (0.0675 \cdot \text{age in years})$

In the case of a 30-year old man, the content of potassium is approximately 2.2 g K per kg body weight. That means a specific activity of: $A = 31.7\,\text{Bq} \cdot \text{g}^{-1} \cdot 2.2\,\text{g} \cdot \text{kg}^{-1} = 69.7\,\text{Bq} \cdot \text{kg}^{-1}$. If we assume 70 kg body weight as a basis, the activity based on the K-content of the human body is:

$$\begin{aligned} A &= m \cdot a \\ a &= 70\,\text{kg} \cdot 69.7\,\text{Bq} \cdot \text{kg}^{-1} = 4879\,\text{Bq} \end{aligned} \tag{13.11}$$

The example shows how the contribution to the total activity in a mans body can be calculated (see also Table 13.4). The human body contains other naturally occurring radio nuclide besides ^{40}K. Therefore, natural radiation activity of the human body on a whole is greater than that calculated on the basis of ^{40}K alone, and has been estimated to be as high as 10,000 Bq, according to reports in the literature as shown below from [2,3]:

Materials, which contain a higher K-content than the human body, possess a natural radiation activity that is likewise higher. For example, pure potassium chloride and potash fertilizer possess a specific activity of 16,000 Bq · kg^{-1} (see Table 13.5).

Plants and animals, as well as foods made of these, contain naturally occurring radio nuclides according to their metabolism and position in the food chain, with the main focus on ^{40}K. Based on equilibrium between the daily

Table 13.5. Specific activities a of some materials containing potassium

material	a/Bq · kg^{-1}
milk	40–50
human body	60–130
granite stone	1000
potash fertilizer	16,000

Table 13.6. Radioactivity of some foods [102]

food	a/Bq · kg^{-1}
milk	40–50
milk powder	400–500
fruit juice concentrate	600–800
instant coffee powder	> 1000

nutritional intake of natural radio nuclides and the concomitant daily biological excretion, the amount of natural radioactivity emitted from the human body, as well as animals, plants and foods is largely constant. The average level of radiation activity emitted from most vegetable and animal-based foods is approximately 40–50 Bq · kg^{-1}. Dry products and concentrates possess an amount which is higher because they are concentrated (see Table 13.6).

13.4.1 Exposure to the Human Body

Exposure to ionizing radiation can have serious detrimental effects on the human body, as well as to all forms of living organisms [6]. The quantity of ionizing radiation energy absorbed by the tissue of the body is a decisive factor for calculating the effects of exposure to radioactivity. This absorbed energy is called absorbed dose of ionizing radiation and is calculated by:

$$\text{absorbed dose of ionizing radiation} = \frac{\text{absorbed energy of radiation}}{\text{mass}} \quad (13.14)$$

The absorbed dose of ionizing radiation has the units of J · kg^{-1}. One J · kg^{-1} = 1 Gy (Gray).

Conversion from the previously used unit of rad (radiation absorbed dose) into the unit of Gray is simply a factor of 100. One rad = 10^{-2} Gy, or one Gy = 100 rads. For conversion of units see also Appendix 15.1.

In addition to the amount of absorbed energy from exposure to radiation, it is just as important to take into account the kind of radiation which is being absorbed. For this purpose, a multiplying factor called a quality factor has been introduced. The absorbed dose of ionizing radiation is multiplied by this quality factor in order to calculate the dose equivalent. In Table 13.7 some examples of quality factors are listed. The dose equivalent of the received dose of radiation reflects the effect of the adsorbed dose of ionizing radiation on the human body, regardless of the type of radiation from which it came (X-ray, γ-ray or β-radiation).

$$\text{dose equivalent} = \text{qualityfactor} \cdot \text{absorbed dose of ionizing radiation} \quad (13.15)$$

The unit of the dose equivalent is Sv (Sievert). Conversion from the previously used unit of rem (roentgen equivalent man) into the new unit of Sv is simply a

Table 13.7. Quality factors for different types of radiation [1]

radiation	quality factor
photons (X-ray, γ-radiation)	1
electrons, positrons (β-radiation)	1
neutrons:	
10 keV	5
10 – 100 keV	10
100 keV–2 MeV	5
2 – 20 MeV	20
protons	5–15
α-particles	20

Table 13.8. Terms used in dosimetry

quantity	definition	SI unit	equivalent to
activity	$\frac{\text{number decays}}{\text{time}}$	Bq	s^{-1}
specific activity	$\frac{\text{number decays}}{\text{mass} \cdot \text{time}}$	$Bq \cdot kg^{-1}$	$s^{-1} \cdot kg^{-1}$
energy		J, eV	
absorbed dose of ionizing radiation	$\frac{\text{absorbed energy}}{\text{mass}}$	Gy	$J \cdot kg^{-1}$
power of absorbed dose of ionizing radiation	$\frac{\text{absorbed energy}}{\text{mass} \cdot \text{time}}$	$Gy \cdot s^{-1}$	$J \cdot kg^{-1} \cdot s^{-1}$
dose equivalent	$\frac{\text{absorbed energy} \cdot Q}{\text{mass}}$	Sv	$J \cdot kg^{-1}$
power of dose equivalent	$\frac{\text{absorbed energy} \cdot Q}{\text{mass} \cdot \text{time}}$	$Sv \cdot s^{-1}$	$J \cdot kg^{-1} \cdot s^{-1}$
dose of ionization	$\frac{\text{absorbed charge}}{\text{mass}}$	$C \cdot kg^{-1}$	$A \cdot s \cdot kg^{-1}$
power of dose of ionization	$\frac{\text{absorbed charge}}{\text{mass} \cdot \text{time}}$	$C \cdot kg^{-1} \cdot s^{-1}$	$A \cdot kg^{-1}$

factor of 100. One rem = 10^{-2} Sv, or one Sv = 100 rems (further values for use in dosimetry are given in Table 13.8).

13.4.2 Irradiation of Food and Packaging Material

It is possible to treat foods with ionizing radiation by exposing them to the radiation energy emitted by γ- and β-radiation. This is called food irradiation.

Table 13.9. Effects of ionizing radiation [109]

dose/kGy	effect of radiation
0.005–0.01	lethal for human body
0.05–0.2	Sprout inhibition in potatoes and onions
0.2–0.1	pest control (insect, trichina)
0.5–1	control of ripening in fruits and vegetables
1–10	destroy pathogenic microorganisms (pasteurization)
10–50	sterilization
10–200	inactivation of viruses
20–1,000	inactivation of enzymes

Radiation treatments of this type have been shown to be effective for the purpose of inactivating enzymes, pathogens, yeasts and moulds, and most non-spore-forming bacteria, as well as destructive weeds and sprouting activity. As a result of this efficacy, the safety assurance and shelf life of many food products can be substantially increased by treatment with ionizing radiation. Table 13.9 shows the order of magnitude of the dose of radiation needed to achieve a specific effect. Details concerning the use of this technology and the related regulatory issues can be found in references [1,2,109].

In cases of high dose irradiation of polymer packaging materials such as for medical devices adverse effects on the physical and chemical properties of the packaging material can occur. For example, at relatively high radiation doses above 50–100 kGy, cross-linking of polymer molecules can occur. This will discolor the plastic film, and cause it to become brittle and easily fracture.

At dose levels of radiation in the range appropriate for most food irradiation, the radiation treatment causes little or no detectable change in any physical, chemical, nutritional or organoleptic (sensory) factor in the treated food. Therefore, it is difficult to devise a test method for the purpose of detecting whether a food had been exposed to ionizing radiation (see Section 13.4.3 below).

Irradiation is used for different goals: It varies from retardation of ripening (onions or exotic fruits) to inactivation of moulds and pathogenic microorganisms, such as *E. coli* and *salmonella*. The irradiation dose has to be chosen in accordance with the objective to be reached. Just as with thermal inactivation kinetics of microbes in the design of heat sterilization or pasteurization processes, the radiation inactivation kinetics of microbes will depend on the specific microbe and the chemical composition of the food product in which it is present.

In the European Union, and United States, as well as many other parts of the world, there are regulations which limit the types of food which are allowed to be irradiated and what dose limits are allowed for each different type of food [4, 5]. When a food is brought into an irradiation facility, the delivered dose of radiation is controlled by the duration of treatment, which can be controlled by the speed of a moving conveyor belt that carries the

packaged food products into the treatment chamber. β-radiation from a linear accelerator or γ-radiation from a radioactive isotope source, such as ^{60}Co, is absorbed by the goods on the conveyor belt as they pass by the beam of radiation being emitted from the source. The depth to which the radiation energy can penetrate into the product depends on the energy of the radiation used and the density of the product material. This depth of penetration is remarkably different for β rays than from γ rays because of the order of magnitude difference in their energy levels.

β-rays are beams of electrons that are normally generated from particle accelerators. In contrast, γ-rays are nuclear energy quanta that can only be emitted by radioactive isotopes. β-rays have relatively limited penetrating ability, typical penetration depths are in the range of a few centimeters, and they cannot penetrate metal. Recall the term penetration depth (Section 10.2.2), which is the depth where the intensity drops to 1/e. Therefore, they are practical for surface treatments only, or in treating small nonmetal food packages individually as they pass under the beam on a conveyor belt. In contrast, γ-rays have substantially greater penetrating ability. They can penetrate into metal cans, as well as into an entire pallet lode of case goods already sealed in shipping cases and stacked into pallet loads.

Although γ-rays have the advantage of much greater penetrating ability, they have the disadvantage of requiring extensive safety shielding to protect workers from inadvertent exposure to radiation. Once a radioactive isotope is brought into a processing facility it continues to emit radiation, and cannot be stopped. When not in use, it is stored at the bottom of a pool of water approximately 4 m deep, and lifted up into the treatment chamber when products are ready to be processed. Alternatively, the radioactive source can be stored in a lead cabinet with walls made of lead approximately 15 cm thick when not in use in the treatment chamber. The treatment chamber, itself, must also be surrounded by a wall that serves as an effective shield to the gamma rays. Concrete walls approximately 2 m thick are used for this purpose. In contrast, no such shielding is required in beta ray facilities because the electron beam accelerator can be simply turned off when not in use, and turned on again when needed. When the beam is operating, the treatment chamber can be easily shielded with thin metal partitions.

It must be clearly understood that foods cannot become radioactive by exposure to ionizing irradiation, just as they cannot becomes heaters (to produce heat) by simply being exposed to heat. The risk of forming radioactive isotopes by applying energies below 10 MeV is very low, and improbable. Below those levels, the main side effects that may possibly occur are the temporary formation of chemical substances known as free radicals. Some of them are well known substances like hydroxyl radicals, which are also sometimes formed upon heating. Other substances that may be formed seem to be specific to ionizing irradiation, and may serve as a possible means for detection of irradiation treatment if performed soon enough after exposure to irradiation.

The main principles responsible for the known formation of radiation side effects in food are summarized here:

When γ-rays, X-rays or β-rays (electrons) are "hitting" food materials (bombardment), their energy is transferred to the molecules and atoms within the material. The energy delivered by this primary bombardment can cause secondary electrons to be formed, as well as ions and free radicals from the surrounding molecules. These radicals may undergo chemical reactions with biochemical molecules in the food material that could damage them irreversibly. Chemical pathways and products depend strongly on water activity, temperature, presence of oxygen and protective substances like antioxidants, as well as storage conditions. Roughly the principle is that irradiation can split molecules, and the resulting fragments can undergo chemical reactions with either the protein, fat or starch molecules in the food, as described below.

Protein: On irradiation, proteins show reactions like the type of denaturation that can be caused by excessive heat or acidity. Peptide molecules can become split into fragments with subsequent alteration in viscosity and solubility of the product. Low molecular weight irradiation products like amines, ammonium (NH_3), and sulphur-volatiles can degrade food quality.

Fat: On irradiation, fats can show reactions like oxidation and the formation of carbonyl-compounds and peroxides.

Starch: High molecular weight polysaccharides like dextrin, amylose, amylopectins and starch can undergo reactions like hydrolysis, resulting in decreased viscosity or firmness of food material [22].

13.4.3 Detection of Food Irradiation

Most food regulations require that irradiated foods be identified as such on their labels so that consumers will always know if a food product has been exposed to irradiation. For this reason, there is a strong need in the food industry to develop reliable methods capable of detecting whether or not a food sample has been exposed to ionizing irradiation. One possibility is the use of electron spin resonance (ESR) spectroscopy or electron paramagnetic resonance (EPR) [7,8]. The procedure is based on the determination of free radicals, which remain in the material after the irradiation treatment. However, a serious limitation to this method is that these free radicals are only short-lived in aqueous materials, and most irradiated foods have high moisture contents. Therefore, this method is mostly applicable to dry materials, like bones and cardboard, in which the life-time of the free radicals is reasonably long. A listing of methods for determination of irradiation in foods is shown in Table 13.10.

Another possibility is thermoluminescence (TL) [9,10]. The scientific principle of this method is that when a crystal lattice of minerals is bombarded by exposure to irradiation, electron–hole pairs can be formed and electrons can get trapped between the valence and electron band in the crystalline structure. By energy uptake these trapped electrons can go into an activated state and when they fall back into their normal state, they emit a photon which can be detected. Because the trapped electrons need a little thermal activation to fall back to their normal state, the sample is placed in an oven and heated up. This

Table 13.10. Methods for detection of food irradiation

practice for dosimetry in gamma irradiation facilities for food processing	[12]
practice for dosimetry in electron and bremsstrahlung irradiation facilities for food processing	[13]
detection of irradiation in food containing bones by ESR spectroscopy	[14]
ESR detection of irradiation in food containing cellulose	[16]
detection of irradiation in food by thermoluminescence (TL)	[17]
biodosimetry based on electron paramagnetic resonance (EPR)	[18]
shellfish: irradiation status by thermoluminescence	[19]
spices and herbs: detection of radiation treatment using thermoluminescence	[20,21]
peppers: irradiation detection by ESR, TL and viscosity	[22]
ethene/butene copolymer: modulated DSC to determine changes by γ -radiation	[23]
potato starch: influence of γ-radiation on gelatinization studied by DSC	[24]
egg products: identification of irradiation pasteurization	[25]
cowpea irradiation: effects on properties of isolated proteins	[26]
rice: effect of gamma irradiation	[27]
detection of irradiated food using photostimulated luminescence	[28]

is why the technique is called thermoluminescence. Detection of single photon emissions during heating is an indicator that the material has been irradiated. This method works only with crystalline minerals, but fortunately with very small amounts which many foods do carry. Using the natural minerals (dust) found on spices, herbs and vegetables, irradiation treatments with doses below 0.1 kGy can be detected with TL. If the TL analysis is negative, this may be due to no irradiation or to no crystalline minerals on the food sample. In that case, the sample is treated with a defined dose of laboratory irradiation. If the analysis is negative after this treatment, the reason is the missing dust particles, and TL is not applicable. If it is positive, then the original sample was not irradiated above the detection limit. A similar technique is the optical stimulated luminescence (OSL) [15]. For specific materials thermal analysis, especially DSC (see Section 7.9) was proposed to detect changes in sample behavior due to irradiation [11]. Because of the irradiation formation of chemical products, analytical techniques like high pressure liquid chromatography (HPLC) or gas chromatography (GC) can also be suited to detect irradiation products. For example dodecyl-cyclobutanone can be used as a specific substance indicating an earlier irradiation of fatty compounds.

13.5 Applications

Most radioactive sources for industrial radiation facilities come from manufactured radioactive isotopes, such as ^{63}Ni and ^{60}Co. One important sensing application is to measure the absorption of radiation by a sample material in order to draw conclusions about its structure (e.g. thickness). Table 13.11 lists some applications.

Table 13.11. Sensing techniques based on radioactivity

term	examples of measurement	nuclide e.g.
β-absorption	on-line thickness of paper, polymers, metal	^{90}Sr, ^{204}Tl, ^{147}Pm
γ-absorption	on-line thickness of thick samples of glass, metal, polymers on belts. Also, on-line fill level	^{241}Am, ^{60}Co, ^{137}Cs
β-backscattering	thickness of thin films (some µm) on solids	^{90}Sr, ^{204}Tl
γ-backscattering	thickness of glass, polymers, light metals and alloys	^{137}Cs, ^{241}Am
static eliminators (dischargers)	elimination of static electric charge from hardware parts, films by blowing of ionized air	^{210}Po
electron capture detector (ECD)	measuring electron current from modulated analyses. Use in gas chromatography.	^{63}Ni
β-radiography	medical imaging of organs, inspection of bank notes	^{14}C PMMA (Polymethylmethacrylate)
γ-radiography	inspection of welding	^{60}Co, ^{192}Ir
n radiography	inspection of materials with low mass number (e.g. turbines, valves, joints) by neutron scattering	^{252}Cf
irradiation	tumour treatment, sterilization of medical devices, treatment of agar and food products	^{60}Co

Literature

1. Airey PL, Loewenthal G (2001) Practical Applications of Radioactivity and Nuclear Radiations. Cambridge University Press, Cambridge
2. Brynjolfsson A (2002) Natural and induced radioactivity in food. International Atomic Energy Agency, IAEA, Vienna
3. Altug T (2002) Introduction to Toxicology and Food. CRC Press Inc, Boca Raton
4. Codex Alimentarius (ed) (2003) Codex Code of Practice for Radiation Processing of Food. CAC/RCP 19-1979, Rev. 2-2003, FAO Rome, Italy,
5. Ehlermann DAE (2005) Four decades in food irradiation. Radiation Phys. Chem. 73:346–347
6. Rusell RS (1962) Radioactivity in human diet. J Med Sci. 439:293–307
7. Schreiber GA, Helle N, Bögl KW (1993) Detection of irradiated food – methods and routine applications. Intern J Radiation Biology 63:105–130
8. Stachowitz W, Strzelczak-Burlinska G, Michalik J, Wojtowicza A, Dziedzic-Goclawska A, Ostrowski K (1002) Application of electron paramagnetic resonance (EPR) spectroscopy for control of irradiated food. J Sci Food Agric 58:407–415
9. Schreiber GA, Ziegelmann B, Quitzsch G, Helle N, Bögl KW (1993) Luminescence techniques to identify the treatment of foods by ionizing radiation. Food Structure 12:385–396
10. DIN EN 1788 (2002) Foodstuffs – Thermoluminescence detection of irradiated food from which silicate minerals can be isolated, in [101]
11. Ciesla K, Eliasson AC (2003) DSC studies of gamma irradiation influence on gelatinization and amylose-lipid complex transition occurring in wheat starch. Radiation Phys. Chem. 68:933–940

12. ASTM 51204 Practice for dosimetry in gamma irradiation facilities for food processing, in [132]
13. ASTM 51431 Practice for dosimetry in electron and bremsstrahlung in irradiation facilities for food processing, in [132]
14. DIN EN 1786 (1997) Foodstuffs – detection of irradiated food containing bone – method by ESR spectroscopy, in [101]
15. Sanderson DCW, Carmichael LA, Naylor JD (1995): Photostimulated luminescence and thermoluminescence techniques for the detection of irradiated food. Food Sci Technol Today 9:150–154
16. DIN EN 1787 (2000) Foodstuffs – Detection of irradiated food containing cellulose by ESR spectroscopy, in [101]
17. DIN EN 1788 (2002) Foodstuffs – Thermoluminescence detection of irradiated food from which silicate minerals can be isolated, in [101]
18. Desrosiers M, Schauer DA (2001) Electron paramagnetic resonance (EPR) biodosimetry. Nuclear Instrum. Methods Phys. Res. Section B 184:219–228
19. Schreiber GA, Hoffmann A, Helle N, Bögl KW (1994) Methods for routine control of irradiated food: determination of the irradiation status of shellfish by thermoluminescence analysis. Rad Phys Chem 43:533–544
20. Khan HM, Delincée H (1995) Detection of radiation treatment of spices and herbs of Asian origin using thermoluminescence of mineral contaminants. Appl Radiat 46:1071–1075
21. Schreiber GA, Helle N, Bögl KW (1995) An inter-laboratory trial on the identification of irradiated spices, herbs and spice herbs mixtures by thermoluminescence analysis. J Am Oil Chem Soc 78:88–93
22. Polónia I, Esteves MP, Andrade ME, Empis J (1995) Identification of irradiated peppers by electron spin resonance, thermoluminescence and viscosity. Radiation Phys Chem 46:757–760.
23. Hälldahl L, Olofsson B (1995) Thermal analysis studies using oscillation DSC to determine changes in LD ethene/butene copolymer induced by gamma radiation treatment. Thermochimica Acta 256:137–149
24. Ciesla K, Eliasson AC (2002) Influence of gamma radiation on potato starch gelatinization studied by differential scanning calorimetry. Radiation Physics and Chemistry 64:137–148
25. Helle N, Schulzki G, Linke B, Spiegelberg A, Bögl KW, Schreiber GA, von Grabowski HU, Pfordt J, Mauermann U, Julicher S, et al. (1993) Identification of irradiated pasteurized egg products: a combined method for use in routine control. Z Lebensm Unters Forsch 197:321–331
26. Oneh Abu J, Müller K, Gyebi Duodu K, Minnaar A (2006) Gamma irradiation of cowpea (Vigna unguiculata L. Walp) flours and pastes: Effects on functional, thermal and molecular properties of isolated proteins. Food Chemistry 95:138–147
27. Sung Wen-Chieh (2005) Effect of gamma irradiation on rice and its food products. Radiation Physics and Chemistry 73:224–228
28. DIN EN 13751 (2002) Foodstuffs – Detection of irradiated food using photostimulated luminescence, in [101]

14 On-line Sensing

In order for the food processing industry to remain competitive in an ever expanding global market place, it is essential that food companies be able to control their processing operations to assure maximum product safety and quality at the least cost possible [1]. The ability to measure processing conditions and product quality parameters while processing is under way on-line is a critical part of successful on-line process control. In any food manufacturing company, process control is only a small part of an overall quality assurance system. A complete quality assurance system for the manufacture of a food product is developed from conducting a hazard analysis of critical control points (HACCP) in following all the steps in the manufacture of a product, beginning with the inspection and approval of raw materials and ingredients all the way to final testing of finished product quality prior to release in the market place.

Process engineers are mostly familiar with the on-line measurement and control of state variables like temperature, humidity and pressure, and the frequent use of in-line probes like thermocouples and resistance thermometric devices (RTD's) and pressure transducers for this purpose. However, this chapter will attempt to identify some of the opportunities that are possible for applications of on-line measuring and monitoring of selected physical properties that may serve as indirect indicators of important product quality attributes in the control of food manufacturing operations.

In order to appreciate the importance of on-line measurement and control, we need to understand the difference between on-line and off-line measurement. First of all, having control of a process means knowing what process conditions are needed in order for the product to be produced within defined quality specifications, and having the ability to adjust the process conditions when needed to assure the desired outcome. Many quality attributes in the final product, such as color, texture, viscosity and solids or moisture content are normally measured off-line by taking samples of finished product to an analytical laboratory for analysis. Laboratory analysis for this purpose can require several hours even days before results are available upon which a process control decision can be made. In large production facilities a delay of one or more hours in obtaining quality information can result in cost prohibitive quantities of off-specification product that may have to be destroyed or reprocessed at economic loss to the factory. Alternatively, if these quality attributes can be measured rapidly and continuously with appropriate instrumentation

in-line, just down-stream of the critical control point that is responsible for each attribute while processing is underway, then the process condition can be adjusted immediately to correct for any changes sensed by the in-line measurement instruments. In this way, very little if any off-specification product is manufactured, and the factory can operate at maximum efficiency. This the most important reason for on-line measurement and control.

The reason for on-line measurement of physical properties is because they can often be measured more easily than chemical or microbiological components, and can often be used as an indirect indicator of the chemical or microbiological condition of the product. Product quality is often related to the concentration of an important ingredient or an unwanted chemical or biological contaminant like toxins or bacteria. Concentrations of chemical and biological contaminants normally have to be performed in a chemical or a microbiology laboratory. Typical response times can be hours or days, so on-line control is not possible. This is the reason for physical sensors. When we can find a way to measure the concentration by a physical sensor, such as a refractometer or a NIR spectrometer, then we can have the results in seconds or microseconds and have the opportunity for on-line process control. Physical sensors normally are faster than chemical and microbiological methods, and they can frequently deliver the result in the form of an electric, pneumatic or hydraulic signal (instead of a chart recording or paper printout) that can be used to actuate a process control device, such as a pump, valve or switch. Therefore, physical sensors are most advantageous when we look for on-line control tools.

When control of physical quality properties like viscosity or particle size is needed, there is no question that physical sensors will be required, and that chemical or biological testing is not applicable. Sometimes physical sensors are assumed to be inappropriate for sensing the concentration of an ingredient of interest to the level capable of a chemical sensor if one existed for that purpose. A situation like this would prompt a search for whether there is an opportunity for indirect measurement of this type of quality attribute using a physical sensor rather than chemical analysis. Sometimes measuring the density, refraction, turbidity, or electromagnetic absorption will do the job. However, physical sensors are not specific for a given analyte. Therefore, we have to make sure that the sensor readings are validated from time to time with appropriate chemical or biological methods which are specific for the specified analyte.

There are two categories of sensor usage. In one category, sensors are used to check or control the status of a machine or piece of process equipment. In the other category, sensors are used to check or control the status of the product being manufactured (quality of the product). Table 14.1 lists the various purposes for sensors in engineering.

Based on the discussion above, we can attempt to categorize the appropriate measurement and sensing methods in accordance with the systematic approach summarized in Table 14.2:

Table 14.1. Purpose of sensors in engineering

purpose for sensors	process control	quality control
goal	proper machine operation	proper product quality
example 1	checking the length of a tool (or level in a tank)	checking the length (size/shape) of a product
example 2	checking the machine oscillation (vibration)	checking the density of a product by oscillation
action (consequence)	adjustment of machine, machine tool, pump speed	adjustment of process parameters

Table 14.2. Terms in on-line sensing [114]

term	description
on-line	real time measurement
in-line	on-line-sensor located in product flow stream
at-line / near-line	fast techniques close to the processing line
off-line	laboratory analysis in facility (on-site) or after sample shipping to another laboratory (off-site)

14.1 Control Systems – Basics

A control system in general is a system where something is continuously adjusted in the right way to reach a prescribed goal. For example, the thermostat control on the heating system in our home can be set to the temperature desired. Then, it will automatically turn the heating system on and off as required in order to keep the temperature constant at the level desired. The means by which it can do this is a simple feed back control system. Similarly in a manufacturing facility, a machine in a production line may be adjusted periodically in order to obtain constant high quality of the products being manufactured.

A simple closed-loop control system is made up of three basic components, sensor, adjustable process device and controller. The sensor is normally located where the goal or end result is required. It continuously measures the specified characteristic of the product or process that must be controlled, and converts this measurement into some type of signal that can be transmitted to and read by the controller, such as a thermocouple converts measured temperature into an electrical signal (voltage). The adjustable process device is normally a piece of process equipment governing the process conditions responsible for the measured product outcome, such as a pump, blower, motor or heater that can be turned on and off or adjusted to alter the process conditions. The controller operates in between the sensor and the adjustable process device. It is an instrument that receives the signal from the sensor and compares it with the desired setting chosen by the operator. When the controller detects a large enough difference between the measured signal coming from the sensor and the set point, it sends a signal to the adjustable process device to make the appropriate adjustment in the process.

All three of these components make up a simple closed-loop control system. The controller is often considered the "nerve center" of the system because it is where settings can be made by the operator, and where decisions are made by complex algorithms on computer software. In simple systems, such as the thermostat in our home heating systems, the controller can be a small box with operator interface (set point adjustment dial) mounted on the wall in a convenient location. In large factories with complex manufacturing and processing operations, the electronics and computer hardware for a controller may be protected in some enclosed remote chamber, while the operator interface with the controller (screen monitor, key pad, dial gauges, printer, etc.) may be located in some centralized control room of the factory.

As explained earlier, in order to develop comprehensive quality assurance systems, so-called critical control points have to be identified from a hazard analysis of the manufacturing process. At each of these control points, a specified property needs to be measured, and the result of this measurement is converted into some type of signal that can be taken as input into the control system. With that input signal and some control algorithms, decisions are made and things can be adjusted in the right way. Quality assurance systems like hazard analysis and critical control points (HACCP) or total quality management (TQM) are based on identifying and controlling critical control points like these. Once critical control points have been identified, they indicate where in the process line something has to be measured and monitored. These are the locations where sensors are needed.

Let us refer back to the example of the heating system in our home. The sensor is a temperature-sensing probe located in the room where the desired temperature is needed. Meanwhile, the furnace with accompanying pump or blower mechanisms that must be turned on and off may be remotely located elsewhere in the building. The switches that ignite the burner in the furnace and turn on the pump or blower are the signal converters for the adjustable process devices. The controller in this system is the thermostat with the set point adjustment dial conveniently located where the residents in the home can read the temperature being sensed in the room, and change the settings when desired.

Recall that the controller is an instrument that receives a signal from the sensor (room temperature from temperature sensing probe) and compares it with the desired setting chosen by the operator (set point temperature on the thermostat). When the controller detects a large enough difference between the measured temperature and the set point, it sends a signal to the adjustable process device (furnace system) to make the appropriate adjustment in the process (turn the furnace system on or off). This type of system is called "closed-loop" or "feed back control" because after an adjustment is made, the system looks back to check and see if the result is what was expected from the adjustment by continuously monitoring and comparing the signal from the measuring sensor.

Another example of a simple closed-loop control system is the cruise control of a car. The speed of the car is continuously measured by a sensor and

compared to the set point chosen by the driver. If there is no difference, there is no action. If there is a difference, the cruise controller sends a signal to the throttle (actuator), and the engine power is adjusted accordingly to keep the difference between measured and set point speeds as small as possible. Note in this case that the signal to the adjustable process device (throttle for controlling engine speed) was not a simple switch for turning the engine on and off. Instead, it was a moveable device that could be used to make a modulated or gradual adjustment in the speed of the engine. Such devices are called actuators in process control systems, and the difference in these types of control responses will be discussed further on.

The opposite of a closed-loop system is an open-loop system, in which the actuator is adjusted to the set point, and the system is allowed to run without feedback from a sensor. For example, when we open a water tap to have water flow at a given rate (set point) and leave the room, the water will flow at that constant rate regardless of anything changing. Often, an open-loop system is combined with a timer which may switch the system on and off, such as with an automated lawn sprinkler system. When we talk about sensors and especially online sensors in this chapter, we will be assuming that we are planning on applications to closed-loop or feed back control systems.

Another issue is the different ways in which the adjustable device in the control system can respond to the signal from the controller. In our previous control system examples, the adjustable devices were the furnace and pump or blower in our home heating system and the engine in our auto cruise control system. The signal converters were the electric switches to turn the furnace, pump and blower on and off and the throttle to adjust the engine speed. There are different ways and different types of signal converters by which to operate these controllable devices. The simplest way is to switch the device on and off in response to the signal from the controller. This type of control would be called "on–off" control. For example, in our home heating system the blower for moving the heated air from the furnace to the living room would be at a set power level to operate at a fixed speed when switched on and off depending on the signal from the controller (thermostat). In this type of "on–off" control system, the room temperature will fall to some level below the set point while the system is off until it reaches some trigger level at which the controller will signal the blower on. Then the room temperature will rise to some level above the set point while the system is on before it is once again turned off. This results in the room temperature oscillating above and below the set point temperature all day long, but keeps the room at the set point temperature "on average."

Another way of operation would be to gradually adjust the blower speed (RPM) in order to modulate the flow rate of heated air entering the living room depending on the signal from the temperature sensor. In this mode, the blower does not run at a fixed speed, stopping and restarting, but runs at variable speeds in a modulated way such that the difference between set point and sensor signal remain as close to each other as possible. In the example of the

modulated blower control, the result would be a smoother and more uniform temperature profile compared to that obtained from a simple on–off switch mode. However, in order to do this, the simple on–off switch would have to be replaced by a rheostat with a movable part (actuator) that would adjust the voltage to the electric motor on the blower in accordance with the strength of the signal coming from the controller.

In order to obtain this type of smooth modulated response in the controlled variable (e.g. room temperature or car speed), different control algorithms and types of actuators can be used to control the adjustable device. Sophisticated control systems include software which gives the system the ability to learn from its actions how best to adjust itself in order to obtain optimum control performance. What type of control system we choose depends again on what we need. An exact temperature–time experience in a freeze drying process for instant coffee or in a retort process for sterilizing baby food is more important than that required in a home heating system. In some cases sophisticated control systems are the key to better product quality in industrial manufacturing operations. On the other hand, for many consumer applications, such as with a household stove or refrigerator, simple switches for "on–off" control are sufficient.

We have now learned that a simple closed-loop control system needs a sensor to measure the controlled variable, a controller which compares the sensor reading with a set point, and an adjustable process device which alters the process according to the result of that comparison. It is also important to note that all these system components will have to respond with some degree of inertia (response time). If for example, we have a controller with high performing sophisticated software, but the sensor signal is always in error because of too much sensor inertia (slow response time), we cannot expect a good result. Or if we have a good sensor and a good control algorithm, but the adjustable device responds much too slowly, we will still get poor results. So, we should keep in mind that all the components of the control system will have to work with compatible and appropriate response times. We can try to understand what causes a control system to have inertia when we consider a temperature sensor: Because of its material properties, it will have given thermal conductivity, thermal diffusivity and heat capacity. A high heat capacity or a low thermal conductivity will make the sensor have excessive thermal inertia. The same considerations apply to the location of the sensor. Based on the thermal properties of the sample material there can be temperature differences between the bulk interior, surface or wall of the material and the location of the sensor. All these factors may contribute to the overall inertia of a control system.

Now that we have a general understanding of the basic principles of a closed loop process control system and how an on-line process control system should work, we can appreciate the important role of the sensor. This is because the technology for operating adjustable process devices like heaters, valves and motors in response to signals coming from a controller is well developed and commercially available on a wide range of levels. However, the need for better

and more sophisticated process control systems is never ending. The development of these better systems is limited by the lack of new and better sensors capable of sensing the wide array of product quality attributes that are needed in process control. For this reason, this chapter will focus on the possibilities for the application of sensors capable of measuring the various physical properties covered in the earlier chapters of this book, that might be used as indirect indicators of the more complex product quality attributes that must be controlled.

14.2 Sensor Types and Applications

A recent survey of process engineers was taken in which they were asked about what types sensors they would wish to have in order to meet all their process control needs. The responses were compiled into a sort of "wish list" of sensors like that shown in Table 14.3.

Table 14.3 is only a snapshot of perceived needs at a moment in time. It cannot be complete or representative of any given industry. Again, we see that sensors are needed for process control and quality control. Many of the process control sensors deal with the position of a body or a part of a machine, such as with length or angle. Many simple sensing techniques are available for detecting position or position over time, or the distance of a body, its velocity or acceleration or the filling level. Further, many sensors for sensing force or mass are based on monitoring the deformation of an elastic part. So, many sensors for pressure, stress (force over area) and mass (weight force) are basically monitoring the difference in length or distance of a moving body or surface. Sensors for temperature and pressure are typical online sensors for process

Table 14.3. Engineers wish list for on-line sensors (after [2]). "I need a sensor for..."

force	power	velocity of a fluid
weight, mass	velocity of a body	volume flow
volume	acceleration	mass flow
density	rotational velocity	concentration
number	rotational acceleration	pH
length	frequency	turbidity
distance	oscillation (amplitude, frequency, form, resonance)	viscosity
position	deformation (extensional, rotational)	creep
angle	stress (extensional, rotational)	relaxation
	torque	temperature
	moment of inertia	pressure
filling height	damping	humidity
thickness	noise	specific analytes, purity/impurity
area	roughness	heat, heat flow

Table 14.4. Examples of on-line sensors and their principles

what sensor must measure	what principle it is based upon
mass	weight force, elastic deformation, change in electric resistance or capacitance, electric current in compensation balances
pressure	elastic deformation, change in electric resistance or capacitance
density	resonance frequency of an oscillator
mass flow	magnetic inductive, CORIOLIS effect, thermal
volume flow	ultrasonic pulse run time,
viscosity	damping of an oscillator, pressure drop, ultrasonic scattering, torque on a rotating body
position	magnetic induction, light reflection, triangulation
thickness	absorption of electromagnetic waves
particle size	laser scattering, in-situ microscopy, camera, ultrasonic spectroscopy,
particle shape	
surface tension	bubble point (pressure measurement)
temperature	IR emission, thermal dilation, change in electric resistance
heat flow, heat conductivity	temperature difference, temperature drop
filling level	pressure, ultrasonic or RADAR distance, electric resistance or capacitance, damping of an oscillation
rotational speed	counting an optical or magnetic inductive signal over time
acidity, concentration	electric resistance or impedance, pH measurement
sugar concentration, salinity, dry substance	refraction index measurement
concentration of dispersed matter	turbidity
water, concentration	permittivity measurement
water, fat, composition	NIR absorption, FTIR spectrometry, UV spectroscopy, NMR
fat in meat	impedance measurement, X-ray absorption
chemical or biological substances	change in electrical, optical or mechanical properties of chemo-sensors or biosensors
metallic contaminant matter	change in magnetic induction
nonmetallic contaminant matter	X-ray absorption, NMR, thermography
color	selective absorption of light
texture	force, acoustic properties
water activity	air humidity measurement
air humidity	change in capacitance of a polymer, dilation of a polymer fiber, dew point measurement, psychrometric measurement
dew point	change in electrical or optical properties of a cooled plate
psychrometry	temperature difference between dry and wet bulb temperature sensor

Table 14.5. Physical properties and related product quality attributes (examples) [3]

physical property	may be used for quality attribute ...
mechanic properties	
length	particle size in powders, emulsions, foams. Texture parameters of chocolate or ice cream.
volume	porosity, bulk density of powders
density	concentration of ingredients, as sugar in juices, alcohol in drinks, water in milk, starch in potatoes.
stiffness, hardness	texture
viscosity, flow yield	flow, consistency, stability
mass	package fill weight
electrical properties	
conductance	water content in grain, honey or milk. Electrolyte concentration of milk. Particle counting.
impedance	microbial growth in liquids, fat in meat
induction	metallic contaminating matter in food
permittivity	water content
acoustic properties	
acoustic impedance	moisture content, ripeness of apple
sound emission	texture of bakery products
ultrasonic impedance	composition of materials, droplet size in emulsions
optical properties	
refraction	water content, sugar content, solid matter in juices and drinks
color	condition, ripeness of fruit and vegetables
angle of light polarization	sugar concentration
NIR absorption	composition of food
electromagnetic properties	
microwave absorption	water content
X–ray absorption	metal and nonmetal contaminating matter
thermal properties	
temperature	shipping condition of food, level of sterilization or pasteurization
crystallization temperature	water content in milk
glass transition temperature	stability
melting temperature	purity and identity of materials
atomic properties	
low resolution	solid fat content, water and fat content in food and feed
isotopic composition	authenticity, origin of food

control. On the other hand, sensors for density, viscosity or concentration are typical sensors for quality control of a material. Table 14.4 shows some examples of online sensors and indicates their working principle.

So, we can see that there are numerous on-line sensors available. When we need to design a control system we would normally go the other way around: We would ask, what properties does my material possess and what information can I derive from knowing that property? After identifying these useful properties, we could then ask for appropriate sensors. Examples of product quality attributes that could be related to easy to measure physical properties are listed in Table 14.5.

14.3 Some Sensors of Relevance

In this chapter we will attempt to introduce only selected types of sensors which are important for automation of food processing operations and quality control. These will include sensors for such applications as in-line measurement of temperature and pressure, flow rates, liquid product density, and dissolved solids, as well as applications for ultrasonic sensors, chemo-sensors and biosensors.

14.3.1 Weighing

Principles of weighing have been explained in Section 2.2. There is process equipment available which measures the weight of raw materials or products online. Belt weigher systems measure the mass of a material while passing the system on a conveyer belt. Besides conventional measurement of the weight force, optical belt check weighing systems are available which measure bulk material quantities by laser scattering or by X-ray absorption.

Multihead weighers consist of several (e.g. 8, 16 or more) compartments which are continuously filled with product, weighed and discharged. By knowing the weight of contents in each compartment a computer calculates what parts of all compartment fillings have to be added to give the final product weight needed. These compartments then are instantly discharged into a funnel which leads the wished amount of product to the next process step, e.g. to packaging. Multihead weighers can be used with free flowing granular food of different particle size ranging from powder to frozen vegetables. Multihead weighers are part of fast and precise dosing equipment.

So-called checkweighers are operated after filling of product into packages to check for correct weight. Checkweighers are fast belt weighing systems connected to devices which automatically reject packages from the packaging line if they are recognized to have incorrect weight. On-line weighing systems like this can also be operated in a way to produce and apply labels with weight and price information for the package.

14.3.2 Density Sensors

Oscillating Systems

On-line density sensors of this type can consist of U-shaped oscillating tubes through which the liquid food sample is pumped. This is a mechanical vibrating device like a tuning fork that has a resonant frequency which is dependent on its mass. So a vibrating system can be used to measure mass and therefore density of a sample if it is part of a system of known volume in which the frequency can be measured and recorded. There are instruments commercially available based on this technology for in-line continuous measurement and monitoring of liquid density. These instruments are calibrated so as to display the density of a fluid on-line while the fluid is flowing through the device.

For density measurement the frequency or the period of vibration is measured. The ideal elastic mechanical vibrating arm has a vibrating period of

$$T = 2\pi \cdot \sqrt{\frac{m}{D}} \tag{14.1}$$

and the frequency is

$$f = \frac{1}{T}$$

or

$$f = \frac{1}{2\pi} \cdot \sqrt{\frac{D}{m}}$$

The angular frequency is

$$\omega = 2\pi \cdot f$$

$$\omega = \sqrt{\frac{D}{m}}$$

where

ω	angular frequency in s^{-1}
f	frequency in s^{-1}
D	elastic constant in $N \cdot m$
m	total mass of the vibrating arm in kg
T	vibration period in s

With a U-tube containing the sample S to be measured, the mass of the vibrating arm is

$$m = m_U + m_S \tag{14.2}$$

and therefore

$$T = 2\pi \cdot \sqrt{\frac{m_U + m_S}{D}} \tag{14.3}$$

so

$$T^2 = 4\pi^2 \cdot \frac{m_U + \rho_S \cdot V_T}{D} \tag{14.4}$$

$$\rho_S = \frac{T^2 \cdot D}{4\pi^2 \cdot V_T} - \frac{m_U}{V_T} = \frac{D}{4\pi^2 V_T} \cdot \left(T^2 - \frac{4\pi^2 \cdot m_U}{D} \right) \tag{14.5}$$

with the following substitutions

$$A = \frac{D}{4\pi^2 V_T} \quad \text{and} \quad B = \frac{4\pi^2 \cdot m_U}{D}$$

the density is a quadratic function of T resp. f

$$\rho = A \cdot \left(T^2 - B \right) \tag{14.6}$$

where

m_U	mass of empty tube in kg
m_S	mass of sample in tube in kg
V_T	inner volume of tube in m^3
A, B	instrument constants

The constants A and B are constants of the instrument used, and can be obtained by calibration of the instrument with reference density materials. When materials with known densities are measured, the vibrating time periods are read out, and a graph of density versus T^2 can be constructed, as shown in Figure 14.1. Calculating the slope from the graph provides A, and the intercept with the horizontal axis is B. Normally, commercial instruments are calibrated to display density directly, and there is no need to calculate A and B. The temperature ϑ of the measurement has to be taken into account and be controlled. When the mathematical function ρ = function(ϑ) for a sample material is known, it is possible to display the density for temperatures other than the temperature of measurement. Modern instruments have built-in software for this type of temperature correction.

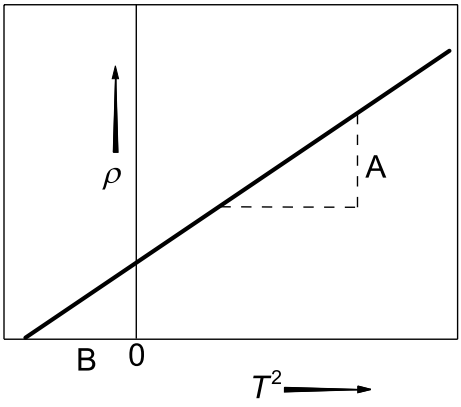

Figure 14.1. Sample density as a function of vibration time period

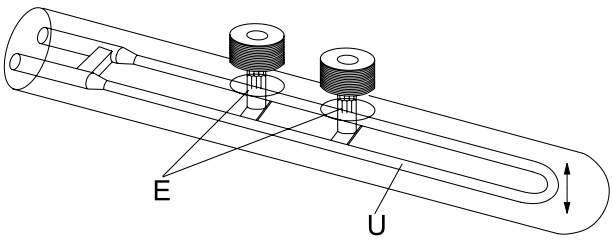

Figure 14.2. Example of a vibrating U-tube system for density measurement. Electromagnetic transducers (E) bring the U-tube (U) into vibration and read the frequency

Figure 14.2 shows an example of the design of a U-tube vibration device. For laboratory equipment the tube often is made of glass. The lower the angular moment of inertia of the vibrating arm, then the higher will be the resolution of the instrument. For process control instrumentation, more robust metal tubes with lower resolution are used. Typical vibration frequencies are 50–1000 Hz. There are "bow" vibrator devices and "angular" devices available.

Example 14.1. Density of beer measured with a U-tube vibrating system
The calibration is performed with two reference materials with the densities ρ_1 and ρ_2. Reference materials should be chosen which will cover the range of densities that are intended to be measured. In case of beer, the values of density may be expected to be slightly higher than that of water. Therefore as reference materials water and a sucrose solution are chosen. The reading of the vibrating time period can be taken in arbitrary units:

reference material	density at 20 °C	reading
H_2O	$\rho_1 = 998.20\,\mathrm{kg \cdot m^{-3}}$	$T_1 = 4.0044$ units
sucrose solution 20% (m/m)	$\rho_2 = 1080.92\,\mathrm{kg \cdot m^{-3}}$	$T_2 = 4.0594$ units

So with

$$A = \frac{\mathrm{d}\rho}{\mathrm{d}T^2} \approx \frac{\Delta\rho}{\Delta T^2} = \frac{\rho_2 - \rho_1}{T_2^2 - T_1^2}$$

$$B = T_1^2 - \frac{\rho_1}{A} = T_2^2 - \frac{\rho_2}{A}$$

A and B are

$$A = \frac{\rho_2 - \rho_1}{T_2^2 - T_1^2} = \frac{(1080.92 - 998.2)\,\mathrm{kg \cdot m^3}}{\left(4.0594^2 - 4.0044^2\right)\ \mathrm{units}^2} = 186.5126\,\mathrm{kg \cdot m^{-3} \cdot units^{-2}}$$

$$B = T_2^2 - \frac{\rho_2}{A} = 4.0594^2\,\mathrm{units}^2 - \frac{1080.92\,\mathrm{kg \cdot m^{-3}}}{186.5126\,\mathrm{kg \cdot m^{-3} \cdot units^{-2}}} = 10.6833\,\mathrm{units}^2$$

The density of the beer sample ($T_{20^\circ} = 4.0045$ units) then is calculated to

$$\rho_{beer}^{20^\circ} = 186.5126\,(4.0045^2 - 10.6833)\,\mathrm{kg \cdot m^{-3}} = 998.35\,\mathrm{kg \cdot m^{-3}}$$

14.3.3 Metal Detectors

The working principle of metal detectors is electromagnetic induction. When an alternating electric field from a sender intrudes into a material having mobile electric charge carriers – like electrons in metals – induction will occur. With electronic means the energy loss from the sender's electric field due to induction can be detected instantly. In this way a food product containing a piece of metal can be identified and rejected in real time. Metal detectors often have the form of a tunnel through which the food product passes on a conveyor, as shown in Figure 14.3. Foods can pass through these detecting tunnels as bulk goods or as pre-packaged goods, or even as flowing liquids. They can be carried on through the tunnel on various types of moving conveyor systems. When they are flowing liquids, they are pumped through nonmetallic tubes. As explained earlier, when the detector senses a metal fragment, it will trigger an alarm and actuate a divert ejection of the contaminated product from the filling line.

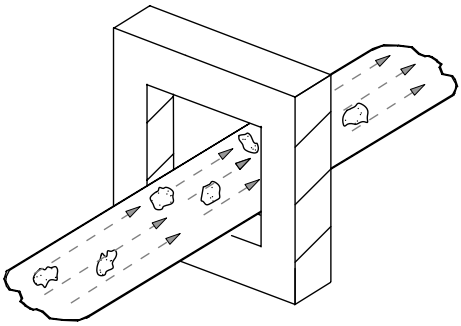

Figure 14.3. Tunnel-type metal detector with food product on a conveyer belt (schematic)

14.3.4 Flow Sensors

The rate at which a liquid product is flowing through a pipeline on its way to being heated or cooled or otherwise being processed is perhaps one of the most important processing parameters that must be kept under critical control in a food processing operation. The need to continuously measure and monitor flow rate is of critical importance to process engineers. Perhaps the simplest type of sensors for this purpose are flow meters based on vertical floating bodies in a supply tank, axial propellers mounted in the flow stream, or some type of simple obstruction in the flow path like a nozzle or orifice that will cause a pressure drop across it proportional to the flow rate.

Another simple type is a thermal flow meter, which consists of a heated location in the pipeline which is in contact with the flowing fluid. With no flow there is no cooling, when flow is present, there will be a cooling effect which

is dependent on the flow velocity and the heat transfer coefficient (see Section 7.6.3). So, monitoring of the temperature at the heated location can be used as an indirect measure of flow rate.

One of the challenges in on-line measurement of the flow rate with liquid food products is that any type of flow meter that introduces any obstruction to the flow path inside the tube or pipeline must be avoided. Such obstructions will cause problems with cleaning operations and will compromise the hygienic or sanitary design of liquid food pipelines, as well as compromise pipelines designed for pigging. The interior of the pipeline must be smooth and free of any obstructions or dead spaces that may harbour the growth of bacteria, etc. For this reason there is great interest in flow rate sensors that do not compromise pipeline integrity or hygiene and assure smooth product flow. The thermal flow meter described above is one such possibility, but it is often not suitable when the product temperature must be kept under tight control. Other interesting possibilities are magnetic inductive flow meters (MID) and ultrasonic flow meters. These have no moving parts, and do not intrude in the product flow through the pipeline in any way.

Magnetic Inductive Flow Meter

Magnetic inductive (MID) flow meters are a useful application of electromagnetism. They work on the principle of the Lorentz force (see Section 9.2.1), which act on the electric charges as the flowing liquid product is passing through a magnetic field. The charge carriers sense the perpendicular forces acting on them, causing them to change direction, which is detected as voltage. Thus, the voltage depends on the velocity of the charge carriers, which in turn, can be directly related to flow rate of the liquid through the detector. A schematic of such an MID probe is shown in Figure 9.5.

Because these MID probes are based on the Lorentz force, they can only work on liquids that carry electrically charged particles. This is often not a problem with most aqueous food liquids since the lower limit of electrical conductivity needed to receive a useful signal can be obtained with normal tap water, alone. More about the theory of magnetic properties and their application to food technology can be found in Chapter 9.

Ultrasound Flow Meter

Ultrasound (see 12.2) can also be used to measure liquid flow rates through pipes and tubes unobtrusively. When an ultrasound pulse is propagated through a flowing liquid, we can measure the velocity of the flow and therefore, the volumetric flow rate, as illustrated schematically in Figure 14.4. The run time of an acoustic pulse is shorter in the direction of the flow than in the opposite direction. From this difference the flow velocity can be calculated [114]. Some ultrasound flow meters allow for estimating the fluid density by simultaneous measurement of the speed of sound. Then, from the volumetric flow rate and liquid density, the mass flow rate can be calculated and displayed. Again,

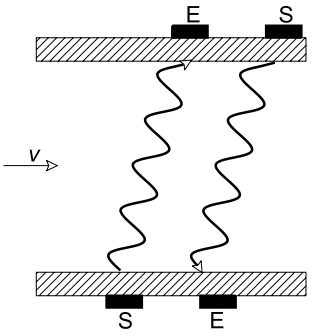

Figure 14.4. Ultrasonic flow meter. The run time of a pulse from sender *S* to receiver *E* is shorter in the direction of the flow than in the opposite direction

flow meters like this, which have no parts protruding into the flowing liquid food, are advantageous from a sanitary and hygienic point of view and good for sanitary pipeline fittings and cleaning operations.

Coriolis Flow Meter

Other types of sensors for in-line density and flow rate measurement rely principally on the CORIOLIS forces that arise in connection with the momentum transfer (movement) of flowing fluids. When a particle or mass of fluid experiences both a translational and rotational motion at the same time the particle or fluid mass will experience the CORIOLIS force. This force has a direction that is mutually perpendicular to both the translation and the vector of the angular velocity, and has a magnitude proportional to the magnitude of both velocities (translational and rotational).

$$\vec{F}_C = 2 \cdot m \times \vec{v} \times \vec{\omega} \tag{14.7}$$

where

F_C	CORIOLIS force in N
m	flowing mass of particle in kg
v	translational velocity of flowing mass particle in $\mathrm{m} \cdot \mathrm{s}^{-1}$
ω	rotational velocity in s^{-1}

Recall that an oscillating tube like that shown in Figure 14.5 performs a rotational movement around an axis (A), while at the time the angular velocity is

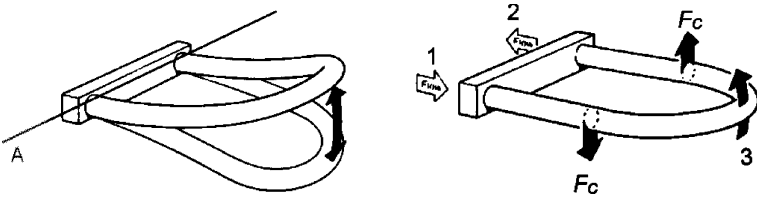

Figure 14.5. A fluid flowing through an U-shaped tube which oscillates around axis A experiences the CORIOLIS force F_C. **1:** flow in, **2:** flow out, **3:** momentary oscillation movement

changing periodically. When we pump a fluid through this vibrating tube, the fluid molecules will experience the CORIOLIS force. This CORIOLIS force will cause the vibrating tube to experience a very slight deformation that can be detected electronically.

With constant oscillation frequency the measuring effect is directly proportional to the velocity of the particles travelling in the oscillating tube. With the cross-sectional area of the tube, we can calculate the volumetric flow rate from the flow velocity.

$$\dot{V} = v \cdot A \tag{14.8}$$

There are in-line density and flow rate sensors commercially available called CORIOLIS flow meters, which operate on this effect. The advantage CORIOLIS flow meters is that they do not obstruct or interfere in any way with the free inner diameter of the product pipeline. Thus, they do not compromise hygienic design and ease of cleaning, just as with MID flow meters.

As we learned earlier (see Section 2.3.4) the resonance frequency of an oscillating tube depends on the density of the fluid in the tube. So by simultaneous measurement of the resonance frequency, it is possible to measure the fluid density together with the flow velocity. Then the measured volume flow can be converted to a mass flow. By this a CORIOLIS sensor can be operated as a volume flow meter and also as mass flow meter.

$$\dot{m} = \rho \cdot \dot{V} \tag{14.9}$$

where

m	flowing mass of particle in kg
v	translational velocity of flowing mass particle in $\mathrm{m} \cdot \mathrm{s}^{-1}$
$\dot{V}$	volume flow in $\mathrm{m}^3 \cdot \mathrm{s}^{-1}$
A	cross-sectional area of tube in m^2
ρ	density of fluid in $\mathrm{kg} \cdot \mathrm{m}^{-3}$

In addition, the damping of the oscillation in a CORIOLIS flowmeter can be detected and may be analyzed for related flow properties (mainly viscosity) of the flowing liquid. Table 14.6 summarizes the effects which can be measured simultaneously.

Table 14.6. Oscillating systems: possibilities of getting information about a sample material or a process

physical quantity to be measured	influenced by…	can be used for calculating…
frequency	mass of the sample	density
CORIOLIS deformation	velocity of the sample mass	mass flow
damping	molecular physical properties of the sample, like viscosity	viscosity

14.3.5 Refraction Sensors

We learned in Section 11.1 on optical properties that the refractive index of light passing through a transparent liquid solution will be affected by the concentration of dissolved solids in that solution. Optical instruments called refractometers are commonly used for this purpose. Laboratory refractometers are small hand-held instruments that are easy to use. They require only a few drops of a liquid sample, and provide results within just a few seconds. However, for industrial process control, the refractive index can also be measured on-line with specially designed sensors consisting of flow cells, as well as with in-line refractometers that are commercially available for process control in industrial manufacturing plants. These in-line refractometers work on the same principle as a hand-held or laboratory refractometer, but with automated means of transmitting a light beam through a window in the flow tube, and detecting and monitoring the refracted light beam electronically and continuously.

An important application of in-line refraction sensors is the fruit juice and soft drink beverage industries. For example, the sucrose concentration in fruit juices and soft drinks can be related directly to the refraction index of the sample solution. Tables listing sucrose concentration and the corresponding refraction index are available for this purpose, as well as commercially available refractometers already calibrated in units of sucrose concentration.

Many commercially available refractometers have built in conversions of sucrose concentrations to other units, such as ∘Bx (degrees Brix), along with published tables with which to calibrate these instruments. When using such tables it is important to remember to check the validity of the calibration. For example, the data in the table are given for a certain temperature and wavelength of the refractometer. When we measure food systems containing different sugars (other than sucrose), we should expect some error because the calibration data were based only on binary sucrose–water mixtures. More information on the use of refractometers and the theory of optical properties related to refractive index can be found in Section 11.1.

14.3.6 Sensing Principles

Before proceeding much further, let us recall some general terms and principles that each sensor and analytical method must have. Each sensor, just as each analytical method, will have a given ability to recognize the substance or component being analyzed (analyte) out of other constituents of a sample. This is called the selectivity of the method. For example a sensor that may respond to dissolved sugars, but not to dissolved electrolytes, will have a higher selectivity than a sensor that responds to all dissolved matter. If the sensor responds to only one specific sugar, e.g. glucose, we call it a specific sensor.

Each sensor, just as with any analytical method has a given sensitivity for an analyte of interest. The sensitivity is defined as the ratio of response

Table 14.7. Terms in analytical work

sensitivity	ability to detect small changes in what is being measured
selectivity	ability to identify what needs to be measured out of others present
specificity	ability to measure only a specific component amidst similar others
detection limit	ability to detect very small levels of what is measured
stability	ability to do all of the above with the same precision consistently

signal to analyte concentration. In other words, sensitivity is the slope of the calibration curve. The detection limit is the lowest concentration which – by use of statistical tools – can be detected reliably.

The stability of a sensor, just as with each analytical method, characterizes its ability to keep properties like its selectivity and its sensitivity consistent over a long time period. For example, the stability of biosensors is strongly dependent on temperature and other conditions of operation.

Another general principle is the distinction between absolute measurement and relative measurement. Absolute measurements give the absolute quantity or level of what is being measured, complete with the appropriate units. In order to obtain absolute measurements, calibration of the sensor against reference materials is always needed. Sensors which give relative measurements are designed to give some type of reading or signal that is simply relative to a predetermined condition. These relative measurements are without units or given with an arbitrary scale. The only calibration needed is a method of adjustment to the arbitrary scale (zero and slope), but no reference material is needed. These types of sensors are usually of a more simple design and less expensive than those designed for absolute measurement.

When we consider either analytical methods or on-line sensors, we should first determine what we really need to learn from the measured result. Often a relative measurement is sufficient. On-line sensors only in certain cases have to show absolute (true) measurements (for example a balance for check weighing on a filling line, or a thermometer in a retail food freezer display case). Distinctive characteristics between absolute and relative measurements are listed in Table 14.8.

Most of the on-line sensors previously described in this chapter are working as relative measurement sensors. For example, magnetic inductive (MID) flow meters measure a voltage (not flow rate). However, this voltage is rela-

Table 14.8. Characteristics of absolute and relative measurements

principle	absolute measurement	relative measurement
display of property with its physical units	yes	not necessary. output of, e.g. voltage as the difference to a set point is sufficient
calibration needed	yes	yes
reference material needed	yes	no

tive, and depends on the velocity of the charge carriers, which in turn, can be directly related to flow rate of the liquid through the detector. Similarly, ultrasound flow meters allow for measurement of the speed of sound as a relative indicator of density. Then, from the volumetric flow rate and liquid density, the mass flow rate can be calculated and displayed. In the case of on-line density measurement, the vibrating tube system for density measurement is a mechanical vibrating device that has a resonance frequency which is dependent on its mass and density. So, the frequency of vibration is measured and recorded as a relative indicator of mass and therefore density of a sample.

14.3.7 Chemosensors and Biosensors

Chemo- and biosensors are sensors which make use of chemical and biological reactions as the means of measurement. They are often more sophisticated than physical sensors, and require more elaborate means of calibration, but they may offer advantages in many situations. By use of chemical and biological reactions, sensors can be designed to have higher selectivity, or to be far more specific for a certain substance [4]. The principle is to combine a sensitive layer of a special substance and a transducer. The sensitive layer is designed to adsorb the analyte when it occurs in the sample. For a better understanding of the mechanism of adsorption, refer to Section 1.2. With the help of special polymers or enzymes in the sensitive layer, or with biochemical tools such as antibodies, the adsorption can be designed to be very specific [5–8]. For example, only one hazardous chemical compound is adsorbed, or only those antibodies responsible for a specified immune reaction. It is often advantageous if the adsorption is not only specific but also reversible. In the case of irreversible adsorption we would have a single use sensor, only.

In these types of chemo- or biosensors, the sensitive layer has to be mounted onto a transducer. The transducer is a device which detects and quantifies the adsorption on the sensitive layer. There are different ways to do this. For example, the sensitive layer can be mounted on an oscillating electronic chip, which is operated at its resonance frequency. On adsorption or desorption of the material at the sensitive layer, there is a shift in frequency which can be measured by the electronics in the chip. Often the biochemical reaction on the sensitive layer results in oxygen consumption or generation. In these cases the transducer can be a miniaturized Clark sensor, which gives an amperage response dependent on dissolved oxygen. Some types of amperometric biosensors use an immobilized enzyme to "recognize" the target molecule. The enzyme interacts with the target, releasing H_2O_2 as a by-product. This electroactive by-product is oxidized at the electrode surface to produce an electric current which is directly proportional to the concentration of target analyte present [4].

There are many possibilities in the design of the transducer, such as measuring the refractive index, electric conductance, polarization, magnetization, pH, optical absorption, etc. For example, there are chips available which carry

a tiny interferometer in a capillary [9]. Because electronic chips are becoming smaller and smaller, it is possible to design chemo-sensors and biosensors consisting of many different sensors, that are specific to many different analytes.

The main advantage of chemo-sensors and biosensors is the combination of a specific reaction (chemical or biochemical "recognition," adsorption) with an on-line measurement of a physical property, which is affected by this reaction. So the speed of physical sensing is combined with the high selectivity of chemical or biochemical reactions. Whereas physical sensors often have a high degree of stability and can be designed to be quite robust to heat and acids, chemo-sensors and biosensors have much lower stability. The sensitive layer often is not sufficiently robust against heat, acids or cleaning agents. The stability of the sensitive layer decreases as we put biological material or sensitive macromolecules like proteins on it. If chemical polymers are used in the sensitive layer, the stability increases whereas the selectivity decreases (see Figure 14.6).

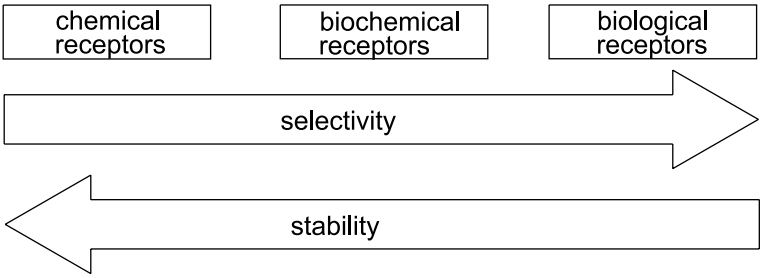

Figure 14.6. In chemo- and biosensors, stability increases while selectivity decreases

One type of biosensor that has made significant impact in the sensory evaluation of food quality is the electronic nose [10]. Aroma detection has always been a challenging area for scientific research because the human nose combines versatility and performance unmatched by any scientific instrument. When people or animals smell something, their noses are acting like sensors with olfactory receptors that are tightly tuned to families of flavors and compounds. Despite this, olfactory receptors respond to overlapping groups of volatile odorants. It is believed that flavor and aroma are signalled by combinations of receptor outputs and interpreted by pattern matching of complex scents in the brain. New biosensor technology research aims to develop a portable "cybernose" instrument. This instrument will combine the advantages of a trained human nose with the convenience and quantitative capability of electronic noses and gas chromatograph-mass spectrometers. Applications of electronic nose technology to the quality evaluation of meat, milk, seafood and spice blends can be found in [11–14]. Many other applications can be found in [10].

Other new and important applications of biosensors are in the detection of pathogenic microorganisms in foods with an unmatched combination of speed and sensitivity. A detection kit for *E. coli* O157:H7 in foods is already commercially available for this purpose [4,15]. These are only examples. There is a great need for scientists and researchers working in the field of sensors and instrumentation applied to food processing to cross the traditional barriers of isolated disciplines and interact and collaborate in interdisciplinary areas in order to accomplish major breakthroughs in on-line sensor technology. Biosensor technology is an exciting new area of biotechnology research, and includes such areas of research as instrumentation and sensors for food quality assurance, sensors and instrumentation for food analysis, biosensors for automation and control in food processing operations, bio-molecular systems/devices for analysis, microarray and nano-biosensors and smart sensors, and applications of instrumental methods of biosensor analysis to color, texture, sensory attributes, rheological properties, and other critical processing parameters important to process automation in the food industry.

14.4 Further Reading

U-tube online refractometer	[16]
coffee differentiation by GC MS aroma patterns	[17]
noninvasive detection of fouling by acoustic and optical techniques	[18]
food authenticity options for online measurement	[19]
dairy products: chemometric analytical tools	[20]
tomato products consistency by in-line absorption photometry	[21]
solid foods inspection by photothermal radiometry	[22]
apples: noncontact bruise detection by thermal imaging	[23]
fiber optical techniques for temperature measurement	[24,25]
fiber optical techniques for refraction measurement	[26]
optical measurement of pH during high pressure treatment of fluid food	[27]

Literature

1. McMeekin TA,Baranyi J, Bowman J, Dalgaard P, Kirk M, RossT, Schmid S, Zwietering MH (2006) Information systems in food safety management. Internat J Food Microbiol 112:181–194
2. Juckenack D (1989) Handbuch der Sensortechnik. Verlag Moderne Industrie, Landsberg/Lech, Germany
3. Figura LO (2005) Lebensmittelphysik. in [131]
4. Scott AO (ed) (1998) Biosensors for Food Analysis. Woodhead Publishing, Cambridge
5. Homola J, Yee SS, Gauglitz G (1999) Surface plasmon resonance sensors: review. Sensors and Actuators B: Chemical 54: 3–15

6. Brecht A, Gauglitz G. Optical probes and transducers (1995) Biosens Bioelectron 10:923–936
7. Mallat E, Barcelo D, Barzen C, Gauglitz G, Abuknesha R (2001) Immunosensors for pesticide determination in natural waters. Trends Analyt Chem 20:124–132
8. Hänel C, Gauglitz G (2002) Comparison of reflectometric interference spectroscopy with other instruments for label-free optical detection. J Anal Bioanal Chem 372:91–100
9. Gauglitz G, Brecht A, Kraus G, Nahm W (1993) Chemical and biochemical sensors based on interferometry at thin (multi-) layers. Sensors and Actuators B: Chemical. Vol. B11:21–27
10. Hurst JW (ed) (1999) Electronic Noses and Sensor Array Based Systems: Design and Applications. CRC Press, Boca Raton
11. Turhan M, Balaban MO, Luzuriaga DA (1998) Potential use of electronic nose technique for detection of meat adulteration: Separation of pork–beef mixtures. Fleischwirtschaft 6:26–28
12. Korel, F., Balaban, M.O. 2002. Microbial and sensory assessment of milk with an electronic nose. J. Food Sci. 67(2):758–764
13. Zhang H, Balaban MO, Portier K, Sims CA (2005) Quantification of spice mixture compositions by electronic nose. Part II. Comparison with GC and sensory methods. J Food Sci 70:E259–264
14. Zhang H, Balaban MO, Portier K, Sims CA (2005) Quantification of spice mixture compositions by electronic nose. Part I. Data analysis using neural networks. J Food Sci 70(4):E253–258
15. Waswa J, Irudayaraj J, DebRoy C (2007) Direct detection of *E. Coli* O157:H7 in selected food systems by a surface plasmon resonance biosensor. LWT – Food Science and Technology 40:187–192
16. Rakowski RT, Gao Y, de Keating-Hart G, Jones BE (1996) Optical transmission properties of a square cross-section U rod refractometer. Measurement 17:91–101
17. Costa Freitas M, Parreira C, Vilas-Boas L (2001) the use of an electronic aroma-sensing device to assess coffee differentiation – comparison with SPME gas chromatography–mass spectrometry aroma patterns. J Food Composition Analysis 14:513–522
18. Withers PM (1996) Ultrasonic, acoustic and optical techniques for the non-invasive detection of fouling in food processing equipment. Trends Food Sci Technology 7:293–298
19. Reid LM, O'Donnell CP, Downey G (2006) Recent technological advances for the determination of food authenticity. Trends Food Sci Technology 17:344–353
20. Karoui R, De Baerdemaeker J (2007) A review of the analytical methods coupled with chemometric tools for the determination of the quality and identity of dairy products. Food Chemistry 102: 621–640
21. Haley TA, Smith RS (2003) Evaluation of in-line absorption photometry to predict consistency of concentrated tomato products. Lebensmittel Wissenschaft und Technologie 36:159–164
22. Gijsbertsen A, Bicanic D, Gielen JLW, Chirtoc M (2004) Rapid, non-destructive and non-contact inspection of solid foods by means of photothermal radiometry; thermal effusivity and initial heating coefficient. Infrared Physics & Technology 45:93–101
23. Varith J, Hyde GM, Baritelle AL, Fellman JK, Sattabongkot T (2003) Non-contact bruise detection in apples by thermal imaging. Innovative Food Science & Emerging Technologies 4:211–218
24. Yun-Jiang Rao (2006) Recent progress in fiber-optic extrinsic Fabry–Perot interferometric sensors. Optical Fiber Technology 12:27–237
25. Jharna Mandal, Tong Sun, Kenneth TV, Augousti At (2005) Fiber laser-based temperature sensor systems using uniform wavelength-matched Bragg grating reflectors. Sensors and Actuators A: Physical 120: 451–461

26. Iadicicco A, Campopiano S, Cutolo A, Giordano M, Cusano A (2006) Self temperature referenced refractive index sensor by non-uniform thinned fiber Bragg gratings. Sensors and Actuators B: Chemical, Volume 120: 231–237
27. Stippl VM (2005) Optical In-Situ Measurement of the pH-Value During High Pressure Treatment of Fluid Food. Dissertation, Technial University Munich

15 Appendices

15.1 The International System of Units (SI)

The international system of units (i.e. Système International d'Unités; SI system) is the modern metric system of measurement. We have two classes of SI units which are called basic units (Table 15.1) and derived units (see Table 15.2).

Table 15.1. Basic units of SI and their definition

quantitiy	name	symbol	definition	relative uncertainty
time	second	s	The second is the duration of 9 192 631 770 periods of the radiation corresponding to the transition between the two hyperfine levels of the ground state of the caesium 133 atom.	10^{-14}
length	meter	m	The meter is the length of the distance travelled by light in vacuum during a time interval of 1/299 792 458 of a second.	10^{-14}
mass	kilogram	kg	The kilogram is the unit of mass; it is equal to the mass of the international prototype of the kilogram	10^{-9}
electric current	AMPERE	A	The AMPERE is that constant current which, if maintained in two straight parallel conductors of infinite length, of negligible circular cross-section, and placed 1 meter apart in vacuum, would produce between these conductors a force equal to $2 \cdot 10^{-7}$ Newton per meter of length	10^{-6}
thermodynamic temperature	KELVIN	K	The KELVIN, unit of thermodynamic temperature, is the fraction 1/273.16 of the thermodynamic temperature of the triple point of water	10^{-6}
luminous intensity	Candela (also: Candle)	cd	The Candela is the luminous intensity, in a given direction, of a source that emits monochromatic radiation of frequency $540 \cdot 10^{12}$ Hertz and that has a radiant intensity in that direction of 1/683 watt per steradian	$5 \cdot 10^{-3}$
amount of substance	mole	mol	The mole is the amount of substance of a system which contains as many elementary entities as there are atoms in 0.012 kilogram of	10^{-6}

Table 15.2. Derived SI units

quantity	symbol
area	m^2
volume	m^3
velocity	$m \cdot s^{-1}$
acceleration	$m \cdot s^{-2}$
wavenumber	m^{-1}
density	$kg \cdot m^{-3}$
specific volume	$m^3 \cdot kg^{-1}$
current density	$A \cdot m^{-2}$
magnetic field strength	$A \cdot m^{-1}$
substance concentration	$mol \cdot m^{-3}$
luminance	$cd \cdot m^{-2}$

Table 15.3. Derived units with special names and symbols

quantity	SI derived unit			
	name	symbol	expressed in terms of other SI units	expressed in terms of SI base units
plane angle	radian	rad		$m \cdot m^{-1} = 1$
solid angle	steradian	Sr		$m^2 \cdot m^{-2} = 1$
frequency	Hertz	Hz		s^{-1}
force	Newton	N		$m \cdot kg \cdot s^{-2}$
pressure, stress	Pascal	Pa	$N \cdot m^{-2}$	$m^{-1} \cdot kg \cdot s^{-2}$
energy, work, heat	Joule	J	$N \cdot m$	$m^2 \cdot kg \cdot s^{-2}$
power	Watt	W	$J \cdot s^{-1}$	$m^2 \cdot kg \cdot s^{-3}$
electric charge	Coulomb	C		$A \cdot s$
electric potential difference	Volt	V	$W \cdot A^{-1}$	$m \cdot kg \cdot s^{-3} \cdot A^{-1}$
capacitance	Farad	F	$C \cdot V^{-1}$	$m^{-2} \cdot kg^{-1} \cdot s^4 \cdot A^2$
electric resistance	Ohm	Ω	$V \cdot A^{-1}$	$m^2 \cdot kg \cdot s^{-3} \cdot A^{-2}$
electric conductance	Siemens	S	$A \cdot V^{-1}$	$m^{-2} \cdot kg^{-1} \cdot s^3 \cdot A^2$
magnetic flux	Weber	Wb	$V \cdot s$	$m^2 \cdot kg \cdot s^{-2} \cdot A^{-1}$
magentic flux density	Tesla	T	$Wb \cdot m^{-2}$	$kg \cdot s^{-2} \cdot A^{-1}$
inductance	Henry	H	$Wb \cdot A^{-1}$	$m^2 \cdot kg \cdot s^{-2} \cdot A^{-2}$
Celsius temperature	°Celsius	°C		K
luminous flux	lumen	lm		$cd \cdot sr$
illuminance	lux	lx	$lm \cdot m^{-2}$	$cd \cdot sr \cdot m^{-2}$

Table 15.4. Derived SI units with special names used in Chapter 13 on Radioactivity

derived quantity	SI derived units			
	name	symbol	expressed in terms of other SI units	expressed in terms of SI base units
activity (of a radionuclide)	Becquerel	Bq		s^{-1}
absorbed dose	Gray	Gy	$J \cdot kg^{-1}$	$m^2 \cdot s^{-2}$
dose equivalent	Sievert	Sv	$J \cdot kg^{-1}$	$m^2 \cdot s^{-2}$

Table 15.5. Examples of SI derived units and their expression in terms of SI base units

derived quantity	SI derived unit	expressed in terms of SI base units
angular velocity	$rad \cdot s^{-1}$	
angular acceleration	$rad \cdot s^{-2}$	
dynamic viscosity	$Pa \cdot s$	$m^{-1} \cdot kg \cdot s^{-1}$
momentum	$N \cdot m$	$m^2 \cdot kg \cdot s^{-2}$
surface tension	$N \cdot m^{-1}$	$kg \cdot s^{-2}$
heat flow (flux) density	$W \cdot m^{-2}$	$kg \cdot s^{-3}$
radiation intensity	$W \cdot sr^{-1}$	$m^2 \cdot kg \cdot s^{-3} \cdot sr^{-1}$
radiance	$W \cdot m^{-2} \cdot sr^{-1}$	$kg \cdot s^{-3} \cdot sr^{-1}$
heat capacity, entropie	$J \cdot K^{-1}$	$m^2 \cdot kg \cdot s^{-2} \cdot K^{-1}$
specific heat capacity, specific entropy	$J \cdot kg^{-1} \cdot K^{-1}$	$m^2 \cdot s^{-2} \cdot K^{-1}$
specific energy	$J \cdot kg^{-1}$	$m^2 \cdot s^{-2}$
thermal conductivity	$W \cdot m^{-1} \cdot K^{-1}$	$m \cdot kg \cdot s^{-3} \cdot K^{-1}$
energy density	$J \cdot m^{-3}$	$m^{-1} \cdot kg \cdot s^{-2}$
electric field strength	$V \cdot m^{-1}$	$m \cdot kg \cdot s^{-3} \cdot A^{-1}$
electric charge density	$C \cdot m^{-3}$	$m^{-3} \cdot s \cdot A$
electric flux density	$C \cdot m^{-2}$	$m^{-2} \cdot s \cdot A$
permittivity	$F \cdot m^{-1}$	$m^{-3} \cdot kg^{-1} \cdot s^4 \cdot A^2$
permeability	$H \cdot m^{-1}$	$m \cdot kg \cdot s^{-2} \cdot A^{-2}$
molar energy	$J \cdot mol^{-1}$	$m^2 \cdot kg \cdot s^{-2} \cdot mol^{-1}$
molar entropy, molar heat capacity	$J \cdot mol^{-1} \cdot K^{-1}$	$m^2 \cdot kg \cdot s^{-2} \cdot K^{-1} \cdot mol^{-1}$
exposure (X and γ-rays)	$C \cdot kg^{-1}$	$kg^{-1} \cdot s$
absorbed dose rate	$Gy \cdot s^{-1}$	$m^2 \cdot s^{-3}$

Table 15.6. SI prefixes for orders of magnitude

factor	name	symbol	factor	name	symbol
10^{24}	yotta	Y	10^{-1}	deci	d
10^{21}	zetta	Z	10^{-2}	centi	c
10^{18}	exa	E	10^{-3}	milli	m
10^{15}	peta	P	10^{-6}	micro	μ
10^{12}	tera	T	10^{-9}	cano	n
10^{9}	giga	G	10^{-12}	pico	p
10^{6}	mega	M	10^{-15}	femto	f
10^{3}	kilo	k	10^{-18}	atto	a
10^{2}	hecto	h	10^{-21}	zepto	z
10	deca	da	10^{-24}	yocto	y

Table 15.7. Non-SI units accepted for use with the International System

name		symbol	value in SI units
minute	(time)	min	1 min = 60 s
hour		h	1h = 60 min = 3600 s
day		d	1 d = 24 h = 86400 s
gon		gon	1 gon = (1/200) rad
degree	(plane angle)	°	$1^\circ = (\pi/180)$ rad
minute	(plane angle)	′	$1' = (1/60)^\circ = (\pi/10800)$ rad
second	(plane angle)	″	$1'' = (1/60)^\circ = (\pi/648000)$ rad
liter		l, L	$1l = 1dm^3 = 10^{-3}\ m^3$
metric ton		t	$1\ t = 10^3$ kg

The unit liter has the symbol *l* and alternative *L* in order to avoid the confusion between the letter l and number 1.

Table 15.8. Other non-SI units currently accepted for use with SI

name	symbol	value in SI units
nautical mile	n.m.	1 nautical mile = 1852 m
knots	kn	1 nautical mile per hour = (1852/3600) $m \cdot s^{-1}$
Ångstrøm	Å	1 Å = 0.1 nm = 10^{-10} m
acre	a	$1\ a = 1\ dam^2 = 10^2\ m^2$
hectare	ha	$1\ ha = 1\ hm^2$
barn	b	$1\ b = 10^{-28}\ m^2$
bar	bar	1 bar = 0.1 MPa = 10^5 Pa
Curie	Ci	1 Ci = 3.7 10^{10} Bq
Röntgen	R	1 R = 2.58 10^{-4} C/kg
rad	rad	1 rad = 1 cGy = 10^{-2} Gy
rem	rem	1 rem = 1 cSv = 10^{-2} Sv

Table 15.9. Old English units and their conversion into SI units

length		**area**	
1 mile	= 1.609 34 km	1 sq mile	= 2.589 99 km^2
1 furlong	= 0.201 168 km	1 acre	= 4046.86 m^2
1 chain	= 20.116 8 m	1 rood	= 1011.71 m^2
1 yd (yard)	= 0.914 4 m	1 yd^2 (square yard)	= 0.836 127 m^2
1 ft (foot)	= 0.304 8 m	1 ft^2 (square foot)	= 0.092903 m^2
1 in (inch)	= 2.54 cm	1 in^2 (square inch)	= 6.4516 cm^2
1 nautical mile	= 1.853 18 km		
1 fathom	= 1.828 8 m	**mass**	
		1 ton (short ton is 909.11 kg)	= 1016.05 kg
volume		1 cwt (hundredweight)	= 50.8023 kg
1 yd^3 (cubic yard)	= 0.764 55 m^3	1 short hundred-weight	= 45.3592 kg
1 ft^3 (cubic foot)	= 28.316 8 dm^3	1 quarter	= 12.7006 kg
1 in^3 (cubic inch)	= 16.387 1 cm^3	1 stone	= 6.35029 kg
1 bu (bushel)	= 36.368 7 dm^3	1 lb (pound)	= 0.45359237 kg
1 pk (peck)	= 9.092 18 dm^3	1 oz (ounce)	= 28.3495 g
1 imperial gal (gallon)	= 4.546 09 dm^3	1 dr (dram)	= 1.77185 g
1 US gal	= 3.785 41 dm^3	1 gr (grain)	= 64.7989 mg
1 qt (quart UK)	= 1.136 52 dm^3	1 troy pound	= 373.24172 g
1 pt (pint UK)	= 0.568 261 dm^3	1 oz tr (troy ounce)	= 31.1035 g
1 gill	= 0.142 065 dm^3	1 drachm	= 3.88793 g
1 fl oz	= 28.413 1 cm^3	1 scruple	= 1.29598 g
1 fluid drachm	= 3.551 63 cm^3	1 dwt (pennyweight)	= 1.55517 g
1 minim	= 59.193 9 mm^3	1 slug	= 14.5939 kg

mass per unit area		**mass concentration**	
1 ton · $mile^{-2}$	= 392.298 kg/km^2	1 gr/ 100 ft^3	= 0.022883 5 g · cm^{-3}
	= 3.922 98 kg/ha	1 oz/ gal	= 6.23602 g · l^{-1}
1 ton · $acre^{-1}$	= 0.251 071 kg/m^2	1 gr/ gal	= 14.2538 mg · l^{-1}
	= 2510.71 kg/ha		
1 cwt · $acre^{-1}$	= 0.012 553 5 kg/m^2	**moment of inertia**	
	= 125.535 kg/ha	1 lb ft^2	= 0.0421401 kg · m^2
1 lb · ft^{-2}	= 4.882 43 kg/m^2	1 lb in^2	= 2.92640 kg · cm^2
1 lb · in^{-2}	= 70.307 0 g/cm^2	1 oz in^2	= 0.182900 kg · cm^2
1 oz · yd^{-2}	= 33.905 7 g/m^2	1slug ft^2	= 1.35582 kg · m^2
1 oz · ft^{-2}	= 305.152 g/cm^2		

area per unit mass		**angular moment of inertia**	
1 sq mile/ ton	= 2 549.08 $m^2 \cdot kg$	1 lb ft/s	= 0.138255 $kg \cdot m \cdot s^{-1}$
1 yd^2/ton	= 0.822922 $m^2 \cdot t^{-1}$		
specific volume		**moment**	
1 in^3/lb	= 36.1273 $cm^3 \cdot kg^{-1}$	1 lb ft^2/s	= 0.0421401 $kg \cdot m^2 \cdot s^{-1}$
1 ft^3/ton	= 0.027869 6 $dm^3 \cdot kg^{-1}$	**force**	
1 ft^3/lb	= 62.4280 $dm^3 \cdot kg^{-1}$	1 tonf (ton force)	= 9 964.02 N
1 gal/lb	= 10.0224 $dm^3 \cdot kg^{-1}$	1 lbf (pound force)	= 4.44822 N
fuel consumption		1 ozf	= 0.278014 N
1 ga · $mile^{-1}$	= 2.824 81 l · km^{-1}	1 pdl (poundal)	= 0.138255 N
1 USgal · $mile^{-1}$	= 2.352 15 l · km^{-1}		
1 mile · gal^{-1}	= 0.354006 km · l^{-1}	**angular moment**	
1 mile · $USgal^{-1}$	= 0.425144 km · l^{-1}	1 lbf ft	= 1.35582 N · m
		1 ton f ft	= 3037.03 N · m
density		1 pdl ft	= 0.0421401 N · m
1 ton · yd^{-3}	= 1.32894 t · m^{-3}	1 ozf in	= 0.706155 N · cm
1 lb·ft^{-3}	= 16.0185 kg·m^{-3}	1 lbf in	= 0.112985 N·m
1 lb·in^{-3}	= 27.6799 g·cm^{-3}		
1 lb·gal^{-1}	= 0.099776 3 kg·l^{-1}		
1 slug·ft^{-3}	= 515.379 kg·m^{-3}		

pressure, stress		**energy**	
1 tonf · ft^{-2}	= 107.252 kPa	1 therm	= 105.506 MJ
1 tonf · in^{-2}	= 15.4443 MPa	1 hp · h (horsepower · hour)	= 2.68452 MJ
1 lbf · ft^{-2}	= 47.8803 Pa	1 Btu (British thermal unit)	= 1.05506 kJ
1 lbf · in^{-2}	= 6 894.76 Pa	1 ft · lbf	= 1.35582 J
1 ft H_2O	= 1.48816 Pa	1 ft · pdl	= 0.0421401 J
1 in H_2O	= 249.089 Pa		
1 in Hg	= 3386.39 Pa		
dynamic viscosity		**power**	
1 pdl · s · ft^{-2}	= 1.48816 Pa · s	1 hp (horsepower)	= 745.700 W
1 lbf · h · ft^{-2}	= 0.172369 MPa · s	1 lf lbf · s^{-1}	= 1.35582 W
1 lbf · s · ft^{-2}	= 47.8803 Pa · s	**heat flux**	
heat flow		1 Btu · ft^{-2} · h^{-1}	= 3.15459 W · m^{-2}
1 Btu · h^{-1}	= 0.293071 W		

specific energy		overall heat transfer coefficient	
$1\ \mathrm{Btu \cdot lb^{-1}}$	$= 2326\ \mathrm{J \cdot kg^{-1}}$	$1\ \mathrm{Btu \cdot ft^{-2} \cdot h^{-1} \cdot {}^{\circ}F^{-1}}$	$= 5.678\ 26\ \mathrm{W/m^2\ K}$
$1\ \mathrm{ft\ lbf \cdot lb^{-1}}$	$= 2.989\ 07\ \mathrm{J \cdot kg^{-1}}$	**thermal conductivity**	
caloric value per unit volume		$1\ \mathrm{Btu \cdot ft \cdot ft^{-2} \cdot h^{-1} \cdot {}^{\circ}F^{-1}}$	$= 1.73073\ \mathrm{W \cdot m^{-1} \cdot K^{-1}}$
$1\ \mathrm{therm \cdot gal^{-1}}$	$= 23.2080\ \mathrm{MJ \cdot l^{-1}}$	$1\ \mathrm{Btu \cdot in \cdot ft^{-2} \cdot h^{-1} \cdot {}^{\circ}F^{-1}}$	$= 0.144228\ \mathrm{W \cdot m^{-1} \cdot K^{-1}}$
$1\ \mathrm{Btu \cdot ft^{-3}}$	$= 0.0372589\ \mathrm{J \cdot cm^{-3}}$	$1\ \mathrm{Btu \cdot in \cdot ft^{-2} \cdot s^{-1} \cdot {}^{\circ}F^{-1}}$	$= 519.220\ \mathrm{W \cdot m^{-1} \cdot K^{-1}}$
		specific thermal resistance	
		$1\ \mathrm{ft^2 \cdot h \cdot {}^{\circ}F \cdot Btu^{-1} \cdot in^{-1}}$	$= 6.933\ 47\ \mathrm{K \cdot m \cdot W^{-1}}$
specific heat capacity		$1\ \mathrm{ft^2 \cdot h \cdot {}^{\circ}F \cdot Btu^{-1} \cdot ft^{-1}}$	$= 57.778\ 9\ \mathrm{K \cdot cm \cdot W^{-1}}$
$1\ \mathrm{Btu \cdot lb^{-1} \cdot {}^{\circ}F^{-1}}$	$= 4\ 186.8\ \mathrm{J \cdot kg^{-1} \cdot K^{-1}}$	**luminous intensity**	
$1\ \mathrm{ft \cdot lbf \cdot lb^{-1} \cdot {}^{\circ}F^{-1}}$	$= 5.38032\ \mathrm{J \cdot kg^{-1} \cdot K^{-1}}$	$1\ \mathrm{lm \cdot ft^{-2}} = 1$ foot candle	$= 10.763\ 9\ \mathrm{lx}$
specific entropy		**luminance**	
$1\ \mathrm{Btu \cdot lb^{-1} \cdot {}^{\circ}R^{-1}}$	$= 4\ 186.8\ \mathrm{J \cdot kg^{-1} \cdot K^{-1}}$	$1\ \mathrm{cd \cdot ft^{-2}}$	$= 10.7639\ \mathrm{cd \cdot m^{-2}}$
heat capacity per unit volume		$1\ \mathrm{cd \cdot in^2}$	$= 1\ 550.00\ \mathrm{cd \cdot m^{-2}}$
$1\ \mathrm{Btu \cdot ft^{-3} \cdot {}^{\circ}F^{-1}}$	$= 0.0670661\ \mathrm{J \cdot cm^{-3} \cdot K^{-1}}$	1 foot lambert	$= 3.426\ 26\ \mathrm{cd \cdot m^{-2}}$

Pound

The TROY system is the system of units used for precious metals and gems:
1 TROY pound = 12 TROY ounces = 240 pennyweight = 5760 grain
The AVOIDURPOIS system defines: 1 (AVOIRDURPOIS) pound = 0.453 592 27 kg

15.2 Distribution Functions

To better understand how distributions are generated and how they work and can be interpreted, some basic examples of velocity distributions are presented here. The first one is very simple and can be used to understand the components of distribution functions without any special mathematical background. Let us assume we have obtained these data from a police speed check in front of our house on a given day:

Example 15.1. Speed check data

$v/\mathrm{km \cdot h^{-1}}$	50	20	40	30	60	80	70

The total number of values is $N = 7$. We can see that the values are not all the same, the velocity is distributed. The median of the distribution is the middle of an ordered listing of the data (from lowest to highest value), so it is apparently $50\ \mathrm{km \cdot h^{-1}}$:

20	30	40	50	60	70	80
			↑			
			median			

Let us now take a larger set of data:

$v/\mathrm{km \cdot h^{-1}}$	50	40	30	60	60	50	40	30	20	40	50	50	60	60	70	60

In this case, the total number of data points now is $N = 16$, the arithmetic average is $\overline{v} = \frac{1}{N}\sum_{i=1}^{N} v_i = 48.1\ \mathrm{km \cdot h^{-1}}$.

Now we can make categories of velocity ranges (in this example we will make five velocity categories), and put the data into these categories, as shown in Example 15.2.

Example 15.2. Sorting the measured velocities into five categories

i	v_i/km · h^{-1}	Δv_i/km · h^{-1}	$\overline{v_i}$/km · h^{-1}	ΔN_i	$\Delta Q_i = \frac{\Delta N_i}{N}$	$Q_{0,i}$	$q_{0,i}$/km · h^{-1}
1	0	21	10.5	1	0.0625	0.000	$3.0 \cdot 10^{-3}$
2	21	14	28.5	2	0.125	0.0625	$8.3 \cdot 10^{-3}$
3	35	17	43.5	7	0.4375	0.1875	$25.7 \cdot 10^{-3}$
4	52	10	57.0	5	0.3125	0.625	$31.3 \cdot 10^{-3}$
5	62	13	68.5	1	0.0625	0.9375	$4.8 \cdot 10^{-3}$
	75					1.0	

$Q = \sum_{i=1}^{j} \frac{\Delta N_i}{N} = Q_0(N_i) = Q_{0,i}$ distribution sum (here number distribution sum)

$N = \sum_{i=1}^{k} \Delta N_i$ sum of the fractions in the classes (here: the sum of a number, not e.g. of a mass)

$q_{0,i} = \frac{\frac{\Delta N_i}{N}}{\Delta v_i}$ distribution density (here: number distribution density)

i category index

$\frac{\Delta N_i}{N} = \Delta Q_{0,i}$ number fraction in category i (here: fraction of number)

$\frac{\Delta \mu_i}{\mu} = \Delta Q_{r,i}$ fraction in any category i (general)

When Q is drawn versus the measured quantity (here the velocity) we get a distribution curve, called the sum distribution curve (see Figure 15.1). The value of Q is between 0 and 1, meaning between 0% and 100%. The histogram bars in Figure 15.2 show us how many categories we have. The smooth sigmoid curve in Figure 15.2 is what the profile of the histogram bars would look like if we were able to make a very large number of categories (approaching an infinite number) with very large amounts of measured data.

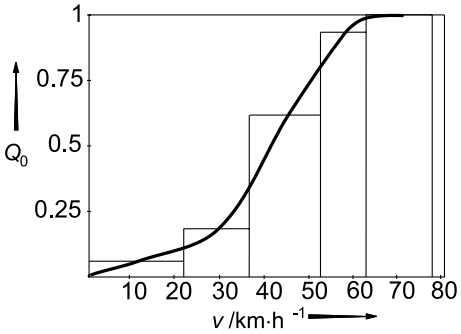

Figure 15.1. Sum distribution curve showing accumulation of sum fraction of speed measurements in velocity class categories as a function of velocity

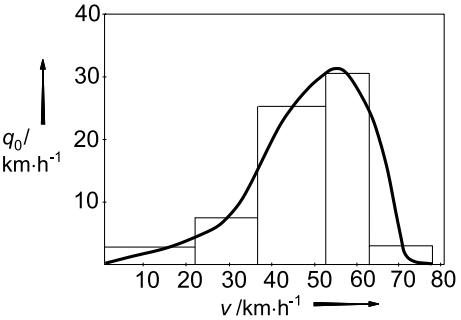

Figure 15.2. Velocity distribution density curve showing the number fraction as a function of velocity in a radar speed check

When q is drawn versus the measured quantity (here the velocity) we will obtain another distribution curve, called the distribution density curve (see Figure 15.2). In this example, it is a number distribution density curve. In mathematical terms q is the derivative of Q. Taking this new histogram shown in Figure 15.2, we see that with only a limited number of categories we have no smooth curve, but a "bell shaped" step-wise curve made up of steps going up and down because of the limited number of categories. Again, the smooth "bell shaped" curve is the one we would get if we could have an infinite number of categories and measured data points.

This example was over a velocity distribution. We measured the velocity, put the data into categories, and counted the number of occurrences. This resulted in a number distribution function. This type of distribution function exercise could be carried out with any other type of measurable quantity. For example, instead of measuring velocities we could have measured the mass of particles in different size categories to get a mass distribution, or measured length to get a length distribution, or areas or volumes to get an area distribution function or volume distribution function. Therefore, it is important to distinguish between what is the distributed quantity (here velocity) and what set (grouping) we use to characterize an individual belonging to a category. The set or grouping can be a number but it can also be another type of set. Recall that when we do a particle size distribution, we perform sieving experiments and then weigh the sample on each of the sieves. This results in a mass distribution and not in a

number distribution of the particle size (understand that in the case of using sieves, we at least only have to weigh the sample and not measure the actual size of the particles to get a particle size distribution).

When we talk about number distributions, then we use terms from probability theory. In our speed check example, the expression $\frac{\Delta N_i}{N} = \Delta Q_0(v_i)$ gives the fraction of cars found travelling in a velocity category i. For example, in category 4 (speed between 52 and 62 km $\cdot$ h^{-1}) of Example 15.2 we found five cars, so $\Delta Q_{0,4} = \frac{5}{16} = 0.3125 = 31.25\%$. If the data were reliable, such as would be the case for a much greater number of measured data points (speed checks), then we say that the probability P to meet a car travelling with a speed between 52 and 62 km $\cdot$ h^{-1} is about 31,25%.

So, we can see that probability is nothing more than:

$$P = \frac{\Delta N_i}{N} = \Delta Q_0(v) \tag{15.1}$$

respectively

$$P = \frac{\mathrm{d}N}{N} = \Delta Q_0(v) \tag{15.2}$$

So when we have a number distribution, we can handle the $Q_0 - v$ function like a probability function. The derivative function then is called a probability density function q_0.

$$q_0 = f(v) = \frac{\mathrm{d}Q_0}{\mathrm{d}v} \tag{15.3}$$

Perhaps the most famous probability density function related to velocity is the Maxwell–Boltzmann function, which describes the velocity distribution of molecules and atoms. Let us have a short look at this more complex example of a velocity function $f(v)$. It is also a number distribution, too. Let us start with some general properties of this function, as listed in Table 15.10.

When the distribution function $f(v)$ is known, many properties of the set of individuals can be obtained by mathematics, e.g.

- the most probable velocity (modal value)
- the average velocity
- the average of the velocity squared
- the median
- the width (or range) of the distribution
- the standard deviation of the mean.

An example of how this can be performed is shown here with the velocity distribution of atoms or molecules in a gas. The function $f(v)$ was first derived by Maxwell and was proven later by Boltzmann. Today it is known as the Maxwell–Boltzmann function defined as follows:

$$f(v) = 4\pi \left(\frac{m}{2\pi kT}\right)^{\frac{3}{2}} \cdot v^2 \cdot \mathrm{e}^{-\frac{\frac{1}{2}mv^2}{kT}} \tag{15.4}$$

Table 15.10. Properties of a velocity distribution $f(v)$

$\int_{v_1}^{v_i} f(v) \cdot \mathrm{d}v = \Delta Q_0$	fraction of individuals in a category i, having a velocity between $v_1 \ldots v_2$. Probability to meet an individual having a speed between v_1 and v_2 by condition of standardization: The fraction of individuals having a speed between $v_{\min} \ldots v_{\max}$ is 1, so the probability to meet an individual having a speed between $v_{\min} \ldots v_{\max}$ is 100%
$\int_{v_{\min}}^{v_{\max}} f(v) \cdot \mathrm{d}v = 1$	
$\int_0^\infty f(v) \cdot v \cdot \mathrm{d}v = \overline{v}$	is the integral mean of the velocity
$\int_0^\infty f(v) \cdot v \cdot \mathrm{d}v = \overline{v} = \int_0^\infty \frac{\mathrm{d}N}{N} \cdot v \cong \frac{1}{N} \sum_{i=1}^{N} \Delta N_i v_i$	is identical to the known arithmetic mean of the velocity
$\int_0^\infty f(v) \cdot v^2 \cdot \mathrm{d}v = \overline{v^2}$	is the integral mean of the velocity squared

where

m	mass of an atom in kg
k	BOLTZMANN's constant
T	temperature in K
v	velocity of an atom in $\mathrm{m} \cdot \mathrm{s}^{-1}$

The maximum of the curve provides us with the velocity which is most probable:

Maximum means:

$$\frac{\mathrm{d}f(v)}{\mathrm{d}v} = 0 \tag{15.5}$$

The condition for this is:

$$\left(\mathrm{e}^{-\frac{mv^2}{2kT}} = \mathrm{e}^{-1}\right) \Rightarrow \left(\frac{\mathrm{d}f(v)}{\mathrm{d}v} = 0\right) \tag{15.6}$$

which means

$$\frac{1}{2}\, m \cdot v^2 = kT \tag{15.7}$$

or

$$E_{kin} = kT \tag{15.8}$$

so the most probable velocity is

$$v_w = \sqrt{\frac{2kT}{m}} \tag{15.9}$$

The mean velocity (arithmetic mean) can be obtained by forming the integral mean. The result often is also called the average velocity $\overline{v}_d$:

$$\overline{v}_d = \int_0^\infty f(v) \cdot v \cdot \mathrm{d}v = \left(\frac{8kT}{\pi m}\right)^{\frac{1}{2}} = \sqrt{\frac{4}{\pi}} \cdot \sqrt{\frac{2kT}{m}} \tag{15.10}$$

so it is slightly different from (15.9)

$$\overline{v}_d = \sqrt{\frac{4}{\pi}} \cdot \sqrt{\frac{2kT}{m}} = 1.13 \cdot v_w \tag{15.11}$$

The integral mean of v^2, the so-called mean velocity squared is obtained by

$$\overline{v^2} = \int_0^\infty f(v) \cdot v^2 \cdot \mathrm{d}v = \frac{3kT}{m} \tag{15.12}$$

so it is

$$v_m = \sqrt{\overline{v^2}} = \sqrt{\frac{3kT}{m}} \tag{15.13}$$

Comparison with (15.9) gives

$$\overline{v^2} = \sqrt{\frac{3}{2}} \cdot v_w = 1.225 v_w \tag{15.14}$$

In Table 15.11 the results are listed and compared with each other.

Table 15.11. Characteristics of the Maxwell–Boltzmann velocity distribution function

velocity	symbol	formula	comparison	description
most probable	v_w	$\sqrt{\frac{2kT}{m}}$	$1 \cdot v_w$	maximum of curve
average	v_d	$\sqrt{\frac{8}{\pi}\frac{kT}{m}}$	$1.128 \cdot v_w$	arithmetic mean
mean	$v_m = \sqrt{\overline{v^2}}$	$\sqrt{\frac{3kT}{m}}$	$1.225 \cdot v_w$	mean v^2

Now we may recognize $v_m = \sqrt{\frac{3kT}{m}}$ which is used in many applications, such as in the basis of the ideal gas law, which is an outcome of the application of mathematics to the Maxwell–Boltzmann distribution function. When we look again at this function (see below), we recognize it is made up of a superposition of a square root function and an exponential function. The last one sometimes is called the Boltzmann factor. At low temperatures the Boltzmann factor is nearly 1, so we simplify to the square root function only. On the

other hand at high temperatures the BOLTZMANN factor is the dominant part of the function.

$$f(v) = 4\pi \left(\frac{m}{2\pi kT}\right)^{\frac{3}{2}} \cdot v^2 \cdot \underbrace{e^{-\frac{\frac{1}{2}mv^2}{kT}}}_{\text{BOLTZMANN factor}} \tag{15.15}$$

In this section, we have learned how to create and work with distribution functions, going from simple to more complex examples. Distribution functions are very important in science and engineering. In the previous exercises, we began with a simple example involving a velocity distribution function from a radar speed check, and progressed to more complex distribution functions that form some of the main principles in thermodynamics, like the basic assumptions behind the ideal gas laws.

15.3 Complex Numbers

Complex numbers are numbers which include a real part and an imaginary part. Imaginary numbers are defined as a multiple of the imaginary unit i:

$$i = \sqrt{-1}$$

Note that this number is imaginary because there exists no real number that can be the square root of a negative number.

Therefore, with:

$$i = \sqrt{-1} \qquad \frac{1}{i} = -i \qquad i^2 = -1 \qquad i^3 = -i \qquad i^4 = +1$$

i and $-i$ are solutions of the quadratic equation $x^2 = -1$ it is:

$$i^5 = i^9 = i$$
$$i^6 = i^{10} = -1$$
$$i^7 = i^{11} = -i$$
$$i^8 = i^{12} = 1$$

The position of the imaginary part of the complex numbers in mathematics is shown in Table 15.12.

A complex number is usually expressed in a CARTESian form. The real part is plotted on the abscissa (real axis) and the imaginary part (as a multiple of i) is plotted on the ordinate (imaginary axis), as shown in Figure 15.3. In general the complex number is expressed as:

$$z = a + i \cdot b \tag{15.16}$$

The representation of complex numbers in polar coordinates looks similar (Figure 15.4), and is also called a trigonometrical representation.

Table 15.12. System of numbers in mathematics

numbers					
real numbers				imaginary numbers	
rational numbers		irrational numbers		pure imaginary numbers	complex numbers
whole numbers	fractional number	algebraic irrational numbers	transcendent numbers	multiple of i $i = \sqrt{-1}$	numbers with real and imaginary parts
1; 2; 3;	$\frac{1}{3}; \frac{1}{2}$	$\sqrt{2}; \sqrt{3}$	$\pi = 3.1416\ldots$	$\sqrt{-4} = 2i$	$4 + 3i$
18; –18	0.25; –6.3	$\sqrt[5]{\frac{27}{4}}$	$e = 2.718\ldots$		
…	…	…	$\sin 2 = 0.9093$		

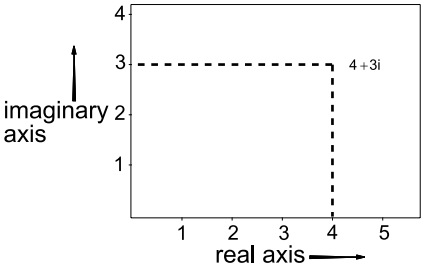

Figure 15.3. Graphical representation of the complex number $4 + 3i$ in a planar diagram (two dimensions)

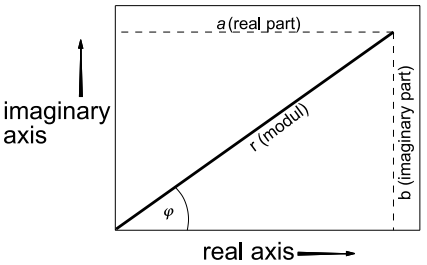

Figure 15.4. Trigonometrical representation of a complex number in polar coordinates

The angle φ in Figure 15.4 is:

$$\cos\varphi = \frac{a}{r} \qquad a = r \cdot \cos\varphi$$

$$\sin\varphi = \frac{b}{r} \qquad b = r \cdot \sin\varphi$$

When put into equation (15.16):

$$z = r(\cos\phi + i \cdot \sin\varphi) \tag{15.17}$$

These also can be written as:

$$\tan\varphi = \frac{a}{b}$$

$$r = \sqrt{a^2 + b^2}$$

Example 15.3. The complex number 3 + 4i
If the complex number z is $3 + 4i$, this means

$$a = 3$$

$$b = 4$$

$$r = \sqrt{a^2 + b^2}$$

$$r = \sqrt{3^2 + 4^2} = 5$$

Also

$$\cos\varphi = \frac{3}{5} = 0.6 \qquad \varphi = 53.13^\circ$$

$$\sin\varphi = \frac{4}{5} = 0.8 \qquad \varphi = 53.13^\circ$$

When constituted into equation (15.17), the calculation can be made in reverse:

$$z = 5 \cdot (\cos 53.13^\circ + i \cdot \sin 53.13^\circ) = 5\,(0.6 + i \cdot 0.8) = 3 + 4i.$$

A very simple expression of complex numbers is to use the relations from Euler. Euler's formulae are:

$$e^{ix} = \cos x + i \cdot \sin x \tag{15.18}$$

$$e^{-ix} = \cos x - i \cdot \sin x \tag{15.19}$$

The Euler's number e is the base of the natural logarithm.

With φ from the trigonometrical representation (Figure 15.4) we have:

$$e^{i\varphi} = \cos\varphi + i \cdot \sin\varphi \tag{15.20}$$

$$e^{-i\varphi} = \cos\varphi - i \cdot \sin\varphi \tag{15.21}$$

With Euler's number, the complex number z can write as:

$$z = |z| \cdot e^{i\varphi} \tag{15.22}$$

$$z = |z| \cdot (\cos\varphi + 1 \cdot \sin\varphi) \tag{15.23}$$

$$z = \underbrace{|z| \cdot \cos\varphi}_{\text{real part}} + \underbrace{i \cdot |z| \cdot \sin\varphi}_{\text{imaginary part}} \tag{15.24}$$

The comparison of these formula to equation (15.17) indicates that the modulus r of the trigonometrical representation in Figure 15.4 is the same as the amount of the complex number z.

$$r = |z| \tag{15.25}$$

The simple advantage for describing a complex number with the Euler's formula is that there is no necessity to use the quantity φ to express the complex number [122] (see right column in Table 15.13).

Table 15.13. Possibilities for expression of the complex number $3 + 4i$

real part	imaginary part	angle φ in $^\circ$	angle φ in rad	EULER	EULER
3	4	53.13°	0.927	$z = \mathrm{e}^{i \cdot 53.13^\circ}$	$z = \mathrm{e}^{i \cdot 0.927}$

Example 15.4. EULER*'s notation of the complex number* $3 + 4i$

$$z = 3 + 4i$$

$$z = a + b \cdot i$$

$$z = \underbrace{|z| \cdot \cos\varphi}_{3} \quad + \quad \underbrace{i \cdot |z| \cdot \sin\varphi}_{4}$$

$$\tan\varphi = \frac{b}{a} = \frac{4}{3}$$

$$\varphi = 53.13^\circ$$

$$z = = \mathrm{e}^{i\varphi}$$

$$z = \mathrm{e}^{i \cdot 53.13^\circ}$$

$$|z| = \sqrt{a^2 + b^2} = \sqrt{9 + 16}$$

$$|z| = 5$$

In general, we can say:

$$\tan\varphi = \frac{\text{imaginary part}}{\text{real part}}$$

$$|z| = \sqrt{(\text{real part})^2 + (\text{imaginary part})^2}$$

Table 15.14. Several phase angles and their interpretation, examples

$\varphi/^\circ$	$\tan\varphi$	description
0	0	real part $\gg$ imaginary part (e.g. when imaginary part = 0)
30	$\frac{1}{3}\sqrt{3}$	real part $>$ imaginary part
45	1	real part = imaginary part
60	$\sqrt{3}$	real part $<$ imaginary part
90	∞	real part $\gg$ imaginary part (e.g. when real part is nearly zero)
135	–1	imaginary part = –(real part)
180	0	see $\varphi = 0^\circ$

Complex Physical Quantities

Physical quantities can also be complex numbers which consist of a real part and an imaginary part. Such a physical quantity is called an apparent quantity, which consists of an effective component (real part) and a loss component (imaginary part). Figure 15.5 illustrates a complex physical quantity with the help of these terms.

When we use "normal" mathematics (without using imaginary parts) we assume the imaginary part is zero, meaning the loss part is zero, and by this observed quantity is equal to the effective component, totally.

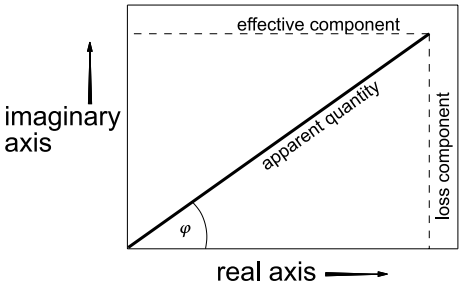

Figure 15.5. Trigonometrical representation of a physical quantity

To help us work with some of the complex properties used in this book, some examples are presented here for the purpose of illustration. We should also recognize that different scientific disciplines or fields of engineering may use their own special terms for the real and imaginary parts, but the mathematics are the same.

Example 15.5. Complex electric resistance
In electric circuits with alternating current, we have real resistances and imaginary resistances, called active resistance and reactive resistance. The apparent quantity – the apparent resistance – is called the impedance, as shown in Table 15.15:

Table 15.15. Terms in a complex electric resistance

impedance	=	effective resistance	+	reactive resistance
Z	=	R	+	$i\left(\omega \cdot L - \frac{1}{\omega \cdot C}\right)$

Table 15.16. Terms in a complex electric conductance

admittance	=	conductance	+	susceptance
Y	=	G	+	$i\left(\omega \cdot C - \frac{1}{\omega \cdot L}\right)$

The inverse quantities are named:

Z, R	resistance in Ω
Y, G	admittance in S
C	capacitance in F
L	inductance in H
ω	angular frequency in s^{-1}

There are cases, in which the reactive resistance is zero, e.g. if the capacitance is zero or the angular frequency is $\omega = 0$. The latter is the case in direct current circuits. We see that all observed resistances are also active resistances, such as OHMic resistances, and we do not have to deal with complex quantities. On the other hand in alternating fields, impedance and resistance is not the same, and we have to take into account both real and imaginary parts of the complex quantities.

Example 15.6. Rheology – oscillation test
By means of mechanic oscillation, it is possible to differentiate between elastic and nonelastic (viscous) properties of a material. The observed behavior can be described as a complex quantity (e.g. complex modulus), which includes both properties, elastic and viscous. Then the elastic properties are represented by the real part and the inelastic (viscous) properties by the imaginary part. In this sense the nonelastic, viscous behavior of the sample is understood as the loss part. A behavior like this can be easily described by the loss angle φ or by the loss tangent, $\tan \varphi$.

It is important to avoid confusion in this regard. For describing rheological behavior, it is also possible to use the apparent viscosity as a complex property which consists of real (viscous) parts and imaginary (elastic) parts. Also sometimes it is useful to use the complex compliance instead of the complex elasticity. When further study of complex rheological properties is needed, it may be helpful to remember to refer to this section once again.

Example 15.7. Modulated DSC
Oscillation tests in thermal analysis are referred to as temperature-modulated tests (MDSC, see Section 7.9.2). These tests result in a complex heat flow which is composed of a real part and an imaginary part. The real part is caused by the heat capacity of the sample; it is a reversible heat flow. The imaginary part is a nonreversible heat flow, in other words the loss component. It may be caused by chemical reactions in the sample. In an analogous way a complex heat capacity can be defined.

15.4 Greek Letters

A	α	*a*	Alpha	*B*	β	*b*	Beta
Γ	γ	*g*	Gamma	Δ	δ	*d*	Delta
E	ε	*e*	Epsilon	*Z*	ζ	*z*	Zeta
H	η	*e*	Eta	Θ	θ, ϑ	*th*	Theta
I	ι	*j*	Jota	*K*	κ	*k*	Kappa
Λ	λ	*l*	Lambda	*M*	μ	*m*	Mu
N	ν	*n*	Nu	Ξ	ξ	*x*	Xi
O	o	*o*	Omikron	Π	π	*p*	Pi
P	ρ	*r*	Rho	Σ	σ	*s*	Sigma
T	τ	*t*	Tau	*Y*	υ	*y*	Ypsilon
Φ	ϕ	*ph*	Phi	*X*	χ	*ch*	Chi
Ψ	ψ	*ps*	Psi	Ω	ω	*o*	Omega

Figure 15.6. Greek block letters and there names

To exercise the notation of Greek letters Figure 15.7 will be helpful:

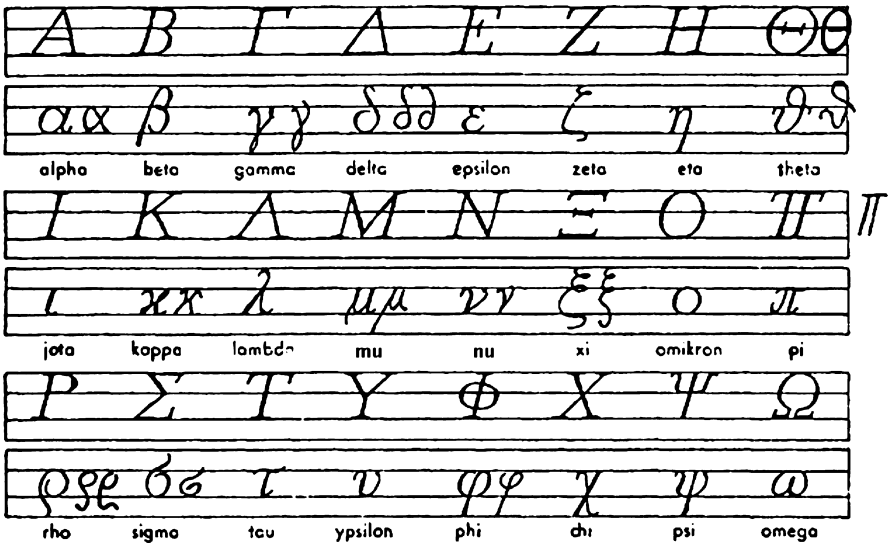

Figure 15.7. Greek script

15.5 Conversion Chart: Temperature

Table 15.17. Conversion of temperatures

given quatitiy in:	required quantity in: °C	required quantity in: °F
°C	1	$\vartheta/°\mathrm{F} = 9/5 \cdot \vartheta/°\mathrm{C} + 32$
°F	$\vartheta/°\mathrm{C} = 5/9 \cdot (\vartheta/°\mathrm{F} - 32)$	1
°R	$\vartheta/°\mathrm{C} = 5/9 \cdot (\vartheta/°\mathrm{R} - 491.67)$	$\vartheta/°\mathrm{F} = \vartheta/°\mathrm{R} - 459.67$
°K	$\vartheta/°\mathrm{C} = T/\mathrm{K} - 273.15$	$\vartheta/°\mathrm{F} = 9/5 \cdot T/\mathrm{K} - 459.67$
	°R	K
°C	$\vartheta/°\mathrm{R} = 9/5 \cdot \vartheta/°\mathrm{C} + 491.67$	$T/\mathrm{K} = \vartheta/°\mathrm{C} + 273.15$
°F	$\vartheta/°\mathrm{R} = \vartheta/°\mathrm{F} + 459.67$	$T/\mathrm{K} = [5/9 \cdot (\vartheta/°\mathrm{F} - 32)] + 273.15$
°R	1	$T/\mathrm{K} = 5/9 \cdot (\vartheta/°\mathrm{R} - 491.67) + 273.15$
°K	$\vartheta/°\mathrm{R} = 9/5 \cdot (T/\mathrm{K} - 273.15) + 491.67$	1

°R degree Rankine, °C degree Celsius, °F degree Fahrenheit, K Kelvin

15.6 Sugar Conversion Chart: Concentration, Density, Refraction

Table 15.18. Conversion table for sugar content, i.e. solid matter (degree Brix, degree Oechsle, degree Baumé, Klosterneuburg degrees)

sucrose concentration °Bx	relative density $d_{20/20}$	degree Oechsle °Oe	degree Baumé °Be	Klosterneuburg degrees
1	1.00389	4	0.56	1.3
2	1.00779	8	1.12	2.0
3	1.01172	12	1.68	2.8
4	1.01567	16	2.24	3.6
5	1.01965	20	2.79	4.4
6	1.02366	24	3.35	5.2
7	1.02770	28	3.91	5.9
8	1.03176	32	4.46	6.9
9	1.03586	36	5.02	7.7
10	1.03998	40	5.57	8.5
11	1.04413	44	6.13	9.3
12	1.04831	48	6.68	10.1
13	1.05252	53	7.24	11.0
14	1.05677	57	7.79	11.9
15	1.06104	61	8.34	12.7

sucrose concentration °Bx	relative density $d_{20/20}$	degree Oechsle °Oe	degree Baumé °Be	Klosterneuburg degrees
16	1.06534	65	8.89	14.4
17	1.06968	70	9.45	14.3
18	1.07404	74	10.0	15.2
19	1.07844	78	10.55	16.0
20	1.08287	83	11.10	16.9
21	1.08733	87	11.65	17.7
22	1.09183	92	12.20	18.6
23	1.09636	96	12.74	19.5
24	1.10092	101	13.29	20.3
25	1.10551	106	13.84	20.9
26	1.11014	110	14.39	21.9
27	1.11480	115	14.93	22.8
28	1.11949	119	15.48	23.6
29	1.12422	124	16.02	24.4
30	1.12898	129	16.57	25.3
31	1.13378	134	17.11	26.1
32	1.13861	139	17.65	26.8
33	1.14347	143	18.19	27.8
34	1.14837	148	18.73	28.7
35	1.15331	153	19.28	–
36	1.15828	158	19.81	–
37	1.16329	163	20.35	–
38	1.16833	168	20.89	–
39	1.17341	173	21.43	–
40	1.17853	179	21.97	–

Conversion of Oechsle Density Unit

The density unit "degree Oechsle" (°Oe) is an unit on a special scale used throughout parts of Europe to characterize fruit juices by their density. Especially in the grape wine industry, vineyard workers use this unit for determining the ripeness of the grapes. The higher the sugar content, the higher is the density. Based upon extensive experience, knowledgeable wine makers can gather valuable information about the quality of the wine they intend to produce from the density reading of the grapes about to be harvested. Based on the relative density d (specific gravity, see Section 2.3.3), the degree Oechsle can be defined as follows:

$$\rho \text{ in } {}^\circ\text{Oe} = (d - 1) \cdot 1000 \tag{15.26}$$

$$d = \frac{\rho \text{ in } {}^\circ\text{Oe}}{1000} + 1 \tag{15.27}$$

Example 15.8. An aqueous solution of sucrose with a concentration of 10% (*m*/*m*) has a relative density of 1.040 and therefore 40°Oe.

There are density meters with OECHSLE scales available. Also, readings from other nondensity instruments like a refractometer (see Section 11.1) can be converted to °Oe.

Table 15.19. Refraction index (20°C, 589 nm) of aqueous sucrose solution. The concentration in °Bx is noted in left column (from [130])

	0	0.1	0.2	0.3	0.4	0.5	0.6	0.7	0.8	0.9
0	1.33299	1.33313	1.33327	1.33342	1.33356	1.33370	1.33385	1.33399	1.33413	1.33428
1	1.33442	1.33456	1.33471	1.33485	1.33500	1.33514	1.33529	1.33543	1.33558	1.33572
2	1.33587	1.33601	1.33616	1.33630	1.33645	1.33659	1.33674	1.33688	1.33703	1.33717
3	1.33732	1.33747	1.33761	1.33776	1.33791	1.33805	1.33820	1.33835	1.33849	1.33864
4	1.33879	1.33893	1.33908	1.33923	1.33938	1.33952	1.33967	1.33982	1.33997	1.34012
5	1.34026	1.34041	1.34056	1.34071	1.34086	1.34101	1.34116	1.34131	1.34146	1.34160
6	1.34175	1.34190	1.34205	1.34220	1.34235	1.34250	1.34265	1.34280	1.34295	1.34310
7	1.34325	1.34341	1.34356	1.34371	1.34386	1.34401	1.34416	1.34431	1.34446	1.34461
8	1.34477	1.34492	1.34507	1.34522	1.34537	1.34553	1.34568	1.34583	1.34598	1.34614
9	1.34629	1.34644	1.34660	1.34675	1.34690	1.34706	1.34721	1.34736	1.34752	1.34767
10	1.34783	1.34798	1.34813	1.34829	1.34844	1.34860	1.34875	1.34891	1.34906	1.34922
11	1.34937	1.34953	1.34968	1.34984	1.34999	1.35051	1.35031	1.35046	1.35062	1.35077
12	1.35093	1.35109	1.35124	1.35140	1.35156	1.35172	1.35187	1.35203	1.35219	1.35234
13	1.35250	1.35266	1.35282	1.35298	1.35313	1.35329	1.35345	1.35361	1.35377	1.35393
14	1.35409	1.35424	1.35440	1.35456	1.35472	1.35488	1.35504	1.35520	1.35536	1.35552
15	1.35568	1.35584	1.35600	1.35616	1.35632	1.35648	1.35664	1.35680	1.35697	1.35713
16	1.35729	1.35745	1.35761	1.35777	1.35793	1.35810	1.35826	1.35842	1.35858	1.35875
17	1.35891	1.35907	1.35923	1.35940	1.35956	1.35972	1.35989	1.36005	1.36021	1.36038
18	1.36054	1.36070	1.36087	1.36103	1.36120	1.36136	1.36153	1.36169	1.36186	1.36202
19	1.36219	1.36235	1.36252	1.36268	1.36285	1.36301	1.36318	1.36334	1.36351	1.36368
20	1.36384	1.36401	1.36418	1.36434	1.36451	1.36468	1.36484	1.36501	1.36518	1.36535
21	1.36551	1.36568	1.36585	1.36602	1.36619	1.36635	1.36652	1.36669	1.36686	1.36703
22	1.36720	1.36737	1.36754	1.36771	1.36788	1.36804	1.36821	1.36838	1.36855	1.36872
23	1.36889	1.36907	1.36924	1.36941	1.36958	1.36975	1.36992	1.37009	1.37026	1.37043
24	1.37060	1.37078	1.37095	1.37112	1.37129	1.37147	1.37164	1.37181	1.37198	1.37216
25	1.37233	1.37250	1.37267	1.37285	1.37302	1.37320	1.37337	1.37354	1.37372	1.37389
26	1.37407	1.37424	1.37441	1.37459	1.37476	1.47494	1.37511	1.37529	1.37546	1.37564
27	1.37582	1.37599	1.37617	1.37634	1.37652	1.37670	1.37687	1.37705	1.37723	1.37740
28	1.37758	1.37776	1.37793	1.37811	1.37829	1.37847	1.37865	1.37882	1.37900	1.37918
29	1.37936	1.37954	1.37972	1.37989	1.38007	1.38025	1.38043	1.38061	1.38079	1.38097
30	1.38115	1.38133	1.38151	1.38169	1.38187	1.38205	1.38223	1.38241	1.38259	1.38277
31	1.38296	1.38314	1.38332	1.38350	1.38368	1.38386	1.38405	1.38423	1.38441	1.38459
32	1.38478	1.38496	1.38514	1.38532	1.38551	1.38569	1.38588	1.38606	1.38524	1.38643

	0	0.1	0.2	0.3	0.4	0.5	0.6	0.7	0.8	0.9
33	1.38661	1.38679	1.38698	1.38716	1.38735	1.38753	1.38772	1.38790	1.38809	1.38827
34	1.38846	1.38865	1.38883	1.38902	1.38920	1.38939	1.38958	1.38976	1.38995	1.39014
35	1.39032	1.39051	1.39070	1.39088	1.39107	1.39126	1.39145	1.39164	1.39182	1.39201
36	1.39220	1.39239	1.39258	1.39277	1.39277	1.39135	1.39333	1.39352	1.39371	1.39390
37	1.39409	1.39428	1.39447	1.39466	1.39485	1.39505	1.39524	1.39543	1.39562	1.39581
38	1.39600	1.39619	1.39638	1.39658	1.39677	1.39696	1.39715	1.39734	1.39754	1.39773
39	1.39792	1.39812	1.39831	1.39850	1.39870	1.39889	1.39908	1.39928	1.39947	1.39967
40	1.39986	1.40006	1.40025	1.40044	1.40064	1.40084	1.40103	1.40123	1.40142	1.40162
41	1.40181	1.40201	1.40221	1.40240	1.40260	1.40280	1.40299	1.40319	1.40339	1.40358
42	1.40378	1.40398	1.40418	1.40437	1.40457	1.40477	1.40497	1.40517	1.40537	1.40557
43	1.40576	1.40596	1.40616	1.40636	1.40656	1.40676	1.40696	1.40716	1.40736	1.40756
44	1.40776	1.40796	1.40817	1.40837	1.40857	1.40877	1.40897	1.40917	1.40937	1.40958
45	1.40978	1.40998	1.41018	1.41039	1.41059	1.41079	1.41099	1.41120	1.41140	1.41160
46	1.41181	1.41201	1.41222	1.41242	1.41262	1.41283	1.41303	1.41324	1.41344	1.41365
47	1.41385	1.41406	1.41427	1.41447	1.41468	1.41488	1.41509	1.41530	1.41550	1.41571
48	1.41592	1.41612	1.41633	1.41654	1.41675	1.41695	1.41716	1.41737	1.41758	1.41779
49	1.41799	1.41820	1.41841	1.41862	1.41883	1.41904	1.41925	1.41946	1.41967	1.41988
50	1.42009	1.42030	1.42051	1.42072	1.42093	1.42114	1.42135	1.42156	1.42177	1.42199
51	1.42220	1.42241	1.42262	1.42283	1.42305	1.42326	1.42347	1.42368	1.42390	1.42411
52	1.42432	1.42454	1.42475	1.42497	1.42518	1.42539	1.42561	1.42582	1.42604	1.42625
53	1.42647	1.42668	1.42690	1.42711	1.42733	1.42754	1.42776	1.42798	1.42819	1.42841
54	1.42863	1.42884	1.42906	1.42928	1.42949	1.42971	1.42993	1.43015	1.43036	1.43058
55	1.43080	1.43102	1.43124	1.43146	1.43168	1.43190	1.43211	1.43233	1.43255	1.43277
56	1.43299	1.43321	1.43343	1.43365	1.43387	1.43410	1.43432	1.43454	1.43476	1.43498
57	1.43520	1.43542	1.43565	1.43587	1.43609	1.43631	1.43654	1.43676	1.43698	1.43720
58	1.43743	1.43765	1.43787	1.43810	1.43832	1.43855	1.43877	1.43900	1.43922	1.43944
59	1.43967	1.43989	1.44012	1.44035	1.44057	1.44080	1.44102	1.44125	1.44148	1.44170
60	1.44193	1.44216	1.44238	1.44261	1.44284	1.44306	1.44329	1.44352	1.44375	1.44398
61	1.44420	1.44443	1.44466	1.44489	1.44512	1.44535	1.44558	1.44581	1.44604	1.44627
62	1.44650	1.44673	1.44696	1.44719	1.44742	1.44765	1.44788	1.44811	1.44834	1.44858
63	1.44881	1.44904	1.44927	1.44950	1.44974	1.44997	1.45020	1.45043	1.45067	1.45090
64	1.45113	1.45137	1.45160	1.45184	1.45207	1.45230	1.45254	1.45277	1.45301	1.45324
65	1.45348	1.45371	1.45395	1.45419	1.45442	1.45466	1.45489	1.45513	1.45537	1.45560
66	1.45584	1.45608	1.45631	1.45655	1.45679	1.45703	1.45726	1.45750	1.45774	1.45798
67	1.45822	1.45846	1.45870	1.45893	1.45917	1.45941	1.45965	1.45989	1.46013	1.46037
68	1.46061	1.46085	1.46109	1.46134	1.46158	1.46182	1.46206	1.46230	1.46254	1.46278
69	1.46303	1.46327	1.46351	1.46375	1.46400	1.46424	1.46448	1.46473	1.46497	1.46521
70	1.46546	1.46570	1.46594	1.46619	1.46643	1.46668	1.46692	1.46717	1.46741	1.46766
71	1.46790	1.46815	1.46840	1.46864	1.46889	1.46913	1.46938	1.46963	1.46987	1.47012
72	1.47037	1.47062	1.47086	1.47111	1.47136	1.47161	1.47186	1.47210	1.47235	1.47260

	0	0.1	0.2	0.3	0.4	0.5	0.6	0.7	0.8	0.9
73	1.47285	1.47310	1.47335	1.47360	1.47385	1.47410	1.47435	1.47460	1.47485	1.47510
74	1.47535	1.47560	1.47585	1.47610	1.47653	1.47661	1.47686	1.47711	1.47736	1.47761
75	1.47787	1.47812	1.47837	1.47862	1.47888	1.47913	1.47938	1.47964	1.47989	1.48015
76	1.48040	1.48065	1.48091	1.48116	1.48142	1.48167	1.48193	1.48218	1.48244	1.48270
77	1.48295	1.48321	1.48346	1.48372	1.48398	1.48423	1.48449	1.48475	1.48501	1.48526
78	1.48552	1.48578	1.48604	1.48629	1.48655	1.48681	1.48707	1.48733	1.48759	1.48785
79	1.48811	1.48837	1.48863	1.48889	1.48915	1.48941	1.48967	1.48993	1.49019	1.49045
80	1.49071	1.49097	1.49123	1.49149	1.49175	1.49202	1.49228	1.49254	1.49280	1.49307
81	1.49333	1.49359	1.49386	1.49412	1.49438	1.49465	1.49491	1.49517	1.49544	1.49570
82	1.49597	1.49623	1.49650	1.49676	1.49703	1.49729	1.49756	1.49782	1.49809	1.49835
83	1.49862	1.49889	1.49915	1.49942	1.49969	1.49995	1.50022	1.50049	1.50076	1.50102
84	1.50129	1.50156	1.50183	1.50210	1.50237	1.50263	1.50290	1.50317	1.50344	1.50371
85	1.50398	1.50425	1.50452	1.50479	1.50506	1.50533	1.50560	1.50587	1.50614	1.50641

15.7 Fundamental Constants

Table 15.20. Fundamental constants

Avogadro's constant	$N_A = 6.023 \cdot 10^{23}\ \mathrm{mol}^{-1}$
Boltzmann's constant	$k = 1.380658 \cdot 10^{-23}\ \mathrm{J \cdot K}^{-1}$
gas constant universal	$R = 8.314\ \mathrm{J \cdot mol}^{-1} \cdot \mathrm{K}^{-1}$
Stefan–Boltzmann constant	$\sigma = 5.670 \cdot 10^{-8}\ \mathrm{W \cdot m}^{-2} \cdot \mathrm{K}^{-4}$
electric field constant	$\varepsilon_0 = 8.854 \cdot 10^{-12}\ \mathrm{C \cdot V}^{-1} \cdot \mathrm{m}^{-1}$
magnetic field constant	$\mu_0 = 4\pi \cdot 10^{-7}\ \mathrm{V \cdot s \cdot A}^{-1} \cdot \mathrm{m}^{-1}$
Planck's constant	$h = 6.6260693 \cdot 10^{-34}\ \mathrm{J \cdot s}$
Euler's number	$\mathrm{e} = 2.71828\ldots$

15.8 Properties of Water

The graph of p_v versus ϑ in Figure 15.8 shows the phase diagram of water. When we cross the p_v–ϑ curve there are distinct terms: 1 sublimation, 2 condensation, 3 evaporation, 4 condensation, 5 melting, 6 freezing.

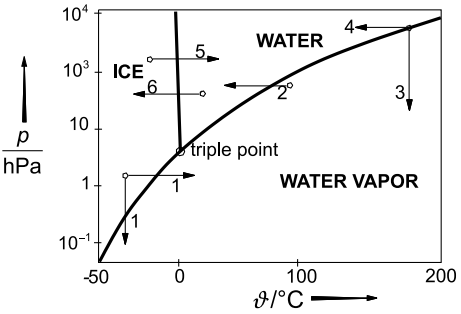

Figure 15.8. Phase diagram of water

Table 15.21. Properties of water: Density ρ, dynamic viscosity η, refraction index at 589 nm n_D, permittivity ε, saturation steam pressure p_v, enthalpy of evaporation Δh_{vap} and surface tension σ at temperature ϑ [105] and [141]

ϑ	ρ	p_v	Δh_{vap}	η	n_D	ε	σ
°C	kg · m^{-3}	kPa	kJ · kg^{-1} · K^{-1}	mPa · s	–	–	mN · m^{-1}
0	999.9	0.610	2501	1.7920	1.3346	87.9	75.6
5	1000.0	0.872		–	1.3346	85.9	74.8
10	999.7	1.228	2520	1.3055	1.3343	84.0	74.1
15	999.1	1.705		–	1.3338	82.1	73.3
20	998.2	2.34	2538	1.0026	1.3333	80.2	72.6
25	997.1	3.17		–	1.3329	78.4	71.8
30	995.7	4.24	2556	0.7984	1.3323	76.6	71.0
40	992.2	7.38	2574	0.6539	1.3309	73.2	69.4
50	988.1	12.33	2592	0.5471	1.3293	69.9	67.7
60	983.2	19.92	2610	0.4660	1.3275	66.8	66.0
70	977.8	31.16	2627	0.4033	1.3255	63.8	64.3
80	971.8	47.34	2644	0.3542	1.3231	60.9	62.5
90	965.3	70.1	2660	0.3148	1.3209	58.2	60.7
100	958.4	101.3	2676	0.2819	1.3182	55.6	58.9
110	951.0	141.4	2692	0.2555	–	–	57.0
120	943.5	195.9	2706	0.2329	–	–	55.0
130	934.8	266.6	2721	–	–	–	52.9
140	926.3	356.7	2734	–	–	–	50.9
150	916.9	469.8	2747	0.1827	–	–	48.7
160	907.6	610.0	2758	–	–	–	46.6
170	897.3	781.6		–	–	–	44.4
180	886.6	989.6	2778	–	–	–	42.2
190	876.0	1238.7		–	–	–	40.0
200	862.8	1534.6	2793	0.1345	–	–	37.7

Table 15.22. Physical data of water

molecular mass	18.01534g · mol^{-1}
melting point at 101.32 kPa (1 atm)	ϑ_{fus} = 0 °C
boiling point at 101.32 kPa (1 atm)	ϑ_{vap} = 100 °C
critical temperature	T_C = 647.15 K
triple point	0.0099 °C and 610.4 kPa
specific gas constant of water	R_S = 461.9 J · kg^{-1} · K^{-1}
Eötvös constant	k_E = 7.5 J · K^{-1} mol^{-1} (at 20 °C)
heat of fusion at 0 °C	334.0 kJ · kg^{-1}
heat of vaporization at 100 °C	2257.2 kJ · kg^{-1}
heat of sublimation at 0 °C	2828.3 kJ · kg^{-1}

15.9 Food Material Data

A comprehensive collection of food material data is something food engineers have been seeking for several years with limited success. The main reason might be that properties of food materials and their raw materials are rarely constant, but often vary with climate, crop conditions, processing and consumer needs. So food engineers often have to work with approximations like assuming a soft drink to behave like an aqueous sucrose solution, etc.

Some advice is given here on where to find compiled food material data, including some tables with information that can be used as a "first aid" measures. Regardless of the approach taken in searching for data on food properties, it is always important to recall that the conditions of the material and testing or measurement methods must be carefully specified (e.g. moisture content, temperature, pH, flow regime, etc.). If these conditions are not specified, there will be considerable chance of obtaining data that is misleading.

[134] Rahman's food properties handbook	valuable presentation of food material data in each chapter
[123] nelfood.com database	commercial online database
[143] data sourcebook for food scientists and technologists	mainly food nutritional data
[145] USDA nutrient database	food composition and nutritional data
[146] sucrose solution database	software for computing physical properties of sucrose, sucrose solutions
[147] thermal conductivity	collection of published data on thermal conductivity of foodstuffs
[148] heat transfer coefficients	collection of published data on heat transfer coefficients in food processing
[149] thermophysical properties	Predictive equations for thermophysical properties and enthalpy during cooling and freezing of food materials
[150] heat transfer data	general data for heating, refrigerating and air conditioning
[151] thermal diffusivity	mathematical functions for estimates of thermal diffusivity of foods
[152] lipid physical data	characteristics of oils, fats and waxes
[153] food powder data	physical properties of food powders

Sorption Data

Table 15.23. BET monolayer moisture data, compiled by [134]

food	$x_{W,a}$	food	$x_{W,a}$
amorphous lactose	0.060	instant starch	0.057
beans	0.042	lima bean	0.054
beef ground	0.061	meat	0.040–0.062
beef soup and gravy	0.024	milk (dried whole)	0.012–0.020
chicken	0.052	milk (instant)	0.057
chicken soup and gravy	0.017	navy bean	0.052
cheese (spray dried)	0.022	nonfat dry milk	0.030
cocoa	0.039	onion powder	0.036
coffee	0.083	pea	0.036
cracker	0.042	potato	0.051–0.078
crystallized sucrose	0.004	potato dice	0.060
dextrin	0.090	potato starch	0.066
egg	0.068	raspberry	0.021
egg albumin	0.050–0.065	rhubarb	0.057
fish	0.049	shrimp	0.056
freeze dried beef	0.040	small red bean	0.045
gelatin	0.087	starch	0.110
instant macaroni	0.059	strawberry	0.048

Table 15.24. BET monolayer data for dehydrated foods, compiled by [167]

material	A/D	$\vartheta/^\circ$C	$x_{W,a}$	product	A/D	$\vartheta/^\circ$C	$x_{W,a}$
amylose	A	28.2	0.070	gel[e]	A	30.0	0.111
amylopectin	A	28.2	0.073		A	40.0	0.090
agar	A	RT	0.135		A	50.0	0.101
CMC	A	25.0	0.095	lactoglobulin[e]	A	25.0	0.059
casein	A	30.0	0.076		A	40.0	0.056
CM	A	37.0	0.044	lactose[e]	A	23.0	0.062
collagen	A	25.0	0.096	maltose[e]	A	23.0	0.050
	A	40.0	0.095	pectic acid	A	29.0	0.073
egg[d]	A	25.0	0.063	pectin, highly esterified	A	29.0	0.108
	A	40.0	0.059	salmin	A	25.0	0.059
egg[d,e]	A	25.0	0.056		A	40.0	0.055
	A	26.5	0.056				
	A	40.0	0.055				
elastin	A	25.0	0.055				
	A	40.0	0.056	starch (maize)	A	25.0	0.075

material	A/D	ϑ/°C	$x_{W,a}$	product	A/D	ϑ/°C	$x_{W,a}$
gelatin	A	20.0	0.133	starch gel[e]	A	20.0	0.092
fish, protein concentrate	A	25.0	0.053		A	30.0	0.082
	A	35.0	0.051		A	40.0	0.078
	A	42.0	0.045		A	50.0	0.072
cheese[e]	A	25.0	0.033	sucrose[e]	A	47.0	0.057
	D	25.0	0.035	yoghurt[e]	A	5.0	0.052
cheese[e]	A	25.0	0.033		A	25.0	0.041
	A	45.0	0.022		A	45.0	0.030
	D	25.0	0.037		D	5.0	0.054
milk (nonfat)	A	1.7	0.101		D	25.0	0.042
	A	15.6	0.075	peanuts	D	25.0	0.043
	A	30.0	0.070	pekanut	A	5.0	0.019
	A	37.7	0.067		A	25.0	0.019
egg (whole)	A	17.1	0.037		A	45.0	0.016
	A	30.0	0.036		A	60.0	0.0085
	A	50.0	0.035		D	5.0	0.020
	A	70.0	0.033		D	45.0	0.017
	D	19.5	0.041		D	60.0	0.0094
paranut	A	5.0	0.022	soybean	A	30.0	0.026
	A	25.0	0.018	walnut	A	22.5	0.0074
	A	60.0	0.011	orange juice	A	25.0	0.011
	D	5.0	0.025	orgeat[e]	A	25.0	0.052
	D	60.0	0.012				

Abbreviations

A	adsorption	*d*	albumin
D	desorption	*e*	freeze dried
CM	microcrystalline cellulose		

Table 15.25. BET parameters for grain and starchy food [134]

material	ϑ/°C	a_W range	$x_{W,a}$	k	C
ADSORPTION					
barley	25	0.43–0.96	0.070	0.827	30.14
corn flower	26	0.11–0.96	0.074	0.794	118.33
corn flower[a]	26	0.11–0.96	0.083	0.748	278.35
flour[b]	27	0.09–0.84	0.080	0.711	32.49
wheat[c]	25	0.33–0.94	0.070	0.821	37.39
maize[d]	25	0.46–0.98	0.067	0.822	14.49
potato[e]	20	0.16–0.99	0.066	0.849	19.10

material	ϑ/°C	a_W range	$x_{W,a}$	k	C
potato[f]	25	0.11–0.86	0.083	0.774	8.50
potato	25	0.11–0.86	0.130	0.700	1.39
sunflower seed	25	0.31–0.89	0.036	0.877	13.47
rice	4	0.10–0.96	0.072	0.735	5.49
rice (A/D, brown)	27	0.20–0.90	0.097	0.654	16.67
rape seed	25	0.52–0.92	0.032	0.923	18.01
wheat	25	0.26–0.96	0.070	0.825	104.60
potato	40	0.05–0.88	0.052	0.830	13.73
	50	0.05–0.88	0.048	0.820	13.41
	60	0.05–0.88	0.036	0.860	21.18
	70	0.05–0.88	0.029	0.900	17.75
wheat	25	< 0.90	0.084	0.743	23.58
sunflower	23	< 0.90	0.022	0.919	28.40
gari[g]	15	0.10–0.90	0.060	0.824	50.40
	25	0.10–0.90	0.056	0.869	45.10
	35	0.10–0.90	0.058	0.877	20.90
DESORPTION					
barley	25	0.26–0.96	0.074	0.811	101.24
flour[b]	27	0.10–0.84	0.100	0.601	33.09
wheat[c]	25	0.26–0.98	0.084	0.756	23.83
maize	25	0.42–0.98	0.073	0.801	16.11
potato[f]	25	0.11–0.87	0.091	0.725	8.62
sunflower seed	25	0.26–0.89	0.043	0.825	11.65
rice	4	0.19–0.92	0.163	0.421	7.44
rice (rough)	25	0.11–0.87	0.100	0.628	17.57
rape seed	25	0.52–0.92	0.035	0.913	28.97
wheat	25	0.26–0.96	0.076	0.807	77.68
wheat	25	< 0.90	0.097	0.698	21.87
potato	40	0.05–0.88	0.059	0.840	12.52
	50	0.05–0.88	0.061	0.820	8.89
	60	0.05–0.88	0.053	0.840	8.57
	70	0.05–0.88	0.057	0.800	4.37
extruded pasta	55	< 0.90	0.054	0.798	10.27

Abbreviations

[a] demerged
[b] Canadian (HRSW)
[c] glenlea
[d] freeze dried
[e] sliced (norchip)
[f] vacuum dried
[g] cassava semolina

Table 15.26. GAB parameters (adsorption), compiled by [134]

material	ϑ/°C	a_W range	$x_{W,a}$	k	C
cocoa bean	28	0.34–0.86	0.033	0.882	903.66
cocoa bean	30	< 0.90	0.161	0.512	11.87
coffee					
freeze dried	20	0.05–0.50	0.039	1.182	19.16
decaffeinated	20	0.05–0.60	0.050	1.048	12.69
spray dried	20	0.05–0.60	0.032	1.285	18.94
roast & ground	20	0.05–0.60	0.033	0.940	61.61
roast & ground	20	0.10–0.95	0.035	0.963	16.65
	25	0.10–0.95	0.032	0.993	15.90
	40	0.10–0.95	0.032	0.987	12.45
	60	0.10–0.95	0.030	0.993	8.59
	80	0.10–0.95	0.028	1.029	5.22
ground	20	< 0.80	0.035	9.963	16.65
green bean	28	0.25–0.88	0.040	0.966	4.86
coffee extract	20	< 0.85	0.029	1.009	3.01
coffee extract	20	< 0.90	0.062	1.023	2.85
tea					
BOP grade	21	0.03–0.99	0.044	0.879	7.49
chamomile	25	0.05–0.80	0.064	0.931	16.76
dust grade	21	0.03–0.94	0.044	0.898	3.20
fennel	25	0.05–0.80	0.043	0.950	3.11
pekoe	28	0.10–0.78	0.065	0.729	26.35
pepper	25	0.05–0.80	0.071	0.831	18.29

Table 15.27. GAB parameters (desorption), compiled by [134]

material	ϑ/°C	a_W range	$x_{W,a}$	k	C
cocoa bean	28	0.12–0.93	0.027	0.918	162.39
tea					
BOP grade	21	0.03–0.96	0.051	0.859	126.65
chamomile	25	0.10–0.80	0.073	0.888	28.40
dust grade	21	0.03–0.95	0.075	0.050	64.25
fanning	28	0.21–0.78	0.044	0.925	25.49
fennel	25	0.10–0.80	0.043	0.929	8.10
pepper	25	0.10–0.80	0.076	0.798	67.68

Density Data

Table 15.28. Density (in $kg \cdot m^{-3}$) of some typical food materials (ϑ in °C)

water:	$\rho = 1000.22 + 1.0205 \cdot 10^{-2} \cdot \vartheta - 5.8149 \cdot 10^{-3} \cdot \vartheta^2 + 1.496 \cdot 10^{-5} \cdot \vartheta^3$
whey:	$\rho = \rho_{water} + 4.039 \cdot dm + 1.273 \cdot 10^{-2} \cdot dm^2 + 9.62 \cdot 10^{-5} \cdot dm^3$
HTST milk:	$\rho = 1040.7 - 0.2665 \cdot \vartheta - 2.3 \cdot 10^{-3} \cdot \vartheta^2$
grape juice:	$\rho = 969 + 0.5715 \cdot dm - (25 + 0.42 \cdot dm) \cdot \vartheta/100$
milk and cream:	$\rho = 2.3 \cdot 10^{-3} \cdot \vartheta^2 - 2.665 \cdot 10^{-1} \cdot \vartheta + 1040.7 - x_1(-4.81 \cdot 10^{-5} \cdot \vartheta^2 + 9.76 \cdot 10^{-3} \cdot \vartheta^2 + 1.011)$

where

dm	dry matter in % (m/m)
ρ	density in $kg \cdot m^{-3}$
ϑ	temperature in °C
x_f	fat content in % (m/m)
ϑ	temperature in °C

Table 15.29. Properties of aqueous $CaCl_2$ solutions [141]

concentration in % (m/m)	specific gravity d at 15.6 °C	density in °Baume at 15.6 °C	freezing point in °C	specific heat capacity c_p in $kJ \cdot kg^{-1} \cdot K^{-1}$
0	1.000	0	0	4.1868
1	1.007	1	–0.6	4.145
2	1.015	2.1	–1	4.061
3	1.024	3.4	–1	4.019
4	1.032	4.5	–2	3.936
5	1.041	5.7	–2	3.894
6	1.049	6.8	–3	3.810
7	1.058	8	–4	3.768
8	1.067	9.1	–4	3.684
9	1.076	10.2	–5	3.643
10	1.085	11.4	–6	3.601
11	1.094	12.5	–7	3.517
12	1.103	13.5	–8	3.475
13	1.112	14.6	–9	3.433
14	1.121	15.6	–10	3.412
15	1.131	16.8	–11	3.329
16	1.140	17.8	–12	3.266
17	1.151	19	–13	3.224
18	1.160	20	–15	3.161
19	1.160	21	–17	3.098

concentration in % (m/m)	specific gravity d at 15.6 °C	density in °Baume at 15.6 °C	freezing point in °C	specific heat capacity c_p in kJ · kg^{-1} · K^{-1}
20	1.179	22	–18	3.256
21	1.188	23	–21	3.014
22	1.198	24	–23	2.973
23	1.208	25	–24	2.931
24	1.218	26	–27	2.889
25	1.229	27	–30	2.868
26	1.239	28	–33	2.847
27	1.250	29	–36	2.805
28	1.261	30	–29	2.784
29	1.272	31	–43	2.763
30	1.283	32	–48	2.721

Table 15.30. Bulk densities and moisture of food, compiled by [134]

food powder	bulk density in kg · m^{-3}	moisture in % (m/m)
baby-food formula	400	2.5
cocoa	480	3–5
coffee (ground, roasted)	330	7
coffee (instant)	330	2.5
coffee (creamer)	470	3
cornmeal	660	12
cornstarch	560	12
egg (whole)	340	2–4
gelatin (ground)	680	12
microcristalline cellulose	680	6
milk	610	2–4
oatmeal	430	8
onion (powdered)	510	1–4
salt (granulated)	960	0.2
salt (powdered)	950	0.2
soy protein (precipated)	280	2–3
sugar (granulated)	800	0.5
sugar (powdered)	480	0.5
wheat flour	480	12
whey	560	4.5

Table 15.31. Specific gravity d of phosphoric acid at different concentrations (m/m) [141]

°C	2%	6%	14%	20%	26%	35%	50%	75%	100%
0	1.0113	1.0339	1.0811	1.1192	–	–	–	–	–
10	1.0109	1.0330	1.0792	1.1167	1.1567	1.341	1.341	–	–
20	1.0092	1.0309	1.0764	1.1134	1.1529	1.216	1.335	1.579	1.9
30	1.0065	1.0279	1.0728	1.1094	1.1484	1.211	1.329	1.572	1.9
40	1.0029	1.0241	1.0685	1.1048	–	–	–	–	–

Table 15.32. Specific gravity d of phosphoric acid at different concentrations (m/m) [141]

%	0 °C	10 °C	25 °C	40 °C	60 °C	80 °C	100 °C
1	1.00747	1.00707	1.00409	0.99908	0.9900	0.9785	0.9651
2	1.01509	1.01442	1.01112	1.00593	0.9967	0.9852	0.9719
4	1.03038	1.02920	1.02530	1.01977	1.0130	0.9988	0.9855
8	1.06121	1.05907	1.05412	1.04798	1.0381	1.0264	1.0134
12	1.09244	1.08946	1.08365	1.07699	1.0667	1.0549	1.0420
16	1.12419	1.12506	1.11401	1.10688	1.0962	1.0842	1.0713
20	1.15663	1.15254	1.14533	1.13774	1.1268	1.1146	1.1017
24	1.18999	1.18557	1.17776	1.16971	1.1584	1.1463	1.1331
26	1.20709	1.20254	1.19443	1.18614	1.1747	1.1626	1.1492

Table 15.33. Fluidization velocities needed for different bulk densities [141]

bulk density in $kg \cdot m^{-3}$	air velocity in $m \cdot s^{-1}$	bulk density in $kg \cdot m^{-3}$	air velocity in $m \cdot s^{-1}$
160	14.7	1120	39.1
240	18.2	1200	40.6
320	20.9	1280	41.9
400	23.4	1360	43.2
480	25.7	1440	44.2
560	27.9	1520	45.7
640	29.7	1600	46.7
720	31.4	1680	48.0
800	33.0	1760	49.3
880	34.5	1840	52.0
960	36.3	1920	53.3
1040	37.8		

Interfacial Data

Table 15.34. Surface tension of skim milk and whole milk lateral to air [109]

ϑ in °C	surface tension σ in N · m^{-1}	
	skim milk	whole milk
0	0.0557	0.0515
10	0.0536	0.0507
20	0.0515	0.0500
30	0.0497	0.0493
40	0.0479	0.0488
50	0.0462	0.0483
60	0.0446	0.0478
70	0.0432	0.0474
80	0.0418	0.0471
90	0.0406	0.0469
100	0.0395	0.0467

Table 15.35. Surface tension of several materials to air at 20 °C [109]

material	σ/N · m^{-1}
cream (30%)	0.0492
whey (dm 5%)	0.0566
egg-white	0.060
skim milk permeate (protein content 0.1%)	0.069
skim milk concentrate (protein content 5%)	0.0513
buttermilk (bm)	0.0489
bm permeate	0.0630
bm concentrate	0.0485
butter fat 99.9% at 30 °C	0.0318

Thermal Data

Table 15.36. Heat capacities and specific gas constants R_S of some gases [141]

gas	molecular mass in $g \cdot mol^{-1}$	R_S in $kJ \cdot kg^{-1} \cdot K^{-1}$	c_p in $kJ \cdot kg^{-1} \cdot K^{-1}$	c_v in $kJ \cdot kg^{-1} \cdot K^{-1}$
air	29.97	0.287	1.0035	0.7665
Ar	39.94	0.208	0.5203	0.3122
CO_2	44.01	0.189	0.8418	0.6529
CO	28.01	0.297	0.0413	0.7445
He	4.00	2.077	5.1926	3.1156
H_2	2.02	4.14	14.2091	10.0849
CH_4	16.04	0.518	2.2537	1.7354
N_2	28.02	0.297	1.0416	0.7448
O_2	32.00	0.260	0.9216	0.6618
H_2O	18.02	0.461	1.8723	1.4108

Table 15.37. Specific heat of food components as a function of temperature [134]

component	equation
water[a]	$c_W = 4.0817 - 5.3062 \cdot 10^{-3}\vartheta + 9.9516 \cdot 10^{-4}\vartheta^2$
water[b]	$c_W = 4.1762 - 9.0864 \cdot 10^{-5}\vartheta + 5.4731 \cdot 10^{-6}\vartheta^2$
ice	$c_I = 2.0623 + 6.0769 \cdot 10^{-3}\vartheta$
protein[c]	$c_p = 2.0082 + 1.2089 \cdot 10^{-3}\vartheta - 1.3129 \cdot 10^{-6}\vartheta^2$
fat[c]	$c_{FA} = 1.9842 + 1.4733 \cdot 10^{-3}\vartheta - 4.8008 \cdot 10^{-6}\vartheta^2$
carbohydrate[c]	$c_{ca} = 1.5488 + 1.9625 \cdot 10^{-3}\vartheta - 5.9399 \cdot 10^{-6}\vartheta^2$
fiber	$c_{FI} = 1.8459 + 1.8306 \cdot 10^{-3}\vartheta - 4.6509 \cdot 10^{-6}\vartheta^2$
ash[c]	$c_{as} = 1.0926 + 1.8896 \cdot 10^{-3}\vartheta - 3.6817 \cdot 10^{-6}\vartheta^2$

Abbreviations

[a] –40 to 0 °C

[b] 0 to 150 °C

[c] –40 to 150°C

Table 15.38. Thermal conductivity λ data of some gases [141]

gas	λ/W · m^{-1} · K^{-1}	ρ/in kg · m^{-3}	ϑ in °C
air	0.024	1.29	0
	0.031	0.94	100
carbon dioxide	0.015	1.98	0
	0.022	1.46	100
nitrogen	0.024	1.3	0
	0.031	–	100

Table 15.39. Thermal conductivity λ of liquids: Polynomial expressions [116]

water	$\lambda/\mathrm{mW \cdot K^{-1} \cdot m^{-1}} = 568.96188 + \vartheta/^\circ C - 8.2 \cdot 10^{-3}\,(\vartheta/^\circ C)^2 + 6.02 \cdot 10^{-6}\,(\vartheta/^\circ C)^3$	
milk products with fat content x_f = 3–62%	$\lambda/\mathrm{W \cdot K^{-1} \cdot m^{-1}} = 0.5406 - 0.0055 \cdot \mathrm{x_f}$	(x_f in % (m/m))
milk products with fat content x_f = 62–100%	$\lambda/\mathrm{W \cdot K^{-1} \cdot m^{-1}} = 0.2309 - 0.00051 \cdot \mathrm{x_f}$	(x_f in % (m/m))

Table 15.40. Heat conductivity λ of main food components [116]

	λ/W · K^{-1} · m^{-1}
air	0.025
protein	0.20
carbohydrate	0.245
fat	0.15
water	0.55
ice	2.21
fat free animal solid matter	0.26
fat free plant solid matter	0.22

Table 15.41. Heat conductivity λ of some frozen foods [116]

product	λ/W · K^{-1} · m^{-1}	
	fresh	frozen
strawberry	0.49	1.12
fruit juices	0.56	2.10
mashed potatoes	0.49	1.10
cucumbers	0.54	1.26
salmon	0.50	1.17
filet of codfish	0.54	1.20
beef	0.48	1.40
fat pork	0.37	0.72
low fat pork	0.50	1.55
bacon	0.19	0.27

Table 15.42. Heat conductivity λ of some foods [116]

food	λ/W · K^{-1} · m^{-1}	ϑ/°C	food	λ/W · K^{-1} · m^{-1}	ϑ/°C
milk	0.55	20			
mashed banana	0.56	16	butter (17% H_2O)	0.2	20
codfish	0.44	0	codfish	1.22	–10
codfish	1.37	–20	vegetable	0.3 . . . 0.6	20
grain (loose)	0.15	20	potatoe	0.55	20
margarine	0.2	20	fruit	0.35 . . . 0.55	20
beef (78.5% H_2O)	0.48	0	beef (78.5% H_2O)	1.06	–5
beef (78.5% H_2O)	1.35	–10	beef (78.5% H_2O)	1.57	–20
beef fat (7% H_2O)	0.2	0	beef fat (7% H_2O)	0.21	–5
beef fat (7% H_2O)	0.23	–10	beef fat (7% H_2O)	0.26	–20
pork (76.8% H_2O)	0.2	0	pork (76.8% H_2O)	0.8	–5
pork (76.8% H_2O)	0.99	–10	pork (76.8% H_2O)	1.29	–20
pork fat	0.19	0	pork fat	0.29	–20
starch (loose)	0.15	20	sodium chloride	7	20
sugar (solid)	0.6	20	(solid)		
sugar (loose)	0.15 . . . 0.35	20	ricinus oil	0.181	20
water	0.596	20	air	0.026	20

Table 15.43. Thermal conductivity λ of freeze-dried gels as a function of pore structure when samples are equilibrated at 52% relative humidity at 41 °C [134]

gel	x^a	porosity ε	pore size range in µm	λ/W · K^{-1} · m^{-1}
starch	0.10	0.93	2 to 10	0.0410
gelatin	0.10	0.93	3 to 15	0.0413
egg albumen	0.10	0.97	3 to 15	0.0418
cellulose gum	0.10	0.89	2 to 10	0.0627
pectin	0.10	0.97	1 to 10	0.0474
pectin	0.05	0.98	1 to 10	0.0391
pectin/glucose	0.10	0.96	1 to 8	0.0500

[a] moisture in gel before drying

Table 15.44. Thermal diffusivity a of some foods at 20 °C

food	$a \cdot 10^6$/m^2 · s^{-1}
ethanol	0.100
beer	0.134
butter	0.086
fat	0.09
fish	0.147
low fat meat	0.15
vegetable	0.14
grain (loose)	0.095
potatoes	0.156
margarine	0.092
oranges	0.150
olive oil	0.115
mineral salt	3.2
sugar (loose)	0.2

Table 15.45. Heat conductivity λ and thermal diffusivity a of some materials at ambient temperature

material	$\lambda/\mathrm{W \cdot K^{-1} \cdot m^{-1}}$	$a \cdot 10^6/\mathrm{m^2 \cdot s^{-1}}$
silver	407	176
copper	384	107
aluminum	220	94.6
glass	0.1 . . . 1.0	
special steel	8 . . . 16	
bronze	62	18.6
iron	74	16.2
glass	1	0.61
quartz glass	1.36	
graphite	169	
constantan	23	
brass	80 . . . 220	
steel (St37)	45	14.7
V2A-steel	15	
titanium	22	
PS	0.15	
PVC	0.16	
EPS (styrofoam)	0.036	
plexiglass	0.19	
PA	0.26	
PE	0.4	
concrete	1.3	0.66
porous concrete	0.3	
earth	0.4 . . . 1.3	
window glass	0.8	0.6
gypsum	0.5	0.47
chalky sandstone	1.1	
marble	2.8	
porcelain	0.9	
sandstone	1.9	1.0 . . . 1.3
chamotte	0.5 . . . 1.2	0.33 . . . 0.69
plaster	0.8	
brick	0.5	0.27
brick wall	0.8	0.55
asphalt	0.7	
roofing paper	0.2	
oak/ beech	0.17 . . . 0.31	0.11
fir	0.14 . . . 0.26	
gum	0.13–0.24	0.1
cork	0.05	
granulated cork	0.036	
mineral faber	0.04	
plant faber	0.05	
asbestos sheet	0.7	
slate	2.1	

Table 15.46. DSC fusion data of some sugars and sugar alcohols [168]

material	$\vartheta_{fus}/^{\circ}C$[1]	$\vartheta_{fus}/^{\circ}C$	$\Delta_{fus}H/kJ \cdot kg^{-1}$
monosaccharide			
L-Arabinose	145	155	260
D-Xylose	140	150	280
D-Ribose	75	90	150
α−D-Glucose · H_2O	70	75	60
α−D-Glucose	140	150	180
β-D-Glucose	140	150	150
D-Glactose	155	165	280
D-Fructose	105	115	180
L-Sorbose	150	160	250
L-Rhamnose · H_2O	90	100	210
L-Fucose	125	130	190
D-Glucoheptose	170	180	270
D-Galacturonic acid · H_2O	100	105	70
	125	130	50
D-Glucoronic acid	130	140	280
D-Glucorono-δ-lactone	150	165	120
disaccharide			
α−Lactose	185	195	220
β-Lactose	210	220	250
Cellobiose	210	220	160
Sucrose	175	185	120
Turanose	155	165	150
Lactulose	145	155	110
oligosaccharide			
Melozitose · $2H_2O$	155	165	140
Raffinose · $5H_2O$	80	85	150
polyol			
Meso-erythritol	115	125	330
L-Arabinitol	90	105	230
Xylitol	90	100	250
Ribitol	100	110	250
D-Glucitol (Sorbitol)	85	95	150
D-Mannitol	155	170	290
Galactitol (Dulcitol)	175	190	330
Maltitol	140	150	150
Isomaltitol	160	175	180
Myo-inositol	215	230	260
polysaccharide			
Inulin	145	150	40
Maize starch	–	–	58
Wheat starch	–	–	53
Waxy maize starch	–	–	61
Potato starch	–	–	60

[1] extrapolated onset temperature
[2] peak temperature

Electrical Data

Table 15.47. Dielectric properties of food materials, adapted from [154]

food	ϑ/°C	moisture	10^7 Hz		10^9 Hz		$3 \cdot 10^9$ Hz	
		in % (db)	ε'	ε''	ε'	ε''	ε'	ε''
beef steak bottom, round	25	–	50	1300	50	39	40	12
beef steak frozen, lean	0	–	–	–	4.4	0.72	3.95	0.3
bacon fat, conventional, rendered	25	–	–	–	2.6	0.16	2.5	0.13
potato, raw	25	–	80	47.8	65.1	19.6	53.7	15.7
turkey cooked	25	–	–	–	46.0	68.0*	40.0	14.0*
butter	0	16.5	–	–	–	–	4.05	0.39
butter	35	–	–	–	–	–	4.15	0.44
ice, pure	–12	–	3.7	0.07	–	–	3.2	0.003
water distilled	25	–	–	–	77.5	1.2*	76.7	12.0
milk powder	30	3.2	–	–	–	–	2.29	0.05
whey powder	30	4.6	–	–	–	–	2.04	0.025

15.10 Color Test Solutions

In conformity with the European Pharmacopoeia [129], five so-called color standard solutions can be prepared from mixtures of three color stock solutions (yellow: $FeCl_3$ solution; red: $CoCl_2$ solution; blue: $CuSO_4$ solution). The five resulting colors are brown, brownish-yellow, yellow, greenish-yellow, and red. Color test solutions can then be prepared from defined dilution levels carried out in six steps. The color stock solutions are very stable, and keep their quality indefinitely. However, the color standard solutions and the color test solutions are not stable, and must be freshly prepared at the time of use. There are two established methods by which to compare a sample color with a color test solution that are described as follows:

method I: 2 cm^3 of each, sample and test solution, are filled in colorless reagent bottles with 12 mm inside diameter and observed under diffuse daylight in a horizontal orientation to a white background.

method II: 10 cm^3 of each, sample and test solution, are filled in colorless reagent bottles with 16 mm inside diameter, and observed under diffuse daylight in a vertical orientation to a white background.

The advantage of method II is that results are more reproducible because of the greater depth of the solutions. It is advisable to use a so-called NESSLER cylinder instead of the reagent bottles. These are translucent, colorless cylinders with 16 mm inside diameter and flat, translucent bottom.

Preparation of Color Stock Solutions

Yellow color stock solution. A quantity of 46 g ferric chloride ($FeCl_3$) is dissolved in ca. 900 ml of a mixture of 25 ml hydrochloric acid and 975 ml water and diluted with this mixture to 1000.0 ml. After analysis to confirm solution composition, the solution is further diluted with sufficient hydrochloric acid–water mixture until there are 45.0 mg $FeCl_3 \cdot 6H_2O$ in 1 ml of the solution.

Analysis of content: A quantity of 10.0 ml of yellow color stock solution and 15 ml water, 5 ml hydrochloric acid and 4 g potassium iodide are mixed in a 200-ml Erlenmeyer flask with glass stopper. Immediately, the flask is closed and placed under darkness for about 15 min. After the addition of 100 ml water the resulting Iodine solution will be titrated with 0.1 N sodium thiosulfate solution. At the end of the titration, 10 drops starch solution has to be added. 1 ml 0.1 N sodium thiosulfate solution conforms to 27.03 mg $FeCl_3 \cdot 6H_2O$.

Red color stock solution. A quantity of 60 g cobalt(II)-chloride ($CoCl_2$) is dissolved in ca. 900 ml of a mixture of 25 ml hydrochloric acid and 975 ml water and diluted with this mixture to a total of 1000.0 ml. After the analysis of contents, the solution will be diluted with sufficient hydrochloric acid–water mixture, until there is 59.5 mg $CoCl_2 \cdot 6H_2O$ in 1 ml of the solution.

Analysis of content: A quantity of 5.0 ml of red color stock solution and 5 ml hydrogen peroxide and 10 ml of a 30 percent (m/V) solution of sodium hydroxide are mixed in a 200-ml Erlenmeyer flask with glass stopper, and heated to low boiling for about 10 min. After cooling down to room temperature, the solution is mixed with diluted sulphuric acid and 2 g potassium iodide, and the flask is immediately closed and shaken slowly to dissolve the iodide. The resulting brownish colored Iodine solution is titrated with 0.1 N sodium thiosulfate solution until the color is pink. Near to the end of the titration, 10 drops of starch solution *R* are added. 1 ml 0.1 N sodium thiosulfate solution conforms 23.79 mg $CoCl_2 \cdot 6H_2O$.

Blue color stock solution. A quantity of 63 g cupric sulfate ($CuSO_4$) is dissolved in ca. 900 ml of a mixture of 25 ml hydrochloric acid and 975 ml water and diluted with this mixture up to 1000.0 ml. After the analysis of contents, the solution is diluted with sufficient hydrochloric acid–water mixture, until there is 62.4 mg $CuSO_4 \cdot 5H_2O$ in 1 ml of the solution.

Analysis of content: A quantity of 10.0 ml blue color stock reference solution and 50 ml water, 12 ml diluted acetic acid and 3 g potassium iodide are mixed in a 200-ml Erlenmeyer flask with glass stopper. The resulting iodine solution is titrated with 0.1 N sodium thiosulfate solution until the solution is blue colored. Near to the end of the titration, 10 drops of starch solution *R* are added. 1 ml 0.1 N sodium thiosulfate solution conforms 24.979 mg $CuSO_4 \cdot 5H_2O$.

Color Standard Solutions

The nomenclature for the five color standard solutions and the color test solutions is given in Table 15.48.

Table 15.48. Color standard solutions [129]

color standard solutions	yellow color stock solutions ml	red color stock solutions ml	blue color stock solutions ml	hydrochloric acid 1% (m/V) ml
B (brown)	3.0	3.0	2.4	1.6
BG (brownish-yellow)	2.4	1.0	0.4	6.2
G (yellow)	2.4	0.6	0.0	7.0
GG (greenish-yellow)	9.6	0.2	0.2	0.0
R (red)	1.0	2.0	0.0	7.0

With these five color standard solutions, the color test solutions are mixed like shown in Table 15.49.

Table 15.49. Color test solutions [129]

color test solutions B		
color test solution	color standard solution B ml	hydrochloric acid 1% (m/V) ml
B_1	1.50	0.50
B_2	1.00	1.00
B_3	0.75	1.25
B_4	0.50	1.50
B_5	0.25	1.75
B_6	0.10	1.90

color test solutions BG		
color test solution	color standard solution BG ml	hydrochloric acid 1% (m/V) ml
BG_1	2.00	0.00
BG_2	1.50	0.50
BG_3	1.00	1.00
BG_4	0.50	1.50
BG_5	0.25	1.75
BG_6	0.10	1.90

color test solutions G		
color test solution	color standard solution G ml	hydrochloric acid 1% (m/V) ml
G_1	2.0	0.00
G_2	1.50	0.50
G_3	1.00	1.00
G_4	0.50	1.50
G_5	0.25	1.75
G_6	0.10	1.90

color test solutions GG		
color test solution	color standard solution GG ml	hydrochloric acid 1% (m/V) ml
GG_1	0.5	1.50
GG_2	0.30	1.70
GG_3	0.17	1.83
GG_4	0.10	1.91
GG_5	0.06	1.94
GG_6	0.03	1.97

color test solutions R		
color test solution	color standard solution R ml	hydrochloric acid 1% (m/V) ml
R_1	2.00	0.00
R_2	1.50	0.50
R_3	1.00	1.00
R_4	0.75	1.25
R_5	0.50	1.50
R_6	0.25	1.75

In the US Pharmacopeia color standard solutions are referred to as color matching fluids and are given letter designations A through T, as shown in Table 15.50.

Table 15.50. Color standards according to USP XII

matching fluid	parts of cobalt chloride CS	parts of ferric chloride CS	parts of cupric sulfate CS	parts of water
A	0.1	0.4	0.1	4.4
B	0.3	0.9	0.3	8.5
C	0.1	0.6	0.1	4.2
D	0.3	0.6	0.4	3.7
E	0.4	1.2	0.3	3.1
F	0.3	1.2	0.0	3.5
G	0.5	1.2	0.2	3.1
H	0.2	1.5	0.0	3.3
I	0.4	2.2	0.1	2.3
J	0.4	3.5	0.1	1.0
K	0.5	4.5	0.0	0.0
L	0.8	3.8	0.1	0.3
M	0.1	2.0	0.1	2.8
N	0.0	4.9	0.1	0.0
O	0.1	4.8	0.1	0.0
P	0.2	0.4	0.1	4.3
Q	0.2	0.3	0.1	4.4
R	0.3	0.4	0.2	4.1
S	0.2	0.1	0.0	4.7
T	0.5	0.5	0.4	3.6

16 General Literature

100. BVL Bundesamt für Verbraucherschutz und Lebensmittelsicherheit (ed) Amtliche Sammlung von Untersuchungsverfahren nach §63 LFGB, Beuth, Berlin
101. DIN Deutsches Institut für Normung (ed), Beuth, Cologne
102. Belitz HD, Grosch W (1987) Food Chemistry. Springer, Berlin
103. Matissek R, Schnepel FM, Steiner G (2006) Lebensmittelanalytik. Springer, Berlin
104. Official Methods of Analysis of AOAC International (2003) 17th Edition, 2nd Revision, Association of Official Agricultural Chemists, Gaithersburg
105. VDI-GVC (ed) (2006) VDI-Wärmeatlas. Springer, Berlin
106. Kohlrausch F (1996) Praktische Physik Band 3. Teubner, Stuttgart
107. Kohlrausch F (1996) Praktische Physik Band 1. Teubner, Stuttgart
108. Grigull U (ed) (1979) Properties of Water and Steam in SI-Units. Springer, Berlin
109. Kessler HG (2002) Food and Bioprocess Engineering – Dairy Technology. A.Kessler, Freising,
110. Nielsen SS (ed) (2003) Food Analysis. Kluwer Academic Press, New York
111. Rauscher K, Engst, R, Freimuth U (1986) Untersuchung von Lebensmitteln. VEB Fachbuchverlag, Leipzig
112. AOCS methods – Official Methods and Recommended Practices of the American Oil Chemists's Society, Boulder
113. Atkins P, de Paula J (2006) Physical Chemistry. Oxford University Press
114. Kress-Rogers E, Brimelow CJB (2001) Instrumentation and Sensors for the Food Industry, CRC Press, Boca Raton
115. Lewis MJ (1996) Physical Properties of Foods and Food Processing Systems. Woodhead Publishing, Cambridge
116. Tscheuschner HD (1996) Grundzüge der Lebensmitteltechnik. Behr's, Hamburg
117. Toledo RT (1991) Fundamentals of food process engineering. Van Nostrand Reinhold, New York
118. Singh RP, Heldman DR (2001) Introduction to Food Engineering, Academic Press, San Diego
119. Kurzhals HA (Hrsg.) (2003) Lexikon der Lebensmitteltechnik. Behr's, Hamburg
120. Loncin M (1969) Grundlagen der chemischen Technik, Die Grundlagen der Verfahrenstechnik in der Lebensmittelindustrie. Sauerländer, Frankfurt am Main
121. Valentas KJ, Rotstein E, Singh RP (1997) Food Engineering Practise. CRC Press, New York
122. Böge A (1990) Das Techniker Handbuch. Grundlagen und Anmerkungen der Maschinenbau-Technik. Vieweg Braunschweig
123. Nesvadba P, Houska M, Wolf W, Gekas V, Jarvis D, Sadd PA, Johns AI (2004) Database of physical properties of agro-food materials. J Food Engineering 61: 497–503
124. Rha C (ed) (1975) Theory, Determination and Control of Physical Properties of Food Materials. Reidel Publishing, Dordrecht

125. Schiweck H, Rymon-Lipinski GW (1991) Handbuch Süßungsmittel. Behr's, Hamburg
126. Okos MR (1986) Physical and chemical properties of food. ASAE Publication, St. Joseph
127. Sharma SK, Mulvaney SJ, Rizvi SS (1991) Food Process Engineering, Theory and Laboratory Experiments. Wiley-VCH, Weinheim
128. Scherz H (ed) Souci Fachmann Kraut (2000) Food Composition and Nutrition Tables. Wiss Verlagsges Stuttgart, Germany
129. Europäisches Arzneibuch (2003) Wiss Verlagsgesellschaft mbh, Stuttgart
130. Whalley HCS (ed) (1964) ICUMSA methods of sugar analysis: official and tentative methods recommended by the International Commission for Uniform Methods of Sugar Analysis (ICUMSA), Elsevier, Amsterdam
131. Frede W (ed) (2005) Taschenbuch für Lebensmittelchemiker und – Technologen, Lebensmittel – Bedarfsgegenstände – Kosmetika – Futtermittel. Springer, Berlin
132. American Society of Testing and Materials (ASTM) (ed) (2005) Annual Book of ASTM Standards. ASTM International, West Conshohocken, PA
133. Mohsenin NN (1986) Physical Properties of Plant and Animal Materials. Gordon and Breach Publishers, Amsterdam
134. Rahman S (ed) (1995) Food Properties Handbook, CRC Press, Boca Raton
135. Sahin S, Sumnu SG (2006) Physical Properties of Food. Springer, Berlin
136. Walstra P (2003) Physical Chemistry of Foods. Marcel Dekker, New York
137. Lide DR (ed) (2006) Handbook of Chemistry and Physics 87th edn. CRC Press, Boca Raton
138. Schwartzberg, Hartel RW (1992) Physical Chemistry of Foods. Marcel Dekker, New York
139. Widlak N (ed) (2000) Physical Properties of Fats, Oils and Emulsifiers. American Oil Chemists' Society Press, Champaign
140. Cui SW (ed) (2005) Food Carbohydrates: Chemistry, Physical Properties, and Applications. CRC Press / Taylor and Francis Group, Boca Raton
141. Hayes GD (1987) Food Engineering Data Handbook. Longman Scientifc and Technical, Harlow
142. Tschubik IA, Maslow AM (1973) Wärmephysikalische Konstanten von Lebensmitteln und Halbfabrikaten. VEB, Leipzig
143. Hui YH (ed.) (1991) Data Sourcebook for Food Scientists and Technologists. VCH Publishers, New York
144. McCance, Widdowson's (1991) The Composition of Foods. Ministry of Agriculture, Fisheries and Food. The Royal Society of Chemistry, London
145. USDA National Nutrient Database, available online: http://www.nal.usda.gov/fnic/foodcomp/search
146. Bubník Z, Henkea S, Kadleca P, Hinkováa A, Poura V (2006) Database of the properties of sucrose, sucrose solution and food. J Food Engineering 77:399–405
147. Krokida MK, Michailidis PA, Maroulis ZB, Saravacos GD (2002) Literature data of thermal conductivity of foodstuffs. Intern J Food Properties 5:63
148. Zogzas NP, Krokida MK, Michailidis PA, Maroulis ZB (2002) Literature data of heat transfer coefficients in food processing. Intern J Food Properties 5:391
149. Fikiin KA, Fikiin AG (1999) Predictive equations for thermophysical properties and enthalpy during cooling and freezing of food materials. J Food Engineering 40:1–6
150. ASHRAE-Handbook (1981) Fundamentals. American Society of Heating, Refrigerating and Air Conditioning Engineers, Atlanta
151. Glavina MY, Di Scala KC, Ansorena R, del Valle CE (2006) Estimation of thermal diffusivity of foods using transfer functions. LWT – Food Science and Technology. 39:455–459

152. Firestone D (ed) (2006) Physical and Chemical Characteristics of Oils, Fats, and Waxes. American Oil Chemists's Society (AOCS), Boulder
153. Barbosa-Cánovas GV, Ortega-Rivas E, Juliano P, Yan H (2005) Food Powders – Physical Properties, Processing and Functionality. Springer, Berlin
154. Hippel AR von (1954) Dielectric Materials and Applications. Technology Press of MIT, Cambridge, MA cited in [141]
155. Baltes W (2000) Lebensmittelchemie. Springer Berlin
156. Gruenwedel DW, Whitaker JR (eds.) (1984) Food Analysis: Principles and Techniques. Vol 2 Physicochemical Techniques. Marcel Dekker, New York
157. Sheehan D (2000) Physical Biochemistry. Wiley-VCH, Weinheim
158. Baianu IC (ed) (1992) Physical Chemistry of Food Processes. Vol 1. AVI, van Nostrand Reinhold, New York
159. Baianu IC, Pessen H, Kumosinksi TF (eds) (1993) Physical Chemistry of Food Processes. Vol 2. AVI, van Nostrand Reinhold, New York
160. Schuchmann H (2005) Lebensmittelverfahrenstechnik: Rohstoffe-Prozesse-Produkte. Wiley-VCH, Weinheim
161. Ebermann R, Elmadfa I (2007) Lebensmittelchemie und Ernährung. Springer, Berlin
162. Saravacos GD, Kostaropoulos A E (2002) Handbook of Food Processing Equipment. Series: Food Engineering Series. Springer, Berlin
163. Heiss R (ed) (2003) Lebensmitteltechnologie. Springer, Berlin
164. Rao MA, Rizvi SSH, Datta AK (2005) Engineering Properties of Food. CRC Press, New York
165. Rao MA, Steffe JF (1992) Viscoelastic Properties of Foods. Elsevier Applied Science, London
166. Rahman MS (1999) Handbook of Food Preservation. Marcel Dekker, New York
167. Iglesias HA, Chirife J (1976) BET monolayer values in dehydratred foods and food components. Food Sci Technol 9:107
168. Raemy A, Schweizer TF (1983) Thermal Behavior of Carbohydrates. J Thermal Analysis 28: 95–108

List of Tables

List of Figures

Index